UNIVERSITÀ
DEGLI STUDI
FIRENZE

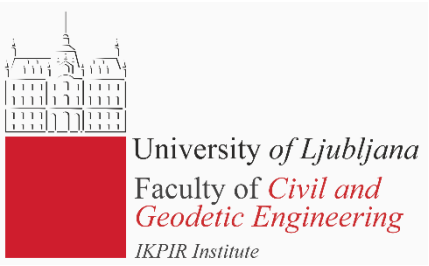

International Doctorate in Civil and Environmental Engineering

CYCLE XXXII

COORDINATOR Prof. Borri Claudio

SEISMIC RESPONSE OF VERTICAL CONCRETE FAÇADE SYSTEMS IN REINFORCED CONCRETE PREFABRICATED BUILDINGS

Scientific Disciplinary Sector ICAR/09

PhD Candidate
Menichini Giovanni

Mentors
Prof. Vignoli Andrea
Prof. Orlando Maurizio
Prof. Isaković Tatjana

Years: 2016/2020

To my parents

Ai miei genitori

Abstract

The design of "non-structural" elements, including the cladding panels for precast RC buildings, plays a key role in the building seismic response. The large damages that occurred in precast RC buildings, during the recent earthquakes in southern Europe were mainly caused by the collapse of the cladding panels. Therefore, is required to revise, to revise the technological and design philosophy the panel-to-structure connection devices in RC precast structures.
Starting from these considerations, the main topic of this thesis is the investigation of such connection devices. Deeply understanding the working principle of these systems makes it possible to open a way to solve the problem.
The influence of the panels to the global response of precast structure is studied for different types of panel-to-structure connections (two types of hammer-head straps) and panels-to-foundation connections (fixed and rocking panels). Numerical models for the in-plane response of connection devices are developed using both existing experimental data from shaking table test performed by University of Ljubljana and result of new tests carried out at the Structures and Materials Testing Laboratory of University of Florence
A new connection device, which better uncouples the in-plane seismic response, is developed and studied analytically and experimentally.
The study highlights that traditional devices fail due to their limited in-plane displacement capacity while the new device has much better behaviour. The study showed that in-plane direction was critical for connection compared to the out-of-plane one. It also showed that fixed-base panels provide a better seismic performance of connection devices.

Keywords: precast reinforced concrete structures, panel-structure connections, out-of-plane connection capacity, cladding panels, seismic response

Acknowledgements

First of all, I would like to thank my mentors Prof. Dr. Andrea Vignoli and Prof. Dr. Maurizio Orlando from the University of Florence for their support, dedication, advice and ideas to carry on the research. A sincere thanks goes to Prof. Dr. Tatjana Isaković from the University of Ljubljana, who hosted me in her department for more than one year and allowed me to work on data from her experimental campaign, constantly following me and offering me valuable advice.
To all of them, Prof. Dr. Andrea Vignoli, Prof. Dr. Maurizio Orlando and Prof. Dr. Tatjana Isaković, thank you for trusting me and allowing me to be involved in your research projects, without which such large-scale experimental research would not have been possible.

I thank Dr. Emanuele del Monte, who was the first to believe in me and suggest me to undertake my PhD career. We often discussed with him about the research issues and he gave me a broader view of the problems related to RC precast structures.

I would also like to thank Baraclit S.p.A., who commissioned the experimental campaign, carried out at the University of Florence and provided specimens and technical support. I also thank the team of the Structural and Materials Testing Laboratory (SMTS) of the Department of Civil and Environmental Engineering of Florence, and the Spin-Off S2R team for their support provided during all phases of the experimental campaign.

During the PhD study, colleagues and friends of my research group at DICEA, as well as those in III / 7 room of the UL-FGG also played an important role in all the ups and downs. Thanks to everyone individually!

I would also like to express my special thanks to my parents, who encouraged me and they were by my side during all my years of study.

Contents

List of figures

List of tables

1 Introduction

From the first post-war period onward, reconstruction policies provided a great opportunity for the industrialization of the construction process. Moreover, in the early fifties, the engineers brought the updated theories of normal and prestressed reinforced concrete to a practical application. Thus the prestressed beams with adherent cables technology started to be produced, then the supply extended to floor panels, columns and gradually to the other construction elements like footings, infill panels, to produce the entire prefabricated system.
During the seventies, the enhancement of technologies led to the production of concrete with high strength and remarkable reliability of performance, at the same time the progress of studies in the theoretical field and the improvement of design practices allowed to cover greater spans, once reserved only for metal structures. At the same time, greater attention was paid to those formal aspects that could guarantee architectural solutions of good quality. These solutions could be obtained at a low price, due both to the rationalization of the building processes and to high competition among the producers. At the start of the nineties, the large roofs tiles winged or with Y-shaped came into the market, and the precast concrete structure solution covered about 85% of industrial construction. Today, the precast reinforced concrete sector employs about 39,000 people only in Italy, which explains the economic impact of research in this field. This production is extremely relevant in terms of civil protection, that is the assessment of life safety standards during seismic events. The last seismic events that struck Italy and southern Europe, in particular, L'Aquila in April 2009, Lorca 2011, Emilia in May 2012 and Central Italy in 2016 caused the collapse or the damage of a great number of industrial buildings. These events draw further attention to the issue of seismic safety of structures built with precast reinforced concrete elements.
Among many reasons for these structural collapses, four main causes can be identified:

- The lack or insufficiency of connection between structural elements, i.e. between tiles and beams and between beams and columns;
- The columns' structural inadequacy, in terms of resistance and ductility;
- The presence of claddings elements (panels) not correctly connected to the structure;
- The presence of non-braced shelving units that carry heavy materials and that can fall down and affect the main structure, causing damage or even collapse.

Many aspects related to the above-mentioned issues have already been addressed in national and European research within the SAFECAST and SAFECLADDING projects. These projects investigated (through a combination of experimental and analytical activity), the seismic behaviour of precast structures with cladding wall panels and also developed some innovative connection devices and new design approaches for a correct fastening system design. These innovations ensure a good structure's seismic performance throughout its service life.
The present work investigates the seismic response of one-storey RC precast structures with vertical cladding panels. Several panel-structure connection systems, based on the isostatic configuration scheme, were studied. An extensive study about the seismic response of the structures with vertical panels layout and traditional hammer-head strap connections was performed by means of the data analysis obtained from a shaking table experimental campaign. In this context, a numerical model was developed to replicate the results obtained from the shaking table and to extend the study to subsequent considerations and further analysis. Within the work, innovative devices for isostatic connections were designed and experimentally catheterized. Simple design rules for single connections were provided. Finally, a study on the relationship between connections demand-capacity for out-of-plane force was performed and analytical formulation for the evaluation of the demand was proposed.

1.1 Historical features on RC precast buildings

The prefabrication of reinforced concrete buildings began in the United States as early as the beginning of the 1900s. In Europe, this technology developed only after the First World War, with the birth and diffusion of new concrete construction systems for structures with large panels and load-bearing supporting frames.
In the period between the first and the second world war some German companies, like for example Philipp Holzmann KG., the Preuss AG., the Dywidag among others, realized different structures introducing innovative constructive systems subsequently adopted throughout the continent. However, in the first half of the twentieth century, the technological evolution in the civil and industrial construction sector was rather slow and conditioned both by the business artisanal structure and by the relatively modest size of the demand. With the end of the Second World War, there was the need to rebuild the urban and productive texture of Europe at low cost and in a short time. Consequently, there was a demand boom for new buildings and infrastructures, both residential and industrial.
What did significantly speed up the construction process was a mass production of standardized building components that could be used for quick on-site assembly. The designers solved the problem by introducing the prestressed tendons technology for concrete and by devising new materials with higher mechanical performances. In this way, they were able to create modular panels, planks and beams needed for long-span floors, roofs, and bridges. Moreover, under controlled factory conditions, plants were able to mass-produce these modular components to standardized specifications, making it far easier to meet the increasing demand for building materials.
When the emergency due to the war was over, the prefabrication system had established itself in such a way that from a situation of need a new and autonomous construction system was born. Also in Italy, prefabrication had a large diffusion starting from the '50s, as a consequence of the mass production of the structural elements. The advantages of this more effective production processes are:

- accelerated construction time, thanks to the possibility of producing the foundations and of assembling the various elements directly on-site;
- less material consumption, due to the possibility of choosing better-designed cross-sections, with a consequent reduction in the weight of the whole structure;
- manpower reduction, since the prefabricated elements are completely made in the factory;
- weather conditions are no longer a problem because the production of the elements can be carried out in closed and air-conditioned environments and therefore the assembly can also be carried out in winter.
- quality improvement offered by industrial manufacturing under constant control of the workshop conditions;

Although also suitable for the construction of residential and office buildings, in Europe and in particular in Italy, prefabrication has always been mainly employed and developed in industrial architecture.
This type of building generally requires the construction of large spanned elements that are repeated with large numbers; it also requires simpler plans and sections of the building as well as less demanding finishes.
In the recent period, to respond to the new demand for sustainable and environmentally beneficial use of buildings and materials, prefabrication has increasingly moved towards systems that improve the thermal performance of buildings and also provide for the energy storage.

1.2 Typologies of RC precast buildings

The static scheme is a key feature of the structures, and it determines their behaviour under the action of static and seismic loads.
About the RC precast structures, it is generally possible to identify three recurrent static schemes:

- *load-bearing panel structures*: which school buildings, hospitals, offices and residences are frequently built with. The characteristic element of this structural typology is the vertical cladding or internal partition panel that works as an element for transferring the loads from each floor to the foundations (Figure 1-1).

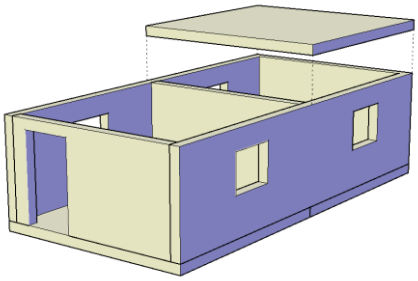

Figure 1-1: Example of a load-bearing panel structure

- *cell structures or spatial load-bearing element structures*: with this system building are made by a rapid assembly of box-shaped or tubular elements, sometimes combined with horizontal panels placed between the overlaying modular elements (Figure 1-2). Due to the volumetric characteristics of the buildings achievable with this system, this structural typology can be used mainly for the construction of residential buildings. This system was born during the fifties and rapidly spread especially in the north-east of Europe, in the United States and Japan

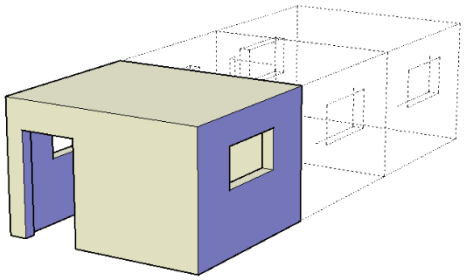

Figure 1-2: Example of a cell structure

- *load-bearing frame structures*: these types of structures are made by assembling linear elements, beams, columns or parts of frames that are connected on site (Figure 1-3).

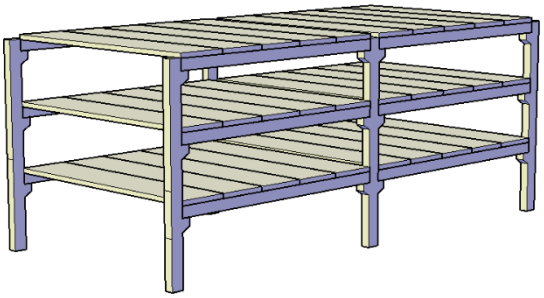

Figure 1-3: Example of a load-bearing frame structure

Depending on the type and arrangement of the connections used, the load-bearing frame structures can be divided into three further subsets (Figure 1-4):

- *Frame with fixed joints* (a): the structure is designed so that it has the typical behaviour of the cast in place RC structures. This behaviour can be obtained with joints that simulate monolithic behaviour or with compatible innovative design solutions usually called Jointed System
- *Scheme with hinged frames* (b): this system usually is mainly typical of industrial buildings. The columns are fixed at the base and the horizontal structures, such as beams, and roofing tiles, are hinged to the columns. Therefore, this scheme has a flexural discontinuity at the joints but it is extremely sensitive to horizontal forces, which could cause large lateral displacements.
- *Isostatic column scheme* (c): Structures with isostatic columns are those that allow free expansion of the roof in the case of, for example, temperature variations, and concentrate on the horizontal forces of columns in the event of an earthquake.

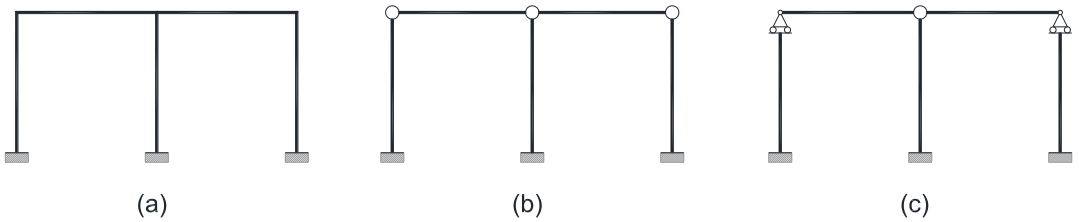

Figure 1-4: Load-bearing frame structure static scheme

A large part of RC precast industrial structures, built both in the past and in present times, have often used the static scheme with hinged frames (b). The considerable lateral displacements, already mentioned above, are a major limitation for verifications at the serviceability ultimate limit states, often leading to not negligible second-order effects (geometric non-linearity).
The type scheme (c) with sliding supports and isostatic pillars is not widely used. The dissipation occurs only at the base of the columns that are not provided with sliding devices.
Introducing in the nodes between the elements some devices capable of reproducing the structural continuity, the scheme (c) becomes to the frame with fixed joints, that is the scheme (a).
This scheme has the advantage, due to its hyperstatic nature, allowing a redistribution of internal forces. Associated with this advantage, there is also a reduction of horizontal displacements and an increase in the number of nodes that are able to dissipate energy. On initial consideration, the frame with fixed joints scheme would appear to be better. But for RC precast structure, it is important to note that the structural design is more complex as it must be defined with a high degree of detail, especially regarding the connections between the various elements of the structure. Indeed, the connections must be able to transmit high flexural and shear stresses. The choice of the static scheme influences the characteristics of the load-bearing components of the structure, and also the types of connection between the vertical and horizontal elements, and those between the horizontal elements themselves.
In this brief introduction, it emerges that the connections are the key elements of the RC prefabricated structures. In particular, the choice of connections defines the static scheme and consequently the response to seismic events.
In this work, the attention will be focused on load-bearing frame structures with hinged frame static scheme, which have been widely employed in south-western Europe and throughout the Mediterranean area for the construction of RC precast buildings, in particular for industrial and manufacturing building.

1.2.1 Connections device classification

As explained above, what characterizes precast RC structures are the connection joints which determine the structural behaviour both for static and seismic loads. Firstly the connections of the prefabricated structures can be divided up into two main categories "*dry joints*" and "*wet joints*" (these are joints with finishing cast)

- Dry joints: the connections are made by interposing metal devices (brackets, plates, threaded bars etc.), to the contact points between the elements; and this allows a bolted or welded connection.
- Wet joints: the connections are generally made up of cast-in-situ concrete and rebar splices. Among the different types of rebar splices, loop splice connections have shown very good mechanical properties. The loop splices are positioned in special housings made up of the elements to be joined and then filled with the concrete casting.

Since the dry joints are immediately efficient, they are better suited for the specific features of RC precast constructions (execution speed, quality control, cost reduction…), and nowadays they are widely used wherever possible. Considering the localized position of dry joints, it is evident that they are used above all where there is no need for continuously distributed connections along the main direction. For this reason, the structural typology in which this type of connection is best included is the load-bearing frame structure.

Another type of classification for the connections, proposed in (ASSOBETON & ReLuis, 2007), is that based on the construction elements that have to be joined, therefore the following categories for the load-bearing frame structure are considered (Figure 1-5):

1. joints between floor elements (JOINT TYPE 1);
2. joints between floor elements and beams (JOINT TYPE 2);
3. joints between beams and columns (JOINT TYPE 3);
4. joints between columns and foundations (JOINT 4 UNION);
5. joints between cladding panels and main structure (JOINT 5 UNION).

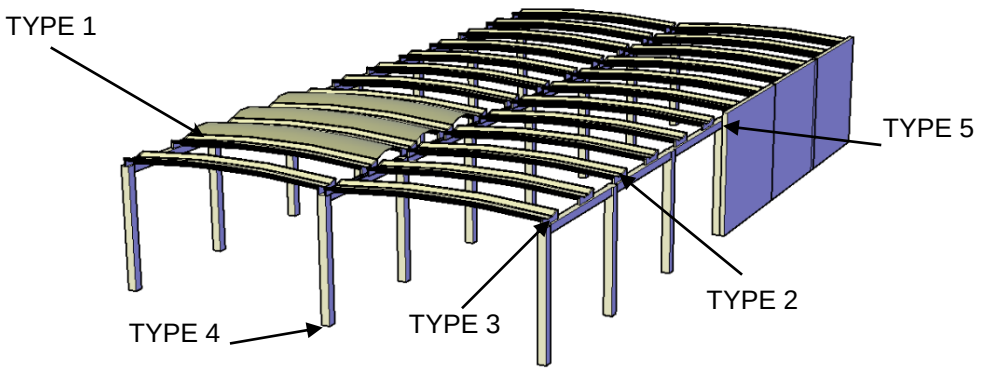

Figure 1-5: Joint types according to Assobeton Catalogue

JOINTS TYPE 1

This category of connections regards the mutual connections between roof or floor elements (Figure 1-6). These joints can change depending on: the shape of the elements that are used and the presence of skylights. Among the most frequently used connections for this typology are those that require a finishing cast on-site or "wet joints". On the other hand, welds, bolts or dowels applied to several steel connecting elements could be used, especially when it is planned to connect adjacent roofing elements or with the presence of flat or curved slabs interposed between the tiles.

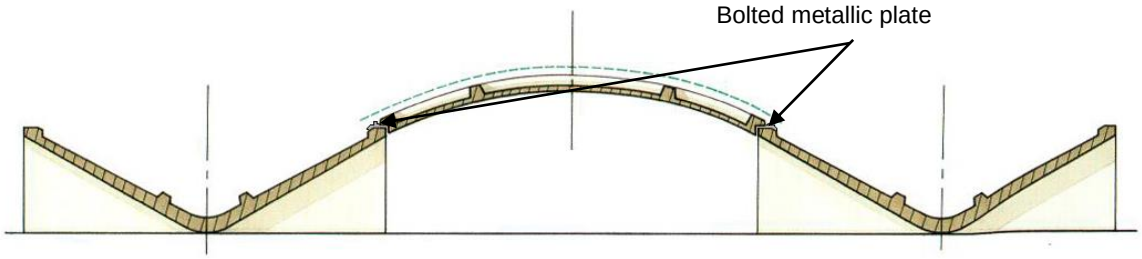

Figure 1-6: Example of type 1 joints (Dassori, 2001)

JOINTS TYPE 2

This category of connections corresponds to the connections between floor elements and beams (Figure 1-7). These type 2 connections are very varied and change depending on the shape of the covering element used as well as on the type of support on the beam: it goes from connections made with only post-inserted elements (as in the case of the constraints that use the blocks) to unions that utilize channel girders or pre-inserted plates to weld or bolt on connecting steel profiles

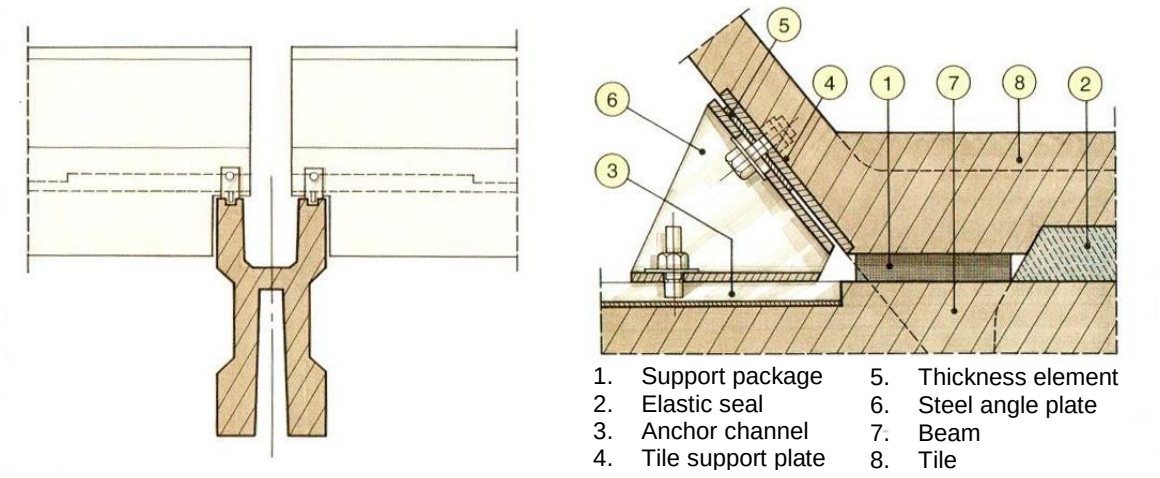

Figure 1-7: Example of type 2 joints (Dassori, 2001)

JOINTS TYPE 3

This category of connections corresponds to the joints between beams and columns (Figure 1-8). Type 3 connections are very varied and change according to the shape of the beam used as well as the type of support on the column: often the column is already shaped to host the beam arranged with appropriate holes or bars emerging from casted concrete and to allow a quick connection once the beam is placed. In general, the most common type is the one that uses a threaded pre-installed pin in the column's casting. This threaded pin screwed to the beam with nuts and washers or with finishing cast.

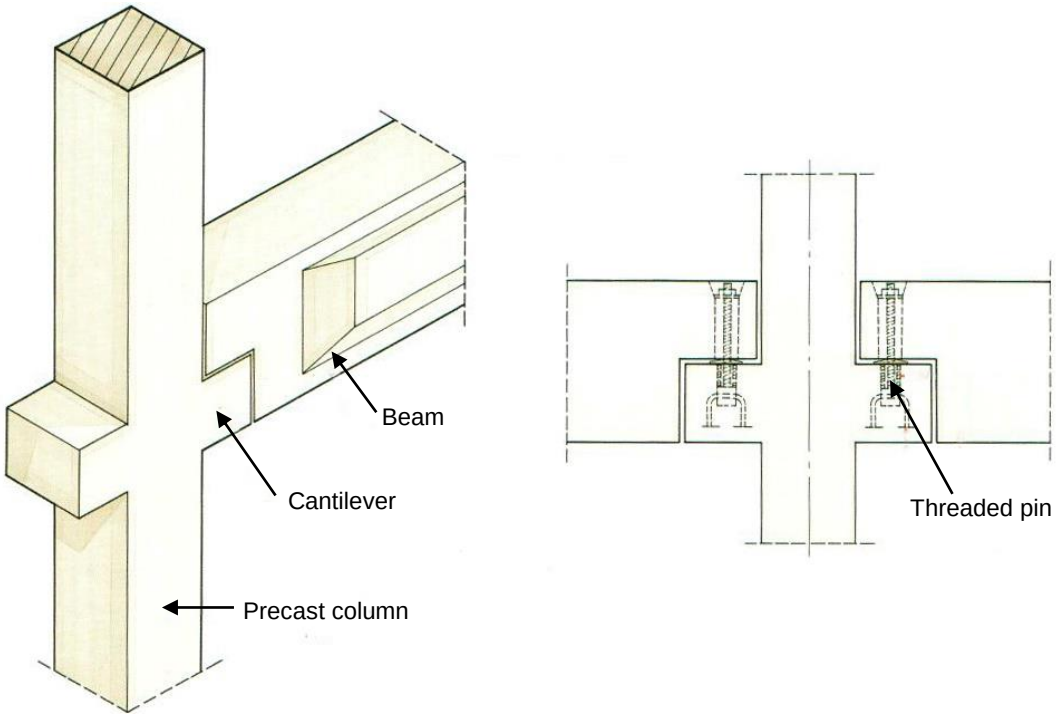

Figure 1-8: Example of type 3 joints (Dassori, 2001)

JOINTS TYPE 4

This category of joints is related to the connections between column segments and foundations (Figure 1-9). The most common type is column-to-foundation joint with a socket footing in which a centering pin is used. The pin is placed at the bottom of the socket so the column can be positioned, then follows a cast made with expansive concrete. A variant of this union is the one used to connect the columns to the foundation mat: the column is equipped with splices at the base that are positioned in special corrugated tubes pre-installed in the foundation and subsequently bound by compensated shrinkage concrete.

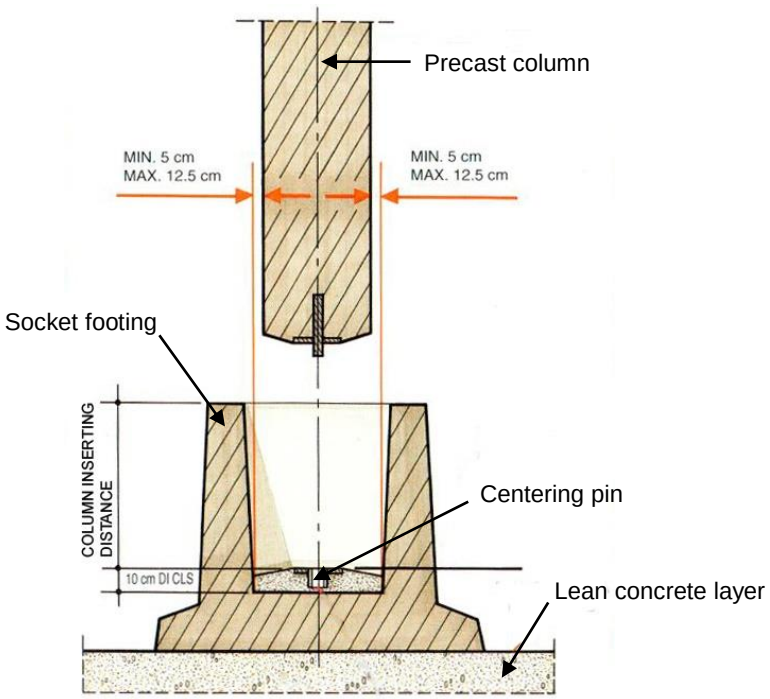

Figure 1-9: Example of type 4 joints (Dassori, 2001)

JOINTS TYPE 5

This set includes connections between wall panels and structure. This includes all the anchoring systems of the RC precast cladding panels to the main elements of the building (Figure 1-10). The panels layout, vertical or horizontal, affects the type of union. In general, the fasteners are placed at the top and bottom of the panels. One of the most frequent op connections for vertical panels is illustrated below. It is made up of hammer-head straps fixed on anchor channels with hammer-head screws.

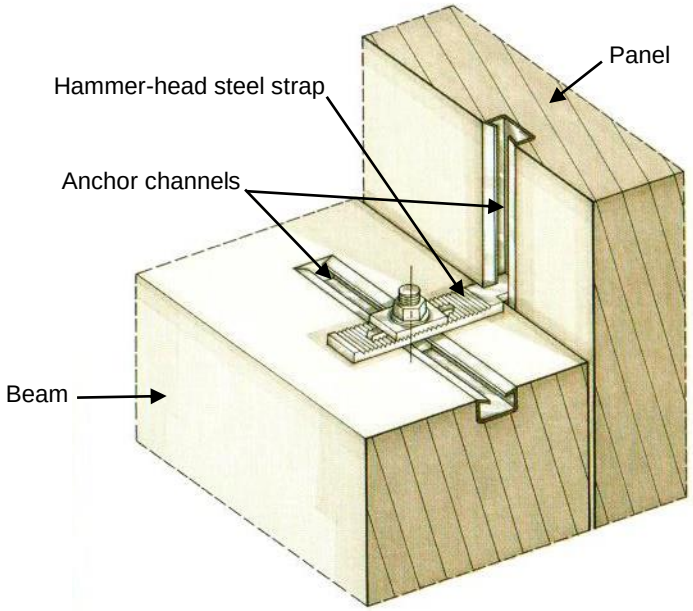

Figure 1-10: Example of type 5 joints (Dassori, 2001)

1.3 Seismic issues of RC precast constructions

The seismic events that struck Mediterranean Europe in the recent period, L'Aquila 2009, Grenada 2010, Emilia 2012 and Central Italy 2016 caused extensive damage to RC precast buildings for industrial and commercial use, in particular, the seismic shocks that occurred in Emilia on 20th and 29th May 2012 hit a highly industrialized area.

In the days following the two main shocks, a direct survey campaign was carried out (Magliulo, et al., 2014). The survey studied the affected areas closest to the epicentre and showed that over half of the existing precast structures had significant damage. Furthermore, the collapse of many non-structural components such as internal partitions, ceilings and high-rack steel structures were immediately evident. High-rack steel structures are widely used in industrial processes to store various types of goods and, in the presence of seismic events, they can be subjected to significant horizontal loads.

The prefabricated buildings built in Italy before the entry into force of the DM, 3-12-1987 were provided only with friction connections between horizontal elements (beams and roof elements), and horizontal (beams) and vertical (columns) elements. This is the main issue to consider when analysing the causes of the collapse. There were practically no connections between beams and columns. Consequently, the main structures collapsed in many cases.

The legal provisions of 1987 were the first to focus attention on the role of connections in precast RC structures. However, the requirements for structural elements and connections were still limited.

1.3.1 Damage of connections between structural components

The lack of connection devices is the main cause of damage following a seismic event since the low resistance offered by the friction mechanism often causes the loss of support both of the roof elements (Figure 1-11a) from the beams and of the beams from the columns (Figure 1-11b).

Figure 1-11: (a) Roof elements collapsed due to the loss of support from the main beam. (b) Loss of support of beam from column (Magliulo et al., 2014).

Moreover, in some prefabricated structures, the connections exhausted its capacity despite the presence of pins due to incorrect connection design (Figure 1-12a, b). However, after the 1999 Kocaeli earthquake in Turkey, the structures showed a better seismic response than those of Emilia because they had an extended presence of dowel connections, instead of just friction-based ones.

Figure 1-12: (a) Pinned beam-to-column connection failure and (b) loss of support of the beam from column (Magliulo et al., 2014).

The damage described above highlights the low robustness of not properly designed precast structures under seismic actions. In most cases, the collapse of only few (even one) connections can cause the collapse of the whole structure and, consequently, the loss of lives and goods (Ercolino, 2014).

1.3.2 Columns damage

In most of the RC precast structures built in Italy, the columns are generally precast elements whose base connections act like a full-fixed joint. In the upper part, they are connected to the beams by a horizontal sliding or translation fixed support. Therefore, it can be assumed that the columns work as cantilever beams. In the presence of strong earthquakes, the precast columns can exhibit:

- The inclination due to a rotation caused by inadequate column-foundation connection. This can be confirmed only by direct inspection of the foundation that is not easy to be carried out. However, this type of damage is unacceptable because it compromises the overall stability of the entire structure (Figure 1-13a).
- Formation of plastic hinges at the base of the column. This type of damage is significant but can be expected in the structure life and it is usually taken into account during the design phase (Figure 1-13b, c).
- Shear failure due to the interaction with traditional masonry infill systems. Due to its extremely brittle mechanism, this type of damage is unacceptable and have to be prevented with appropriate detailing during the design phase.

Figure 1-13: Columns damage: (a) Column loss of verticality due to rotation in the foundation element; (b) cracking of the base section in a column; (c) plastic hinge at the bottom of the column and buckling of a longitudinal reinforcement bar at the base (Magliulo et al., 2014).

1.3.3 Infill and precast panel damages

The infill system of precast single-storey industrial buildings is mainly made up of RC precast cladding panels. The collapse of the horizontal or vertical panels is the damage that occurs most frequently during an earthquake (Figure 1-14a, b).
The causes of the collapse can be attributed to:

- The lack of an adequate design concerning the seismic action in the connection between panel and structural element devices.
- The pounding of roof elements, columns or other prefabricated panels.
- Possible panel-to-structure interaction that causes additional lateral forces in the connection devices. Forces often not considered during the design process.

(a) (b)

Figure 1-14: (a) Collapse of vertical precast panels (b) Collapse of horizontal precast panels.

2 State of the art and main goal of the thesis

2.1 Panels configuration

The precast RC industrial buildings, mainly one-storey, are provided with RC cladding panels. The panels, regardless of their shape, are typically designed to support only their self-weight, the wind forces to which they are directly exposed and the seismic forces associated with the panel's mass. However, in most cases, the design of the panel and its steel reinforcement is determined by the forces that are generated during the construction phase for the lifting and installation on the structure. Four levels of structural participation of cladding system can be distinguished. The participation levels were defined by (Arnold, 1989) and also by (NIST, 1995), namely:

1. *Theoretical detachment* (push-pull connections). The push-pull connections should, in theory, detach the cladding system from the structure, but in a building with hundreds of cladding panels the detachment cannot be complete, and there is a certain transmission of forces from the structure to the panels and vice versa.

2. *Accidental participation* (grooved connections and sliding joints). Due to the deterioration of the connection devices or installation mistakes, the separation between the cladding panels and the structure is not effective. This is uncontrolled participation.

3. *Stiffening or controlled damping*. This involves the use of devices to connect the lining to the structure in such a way that the damping of the structure is modified (generally increased) or the structure is stiffened.

4. *Complete structural participation*. The cladding and the structure become a new integrated composite structure in which each element plays an assigned role. The cladding system can participate in the vertical support and certainly contributes to opposing lateral forces.

This classification refers to existing panels. However, for new buildings, the cladding system accidental participation should not be taken into account because it can lead to serious damage during a seismic event. Particular attention must be paid to sliding-type connections to make their behaviour stable and reliable, and therefore guarantee an effective detachment effect.

In the PhD. thesis of Dal Lago, (2015), a new classification of the panels is proposed based on the possible connection systems that can be used in new constructions This new classification was made focusing on the structure-panel interaction. The proposal is also reported in (Biondini, et al., 2010), (Biondini, et al., 2013) and also in (Toniolo, 2014). The following four categories are considered:

1. *Isostatic system*. The panels are isolated or partially (mostly) isolated from the main structural system by the connection devices. This category also includes those connection systems that, under seismic action, involve a rigid motion of the panels or allow relative displacements between structure and panels. An example of this could be the correctly efficient sliding connections.

2. *Integrated system*. The connection system provides a complete interaction between the structure and the panels. In the connection devices, forces arise which depend on the

intensity of the seismic action. It is preferable that the connections and the panels remain in the elastic field but a small amount of damage is allowable in the ductile connections or in the panels. In this case, the panels must be considered as part of the structural system of the building. They and their connections to the rest of the structure should be designed to resist the demand caused by the seismic action.

3. *Dissipative system.* The cladding panels and the main structural system are connected to the devices, which are designed as the main source of the energy dissipation when the building is subjected to the seismic action. The forces in these devices increase with the intensity of the seismic action until the resistance threshold is reached. After that, the dissipation of the energy considerably increases due to the plastic deformations in the connections. This category includes connection systems with highly ductile connection devices or those made using special dissipative devices. Within the building design, the cladding panels may be considered explicitly or with simplified methods, and their connections may be designed according to their subassembly static scheme.

4. *Second-line system.* The second line systems consist of additional safety devices that connect the structure and the panel in order to prevent them from falling down in case of failure of the primary connection system. This solution can be added to one of the previous ones but cannot replace any of them. It can be used for temporary safe restraint of existing panels damaged by a seismic event. Since the devices come into action only after the panel tends to fail, they can be omitted in the building design. The design procedure for the restrainers, which can be designed as the second-line protection systems, is proposed in (Zoubek, et al., 2018), some other technological examples of such connections are included in Civil Protection (2012).

Some sketches illustrating the working principle of precast buildings with isostatic or integrated vertical cladding panels are illustrated in Figure 2-1 and for horizontal panels, in Figure 2-2. A typical precast single-story structure is highly flexible due to its cantilever column static scheme designed without bracing. An isostatic solution, for example, provided with fixed hinge connections positioned to create a truss element, fully allows the structure to move without adding stiffness. The integrated solution, for example, equipped with four fixed connections positioned at the panel's corners to create a double beam blocked element, introduces a large additional stiffness in the plane linked with the displacement of the frame, to which large forces that arise in the connections and in the panels correspond.
However, the integrated panel system is not easy to construct and it is very difficult to have an adequate dissipation of energy in panels. On the contrary, the displacements of the structures with an isostatic configuration of panels can be limited with the proper dimensions of columns and/or by building RC wall cores, which limit the displacements. For one-storey buildings, the displacements are not problematic (also without RC wall cores). The problems arise and are quite considerable in multi-storey buildings with isostatic panels. Such structures are dangerous in the seismic regions when the RC wall cores are not used.

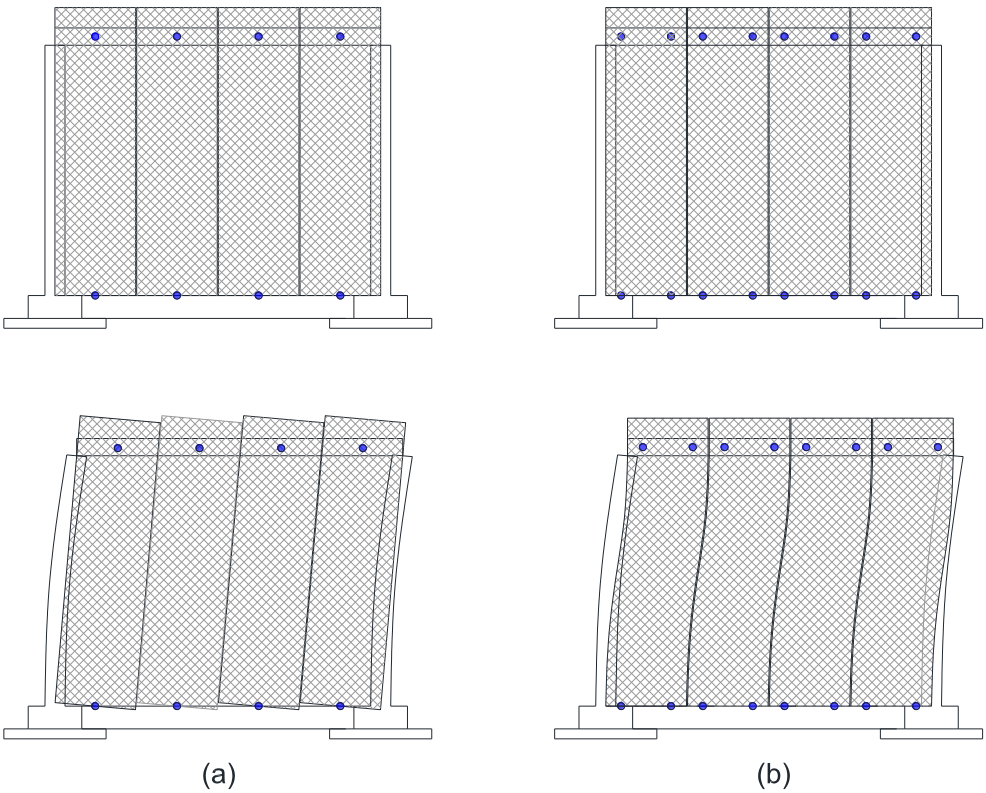

Figure 2-1: Vertical cladding panels: (a) isostatic connection system and (b) integrated connection system

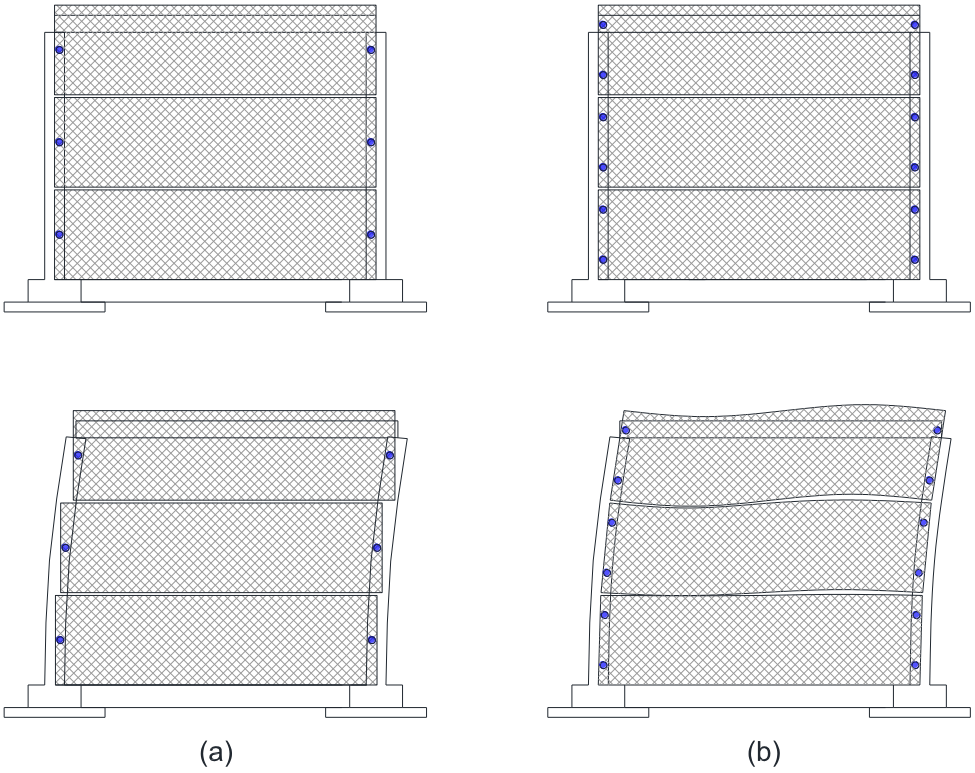

Figure 2-2: Horizontal cladding panels: (a) isostatic connection system and (b) integrated connection system

The following symbols according to (NIST, 1995) and (Dal Lago, 2015) are used in order to identify the degrees of freedom and of restraint of a connection:


restrained displacement in the direction of the triangle enlargement.


free displacement in the arrow direction. Large displacement is expected to occur.


free displacement in the arrow direction. Small speed displacement may occur.


displacement direction of dissipative connection.


Restrained rotation around the axis indicated by the double arrow.

2.1.1 Isostatic systems

Within the panels, several isostatic connections arrangement can be used. The most common isostatic connection arrangements are presented hereafter. This does not mean that additional degrees for restraints could not be added but only when they do not modify the correct kinematic of the panel.

Pendulum arrangement or double hinged pendulum. The pendulum connection system for vertical panels is realized with a central restraint at the base around which the panel can rotate in its plane and a top panel-beam shear connection allows vertical deformation at low speed. For the correct operation of this system, it is essential to leave the panel free to move vertically even in the downward direction at its base. The downward displacement at the base can be guaranteed by adding some soft material under the panel bottom. This solution is not commonly used in design practice. Within this structural arrangement, it is important to limit the rotation around the panel's vertical axis or the torsion of the panel. To do this it is possible to proceed with two solutions, which can also be combined. Figure 2-3a shows a solution with a rotational restraint included in the basic connection, while Figure 2-3b shows a configuration with added push-pull connections that must be able to allow large vertical movements.

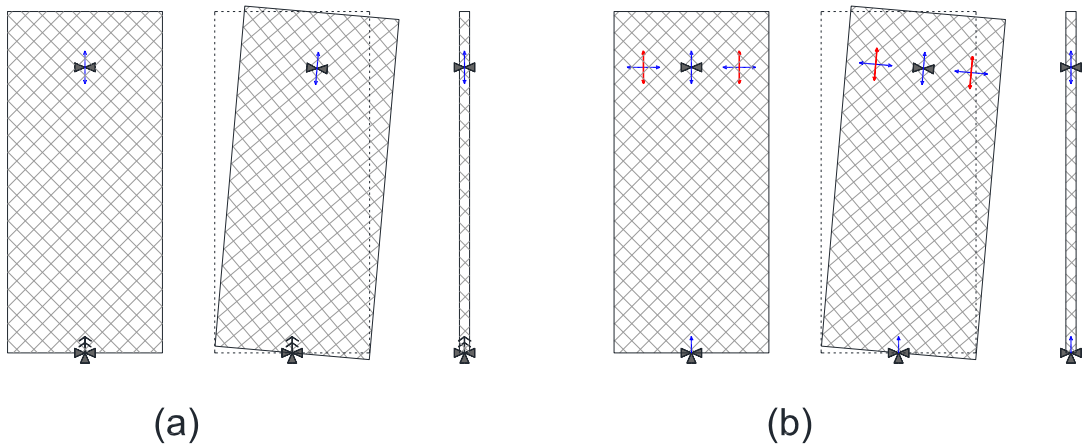

Figure 2-3: Isostatic pendulum arrangement for vertical panels: (a) base torsional restraint and (b) with push-pull connections

Rocking arrangement. The connection system with rocking for vertical panels consists of base supports and panel-to-upper cutting connections that must allow a vertical movement at high speed. The panel can simply be supported on its base. In the case of simple support, it is always a good solution to use out-of-plane additional restraint systems. Figure 2-4 shows the flat and out-of-plane behaviour of the rocking arrangement.

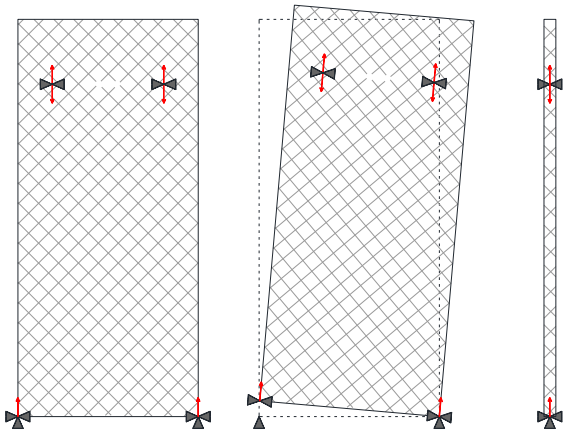

Figure 2-4: Isostatic rocking arrangement for vertical panels

Cantilever arrangement. The cantilever connection system for vertical panels consists of base supports and top horizontal sliding connections that allow a relative displacement at high speed between the beam and the panel. The panel can simply be supported on its base but lifting should be prevented. Figure 2-5 shows the flat and out-of-plane behaviour of the cantilever arrangement.

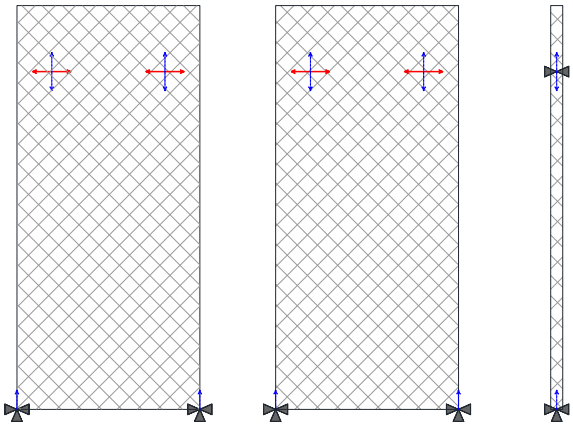

Figure 2-5: Isostatic cantilever arrangement for vertical panels

The cantilever or rocking configuration are theoretical arrangements to which the designers try to refer. However, in real buildings, an intermediate configuration can also be reached due to the difficulty of realizing supports that work as in the supposed theoretical scheme

Swaying arrangement. The swaying connection system for horizontal panels consists of panel-to-foundation or panel-to-column supports and horizontally sliding connections that can allow large relative displacement between the panel and the column or the beam. Four solutions are foreseen. Figure 2-6a shows a solution with bottom sliding supports and top shear connection, provided with additional push-pull connections, in Figure 2-6b the solution is similar to the previous one with supports at the top and shear and push-pull connections at the bottom, Figure 2-6c shows a solution with bottom supports and horizontal restrainers and top sliding connections and in Figure 2-6d the solution is similar to the previous one with supports at the top and shear and sliding connections at the bottom.

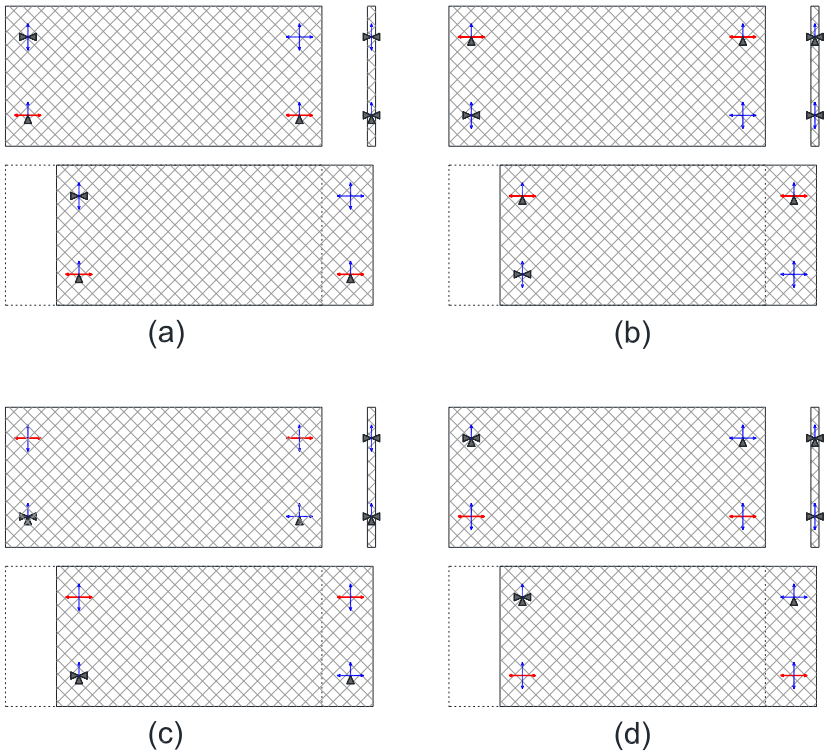

Figure 2-6: Isostatic swaying arrangements for horizontal panels: (aa) sliding bottom supports, (b) sliding top supports, (c) sliding top connections and (d) sliding bottom connections

Stacked panels arrangement. This connection system for horizontal panels consists in panel-to-foundation or panel-to-panel fixed connections, that may also be simple supports on the panel underneath or on the foundation and horizontally sliding connections that shall allow high-speed relative displacement between the panel and the column or the beam. Figure 2-7 shows the in-plane and out-of-plane behaviour of the arrangement of the stacked panels. This solution may be used only for a low number of stacked panels.

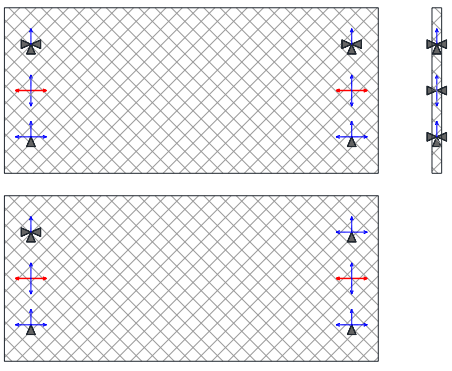

Figure 2-7: Isostatic stacked panels arrangement for horizontal panels

2.1.2 Integrated systems

It is possible to use different integrated connection devices for both vertical and horizontal panels. In the following sections, some of the most common integrated connection provisions for vertical panels will be illustrated. Additional degrees of restraint can be added to strengthen the system.

Hampered rocking arrangement. The rocking connection system obstructed for vertical panels can be obtained through two solutions. The first solution with a locked panel base and a higher cut connection (Figure 2-8a). A second solution with a supported base and upper fixed connection (Figure 2-8b). In the latter case, it is advisable to use only non-composite panels to compensate for the hampered deformation of temperature.

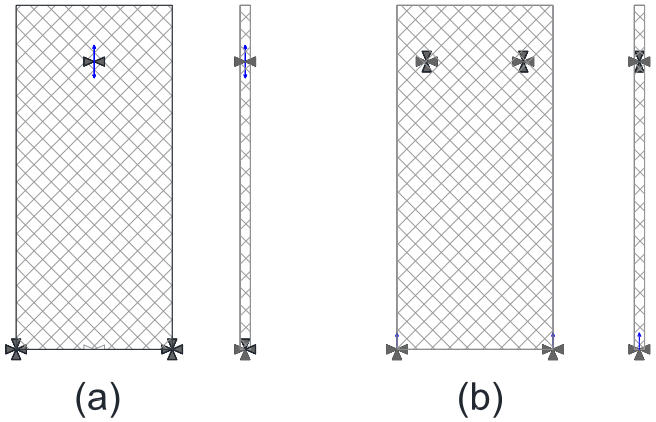

Figure 2-8: Integrated hampered rocking system for vertical panels: (a) fixed at the base and (b) fixed at the top

Fixed arrangement. The fixed connection system for horizontal panels consists in the application of fixed connections in correspondence of the panel corners. Figure 2-9 illustrates a possible solution. Only the use of non-composite panels is suggested to compensate for the hampered temperature deformation.

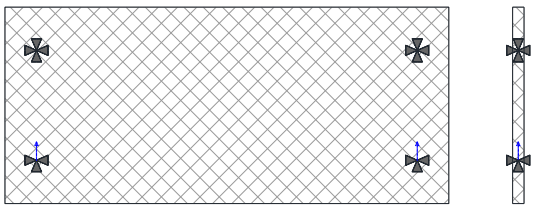

Figure 2-9: Integrated fixed arrangement proposed for horizontal panels

2.1.3 Dissipative systems

The dissipative connections can be inserted between the panels or between the panels and the elements of the main frame structure (or its foundation). It is possible to add further degrees of constraint only if they do not modify the correct kinematics of the panel.

Pendulum arrangement. The dissipative pendulum connection system for vertical panels can be obtained on each of the solutions considered for the isostatic configuration.
Figure 2-10a shows the relative displacement of the panel that can be used for the exploitation of dissipative shear devices.

Rocking agreement. The scheme of operation of the oscillating dissipative connection system is illustrated in Figure 2-10b together with the relative one

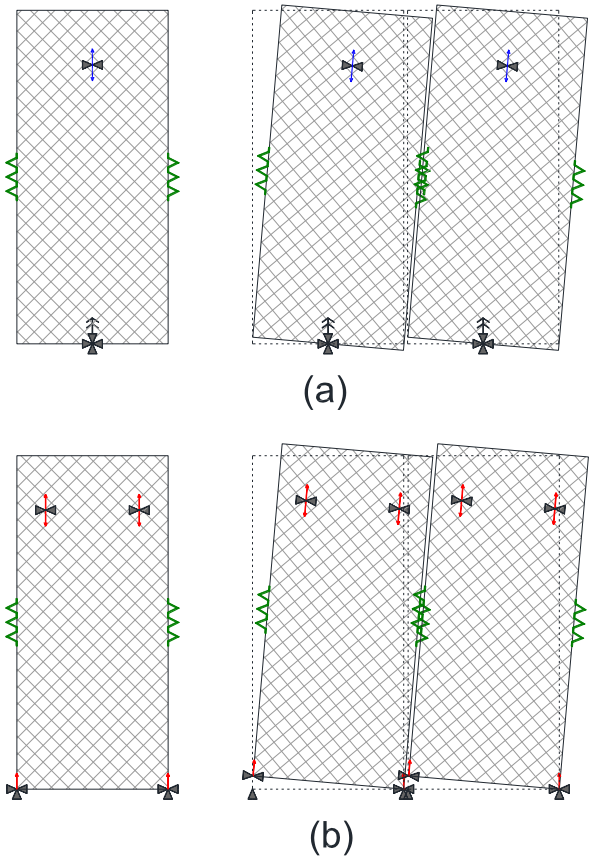

Figure 2-10: Dissipative arrangement for vertical panels: (a) pendulum system and (b) rocking system

Swaying arrangement. The swaying dissipative connection system for horizontal panels working scheme is illustrated in Figure 1.17 together with the relative panel displacement that can be used for the exploitation of shear dissipative devices.

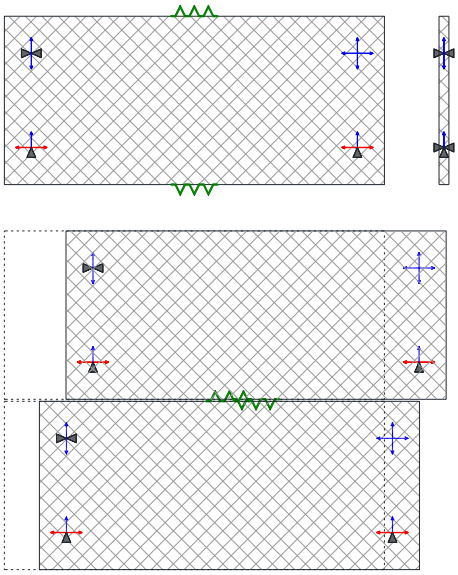

Figure 2-11: Dissipative swaying arrangement for horizontal panels

2.2 Overview of literature

The state of the art regarding both the practice and the research on precast concrete structures will be described in this paragraph. First, a brief overview of the research history carried out on dry-assembled precast concrete structures will be provided. Then, the specific behaviour of the usual prefabricated frame connections and their role on the seismic response of the structure will be addressed. And lastly, there will be an in-depth study about the practice of the vertical cladding panel layouts, about the research activity carried out on the connections of the dissipative cladding panel and about the existing philosophies and design methods for connections.

2.2.1 Research history on dry-assembled precast structures

The reinforced cast in situ concrete structures have been carefully studied in the past as far as their seismic behaviour is concerned: with the knowledge currently gathered, their seismic performance can now be reliably predicted, even when complex and/or irregular structures are involved. Furthermore, unified design philosophy was developed for optimal seismic performance of traditional concrete structures: the so-called "capacity design" approach, which was also codified in the most recent versions of the relevant codes, such as Eurocode 8 (EN 1998-1-1, 2005).
Moreover, the precast structure, due to their great diffusion, their peculiar features and, in particular, their response to seismic excitation, have carefully been studied in over the years.
Since the 1980s, important research has been carried out on prefabricated buildings and connections. In particular, the following works are worth mentioning: the "*Joint U.S.-Japan Cooperative Research Program*" (Wang, 1987) and the "*Seismic behavior and Design of Precast Facades / Claddings and Connections in Low-Medium Rise Buildings*" (Rihal, 1988) for the United States. And "The Building Construction Under Seismic Conditions In The Balkan Region" (Simeonov, 1985) for the region of the former Yugoslavia, although the Balkan project was strongly oriented towards load-bearing panel systems, which were widely used in Eastern Europe and the Russian Federation
The most recent state of the art report was published by the activity group FIB 7.3 in Bulletin n. 27 (International Federation for Structural Concrete, 2003) and it reports the latest developments in New Zealand, Mexico, Indonesia, Chile, the United States, Slovenia, Japan and Italy. A separate chapter is devoted to modelling and analytical methods.
However, although these are the most complete existing documents, they only cover some specific prefabricated structural systems and connections.

Over the past two decades, extensive research has been carried out on the seismic behaviour of prefabricated concrete structures on a European scale. The results of this activity made it possible to achieve a good knowledge of the seismic behaviour of precast systems and contributed to an increase in the quality and reliability of prefabrication in Europe
The first phase of this research was developed between 1992 and 1996 during the drafting of the first ENV version of Eurocode 8. In the initial code's draft, a very bad seismic behaviour for RC precast structures was supposed. One-storey industrial precast buildings were defined as inverted pendulum structures to which a low value of the behaviour factor was attributed.
Some research programmes worked to demonstrate the good seismic response of precast structures through experimental campaigns and numerical analysis.
A first series of tests were conducted at ELSA laboratory of Joint Research Centre of the European Commission where cyclic and pseudo-dynamic tests were performed on a precast

cantilever column with different imposed axial load (Saisi & Toniolo, 1998). The results showed a good ductile behaviour of the precast columns as typical of cast-in-situ ones.

The Ecoleader project

The objective of the project is to provide specific experimental evidence of the seismic behaviour of precast one-storey frames for industrial buildings as compared with cast-in-situ analogous structures.
Within the Ecoleader programme for the free use of the large European testing facilities, two pseudo-dynamic tests on full-scale prototypes (Figure 2-12) have been performed at ELSA Laboratory (Biondini, Ferrara, Negro, & Toniolo, 2004). The Ecoleader project was supported by the 3 associations ANDECE of Spain, ANIPC of Portugal and "Progetto Ulisse" (AITEC+ATECAP+ASSOBETON) of Italy, while the research providers were Politecnico di Milano and the University of Ljubljana.
The tests consisted in an experimental comparison of the seismic capacities of cast-in-situ and precast structures. The results confirmed the great seismic capacities that were expected from this type of structures and highlighted the overall equivalence of the seismic behaviour of precast and cast-in-situ structures.

(a)

(b)

Figure 2-12: Ecoleader project (a) cast-in-situ frame and (b) precast frame with hinged beam-to-column connections (Dal Lago, 2015).

The European Growth programme

The project aimed at presenting new indications for Eurocode 8 about the precast RC buildings. In particular, it provides reliable quantification of the behaviour factors q of this type of structures.
In the meantime, BIBM, the international association of prefabrication industry, has shown its interest in the research so that another wider testing campaign has been launched within the European Growth programme. Ten partners are involved in the programme.
For Portugal: LNEC Laboratorio National de Engenharia Civil of Lisbon and Civibral Systemas de Construcao of Sao Pedro Fins. For Italy: Politecnico di Milano, Magnetti Building of Carvico and Gecofin of Verona. For Greece: NTUA National Technical University of Athens and Proet of Athens. For Slovenia: University of Ljubljana. For Cina: Tongji University of Shanghai. For the European Community: ELSA European Laboratory of Structural Assessment.
Two prototypes consisting of six columns and a set of beams and roof elements were designed to investigate the seismic behaviour of precast structures with roof elements placed side by side. Figure 2-13 shows a view of the prototypes.

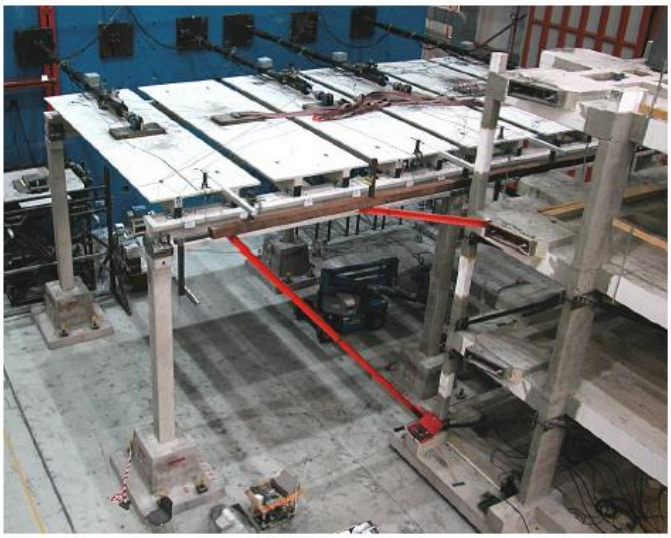

(a)

(b)

Figure 2-13: Growth project: precast frame specimen with (a) diaphragm elements oriented parallel and (b) orthogonal to the direction of seismic action (Dal Lago, 2015).

The results of the investigations carried out under the Growth research projects showed once again the good seismic performance of precast structures but the connections have to be properly over-dimensioned (Biondini & Toniolo, 2009).
The problem of the influence of the connections was investigated in Fabbrocino et al. (2006) and Biondini et al. (2013c), in which the seismic response of industrial prefabricated buildings with weak connections is studied. Within the project, (Fischinger, et al., 2008) and (Magliulo, et al., 2008) some indications for the seismic evaluation of existing industrial buildings are given.

The SAFECAST programme

The investigations continued in the SAFECST project and showed that prefabricated systems can have energy dissipation/seismic performance capabilities comparable to cast-in-situ systems, but only if the connections are properly designed and the drift limitations are respected together with other minimum requirements set by Eurocode 8. The analytical investigations described in (Kramar, et al., 2010) support this fact, underlining also the great seismic resistance that the prefabricated frames can provide.
In recent years, there has been a growing interest of the scientific community for the seismic behaviour of the so-called non-structural components in general and not exclusively for the behaviour of cladding panels.

2.2.2 Research activity on connection systems

The connections play a fundamental role in the seismic response of RC precast buildings as already underlined in the previous paragraphs. Following the classification proposed by ASSOBETON and described in subsection 1.2.1, the research works on the various types of connections will be briefly illustrated, while a separate section will be devoted to the structure-panel connections.

Column-foundation connection

The column-foundation connection plays a fundamental role in the static scheme of prefabricated buildings traditionally built in Europe, in which the cantilever columns concentrate at their base all the seismic demand for ductility and energy dissipation.
The equivalent monolithic wet-assembled connections mounted wet with pocket foundation have been studied by (Saisi & Toniolo, 1998) and in an experimental campaign described in (Popa, et al., 2015), In (Angotti, et al., 2010) and (Orlando & Piscitelli, 2018) the behaviour of dry-assembled mechanical connections, which are becoming increasingly common in the construction practice, have been studied. Moreover, some innovative solutions of bolted sockets have been designed and tested in order to improve their mechanical behaviour (Dal Lago, et al., 2013).
The effect of HFRP reinforcement was studied for existent precast columns with a socketed foundation (Germano, et al., 2015).
(Metelli, et al., 2011) proposed a solution with a concentration of damage in the foundation rebars. The proposed connection was characterized by the use of high strength threaded steel bars partially un-bonded in grouted sleeves and by steel support elements which allow an easy assemblage and centring of the column. The authors underlined that the damage was localized at the column base thus allowing a simple retrofitting after a seismic event.

Column-beam connection

In the past, the beam-to-column connections were commonly realized with a simple support contact or with dowels that were not designed to withstand lateral forces, sometimes a support layer was interposed, usually in neoprene or plumb, in order to better distribute the load. This simple technology has been shown to be largely inadequate for seismic loading and it was studied among the others by (Magliulo, et al., 2011).

Typical beam-to-column connections largely diffused in all dry-assembled precast frames all around the world are dowel connections, made with large diameter rebars protruding from the bearing member (or screwed in pre-installed bushes) and grouted once the supported member is placed in position. Usually, a neoprene pad was interposed between the beam and the column supporting corbel. The dowel shows negligible entirely flexural stiffness, allowing relative rotations between the members, but should resist the shear force, which could be larger than the shear force in the column. Among the first to conduct an experimental study on this type of connections (Vintzeleou & Tassios, 1985) and (Soroushian, et al., 1987) should be mentioned.

Within the SAFECAST project, Psycharis & Mouzakis performed an extensive experimental campaign, with local pure shear tests (Psycharis & Mouzakis, 2012b) and full-scale shaking table tests, (Psycharis & Mouzakis, 2012a) on beam-to-column structural sub-assemblies with dowel connections of different geometries. The campaign has highlighted that there exists a large resistance reduction in case of cyclic load in comparison with monotonic load and a ductile behaviour of the connection if adequately provided with a considerable amount of transversal reinforcement around the dowel. In the end, the researchers published a book that summarizes all the investigation conducted on this connection type (Psycharis, et al., 2012).

(Fischinger, et al., 2012) performed an experimental campaign within the same research project regarding the behaviour of dowel connections at large relative rotations, through monotonic and cyclic tests (Figure 2-14). The results of this study are that a non-negligible resistance reduction occurs at large relative rotations, identifying similar failure modes with respect to pure shear tests. A robust numerical 3D model (Zoubek, et al., 2014) has been used to get and to interpret the experimental results and a strut-and-tie scheme (Figure 2-15) was proposed to produce more reliable design guidelines for these connections (Zoubek, et al., 2014).

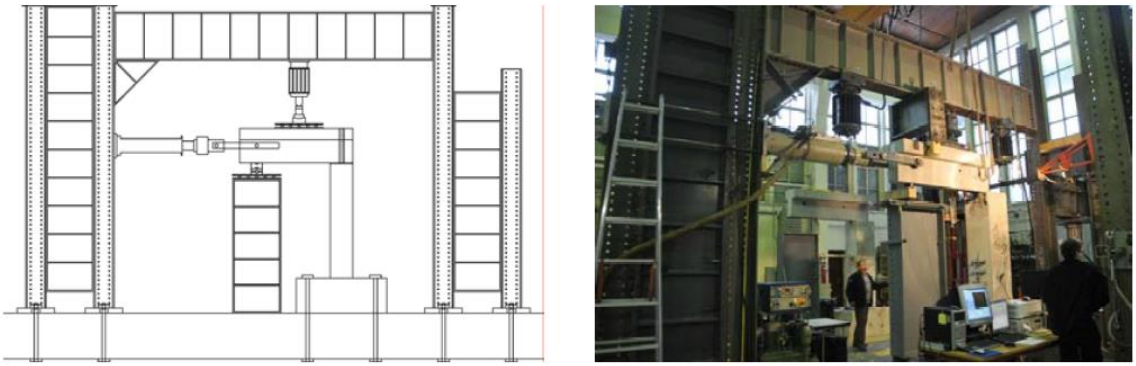

Figure 2-14: Experimental campaign performed at the University of Ljubljana (Fischinger et al., 2012).

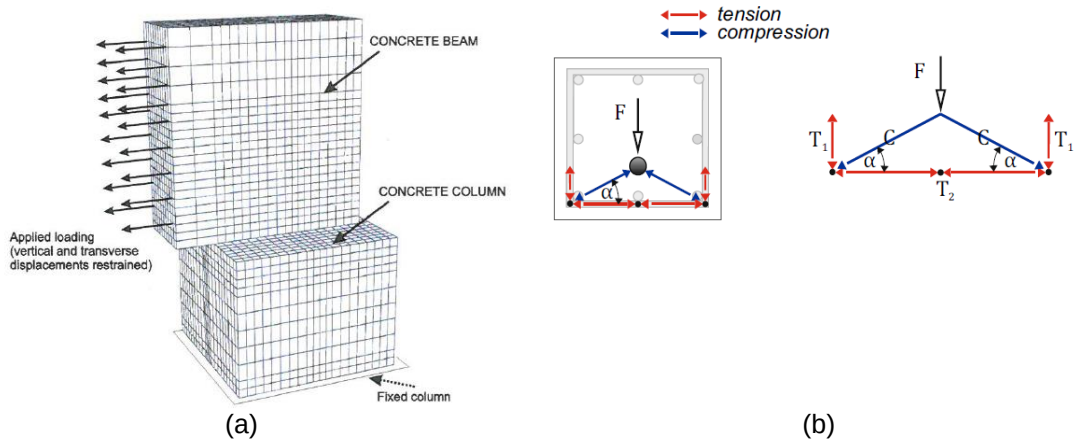

Figure 2-15: The robust numerical model (a) and one of the strut-and-tie models proposed (b)

Tiles-beam connections

About the tile-beam connection, an innovative device based on energy dissipation by friction was designed by (Marinini et al., 2008). This device is composed of a series of different material disks and layers that allow for a very limited free displacement and this contributes to accommodate movements of the static loads. For larger displacement, the disks go into action and the energy dissipation for friction starts.

Another type of tile-beam connection are the bow-shaped dissipators designed by (Beschi, et al., 2010). These devices belong to the category of metallic dissipator and they are activated by the relative displacement between the elements to which they are connected. For this device, two design strategies are proposed by (Belleri, et al., 2013): an elastic approach, with the connection designed as elastic in a seismic event corresponding to the No-Collapse Requirement, and a dissipative approach, with the connection designed to yield and dissipate energy

The behaviour of traditional steel plate angle connection for wing-shaped tiles was studied in (Menichini, 2016) and a new comb-shaped steel plate (Figure 2-16) that can gain a high ductility due to its particular shape was analysed and discussed in (Menichini, et al., 2017)

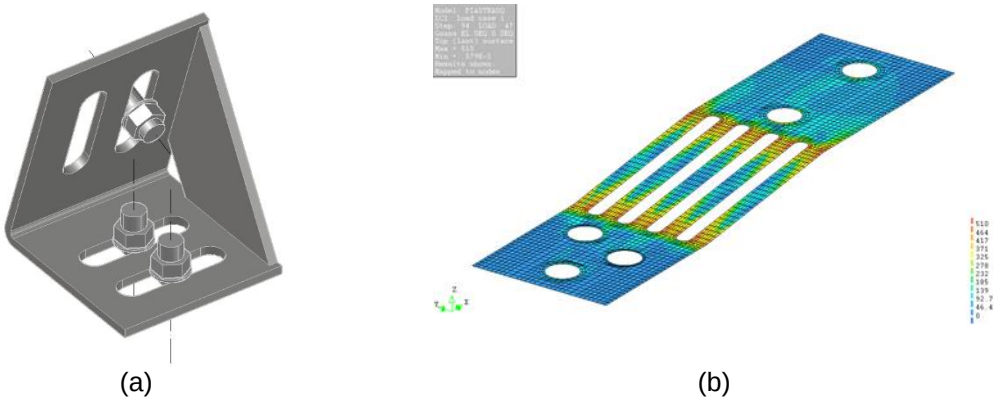

Figure 2-16: Tile beam connections: traditional steel plate angle (a) and comb-shaped steel plate (b)

At the global level, the role played by beam-tile connections for the definition of the diaphragm behaviour of one-storey precast building roofing systems was studied in the work of (Belletti, et al., 2013).

The results obtained show that the structure's behaviour is strongly influenced by the roof modelling. Furthermore, the shear forces on the beam-tile connections were compared, in the hypothesis of both finite and infinite stiffness of the connections. The results show that if you assume a finite stiffness of the connections then a greater redistribution of stresses is obtained. The stresses are then more homogeneous and smaller than in the case of connections with infinite stiffness.

Floor-to-floor connections

Within floor-to-floor connections, typically, welded plates with various shape are used. Large experimental research was performed at in the European Laboratory for Structural Assessment laboratory (ELSA) where a full-scale three-storey precast building was subjected to a series of pseudo-dynamic tests (Bournas & Negro, 2012).

The welded floor-to-floor connections showed an elastic response (stronger connections than elements) and allowed for equal distribution of the storey forces among all columns.

2.2.3 Precast RC panels

The RC cladding panels can be divided into:

- *monolithic*: are panels composed of a single layer of ordinary or lightweight concrete with a minimum thickness of not less than 8 cm (Figure 2-17a).
- *lightened*: are panels realized with two external concrete layers connected together by ribs or point connections with interposed layers of insulating material (Figure 2-17b).
- *sandwich*: are panels made up of a set of layers with different functions. Usually, there is an external protective and finishing layer (thickness 4-6 cm), an intermediate insulating layer (thickness 4-20 cm), an internal bearing layer (with variable thickness starting from 8 cm) (Figure 2-17c,d). More well-structured solutions provide for the presence of air chambers obtained by shaping the insulating layer (Figure 2-17e). If the connection elements between the outer and inner concrete layer allow the free movement of the first with respect to the second, the panel is defined as *freely expandable*. In the reverse case, the panel is defined as *rigidly connected*. This difference gives rise to different mechanical behaviours.

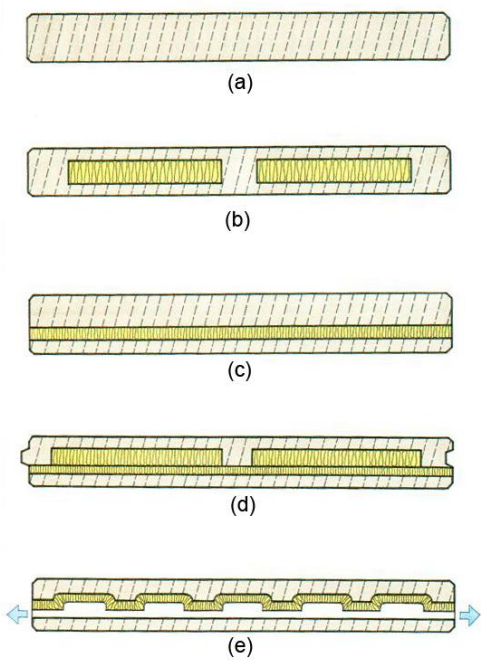

Figure 2-17: Panels type categories from (Dassori, 2001)

Even if different technologies of connections are generally used in many countries, a common distinction is made among bearing, shear and tie-back connections.

- Bearing connections have the function of sustaining the gravity weight of the panel.
- Shear connections restrain horizontal relative displacements between panel and structure
- tie-back connections restrain out-of-plane relative displacements.

A single connector device can provide multiple functions.

In European practice, in general, vertical and stacked horizontal panels are simply placed on the foundation beam and jointed by bearing connections. The suspended horizontal panels are generally equipped with bracketed bearings connections. All panels are then equipped with tie-back connections designed with various technologies, the most diffused of which is the steel strap type.

It is important to note that, while some brackets are designed to allow horizontal sliding, tie-back connections are for the large majority fixed, possibly acting unintentionally as shear connectors. An overview of the Italian typical cladding connections with reference to their specific technology is available in (Mandelli Contegni, Palermo, & Toniolo, 2007).
Furthermore, some reference to the specific technologic products available in Europe can be found in the official reports of the SAFECLADDING project.
In the US practice, cladding panels are traditionally designed with two combined bearing-shear connections positioned in a row and several tie-back connections, positioned in order to leave the panel in its position during a lateral load event. Usually, the tie-back connections are made with fixed slender steel rods that can provide large out-of-plane axial resistance while sustaining large in-plane deformation demand, or with sliding devices obtained through slotted profiles.
Relevant technical details of typical connections can be found in (NIST, 1995) and (PCI, 2007), (NPCA, 2012)
Japanese connections are largely employed in a static scheme that allows the panel to the rocking movement around the base connections. The typical connections are placed in four symmetric positions along with the panel, two at the top and two at the base, and all of them are load-bearing. Technical details can be found again in the document (NIST, 1995)

Structure-panels interaction
The cladding panels are usually designed as non-structural components (referring to the seismic action) since they are fastened to the main structure in a such a way that they can respond to the seismic action independently of the main resisting structure. Therefore, they are usually completely disregarded when the seismic analysis of the frame precast structures is performed, with exception of their mass, which is added to the total mass of the structure according to the panel static scheme.
A noteworthy state of the art report can be found in, (Hunt & Stojadinovic, 2010) and (NIST, 1995). (Goodno & Craig, 1989, 1998) provide an overview of the studies devoted to the cladding-frame collaboration for typical U.S.A cladding system.
Among the first to promote the idea of using cladding as an integral part of the wind bracing system were (Gjelsvik, 1974; Oppenheim, 1973; Weidlinger, 1973). They observed that cladding panes can be incorporated into the structural resistance system to increase the lateral stiffness of high-rise buildings. They also studied the shear behaviour of panels as well as the interaction between frames and precast panels, by focusing on the effect of cladding on the lateral strength capacity of a frame with simple beam-column connections.
An extensive study was performed by the research team at the Georgia Institute of Technology on the influence of the cladding systems on the seismic response and vibration properties of multi-storey buildings. (Goodno, et al., 1980; Goodno & Craig, 1989; Goodno & Palsson, 1986; Palsson & Goodno, 1988; Palsson, et al., 1984). A 25-storey steel-framed office structure was studied. Three sets of ambient tests and one forced vibration test were performed on the building to find frequencies and mode shapes and also a numerical study was carried out. Since the analytical and measured periods did not agree, the research of the effects of the claddings on the overall structural response was performed. The analytical periods of the bare frame structure without claddings were up to 34% and 48% greater than the measured translational and torsional periods, respectively. The corrected numerical model with added claddings gave similar results if compared to the experimental. The above references include also the study of the claddings, the roof displacements and the damping.
Cladding-frame interaction on the modal properties of a multi-storey concrete framed building was analytically investigated by (Henry & Roll, 1986) through a case study. They analysed a two-dimensional, nine-storey, three-bay concrete moment-resisting frame structure. The cladding system consisted of spandrel panels attached to the structural frame at the panel four corners. The fundamental period of the model with cladding was 18% - 55% smaller than the

fundamental period of the bare frame model, depending on the bay width, the panel height and weight. According to what stated by (Hunt & Stojadinovic, 2010), the approach proposed by Henry and Roll is not completely correct because the authors assumed that all of the deformations in the cladding system occur in the panels themselves. Modelling the cladding system in this manner overestimates the contribution of the cladding to the lateral stiffness of the building. In reality, the shear stiffness of the cladding connectors is much lower than that of the panels, which can be assumed to act as rigid blocks.

Henry & Roll tested also the influence of the claddings on the frame drifts. The lateral roof displacement decreased as the height of the panel increased. The lateral roof displacement decreased up to 75% comparing to the model, which consisted of a bare frame only.

The contribution of cladding to the lateral stiffness of bare frame structures was also studied by (Gaiotti & Smith, 1992; Smith & Gaiotti, 1989). They compared the drifts of frames with and without cladding panels. Rather than analysing a multi-storey multi-bay structure, a single-story module was analysed, which was designed to behave like a typical end-bay-width story of the frame. The cladding system, described as typical of low seismicity areas, consisted of one panel constructed over the full storey height and a full bay width with two window openings. The cladding panels reduced the displacement from 12,6 cm to 3,6 mm. In the opinion of (Hunt & Stojadinovic, 2010) these results seem to be, however, unrealistic, since the stiffness values assigned to the connectors were unrealistically large.

The role of cladding panels in the lateral load resistant design of buildings was also evaluated by (Charney & Harris, 1989). In the study, a four-storey two-bay steel moment-resisting frame building was analysed. The 2 inches thick panel decreased the lateral displacement of about 28%. The connectors and panels contributed 14,4% and 8,4%, respectively, to the total drift. When the panel thickness was increased to 6 inches, these contributions were changed to 20,3% and 4,3% for the connectors and panels, respectively. For the 60 inches thick panel (which represents the infinitely rigid case), the connector was responsible for 24,4% of the total drift.

(Thiel et al., 1986) studied the effect that the cladding system has on the damping properties of a ductile steel moment-frame. The researchers performed nonlinear time-history analyses of a benchmark 15-storey building. The cladding was modelled as dampers lumped at each floor and idealized as having elastic-perfectly plastic behaviour. The main conclusions showed that, as reported in (Hunt & Stojadinovic, 2010) the effectiveness of the dampers, which represented the cladding system, increased with increasing yield level. The cladding dampers required relatively high stiffness, when comparable to the structure's stiffness, in order to be most effective. With high yield levels and 2% viscous damping in the frame, the cladding damper reduced the response of the structure by approximately 40% of the maximum roof displacement and 45% of the base shear. In the summary, the authors argue that the effective damping of a building can be increased through activation of part of the lateral force resistance capacity of the cladding panels and controlled hysteretic behaviour of their connections to the structure. However, as stated in their paper, the cladding connections require very high stiffness to be effective, which is not feasible given the connection details and design approach currently used at that time and today.

Wolz et al. (1992) used an analytical model and time-history analyses to study the seismic response of a six-storey, 1:4 scale model of a moment-resisting frame provided with two cladding panels on each bay. The time-history displacement of the roof with and without claddings was recorded. The maximum roof displacement of the model with cladding was approximately 33% less than the roof displacement of the bare frame model.

(Cohen & Powell, 1993) performed a design study to explore the use of structural cladding panels with the energy dissipating cladding-to-frame connections in order to enhance the seismic behaviour of the frame itself. They showed by means of non-linear dynamic analyses how a dissipative cladding solution could improve the global seismic behaviour of the building.

(Pinelli, et al., 1995; Pinelli, et al., 1993) developed a design method for the optimisation of energy dissipative cladding connections by choosing the device that provides the largest energy dissipation within the building façade. The validity of the proposed design criterion has been validated through a parametric investigation on case studies, with non-linear dynamic analyses and with reference to a plasticity-based tapered connector, which mechanical behaviour can be defined according to the elastic stiffness and the yield force.
(Memari, et al., 2004) carried out a numerical investigation on the effect of near-source vertical ground motion on the demand on cladding connections, finding that vertical ground acceleration in near-source regions can increase the design forces for connections of heavy non-structural cladding panels and suggesting to consider vertical ground acceleration spectra for a more conservative design.
(Singh, et al., 2006a, 2006b) extensive work has been done in order to validate and improve the methodology of evaluation of the out-of-plane forces of non-structural components, both for rigid and flexible components. In their work, Singh, et al., perform a large parametric numerical investigation on forces on non-structural components that arise in tall buildings with non-linear dynamic analyses. As a final consideration, the authors state that the formulation provided by the US standards appears to be very conservative since it does not take into account the real complex dynamic interaction between structure and component. More accurate formulations are proposed in the cited papers
In more recent times, (Baird, et al., 2011b) carried out a parametric study of the interaction between cladding panels and the bearing structure. Different failure mechanisms and various configurations were considered in order to show the effect of the entire cladding system upon a structure's seismic behaviour. The results showed that there was an increase in strength of at least 10-20% for all systems when the influence of cladding panels was taken into account.
This contribution was greater when panels were attached to the columns rather than to the beams because the beams deflected more and activated the connections later. An increase in hysteretic damping for all systems has also been observed. Frame height to span length ratio did not largely affect the yield force of the system. However, increasing the frame height allowed for a higher deflection/drift of the system at yield. When both panel and connections were strong, the capacity of the system increased but the ductility decreased. The authors of the study further concluded that it was apparently more advantageous to design for a connection governed failure mechanism instead that for a failure mechanism governed by either the panel or the frame.
Connection governed failure allowed greater damping, strength and stiffness over many cycles, provided that the connections are able to achieve large ductility. The post-earthquake substitution of failed connections is seen to be more favourable than having to replace entire damaged panels or to repair the frame.
A special investigation was carried out by (Baird, et al., 2012) in order to analyse in detail the damage sustained by cladding systems in the earthquake that struck Christchurch on the 22nd of February. The cladding panels were attached to the frame using two fixed connections at the base and two flexible tie-back connections at the top. Static push-over analyses were used to determine the change in strength and stiffness of the system.
Results showed that when cladding interaction is taken into account, the frame is provided with larger stiffness and strength, though with an earlier onset of collapse. The time-history nonlinear analysis was also performed. The maximum inter-storey drift and subsequent cladding connections damage were reported. Results confirmed the high influence of cladding systems upon the seismic behaviour of multi-storey buildings. Some additional details concerning this research can also be found in (Baird, et al., 2011a)
With specific reference to the technology used in Southern Europe, (Ercolino et al., 2013) carried out a numerical investigation on the influence of infilled vertical cladding panels on the dynamic behaviour of one-storey precast industrial buildings. The parametric study shows a

high influence of the panels on the first period of the structure, as well as the inadequacy of the code relationships (i.e. NTC, 2008) for the evaluation of the natural period for such typology of structure. More suitable relations are proposed in order to evaluate the seismic demand of one story precast buildings both in the case of bare and infilled system. The stiffening effect of cladding panels provided with interactive connection systems provides a shift in the vibration frequencies of precast buildings, possibly increasing the seismic demand on them, as presented in (Magliulo, et al., 2015)

Precast cladding seismic performance: the field investigation

During the recent L'Aquila (2009), Lorca (2011), Emilia (2012) and partly Central Italy 2016 earthquakes, a reliable number of data about the response of the panel connections, typically used in Southern Europe, was collected. In the L'Aquila (Menegotto, 2009; Toniolo & Colombo, 2012) and Lorca (Romão et al., 2013) earthquakes, the precast frame structures showed a quite satisfactory behaviour, with heavy damage observed only in very few buildings located nearby the earthquake epicentres.

On the contrary, after the Emilia earthquake (Magliulo et al., 2014; Savoia, et al., 2017), poor performance of both precast structures and cladding panels was observed. However, it is worth remembering that, while L'Aquila area has been considered seismically active in the Italian national standards since the beginning of the diffusion of precast structures, the area surrounding Modena has been classified as significantly seismically active only since 2005.

As already illustrated in §1.3, in the majority of the cases, there were no dowels between beams and columns. Because of that, the main structural system collapsed and consequently the panels fell down.

In the USA, after the Northridge earthquake (Cohen, 1995) and (Iverson & Hawkins, 1994) described the damage of cladding panels observed during the Northridge earthquake. They concluded that cladding panels and connections unintentionally participated in lateral load-resisting structural systems. As a consequence, unexpected cladding damage occurred, including life-safety problems when a large number of panels fell down and others were left hanging precariously. Despite the fact that the experimental and analytical investigation had proved that the claddings played an important role in the overall response of the buildings, they were usually completely neglected by the designers. Cohen further concluded that multidisciplinary efforts are needed to change the codes and practice in order to ensure predictable, reliable, and safe performance of cladding during seismic events.

A report about the behaviour of precast structures, with a focus on parking facilities, stricken by the Christchurch (New Zealand) earthquake of February 2011 was made by (Restrepo, et al., 2012) and (Wilkinson et al., 2013).

Experimentation on cladding panels and connections

In the (NIST, 1995) mostly cladding connections typical for the US and Japan practice were examined.

At the start of the 80s, a cooperative US-Japan testing program was performed on a full-scale steel structure to determine the seismic performance of non-structural elements (Wang, 1986a, 1986b, 1987; Wang, Sakamoto, & Bassler, 1992). A full-scale six-storey steel building was tested. It consisted of two bays frame in each direction of the building. Free vibration tests were performed before and after the construction of the non-bearing components. The non-structural elements reduced the natural period of the building by 30%, which suggested that the overall structural stiffness was increased by more than 100%. The stiffness decreased when the non-structural elements were damaged. At storey drift of 0,3%, most of the additional stiffness was lost.

Regarding the connections, some observations obtained within the presented tests are summarized below.

- Long ductile rods used for lateral connections (Figure 2-18a), typical in the U.S.A., can accommodate very large storey drift. Sliding connections (Figure 2-18b), typical in Japan, may have problems either because of insufficient slot length or due to impedance of the sliding mechanism. Although it is possible to design a sliding connection that enhances their reliability, they are still potentially fraught with problems ranging from weathering and ageing of the connection, to improper installation, or poor detailing. Lateral connections, in particular, should not depend upon subjective criteria for installation such as tightening of nuts which cannot be easily perceived during inspections. Once the connection's sliding mechanism gets tangled, the failure of the connection may be sudden and dangerous. If sliding connections are to be allowed, they must be detailed, so that correct installation does not require great experience and skill on the part of the installer. Slot length needs to be large, to avoid the imposition of large stresses in panels and connections.
- Bearing connections must be sufficiently flexible to avoid conveying stress to the panel, resulting from inter-storey drift in regard to both in-plane and out-of-plane components of direction. The choice of tube or angle connections makes a great difference in the degree of cracking of the panels. Care should be taken not to inadvertently stiffen connections, for example by pouring new concrete around the connection body.
- Panels should be "hung" so that bearing connections are at the top and lateral connections are at the bottom, whenever possible. The common practice of bottom bearing connections may result in the falling out of panels if the tie-back connections fail.
- Connections from a panel to frame should be oriented in the same horizontal direction, otherwise extensive warping and cracking of the panel will occur. This caution is particularly noteworthy in the design of cladding for corner conditions.
- Joints must be wide enough to avoid contact between panels as a result of drift. Adjacent panels should be designed to respond to drift, in a similar manner whenever possible. Thus, placing wall panels attached to girders, next to column covers attached to columns, must be detailed with extreme caution, to avoid the pounding of adjacent panels.

Despite the limitations of the test, this research provided some reasonable indications of the behaviour of the elements under large storey drifts and the effects of the elements on the strength and stiffness of the structure. Moreover, a basis to decision making in seismic design of cladding was given.

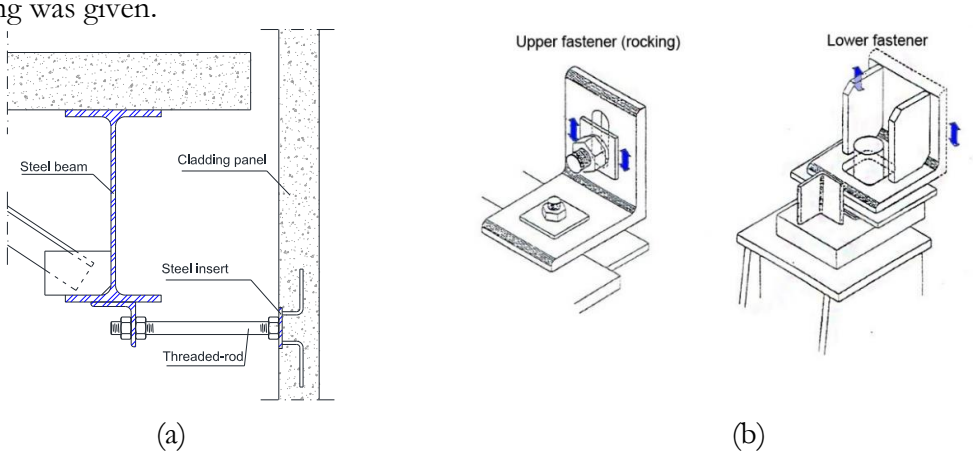

Figure 2-18: Example of: Tie-back lateral connection (a) and Japanese rocking connection (b)

A series of static tests were performed, by (Rihal, 1988, 1989), on threaded-rod lateral (push-pull) cladding connections in order to investigate the strength and behaviour of these connections (Figure 2-19). Cyclic in-plane racking tests were carried out on a precast concrete cladding panel with bearing connections at the bottom and threaded-rod lateral connections at the top. The in-plane resistance was controlled by the bending deformation of the top threaded rod connections. The 8-inches long threaded rod failed at an applied load of 1.2 kips (5.33 kN) and an inter-storey drift ratio of 1.2%. The in-plane lateral forces in the top connections were approximately 0.25–0.40 times the panel weight at a drift ratio of 1.0%. The load capacity of the push-pull connectors decreased with increasing rod length

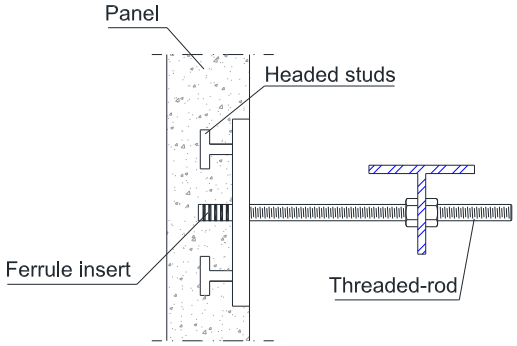

Figure 2-19: Ductile connection tested by (Rihal, 1988)

(Sack, et al., 1989) tested various basic connection assemblies to obtain static stiffness properties and a limited amount of low cycle fatigue data. The connection types consisted of ferrule inserts with threaded rods and standard angles with welded inserts and face plates. The results of the test demonstrate that the panel connections perform as ideally elastic perfectly-plastic materials. It was noted that the steel face plates did not enhance the behaviour of connections using single inserts and threaded bars, and the energy dissipation characteristics of the connections could be based on the product of the inter-storey drift and the plastic load limit. During the cyclic tests, the concrete of the panels maintained its integrity.
(Craig, et al., 1986)and (Craig, et al., 1988) carried out particular tests of the behaviour of steel inserts in cladding panels. These tests had the aim to determine the connections' lateral stiffness, energy dissipation, and ductility. The method of failure was the undesirable mode of concrete fracture, and therefore the authors point out that an improvement in the connections should be considered.

(Pinelli & Craig, 1989) investigated on seven concrete panels with steel plate inserts. The embedded inserts were supported with either welded 90-degree rebar J-hooks or welded rebar parallel to the surface of the concrete (Figure 2-20). The inserts showed limited energy dissipation. The cyclic load tests revealed pinching in the hysteretic loops. Low levels of load were resisted primarily by the surrounding concrete, and as the lateral movement increased, the stiffness increased as the rebar engaged the concrete. After the failure of the surrounding concrete, the inserts behaved as a hinge. Failure resulted from either failure of the concrete or fracture of the weld between the rebar and plate.

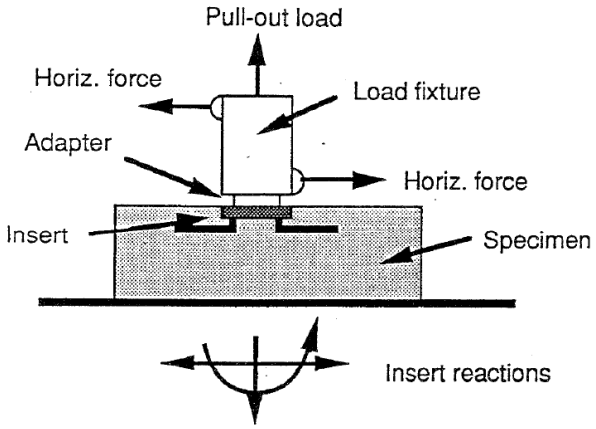

Figure 2-20: Test arrangement from (Pinelli & Craig, 1989)

(Pall, 1989) developed friction-damped connections to attach the cladding panels to the structure (Figure 2-21). As explained in (Pantoli, 2016), these connections should be designed not to slip during service level conditions - thus controlling deflections- and slipping during a major earthquake to dissipate energy. A nonlinear time-history dynamic analysis was performed on a typical ten-storey concrete frame, and it was concluded that cladding installed using advanced connections could increase the torsional resistance of the building, dissipate a large amount of energy during an earthquake, decrease drifts, help preserve the structural integrity and reduce floor accelerations

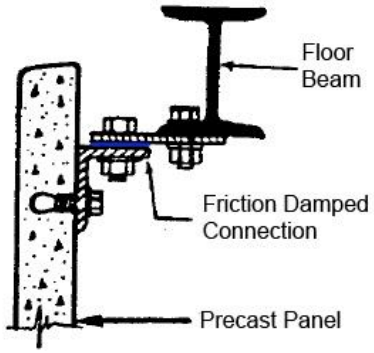

Figure 2-21: Typical friction damped connection from (Pall, 1989)

(Pinelli, et al., 1992, 1996) performed experimental testing for the mechanical characterisation of a cladding-to-structure dissipative connection based on plasticity that is called "tapered tube" (Figure 2-22). The results obtained showed that the connection behaviour is satisfactory for what concerns ductility, strength, dissipation and cyclic stability. The authors provide a design guideline and a design chart for the connection.

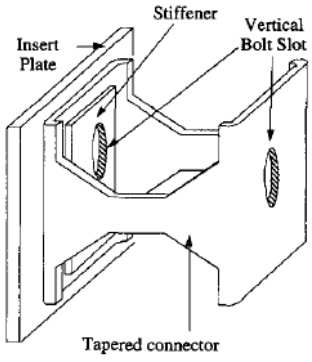

Figure 2-22: Advanced tapered connector from (Pinelli et al., 1996)

(Chan, 2003) performed four monotonic experiments on push-pull connections in two orthogonal directions. The main goal was to investigate the behaviour under bending and axial load. Axial tension and compression occurs as a result of out-of-plane panel movements, and represent the forces that the rods are intended to resist. Bending of the rods occurred as a result of in-plane panel movements. Although push-pull rods were not intended to resist lateral forces on panels via shear, their bending was significant, particularly if they were short. Concerns about their fracture due to bending would not seem justified until deflections exceed 25% of their length.
(McMullin, et al., 2004) carried out eight full-scale tests on cladding connections. Tie-back push-pull threaded rod connections and welded plate lateral seismic connections were subjected to monotonic loading. All connections tested showed ductile failure modes, with some amount of energy dissipation before final failure. Weld fracture was always the failure mode for the lateral seismic connection except for the threaded rod tie-back push-pull connections. However, the push-pull connection showed significant stiffness when subjected to out-of-plane loading, and it failed at a limited deformation.

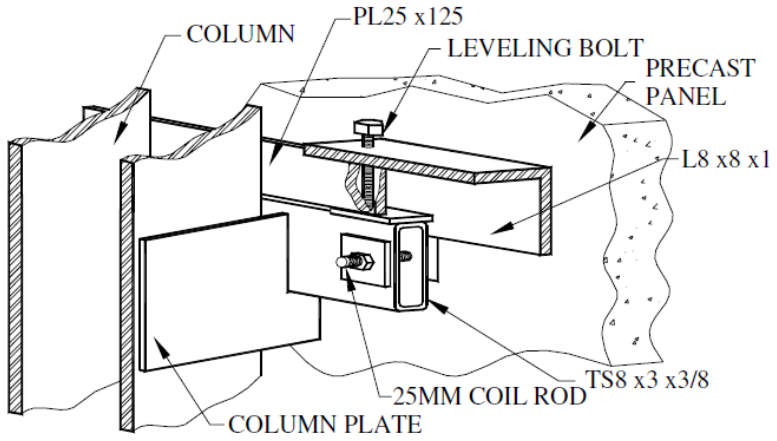

Figure 2-23: Connection detail from (McMullin et al., 2004)

At the San Diego University (UCSD), in cooperation with the Network for Earthquake Engineering Simulation (NEES), a shaking table experimental campaign of a benchmark full-scale 5-storey precast building provided with non-structural components was performed (Chen et al., 2015; Pantoli, 2016; Pantoli et al., 2015).
The cladding panels were installed at upper two storeys. Three full-scale experiments have been carried out, two of which include precast concrete cladding panels (Figure 2-24a). Seismic base isolation has been tested, together with clamped foundations. Different types of damage and failure are investigated, including loss of air seal at joints, the closing of the slip connection at the top of column cover panels, damage to the corners of concrete panels when excessive rotation results in the contact between adjoining panels, damage including possible bolt fracture to the pin connections at the base of the column cover panels, cracking of the window glass due to crushing and damage to the connections supporting the return panels resulting in potential instability of panels. Two types of push-pull connections were tested (Figure 2-24b,c) and their capability to accommodate in-plane storey drifts was assessed. Namely, fixed rod and sliding rod connections of varying rod lengths were installed and tested in an effort to understand the relationship between rod length and connection performance. Inspection of residual damage after each test motion revealed that the connections did not undergo any substantial damage in the isolated configurations. During the clamped foundation tests, however, plastic yielding of both the fixed rod and sliding rod connections were observed,

with the exception of the sliding short rod connections, which showed no signs of damage under any test.

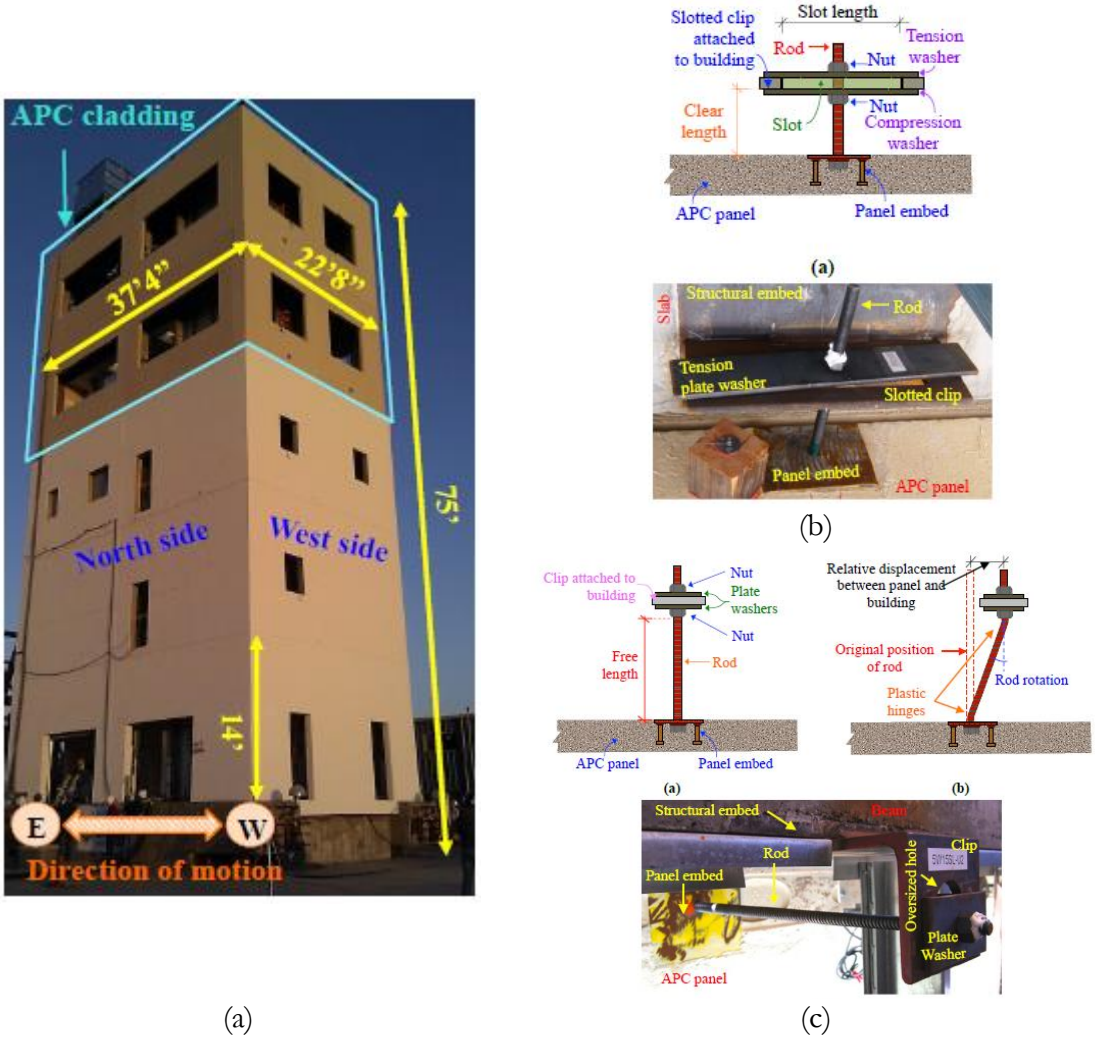

Figure 2-24: Full-scale test arrangement (a). Sliding connection for panels (b). Flexing connection (c) from (Pantoli, 2016)

The European construction practice for RC precast buildings is quite different from the US one. In Europe, most of the precast RC buildings are of a single-storey type and mainly house industrial activities, while in the United States the prefabricated system is also widely used for residential and offices buildings. The infill panels of these European industrial buildings can be up to 15 m high, up to about 2.5 m wide and up to 400 kg/m^2 in weight, while smaller panels, spandrel and column-cover, are used in the United States. Panels of this size can almost be considered as a separate structure. For this reason, in Europe, connections commonly used are substantially different from those in the US practice.
(Ferrara, Felicetti, Toniolo, & Zenti, 2011) focused on the design and experimental assessment of the behaviour of friction dampers to be used along the edges of cladding panels. The concept and design of such devices is based on a no-slip requirement under wind and moderate earthquake loadings, while allowing large displacements and consequent significant energy dissipation due to friction for higher intensity earthquakes (Figure 2-25). Elements were custom-built by assembling, by means of bolted connections, three steel plates, in case, with interposed brass plates. The result confirmed that a steel-brass friction coupling provides a

more stable hysteretic behaviour than a steel-steel one. Moreover, the original capacity of the whole devices can be effectively restored through simple surface treatments, such as brushing or sandpaper abrasion

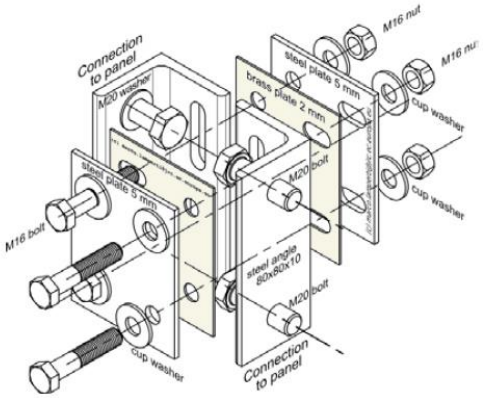

Figure 2-25: Dissipative device from (Ferrara et al., 2011)

Isakovic, et al., (2014), Starešinič, (2020) and Belleri, et al., (2016a) investigate experimentally and numerically, the in-plane performance of horizontal precast reinforced concrete cladding panels, typically adopted in one-storey precast industrial and commercial buildings. They performed experimental tests on full-scale panels sub-assembly under quasi-static cyclic loading. The study confirmed that a key characteristic of the connections is the tightening of the sliding element. When this element is to tight, it could lead to premature fracture of the connections.

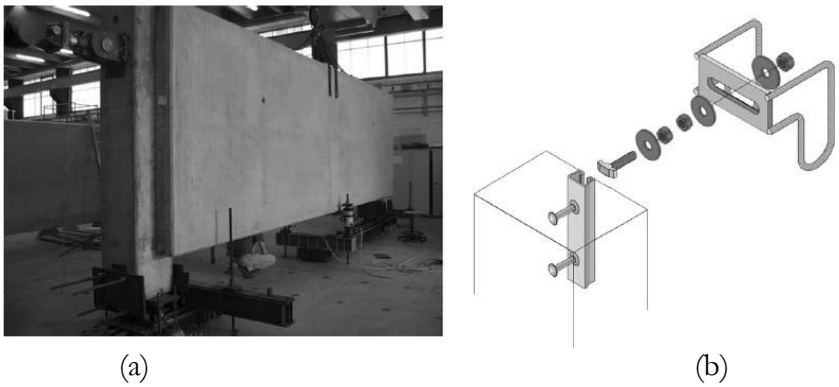

(a) (b)

Figure 2-26: Sub-assembly test set up (a) tested connection device (b) from (Belleri, Torquati, Marini, & Riva, 2016b)

(Zoubek, et al., 2016) performed an experimental and numerical investigation on hammer-head strap connections that are most commonly used in the current European design practice. The authors tested a panel-connection-beam sub-assembly by means of cyclic uniaxial shear tests and biaxial shear tests, in order to evaluate the influence of out-of-plane force on the in-plane response of the hammer-head strap connections. And a series of uniaxial sliding tests were also carried out in order to investigate the response of the connections along their vertical axis. The results obtained from experimental studies were used to develop reliable numerical models of typical connections. Appropriate procedures for the safe design of in-use connections were also defined.

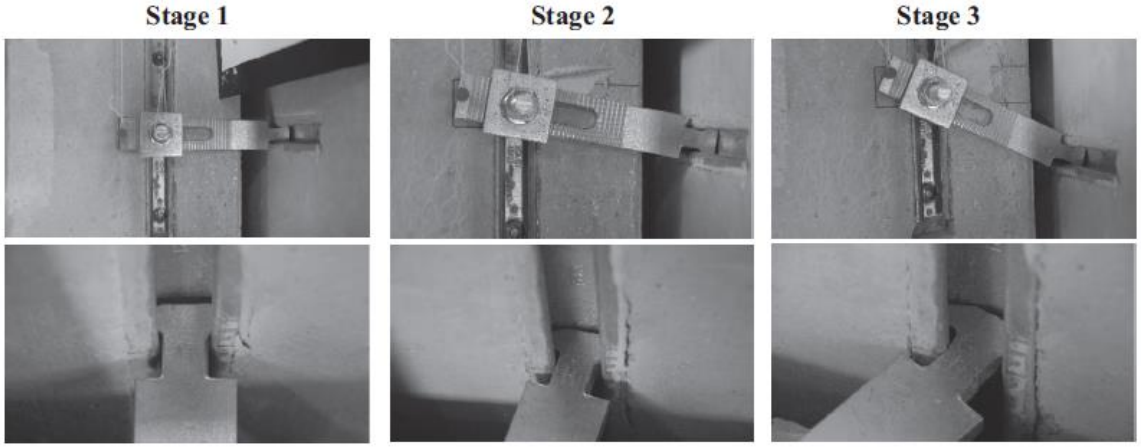

Figure 2-27: Hammer-head strap connections tested at the University of Ljubljana. Courtesy of (Zoubek et al., 2016)

Within the SAFECLADDING research project (Biondini, et al., 2017; Dal Lago, et al., 2018) presents the main results of an experimental campaign carried out on different types of dissipative connections, including a panel-to-column connector for horizontal panels and two panel-to-panel connection devices for both vertical and horizontal panels.

- The panel to-column Folded Plate Device (FPD) consists of a steel plate folded at right-angle along three lines to get a W-shaped profile (Figure 2-28a). This dissipative connection system provides stiffness and strength against out-of-plane loading, as well as flexibility and ductility to accommodate in-plane panel-to-structure relative displacements.
- The plasticity-based Multiple Slit Device (MSD) consists of steel plates with slits of various shapes and sizes which realize a set of elementary beams (Figure 2-28b). The MSD device exhibits a relevant elastic stiffness and a plastic behaviour characterized by a pronounced hardening. A stable dissipation of energy is attained through plasticity up to a drift ratio of about 20% with respect to the length of the slits.
- The Friction Based Device (FBD) is made by the assemblage of brass sheets, cover steel plates, and support steel profiles, as shown in (Figure 2-28c). This device is characterized by a pseudo-plastic behaviour with high initial stiffness and a plateau associated with the friction load threshold, after which relative sliding of the supports occurs. This friction mechanism leads to large dissipation of energy.

(a) (b) (c)

Figure 2-28: Folded Plate Device (a), Multiple Slit Device (b) and Friction Based Device from (Biondini et al., 2017)

Extensive experimental and numerical studies on an energy-dissipative steel cushion (SC) connection (Figure 2-29a, b) device were carried out in the framework of the SAFECLADDING project by (Karadogan, et al., 2012) at Istanbul Technical University.
It emerges that higher structural damping could be achieved by appropriately selecting the thickness and locations of the SCs in the RC cladding system. And also that the out-of-plane deformations of the cladding panels can be reduced by using double SCs in the panel-foundation connection as well as a thick SC in the panel-beam connection.

(a) (b)

Figure 2-29: Steel Cushion connection test: sub-assembly test arrangement (a) and test picture (b). From (Karadoğan et al., 2019)

At the Laboratory for Earthquake Engineering of the National Technical University of Athens, Greece panels with integrated arrangements were studied (§2.1.2) by (Psycharis, Kalyviotis, & Mouzakis, 2018).
The authors provided some basic suggestion for the integrated panels' design.
In buildings with integrated cladding panel walls, plastic deformation of the panel connections occurs for large lateral displacements. However, the experimental investigation showed that this is typically accompanied by horizontal slippage at the panel-to-beam joint and by considerable pinching during the cyclic response.

- Due to the above-mentioned unwanted effects, it is suggested that the panels' connections should be overdesigned by applying the capacity design concept. To this end, it is suggested that the over-proportioning of the connections shall be based on the forces derived from a structural analysis performed with behaviour factor q not larger than 1.5.
- For the design of the columns, the behaviour factor that corresponds to wall or wall-equivalent dual systems should be applied.
- Large forces might also develop in other connections of precast members (such as roof-to-roof, roof-to-beam etc.). In order to accurately estimate these demands, accurate numerical simulation is required.

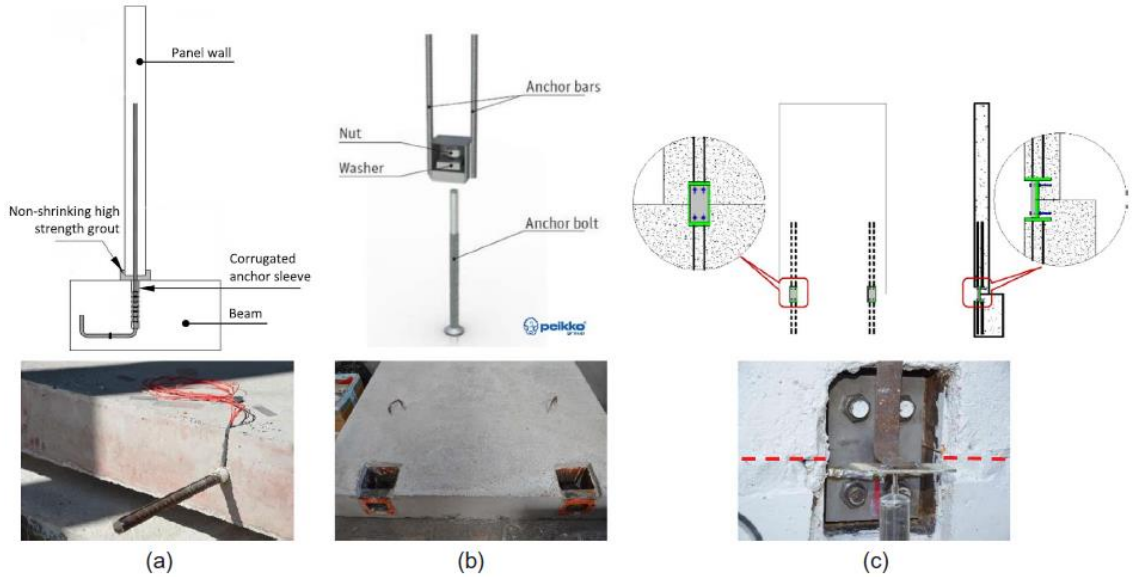

Figure 2-30: Connection types considered in the experimental investigation: (a) 'Rebar' connections; (b) 'Wall shoe' connections; (c) 'Steel plate' connections. From (Psycharis et al., 2018)

Experimental campaign on second-line system connections (§2.1) was performed by (Zoubek et al., 2018). The system consists of special anchoring elements and a rope restrainer (Figure 2-31). The connection is activated only in the case when the existing connections between the primary structure and the panel fail. The authors proposed an analytical procedure to estimate the maximum possible impact forces acting in a restrainer. The procedure is based on the estimation of the maximum relative velocity between the main structure and the panel and the acceleration of the primary structure at the moment of activation of the restrainer.

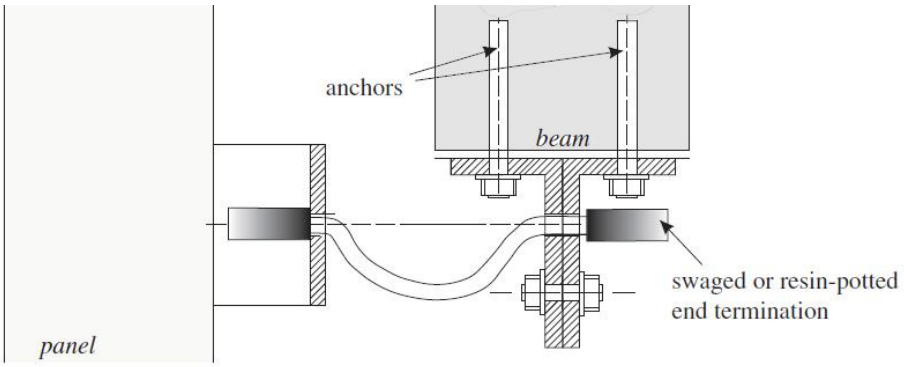

Figure 2-31: Restrainer system as a second-line back-up device for the prevention of the collapse of concrete cladding. From(Zoubek et al., 2018)

Finally, (Dal Lago, et al., 2017; Negro & Lamperti Tornaghi, 2017) investigated the effect of silicone sealant that is usually interposed between panels of precast facades. The study about the effects of the silicone sealant placed between the cladding panels is relevant because it is necessary to assess if the sealant can influence the seismic performance of the structure and of the connections. It is also important to understand and if there is a stiffness contribution due to the presence of the silicone between alongside panels. The experimental campaign consisted of local tests on small specimens of silicone sprayed in between concrete blocks (Figure 2-32a), sub-assembly tests on panels sealed with long silicone strips (Figure 2-32b), and full-scale prototype tests on a precast building with vertical cladding panels sealed with silicone. The researchers concluded that the silicone sealant placed in between cladding panels can influence

the seismic performance but only at the serviceability limit state and can increase the load demand on the panel connections. However, the silicone stiffening contribution is limited and not reliable, since the variability of the mechanical characteristics of this type of product is large. The study also shows that silicone is not suitable to sustain the large drifts typically associated with the ultimate limit state.

(a) (b)

Figure 2-32: Local test on silicone (a) and pseudo-dynamic test on vertical panels sub-assembly

2.3 Design procedures for cladding panels

The design of the precast cladding panels and their connections to the main structure is in the majority of codes limited to the application of equivalent static forces defined on the basis of the mass of the single panel. In many cases, only the resistance with respect to out-of-plane seismic forces is provided. Mostly, no requirements are defined for the in-plane direction of panels, with an exception of the drift limitations.
The reason for the lack of specific recommendations can be found in the fact that most of the codes consider the panels as non-structural elements. However, the classification of panels as non-structural elements should depend on the type of their connection with the main structural system and their influence on the response of the precast building.

2.3.1 Eurocode 8 and Italian code requirements

Eurocode 8 considers cladding panels as non-structural elements. The out-of-plane equivalent static action is calculated according to the following equation:

$$F_a = \frac{S_a W_a \gamma_a}{q_a} \qquad (2.1)$$

where: F_a is the out-of-plane horizontal force, W_a is the weight of the element, q_a is the maximum behaviour factor (equal to 2,0 for façade elements), γ_a is the importance factor (equal to 1,0 for façade elements) and S_a is the seismic coefficient, which can be determined according to the following equation:

$$S_a = \alpha S \left[\frac{3\left(1+\frac{z}{H}\right)}{1+\left(1-\frac{T_a}{T_1}\right)^2} - 0.5 \right] \geq \alpha S \qquad (2.2)$$

where α is the ratio of the design ground acceleration, a_g, on subsoil type A, and the acceleration of gravity *g*, *S* is the soil factor, *z* is the height of the non-structural element centroid above the level of application of the seismic action, *H* is the building height measured from the foundation or from the top of a rigid basement, T_a is the fundamental vibration period of the element and T_1 is the fundamental vibration period of the building in the relevant direction.

The structural standards until the 90s (for example the Italian code DM, 1996) only required that, in case of seismic/wind drift, the stability of non-structural elements was guaranteed. No information or explicit instructions were provided about the calculation of the seismic load on non-structural elements. Subsequently, European member countries accepted the Eurocode 8 (EN 1998-1-1, 2005) rules for the design of non-structural elements as the cladding panels and their connections.
Starting from the indications provided by Eurocode 8 (EN 1998-1-1, 2005), the Italian code (NTC, 2018) requires, in addition to the seismic resistance calculation, that non-structural elements have to accommodate the drift of the structure subjected to design seismic excitation. Therefore, the formulation based on spectra is introduced according to (Sullivan, et al., 2013) for the assessment of the acceleration which is to be applied to the secondary elements.
For load-bearing frame structures, the maximum spectral acceleration $S_a(T_a)$ could be determined by:

$$S_a(T_a) = \begin{cases} \alpha S\left(1+\frac{z}{H}\right)\left[\frac{a_p}{1+(a_p-1)\left(1-\frac{T_a}{aT_1}\right)^2}\right] \geq \alpha S & for\ T_a < aT_1 \\ \alpha S\left(1+\frac{z}{H}\right) & for\ aT_1 \leq T_a < bT_1 \\ \alpha S\left(1+\frac{z}{H}\right)\left[\frac{a_p}{1+(a_p-1)\left(1-\frac{T_a}{bT_1}\right)^2}\right] \geq \alpha S & for\ T_a \geq bT_1 \end{cases} \qquad (2.3)$$

Where the symbols are the same explained above, except for *a*, *b*, a_p, that are parameters depending on the fundamental vibration period of the building in the relevant direction T_1.

2.3.2 U.S.A. codes requirements

The 1967 Uniform Building Code already introduced some regulations about the cladding panel connections. For what concerns drift allowance, it was indicated to that it should be larger than twice the maximum drift caused by wind or seismic load, or one-fourth of an inch (6.4 mm), whichever is the greater. The seismic forces acting on the single panel were estimated according to the following equation:

$$F_p = ZC_pW_p \qquad (2.4)$$

where F_p is the total lateral design seismic force acting on the component, Z is the seismic zone factor and it could be determined from seismic zone map (Figure 2-33), C_p is the horizontal force factor (equal to 1.0 for non-structural components) and W_p is the panel weight.
In the 1979 UBC version, only the introduction of the multiplying factor I, namely the importance factor, has been adopted as a modification of the previous formula. It was suggested that the value of the importance factor should be equal to 1.0. However, an important distinction is added for what concerns the force factor C_p. Indeed, a unity value is given for all elastic portions of the connections, while the body of the connection could be made with ductile devices which could be calculated according to a larger force factor, equal to 3.0
In the following 1991 UBC version, the formula for lateral forces remained unchanged, while the drift allowance lower limit doubled to half an inch.
The 1997 UBC version introduced several important changes in the calculation methodology (Bachman & Bonneville, 2000). While the drift allowance remained unchanged but with indications on how to compute the drift, two alternative formulae were provided for the evaluation of seismic lateral forces, described in the following equations, together with a lower and higher limitation.

$$4.0C_aI_pW_p \geq F_p = 4.0C_aI_pW_p \geq 0.7C_aI_pW_p \quad (2.5)$$

$$4.0C_aI_pW_p \geq F_p = \frac{a_pI_pC_a}{R_p}\left(1+\frac{3h_x}{h_r}\right) \geq 0.7C_aI_pW_p \quad (2.6)$$

where a_p is the in-structure component amplification factor (equal to 1.00 for rigid components), R_p is the component response modification factor (equal to 3.00 for the body of the connection and to 1.00 for other non-ductile connections), h_x is the element attachment elevation with respect to ground and h_r is the structure roof elevation with respect to ground and C_a is the beginning value of the design response spectrum.

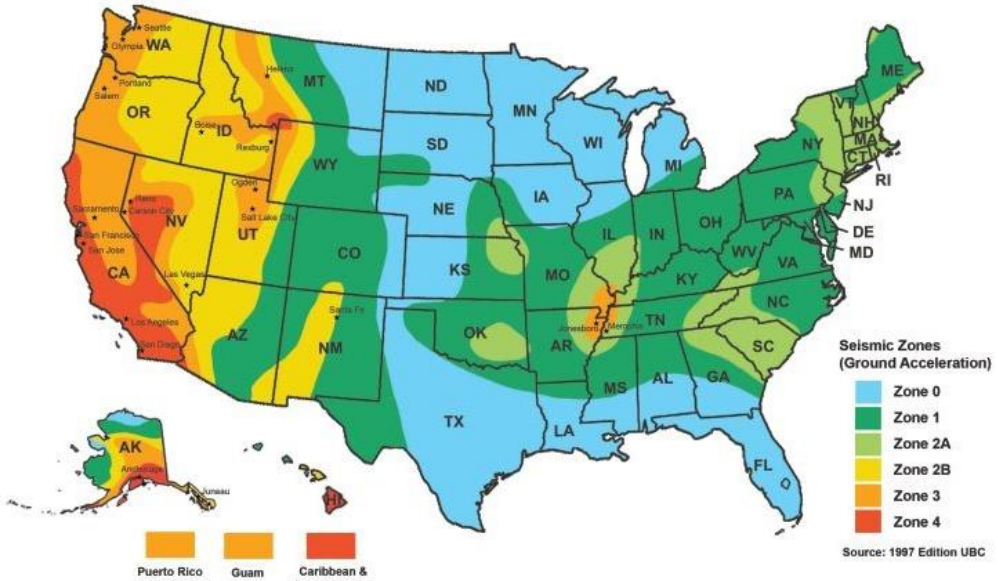

Figure 2-33: The UBC 1997 seismic zone map

The 2000 and 2003 UBC versions converged on a slightly different version, introducing the design earthquake spectral design acceleration at short period S_{DS}. The calculation is then modified as the following equation:

$$1.6S_{DS}I_pW_p \geq F_p = \frac{0.4a_pS_{DS}I_pC_a}{R_p}\left(1+\frac{2z}{h}\right)W_p \geq 0.3S_{DS}I_pW_p \quad (2.7)$$

The most recent version of the IBC refers to ASCE 7 Standard for the seismic requirements on non-structural components. Version ASCE 7-10, includes the computation of the vertical seismic component F_{pv}, calculated as per the following equation.

$$F_{pv} = \pm 0.2S_{DS}W_p \quad (2.8)$$

In addition to the calculation rules, FEMA 461 provides instructions about standard experimental tests aimed at assessing the correct functioning of non-structural elements and connections. Finally, general approaches for non-structural building components can be found in (Filiatrault & Christopoulos, 2001).

2.4 The main goals of research

As discussed in the previous paragraphs, understanding the behaviour and the influence of the connections between the cladding panels and the main structure in RC precast buildings, especially in seismic conditions, has been the subject of many research works.
The aim of this thesis is to propose appropriate solutions and to improve the current knowledge and technical practices related to the connections of vertical cladding panels to the main structure.
The widely used hammer-head strap connections and their influence on the seismic response of the structure are studied, both when the panels have a cantilever configuration and when they have a rocking one.
This thesis also illustrates the results of a previous shaking table experimental campaign for an RC precast structure prototype with vertical panels and hammer-head strap connections. The procedure for making-up a numerical model that is able to reliably replicate the results obtained during the real tests are described. This numerical model makes it possible to extend the results of the experimental evidence also to real structures that, by their nature, can not directly be tested in a laboratory. By extending the calibrated numerical model the influence of silicone sealant on the seismic behaviour of precast vertical cladding panels was evaluated.
Subsequently, an innovative connection device is described and a series of experimental tests for the characterization of its mechanical behaviour is illustrated
Finally, a purely numerical study is carried out to understand the force that stresses the vertical panel-structure connection in the out-of-plane direction. A parametric study allows to evaluate the force that acts in the connection in the function of the mass and the period of the structure, generalizing in this way the field of investigation. Following this study, a preliminary design rule is proposed.

3 The in-plane seismic response of vertical cladding panels

In this chapter, there is an overview of a shaking table experimental campaign, performed at UL FGG and studying the seismic response of single-storey RC precast buildings with vertical panels. A numerical model that reliably replicates the results of the experimental tests is developed. Some considerations are carried out regarding the results obtained.
Furthermore, an analytical and experimental study of an innovative connection device that dissipates energy by friction mechanism is presented.

3.1 Shaking table experimental test

The experimental investigation of structures on a seismic shaking table is the most effective way of investigation regarding the dynamic structural behaviour during real earthquakes. Within the project "*Seismic resilience and strengthening of precast industrial buildings with concrete claddings"* the department of Civil Engineering from the Faculty of Civil and Geodetic Engineering of University of Ljubljana (UL-FGG) designed and conducted a set of full-scale shaking table tests of a RC precast prototype building with claddings. All the tests were performed at the shake table of Institute of Earthquake Engineering and Engineering Seismology (IZIIS) in Skopje, Republic of North Macedonia (Isaković, et al., 2018)

3.1.1 Design and aim of full-scale shaking table tests conducted by UL-FGG

The shaking table tests campaign was carried out in July 2017. The experimental work had the aim of evaluation the influence of several parameters on the dynamic response of precast industrial building with concrete cladding panels. The investigated parameters in this study included:

- The orientation of the panels.
- The type of connections between the panels and the main structural system of the building (long or short hammer-head strap).
- The type of the panels' connections with the footings

Altogether, eight different prototype configurations were tested. The tests differ in the panels' orientation (horizontal or vertical configuration), the type of the panel-to-structure connections, the type of the connections between the vertical panels and the footings (cantilever or rocking panels) and the number of the panels (on both sides or only on the one side). The main frame structure was the same for all eight configurations. In the following table, the complete testing sequence is summarized:

Label	Consecutive number	Claddings orientation	Claddings-structure connections	Claddings-foundation connections	Number of panels
V1	1	Vertical	Hammer-head strap (long)	Rocking (dowels)	2
V1e	2	Vertical	Hammer-head strap (long)	Rocking (dowels)	1
V2	3	Vertical	Hammer-head strap (short)	Rocking (dowels)	2
V2e	4	Vertical	Hammer-head strap (short)	Rocking (dowels)	1
V3	5	Vertical	Hammer-head strap (long)	Fixed (couples)	2

V4	6	Vertical	Hammer-head strap (long)	Fixed (couples)	2
H	7	Horizontal	Nodo7 (top) Hop (bottom)	/	2
He	8	Horizontal	Nodo7 (top) Hop (bottom)	/	1

Table 3-1: Summary of the tested connection

In the tests V1e and V2e the tested structure was equipped with only one panel so that the structural configuration was not symmetrical. The connection devices, used during the tests, will be described in detail within the sub-section 3.1.3 as well as the panels support condition. Since this work aims to characterise the seismic response of vertical panels, only the tests arranged with vertical panels will be discussed and commented upon this thesis.

3.1.2 Geometry and configuration of the prototype

The tested prototype consisted of four 4.5 m high RC columns, with 0.3 × 0.3 m square cross-section, cast together with pad foundation (1×1×0.5m), two vertical or horizontal 0.15 m thick concrete cladding panels (Figure 3-1). The whole structure was covered by an RC slab (4.3×1.7×0.36m). The dimensions of the slab were chosen in order to simulate the roof mass of a real building. The construction of the prototype structural elements and the panels were carried out in Kolektor CPG d.d, Nova Gorica, Slovenia. In this thesis, only the vertical panel configuration are addressed.

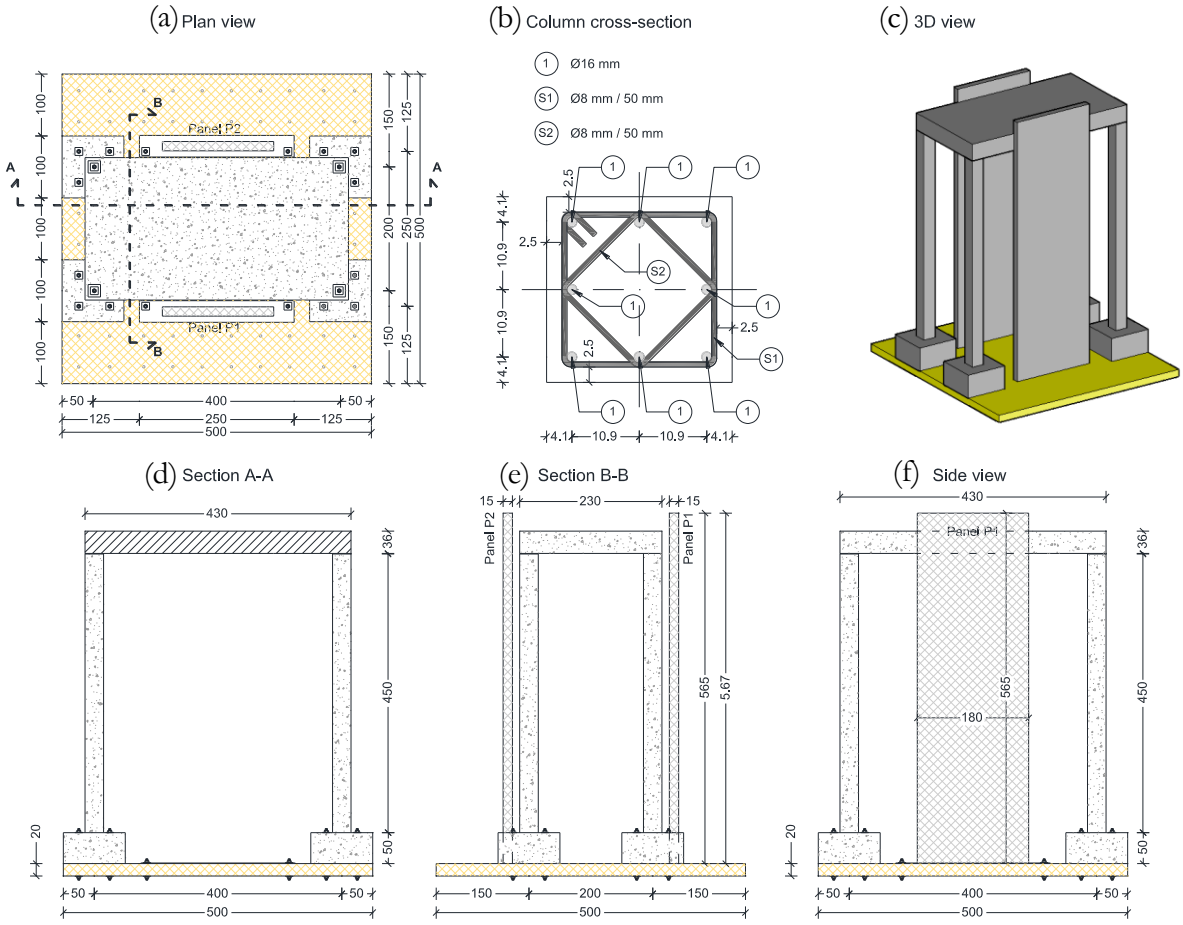

Figure 3-1: Geometry and configuration of the specimen with vertical panels

Each pad foundation was fixed to the shaking table by means of four Φ38 anchors. The slab was fixed to the columns by means of dowel connection. One Φ25 bar, protruding out from the column top face, was used as connection. A neoprene bearing pad 1.00 cm thick was placed between the top face of the column and the slab to allow for relative rotation.
The thickness of the panels P1 and P2 was 15 cm (the insulation layer was not included). They were reinforced by means of two Q355 reinforcing meshes (steel ribbed bars ϕ8 mm/15 cm in both directions used at both sides of a panel. The class of concrete was C40/50 and the class of steel was S500.

3.1.3 Connection between cladding panels and the main structural system

In this sub-section, the panel-to-structure connections devices and panels support conditions will be described.

Typical hammer-head strap connections were studied. They are the most common type of connections, used in Central Europe and Italy.
Each vertical panel was attached to the RC slab by means of two hammer-head strap connection (Figure 3-2). Panels were founded on steel plates, which were fixed to the shaking table by two Φ38 anchors. Four panels' configurations were tested. They differed in the type of connections between the panel and the foundation (rocking and fixed), as well as the length of the hammer-head straps (long and short), as explained in Table 3-1.
In the first two configurations (V1 and V2) the panels simply were supported by two steel bars, which were welded to the steel foundation plate (see Figure 3-4a). Long and short hammer-head strap connections were applied at the top. This was the rocking configuration for vertical panels.
In the third and fourth configuration (V3 and V4), the steel bars, which were cast in the panels were connected to the foundation steel plate by means of the mechanical couplers. In this way, the panels were fixed to the foundation plate. The top connections were long and short hammer-head strap.
This was the isostatic cantilever configuration for vertical panels.

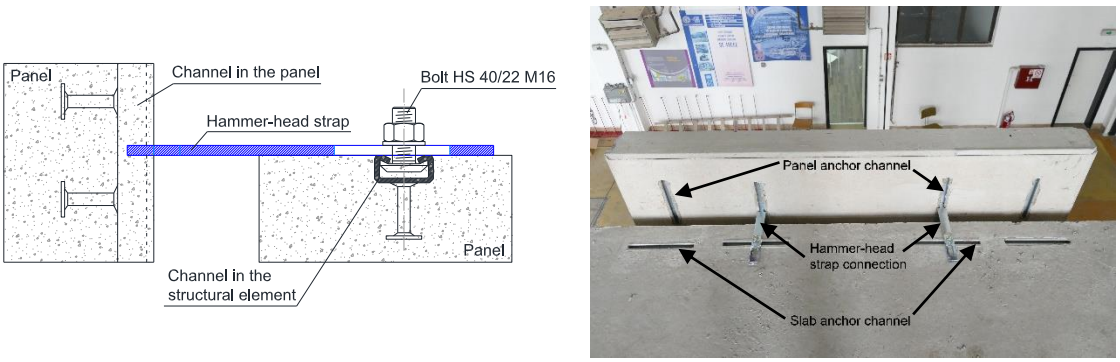

(a) (b)

Figure 3-2: Hammer-head strap connection: assembly scheme (a) and connected panel (b) Courtesy of UL-FGG.

The assembly of the hammer-head strap connection is shown in (Figure 3-3) and the dimensions are described in Table 3-2. The connection consists of a special steel strap (TA-210 or TA-290) a toothed washer, a bolt (HS 40/22; M16; class 4.6) and two hot-rolled steel channels with anchors (HTA 40/22 - 25cm) which were installed before casting the elements.

One of the channels was cast in the panels whereas the other was cast into the slab. The strap is fastened to the slab's channel by means of a toothed washer and a bolt (see Figure 3-3). Finally, the strap was fixed inside the channel on the panel side. In this way, the connection between the panel and slab is created.

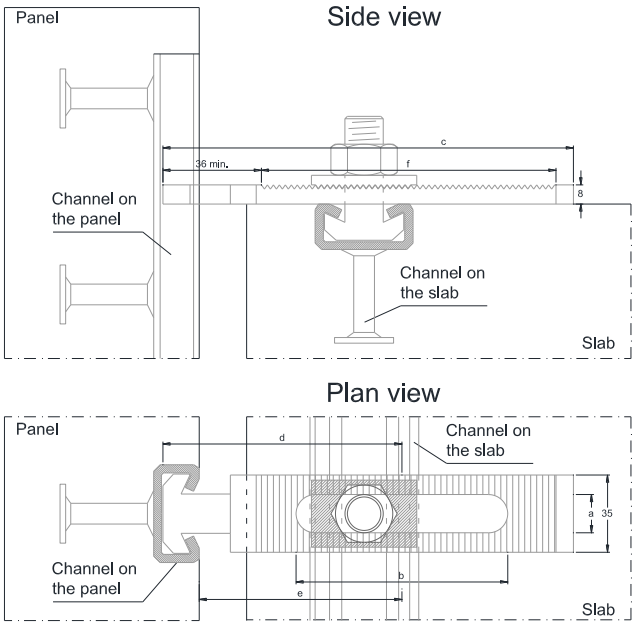

Figure 3-3: Dimension of the strap in the connection

Label	c [mm]	a [mm]	b [mm]	d [mm]	e [mm]	f [mm]	Bolt-channel distance [cm]	Panel-slab gap [cm]
TA-210	210	17	80	140	122	124	10	3
TA-290	290	17	80	220	202	124	13	7

Table 3-2: Dimension of the straps used

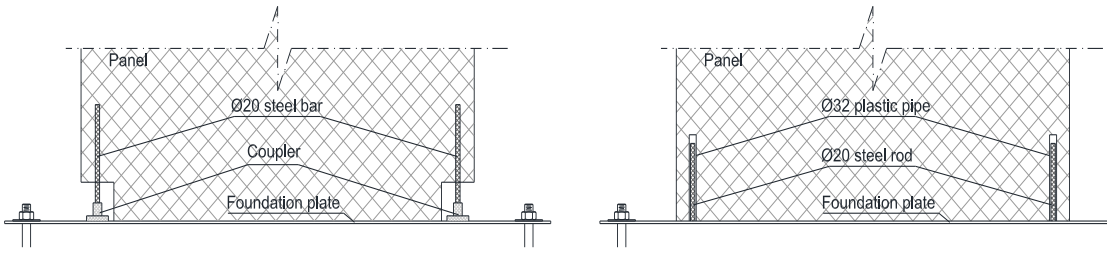

Figure 3-4: Rocking panel arrangement (a) and fixed panel arrangement (b). Courtesy of UL-FGG.

3.1.4 Test structure assembling

In Figure 3-5 different phases of the construction of the test assembly are presented:

The four columns with Φ25 bar at the top for slab anchoring

Columns installed on the shaking table

Slab placing on columns' top

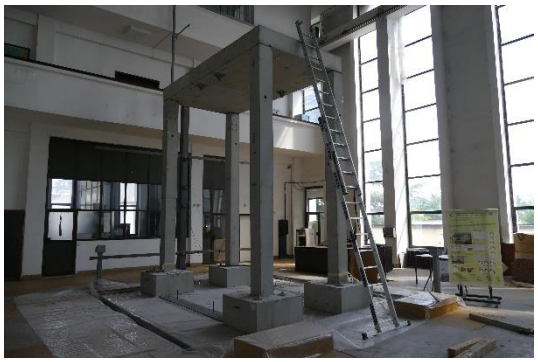

The whole main structure assembled

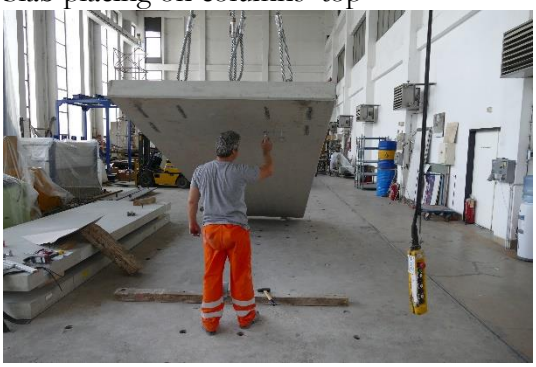

Panel lifting

Complete structure with vertical panels assembled

Figure 3-5: Assemblage of the prototype. Pictures courtesy of UL-FGG.

In the following Table 3-3 the element's dimensions, weight and assembly method are described:

Element	Dimensions [cm]	pcs	Mass [t]	Assembly method
Column S footing column	100/100/50 cm 30/30/450 cm	4	2.18	The columns were lifted by using a portal crane of maximum capacity 10 t. The columns are then fixed to the shaking table through 4 Φ32 threaded bars.

Slab P1	230/430/36 cm	1	8.56	The slab was placed at the top of the four columns by using the portal crane and four Φ20 hooks cast in the slab.
Panel V1	180/565/15 cm	4	3.65	The panel is erected by using the portal crane and four hooks cast at the back face of the panel.
Panel V2	180/565/15 cm	2	3.65	

Table 3-3: Precast elements: dimensions, weights and assembly methods

The total mass of the prototype without panels was 17.28 t. The total mass of the precast structure with two vertical panels 24.6 t

3.1.5 Test procedure and applied earthquake excitation

In order to understand the behaviour of the connection considering realistic boundary conditions at large relative drifts during a strong earthquake and their interaction with the structure, a testing program consisting of several test phases was prepared.
The testing procedure for each of the eight configurations consisted of a series of the seismic response tests applying the selected earthquake record. The tests were performed in several steps increasing the input intensity of the earthquake and monitoring the response of the panels and the main structural system. In between these tests, the periods of vibrations of the tested structure were estimated by means of the special vibration tests (Table 3-4).

Original test label	Panels numbers	Config. type	Connections length [mm]	Number of excitations/ applied intensities PGA [g]	First vibration period at the end of the test [sec]
V1	2	Rocking	290 (long)	4/ PGA = 0.1g, 0.2g, 0.3g, 0.4g	0.67
V1e	1	Rocking	290 (long)	3/ PGA = 0.1g, 0.3g, 0.4g	0.77
V2	2	Rocking	210 (short)	3/ PGA = 0.2g, 0.4g, 0.5g	0.73
V2e	1	Rocking	210 (short)	2/ PGA = 0.2g, 0.4g	0.74
V3	2	Fixed	210 (short)	4/ PGA = 0.1g, 0.2g, 0.4g, 0.5g	0.74
V4	2	Fixed	290 (long)	3/ PGA = 0.2g, 0.4g, 0.5g	0.65

Table 3-4: Experimental programme summary

Considering the significant weight of the tested structure, as well as the capacity of the shaking table, one of the issues was to select a suitable ground motion, which would generate displacement of the prototype, at which the existed hammer-head stop connections were expected to fail (at about 10 cm).
Therefore, an artificial accelerogram generated based on the Petrovac E-W (Luzi, Pacor, & Puglia, 2019) ground motion registered during Montenegro earthquake in 1979, was applied in all tests. The record was modified to match the Eurocode 8 spectrum for soil type B. Filtering and baseline correction was applied to limit residual displacements.

The accelerogram used in the tests, corresponding to PGA=1.0 g and the correlated response spectra are plotted in Figure 3-6:

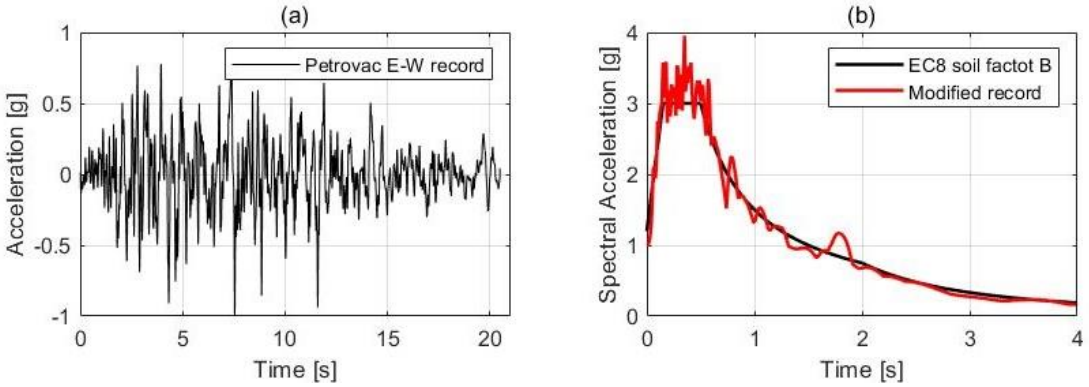

Figure 3-6: Pertovac E-W record (a) and spectrum modified to match EC8 (b)

3.2 Main results and observation

3.2.1 Comparison of the response of rocking and fixed panels

Since the experimental campaign was designed and conducted by the University of Ljubljana, from now on only the main results and observations are reported. As it can be seen from the summary Table 3-5, horizontal displacement measured at the top of the rocking panels was about 10 times greater than that of the fixed panels. Their response was completely different. For further details see the work of (Isaković et al., 2018)
Although in both cases (fixed and rocking panels) the response was qualitatively different, the maximum relative displacements between the panels and the main structure were quantitatively quite similar. Since the fixed panels had large stiffness, compared to the rocking panels, their displacements were consequently small and their vibration period was considerably shorter than that of the main structure. Instead, the vibration period of rocking panels was mainly controlled by the main structure, consequently their displacement was larger than that on the fixed panels Furthermore, the interaction between the main structure and the panels was considerably week because the connection stiffness and strength are quite limited. It can be concluded that the connections isolated the panels from the main structure and they allowed panels to vibrate differently from the main structure.

Test	**V1**	**V1e**	**V2**	**V2e**	**V3**	**V4**
Horiz. displacements of the slab [mm]	94	92	84	89	82	72
Horiz. displacements of panel P1[mm]	135	121	93	101	13	16
Horiz. displacements of panel P2[mm]	107	-	77	-	12	12
Relative horiz. displacements P1-slab [mm]	70	67	39	33	58	571
Relative horiz. displacements P2-slab [mm]	57	-	48	-	62	70
Vertical displacements of panel P1 [mm]	28	29	25	25	-	-
Vertical displacements of panel P2 [mm]	26	-	22	-	-	-
Horiz. acceleration of the slab [g]	0.85	0.74	0.72	0.66	0.70	0.66

Horiz. acceleration of the panel P1 [g]	1.73	1.49	1.39	1.42	1.18	1.05
Horiz. acceleration of the panel P2 [g]	2.06	-	1.33	-	0.96	1.08

Table 3-5: Summarizing table for maximum displacements of all test performed at 0.4g

Observing the results of maximum displacement in Table 3-5 in can be noticed that in the case V1 and V4, when the long straps were used, the maximum relative displacements were almost the same (about 70 mm at the seismic intensity of 0.4g) in both cases (V1 and V4) during the tests with higher intensity, significant deformations of the hammer-head straps were observed. In the case of rocking panels, the hammer-head straps were deformed in both horizontal and vertical direction. In the case of fixed panels, the straps were deformed only in the horizontal direction.
When the short straps were used (tests V2 and V4) the maximum relative displacements were slightly greater in the structure with fixed panels (62 mm against 48 mm at the seismic intensity at 0.4 g). In test V3 (short straps with fixed panels), the ultimate capacity of the straps was gained at the seismic intensity of 0.5 g. In the other test cases, the straps were able to satisfy the displacement demand even for rather high seismic intensities (0.5 g and 0.4 g).
The long straps were more beneficial in structures with fixed panels arrangement. Indeed, in the case of rocking panels, the use of long straps significantly increased the panels' displacement demand, which in some cases exceeded the displacements of the main structure. Despite the failure of the straps in the test V3 at 0.5g, it can be stated that the configuration with fixed panels could be more appropriate for two reasons, as explained in (Isaković et al., 2018):

1. The hammer-head steel straps are deformed only in their horizontal plane (contrary to the rocking panels, where vertical deformations can occur).
2. The response of the fixed panels is less sensitive to the random factors caused by imperfections during the assembling phase and it is more predictable.

In all the tested structures configuration, the stiffness of the panels did not significantly influence the response of the main structure. This was due to the connections since their stiffness and resistance was small compared to that of the panels and the structure. This can be seen in Figure 3-7, where the displacement response history of the main structure recorded during the tests V1 (oscillating panels, long straps), V2 (oscillating panels, short straps), V3 (fixed panels, short straps) and V4 (fixed panels, long straps) is presented. Despite the great differences among the tested panel configurations, the vibration periods and the displacement of the main structure are essentially the same. Therefore, it is possible to conclude that the connections isolated the panels from the main structure and allowed the panels to vibrate differently from the latter.

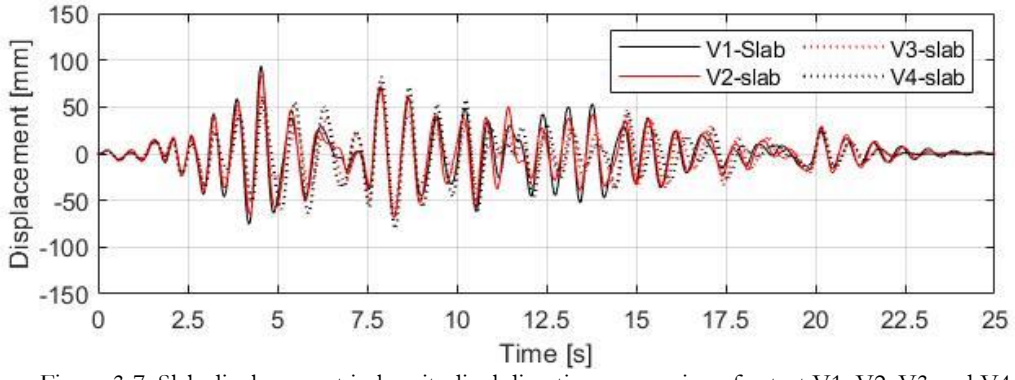

Figure 3-7: Slab displacement in longitudinal direction comparison for test V1, V2, V3 and V4

3.2.2 The response of fastenings

During the execution of the V1 and V1e tests, no failure of the panel-to-structure connection was observed, even in tests at the greater intensity of 0.4 g. When they were subjected to weaker seismic excitations, the hammer-head straps rotated in the horizontal plane around the bolt, which was used to fix them to the anchor channel installed in the slab. The connections do not show any displacement along this channel.
During the tests with higher seismic excitations, the straps were deformed both horizontally and vertically (see Figure 3-8). The deformations of the straps in the horizontal direction was one expected before the tests, according to the experimental campaign, performed at UL-FGG on single components of the panel fasteners (Zoubek et al., 2016). The steel straps were deformed also in the vertical direction, due to the vertical displacement of the panels caused by their rocking movements of the panels. As long as the rotation of the straps in the horizontal plane remained limited and the straps were not deformed, the relative vertical displacements between the strap head and the panel channel were enabled. When the relative horizontal and vertical displacements between the panel and the slab considerably increased, the heads of the straps were deformed in a horizontal direction (Figure 3-8c) and consequently they were stacked in the anchor channels of the panels' side. When the panels started moving downwards, the straps were deformed also in the vertical downward direction (see Figure 3-8a,b). In the tests V2 and V2e, the straps were deformed in the same way as in the tests V1-R and V1e-R tests as described before. In these tests, the connections did not undergo any failure even when the maximum seismic excitation was increased to0.5 g.

(a) (b) (c)

Figure 3-8: Hammer-head strap deformation: vertical deformation (a), (b) and horizontal deformation of the head (c). (Test V1: rocking panels, long straps, maximum seismic intensity of 0.4 g). Pictures courtesy of UL-FGG.

3.3 Numerical modelling of the seismic response of cladding panels

3.3.1 Numerical model overview

The computational framework *Open System for Earthquake Engineering Simulation* (OpenSees) (Mazzoni, McKenna, Scott, & Fenves, 2006a) was used to develop a numerical model of the structure, panels and connections. The following Figure 3-9 illustrates a scheme of the numerical model.

The four columns were modelled by means of non-linear elements that could also take into account the P-Delta effect. They are described in section 3.3.4.

The panels were modelled with elastic elements. The section assigned to the elastic elements had the inertial characteristics of the panel's real cross-section. For more details see Section 3.3.3. The roof slab, since it is very rigid in its plane (rigid diaphragm) was modelled through a horizontal truss system. A very large axial stiffness was defined for the trusses so the mutual displacements along the horizontal x and y axes, as well as rotation around the vertical z axis, of the nodes connected by the trusses, are restrained. The foundation pads were modelled using elastic elements to which a very rigid behaviour was assign. This happens because foundation pads were bolted to the shaking table and the bolts prevented the activation of their flexural behaviour. As further proof, a very limited displacements were measured at the foundation pads during the shaking table tests. Structure-to-panels, slab-to-columns and panels-to-foundations connections, were modelled by means of link elements to which it was possible to assign an appropriate hysteretic behaviour. The whole mass of the structure was modelled as a lumped mass that could be assigned to each node (see Figure 3-9 and Section 3.3.2 for more details).

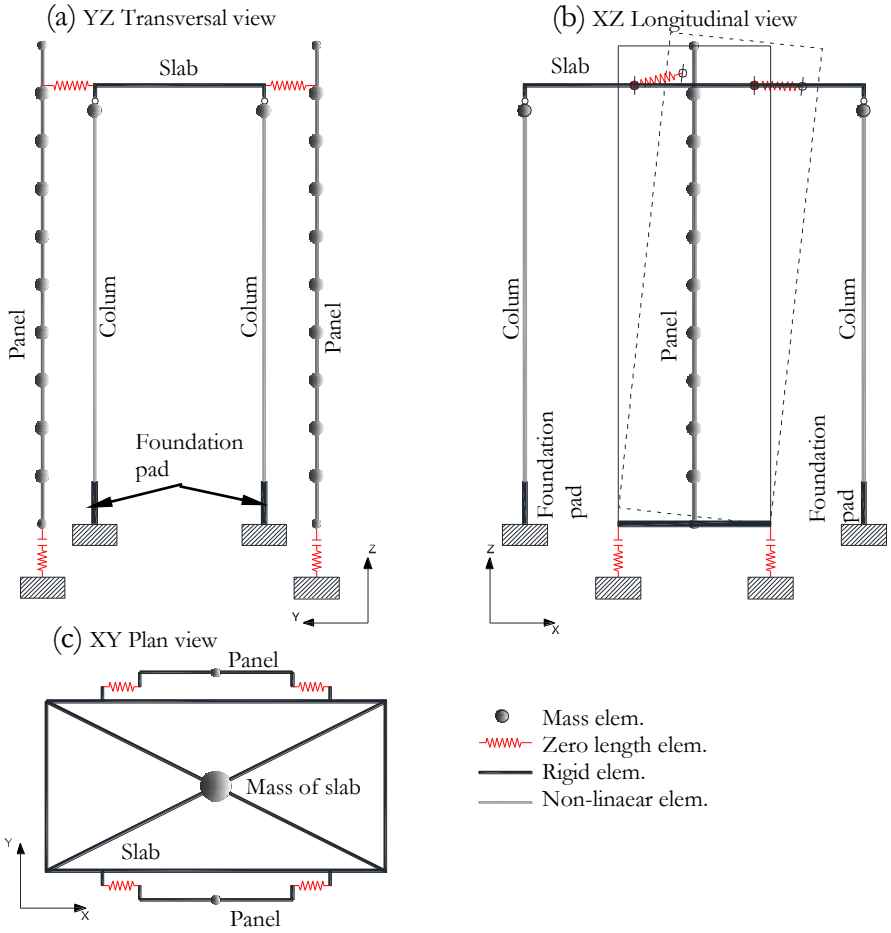

Figure 3-9: Numerical model overview

3.3.2 The model of Masses

Mass of the slab was concentrated in the centre of the mass at the roof level (Figure 3-9c). The panels' mass was discretized over the height by using an 11-node lumped-mass model (Figure 3-9a,b). Half of the columns' mass was lumped at the top of the columns element (Figure 3-9a,b). Masses of different elements of the specimen are summarized in Table 3-6.

Mass position		Mass value [t]
Centre of slab	m_s	8.60
Top of columns	m_c	0.50
Top and bottom of panels	$m_{p,tb}$	0.18
Middle joints of panels	$m_{p,m}$	0.36

Table 3-6: Elements' masses value

3.3.3 The model of panels

In the panels, no yielding or plastic deformations were observed during all performed shaking table tests. For this reason, OpenSees' *elasticBeamColumn* element was used to model the panels. The properties of the element cross-section are presented in Table 3-7:

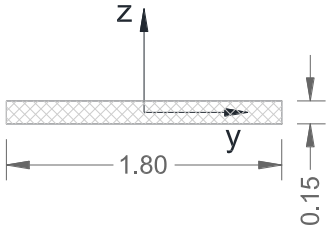

Figure 3-10: Panel's cross-section

Properties	A [m^2]	J [m^4]	I_z [m^4]	I_y [m^4]
Panel	0.27	$2.02 \cdot 10^{-3}$	0.05	$3.54 \cdot 10^{-4}$

Table 3-7: Inertial characteristic of panel's elastic section

A is the area of cross-section, J is the torsional moment of inertia and I_z, I_y are the bending moments of inertia in respect to the main axes of the section (Figure 3-10). In general, since some cracking of the panels would be expected, the moments of inertia I_z, I_y were reduced by 30% respect to the uncracked value.
The elastic modulus od C45/50 concrete is assumed 34.64 GPa and the shear modulus, with a Poisson coefficient ν=0.2, is G= 14.43 GPa.

3.3.4 The model for columns

To model the columns, three different types of elements were taken into consideration and compared:

1. A classic displacement- based nonlinear fibre beam-column element (Spacone, Filippou, & Taucer, 1996).
2. Giberson element with lumped plasticity consisting of non-linear springs at the end of elements and elastic element between these two springs, (1967). The response of the non-linear hinges (springs) was defined by Takeda's hysteretic rule (Takeda, et al., 1970).
3. A nonlinear force-based beam-column element where the non-linear response was defined with moment-curvature behaviour.

1. Displacement based nonlinear beam-column fibre element

This modelling approach is widely used due to its capability for describing nonlinear structural behaviour. The non-linear behaviour of the element is monitored at several control sections (Gauss-Lobatto integration sections) that are, in turn, discretized into certain number of steel and concrete fibres (Figure 3-11). The non-linear moment-curvature section behaviour, is derived taking into account the non-linear stress-strain behaviour of the fibres. When this fibre element approach is used some overestimation of the stiffness problem could arise. If it is supposed to have an element initially cracked the use of fibres approach does not easily allow to reduce the initial uncracked stiffness

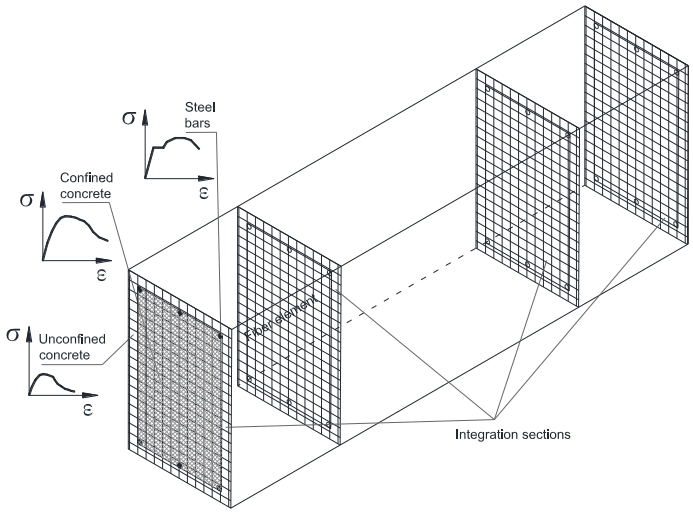

Figure 3-11: Example of fibre element

2. Giberson's lumped plasticity model with Takeda's hysteretic rules used to define the nonlinear response of plastic hinges

The Giberson lumped plasticity model is presented in Figure 3-12. An elastic beam-column element is combined in series with two zero-length plastic hinges at the ends of the elastic element. In this model, the damage is lumped at the two ends of the column, or in one end, in the case of cantilever columns. This is a realistic situation in seismic conditions because the damage is mainly concentrated in the areas where the bending moments are large.

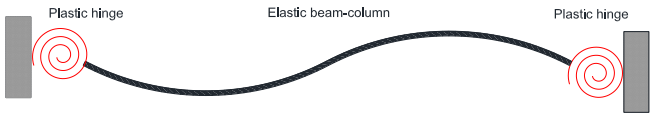

Figure 3-12: The Giberson model with concentrated plastic hinges

With this kind of model, the non-linear response of the element is limited to the plastic hinge only. The hysteretic behaviour of the hinge can be defined according to different rules that is possible to find in the scientific literature. In general, input parameters for these rules are ordered pairs of moments and rotations that define the envelope of the column response

In this work, the response of the hinges was defined according to the work of Fischinger et al., (2008) considering the formula of Fardis and Biskinis, (2003) for yielding. Three couples of moment-rotation parameters have to be defined corresponding to the level of cracking, yielding and ultimate limit state of the column.

When this approach is used some basic assumptions need to be made:

1. The distribution of the bending moment along the element has to be linear
2. The plastic curvature is assumed to be essentially constant along the length of the equivalent plastic hinge
3. The axial force of the element does not change appreciably during the analysis.

To define the properties of plastic hinges, the moment-curvature relationship of the cross-section was firstly defined (Figure 3-13b). The geometry and reinforcement of structure cross-section presented in Figure 3-13a were taken into account. Section moment-curvature analysis was done with OpenSees (Mazzoni et al., 2006a). For concrete, the model proposed by Mander et al,. (1988) was used and it is also included in Eurocode 8-2 - Appendix E, (EN 1998-2, 2009), and the steel of the reinforcement bars were modelled with the Giuffré-Menegotto-Pinto model (Giuffrè et al., 1970). The average values of the material characteristics are taken into account (f_{cm} = 48 MPa, f_{ym} = 575 MPa, f_{tm} = 690 MPa).

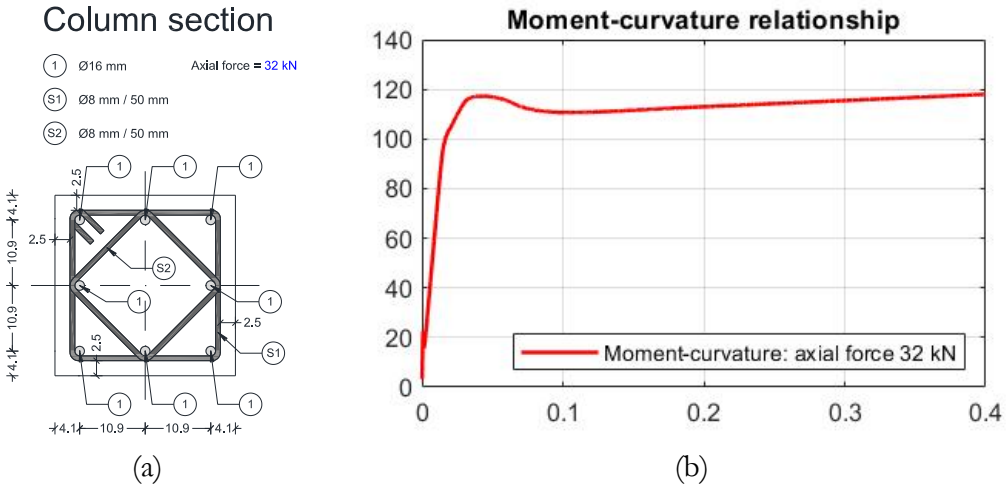

(a) (b)

Figure 3-13: Building column section (a) and moment-curvature relationships (b)

Starting from the cracking point (green point in Figure 3-14), the moment-curvature relationship was idealized through the principle of area equivalence, and imposing the linear post cracking branch passing through the first yield point (blue point in Figure 3-14), in this way the equivalent yielding point, $Ø_y$-M_y, is obtained.
The ultimate section curvature $Ø_u$ and the ultimate moment M_u were determined considering that the failure occurs when the maximum deformation is reached in the tensile reinforcement (red point in Figure 3-14). Deformation of 7.5% was taken into account. It corresponds to steel of ductility class C
Once the linearized moment-curvature diagram has been obtained, the moment-rotation relationship can be calculated as follows:

Cracking rotation $$\theta_{cr} = \frac{\phi_{cr} L_v}{3} \quad (3.1)$$

Yielding rotation $$\theta_y = \frac{\phi_y L_v}{3} + 0.00275 + a_{sl} \frac{0.2 d_{bL} f_y \varepsilon_y}{\sqrt{f_{cc}(d - d')}} \quad (3.2)$$

Ultimate rotation $$\theta_u = \left(\theta_y + (\phi_u - \phi_y) L_{pl} \left(1 - \frac{0.5 L_{pl}}{L_v} \right) \right) \quad (3.3)$$

where the equation (3.1) is the theoretical formulation to obtain the column chord rotation. Equation (3.2) is the formula proposed by Fardis and Biskinis, (2003) and the equation (3.3) is the formulation proposed by Eurocode 8 (EN 1998-1-1, 2005) for the ultimate rotation. In which:

$\emptyset_{cr}$	Cracking curvature
$\emptyset_{y}$	Yielding curvature
$\emptyset_{u}$	Ultimate curvature
L_{v}	is the shear span
a_{sl}	variable indicating slip of the longitudinal bars (1=slip, 0=no slip);
d_{bL}	diameter od longitudinal reinforcement
$(d-d')$	is the distance between the tension and compression reinforcement
ε_{y}	is the yield strain of the tension reinforcement
f_{y}	is the yield stress of the tension reinforcement in MPa
f_{c}	is the compressive strength of the concrete in MPa.

For the plastic hinge length L_{pl}, it was suggested by Park and Paulay, (1975) that the equivalent plastic hinge should not be longer than $0.5h_c$, where h_c is the height of the cross-section in the direction of the loading:

$$L_{pl} = 0.5h_c \qquad (3.4)$$

The idealized moment-rotation relationship of Figure 3-14b was assigned to the plastic hinge. The parameters of the moment-rotation backbone curves are defined in Table 3-8.

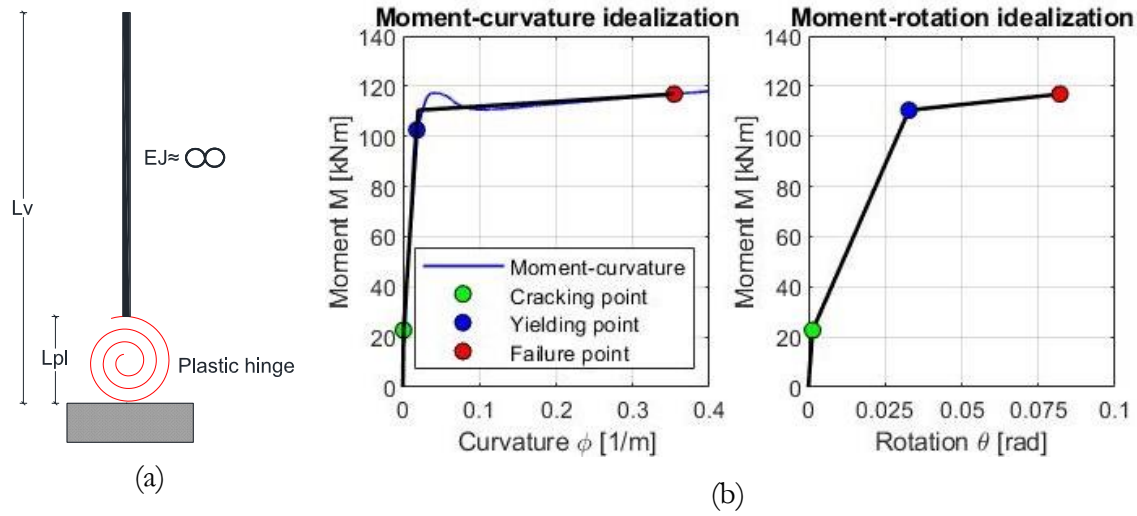

Figure 3-14: Spring and element connected in series (a) and moment-rotation and moment-curvature idealization for the plastic hinge (b)

Since the column member was composed of a nonlinear spring and an elastic element connected in series (Figure 3-14a), the rotational stiffness of the member, K_{mem}, should be related to the stiffness of the spring, K_s, and to the stiffness of the beam-column, K_{bc} according to the following equation:

$$K_{mem} = \frac{1}{\frac{1}{K_s} + \frac{1}{K_{bc}}} \qquad (5)$$

A large stiffness, K_{bc} was considered for the elastic part of the element, in this way the deformations were forced to occur only into the plastic hinge. Therefore the global stiffness of the column member K_{mem} was the same assigned to the plastic hinge K_s.

	Moment-rotation parameters
M_{cr} [kNm]	22.67
M_y [kNm]	110.41
M_u [kNm]	116.83
θ_{cr} [rad]	0.0013
θ_y [rad]	0.0327
θ_u [rad]	0.0820

Table 3-8: Parameters of the moment-rotation backbone

3. Force Beam-column element using moment-curvature approach

At each *forceBeamColumn* element integration point the response was defined by the moment-curvature relationship, provided as input data. To obtain the moment-curvature diagram, an OpenSees procedure was used as described before. Later on, the curvature-moment relationship was idealized with a two linear branch according to the principle of area equivalence.

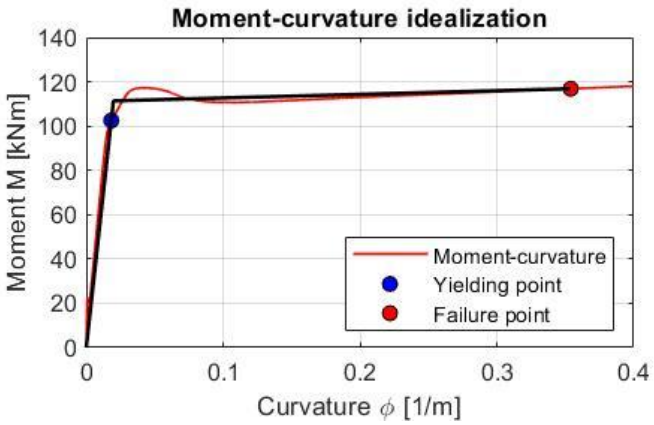

Figure 3-15: Bi-linearized moment-curvature relationship

The idealized moment-curvature relationship depicted in Figure 3-15 was assigned to each integration section of *forceBeamColumn* element. The parameters of the moment-rotation backbone curves are defined in Table 3-9.

	Moment-rotation parameters
M_y [kNm]	111.36
M_u [kNm]	116.83
$Ø_y$ [1/m]	0.0198
$Ø_u$ [1/m]	0.3540

Table 3-9: Parameters of the moment-curvature backbone

Comparison of the three different types of elements for column modelling

Considering the structure with fixed panels (test V3) like the one schematically illustrated in Figure 3-1c, a non-linear dynamic analysis was performed using as input the Petrovac earthquake accelerogram, depicted in Figure 3-6 and scaled to intensity of 0.4g.
The structure response, with different column modelling approaches, is compared in Figure 3-16. The fibre model (approach 1.) has a higher initial stiffness because the steel fibres stiffness can not be reduced without incurring numerical problems. As it was observed in the majority of the tests carried out on concrete structures, the initial stiffness is much lower than the theoretical one, for this reason, the stiffness needs to be reduced. In the shaking table test, the initial stiffness was much lower, a value of 30% of the value of the gross cross-section was observed. It was an issue to reduce the initial stiffness in the fibre model. Some numerical issues were also observed in this fibre model: a quite large and unreal vertical acceleration was recorded using this model. Instead, in the presented 2. ad 3. approaches, the initial stiffness can be easily reduced without any numerical problems. The reduction can be obtained by modifying the slope of the elastic branch.

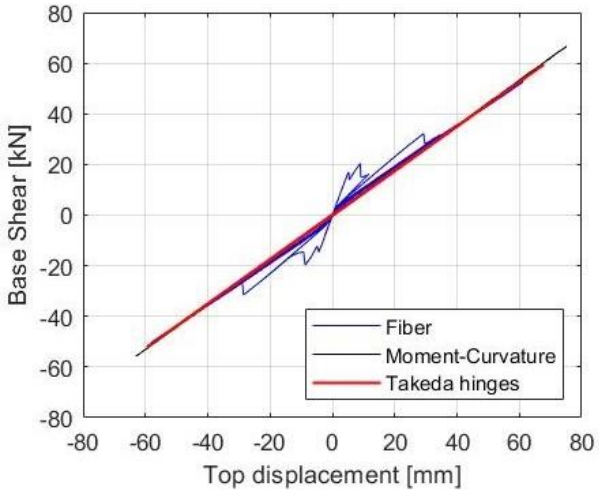

Figure 3-16: Columns' modelling approaches comparison

In the following numerical analyses, performed within this work, the Giberson's lumped plasticity model was used. And the plastic-hinge behaviour was defined according to the work of Fischinger et al., (2008) considering the formula of Fardis and Biskinis, (2003) for yielding. In such way, the nonlinear response of column member was defined.

3.3.5 The model of panels' connection with the main structure

Hammer-head strap behaviour in the horizontal direction

When the hammer-head straps are used to connect the cladding panels and the structure, the response of this type of connections in the horizontal direction, parallel to the panel's plane, was modelled taking into account the findings and the model proposed by Zoubek et al., (2016). The complete cyclic response of the connection can be simulated by combining three different hysteretic models, which are included in the OpenSees material library: *ElasticPP*, *ElasticPPGap* and *Hysteretic*. These hysteretic models are combined as shown in Figure 3-17:

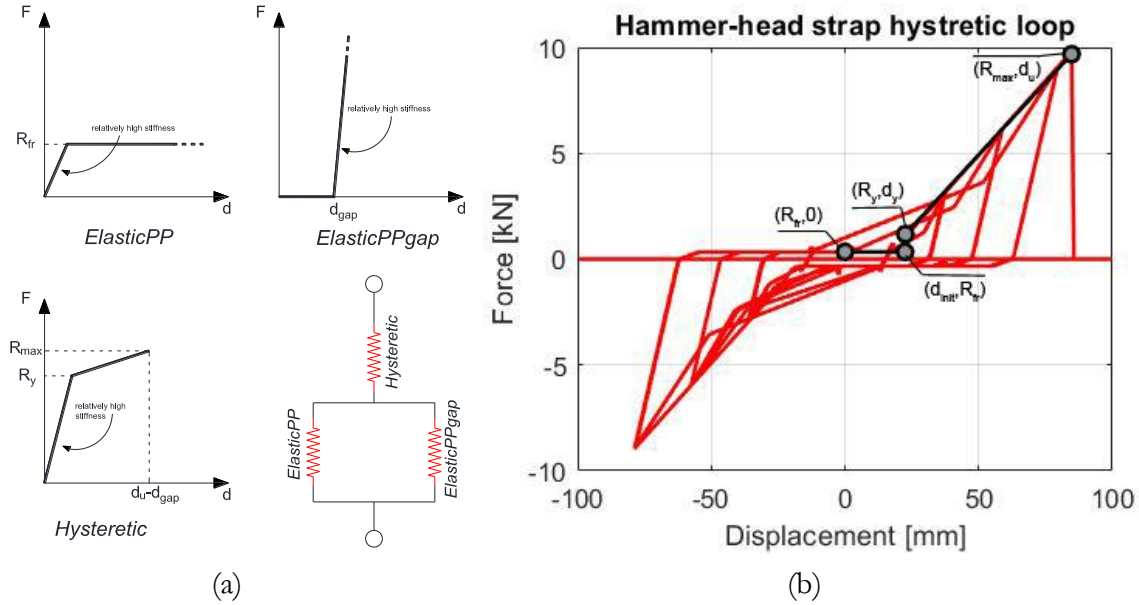

(a) (b)

Figure 3-17: Materials combination for the numerical model of the hammer-head strap behaviour in the horizontal direction (a) and hysteretic loop (b)

The first *ElasticPP* material simulates the friction force between the straps and the RC beam, or slab in this case, due to the tightening torque in the fixing bolt. R_{fr} is calculated as:

$$R_{fr} = \frac{M_{fr}}{L} \quad (3.6)$$

Where M_{fr} is the tightening torque in the bolt and L is the distance between the fixing bolt and the anchor channel profile installed on the panel (Figure 3-18).

The *ElasticPPGap* material is added in parallel to simulate the stiffness increase that occurs when the strap head is stuck inside the anchor channel. The size of the gap d_{gap} can be calculated as:

$$d_{gap} = \theta_{init} \cdot L \quad (3.7)$$

where θ_{init} is the strap rotation that can be initially admitted due to the tolerances inside the anchor channel

The *Hysteretic* material is added in series to simulate the strap's non-linear response. Where:

$$R_y = \frac{M_{y,N} + d_y \cdot N + M_{fr}}{\sqrt{L^2 + d_y^2}} \quad (3.8)$$

with:

$$d_y \approx d_{init} \quad (3.9)$$

furthermore

$$R_{max} = \frac{M_{pl,N} + d_u \cdot N + M_{fr}}{\sqrt{L^2 + d_u^2}} \quad (3.10)$$

and:

$$d_u = (\theta_{init} + \theta_{st}) \cdot L \quad (3.11)$$

In which: $M_{y,\,N}$ and $M_{pl,\,N}$ are respectively the resistance to yield bending moment and the plastic bending moment of the narrowest part of the steel strap, the one just below the hammer-head, called "neck". The two bending moments must take into account the possible axial force N in the strap. θ_{st} is the rotation of the straps due to the flexural deformation of the neck and can be estimated as the ultimate curvature multiplied by the length of the neck.
With the reference to Table 3-2 for the strap geometric features, the main parameters to be used as input for the correct definition of the connection behaviour are listed in Table 3-10 below:

Strap type	Input parameters											
	M_{fr} [Nm]	L [mm]	θ_{init} [°]	L_{neck} [mm]	θ_{st} [°]	M_y [kNm]	M_{pl} [kNm]	d_{gap} [mm]	d_u [mm]	R_{fr} [kN]	R_y [kN]	R_{max} [kN]
TA-210	45	135	9	18	39	0.72	1.07	21.20	85	0.34	1.18	9.90
TA-290	45	170	9	18	39	0.72	1.07	26.70	143	0.26	0.72	8.11

Table 3-10: Input parameters for connections modelling in the horizontal direction

Test V1 (long straps)

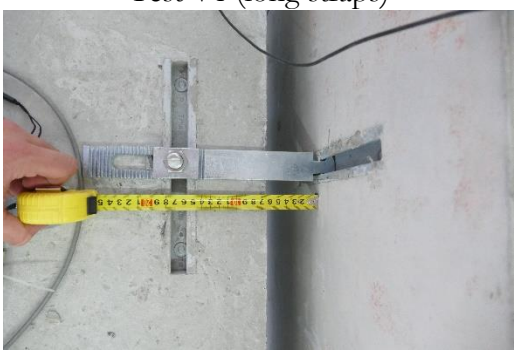

Test V3 (short straps)

Test V2 (short straps)

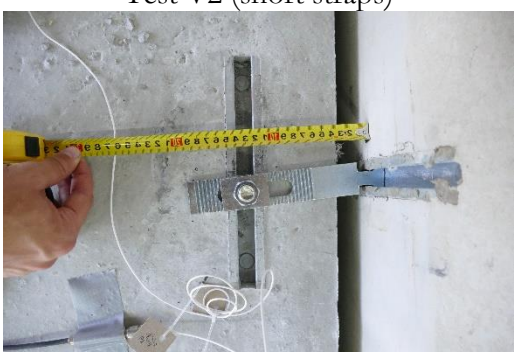

Test V4 (long straps)

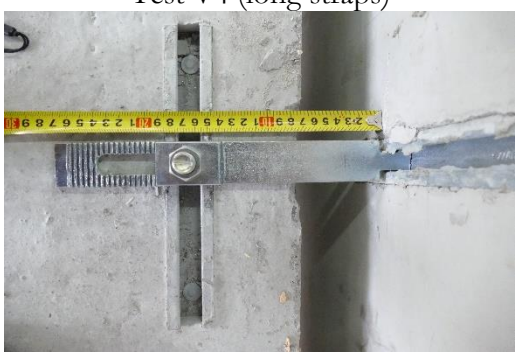

Figure 3-18: Measured distance L between the fixing bolt and the anchor channel profile. Pictures courtesy of UL-FGG.

Hammer-head strap vertical behaviour

A new contribution of this thesis is the introduction of vertical behaviour for the hammer-head strap connections.

The rocking panels can rotate around their bottom outer corners (Figure 3-19). This movement induces relative horizontal and vertical displacements between the panels and the main structure. For this reason, straps vertical deformation, can occur during the panels' rocking movement.

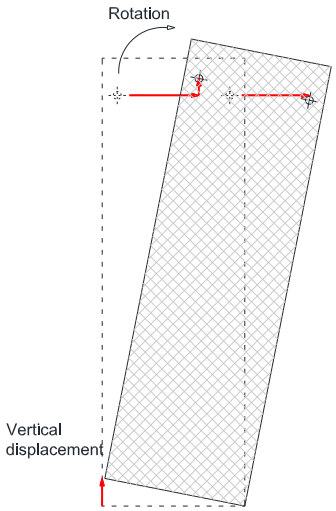

Figure 3-19: Rocking panel: rotation and displacement

Within numerical modelling, it is important to not disregard the straps vertical deformation to correctly obtain the structural response. A numerical model for straps vertical behaviour is proposed by combining in series two different hysteretic models, which are included in the OpenSees material library: *ElasticPPGap* and *Hysteretic,* see Figure 3-20a:

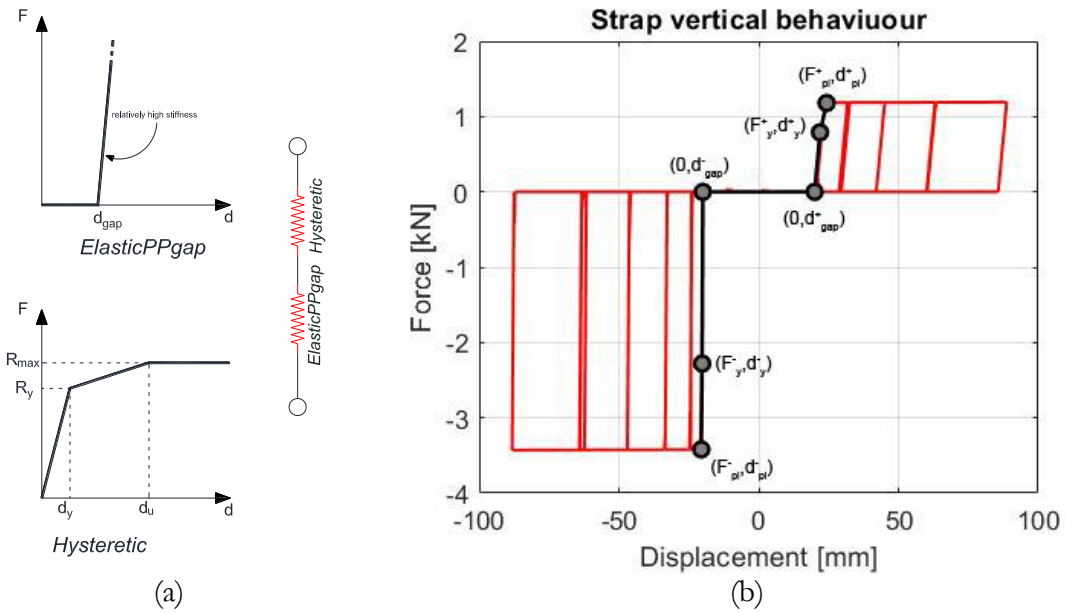

(a) (b)

Figure 3-20: Materials combination for the numerical model of the hammer-head strap behaviour in the horizontal direction (a) and hysteretic loop (b)

The strap in the vertical direction behaves like a cantilever beam, and it has two different deflection spans L1 and L2, as shown in Figure 3-21a below:

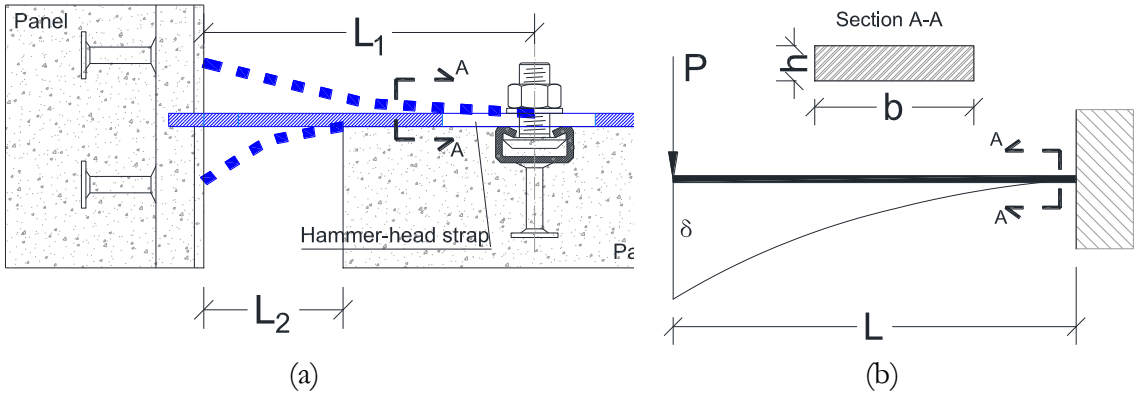

Figure 3-21: Upward deflection span L1 and downward deflection span L2 (a) and the assumed cantilever static scheme (b)

Therefore, the strap has, in the upward and in the downward direction two similar behaviours but with different stiffness and strength.
The hammer-head straps are made by S275 JR steel; the material can be idealized as elasto-plastic material. The assumption of perfect plasticity, after the yield stress is reached, means that the effects of strain hardening are disregarded, but since strain hardening provides an increase in the strength of the steel, it is generally safe to disregard it.

The *ElasticPPGap* material simulates the stiffness increase that occurs when the strap head is stuck inside the anchor channel. The size of vertical gap d_{gap} can be assumed about 25-35mm in the upward direction and about 5 mm in the downward direction according to the experimental result reported in SafeCladding Project (Isaković et al., 2013).
The *Hysteretic* material is added in series to simulate the strap's non-linear response

For a cantilever beam of rectangular cross-section (Figure 3-21b), such as the straps are, the yield moment is:

$$M_y = \frac{f_y b h^2}{6} \quad (3.12)$$

and the plastic bending moment is:

$$M_{pl} = \frac{f_y b h^2}{4} \quad (3.13)$$

The yield load P_y that first produces the yielding of the beam is given by the equation:

$$P_y = \frac{M_y}{L} \quad (3.14)$$

The P_{pl} load corresponding to the plastic moment M_{pl} can be calculated as:

$$P_{pl} = \frac{M_{pl}}{L} \quad (3.15)$$

The deflection δ_y caused by this load is:

$$\delta_y = \frac{P_y L^3}{3EJ} \quad (3.16)$$

According to the plastic bending theory the deflection δ_{pl} that corresponds to the load P_{pl}, in the case of a cantilever beam with rectangular cross-section, can be assumed as:

$$\delta_{pl} = \frac{20}{9}\delta_y \quad (3.17)$$

In Figure 3-20b the displacement d^+_y and d^+_{pl} are, the deflection corresponding to the length L_1, at the yielding point δ_y and at the plastic point δ_{pl} respectively, to which the upward d^+_{gap} is added. Instead, the displacement d^-_y and d^-_{pl} are the deflection corresponding to the length L_2, at the yielding point δ_y and at the plastic point δ_{pl} respectively, to which the downward gap d^-_{gap} is added.
The main parameters to be used as input for the definition of the connection vertical behaviour are listed in following Table 3-11:

Strap type	Cross-section characteristics					Input parameters							
	h [mm]	b [mm]	J_x [mm^4]	My [Nmm]	Mpl [Nmm]	L [mm]	Py [kN]	Ppl [kN]	δ_y [mm]	δ_{pl} [mm]	d_{gap} [mm]	d_y [mm]	d_{pl} [mm]
TA-210	8	35	1493	102667	154000	L_1=135	0.76	1.14	2.09	4.64	35.00	37.09	39.64
						L_2=45	2.28	3.42	0.23	0.52	5.00	5.23	5.52
TA-290						L_1=170	0.60	0.91	3.31	7.36	35.00	38.31	42.36
						L_2=65	1.58	2.37	0.48	1.08	5.00	5.48	6.08

Table 3-11: Input parameters for connections modelling in the vertical direction

3.3.6 The model of panels' connection with foundations

The rocking panel case

In the case of rocking panels, a nonlinear elastic behaviour was assigned to the panel base spring such that they had a high stiffness in compression and very low stiffness in tension. In this way, the two springs were able to simulate unilateral support to allow the panel to freely uplift. To simulate the correct rocking behaviour it is possible to follow two simplified modelling strategies proposed by Vassiliou et al., (2014) and Vassiliou et al., (2016), however, more realistic modelling has been studied by introducing two elements at the panels' ground corners that could simulate a dissipation of energy due to the impact. In the following Figure 3-22, the full fixed restraints are marked with the red arrow, the nonlinear impact behaviour directions are highlighted with a magenta arrow and the green arrows denotes a free movement allowed. It is worth stressing that that the impact can occur only in the negative Z direction of the magenta arrow

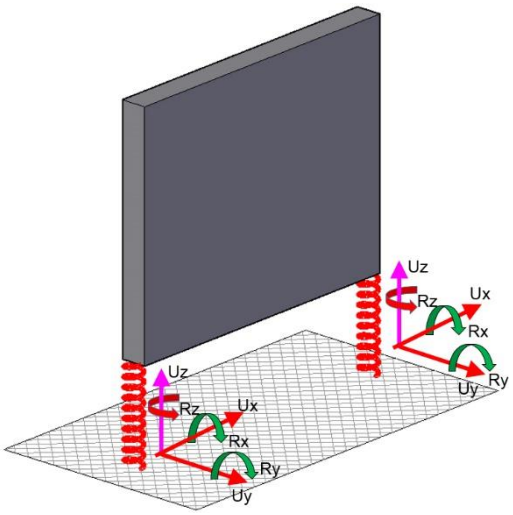

Figure 3-22: Rocking panel support conditions

The energy dissipation from the impact was simulated with the *Impact Material* of the OpenSees library (Figure 3-23b) which is an approximation of the Hertz contact model and whose parameters are calibrated according to the work of Muthukumar & DesRoches, (2006). In their model, the two colliding bodies are represented as two elastic isotropic spheres of radii R_1, R_2 (Figure 3-23a) and the stiffness parameter of the hertz model k_h can be expressed as:

$$k_h = \frac{4}{3\pi(h_1 + h_2)} \cdot \left[\frac{R_1 R_2}{R_1 + R_2}\right]^{1/2} \quad (3.18)$$

where h_1 and h_2 are material parameters defined as:

$$h_i = \frac{1 - \upsilon_i^2}{\pi E_i}; \quad i = 1,2 \quad (3.19)$$

where ν_i and E_i are the Poisson's ratio and modulus of elasticity, respectively, of sphere i. Assuming the colliding bodies to be spherical, the radius of an equivalent colliding sphere can be estimated as

$$R_i = \sqrt[3]{\frac{3m_i}{4\pi\rho}}; \quad i = 1,2 \tag{3.20}$$

where m_i is colliding bodies mass and ρ is the density of concrete.

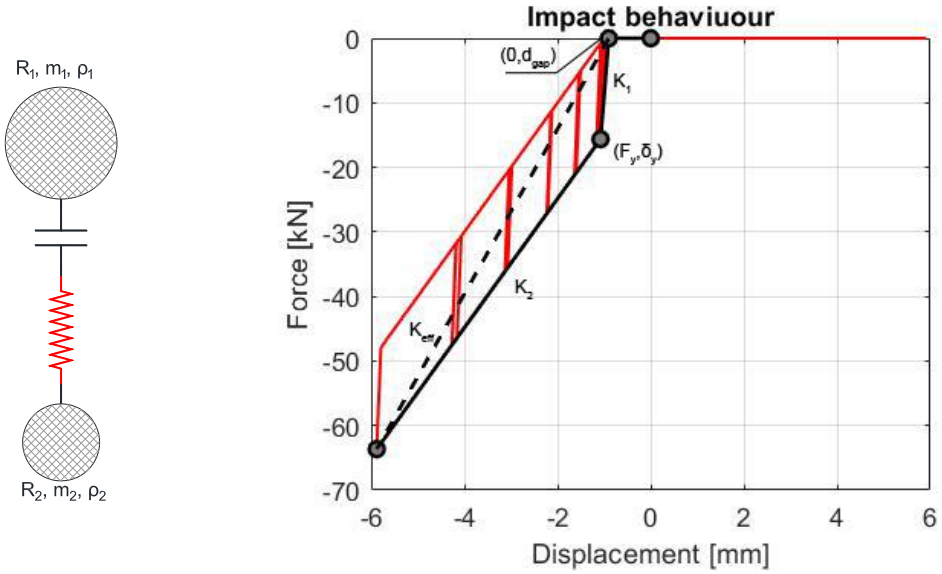

(a) (b)

Figure 3-23: Impact material hysteretic loop (a) and the two colliding spheres

Once k_h was defined it was possible to calculate the two stiffness K_1 and K_2 that are needed to define the impact material behaviour.
First, it is necessary to define the energy, which is dissipated during the impact. According to OpenSees reference manual (Mazzoni, et al., 2006b) this energy can be estimated as:

$$E = k_h \cdot \delta_m^{(n+1)} \cdot \frac{(1-e^2)}{(n+1)} \tag{3.21}$$

where *n* is typically taken as 3/2 for the exponent associated with the Hertz power rule; *e* is the coefficient of restitution, with typical values from 0.6-0.8; and δ_m is the maximum penetration during the pounding event. The effective stiffness, K_{eff}, is:

$$K_{eff} = k_h \cdot \sqrt{\delta_m} \tag{3.22}$$

The yield displacement is:

$$\delta_y = a \cdot \delta_m \tag{3.23}$$

where *a* is typically taken as 0.1. The initial stiffness, K_1, and secondary stiffness, K_2, are then defined such a way that the *Impact model* dissipates an amount of energy during a pounding event that is consistent with the associated energy dissipated in the Hertz model.

$$K_1 = K_{eff} + \frac{E}{(a \cdot \delta_m^2)} \tag{3.24}$$

$$K_2 = K_{eff} - \frac{E}{((1-a)\cdot\delta_m^2)} \quad (3.25)$$

The shaking table used in the experimental campaign performed by the University of Ljubljana was made with a concrete plate with a plane size of 5x5m and 20 cm thick as shown in Figure 3-1. Therefore, its mass m_1 is 39.75 kN·s^2/m.
The RC panels of dimensions 1.80x5.56 m and 15 cm thick have a mass $m_{2\,of}$ 3.64 kN·s^2/m. The Poisson coefficient for reinforced concrete can be assumed to be 0.2.
With these quantities, according to the eq. (3.18) it is possible to calculate the Hertz impact model's material and stiffness parameters that are shown in the following Table 3-12:

	Mass [kN·s^2/m]	Poisson coefficient ν	Elastic modulus E_{el} [kN/m^2]	Equivalent radius R [m]	Hertz material parameter h	Hertz stiffness parameter k_h [kN/m$^{3/2}$]
Shaking table	39.75	0.30	2.10·10^8	0.73	1.44·10^{-9}	1.96·10^7
Panel	3.64	0.20	3.46·10^7	0.33	8.82·10^{-9}	

Table 3-12: Material and stiffness parameter for the Hertz model

During the rocking movement, the panels pounded on the shaking table and some energy was dissipated due to the concrete damage that occurred at the panel bottom corners (Figure 3-24a,b)

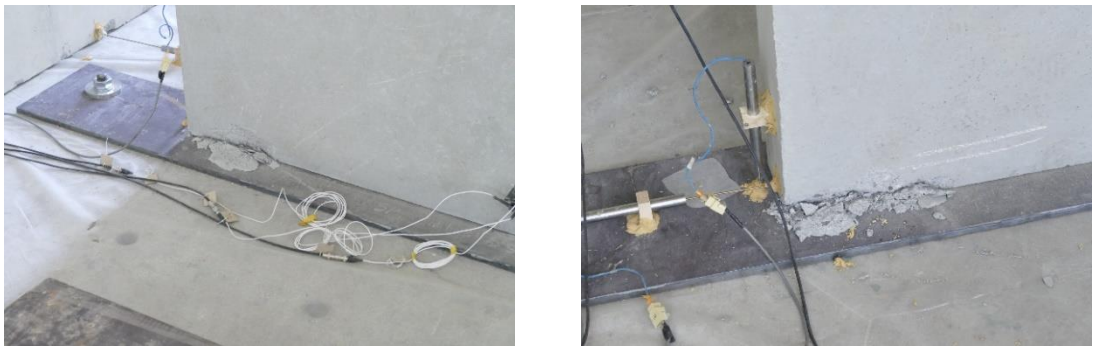

(a) (b)

Figure 3-24: Panel damage at the bottom corner due to rocking: Panel P1 (a) and P2 (b). (test V1 at 0.4g). Pictures courtesy of UL-FGG.

Due to the small amount of damage occurred, the maximum penetration δ_m during the pounding event could be estimated at 5.0 mm. In this way, the dissipated energy during the impact E and the effective stiffness K_{eff} can be calculated following the eq. (3.22) The values are reported in the following Table 3-13:

Coefficient of restitution e	Maximum penetration δ_m [m]	Dissipated energy E [kJ]	Effective stiffness K_{eff} [kN/m]
0.6	5.00·10^{-3}	2.05·10^{-3}	1.56·10^6

Table 3-13: Coefficient of restitution, Maximum penetration, dissipated energy and effective stiffness values

Following the eq. (3.23), (3.24) and (3.25) and using the values of Table 3-13 it is possible to define 4 parameters which can be used to describe the properties of the *Impact material* (Figure 3-23b): the initial gap, the displacement at yield δ_y and the two stiffnesses K_1 and K_2 whose values are reported in Table 3-14:

Input parameters for Impact material			
gap [m]	δ_y [m]	K_1 [kN/m]	K_2 [kN/m]
$1 \cdot 10^{-3}$	$5 \cdot 10^{-4}$	$5.84 \cdot 10^{6}$	$1.17 \cdot 10^{6}$

Table 3-14: Input parameters for Impact material

Although the amount of dissipated energy is relatively small and the effective stiffness is large, as shown in Table 3-13, the modelling of the impact between the foundation and the panel allowed to capture the seismic response of the structure more accurately.

The fixed panel case

Two elastic springs were used at the base of the panels to model their interaction with the foundation. In case of fixed panels, the stiffness given to the springs was considerably high, so that these could be considered as full fixed restraints in the directions marked with the red arrow within Figure 3-25

Instead, the green arrow highlights the free movement allowed. Since the panels are fixed to the foundation by means of the mechanical couplers connecting the panel rebar to the foundation steel plate (Figure 3-4a), therefore in can be assumed a hinge support at least in the field of small rotation.

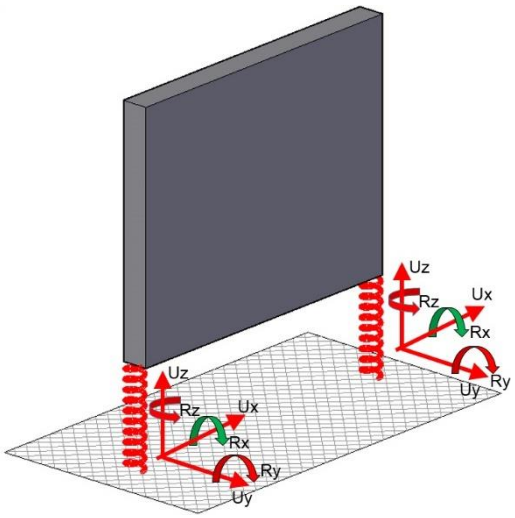

Figure 3-25: Fixed panel support conditions

3.3.7 System damping

In the dynamic analysis of structures and foundations damping plays an important role.

For the structure considered in the following, the damping ratio ξ was assumed equal to 0.02.

3.3.8 Comparison of the analysis and experiments in the case of fixed panels

Response of panel and main structure for test V3

In the tests with the panels fixed to the base (V3 and V4) no damage was observed either in the structure or in the panels as mentioned in (Isaković et al., 2018). However, during the V3 test, when the maximum seismic intensity of 0.5 g was applied, one of the short straps reached the failure for a displacement request of about 85 mm. With the numerical model developed, it was possible to replicate the response obtained during the real tests and also the failure of the connections in quite accurately way. After the failure of the straps, there is a noticeable acceleration increase both in the structure and in the panels, which cannot be correctly approximated by prepared OpenSees numerical model.

Within the numerical model results, the connection failure could be recognised by examining the relative displacement between the panel and structure. If the relative displacement is greater than d_u, as defined in Table 3-10, the connection capacity can be considered exhausted.
The results are illustrated in terms of acceleration at the top of the main structure and at the top of panel P1 and P2 (Figure 3-26a,b,c). In the figures, the black line shows the acceleration recorded during the shaking table tests while the red line shows the acceleration computed with the numerical model.

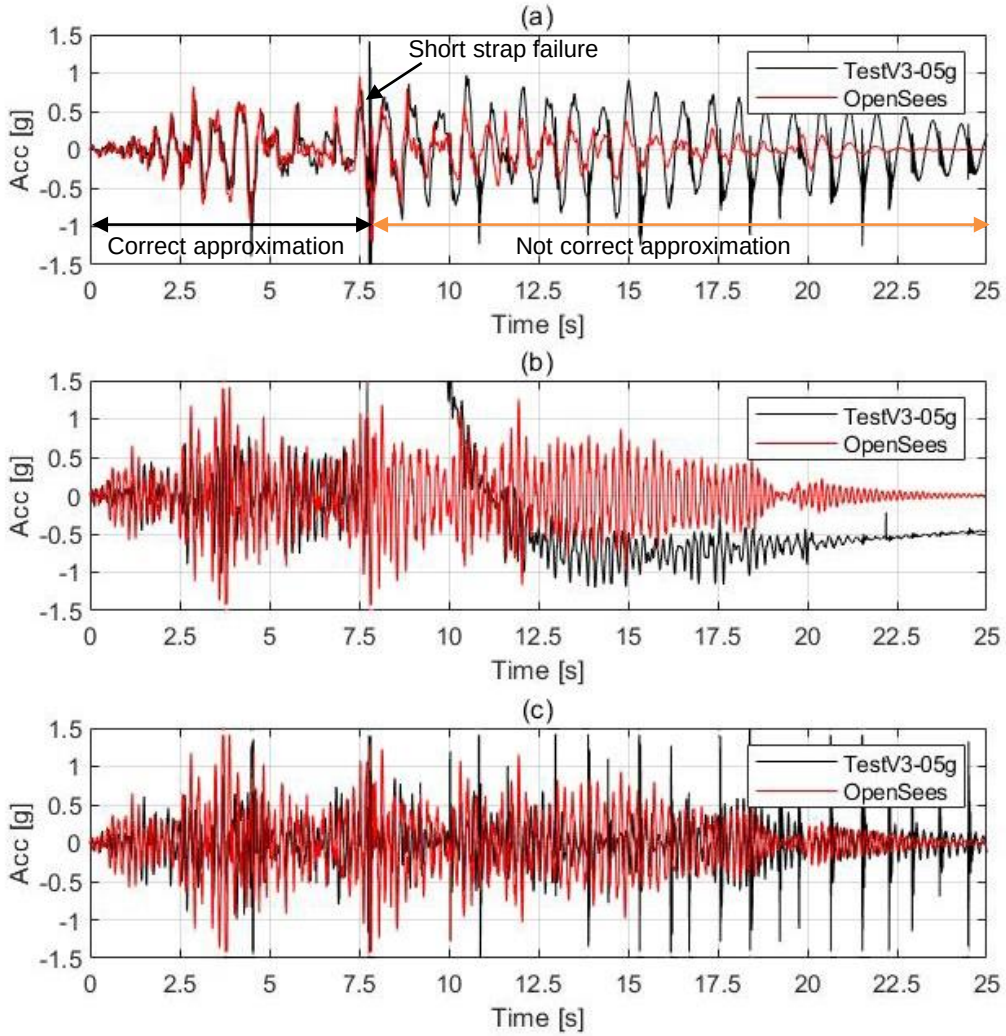

Figure 3-26: Accelerations comparison for test V3 (short strap at 0.5g) and numerical model: for slab (a), panel P1 (b) and panel P2 (c)

The results can also be depicted in terms of structure slab displacement and top of panel P1 and P2 displacement. In Figure 3-27a,b, c, it can be observed that, after the connections failure in the V3 test, the numerical curve and the experimental curve considerably differed. According to Figure 3-27a, it could be concluded that the damping in the main structure is not properly modelled after the strap failure.
The displacement at the top of the panels was very limited both in the case of the real test and of the numerical model. This is because the panels were fixed to the base.

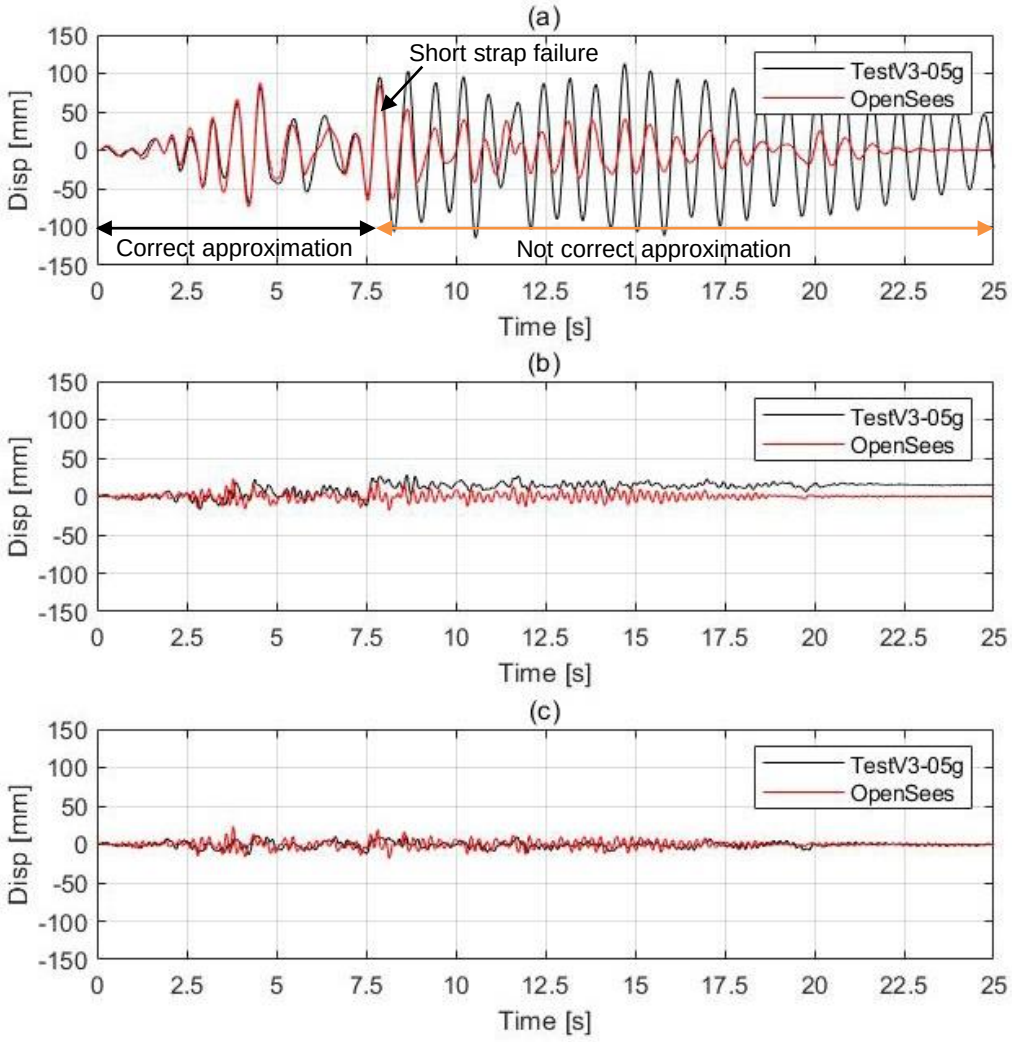

Figure 3-27: Displacements comparison for test V3 (short strap at 0.5g) and numerical model: for slab (a), panel P1 (b) and panel P2 (c)

The response of connections for test V3

Since the numerical model approximates quite well the response of the structure and panels both in terms of acceleration and displacement, it is reasonable to suppose that the elastoplastic model of the connections presented in paragraph 3.3.5 is appropriate.
Figure 3-28 shows that the stiffness increases at large displacement due to the impact between the strap's head and panel.

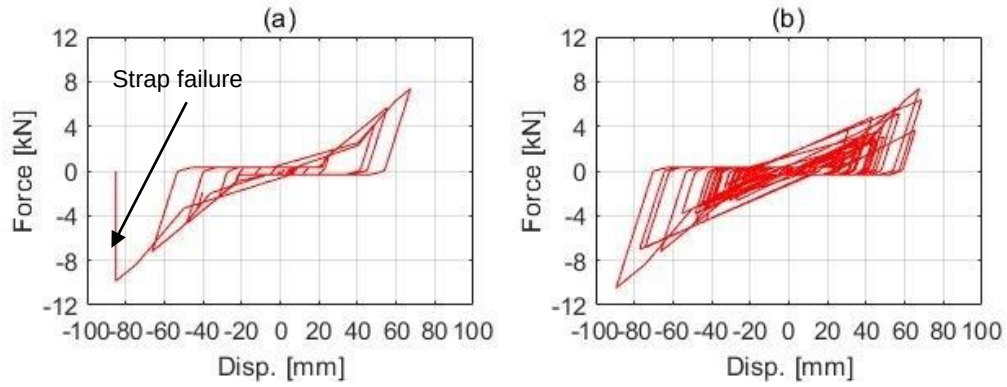

Figure 3-28: Numerical response of connection: for Panel P1 (a) and panel P2 (b)

To get a direct measurement of the connection displacement, the analytical and experimental relative displacements between the panels and the main structure are compared in Figure 3-29.

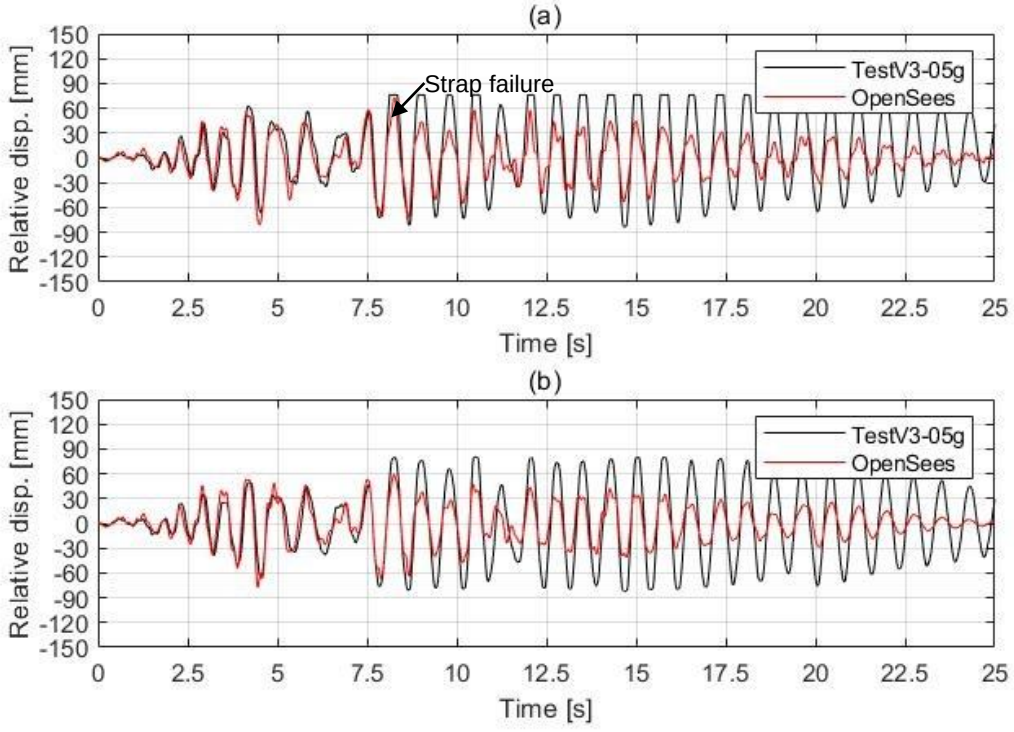

Figure 3-29: Test V3 (short strap at 0.5g), the relative displacement between structure and panel P1 (a) and panel P2 (b)

Around 7.5 the relative displacement between panel P1 and structure (Figure 3-29a) reached the connection displacement capacity (about 82mm) and the connection failed. After that, the numerical model does not correctly approximate the real response.

The response of panel and main structure for test V4

The results are displayed for test V4 (strap and fixed panels) at seismic intensity of 0.5 g. With the developed numerical model, it was possible to very accurately replicate the response history obtained during the real tests.
In the subsequent Figure 3-30a, the comparison between the numerical and experimental slab acceleration is shown. It is possible to notice that the numerical response well matches the experimental one. In Figure 3-30b and c the comparison between the numerical and experimental panels acceleration measured at their top are depicted. Observing the figures, it is possible to see the rather good matching between the numerical and experimental response except for the last part (time interval within 16 seconds and the end of the response). It can be assumed that this is due to a modelling of the damping which is not completely appropriate. Another reason could be that the panel base restraints are not perfectly full-fixed as in the model but in reality, they could allow very small displacements. In the test V4, the long straps never reached the failure. The results are illustrated in terms of acceleration at the top of the main structure, panel P1 and P2

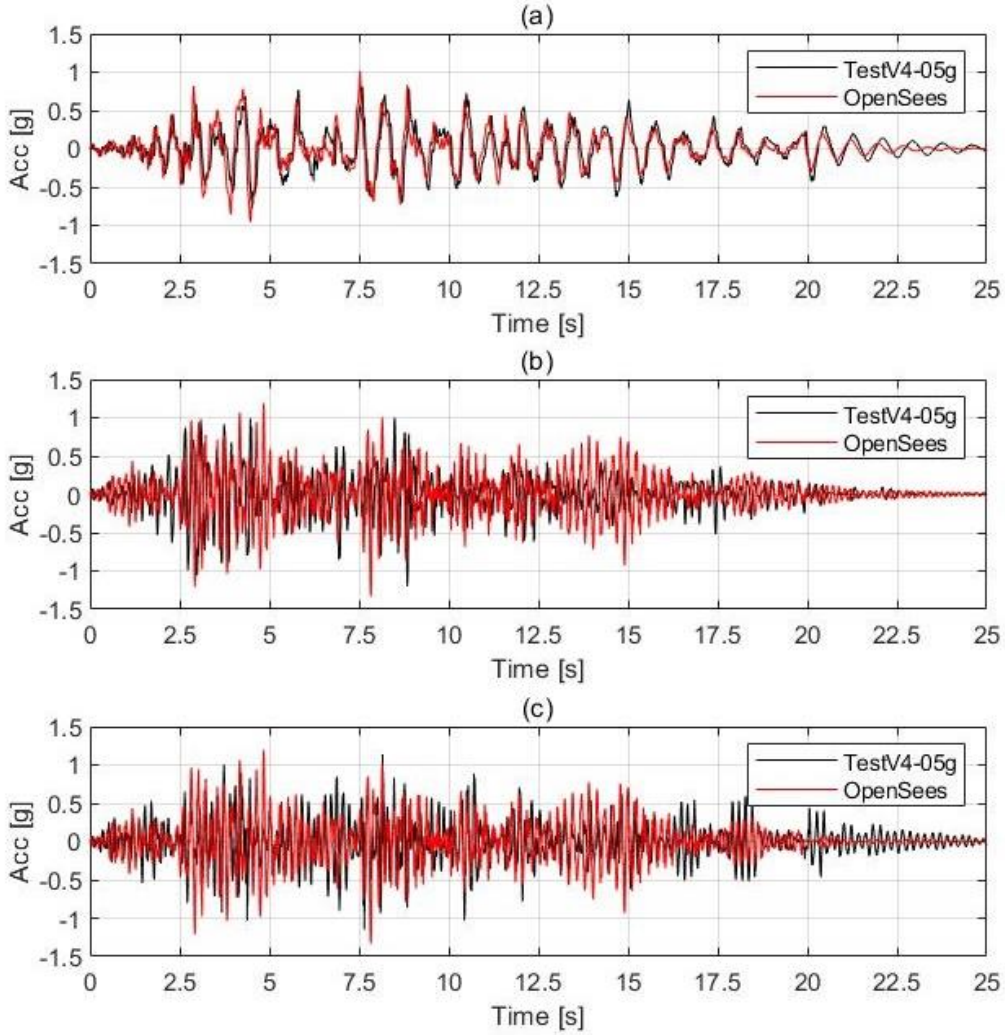

Figure 3-30: Accelerations comparison for test V4 (long strap at 0.5g) and numerical model: for slab (a), panel P1 (b) and panel P2 (c)

Also in terms of displacement, the numerical results show a good matching with the experimental ones. The comparison between the experimental and numerical recorded displacement for the main structure, panel P1 and P2 are presented in the following Figure 3-31a,b,c:

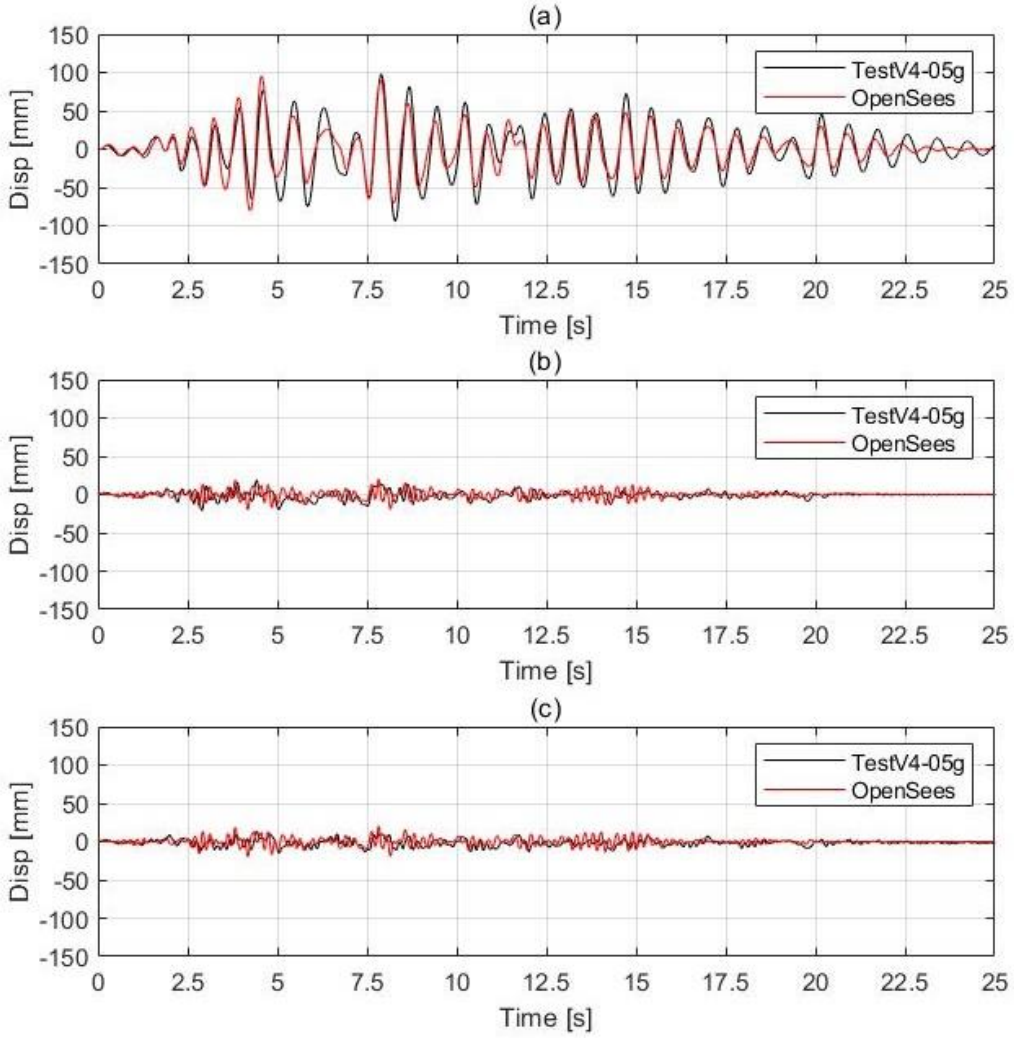

Figure 3-31: Displacements comparison for test V4 (long strap at 0.5g) and numerical model: for slab (a), panel P1 (b) and panel P2 (c)

The response of connections for test V4

The connections' hysteretic loop for test V4 at an input acceleration scaled to 0.5g, is presented in Figure 3-32a, b. The displacement capacity of long straps is significantly larger than that of the short ones, and therefore they were able to sustain a larger demand and didn't reach the failure point.

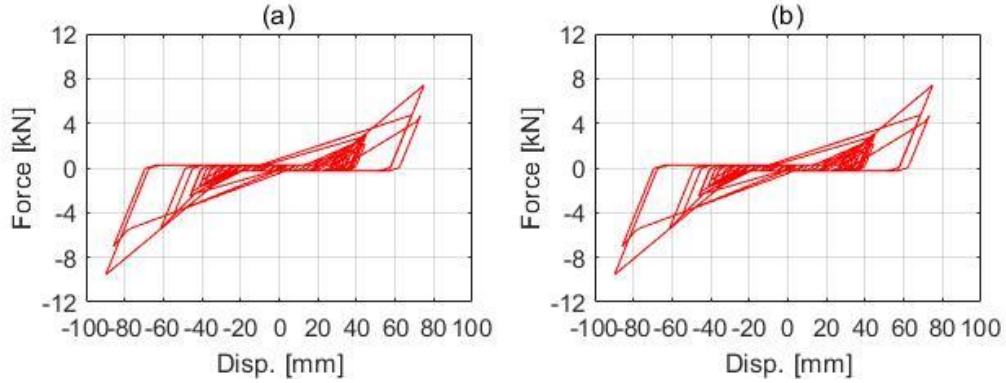

Figure 3-32: Numerical response of connection: for Panel P1 (a) and panel P2 (b)

To get a direct measurement of the connection displacement, the analytical and experimental relative displacements between the panels and the main structure are compared in Figure 3-33.

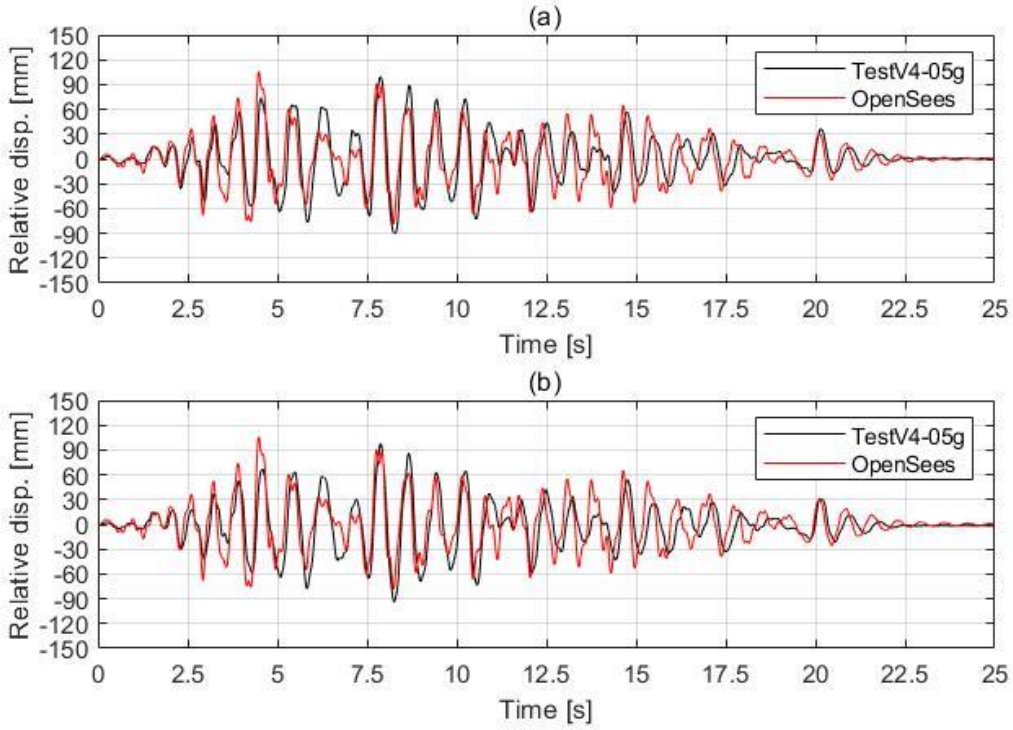

Figure 3-33: Test V4 (long strap at 0.5g), the relative displacement between structure and panel P1 (a) and panel P2 (b)

In this case, the connections never reached the failure. The numerical model was able to approximate the real response in quite a good way compared to the test V3 (Figure 3-29a), in which the connection between panel P1 and structure exhausted its displacement capacity.

3.3.9 Comparison of the numerical analysis and experiments in the case of rocking panels

The response of panel and main structure for test V1

Also in the case of rocking panels, by the developed numerical model, it was possible to replicate the response obtained during the real tests quite accurately. The figures below illustrate the numerical results (red) in terms of displacements (Figure 3-34a,b,c) and horizontal accelerations (Figure 3-35a,b,c) for the structure and the panels. The results are compared with the recorded response during the tests (black).

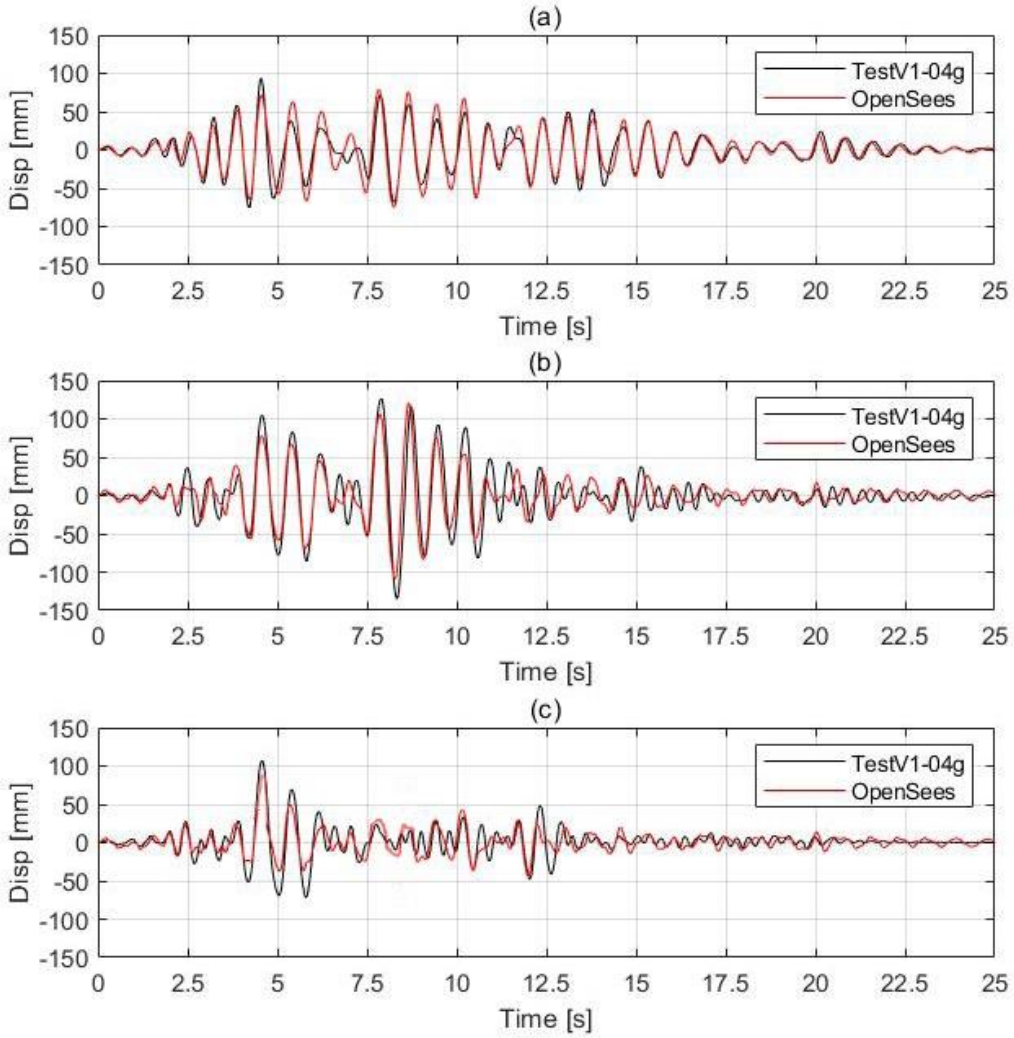

Figure 3-34: Displacements comparison for test V1 (long strap at 0.4g) and numerical model: for slab (a), panel P1 (b) and panel P2 (c)

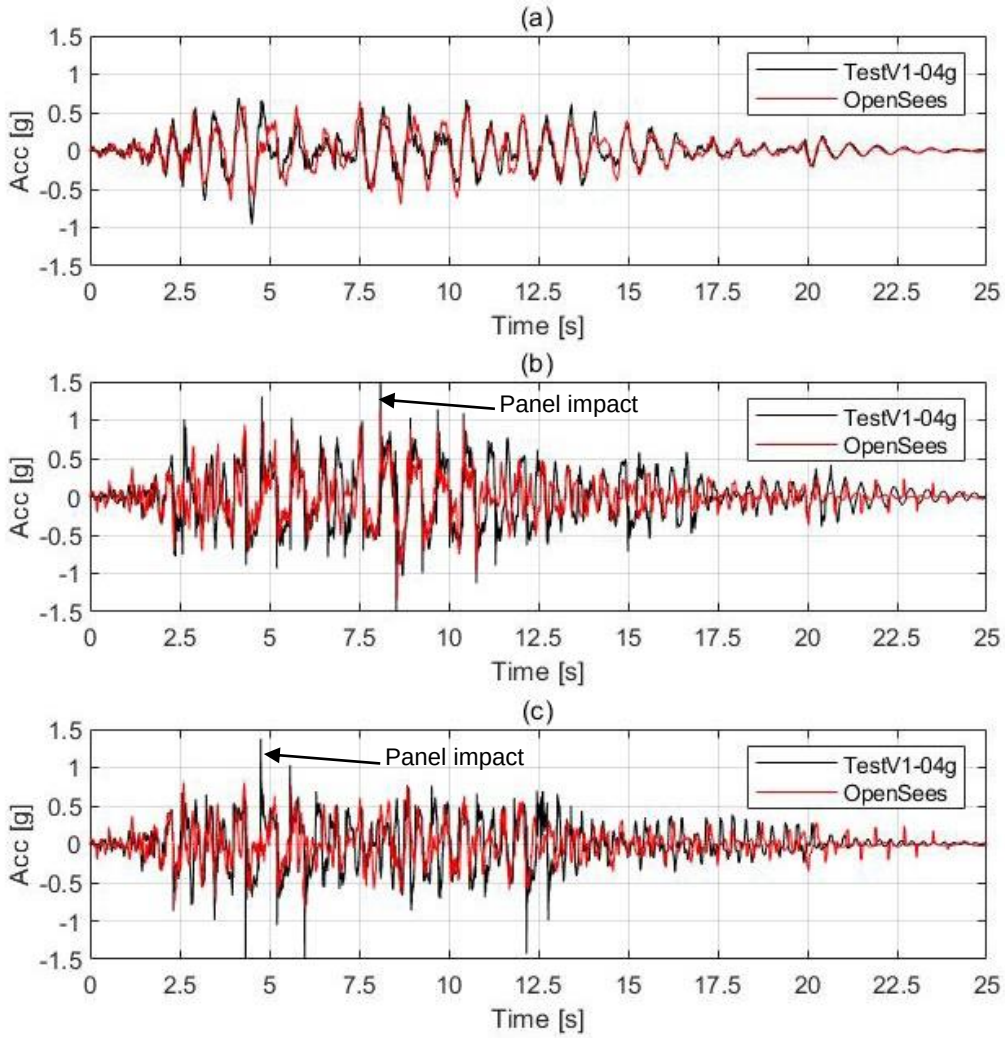

Figure 3-35: Horizontal accelerations comparison for test V1 (long strap at 0.4g) and numerical model: for slab (a), panel P1 (b) and panel P2 (c)

Due to the rocking movement of the panels, it is important to also evaluate the vertical acceleration of both the panels and the structure. The vertical acceleration response-history (Figure 3-36) highlights the impacts of the panels on the shaking table (acceleration peaks) and it also possible to understand if the numerical model correctly approximates the rocking movement.

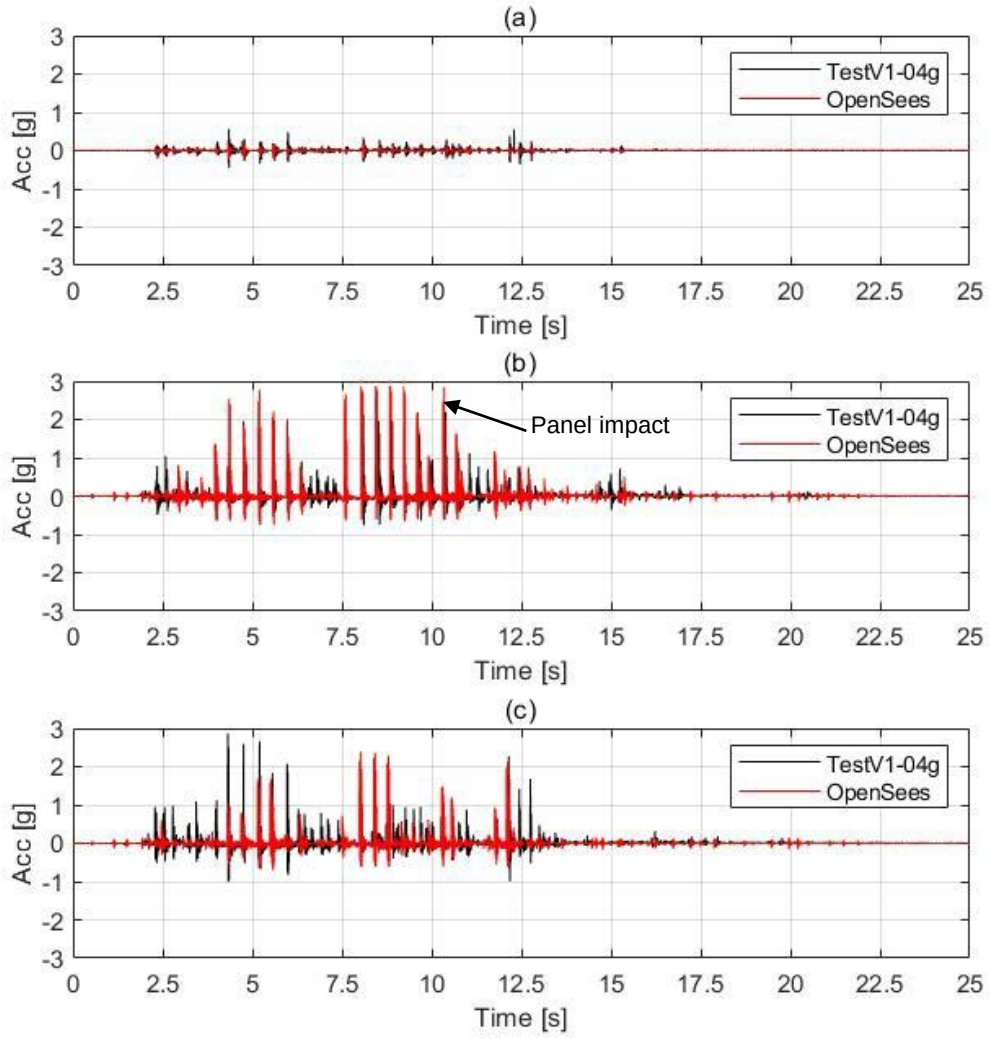

Figure 3-36: Vertical accelerations comparison for test V1 (long strap at 0.4g) and numerical model: for slab (a), panel P1 (b) and panel P2 (c)

From the experimental results is was observed that the response of rocking panels was quite sensitive to different coincidences during the response, due to various construction imperfections. For example, channels were not mounted into the panels in the perfectly vertical direction, channels mounted in the beam (slab) were not perfectly parallel to the beam edge, etc. Despite that, the experimental and numerical results were in rather good agreement both in terms of displacement (Figure 3-34) and horizontal (Figure 3-35) as well as vertical (Figure 3-36) acceleration. In particular, the panels acceleration peaks, due to the impact between the panel and the foundation during the rocking movement, were correctly approximated by the numerical response because of the introduction of the impact behaviour described in section 3.3.6.

The response of connections for test V1

Concerning the response of the connections, also in this case, a direct measure of force was not possible during the experimental test. However, the relative displacement between panel- and structure could be measured (Figure 3-39) and it reveals the connection displacement. The numerical responses of connections are reported in Figure 3-37

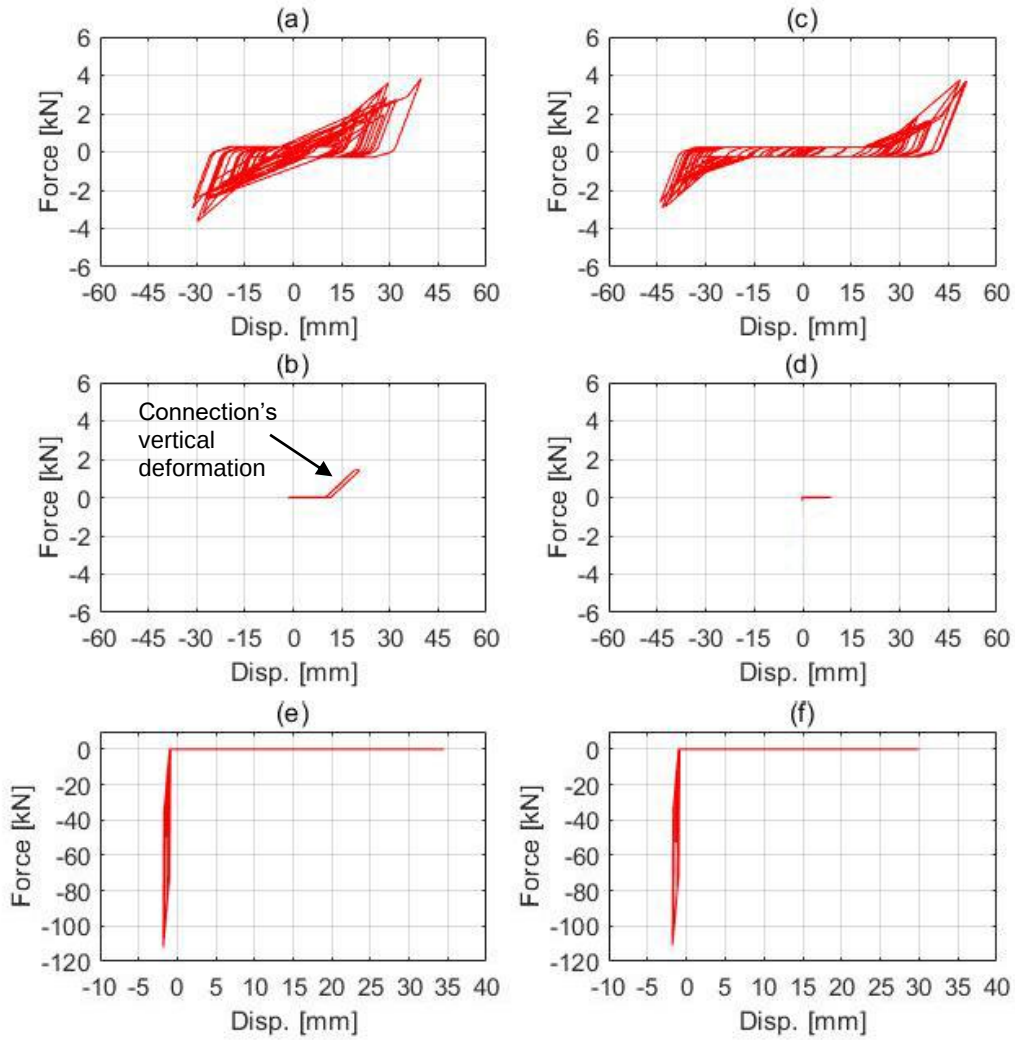

Figure 3-37: Numerical response of connection: for Panel P1 in the horizontal direction (a) in the vertical direction (b) and impact at the base (e). For Panel P2 in the horizontal direction (c) in the vertical direction (d) and impact at the base (f).

As shown in Figure 3-37, the connections' response on panel P1 (Figure 3-37 a,b,e) and on panel P2 (Figure 3-37 c,d,f) are different. The difference is due to the different assembly tolerances on the connections (Figure 3-38). In particular, the connection on panel P1 was also deformed vertically as it happened during the experimental test. The occurred vertical deformation is shown in Figure 3-8a, b.

Panel P1: Connection 1

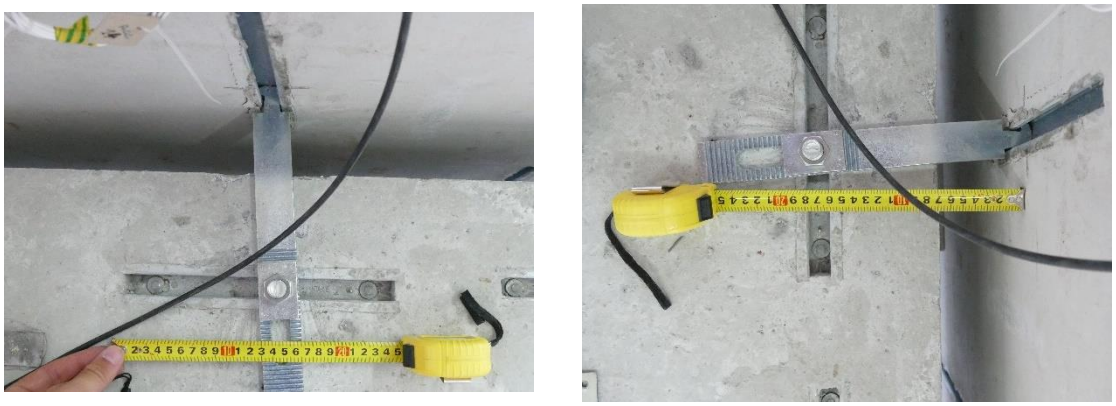

Panel P1: Connection 2

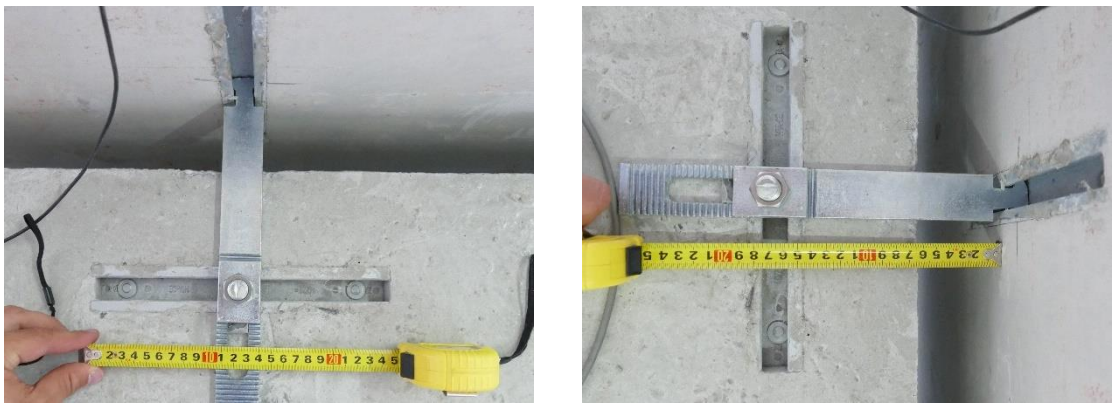

Panel P2: Connection 1

Figure 3-38: Connections' assembly tolerances. Pictures courtesy of UL-FGG

The analytical and experimental relative displacements between the panels and the main structure are compared in Figure 3-39

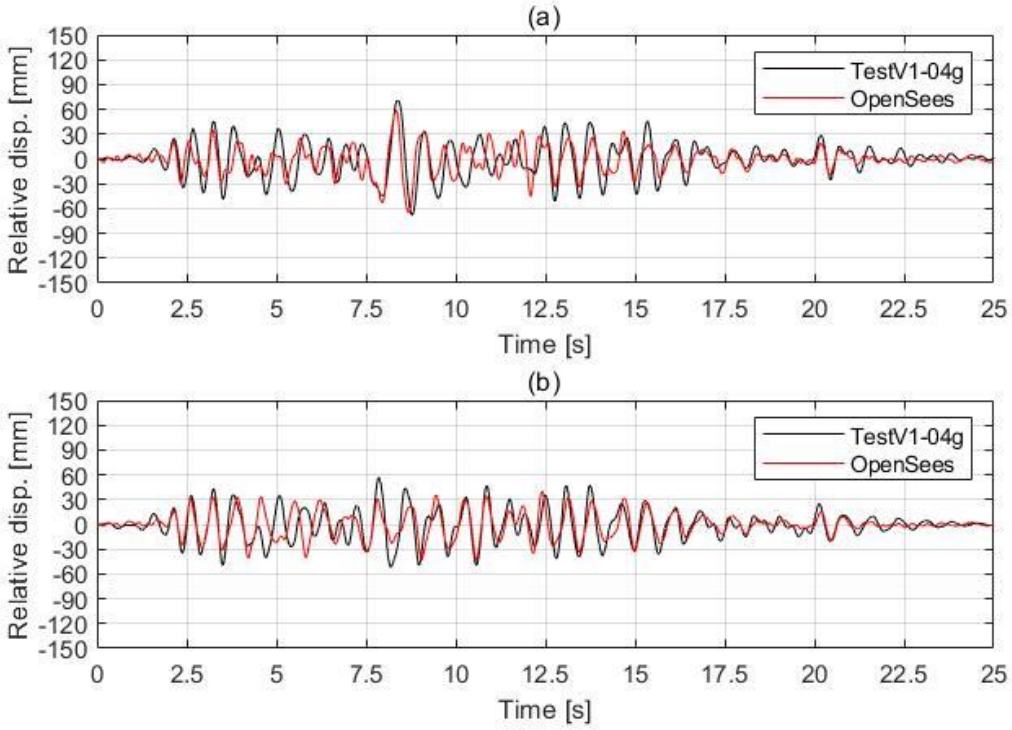

Figure 3-39: Test V1 (long strap at 0.4g), the relative displacement between structure and panel P1 (a) and panel P2 (b)

It can be observed that the numerical response (red) approximates the experimental response (black) in quite a good way although the response of rocking panels was quite stochastic and influenced by different coincidences and construction imperfections as explained in the previous paragraph.

The response of panel and main structure for test V2

The same results are displayed for test V2 (short strap and rocking panels) at seismic intensity of 0.4 g. With the numerical model developed, it was possible to replicate the response histories obtained during the real tests in quite an accurate way.
The results are illustrated in terms of displacement (Figure 3-40a,b,c) and horizontal acceleration (Figure 3-41a,b,c) for the main structure and for the panel P1 and P2.

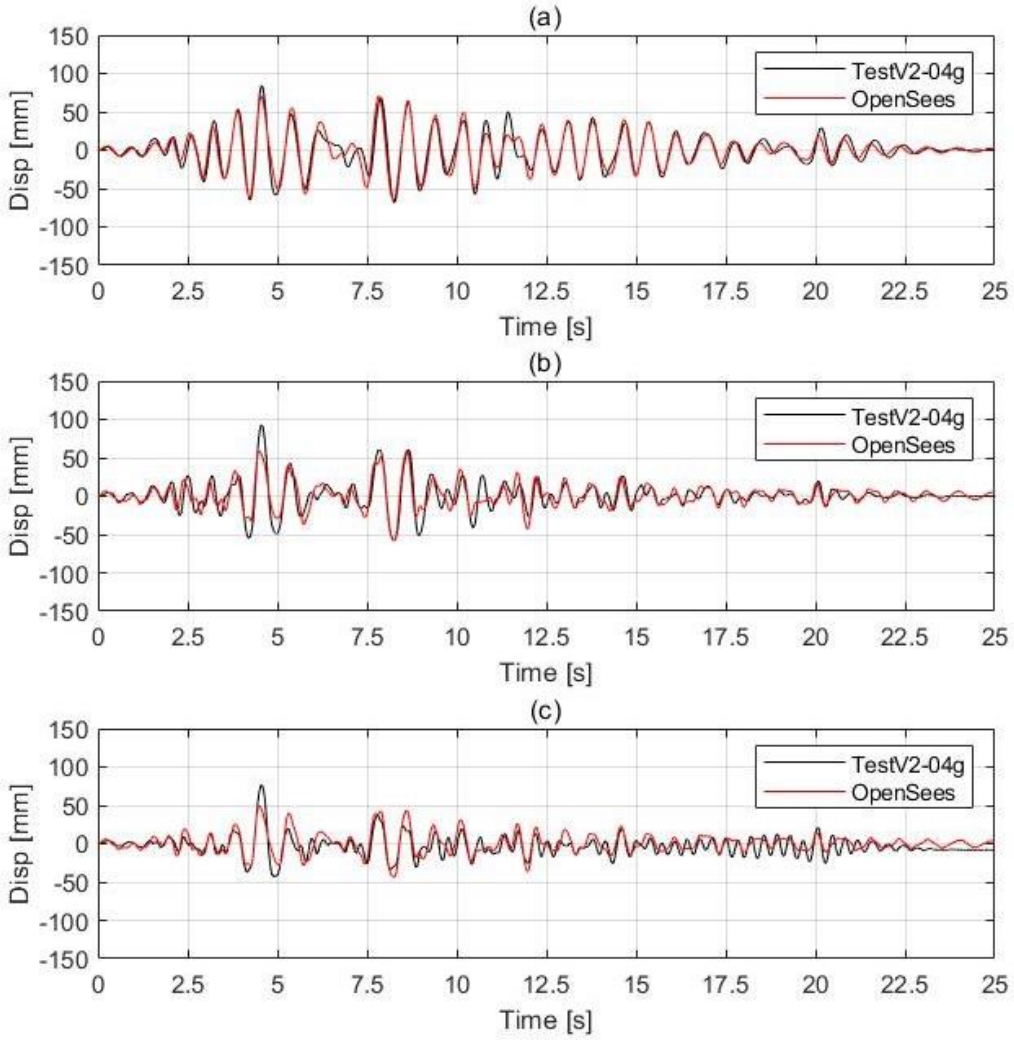

Figure 3-40: Displacements comparison for test V2 (short strap at 0.4g) and numerical model: for slab (a), panel P1 (b) and panel P2 (c)

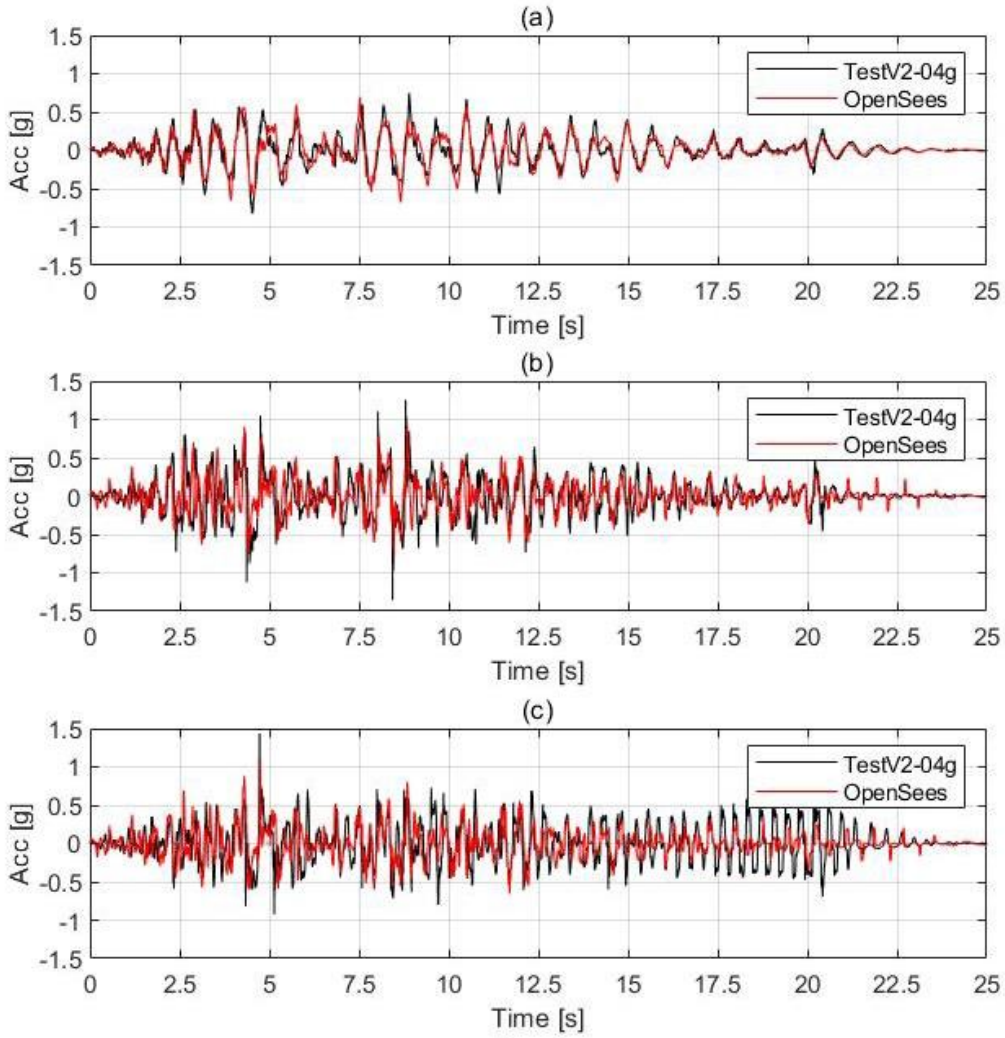

Figure 3-41: Horizontal accelerations comparison for test V2 (short strap at 0.4g) and numerical model: for slab (a), panel P1 (b) and panel P2 (c)

The vertical acceleration response-history highlights the impacts between the panels and the on the shaking table (Figure 3-42a,b,c). However, the acceleration peaks, due to impacts, are lower than those measured in the test V1 (long straps with fixed panels) because the short straps limit the rocking movement.

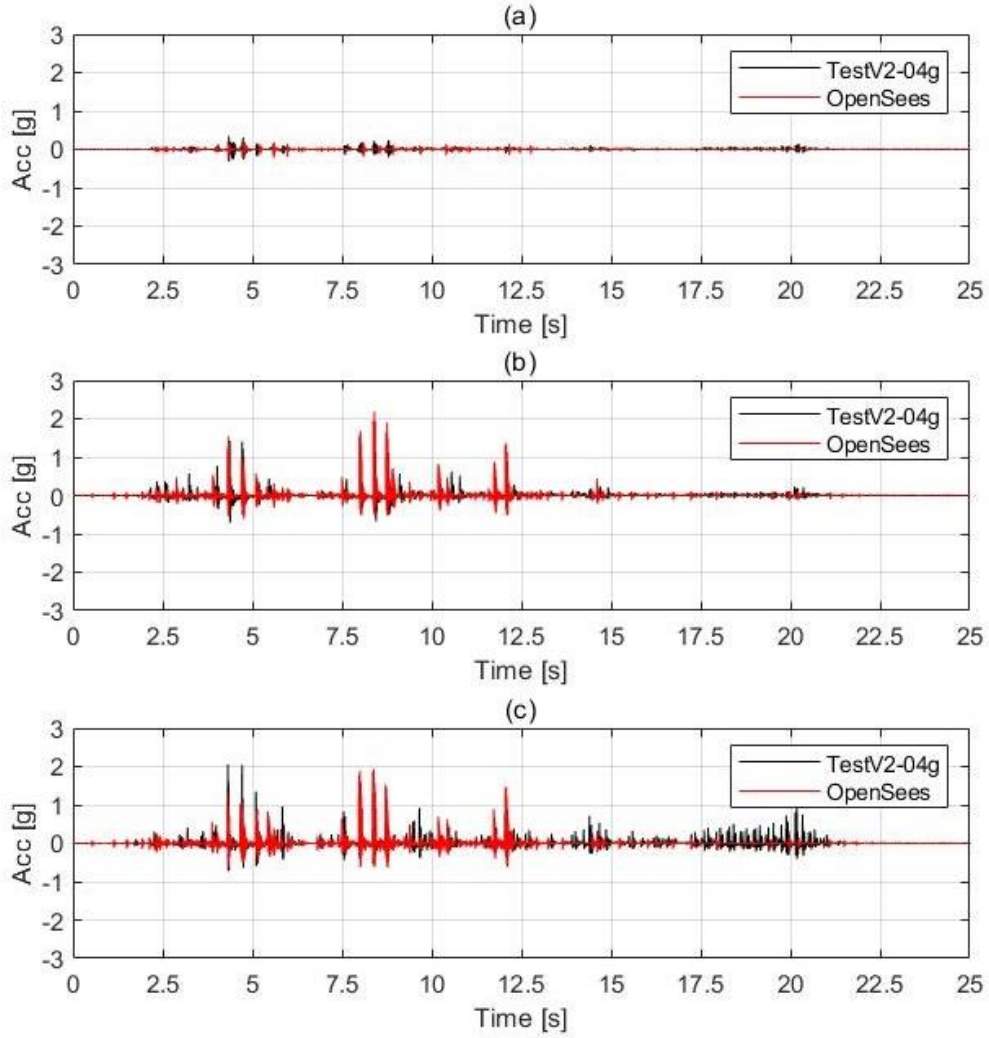

Figure 3-42: Vertical accelerations comparison for test V2 (short strap at 0.4g) and numerical model: for slab (a), panel P1 (b) and panel P2 (c)

The response of connections for test V2

The fact that the short straps limit the rocking movement can be also noted from the response of the connections. Within the numerical response as well as in the real experimental test, the connections didn't show vertical deformations (Figure 3-43b, d).
Because of the limited rocking movement, the energy dissipation due to the panel-shaking table impact is more limited compared to the test V1. (Compare Figure 3-43e, f and Figure 3-37e, f)

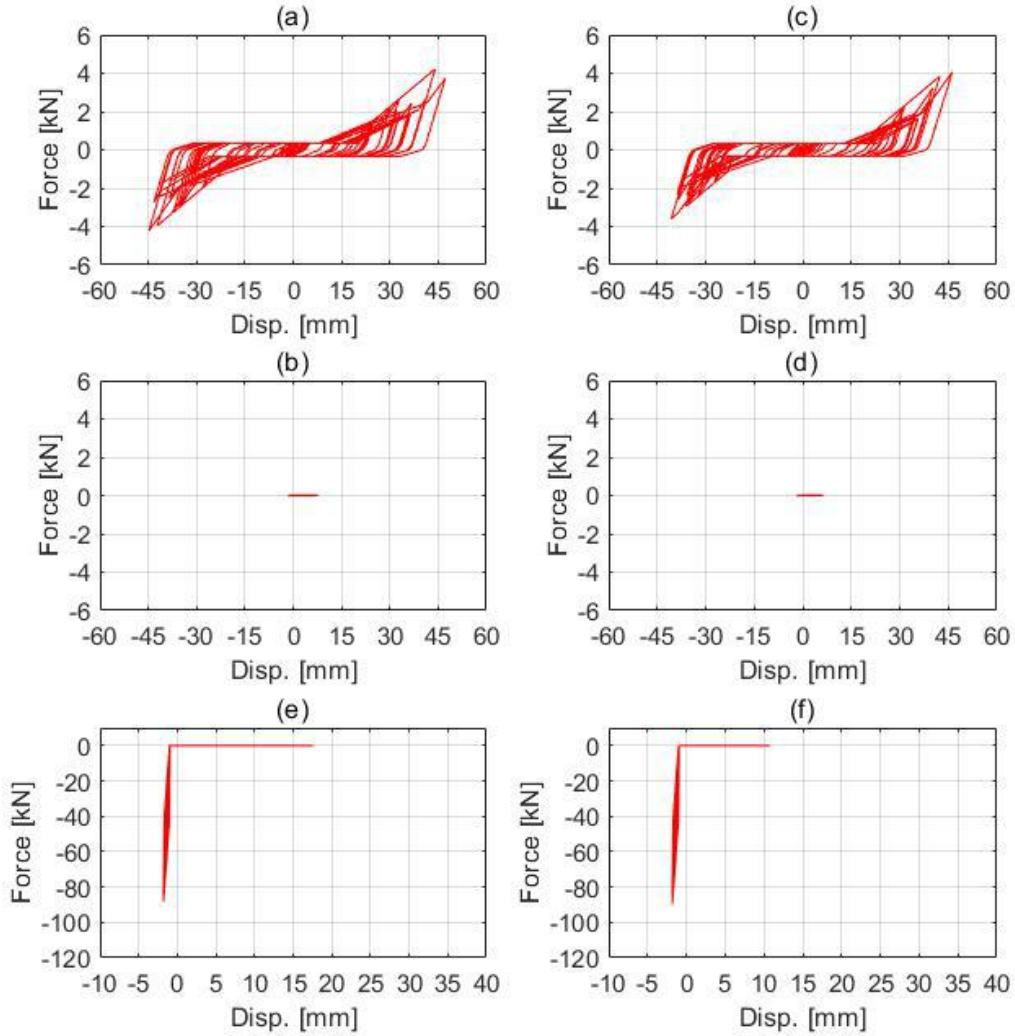

Figure 3-43: Numerical response of connection: for Panel P1 in the horizontal direction (a) in the vertical direction (b) and impact at the base (e). For Panel P2 in the horizontal direction (c) in the vertical direction (d) and impact at the base (f).

The analytical and experimental relative displacements between the panels and the main structure are compared in Figure 3-44.

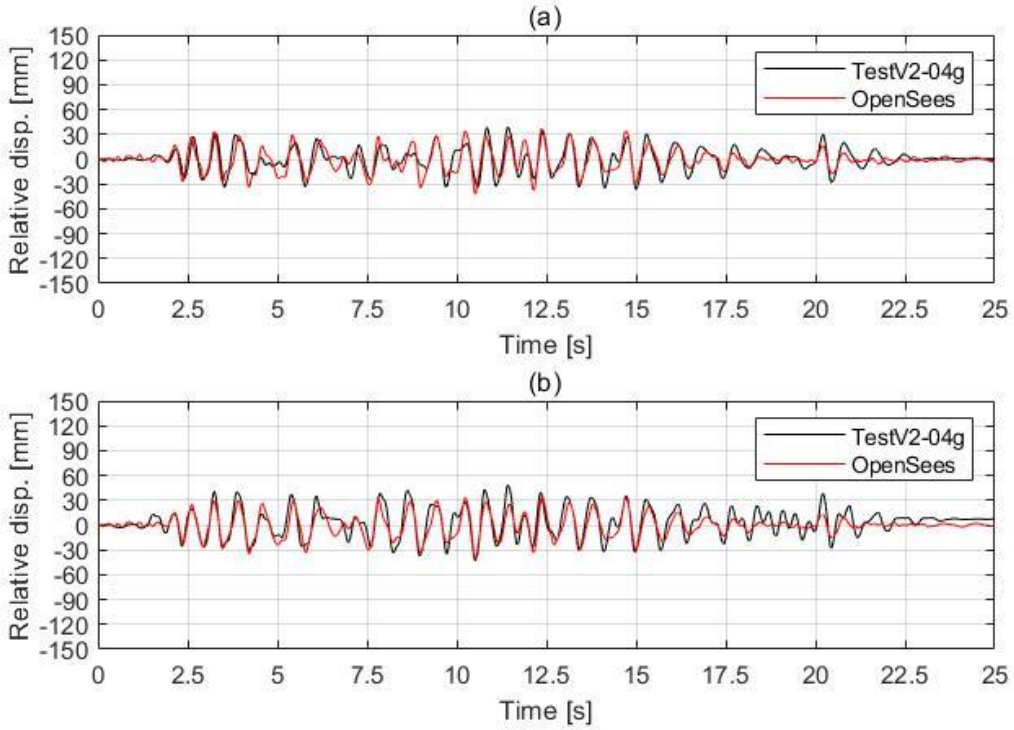

Figure 3-44: Test V2 (long strap at 0.4g), the relative displacement between structure and panel P1 (a) and panel P2 (b)

The numerical result matches the experimental response in quite a good way. The correspondence between numerical and experimental result is better if compared with the same results for tests V1 (Figure 3-39) because the rocking movement was more limited due to the short straps.

3.3.10 Conclusions

The results of a shaking table experimental campaign, designed and conducted by the University of Ljubljana, were analysed.
The numerical modelling of this experimentation was discussed in this section.

The numerical models realized through the OpenSees software were able to replicate the experimental data with good approximation both in the case of fixed and of rocking panels. This was possible through the implementation of the hysteretic model of connections.
Specifically, the model for hammer-head strap connections presented in a previous work performed by University of Ljubljana (Zoubek et al., 2016) was improved by introducing adequate modelling of the connection vertical behaviour which is able to take into account their elastic and plastic strength and deformation.
In this way, the numerical model was able to simulate the experimental response of both the structure and the panels in terms of displacements and accelerations.
Moreover, in the case of rocking panels, some limited damage to the lower corner of the panels was observed during the tests. To numerically simulate this behaviour, a hysteretic model capable of catching the impact between the panel and the foundation was introduced and calibrated. Thus, it was possible to simulate the correct impact between the shaking table and the panels.
However, it was noticed from the obtained results that the numerical model was able to very well approximate the real response of panels, when they were fixed at the base but the approximation was less accurate in the case of rocking panels, particularly when long straps were used. This was because the response of the panels significantly depended on the boundary conditions at the foundations. The response of the rocking panels was quite stochastic and influenced by various coincidences and construction imperfections that cannot be fully modelled.

The numerical model can be used for future analytical studies that can investigate, for example, the behaviour of larger structures or the interaction between several panels mounted on the same side of the structure, whether they have a fixed or a rocking arrangement.

3.4 Study on the influence of silicone sealant

Silicone sealant is commonly used for completion of precast RC panel façade systems. Generally, silicone is used to seal the joints between the adjoining cladding panels and between the panels and other components of the main structure. The silicone is installed in strips either on the outside of the panel or both inside and outside.
In the rocking panels configuration (see also section 2.1.3), a relative sliding, between the adjoining panels, can occur under seismic actions. Shear drift and consequently the shear strain arises in the silicone strips. In this section, the deformations and shear stresses in the silicone strips can lead to an increase in displacement demand in the panel-to-structure connections and can influence the seismic behaviour of the structural system, are investigated.

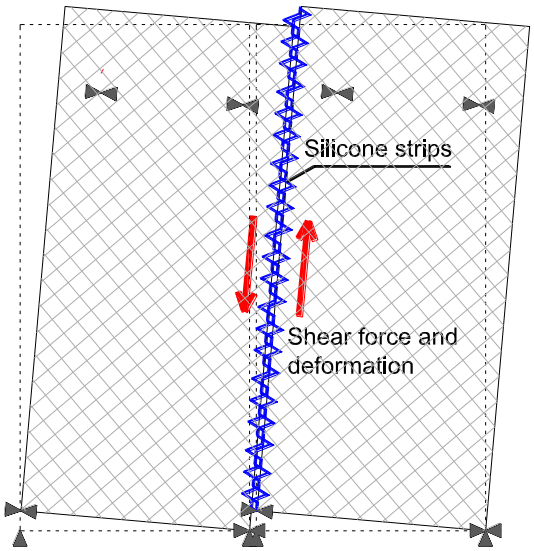

Figure 3-45: The shear drift of the silicone strips

In order to assess the influence of silicone sealant on the seismic response, we started from the numerical model with rocking panel configuration and short hammer-head strap that was well-calibrated on the real response obtained during the shaking table tests (Test V2_0.4g, see section 3.3.9).

The numerical model of the structure used, used in this study, is the same to the one described in section 3.3 The only difference lies in the fact that one panel on each side, with the same dimensions as the existing panel, was added (Figure 3-46a).

The panels, which had a rocking configuration, were joined together with a link element (blue) to simulate the silicone sealant (Figure 3-46b). The link element is concerted at mid-height of the panel interface because the stiffness of the silicone is much lower than the stiffness of the concrete panels, this hypothesis is not expected to have a significant influence on the overall seismic behaviour of the structure.

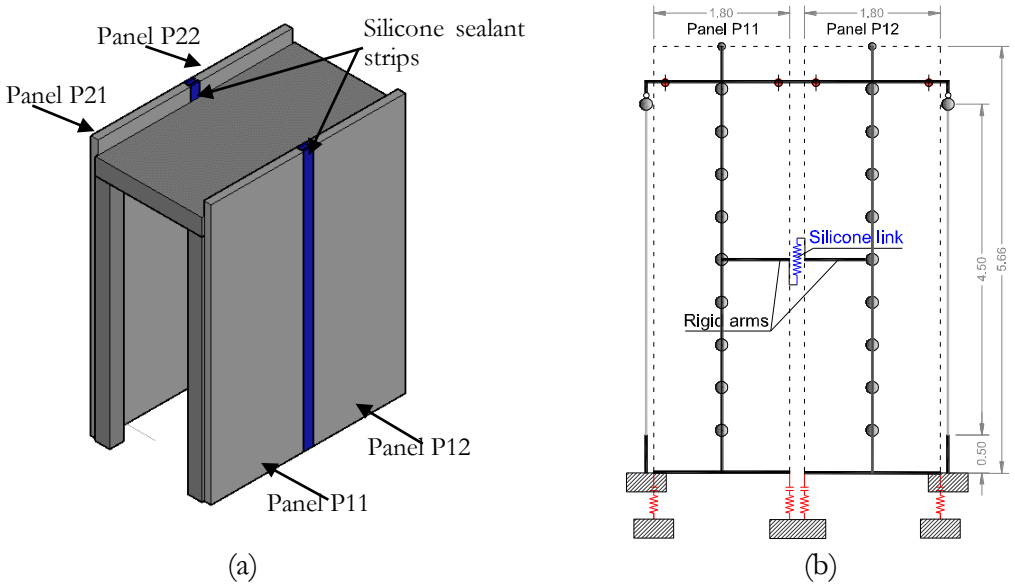

Figure 3-46: 3D view (a), numerical model scheme (b)

3.4.1 Silicone sealant numerical model calibration

The numerical model of the silicone sealant was calibrated based on the results obtained by Dal Lago et al., (2017). In their work, the authors investigated the behaviour of silicone sealants both through local, monotonic and cyclic tests, on small specimens and a full-scale prototype of a precast building with silicone sealed cladding panels.

From the tests, the failure mechanism of the silicone strips for both low and high deformation ratios was detected.
In particular, it was observed that the silicone exhibited a great displacement capacity with an elastic behaviour up to 50% - 80% of the imposed drift. The failure occurred between 150 and 300% of the imposed drift.
The results on the hysteretic behaviour of silicone are reported in the work of Dal Lago et al., (2017) in terms of shear stress versus shear deformation, defined as follows:

$$\gamma = \frac{d}{s}$$

$$\tau = \frac{V}{s \cdot L_{tot}} \qquad (3.26)$$

where:

L_{tot} is the total length of the silicone strips.
d is the applied drift.
V is the measured shear force.
s is the contact thickness of the silicone strip.

Based on Dal Lago et al., (2017) results, the hysteretic bond of the silicone was calibrated using a *Hysteretic* material from the OpenSees material library. The OpenSees *Hysteretic* material was chosen because it is easier to calibrate than others that require more parameters. However, this material allowed to replicate the actual behaviour of the silicone sealant satisfactorily.
The *Hysteretic* material requires 6 points for the definition of the backbone envelope curve (3 if the behaviour is symmetrical) 2 parameters for the definition of the hysteresis cycle pinching: *PinchX* is the pinching factor for strain, *PinchY* is the pinching factor for stress. And 2 parameters for the definition of the damage: *damage1* is the damage due to ductility, *damage2* is the damage due to energy.
The data for *Hysteretic* material calibration are reported in Table 3-15 and the calibrated silicone hysteretic loop is depicted in Figure 3-47.

Hysteretic material		
Point	Shear stress [N/mm^2]	Shear strain
1	0.025	0.10
2	0.220	1.90
3	0.186	2.53
Pinching X	1	
Pinching Y	0.2	
Damage1	0.0	
Damage2	0.045	

Table 3-15: *Hysteretic* material parameters in terms of stress-strain

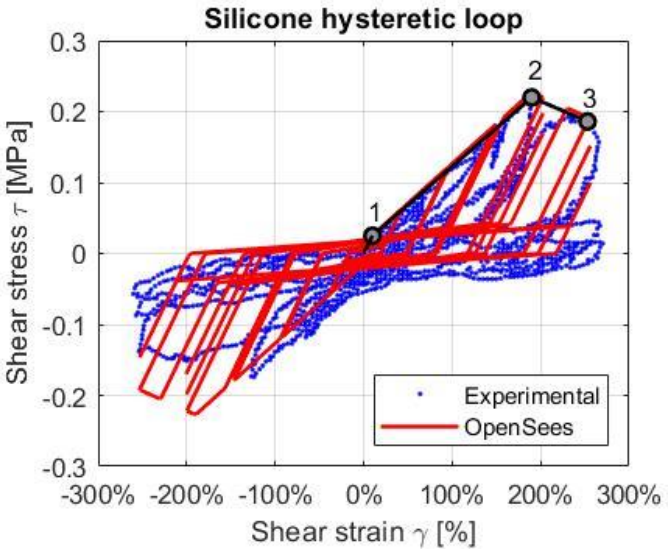

Figure 3-47: Numerical and experimental silicone sealant behaviour

Since the silicone behaviour are lumped in one link element (Figure 3-46b), the shear stress and strain values reported in Table 3-15 have to be converted into force shear V and shear drift d by manipulating the equations (3.28) as follows:

$$d = \gamma \cdot s$$
$$V = \tau \cdot s \cdot L_{tot} \qquad (3.27)$$

In the considered building, two strips of silicone that connect the adjoining panels are taken into account The two strips had a total length L_{tot} =11.30m and a contact thickness s of 10 mm (Figure 3-48). Therefore, the parameter values for *Hysteretic* material are obtained in terms of force shear V and shear drift d as reported in Table 3-16.

Hysteretic material		
Point	Shear force [kN]	Shear deform. [m]
1	2.82	0.001
2	24.86	0.019
3	21.01	0.0253
Pinching X	1	
Pinching Y	0.2	
Damage1	0.0	
Damage2	0.045	

Table 3-16: *Hysteretic* material parameter in terms of force-displacement

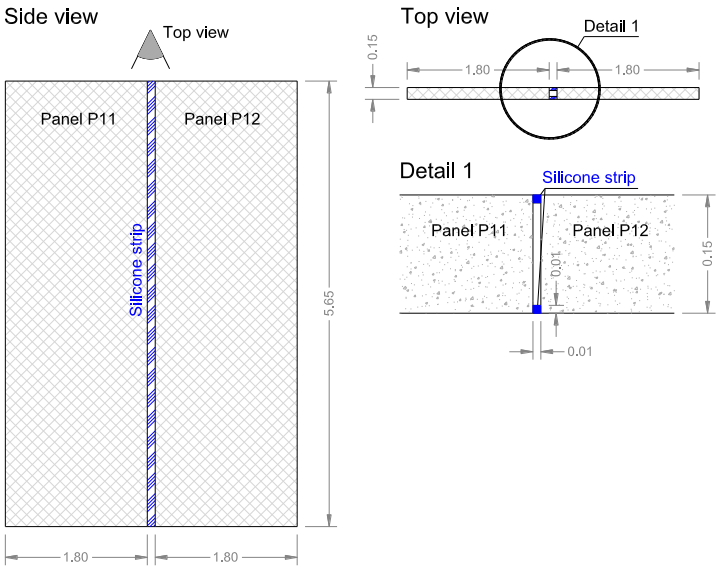

Figure 3-48: Silicone strips dimensions

To the structure numerical model with 2 panels on each side (as described in Figure 3-46) the Pertovac earthquake (Figure 3-6) scaled to 0.4g was applied as input acceleration.
The results of the non-linear dynamic analysis are reported in terms of displacement and acceleration of the structure as well as of the panels and relative displacement between structure and panels are also reported. The hysteretic behaviour of the panel structure connections was also shown. In all cases, the response of the structure with the panels joined by a silicone sealant was compared with the response of the structure in which the two adjoining panels were not sealed by silicone.

3.4.2 Analysis results

From the results, depicted in terms of displacement in Figure 3-49 it is possible to observe a reduction in the maximum longitudinal displacement of the panels in the case of silicone sealant (blue line) compared to the case without silicone (red line). While the displacements of the main structure are practically the same in the two cases.

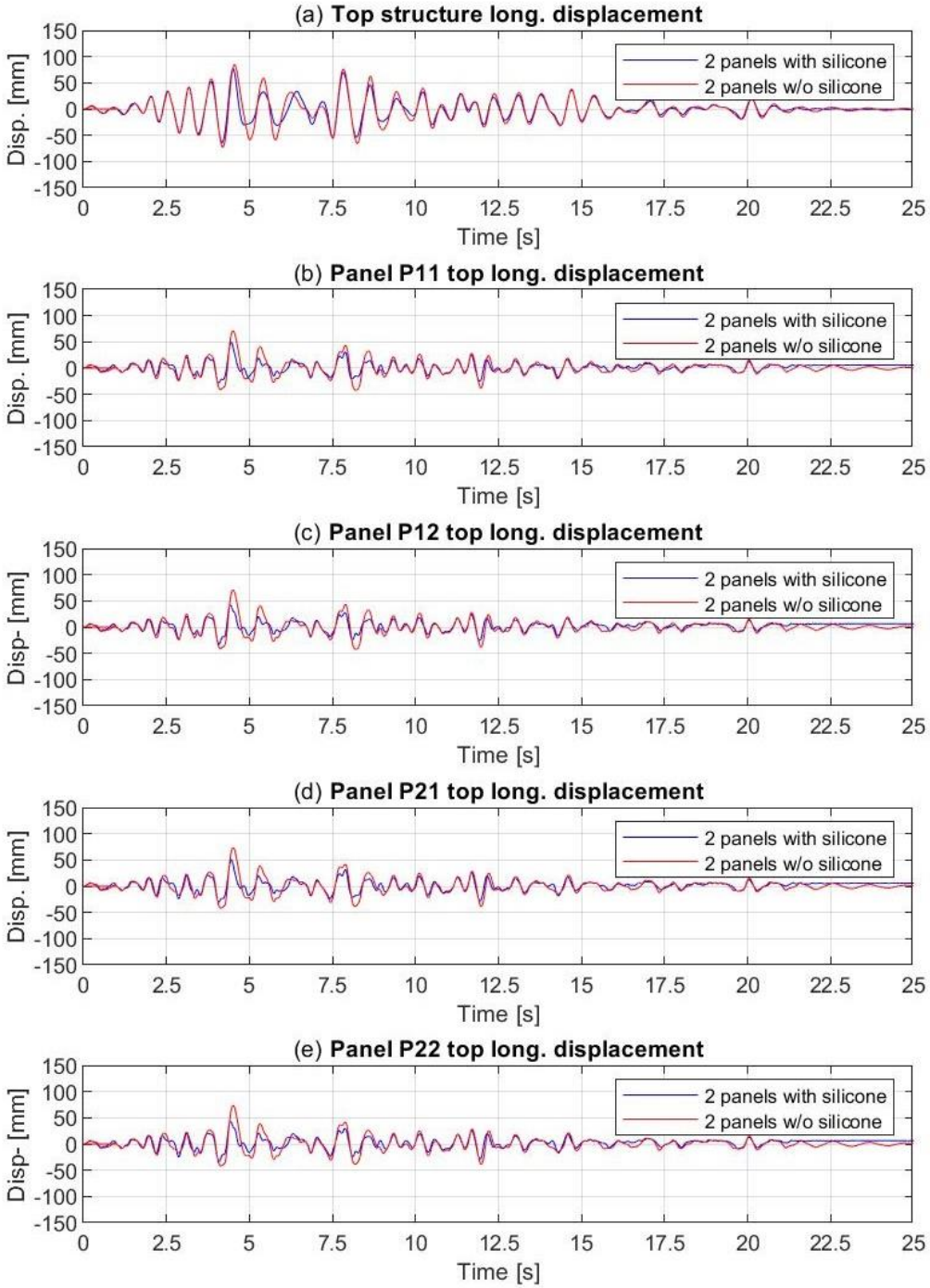

Figure 3-49: Longitudinal displacements comparison between panels with and without silicone sealant: for slab (a), panel P11 (b) panel P12 (c), panel P21 (d) and panel P22 (e)

The same considerations carried out for the longitudinal displacements can be made for the longitudinal accelerations of the panels (Figure 3-50). The longitudinal accelerations, in the case with silicone (blue line), show a small reduction in the maximum peaks compared to the case without silicone (red line). While the longitudinal acceleration of the main structure is practically the same in both cases.

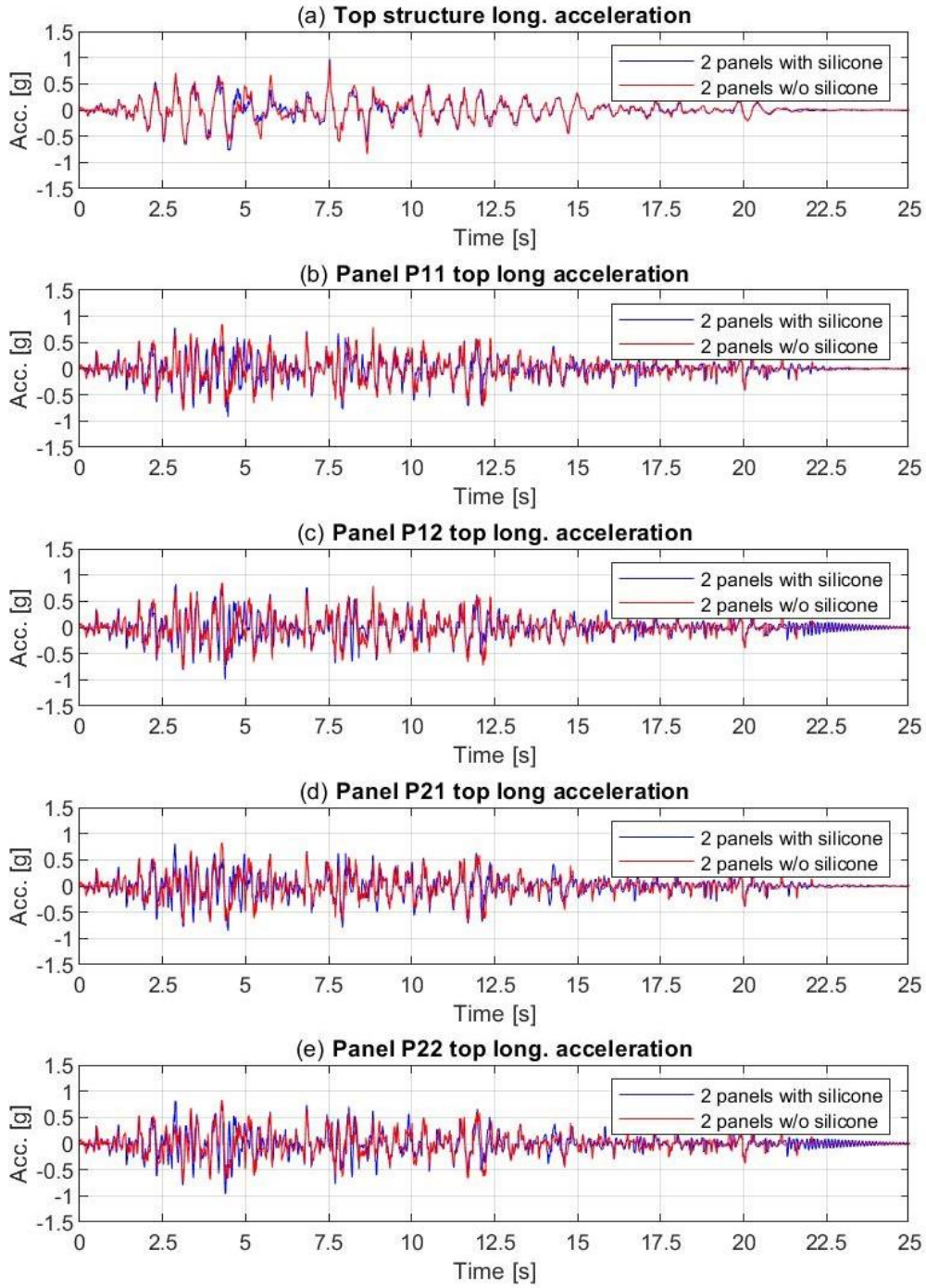

Figure 3-50: Longitudinal accelerations comparison between panels with and without silicone sealant: for slab (a), panel P11 (b), panel P12 (c), panel P21 (d) and panel P22 (e)

Since we are in the configuration in which the panels and allowed rock around their lower corner, it is appropriate to also report the vertical accelerations, both for the panels and the main structure (Figure 3-51). The vertical acceleration of the structure and the same in the case with silicone. Concerning the panels, in the case of silicone sealant, the maximum peaks of vertical acceleration are reduced compared to the case without silicone.

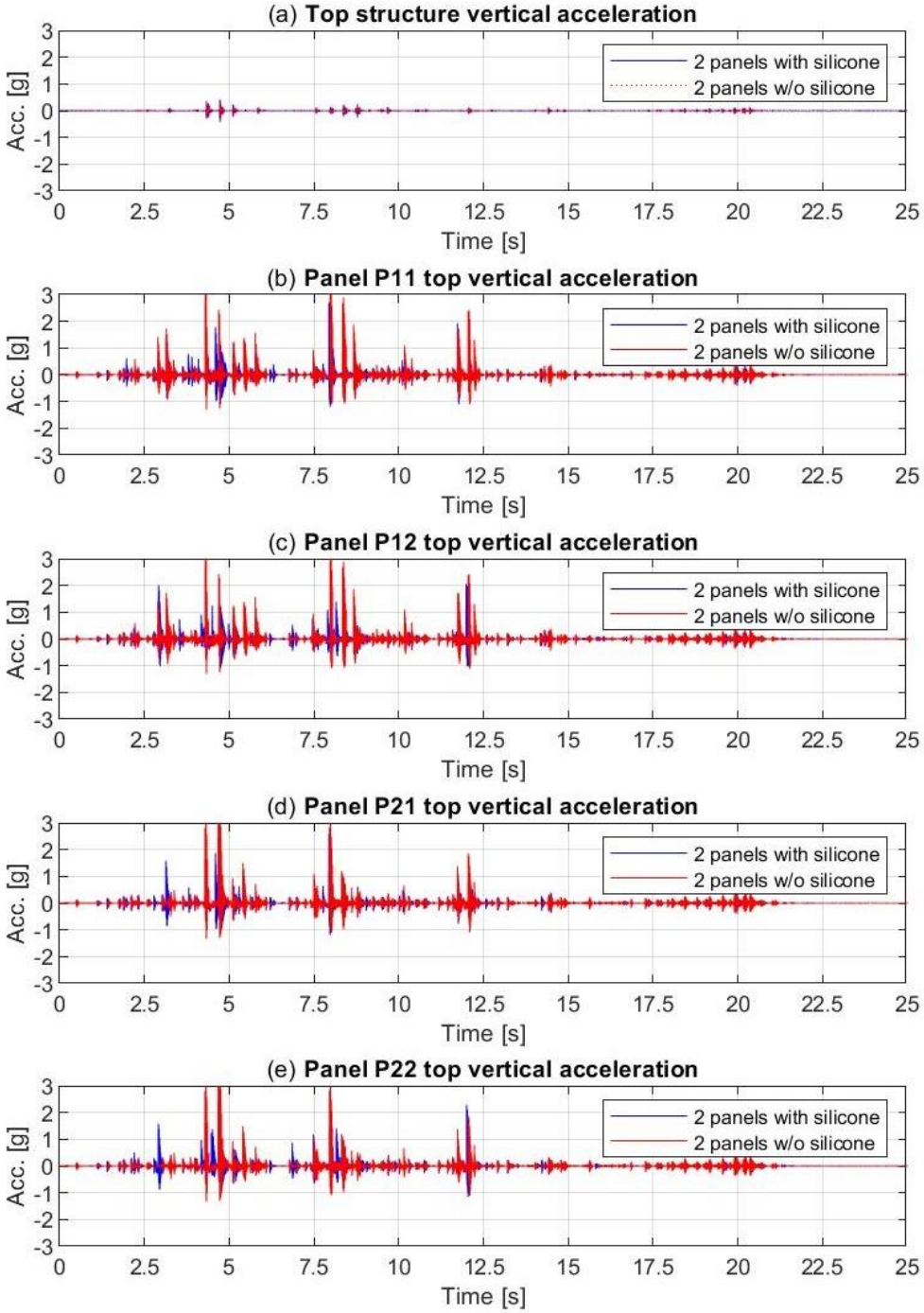

Figure 3-51: Vertical accelerations comparison between panels with and without silicone sealant: for slab (a), panel P11 (b), panel P12 (c), panel P21 (d) and panel P22 (e)

Observing the relative displacement between the panels and the structure it can be noted that if silicone sealant is used the relative displacement slightly increases compared to the case without silicone (Figure 3-52). This leads to an increase in displacement demand in the panel-to-structure connections as is also possible from the figure in which the hysteretic loop connection devices are represented.

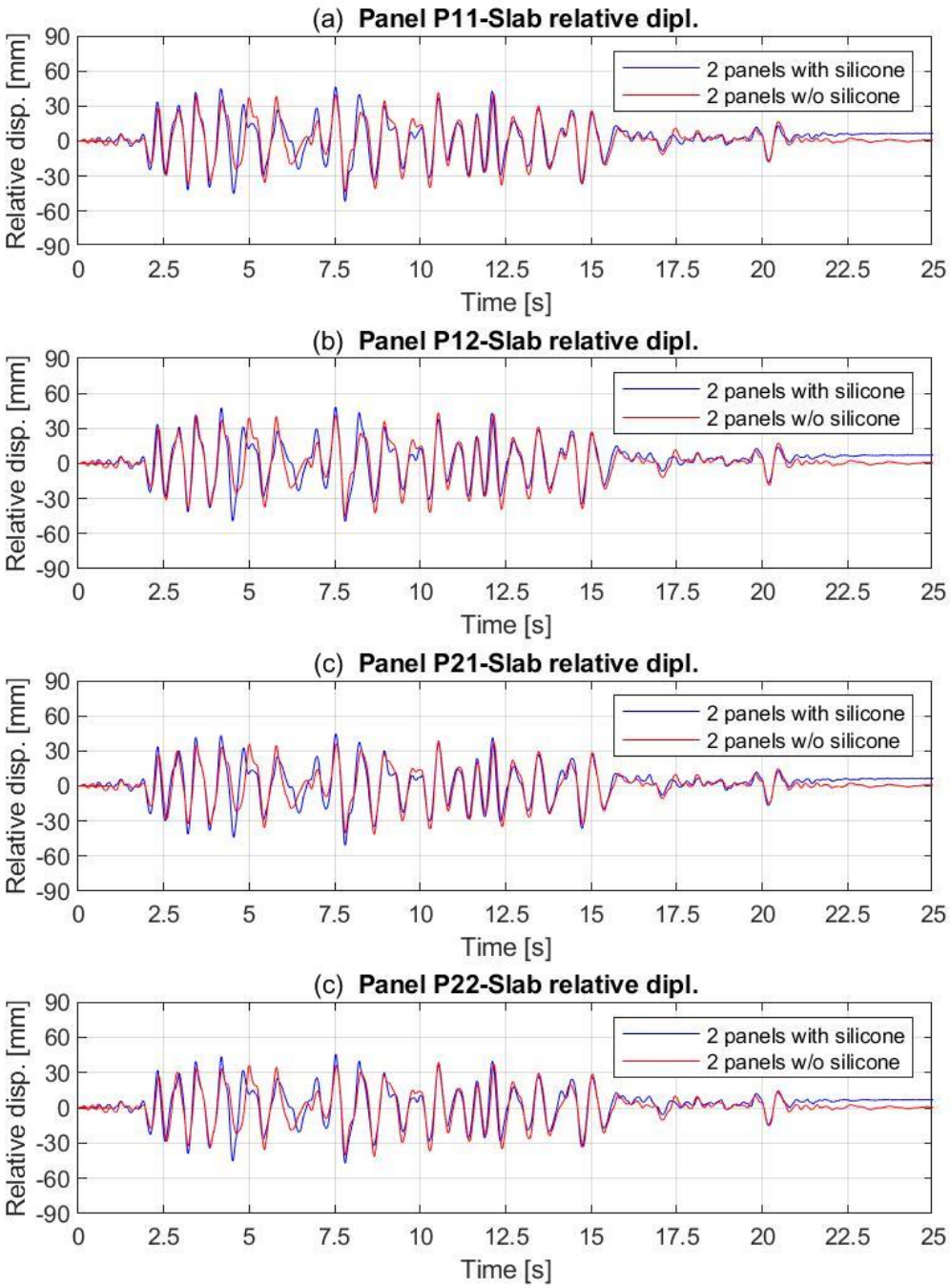

Figure 3-52: Panel-structure relative displacements comparison between the case with and without silicone sealant. Relative displacement slab-panel P11 (a), slab-panel P12 (b), slab-panel P21 (c) and slab-panel P22 (d)

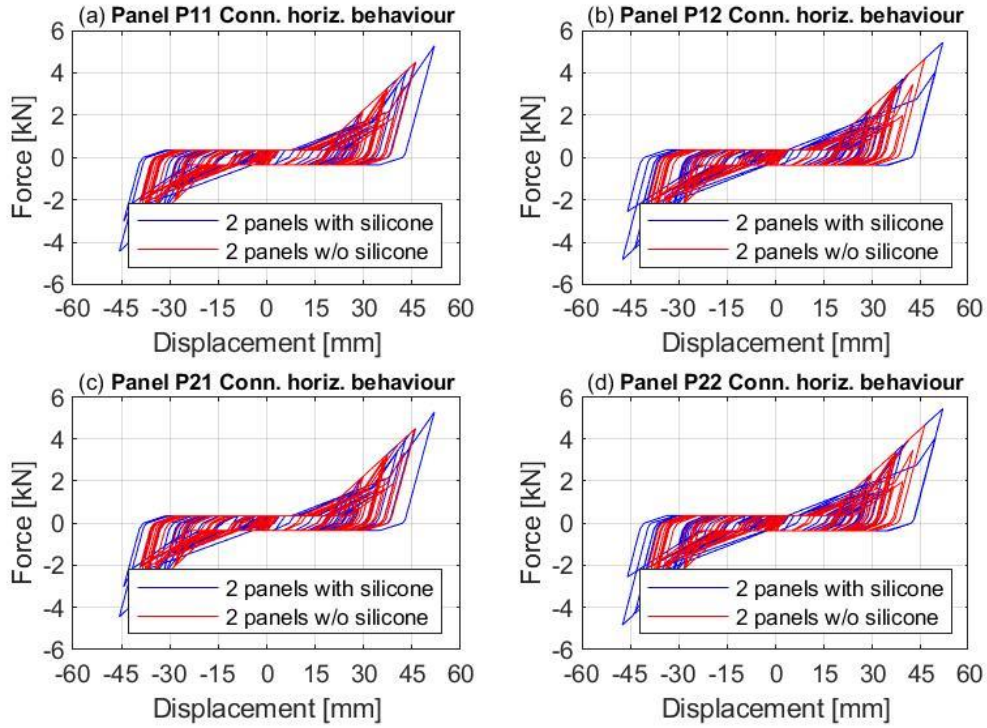

Figure 3-53: Hammer-head straps hysteretic loop comparison between the case with and without silicone sealant. Connection on panel P11 (a), on panel P12 (b), on panel P21 (c) and on panel P22 (d)

In the end, a final consideration can be carried out about the main structure.
The main structure is very slightly affected by the presence of the silicone between the adjoining panels and the contribution in stiffness (compare the blue dotted line with the red one in Figure 3-54a) could be neglected. Finally, as an example, the hysteretic diagram of the silicone obtained during the analysis is shown in Figure 3-54b.

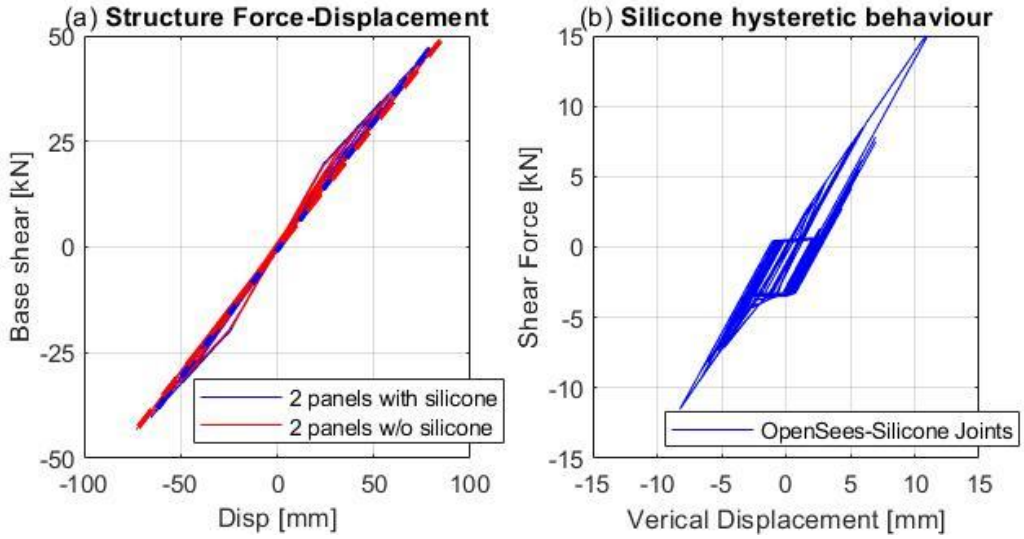

Figure 3-54: Structure base shear-displacement diagram (a) and silicone hysteretic loop (b)

3.4.3 Concluding remarks

Some considerations can be carried out from the results of the numerical analysis.
First of all, it can be stated that the longitudinal displacement of the panels, when silicone sealant is used, is limited compared to the longitudinal displacement of panels without silicone. This is due to the fact that the adjacent panel stabilises the rocking movement of the next one due to the shear force that develops in the silicone strips.
The silicone strips installed between adjoining panels can certainly be useful at the serviceability limit states although they contribute to increasing the displacement demand in the panel-to-structure connection devices. Therefore, at the serviceability limit states the silicone sealant can influence the seismic performance of the cladding panels system.
However, silicone is not an engineered material and there can be great variability in mechanical properties between different products on the market. Furthermore, it is not clear what are the effects of ageing on the silicone sealant, this contributes to additional uncertainty in its mechanical properties.
Besides, silicone is not suitable for supporting large drifts between panels, such as those occurring at the ultimate limit states.
According to the indication provided by Dal Lago et al., (2017), it is advisable to disregard the silicone effect when it has a possible beneficial effect on the seismic performance of the structure. On the contrary, the effects of the silicone sealant between adjoining panels should be considered when they are on the unsafe side, for example when assessing the displacement demand of the connections.
However, this is an initial study on this topic and further investigation and future analyses would be necessary to deeply investigate the effects on the seismic response of silicone sealant.

3.5 SismoSafe connection experimental campaign

An experimental campaign focused on the Isostatic Sliding-Frame system (§2.1.1) for vertical or horizontal panels was carried out at Laboratory of Tests and Materials of the Department of Civil and Environmental Engineering at the University of Florence.
Both in-use commercial steel hammer-head strap connections (called "Standard" in the following) and innovative ones (called "SismoSafe") were tested.

3.5.1 Design and aim of the tests

During recent Italian earthquakes, in "Standard" connections, constituted by hammer-headed straps, relative displacements between panels and the structure often did not occur, leading to heavy actions in the straps and a strong cladding-structure interaction as explained in §1.3. In a different way, experimental tests on these innovative connections showed the achievement of the isostatic sliding-frame behaviour with quite low friction forces in the connections.
Table 3-17 lists restrained degrees of freedom in the three directions x, y and z, where x-z is the plane of panels; restraints are denoted by letters as shown in Figure 3-55. Restraint conditions allow for horizontal panels to transmit their inertial forces to the structure in both horizontal directions, since, except the lowest panel, they are supported on RC corbels jutting out from columns. Connections of horizontal panels should permit much smaller relative displacements than connections of vertical panels, since the height of horizontal panels is equal to about 2 m, against 7m - 10m of vertical panels.

Direction	A	B	C	D	G	H	I	L
x	⊗	⊗			⊗	⊗		
y	⊗	⊗	⊗	⊗	⊗	⊗	⊗	⊗
z	⊗	⊗			⊗	⊗		

Table 3-17: Restrained ⊗ translational degrees of freedom for horizontal and vertical panels (see Figure 3-55).

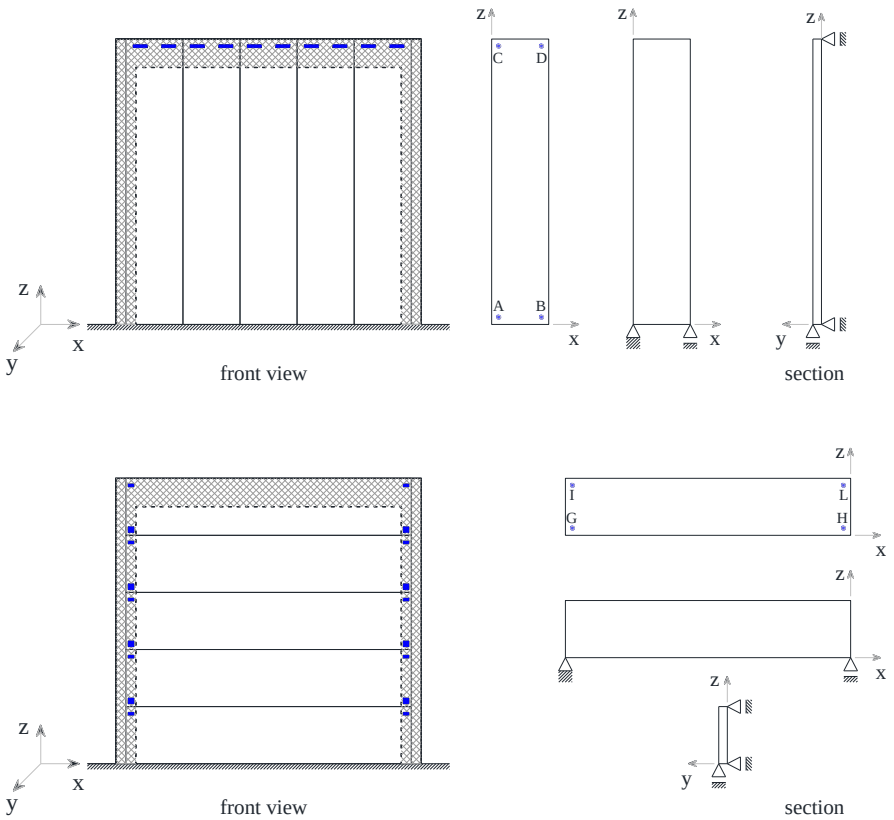

Figure 3-55: Static schemes for vertical (above) and horizontal (below) cladding panels

The experimental campaign consisted of more than 60 tests and involved different types of connections at varying the load-time history and applying or not an out-of-plane load (Table 3-1).

Tests differed for the following aspects:

- *Panels*. Connections of vertical panels or horizontal panels were tested. Besides tests on connections of vertical panels to horizontal beams, some tests were also carried out on connections capable of uncoupling both vertical and horizontal displacements to simulate the case of vertical panels fixed to the inclined top face of a roof tile; these tests are denoted by the acronym AT (Aliant Tile). In general, this configuration is also representative of vertical panels fixed to horizontal beams exhibiting significant rotations and displacements in the vertical plane; in summary the experimental campaign concerning connections of horizontal panels (HP), vertical panels (VP) with a horizontal beam and vertical panels with the inclined top face of a roof tile (AT).
- *Connections*. Within each of the above three typologies, connections to be tested were chosen among available commercial joints ("Standard" joints) or designed by the authors ("Prototype" joints). By geometrically/mechanically improving the "Prototype" connections, new connections were designed ("SismoSafe" joints).
- *Type of in-plane load*. Two different load-histories were considered for the in-plane load: sinusoidal or three cycles of increasing amplitude.
- *Intensity of the out-of-plane load*. The intensity of the out-of-plane seismic load was chosen as 30% of the out-of-plane strength of investigated joints. This choice derives from the rule for the combination of the effects of horizontal components of the seismic action (1.0 E_x + 0.3 E_y), being the x-axis parallel to the plane of panels.

Number of tests	Test designation	Connection type	Fastening type
3	F05_01, F17_01, F18_01	HP	Standard_01
2	F04_01, F04_02	HP	Prototype_01
3	F14_01, F14_02, F14_03	HP	SismoSafe®
9	F01_01, F01_02, F01_03, F01_04, F01_02, F16_01, F16_02, F16_03, F16_04	VP	Standard_01
1	F09_01	VP	Standard_02
1	F10_01	VP	Standard_03
1	F02_01	VP	Prototype_01
2	F03_01, F03_02	VP	Prototype_02
2	F08_01, F08_02	VP	Prototype_03
12	F11_01, F11_02, F11_02A, F11_02B, F11_02C, F11_02D, F11_02E, F11_02F, F11_02G, F11_02H, F11_02I, F11_02L	VP	Prototype_04
4	F12_01, F12_02, F12_03, F12_04	VP	SismoSafe®
9	F15_01, F15_02, F15_03, F15_04, F15_05, F15_06, F15_07, F15_08, F19_01	VP	SismoSafe®
5	F06_01, F06_02, F06_03, F06_04, F06_05	AT	Standard_01
2	F07_01, F07_02	AT	Prototype_01
4	F13_01, F13_02, F13_03, F13_04	AT	SismoSafe®

Table 3-18: Summary of tests

3.5.1.1 Experimental setup

Experimental tests were performed at the Structures and Materials Testing Laboratory (SMTS) of the Department of Civil and Environmental Engineering of Florence. The test setup is the same for connections of both vertical and horizontal panels and it consists of the following elements (Figure 3-56 and Figure 3-57):

- a horizontal or vertical panel specimen supported on rollers;
- a RC beam supported on a roller oscillating under a displacement history imposed through a horizontal actuator;
- a hydraulic jack;
- a steel lever to amplify the displacement imposed by the hydraulic jack to the beam;
- a mechanical joint between the panel and the beam;
- an out-of-plane horizontal loading system composed of two ropes passing through two pulleys and having one end fixed to the upper edge of the panel specimen and a weight suspended at the other end; this system was utilized to apply an out-of-plane static load to the panel;
- a load cell fixed to the beam to measure the force required to produce an assigned horizontal displacement of the beam;
- a load cell fixed to the panel to measure the load on the panel due to the friction resistance of the joint;
- a displacement transducer to measure the beam horizontal displacement.
-

Each panel specimen was fixed to the testing apparatus. A displacement history was imposed to the lateral beam to simulate the oscillation of the structure and an out-of-plane load was applied to the specimen's upper edge to simulate out-of-plane seismic inertial forces. The installation of all specimens in the test machine was executed carefully to reduce as much as possible the influence of installation defects on test results.

(a) (b)

Figure 3-56: Pictures of the experimental setup. Front view (a) and back view (b)

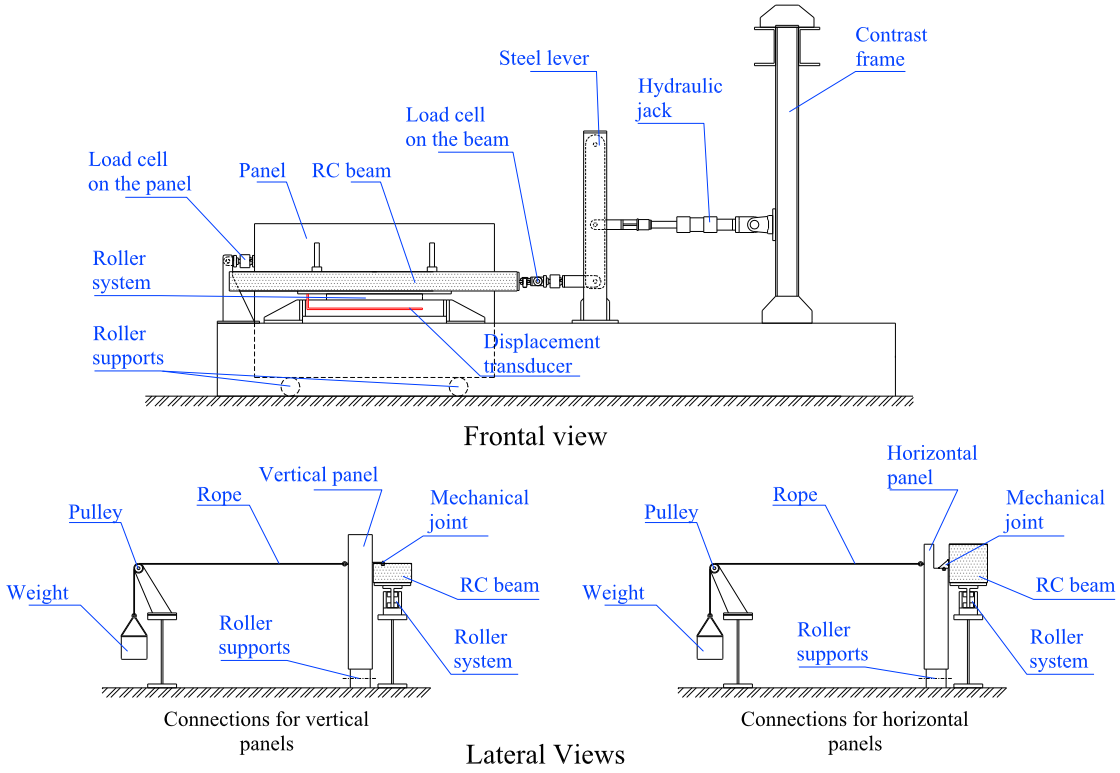

Figure 3-57: Test setup and instrumentation details: frontal (above) and lateral (below) views.

3.5.1.2 Experimental campaign

Experimental tests were performed imposing two different sinusoidal time-displacement histories to the lateral beam along its axis (Table 3-19), while the panel specimen was fixed to the beam with the investigated connections and supported on rollers. A maximum frequency of 0.86 Hz and a minimum of 0.52 Hz were considered. These frequency values are typical for one-storey industrial buildings with height of 7.00 m or 10.00m, square column section of 40×40cm or 60×60cm, respectively, and span of 18.00m, designed according to EN1998-1 (CEN 2005). The maximum amplitude of the displacement to be used in tests was chosen as the horizontal displacement of the roof at the onset of the first plastic hinge at the base of columns, whose longitudinal reinforcement ratio was assumed equal to 1%. This value resulted equal to about 100mm for 7.00m high buildings and 170mm for 10.00m high buildings.
Table 3-19 lists the frequency values of the sinusoidal displacement-time histories and the corresponding maximum relative displacements used in tests.

	Frequency [Hz]	Maximum displacement [mm]
Sin 1	0.86	100
Sin 2	0.52	170

Table 3-19: Frequencies and maximum relative displacements used in tests.

To evaluate the maximum capacity of connections, in case that their behaviour is mainly controlled by the hysteresis of the material, a cyclic push-over test was also performed under a displacement time history consisting of groups of three cycles of the same amplitude, with subsequent increment Δd between two successive groups up to the ultimate limit. The amplitude d_1 of the first group was taken as 1/10 of the maximum expected displacement; the

amplitude increment Δd from one group of cycles to the subsequent group was taken equal to d_1 (Figure 3-58).

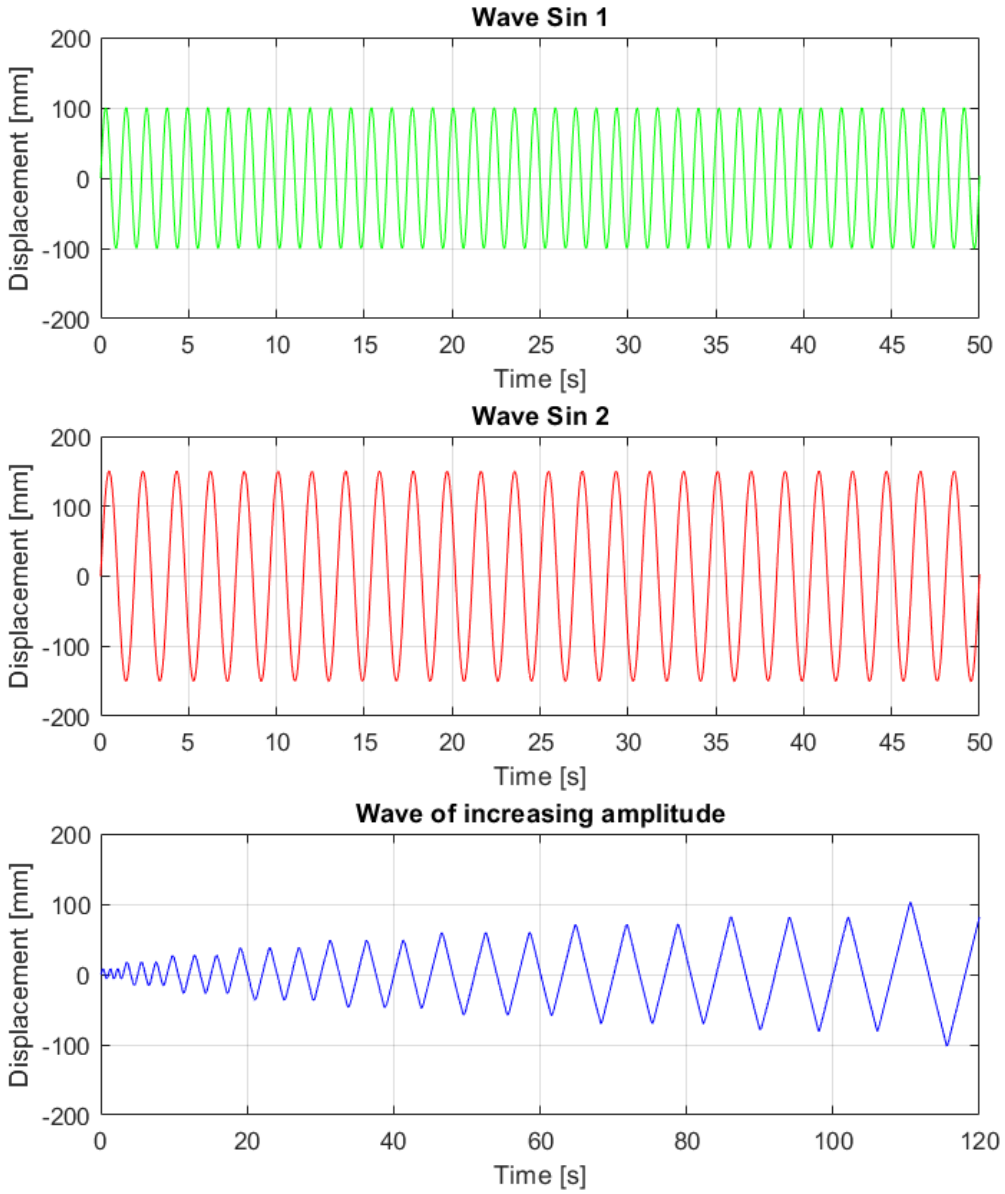

Figure 3-58: Imposed displacement history with groups of three cycles of increasing amplitude.

Among all tests, the most significant tests are selected and reported in Table 3-20 and Figure 3-59., Figure 3-60. and Figure 3-61. Table 3-20 lists the test designation, the connection type, the displacement-time history and the value of the out-of-plane load.

Test designation	Connection type	Fastening type	Displacement-time history	Out-of-plane load [kN]
F17_01	HP	Standard	Three cycles of increasing amplitude	7.40
F14_01	HP	SismoSafe®	Sinusoidal 0.86 Hz	7.40
F16_04	VP	Standard	Three cycles of increasing amplitude	7.40
F15_04	VP	SismoSafe®	Sinusoidal 0.86 Hz	7.40
F06_04	AT	Standard	Three cycles of increasing amplitude	7.40
F13_04	AT	SismoSafe®	Sinusoidal 0.52 Hz	7.40

Table 3-20: List of most significant tests.

(a) (b)

Figure 3-59. Experimental test setup: F17_01 (a) and F14_01 (b).

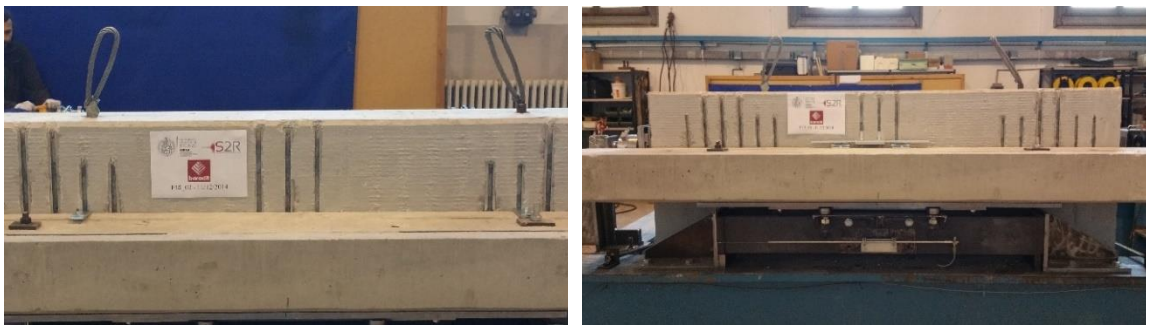

(a) (b)

Figure 3-60. Experimental test setup: F16_04 (a) and F15_04 (b).

(a) (b)

Figure 3-61. Experimental test setup: F06_04 (a) and F13_04 (a)

The "Standard" connection for horizontal panels consists of a steel angle plate with a stiffener, which is fixed with hammer-head bolts to anchor channels pre-installed both on the column and on the panel side. Bolts are provided with sliding blocks to prevent them from locking, so they can freely slide inside the channel profiles (Figure 3-62).

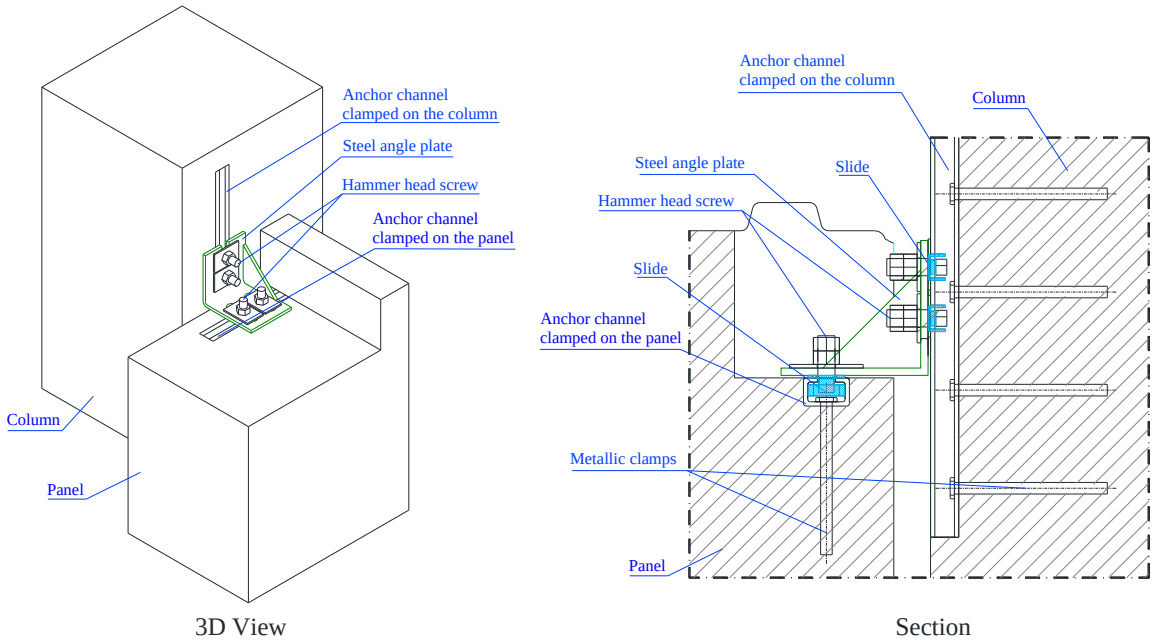

Figure 3-62: Layout of a "Standard" connection of horizontal panels to columns.

The "SismoSafe" connection represents an improvement of the "Standard" connection (Figure 3-63) from which it differs because the steel angle plate has not a stiffener and on the column side it has a horizontal slotted hole to allow for in-plane relative horizontal displacements.

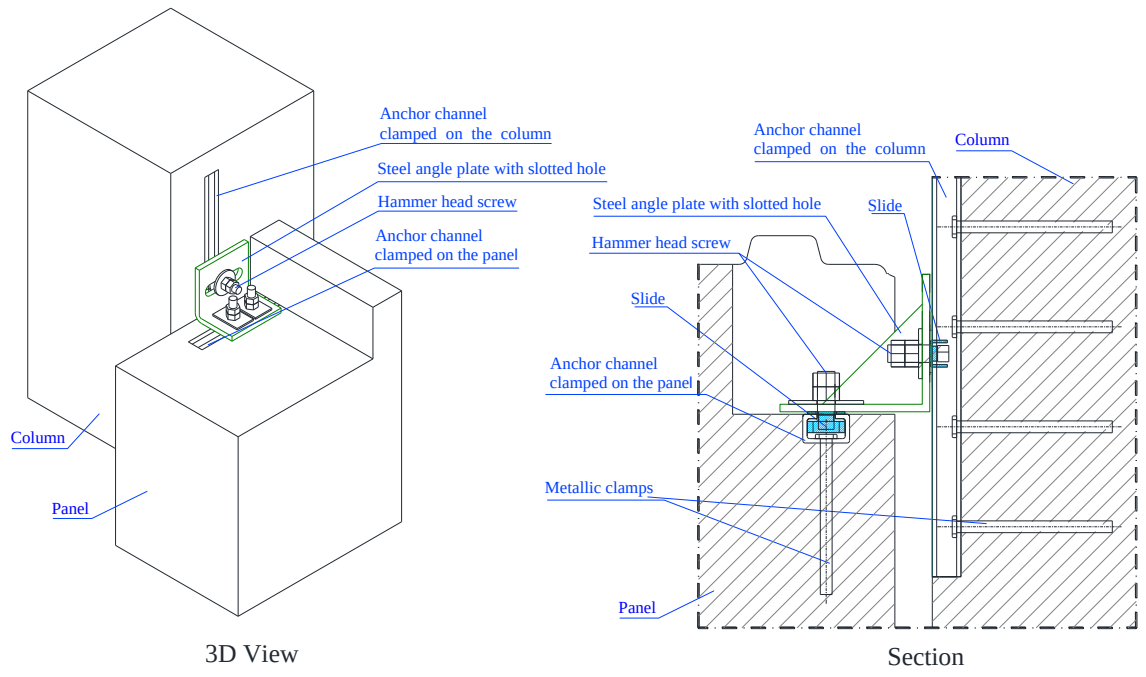

Figure 3-63: Layout of a "SismoSafe" connection between a horizontal panel and a column.

For vertical panels, the "Standard" connection consists of a steel strap (hammer-head strap), a washer, a sliding block, a hammer-head bolt, and two steel channels with anchors, which are pre-installed (Figure 3-64) in the panel and in the beam or column to which the panel is fixed. The strap is fastened to the channel on the structural element side by means of a hammer-head bolt with a washer, but the sliding block prevents it from locking, leaving the bolt free to slide inside the channel profile. Finally, the head of the strap is fixed inside the channel on the panel side.

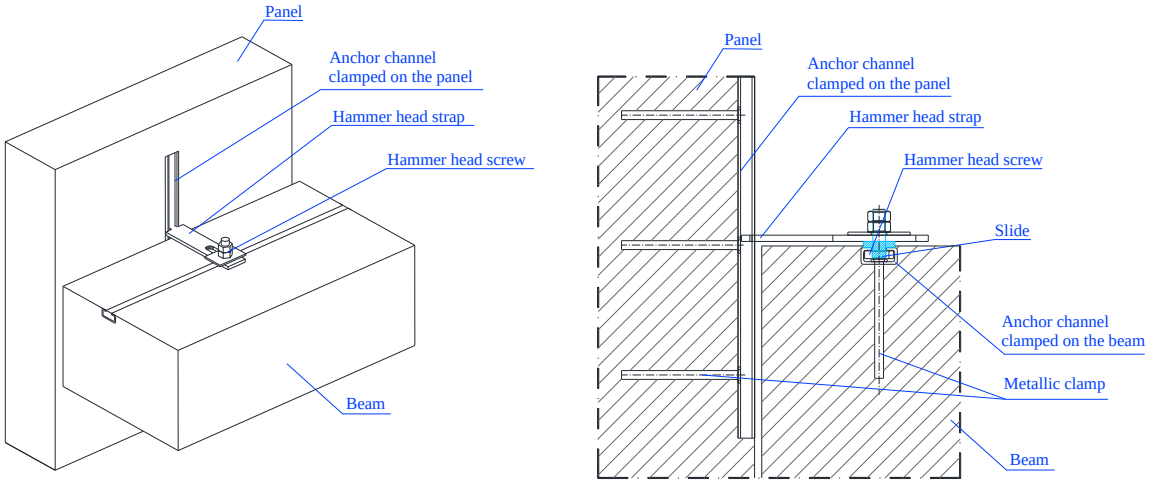

Figure 3-64: Layout of a "Standard" connection between a vertical panel and a beam.

The "SismoSafe" connection of vertical panels has a completely different fastening apparatus. It consists of two vertical steel channel profiles fixed on the panel before it is cast. Inside these two channels a sliding block, to which a mobile guide rail is welded, can slide vertically. The profile of the movable guide rail is suitable to receive a fixed guide rail, which in turn is fixed to the beam through two self-tapping screws (Figure 3-65).

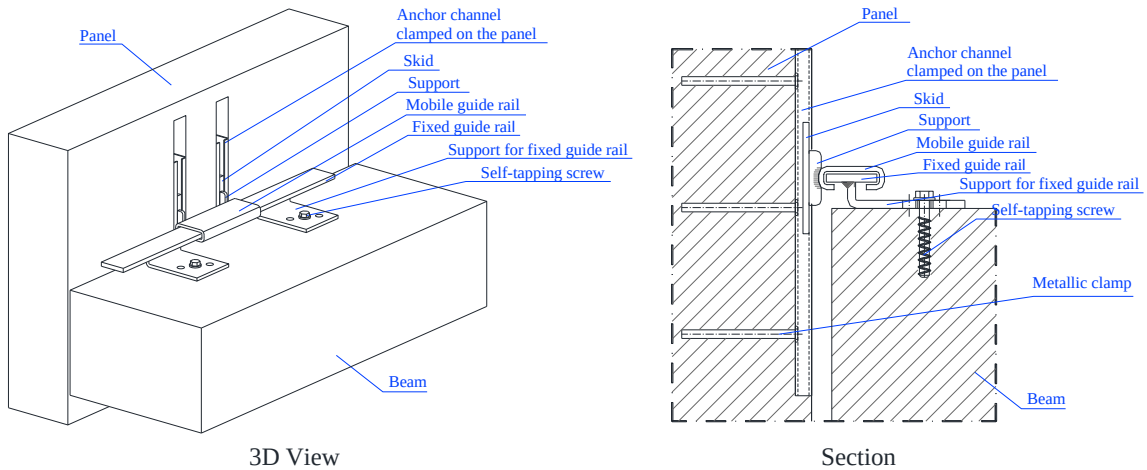

Figure 3-65: Layout of a "SismoSafe" innovative connection between a vertical panel and a beam

The configuration of TA devices, both for "Standard" and "SismoSafe" joints, is identical to vertical panels, with the only difference that the face of the beam, where the connections are fixed, is inclined by an α angle (equal to the slope of the roof) with respect to the horizontal.

Regardless of the in-plane stiffness of the roof system, whether it is rigid or flexible, the mobile guide rail of "SismoSafe" connections have a clearance of about 10 mm to compensate for deflections of support beams in the roof plane. However, the out-of-plane deformation of beams should be limited in the design. The authors checked that the 10mm clearance was sufficient for the structural system for which connections were designed, even if different structures may require different values of the clearance

3.5.2 Experimental results

With the aim of analysing the behaviour of connections, forces acting on them were evaluated from data measured during tests.

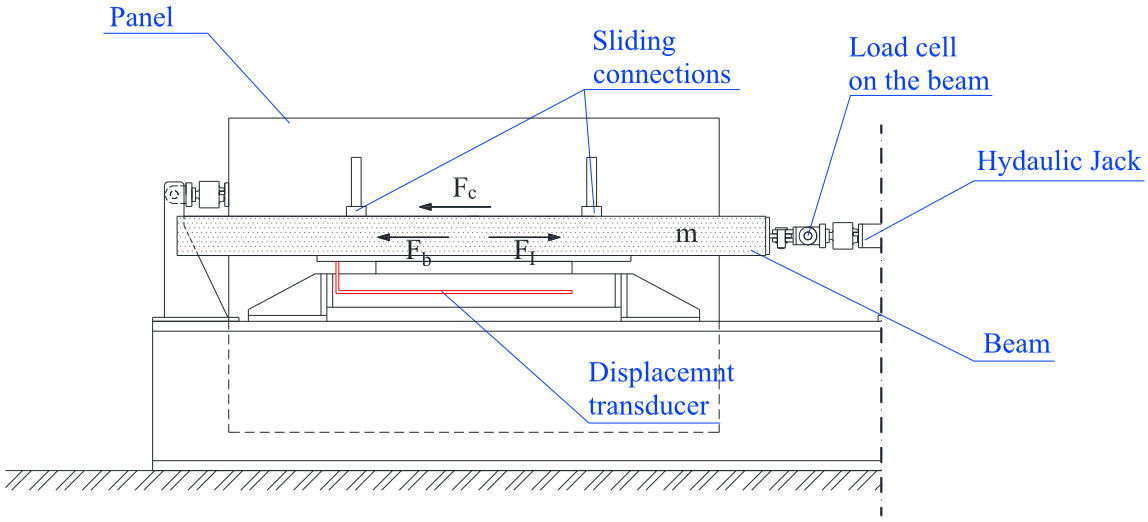

Figure 3-66: Forces acting on the connection and the beam.

With reference to Figure 3-66, the force F_c acting on the connection can be calculated through the equilibrium of forces:

$$F_c = F_I - F_b \quad (3.28)$$

where:
F_c is the force on the connection,
F_I is the inertial force of the moving beam,
F_b is the force on the beam measured by the load cell.

The inertial force can be calculated through the equation:

$$F_I = m \cdot \ddot{x} \quad (3.29)$$

where:
m is the beam mass,
$\ddot{x}$ is the moving beam acceleration calculated starting from the displacement measured on the beam and getting its derivative twice with respect to time by using the central difference method.
For horizontal panels, the "Standard" connection (test F17_01) showed a hysteretic behaviour (see the force-displacement curve in Figure 3-67). During the test, the rotation and the sliding inside the channel of the steel angle plate were only visible initially at small displacements. At larger displacements, deformations of the angle plate were observed together with a considerable cracking of the concrete and deformations of the channel fixed to the column. A

further increase of displacements resulted in an increase of the damage of the concrete around the channel on the column side, and in a growth of plastic deformations of the channel. Due to the rotation of the angle plate, some compression forces arose at one edge of the angle in contact with the column and, for equilibrium, tension forces arose in the hammer-head screws. The failure of the connection typically occurred due to the failure of the channel fixed to the column. The hammer-head screw was pulled out of the channel (Figure 3-68). Despite the presence of sliding blocks under the screws, only a limited sliding of the angle plate was observed.
The stiffness of the steel angle connection is not negligible, and it should be considered in the global analysis of the structure before as well as after yielding of the connection.

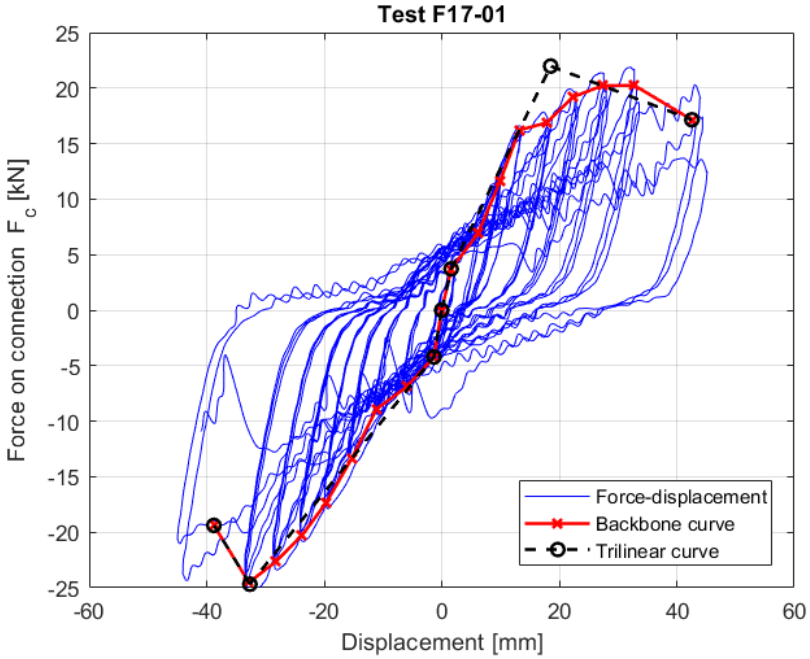

Figure 3-67: Test F17-01 (horizontal panel with "Standard" connection): force-displacement curve.

Figure 3-68: Test F17-01: the collapse of the anchor channel.

The graph in Figure 3-67 shows the connection hysteretic behaviour, the backbone curve and its trilinear approximation for the test F17_01. Each point of the backbone curve is calculated as the average force in the three displacement cycles having the same amplitude. For the trilinear approximation on the positive side, equations of each branch are expressed in the form $y = m \cdot (x - x_1) + y_1$ (being x the force in the connection in Newton and y the displacement in mm):
1st branch:

$$y = 2.31x \quad (3.30)$$

2nd branch:

$$y = 1.07(x - 1.60) + 3.71 \quad (3.31)$$

3rd branch:

$$y = -0.20(x - 18.54) + 21.98 \quad (3.32)$$

The behaviour of the connection is almost the same on the positive and negative side. The not perfect symmetry is due to slight imperfections of the test setup during the loading phase.
A similar connection (Figure 3-69) was studied at the University of Ljubljana (UNI-LJ), as the same typology tested at the University of Florence (UNIFI), a bolted angle tied together channels mounted in the panel and in the beam. The study developed at UNI-LJ is reported in (Isaković et al., 2013).

Figure 3-69: Angle connection tested at UNI-LJ (Isaković et al., 2013)

By comparing the result obtained at UNIFI and at UNI-Lj it is possible to see that the hysteretic behaviour of the two connectors is quite similar even if they are made by two different producers (Figure 3-70).

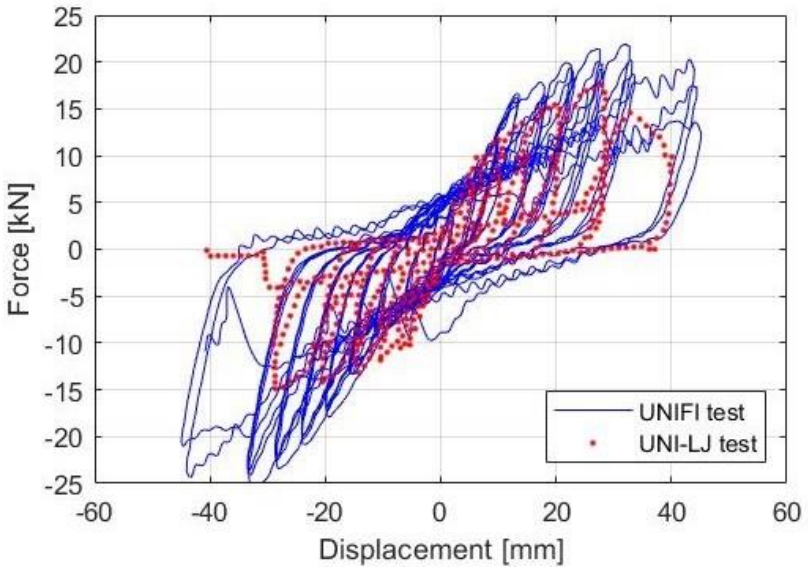

Figure 3-70: Comparison between test F17_04 (UNIFI and test P2.3-27 (UNI-LJ)

In the "SismoSafe" connection for horizontal panels (test F14_01), the angle plate, on the column side, is provided with a horizontal slotted hole along the direction of the shear force, so the connection showed to be able to slide without damaging neither the angle plate nor the channel profile. Therefore, the force transmitted by this connection is mainly due to the friction that arises, during sliding, between the steel angle and the bolt washer. Nevertheless, in this case the slotted hole should be larger than the imposed displacement to avoid that the bolt shank comes in touch with the hole contour and the behaviour changes from friction to hysteretic.

The friction force can be represented through its coefficient μ calculated dividing the force on the connection F_c by the out-of-plane force imposed by the weight F_w (Figure 3-71):

$$\mu = \frac{F_c}{F_w} \qquad (3.33)$$

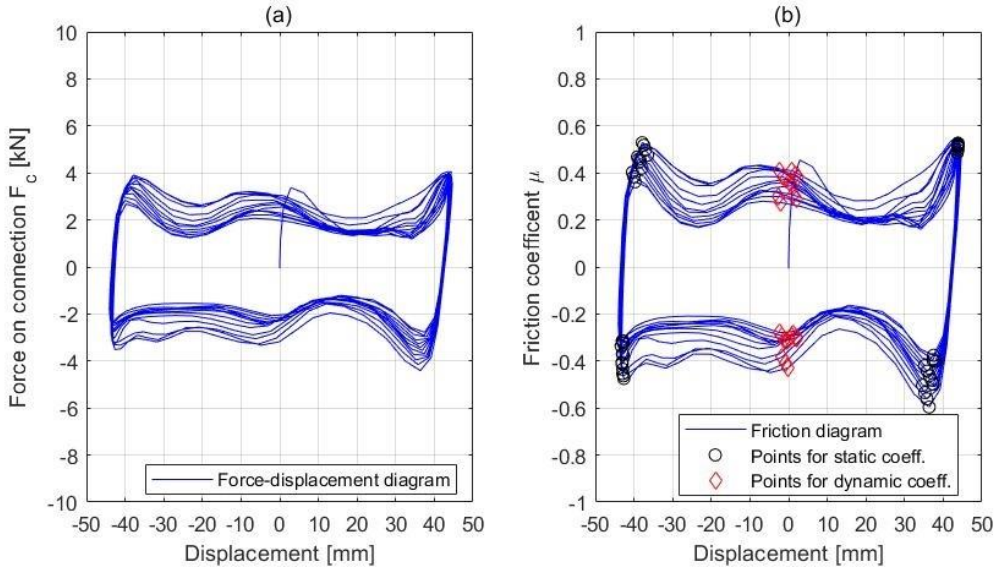

Figure 3-71: Test F14-01 (horizontal panel with "SismoSafe" connection): (a) force-displacement curve;(b) friction-displacement curve.

From the diagram, the two friction coefficients μ_s and μ_d are evaluated. The first is calculated at points where the absolute value of the acceleration is maximum, i.e. when the displacement is maximum d_{max} or minimum d_{min}; the second is calculated at points where the velocity is maximum or at points where the displacement is zero with respect to the reference system d_0 (Figure 3-72). For test F14-01, the friction coefficients had the following average values:

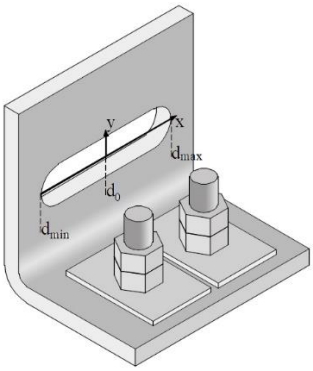

$$\mu_s = 0.45$$
$$\mu_d = 0.33 \qquad (3.34)$$

Figure 3-72: Definition of d_{max} and d_{min} displacements.

Figure 3-73 shows the main failure mechanisms of vertical panels with the "Standard" connection when subjected to shear loading (test F16_04). During the test, the metallic strap did not rotate around the fastening bolt due to its tightening torque and the sliding in the beam channel did not occur, so the strap showed a hysteretic behaviour also at relatively low displacements (10 mm). At a displacement of 20 – 30mm, the yielding of the strap occurred in the narrow part just below its head. Finally, the connection failed due to flexural failure of the neck of the strap. In all tests on this type of connection, the gap between the beam and panel never closed before the failure of the strap or of the channel. However, it was noticed that, due to very large rotations, straps pulled the panel against the beam, and if the gap between the panel and the beam was not large enough to accommodate out-of-plane relative displacements, the gap closed and friction between the panel and the beam was activated. Consequently, the stiffness of the connection widely increased.

Figure 3-73: Test F16_04 (vertical panel with "standard" connection): the collapse of the neck of the hammer-head strap.

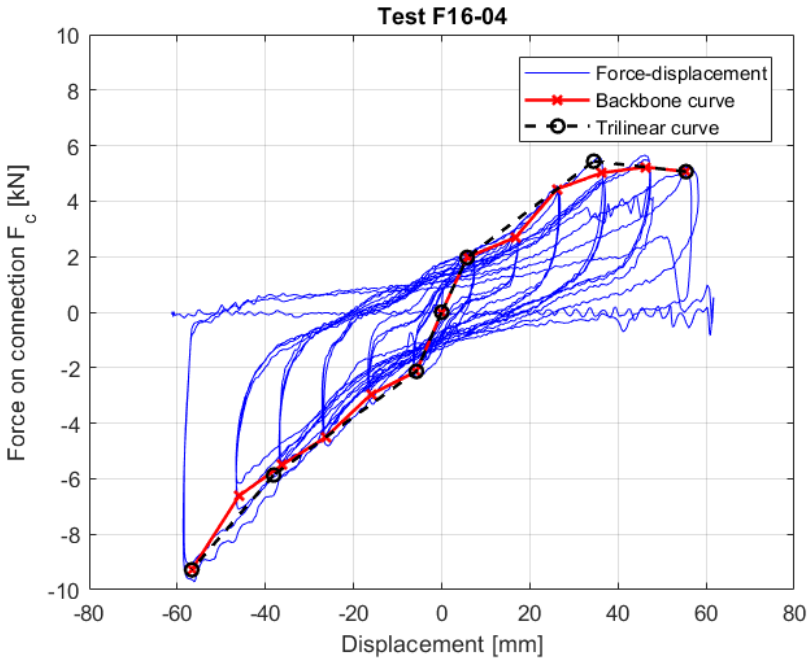

Figure 3-74: Test F16-04 (vertical panel with "standard" connection): force-displacement curve.

The graph in Figure 3-74 shows the connection hysteretic behaviour, the backbone curve and its trilinear approximation of test F16_04.

For the trilinear approximation, equations of each branch on the positive side are (x - force on the connection in N, y - displacement in mm):
1st branch:

$$y = 0.34x \quad (3.35)$$

2nd branch:

$$y = 0.12(x - 5.76) + 1.97 \quad (3.36)$$

3rd branch:

$$y = -0.01(x - 34.48) + 5.43 \quad (3.37)$$

As already illustrated before for horizontal panels' connection devices, also in this case a similar connection (Figure 3-69) was studied at the University of Ljubljana (UNI-LJ), as the same typology tested at the University of Florence (UNIFI), a bolted angle tied together channels mounted in the panel and in the beam. The study developed at UNI-LJ is reported in (Isaković et al., 2013)

Figure 3-75: Hammer-head strap connection tested at UNI-LJ (Isaković et al., 2013)

By comparing the result obtained at UNIFI and at UNI-Lj it is possible to see that the hysteretic behaviour of the two connectors is quite similar in term of stiffness even if they are made by two different producers (Figure 3-76).

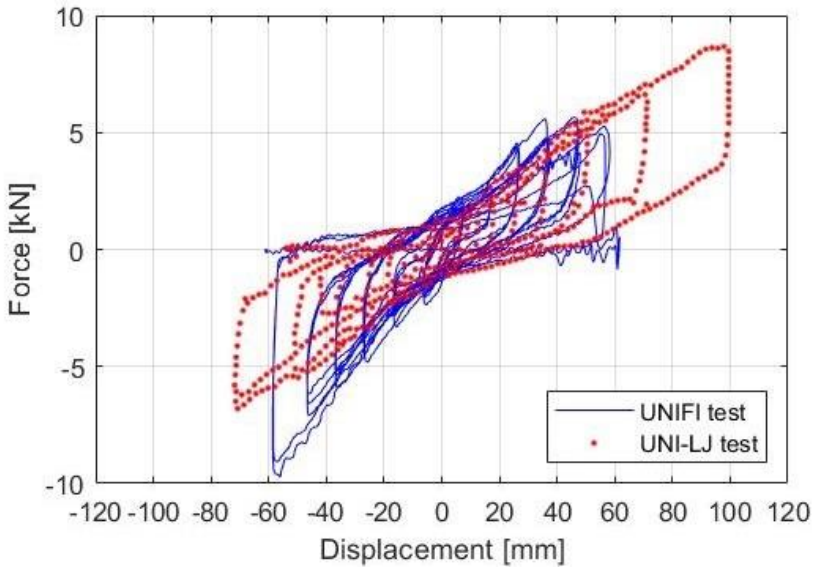

Figure 3-76: Comparison between test F16_04 (UNIFI and test P3.2-10 (UNI-LJ)

In the "SismoSafe" connection for vertical panels (test F15_04), the mobile guide rail mounted on the panel can slide along the fixed guide rail mounted on the beam; the connection did not show any damage on the sliding components and channel profiles. Therefore, the force transmitted by this connection is mainly due to the friction which arose during sliding, between the two guide rails. That force can be represented through its static and dynamic friction

coefficients.

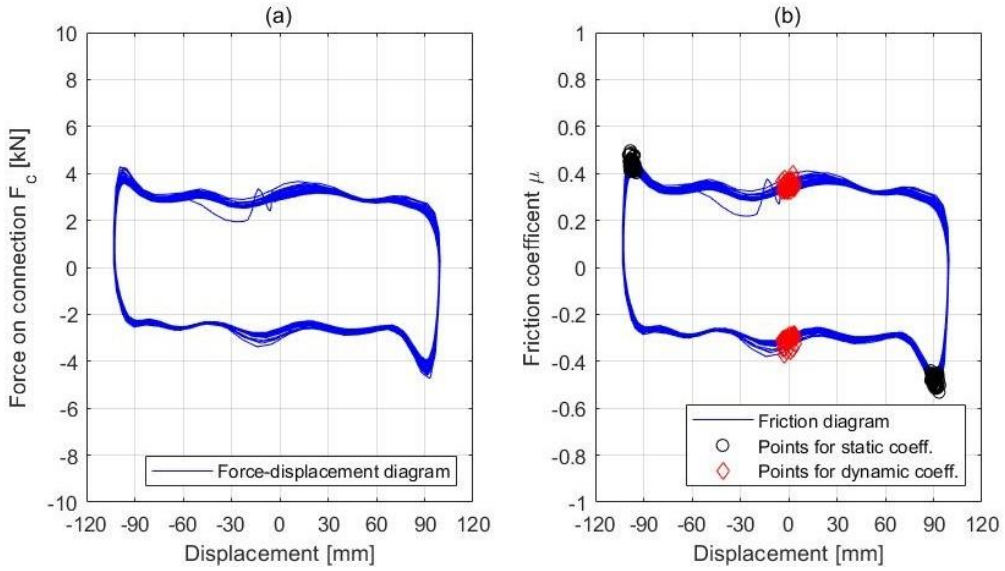

Figure 3-77: Test F15-04 (vertical panel with "SismoSafe" connection): (a) force-displacement curve; (b) friction-displacement curve.

From the force-displacement curve (Figure 3-77), the static μ_s and dynamic μ_d friction coefficients are evaluated. Again, the first is calculated at points where the acceleration modulus is maximum, i.e. when the displacement is maximum d_{max} or minimum d_{min}; the second is calculated at points where the velocity is maximum or the displacement is zero with respect to the reference system d_0 (Figure 3-78). For this test, friction coefficients had the following average values:

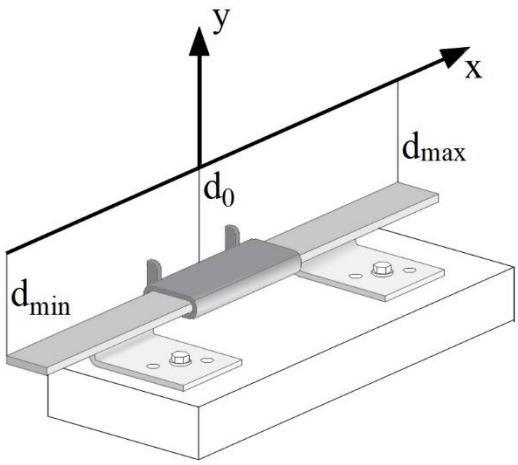

$$\mu_s = 0.46 \qquad \mu_d = 0.32 \qquad (3.38)$$

Figure 3-78: Vertical panel with "SismoSafe" connection: identification of d_{max} and d_{min} displacements.

The following Figure 3-79 shows the main failure mechanism of metallic straps (test F06_04) in "Standard" connections of vertical panels with an inclined roof tile when they are subjected to a shear loading. The behaviour of the connection is qualitatively the same as the horizontal ones (test F16_04). At a displacement of 20 – 30mm, the yielding of the strap occurs in the narrow part just below its head. Finally, the connection fails due to flexural failure of the strap. The gap between the beam and panel never closed before the failure of the strap or the channel.

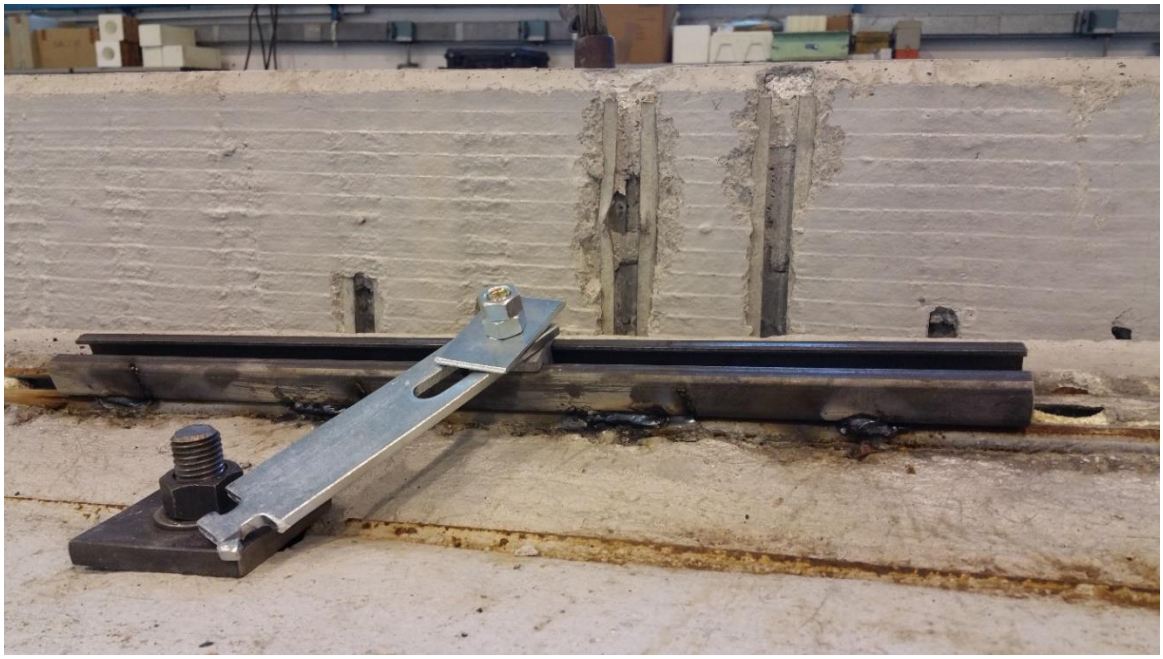

Figure 3-79: Test F06-04: failure of the hammer-head strap.

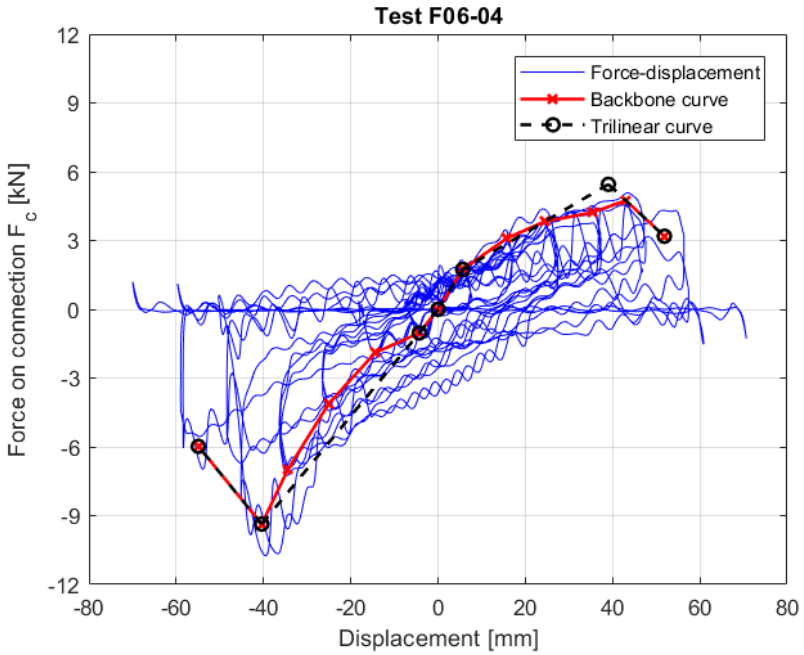

Figure 3-80: Test F06-04 (panels jointed to a tile roof beam with "standard" connection): force-displacement curve.

Figure 3-80 shows the connection hysteretic behaviour, the backbone curve and its trilinear approximation. Equations of each branch of the trilinear approximation on the positive side are (x - force on the connection in Newton, y - displacement in mm):
1st branch:

$$y = 0.30x \quad (3.39)$$

2nd branch:

$$y = 0.11(x - 5.64) + 1.74 \quad (3.40)$$

3rd branch:

$$y = -0.17(x - 39.03) + 5.44 \quad (3.41)$$

Even if the hysteretic behaviour is approximately the same as connections without inclination, both in forces and displacement, the graph shows a much noisier trend due to the vertical displacement of the straps.
In "SismoSafe" connections used to connect vertical panels to the inclined top face of a roof tile (AT), the mobile guide rail was fixed to the panel and the fixed guide rail on the inclined top face of the beam. Besides two displacement transducers, d_{v1} and d_{v2} were installed on the mobile guide rail of the two SismoSafe devices to evaluate the connection possibility to move in the vertical direction (Figure 3-81a, b).

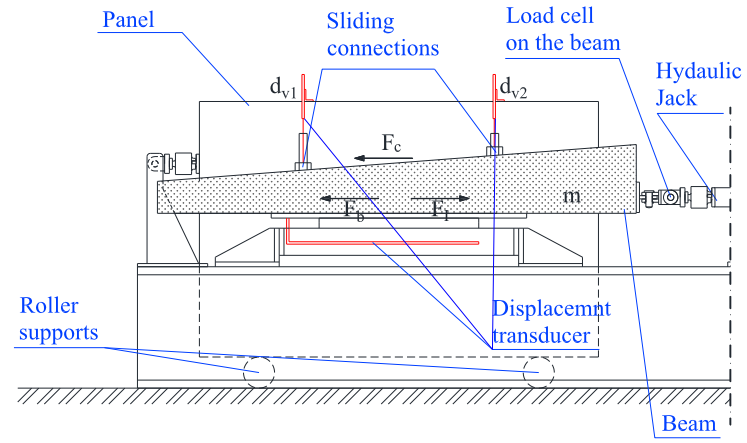

(a)

(b)

Figure 3-81: Test setup with the inclined beam (a) and (b); and forces acting on the connection and the beam and the two vertical displacement transducer d_{v1} and d_{v2}.

In this case, the connection did not show any damage either on sliding components or channel profiles. The force transmitted by this connection is mainly the friction force which arises,

during sliding, between the two guide rails. In that case friction coefficients, calculated as described above and represented in Figure 3-82, hold:

$$\mu_s = 0.44$$
$$\mu_d = 0.35 \quad (3.42)$$

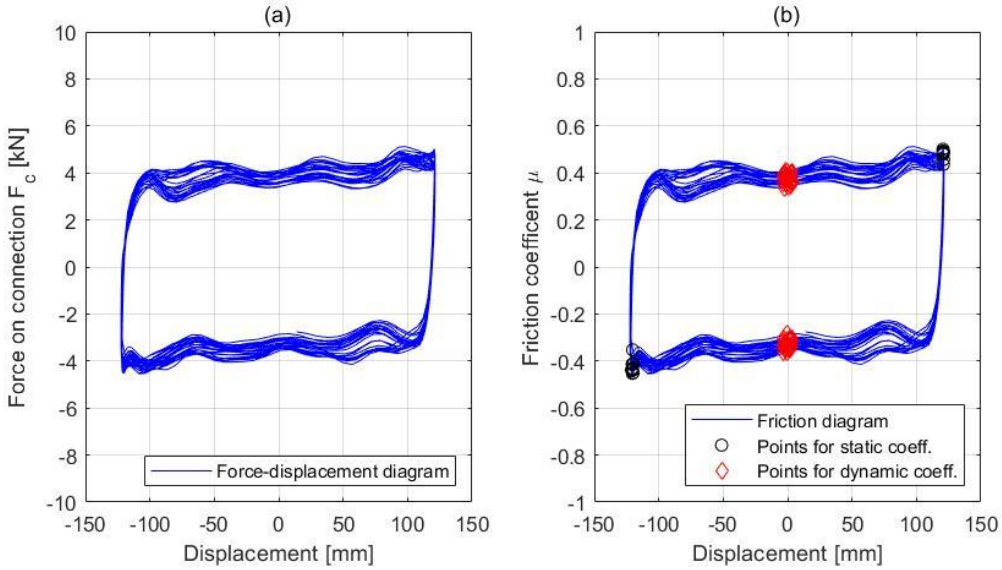

Figure 3-82: Test F13-04 (panels jointed to a tile roof beam with "SismoSafe" connection): (a) force-displacement curve; (b) friction-displacement curve.

During the cyclic test F13-04, the mobile guide rail showed the possibility to move vertically, within the anchor channels installed on the panel, without suffering any damage as confirmed by the displacement recording of the two transducers d_{v1} and d_{v2} (Figure 3-83).

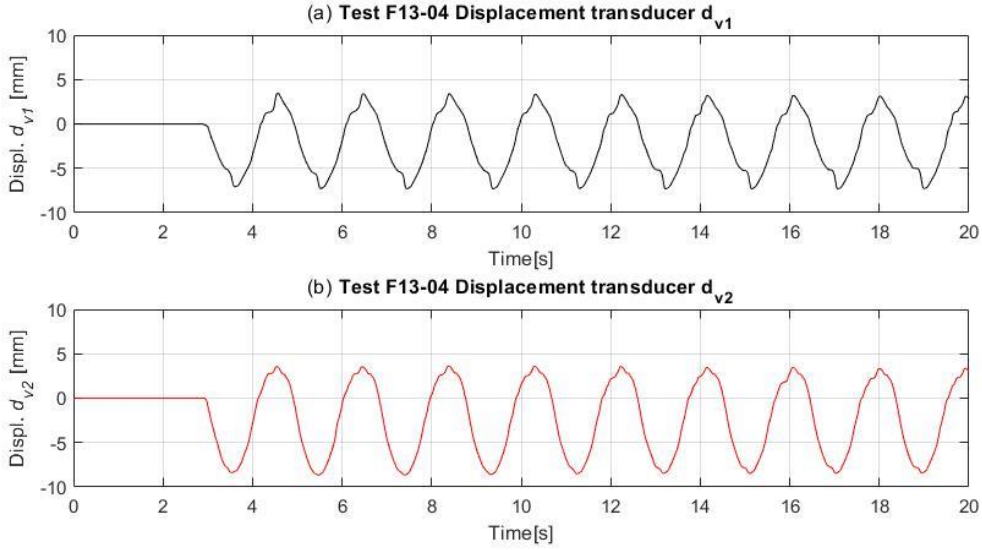

Figure 3-83: Recorded displacement at transducer d_{v1} (a) and d_{v2} (b)

For tests that showed friction behaviour, it can be worthy to emphasize the friction coefficient trend during the cycles. For each test, two sets of points can be identified in the cycle-friction coefficient μ) plane: one for the static friction coefficient s and the other for the dynamic friction coefficient μ_d. Each point of the two sets is calculated as the mean of the absolute values of the four points per cycle for s or two points per cycle for μ_d. To gather a mean trend of friction coefficients during cycles, the least-squares method was used, whose regression lines are shown in Figure 3-84:

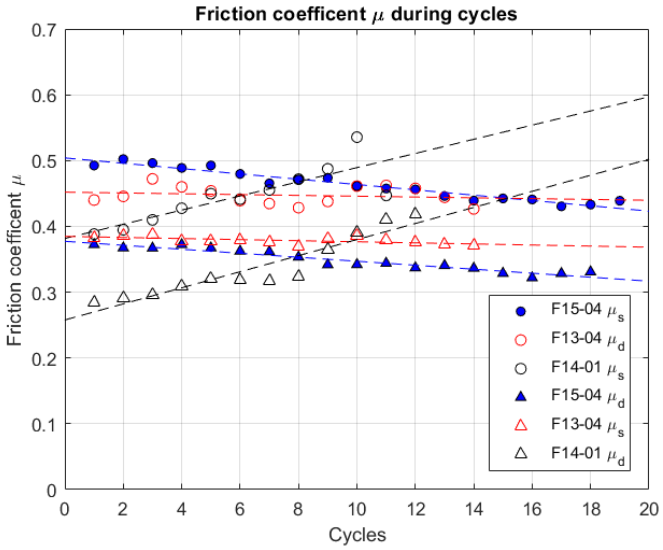

Figure 3-84: Friction coefficient-cycle curves for HP (test F14_01), VP (test F15_04) and AT (test F13_04) connections.

For tests F15_04 and F13_04, both static and dynamic friction coefficients showed a decrease with time due to the wear of contact surfaces between the mobile and fixed guide rails.
For test F14_01, both friction coefficients showed an increase with time because during the cyclic sliding the bolt washer underwent a deep-drawing deformation, which significantly increased friction forces.

3.5.3 Conclusions

An experimental campaign on dry joints of both horizontal and vertical cladding panels to precast structures was carried out at the University of Florence. The experimental campaign concerned more than 60 tests on 20 different typologies of mechanical joints, some of which were chosen among available in-use commercial joints (called "Standard") and some others (called "SismoSafe") were designed by the author in collaboration with Baraclit company. Collected experimental data allowed for the cyclic response of each tested mechanical joint to be assessed. Tests confirmed those critical issues of "Standard" devices highlighted by recent Italian earthquakes. They are able to uncouple in-plane displacements of the cladding system and the structure but they have quite limited displacement capacity. They show hysteretic behaviour until the collapse typically due to the flexural failure of the strap, in the narrow part just below the head, or to the failure of the anchor channel installed on beams or columns and the expulsion of the hammer-head screws. Moreover, the results for "Standard" connections test were compared with the result obtained from experimental camping conducted at the University of Ljubljana on the same type of connection. The comparison shows that the connections tested, both in Florence and in Ljubljana, showed the same stiffness but different displacement capacities. This may be due to the fact that the connections, although similar, are made by two different producers.

Experimental tests highlighted that proposed innovative joints are able to uncouple in-plane displacements of cladding panels and the main structure with grater displacement capacity than the "Standard" one. These new devices, patented by the company Baraclit S.p.A. and called "SismoSafe WALL", did not show significant damage in their metallic components during all the tests, thanks to very low friction forces. Values of the friction static coefficient μ_s were about 0.45, while dynamic ones μ_d were in the range 0.32 - 0.35.
"SismoSafe" joints are slightly more expensive but oriented in favour of greater structural safety. However, the increase in costs is limited because "SismoSafe" connections do not need pre-installed elements on the beam (with a reduction of labour costs, too) and, since they have a higher capacity against out-of-plane loads than traditional joints, a lower number of fixing devices is required for each panel.

4 Out-of-plane vertical panels behaviour

Within the experimental campaign carried out at the University of Florence, the in-plane displacement capacity of commercial steel hammer-head strap connections (called "Standard" in the following) and of innovative ones (called "SismoSafe") was investigated. However, during a seismic event, the panels have also to sustain out-of-plane actions that stress the connections. In the design phase, the panel-structure connections are generally considered to be rigid due to out-of-plane forces and therefore dimensioned taking into account their resistance capacity instead of displacement one. To understand what was the resistance capacity for out-of-plane actions of both for "Standard" (Figure 4-1a) and "SismoSafe" (Figure 4-1b), connections for vertical panel layout, a series of tests were carried out within the experimental program above mentioned.

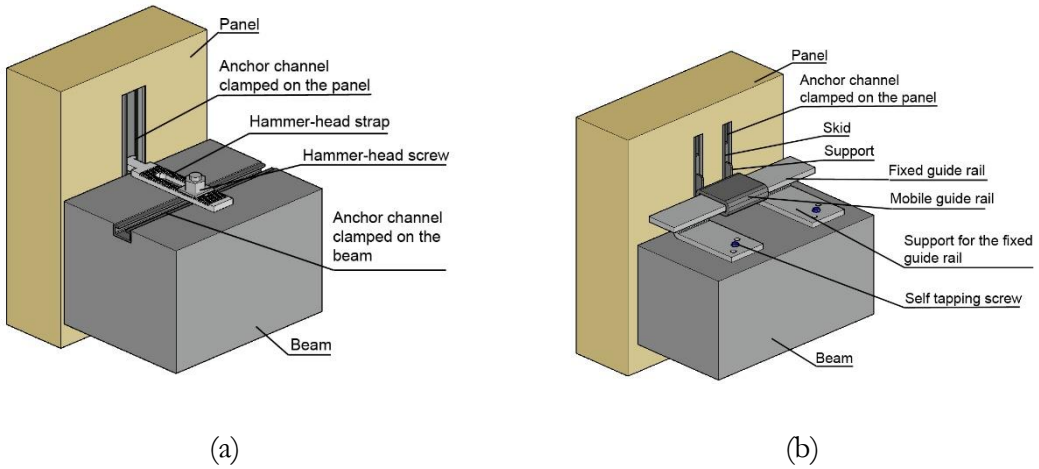

(a) (b)

Figure 4-1: The hammer-head strap "Standard" connection (a) and the SismoSafe connection (b)

To define a design rule for out-of-plane forces and then determine the demand that these connections require during a seismic event, a parametric analysis was conducted on a simplified structure model. The force that out-of-plane stress the connections was determined as a function of the mass and stiffness of the structure, once the characteristics of the panel have been established.

4.1 Experimental campaign

During a seismic event, panel-to-structure connections should accommodate relative displacements between panels and the main structure, but they should also support out-of-plane forces. In the design phase, these connections are generally considered to be rigid in the out-of-plane direction, along with they are dimensioned considering their resistance capacity. To assess the out-of-plane resistance capacity of both Standard and SismoSafe devices, a series of tests were carried out.

The experimental campaign consisted of 30 tests: 6 tests were performed on Standard devices and 24 tests on SismoSafe devices. The large number of tests on SismoSafe devices was needed to identify a suitable geometry, with special attention to the curvature of the fixed guide rail supports and the welding length, to avoid the brittle failure of devices. In the present work, only the 6 tests on devices with the final geometry are illustrated and discussed. For each type, both monotonic and cyclic load time-histories were considered.

- *Type of device*. Standard or SismoSafe
- *Side of the connection*. For each device both the connection to the cladding panel and the connection to the beam were tested.

Table 4-1 lists the six tests on Standard devices and the six tests on SismoSafe devices with the final geometry. The designation of each test has been chosen to easily identify the connection tested ("P" for panel connection, "B" for beam connection), the type of device ("St" for Standard device, "Sismo" for SismoSafe device) and the loading type ("M" for monotonic loading, "C" for cyclic loading); moreover, a digit (1 or 2) identifies the first or the second test performed on the same connection under the same input motion type, monotonic or cyclic.

Number of tests	Test designation	Connection side	Type of device
3	P_St_M1, P_St_C1, P_St_C2	Panel	Standard
3	B_St_M1, B_St_C1, B_St_C2	Beam	Standard
3	P_Sismo_M1, P_Sismo_C1, P_Sismo_C2	Panel	SismoSafe®
3	B_Sismo_M1, B_Sismo_M2, B_Sismo_C1	Beam	SismoSafe®

Table 4-1: Summary of tests

4.1.1 Connection components and measurements

Hammer-head strap

The hammer-head "Standard" strap used within the experimental campaign had the size depicted in Figure 4-2 and it was made with steel S 275 JR: yield strength f_y = 275 MPa; Ultimate strength f_u = 430 MPa

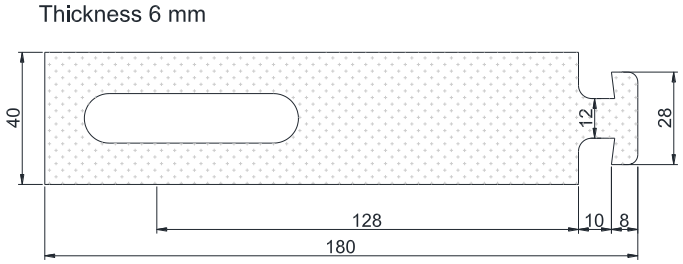

Figure 4-2: Geometry of the hammer-head "Standard" connection used during the test

The hot-rolled anchor channel used during the test had the geometry illustrated in Figure 4-3.

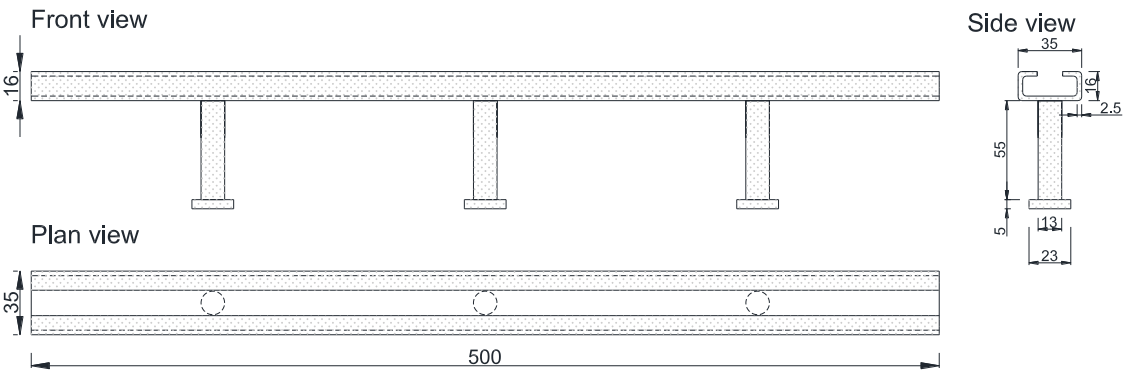

Figure 4-3: Geometry of the hot-rolled anchor channel used during the test

SismoSafe device

The fixed guide rail of the SismoSafe device was made with steel S 275 JR and the geometric features are described in Figure 4-4.

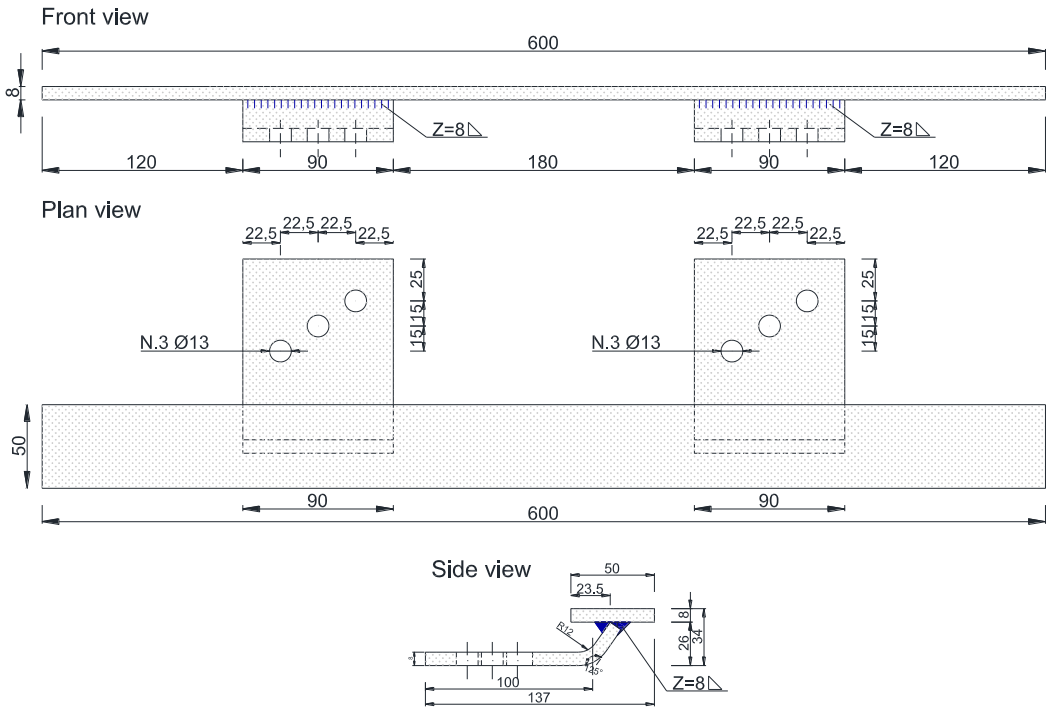

Figure 4-4: Geometry of the fixed guide rail

The mobile guide rail of the SismoSafe device was made with steel S 275 JR and the geometric features are described in Figure 4-5.

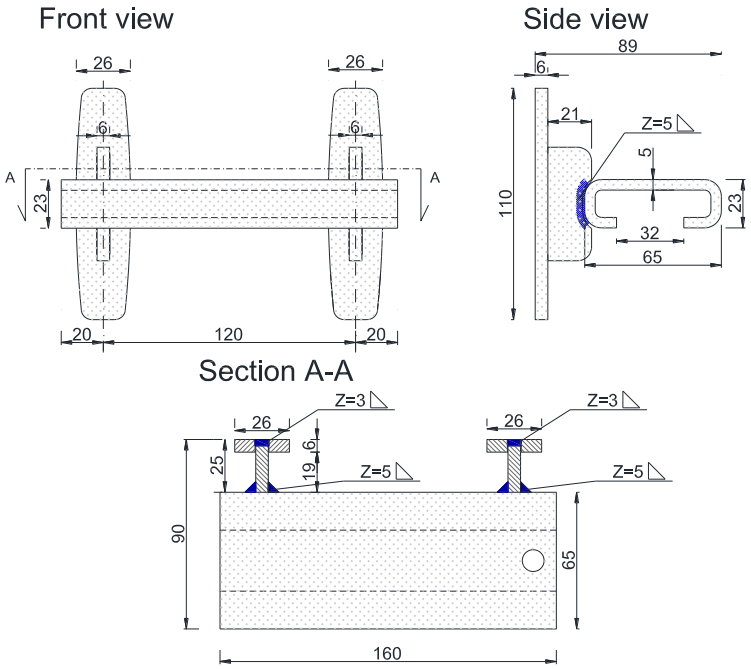

Figure 4-5: Geometry of the mobile guide rail

4.1.2 Experimental setup

The test setup consists of the following elements (Figure 4-6):

- the specimen (RC beam or panel) suitably equipped with channel profiles to host the connection device;
- a hydraulic jack;
- a steel sleeve to join the tested device to the hydraulic jack;
- a load cell mounted on the hydraulic jack.

Each panel or beam specimen was fixed to the testing apparatus, which was formed by an MTS machine with a loading capacity of 500 kN. The hydraulic jack was placed closer to the specimen, as the crosshead could be moved up and down by lowering or lifting the extendable columns. All tests were performed under displacement control.

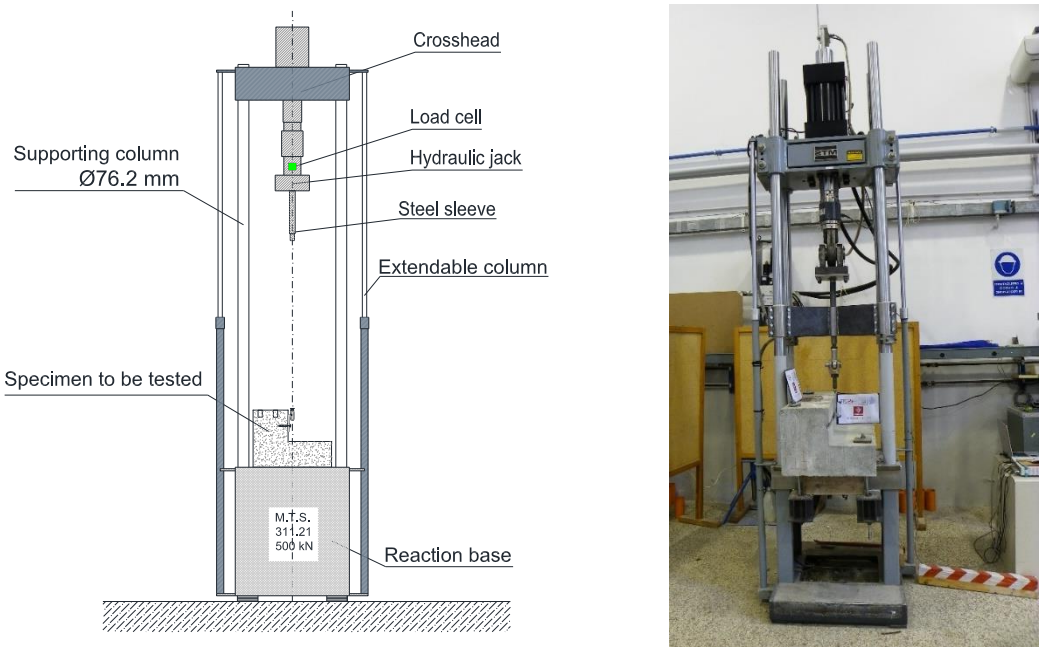

Figure 4-6: M.T.S. 311.21 testing apparatus

4.1.3 Experimental tests

To evaluate the maximum capacity of connections, both monotonic (Figure 4-7a) and a cyclic (Figure 4-7b) test was performed under displacement control. The cyclic tests consisted of groups of three cycles of the same amplitude, with subsequent increment Δd between two successive groups up to the ultimate connection capacity. The amplitude d_1 of the first group was taken as 1/20 of the maximum expected displacement; the amplitude increment Δd from one group of cycles to the subsequent group was taken equal to d_1.

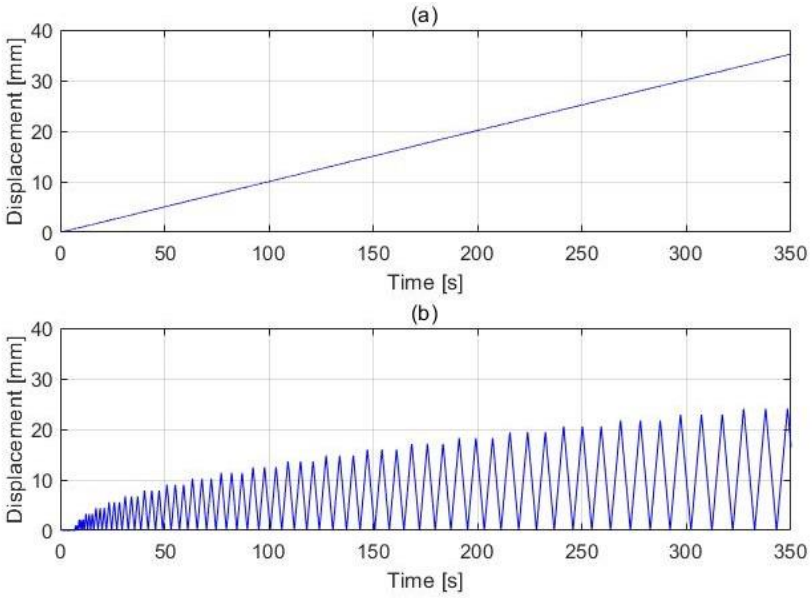

Figure 4-7: Applied displacement history: three cycles of increasing amplitude (a) and constant increasing displacement (b)

In the cyclic displacement history, the amplitude d_1 of the first group, as well as the increase Δd between one cycle and the next, was assumed equal to 1 mm. For monotonic tests, a very low relative velocity of 0.1 mm/s was used to exclude as much as possible dynamic effects, while during cyclic tests a value of 5 mm/s was chosen as it is of the same order of magnitude of the maximum relative velocity registered in real one-story precast buildings under medium seismic excitation. The adopted value of 5 mm/s is also close to the relative velocities between cladding panels and the main structure provided by the numerical model of the case study presented within this work for different seismic inputs. Figure 4-8. shows the specimens of a Standard connection ready for the test, while Figure 4-9. shows the specimens of a SismoSafe connection.

(a) (b)

Figure 4-8. Experimental test setup: P_St_M (a) and B_St_M (b).

(a) (b)

Figure 4-9. Experimental test setup: P_Sismo_C1 (a) and B_Sismo_M1(b).

For the panel connections of Standard devices, the hammer-head strap, provided with a welded end bolt fixed to the testing apparatus, was inserted in a hot-rolled anchor channel pre-installed on the panel specimen (Figure 4-10a). For the beam connection of Standard devices, the hammer-head strap was fixed to the testing apparatus by means of a bolt welded on the hammer-head side. On the other side, the strap was fastened to the beam specimen through a hammer-head bolt which was inserted into a channel profile previously installed on the beam. The hammer-head bolt was provided with a slide to prevent the locking in the channel profile (Figure 4-10b).

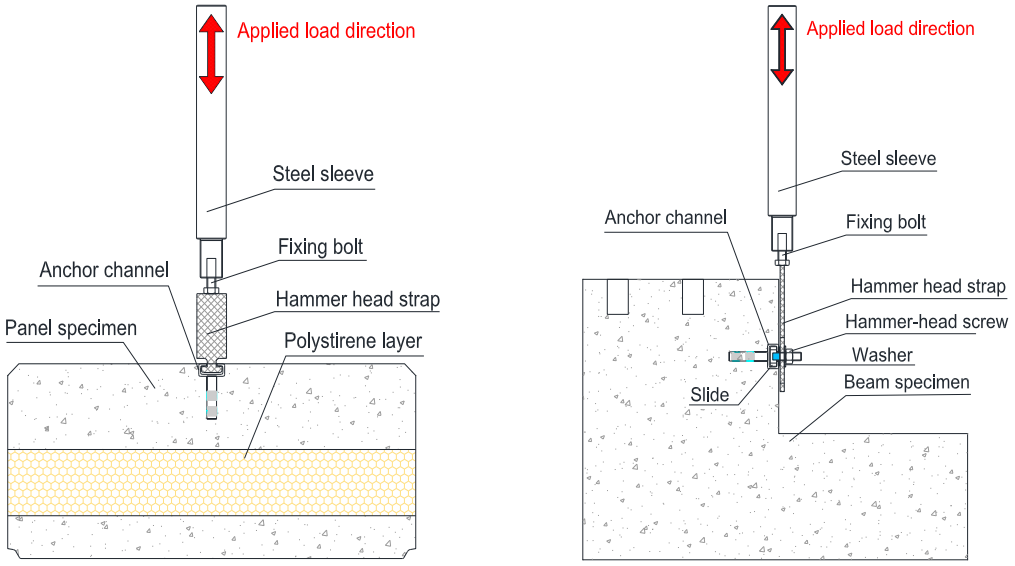

(a) (b)

Figure 4-10: Layout test of a Standard connection for vertical panels to evaluate the resistance on the panel side (a) and on the beam side (b).

Concerning the test setup for panel connections of SismoSafe devices, the mobile guide was mounted on the panel specimen by inserting the two skids in the pre-installed hot-rolled anchor channel profiles, and the mobile guide had a welded bolt that was screwed into the test apparatus connection sleeve (Figure 4-11a).
For beam connections, the fixed guide was installed on the beam specimen by means of two self-tapping screws. Then the mobile guide was mounted on the fixed guide. The mobile guide was provided with a welded bolt to fix onto the test equipment (Figure 4-11b).

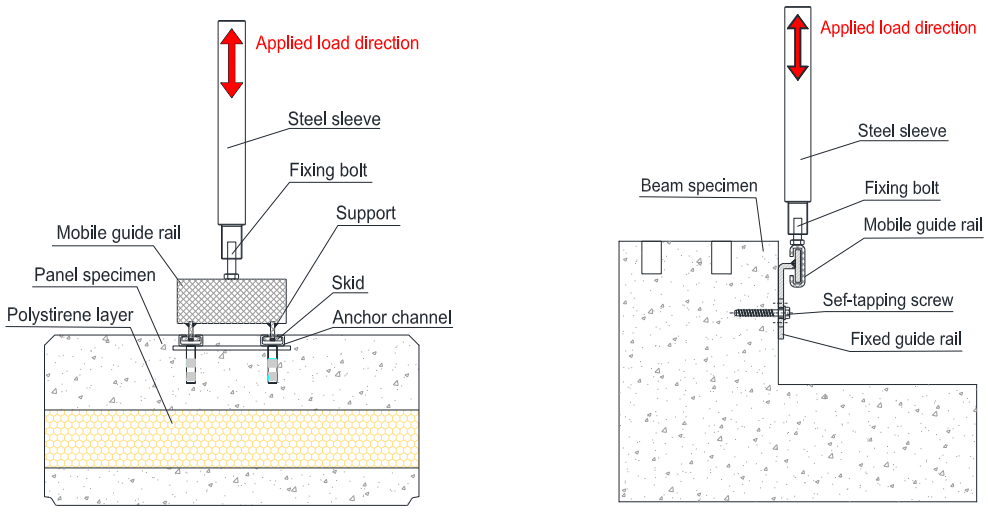

(a) (b)

Figure 4-11: Layout test of a SismoSafe connection for vertical panels to evaluate the resistance on the panel side (a) and on the beam side (b).

4.1.4 Experimental result.

The Standard devices showed initially a quite stiff behaviour on the panel side: the stiffness was about 3500 kN/m (Figure 4-12a). During the monotonic test (P_St_M), some cracks started to appear on the concrete around the fixing point of the steel strap at the displacement of 3÷4 mm. As the imposed displacement increases, cracks become wider until the complete detachment of the concrete surface layer (about 10 mm). Then, the channel profile began to bend upwards until the head of the steel strap opens the edges of the anchor channel profile (Figure 4-12b). During the cyclic test (P_St_C1 and P_St_C2) initially a rather rigid elastic branch was observed. By increasing the amplitude of the cyclic displacement some cracks began to appear around the channel profile, gradually extending along the whole length. Later, the concrete surface layer (about 10 mm) detached and the channel profile was bent, alternately upwards and downwards, by the cyclic load. Finally, the channel profile was detached from the concrete due to the failure of its fastening clamps (Figure 4-12c, d).

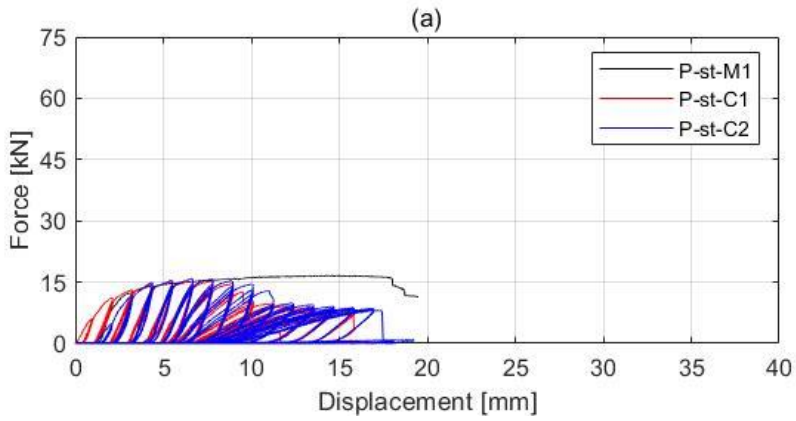

(b) (c) (d)

Figure 4-12: Standard connection test on panel side: force-displacement relationship (a) anchor channel edge failure in monotonic test P_St_M1 (b). Anchor channel clamps failure in cyclic test P_St_C1 (c) and P_St_C2 (d)

The maximum values of forces and displacements of each test are listed in Table 4-2.

Test label	Displ. time history	F_{max} [kN]	d_{max} [mm]
P_St_M1	Monotonic	16.62	14.21
P_St_C1	Cyclic	15.22	6.57
P_St_C2	Cyclic	15.84	6.59

Table 4-2: Maximum values for P_St_M, P_St_C1 and C2 tests

The beam connection also exhibited a rather rigid elastic behaviour, the stiffness was approximately equal to 4000 kN/m (Figure 4-13a). During the monotonic test (B_St_M), the displacement of 1-2mm, some semi-circular cracks started to appear on the concrete around the fixing point of the steel strap. With the increase of the imposed displacement, the strap began to bend around the hammer-head fixing bolt. The inflexion became larger and larger below the bolt washer until the slide pushed against the anchor channel edge, opening it and detaching the steel strap from the beam (Figure 4-13b).
In the cyclic test (B_st_C1 and B_st_C2) the behaviour was similar to the monotonic test with the formation of semi-circular cracks on the concrete around the hammer-head fixing bolt on the channel profile. The cyclic load effect caused the anti-lock slide to push against both edges of the channel profile, opening them and causing the slide to break into two parts. The steel strap was thus detached from the beam (Figure 4-13c, d).

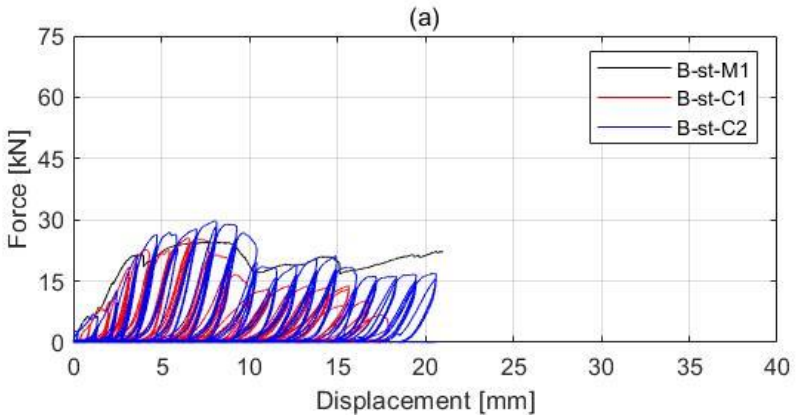

(b) (c) (d)

Figure 4-13: Standard connection test on the beam side: force-displacement relationship (a) anchor channel edge failure in monotonic test B_St_M1 (b). Anchor channel opening and slide failure in cyclic test B_St_C1 (c) and B_St_C2 (c)

The maximum values of forces and displacements for each test are listed in Table 4-3.

Test label	Displ. time history	F_{max} [kN]	d_{max} [mm]
B_St_M1	Monotonic	24.64	7.47
B_St_C1	Cyclic	25.60	6.55
B_St_C2	Cyclic	29.80	9.88

Table 4-3: Maximum values for B_St_M, B_St_C1 and C2 tests

The SismoSafe device showed on the panel connection a stiffer behaviour than the Standard type, as the stiffness was equal to 9830 kN/m, about 2.8 times higher (Figure 4-14a). During the monotonic test (P_Sismo_M), after the elastic phase, some cracks started to arise on the concrete between the two anchor channels in the transversal direction. Cracks developed from the point where the two slides of the mobile guide rail were inserted into the channel profile, when the displacement increased, cracks also developed outside the two anchor channel profiles. Later, the welding between the fixing clamps and the channel profile reached the failure. The anchor channels were lifted upwards by the applied force and were progressively detached from the panel (Figure 4-14b).
In the cyclic tests (P_Sismo_C1 and P_Sismo_C2) the behaviour was completely like the monotonic test with the formation of cracks in the concrete around the fixing skids of the mobile guide. The load cyclic effect bent the two anchor channel profiles upwards and downwards causing the welding failure between the fixing clamps and the channel profile. Finally, both anchor channels were torn off from the concrete (Figure 4-14c, d).

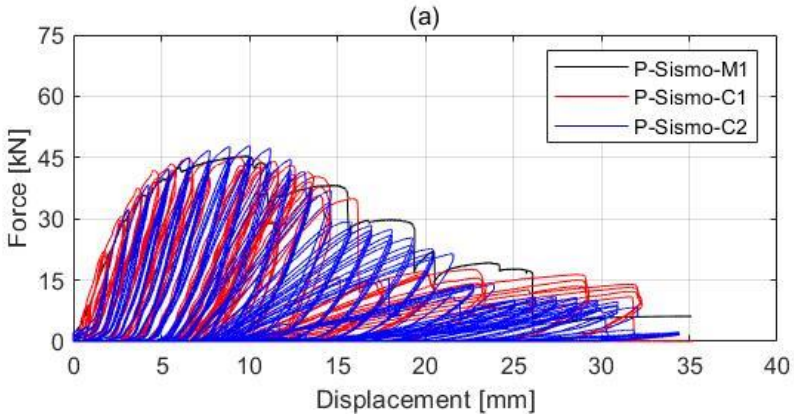

(b) (c) (d)

Figure 4-14: SismoSafe connection test on the panel side: force-displacement relationship (a) anchor channel clamps failure in monotonic test P_Sismo_M1 (b). Anchor channel clamps failure in cyclic test P_Sismo_C1 (c) and P_Sismo_C2 (d)

The maximum values of forces and displacements for each test are listed in Table 4-4. It is worth noting that the maximum force values are about three times higher than Standard devices (see Table 4-2).

Test label	Displ. time history	F_{max} [kN]	d_{max} [mm]
P_Sismo_M1	Monotonic	45.42	10.57
P_Sismo_C1	Cyclic	45.16	9.84
P_Sismo_C2	Cyclic	47.84	11.31

Table 4-4: Maximum values for P_Sismo_M, P_Sismo_C1 and C2 tests

The beam connection of the SismoSafe devices was more rigid than the panel connection (about 11775 kN/m), as shown in Figure 4-15a.
During the monotonic test (B_Sismo_M1 and B_Sismo_M2), no crack developed in the concrete not even around the self-tapping fixing screws. The fixed guide rail was dragged by the displacement imposed on the mobile guide rail and it was bent upwards. As the displacement increased, it was possible to observe an opening of the edges of the mobile guide rail. Due to its increasing opening, in the end, the mobile guide rail was slipped out from the fixed guide (Figure 4-15b).
In the cyclic test (B_Sismo_C) the behaviour was the same as the monotonic test. The cyclic effect of the load caused the fixed guide to bend both downwards and upwards and the failure occurred due to the bending of the bolt fixing the mobile guide rail to the test apparatus (Figure 4-15c, d).

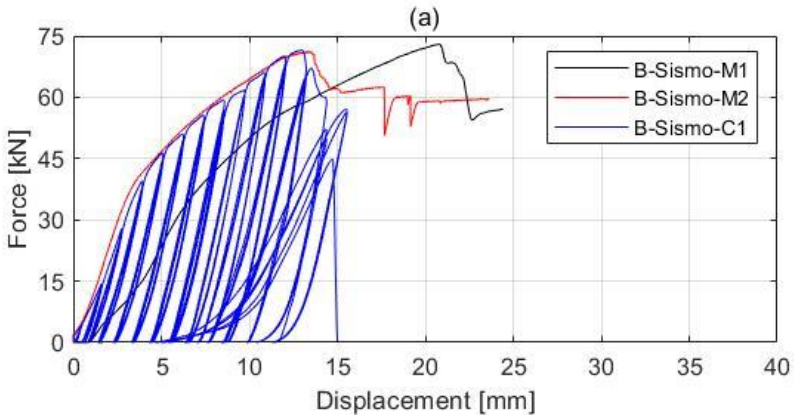

(b) (c) (d)

Figure 4-15: Test on a SismoSafe beam connection: force-displacement relationship (a) fixed guide upward bending (b) mobile guide edge opening (c) and fixing bolt deflection (d)

The maximum values of forces and displacements for each test are listed in Table 4-5.
The maximum force values are about double times higher than Standard devices (see Table 4-3).

Test label	Displ. time history	F_{max} [kN]	d_{max} [mm]
B_Sismo_M1	Monotonic	72.96	20.76
B_Sismo_M2	Monotonic	71.27	13.86
B_Sismo_C1	Cyclic	71.50	13.42

Table 4-5: Maximum values for B_Sismo_M1, B_Sismo_M2 and C tests

4.2 Case study

A case study is presented to investigate the seismic behaviour of SismoSafe connections in a one-storey precast industrial building. The study is aimed at understanding the distribution of out-of-plane seismic forces on SismoSafe connections. The interaction between the cladding panels and the main structure is investigated considering the in-plane friction forces transmitted by the connections or neglecting the friction. The four among the strongest seismic events which struck the Italian territory in the last 12 years and caused significant damage to the RC precast structures were considered in the numerical analysis (Ercolino et al. 2016, Savoia et al. 2017).

4.2.1 Building geometry

The case study of an industrial building with a rectangular plan of dimensions 69.36x36.62m ad fixed panels is considered (Figure 4-16). It is made of precast RC columns and beams, prestressed RC roofing beams and vertical RC cladding panels.
Columns are 10.30 m high, while vertical cladding panels are 11.40 m high, so they cover the roof elements, as shown in the front views of the building in Figure 4-16. The building was designed according to Eurocode 2 (EN 1992-1-1, 2004) and Eurocode 8 (EN 1998-1-1, 2005) adopting C40/50 grade concrete and S500 steel grade with ductility class C for reinforcing bars.
Each roof beam had a dead weight 5.4 kN/m, according to the specification provided by the producers. Considering that the structure had 24 roof beam each 18.31m long, the total dead weight is 24·5.5·18.31=2373 kN. By dividing the total dead weight by the roof area the distributed dead weight is obtained: 2373/(36.62·69.36)=0.93 kN/m^2. The secondary roof elements are made of lightened vault shell elements. They have a dead weight of 0.1 kN/m^2; moreover, a super dead load due to electrical/hydraulic systems of 0.11 kN/m^2 is considered.

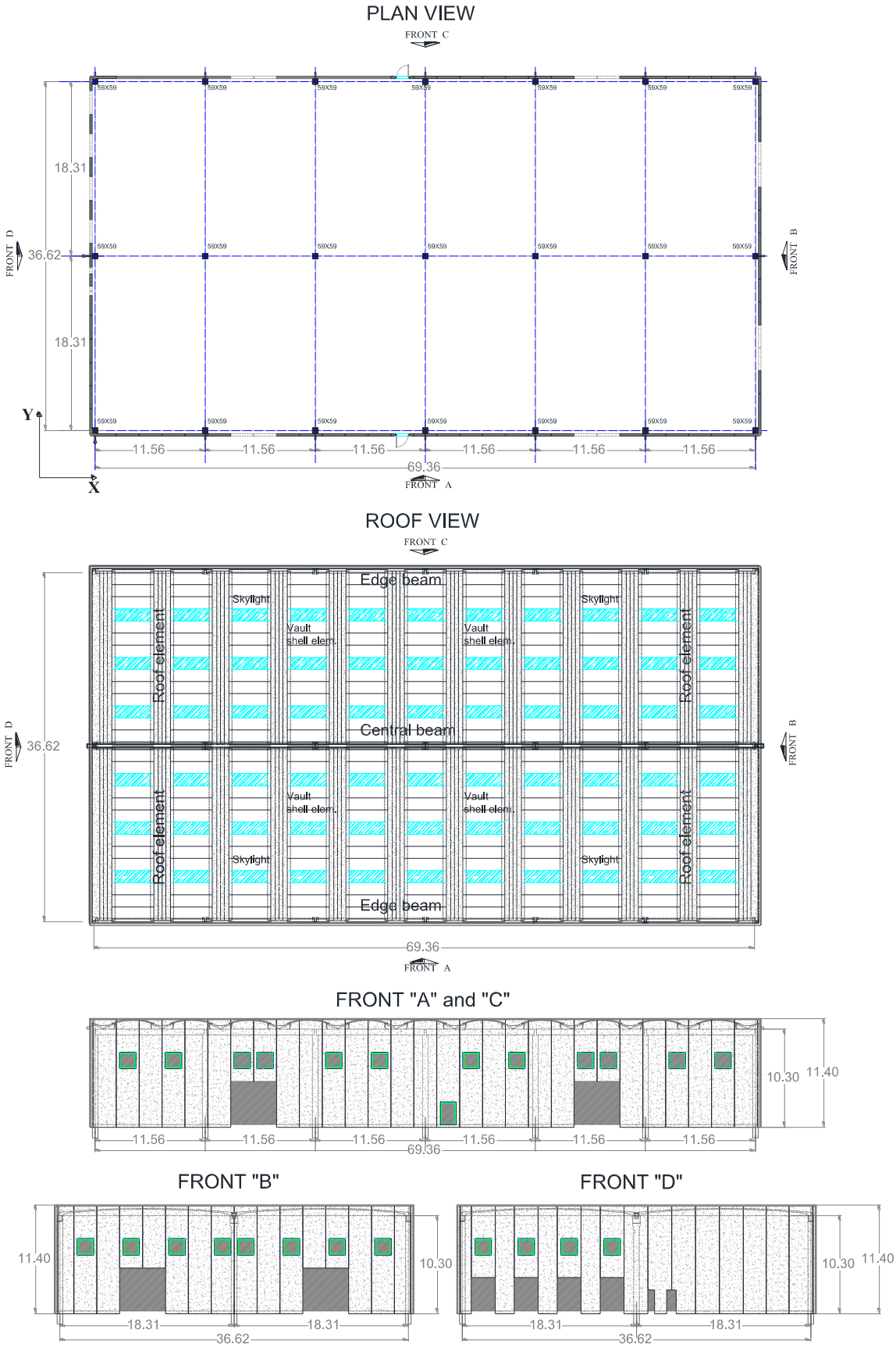

Figure 4-16: Building plan and front views

The cross-sections of the main structural element, with their weight per unit length, are described in Figure 4-17, which also reports the material characteristics.

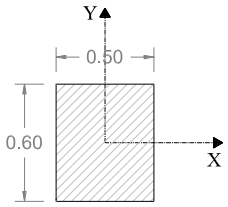

Edge beam (7.50 kN/m)

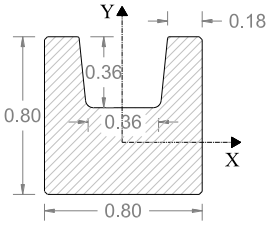

Central beam (10.3 kN/m)

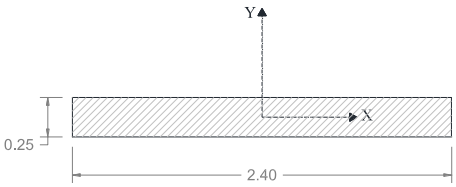

Vertical cladding panel (3.10 kN/m^2)

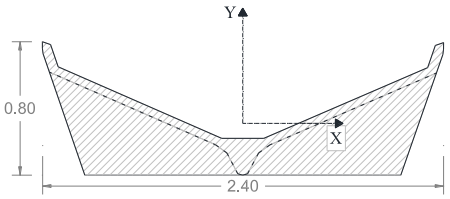

Wing-shaped roof element (5.40 kN/m)

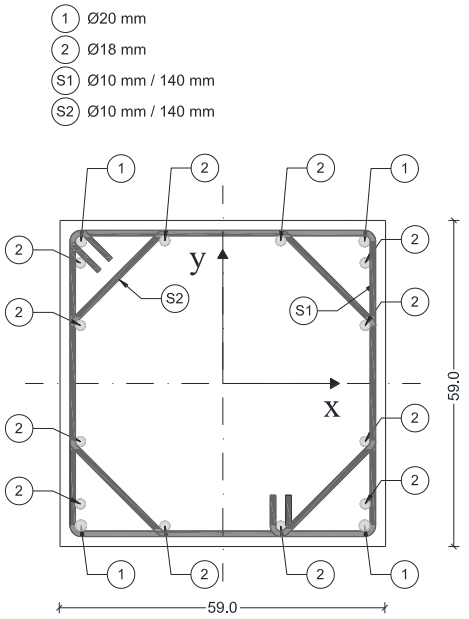

Column (8.70 kN/m)

Materials

Reinforcements: S500 steel
Concrete: C 40/50

Figure 4-17: Cross-sections of main structural elements with their weight per unit length

The RC columns are fixed at the base in socketed footings; at the top, they are connected to the beams through pinned connections. The vertical cladding panels, at the base, are hinged in the out-of-plane direction and fully restrained in their plane. At the top, they are connected to the beams with SismoSafe devices shown in the previous Figure 4-1b.
Each end of the roof-beam is placed on a cast-in-situ mortar bed and connected to the main beam through two steel angle plates, one on each side of the end section. Each angle plate is fixed to the main beam through a hammer-head bolt, inserted in an anchor channel profile, so that its positioning is adjustable, while the angle plate is fixed to the roof beam through a fixing bolt (Figure 4-18).

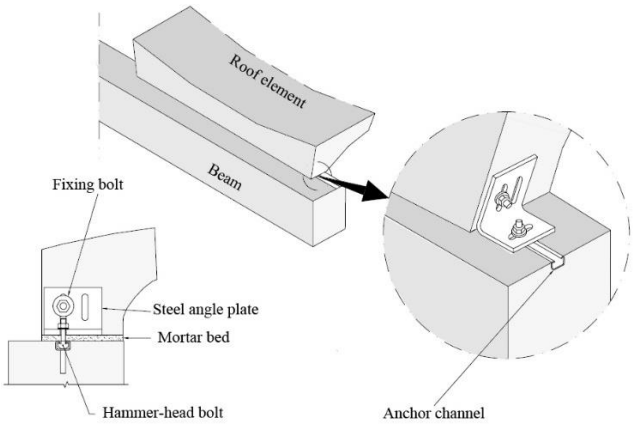

Figure 4-18: Beam-roof element connection, courtesy of (Mandelli Contegni et al., 2007)

The two connections not only restraint the displacements of the end section of the roof beam with respect to the main beam, but also its rotation in the horizontal plane, through the transmission of a couple of shear forces; according to Belletti, Gasperi, & Spagnoli (2015), the connection can be defined as a hyper-static connection. Due to the double connection of each end section of the roof beams, under longitudinal seismic loading the relative displacement between the edge frames and the central frame is opposed by the flexural stiffness of the double-fixed roof beams (Figure 4-19a), while for transversal seismic loading the roofing system behaves as a Vierendeel beam (Figure 4-19b). IBC (IBC, 2018) states that diaphragms are rigid for distribution of story shear and torsional moment when the ratio of the lateral deformation of the diaphragm and the average of the story drift is less than or equal to two. In the present case, considering the strongest among the selected ground motions, the ratio is equal to 0.052 in the longitudinal direction and to 0.116 in the transversal direction, therefore the roof diaphragm can be assumed to be rigid. The high in-plane stiffness of the roof can cause high horizontal shear forces in the roof beams connections under horizontal seismic load (Figure 4-19c); nevertheless, in all the numerical analyses, those shear forces never exceeded the resistance of the connections. The presence of a rigid roofing system allows for the seismic loads to be distributed proportionally to the stiffness of the columns, which are subjected to the same shear and bending moment. Therefore, the most vulnerable columns are the corner ones, which are subjected to the lowest axial forces.

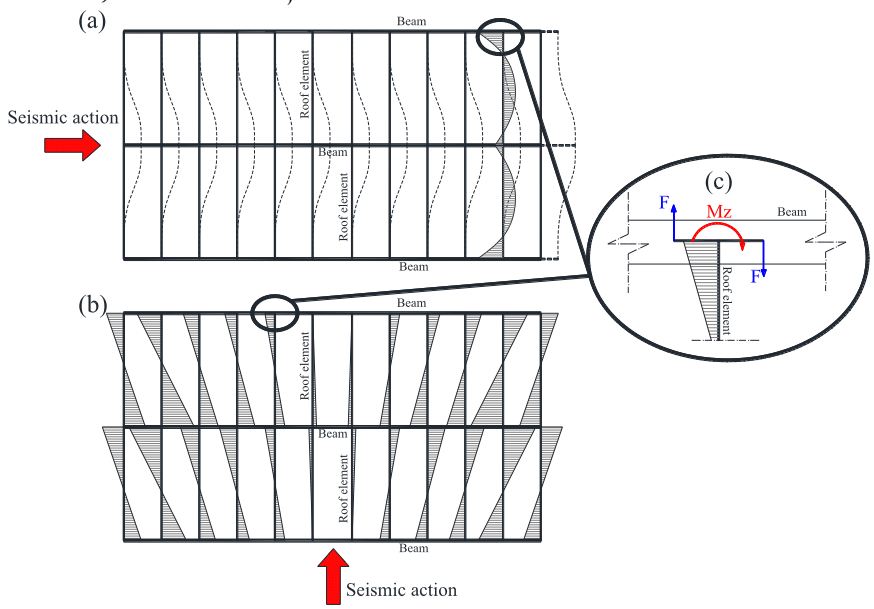

Figure 4-19: Bending moment distribution in the roof beams due to longitudinal (a) or transversal (b) seismic loading and horizontal shear forces in the connections (c)

4.3 Numerical model

The numerical model was created using the OpenSees software (Mazzoni et al., 2006a). All prismatic elements were modelled with elastic elements, except for the columns, which were modelled using fibre elements since they are the main location of the inelastic behaviour of the structure. The non-linear behaviour of the column elements is monitored at 3 control sections (Gauss-Lobatto integration sections) that are, in turn, discretized into longitudinal steel and concrete fibres. The non-linear section behaviour, thus, derives from the integration of the non-linear stress-strain behaviour of the fibres. The constitutive relationships used in the model for the concrete and steel rebars are illustrated in Figure 4-20. For columns, the stirrup confinement effect was considered through the confinement effectiveness factor α provided by Eurocode 8 (EN 1998-1-1, 2005). Considering the column geometry and reinforcements depicted in Figure 4-17, α holds 0.63, then the confining pressure σ_2 is equal to 0.95 N/mm^2 and substituting in the expression of $f_{ck,c}$ provided by EN 1992-1-1 (EN 1992-1-1, 2004), the ratio K between the resistance of confined ($f_{ck,c}$) and unconfined (f_{ck}) concrete is equal to $K = f_{ckc}/f_{ck} = 1.1$.

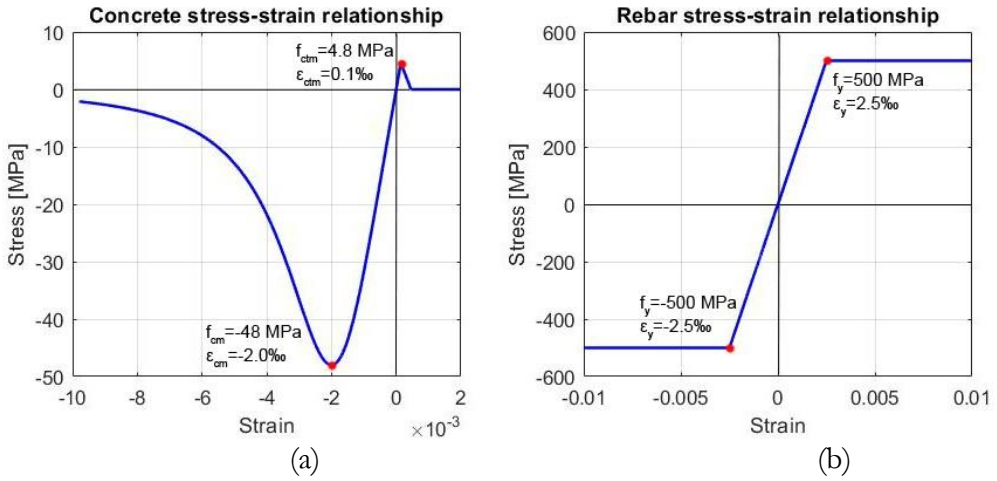

Figure 4-20: Mander model (Mander et al., 1988) for concrete (a) and elasto-plastic model for rebar (b)

The SismoSafe panel-to-structure connections are modelled through link elements. At the base, the columns are fully fixed, as well as the panels(Figure 4-21).

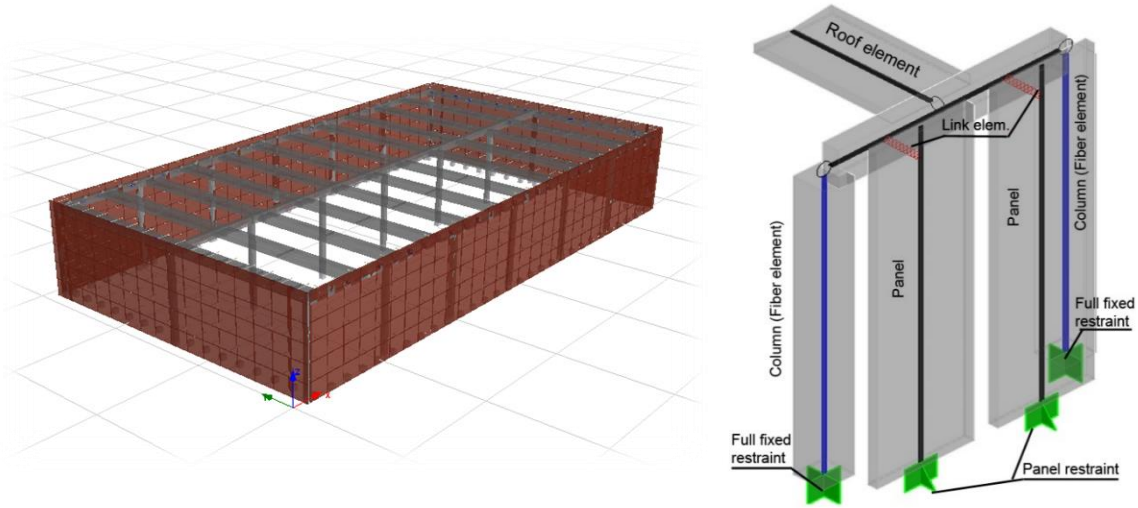

(a) (b)

Figure 4-21: Numerical model: 3D view (a) and details of non-linear and linear elements assembly (b)

The friction force F_μ generated during the relative sliding between the panel and the structure depends on the out-of-plane force F_c (Figure 4-23b).

$$F_\mu(t) = \mu \cdot F_c(t) \quad (4.1)$$

The *Flat Slider Bearing Element* was used to simulate the frictional behaviour. Its axial elastic stiffness was evaluated from the experimental values of the beam connection stiffness and panel connection stiffness (Figure 4-22), assuming that the two stiffnesses are in series. As the beam connection stiffness holds 11775 kN/m and the panel connection stiffness 9830 kN/m, the total axial elastic stiffness holds 5357 kN/m.

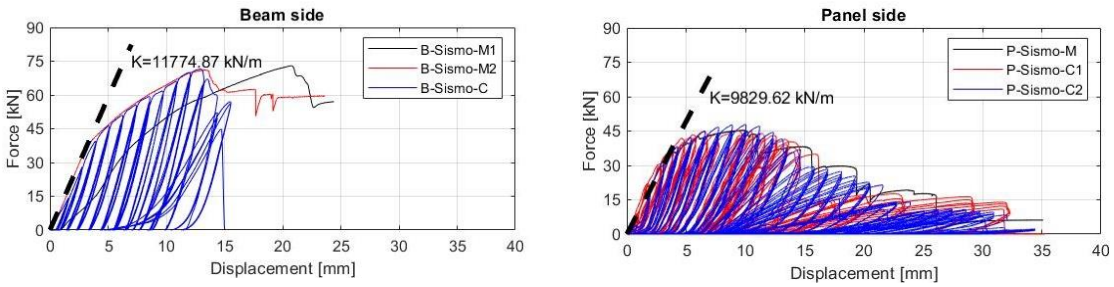

(a) (b)

Figure 4-22: Tangent elastic stiffness measured during the experimental test on the beam side (a) and on panel side (b)

The frictional behaviour is defined by associating a Coulomb friction model to the horizontal sliding direction (Figure 4-23a). In this model, the kinetic friction is independent of the sliding speed.

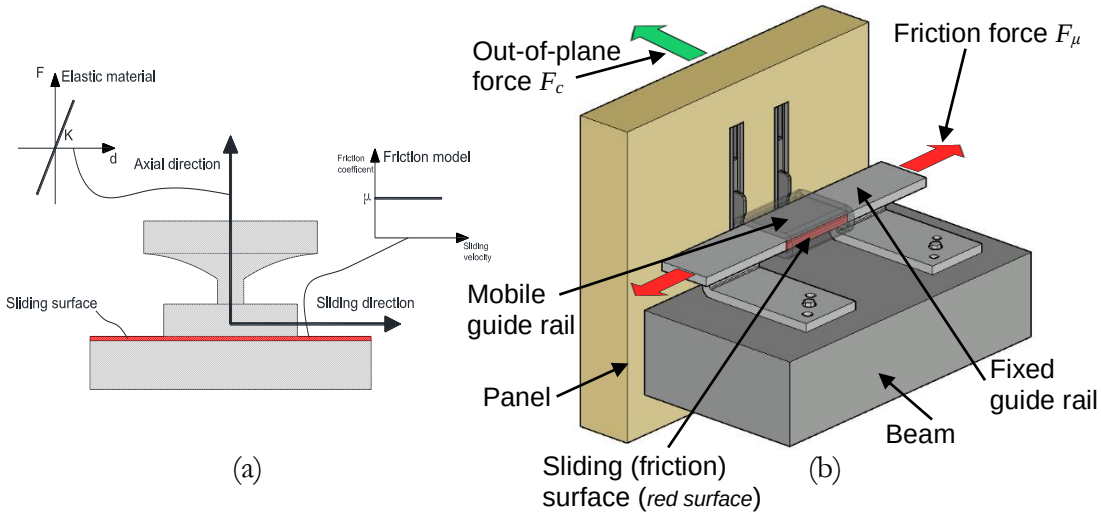

(a) (b)

Figure 4-23: Flat slider bearing element (a) and sliding surface and direction of friction force in the connection device (b)

Using the same imposed displacement function and the same out-of-plane force of the test F15-04 described in the previous §3.5.2 (see also Figure 3-77) and assuming the friction coefficient μ equal to 0.4, the numerical and the experimental result for a single SismoSafe device are in good agreement, as shown in Figure 4-24.

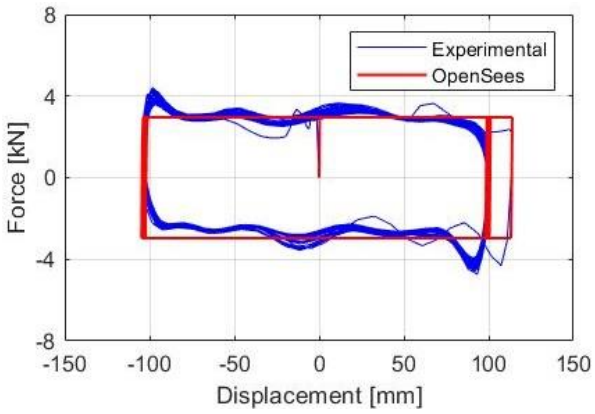

Figure 4-24: SismoSafe device: comparison between the numerical and experimental result

The OpenSees numerical model of the whole structure was used to evaluate the out-of-plane force in the connection devices through nonlinear dynamic analyses. Three cases have been studied according to the behaviour assigned to the link that connects the panels to the edge beams:

- case 1: the experimental in-plane stiffness was assigned to the link element in the axial direction, while it was left free to move in the in-plane direction,
- case 2: the same as case 1, with the assignment of the friction coefficient μ=0.4 in the in-plane direction,
- case 3: the same as case 2, with the assumption that the roof behaves like a rigid diaphragm.

4.3.1 Seismic action

The four strong earthquakes that stroke the Italian territory in the period between 2009 and 2016 were taken from the ITACA Database (Luzi et al., 2019). The main feature of the chosen unscaled accelerograms are reported in Table 4-6, where R is the epicentral distance and M_w is the moment magnitude and t_D the record duration.

Number	Event name	Station name	Date	PGA [g]	Mw	R [km]	$V_{s,30}$ [m/s]	Duration t_D [s]
1	L'Aquila	AQK	2009-04-06	0.353	6.1	1.8	705	100.00
2	Emilia 1st shock	MRN	2012-05-20	0.263	6.1	16.1	208	130.15
3	Central Italy	NRC	2016-10-30	0.485	6.5	4.6	498	50.00
4	Emilia 2nd shock	MRN	2012-05-29	0.218	6.0	4.1	208	68.00

Table 4-6: Accelerograms utilized in nonlinear dynamic analysis

The acceleration spectrum S_A and the displacement spectrum S_D of the chosen unscaled accelerograms are reported in following Figure 4-25:

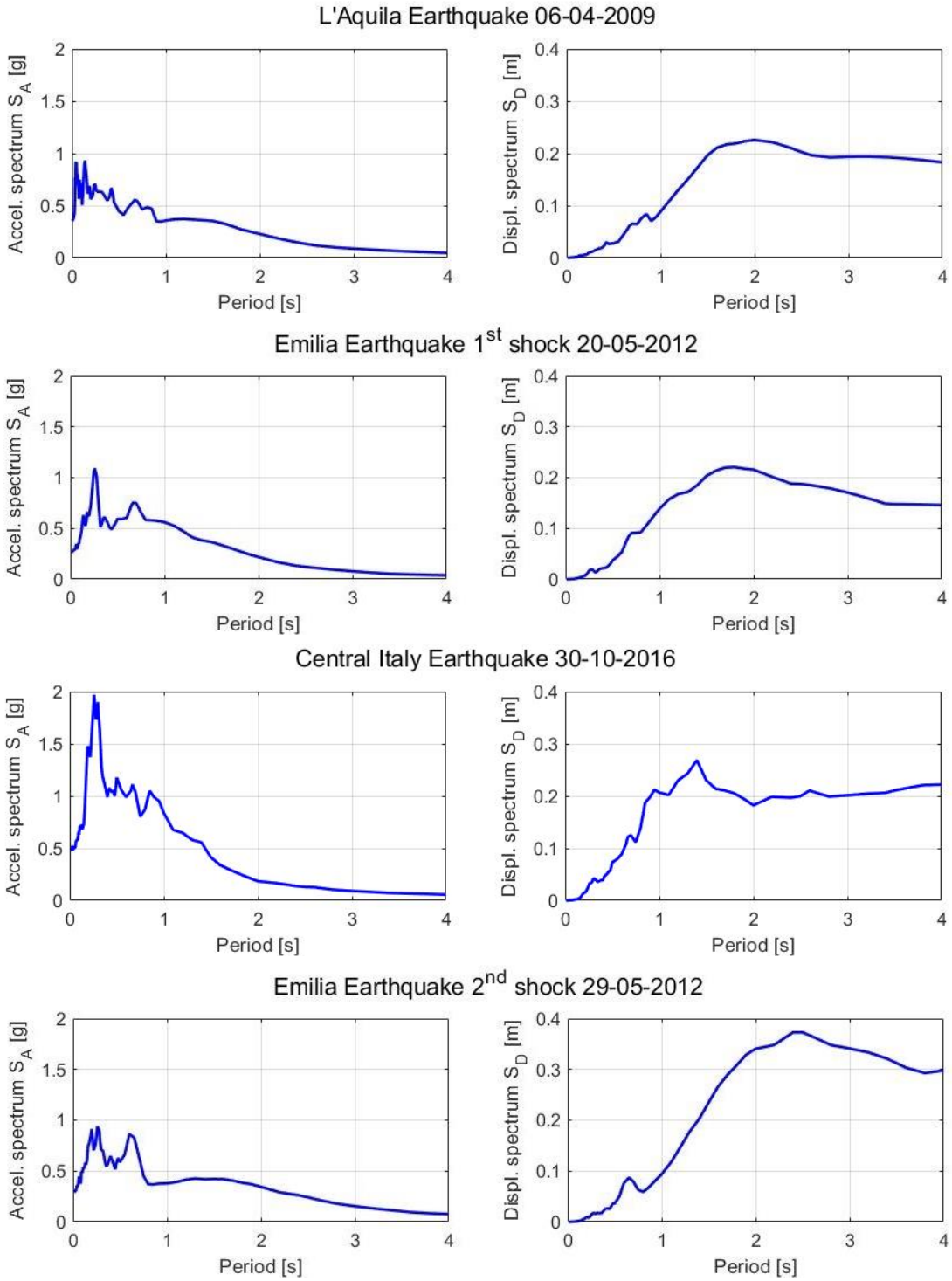

Figure 4-25: Spectrum acceleration and displacement for the chosen seismic events

4.3.2 Results

Fixed a cartesian reference system (Figure 4-26), Figure 4-27, Figure 4-28, Figure 4-29 and Figure 4-30 show the graphs of the structure displacements, the chord rotation of the most stressed column, the out-of-plane forces on the connections, the lifting force on the panels and the shear force at the panel bases.

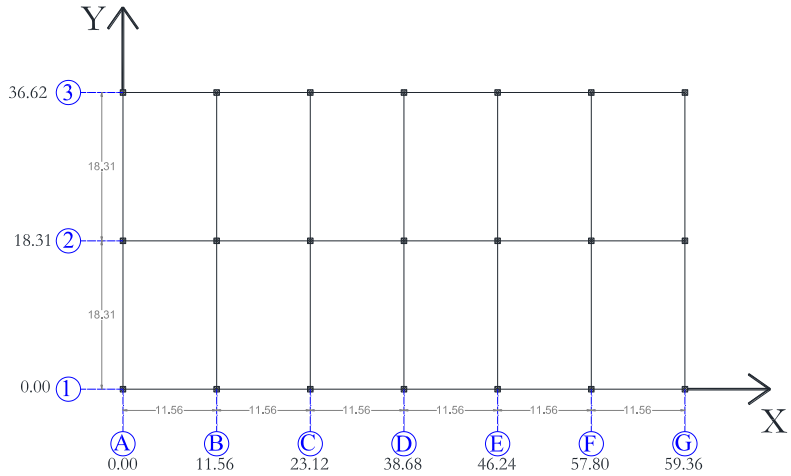

Figure 4-26: Wireframe plan view of the building and the coordinate reference system

In the graphs of Figures 4-23 ÷ 4-26 the values of *X* and *Y* identify the position of the frames arranged in the Y and X direction, respectively. The graphs show the maximum values over time of the studied quantities.

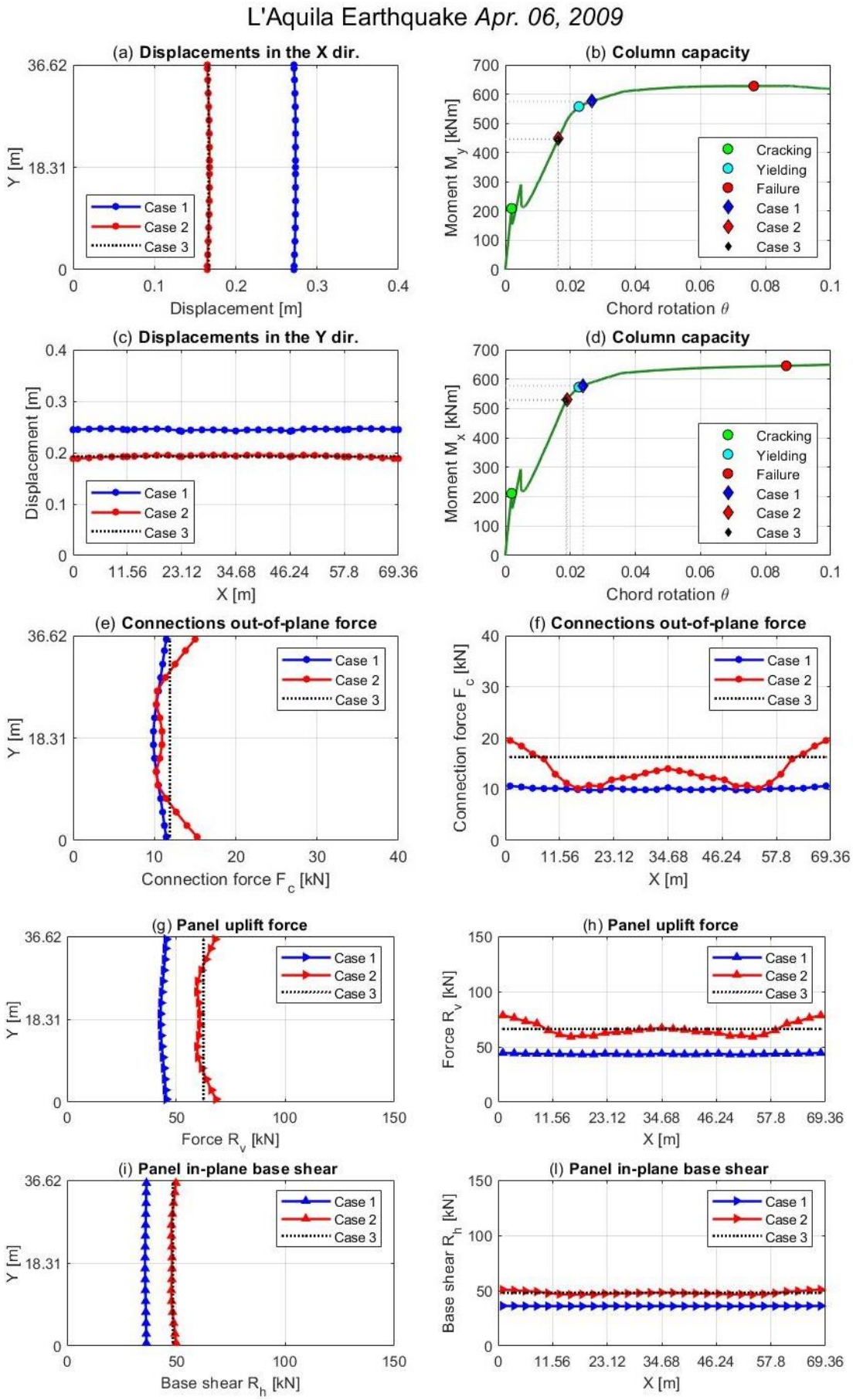

Figure 4-27: Results for the L'Aquila earthquake

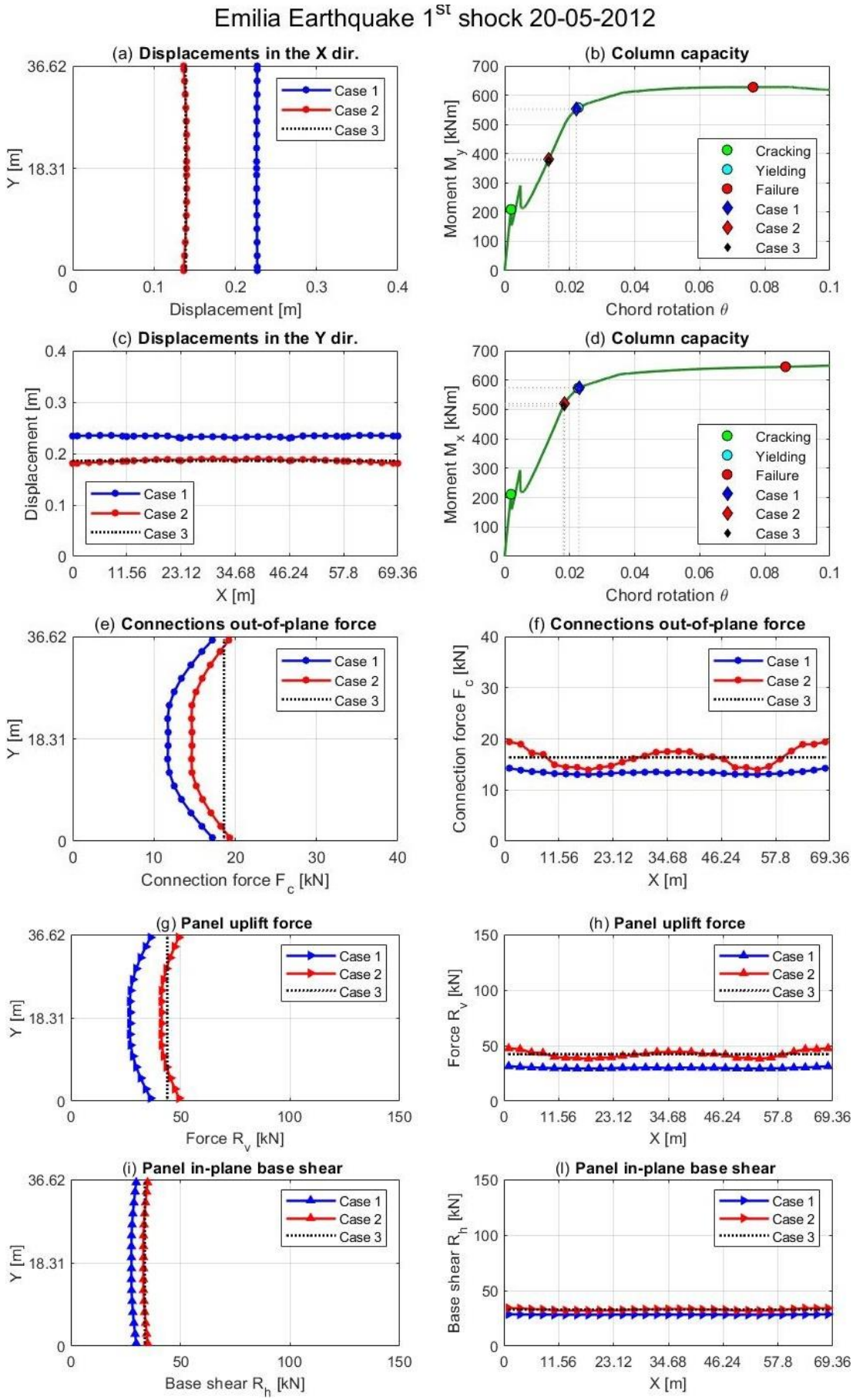

Figure 4-28: Results for the Emilia 1st shock earthquake

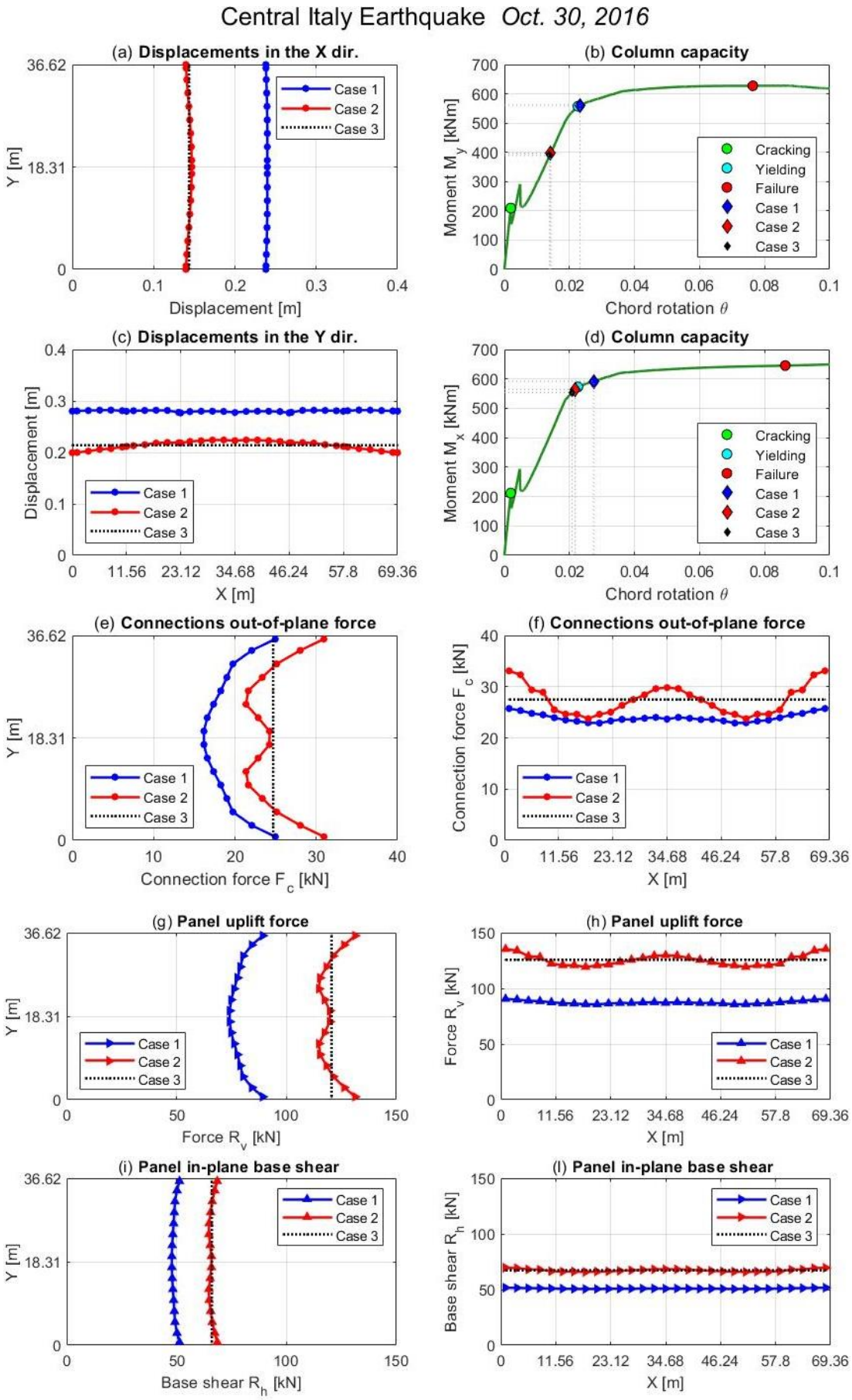

Figure 4-29: Results for the Central Italy earthquake

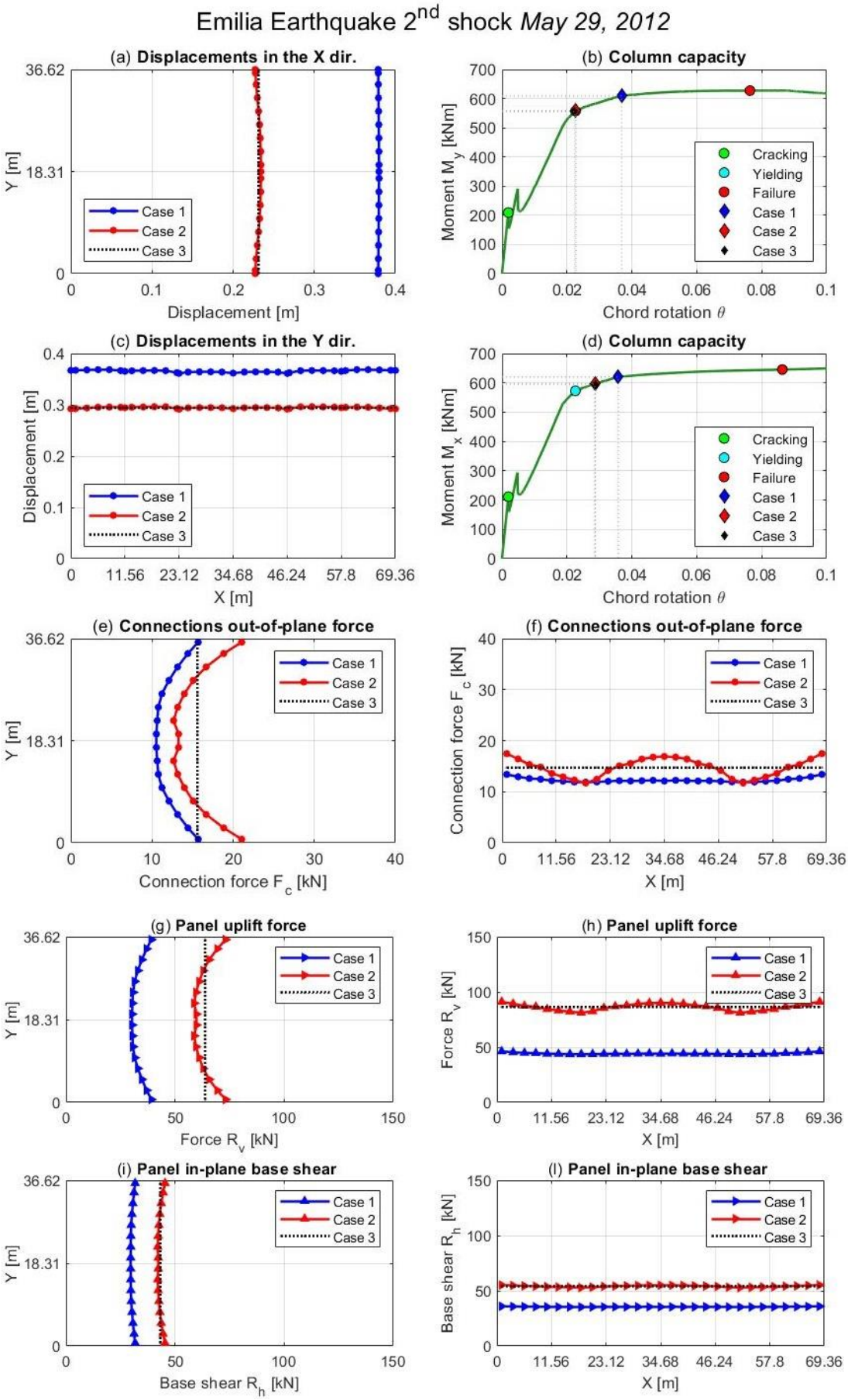

Figure 4-30: Results for the Emilia 2nd shock earthquake

4.3.3 Discussion of the case study results

Structure displacements

The mean displacement of the structure in the Case 1, where in-plane friction forces in the connections are neglected, is about 65% and 25% greater in the X and Y direction, respectively, compared to the Case 2, where friction at connections is considered (see Figure 4-27, Figure 4-28, Figure 4-29, Figure 4-30 a and c). The difference is evidently due to the constraint force produced by the friction in the connections. In Table 4-7, for each case study, each direction of seismic action (X or Y) and each seismic event, the maximum, minimum, mean displacement value and the percentage difference respect to Case 3, are listed.
For Case 3, since the roof behaves like a rigid diaphragm, the maximum, minimum, mean displacement value are the same and only the latter is reported in Table 4-7.

Case study			Seismic event							
			L'Aquila		Emilia 1st shock		Central Italy		Emilia 2nd shock	
Case 1	X displ [m]	Max	0.273	63.5%	0.227	65.7%	0.240	66.7%	0.380	63.8%
		Min	0.271	62.3%	0.225	64.2%	0.238	65.3%	0.378	62.9%
		Mean	**0.272**	**62.9%**	**0.226**	**65.0%**	**0.239**	**66.0%**	**0.379**	**63.4%**
	Y displ [m]	Max	0.246	26.8%	0.235	27.7%	0.282	31.8%	0.368	24.7%
		Min	0.241	24.2%	0.230	25.0%	0.276	29.0%	0.361	22.4%
		Mean	**0.244**	**25.8%**	**0.233**	**26.6%**	**0.280**	**30.8%**	**0.365**	**23.7%**
Case 2	X displ [m]	Max	0.168	0.6%	0.140	2.2%	0.146	1.4%	0.234	0.9%
		Min	0.164	-1.8%	0.136	-0.7%	0.139	-3.5%	0.227	-2.2%
		Mean	**0.166**	**-0.6%**	**0.138**	**0.7%**	**0.143**	**-0.7%**	**0.231**	**-0.4%**
	Y displ [m]	Max	0.195	0.5%	0.190	3.3%	0.224	4.7%	0.296	0.3%
		Min	0.188	-3.1%	0.181	-1.6%	0.199	-7.0%	0.291	-1.4%
		Mean	**0.192**	**-1.0%**	**0.186**	**1.1%**	**0.213**	**-0.5%**	**0.294**	**-0.3%**
Case 3	X displ [m]	**Mean**	**0.167**		**0.137**		**0.144**		**0.232**	
	Y displ [m]	**Mean**	**0.194**		**0.184**		**0.214**		**0.295**	

Table 4-7: Structure displacement for Case 1, 2 and 3 and percentage differences compared to Case 3

Column chord rotation

In Case 1, where connection friction forces are neglected, the chord rotation demand on the columns exceeds the yielding chord rotation θ_y for all the four seismic events. While, in the Case 2 with the friction in the connections, the chord rotation demand in the columns is lower and the yielding chord rotation θ_y is only achieved for the two most severe seismic events (Central Italy and Emilia 2nd shock), as shown in Figure 4-27, Figure 4-28, Figure 4-29, Figure 4-30 b and d. The chord rotation demand reduction can be positive to preserve the integrity of the columns or some column-foundation mechanical connection devices such as those studied in Dal Lago, et al., (2016) and Orlando & Piscitelli, (2018).
However, if on one hand, the friction at the connections parallel to the seismic excitation reduces the structure mean displacement and the chord rotation demand in the columns, on the other hand, it increases the in-plane force demand at the base of panels, as depicted in

Figure 4-27, Figure 4-28, Figure 4-29, Figure 4-30 g, h, i and l). This aspect is discussed in detail in the next sub-section 4.3.4.

Connection out-of-plane forces

When the frictional behaviour is considered (Case 2) the connection out-of-plane forces increase compared to Case 1 without friction (see Figure 4-27, Figure 4-28, Figure 4-29, Figure 4-30 e and f). Nevertheless, the demand for out-of-plane forces never exceeds the capacity of the SismoSafe devices, which is equal to 45 kN (see Table 4-4). Moreover, if the roof system is considered as a rigid diaphragm (Case 3), the out-of-plane forces assume a constant value, which is equal to approximately the mean value of Case 2.

In Table 4-8, for each case study, each direction of seismic action (X or Y) and each seismic event, the maximum, minimum, mean out-of-plane force value on connections and the percentage difference respect to Case 3, are listed.

For Case 3, since the roof behaves like a rigid diaphragm, the maximum, minimum, mean out-of-plane force are the same and only the latter is reported in Table 4-8.

Case study			Seismic event							
			L'Aquila		Emilia 1st shock		Central Italy		Emilia 2nd shock	
Case 1	X dir. [kN]	Max	11.45	-4.2%	17.19	6.0%	24.96	0.8%	15.70	0.4%
		Min	9.88	-17.3%	11.68	-28.0%	16.18	-34.6%	10.54	-32.6%
		Mean	**10.63**	**-11.0%**	**13.60**	**-16.1%**	**19.27**	**-22.1%**	**12.32**	**-21.2%**
	Y dir [kN]	Max	10.64	-21.7%	14.27	-13.2%	25.73	-6.5%	13.40	-9.1%
		Min	9.82	-27.8%	13.04	-20.6%	22.89	-16.8%	11.87	-19.4%
		Mean	**10.10**	**-25.7%**	**13.42**	**-18.3%**	**23.93**	**-13.0%**	**12.28**	**-16.6%**
Case 2	X dir. [kN]	Max	15.25	27.6%	19.31	19.0%	30.95	25.0%	21.05	34.6%
		Min	10.20	-14.7%	14.63	-9.8%	21.36	-13.7%	12.66	-19.1%
		Mean	**11.91**	**-0.4%**	**16.19**	**-0.2%**	**24.70**	**-0.2%**	**15.59**	**-0.3%**
	Y dir [kN]	Max	19.53	43.7%	19.41	18.2%	33.09	20.3%	17.46	18.5%
		Min	10.12	-25.5%	13.93	-15.2%	23.74	-13.7%	11.71	-20.5%
		Mean	**13.56**	**-0.2%**	**16.38**	**-0.3%**	**27.49**	**-0.1%**	**14.72**	**-0.1%**
Case 3	X dir. [kN]	**Mean**	**11.95**		**16.22**		**24.75**		**15.64**	
	Y displ [m]	**Mean**	**13.59**		**16.43**		**27.51**		**14.73**	

Table 4-8: Out-of-plane forces for Case 1, 2 and 3 and percentage differences compared to Case 3

The connection out-of-plane forces show both in the X and Y direction a wavy trend: the force is higher in the connections close to the edge frames, especially in Case 2 where the friction is considered. For panels lying in the transversal Y direction, that trend can be explained by schematizing the building as an equivalent transversal beam having the flexural stiffness of the roofing edge transversal beam (A or G in Table 4-9) to which the top of panels is fixed. For panels lying in the longitudinal X direction, a longitudinal beam with the flexural stiffness of the edge main beam (1 or 3 in Table 4-9: Computation of masses and relative tributary areas

can be considered. Those beams are supported on springs with stiffness K_{ix} or K_{iy}, which are equal to the translational stiffness of frames in the considered direction: three equal springs in

the X direction ($K_{1x} = K_{2x} = K_{3x}$) and seven equal springs in the Y direction ($K_{Ay} = K_{By} = \dots = K_{Gy}$). Moreover, in the horizontal *x-y* plane the rotations of the three supported sections of the equivalent transversal beam are neglected (see the qualitative deformed configuration of the roof in the longitudinal direction in Figure 4-19a); this hypothesis derives from the much higher bending stiffness in the horizontal plane of main beams compared to roof beams.
The tributary masses of each frame in the considered direction are applied on the beam. The masses of the panels are connected to the beam through springs whose stiffness k_c is given by the out-of-plane stiffness of connections. In the equivalent beam schematization, half of the mass of each panel ($m_p/2$) was considered. All masses were calculated using uniform loads described in section 4.2.1 and their values are provided in Table 4-9 with reference to tributary areas shown in Figure 4-31. Then the mass and stiffness values used in the equivalent beam schematization are listed in Table 4-10.

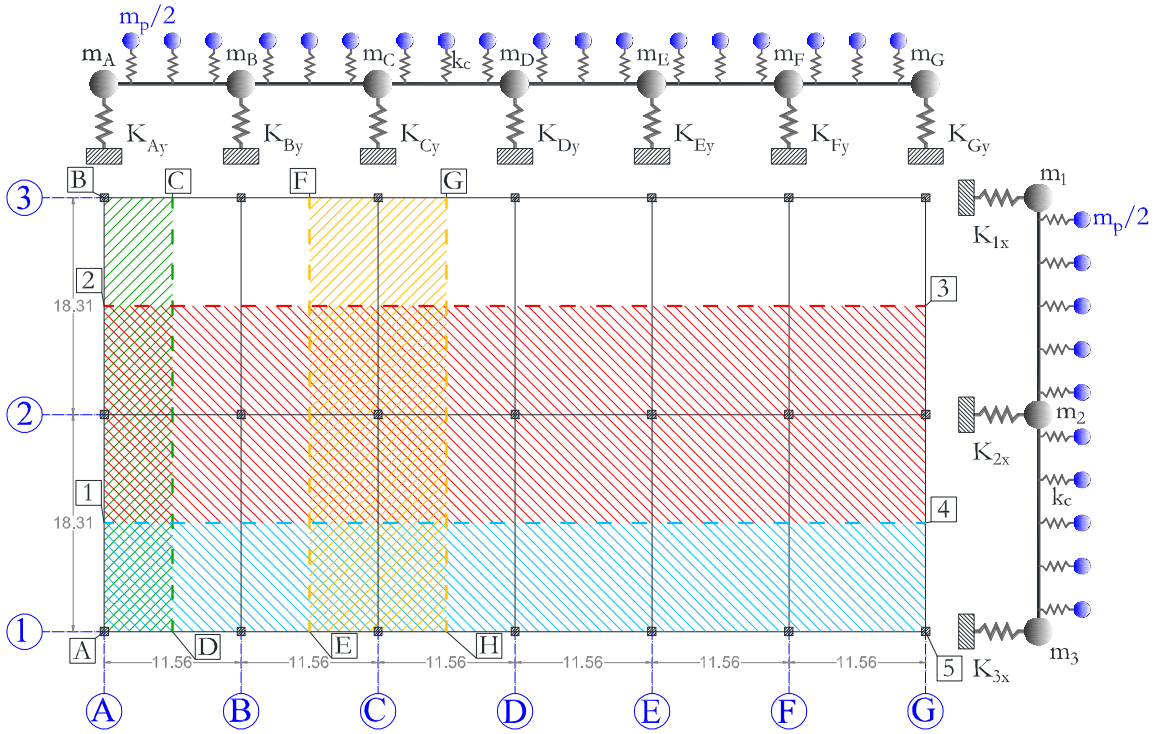

Figure 4-31: Schematization with spring supported beams and tributary areas for mass calculation (each vertex is marked with a capital letter inscribed in a square)

	Mass m_A [kg·s²/m]	Mass m_C [kg·s²/m]	Mass m_3 [kg·s²/m]	Mass m_2 [kg·s²/m]
Tributary area (vertexes)	ABCD	EFGH	A145	1234
Roof elements	2006.60	4013.19	6019.79	12039.58
Vault shell elements	222.24	444.47	666.71	1333.42
Superdead	237.34	474.68	712.02	1424.04
Columns	1370.18	1370.18	3197.09	3197.09
Beams	1490.66	2981.33	5302.75	7282.45
Total	**5327.02**	**9283.85**	**15898.36**	**25276.57**

Table 4-9: Computation of masses and relative tributary areas

When the beam is subjected to the earthquake acceleration, its response is a function of the frame stiffnesses K_x and K_y, of the participating masses m_j and m_i and of the frequency content of the applied excitation, which can make half of the mass of each panel $m_p/2$ to respond in phase or in counterphase with masses m_j and m_i of the frames. However, when the connection frictional behaviour is taken into account, the stiffnesses K_{Ay} and K_{Gy} of the two edge frames in the Y direction and the stiffnesses K_{1x} and K_{3x} of the two edge frames in the X direction

increase significantly compared to Case 1, because the displacement of edge frames is reduced by the friction forces transmitted by the cladding panels. That assumption requires to check the in-plane resistance of the base connection of the panels, otherwise, the stiffening effect of panels could not be considered. To this aim, in sub-section 4.3.4 the resistance verification of the base connection is dealt with.
In Case 2, due to the increase of the translational stiffness of edge frames, the displacement of the end joints of the equivalent beam decreases, so the connections close to the edge frames are subjected to higher out-of-plane forces than the other connections.

Equivalent beam parameters		
$m_p/2$	440.52	$kg \cdot s^2/m$
$m_1=m_3$	15898.36	$kg \cdot s^2/m$
m_2	25276.57	$kg \cdot s^2/m$
$m_A=m_G$	5327.02	$kg \cdot s^2/m$
$m_B=m_C=m_D=m_E=m_F$	9283.85	$kg \cdot s^2/m$
K_{ix}	6319	kN/m
K_{iy}	2708	kN/m
k_c	5357	kN/m

Table 4-10: Equivalent beam parameters

4.3.4 In-plane forces at the base of panels

Panels are fully-fixed at the base, that is they are equipped with connection devices capable of preventing the panel rocking and horizontal sliding, so they can withstand the uplifting reaction force R_v and the shear reaction force R_h shown in Figure 4-32.

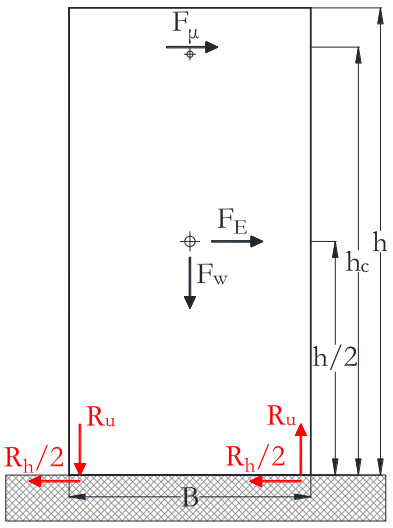

Figure 4-32: Forces acting on the panel for seismic force to the right: $F\mu$ friction force transmitted by the panel-to-structure connection (due to a relative displacement of the structure to the right), F_E inertial force of the panel, F_w dead weight of the panel, R_h and R_v horizontal and vertical reaction of fixing devices

The connection devices at the top of the panel, which develop a friction force F_μ, increase the demand for both the uplifting force R_v and the shear force R_h. Those reaction forces can be evaluated through the equilibrium of the forces acting on the panel (Dal Lago, et al., 2012). The shear force R_h can be calculated by imposing the translational equilibrium of the panel:

$$R_h(t) = F_\mu(t) + F_E(t) - R_f \quad (4.2)$$

where:
F_μ, defined in the Eq. (4.1), is the friction force that develops in the connection device at the top of the panel and is equal to the out-of-plane force F_c of the connection multiplied by the friction coefficient μ
F_E is the horizontal force imposed by the earthquake equal to the mass of the panel m_p multiplied by the seismic acceleration a_E:

$$F_E(t) = m_p \cdot a_E(t) \quad (4.3)$$

R_f is the friction force at the base of the panel, which in safety could be neglected; in any case it should be taken not higher than the weight force F_w multiplied by the static friction coefficient of concrete-to-concrete μ_{cc} (typically equal to 0.65):

$$R_f \leq \mu_{cc} \cdot F_w \quad (4.4)$$

With reference to Figure 4-27, Figure 4-28, Figure 4-29, Figure 4-30 i and l, Table 4-11 lists the maximum, minimum and mean shear force R_h at the base of panels and the percentage difference compared to Case 3. For Case 3, since the roof is supposed to behave like a rigid diaphragm, the maximum, minimum and mean values of R_h are the same, so only the latter is reported in Table 4-11.

Case study			Seismic event							
			L'Aquila		Emilia 1st shock		Central Italy		Emilia 2nd shock	
Case 1	X dir. [kN]	Max	36.40	-17.8%	36.38	-17.5%	89.21	-26.2%	39.19	-38.8%
		Min	35.77	-19.2%	26.92	-39.0%	74.14	-38.7%	30.32	-52.6%
		Mean	**36.07**	**-18.6%**	**30.22**	**-31.5%**	**79.45**	**-34.3%**	**33.38**	**-47.8%**
	Y dir [kN]	Max	36.23	-9.9%	31.42	-26.0%	90.54	-28.1%	46.19	-46.7%
		Min	35.90	-10.7%	29.31	-30.9%	85.67	-32.0%	43.57	-49.7%
		Mean	**36.02**	**-10.5%**	**29.96**	**-29.4%**	**87.46**	**-30.6%**	**44.27**	**-48.9%**
Case 2	X dir. [kN]	Max	45.46	2.7%	49.36	11.9%	131.21	8.5%	73.16	14.3%
		Min	43.44	-1.9%	41.32	-6.3%	114.75	-5.1%	58.75	-8.2%
		Mean	**44.13**	**-0.4%**	**44.01**	**-0.2%**	**120.48**	**-0.3%**	**63.79**	**-0.3%**
	Y dir [kN]	Max	42.39	5.4%	47.50	11.9%	135.27	7.4%	91.04	5.1%
		Min	38.63	-4.0%	38.09	-10.2%	119.23	-5.3%	81.17	-6.3%
		Mean	**40.01**	**-0.5%**	**42.29**	**-0.3%**	**125.65**	**-0.2%**	**86.34**	**-0.3%**
Case 3	X dir. [kN]	**Mean**	**44.29**		**44.12**		**120.88**		**63.99**	
	Y displ [m]	**Mean**	**40.22**		**42.43**		**125.95**		**86.64**	

Table 4-11: Mean shear forces for Case 1, 2 and 3 and percentage differences compared to Case 3

The uplifting force R_v can be calculated by imposing the equilibrium on the rotation for the panel in which F_μ and F_E are overturning forces while the weight force F_w is the stabilizing force.

$$R_v = \left[F_\mu(t) \cdot h_c + F_E(t) \cdot \frac{h}{2} - F_w \cdot \frac{B}{2}\right] \cdot \frac{1}{B} \quad (4.5)$$

where:

$$F_w = m_p \cdot g \quad (4.6)$$

is the weight force, equal to the mass of the panel m_p multiplied by the acceleration of gravity g. And h is the total height of panel h_c is the height of the top connection with respect to the panel base and B is the panel width.

By observing the graphs in Figure 4-27, Figure 4-28, Figure 4-29, Figure 4-30 g, h, i and l, it can be noticed that the trend of the R_v and R_b forces has the same shape as that of the out-of-plane forces on the connections F_c. This is caused by the fact that F_μ is proportional to the out-of-plane force F_c and that the forces F_w (weight) and F_E (earthquake) are constant for all panels. As for F_c, it is noted that the values of R_v and R_b increase at the panels closest to the edge of the building. Table 4-12 lists the maximum, minimum, mean uplift force value R_v at the panels' base and the percentage difference respect to Case 3. Again, for Case 3, since the roof behaves like a rigid diaphragm, the maximum, minimum, R_v force are the same and only the latter is reported in Table 4-12.

Case study			Seismic event							
			L'Aquila		Emilia 1st shock		Central Italy		Emilia 2nd shock	
Case 1	X dir. [kN]	Max	45.55	-27.4%	17.19	6.0%	24.96	0.8%	15.70	0.4%
		Min	42.85	-31.7%	11.68	-28.0%	16.18	-34.6%	10.54	-32.6%
		Mean	**44.15**	**-29.6%**	**13.60**	**-16.1%**	**19.27**	**-22.1%**	**12.32**	**-21.2%**
	Y dir [kN]	Max	44.51	-19.6%	14.27	-13.2%	25.73	-6.5%	13.40	-9.1%
		Min	43.09	-22.1%	13.04	-20.6%	22.89	-16.8%	11.87	-19.4%
		Mean	**43.57**	**-21.3%**	**13.42**	**-18.3%**	**23.93**	**-13.0%**	**12.28**	**-16.6%**
Case 2	X dir. [kN]	Max	68.27	8.8%	19.31	19.0%	30.95	25.0%	21.05	34.6%
		Min	59.59	-5.0%	14.63	-9.8%	21.36	-13.7%	12.66	-19.1%
		Mean	**62.53**	**-0.3%**	**16.19**	**-0.2%**	**24.70**	**-0.2%**	**15.59**	**-0.3%**
	Y dir [kN]	Max	65.35	18.1%	19.41	18.2%	33.09	20.3%	17.46	18.5%
		Min	49.20	-11.1%	13.93	-15.2%	23.74	-13.7%	11.71	-20.5%
		Mean	**55.10**	**-0.4%**	**16.38**	**-0.3%**	**27.49**	**-0.1%**	**14.72**	**-0.1%**
Case 3	X dir. [kN]	**Mean**	**62.73**		**16.22**		**24.75**		**15.64**	
	Y displ [m]	**Mean**	**55.33**		**16.43**		**27.51**		**14.73**	

Table 4-12: Mean uplift forces for Case 1, 2 and 3 and percentage differences compared Case 3

4.3.5 Concluding remarks

The out-of-plane capacity of isostatic panel-to-structure connections of one-storey precast structures was investigated through an experimental campaign. The experimental campaign consisted of 30 tests on two different typologies of mechanical connections, one typology was chosen among available in-use commercial joints (hammer-head strap type) and the other one was proposed as a new solution in this thesis. The first are the typical hammer-head steel straps, the second is made of a mobile guide which can slide along a fixed guide rail.
Under in-plane seismic forces, isostatic connections should be able to accommodate high relative displacements between the panels and the structure, therefore, it is important to test and evaluate their displacement capability. Under out-of-plane seismic forces, the connections should have a satisfactory out-of-plane resistance and restrain out-of-plane relative displacements between the cladding panels and the structure to preserve the structural integrity. The experiments allowed to evaluate the capacity of the studied devices for out-of-plane forces both on the beam side and on the panel side. The lesser between the two resistances is always given by the connection on the panel side, which represents the ultimate resistance of the device.
The tests highlighted that the Standard devices have a lower out-of-plane resistance than the SismoSafe devices: on the panel side, they exhibited an ultimate resistance about three times lower than SismoSafe connections under both cyclic and monotonic load. Moreover, the actual capacity of Standard connections is even lower than the experimental one, as they are damaged by in-plane seismic forces, as already highlighted in a previous section 3.5. The SismoSafe devices do not suffer damage due to relative in-plane displacements, so the experimental out-of-plane capacity could be considered reliable.
A series of non-linear dynamic analyses were also carried out to evaluate the out-of-plane forces in the SismoSafe panel-to-structure connections of a one-storey industrial building, considering the four strongest Italian earthquakes of the last 12 years. Numerical results confirmed that the new SismoSafe connections could safely withstand the out-of-plane forces for all the four seismic events whether the in-plane friction force is considered or not. The numerical analyses allowed to highlight the influence of friction at the connections on the seismic response of the structure. At increasing the friction force, the uplift and shear reaction forces at the base of panels parallel to the earthquake direction increase, as well as the out-of-plane forces at the top of panels normal to the earthquake. Therefore, a very low friction is preferable. Nevertheless, the manufacturing of low friction devices could be very expensive and not convenient for industrial production.
The effect of friction is very pronounced on the panel-to-structure connections arranged along the transversal edge of the building. Here the panels are connected to the edge roof beam, which has a rather large span and great flexibility, so the out-of-plane forces on those connections due to longitudinal seismic loading have a very pronounced non-uniform distribution, much more than connections of panels fixed to the edge longitudinal beams for transversal seismic loading. Vice versa, in one-storey precast buildings with a rigid diaphragm roofing system, the distribution of out-of-plane forces on the connections is uniform without peaks at the edge frames.
Traditional panel-to-structure connections made with hammer-head strap devices could not withstand the demand for out-of-plane force and in-plane displacement required by those four seismic events. The hammer-head strap devices have a limited in-plane displacement capacity for available on the market devices and a limited out-of-plane capacity ($\approx$ 15 kN). Furthermore, during a seismic event, they are susceptible to in-plane damage, which could reduce

significantly the out-of-plane capacity of the standard connections. On the contrary, the SismoSafe devices, even if they transmit in-plane friction forces, can sustain very large displacements in the plane, which depend on the length of the fixed guide inside which the mobile cursor slides. The out-of-plane resistance capacity of the SismoSafe devices is about 45 kN, as evaluated through the experimental campaign, so the number of devices required to withstand the out-of-plane seismic actions is three times lower than standard connections. In none of the four considered seismic events, the in-plane displacement capacity, as well as the out-of-plane resistance capacity, were never exceeded. Moreover, the out-of-plane resistance of the SismoSafe connections is not affected by the in-plane sliding behaviour, so they could work correctly even in the presence of randomly inclined seismic actions

4.4 Out-of-plane seismic demand evaluation

The correct design of the non-structural elements, including the cladding panels for precast RC buildings, plays a role of primary importance in the suitable response of the building to seismic action. Indeed, the aforementioned elements, if not correctly designed, could generate brittle and premature collapses that may significantly reduce the safety of the buildings as well as that of the people.
The capacity of non-structural elements, including the connections device that supports and join them to the main structure, must be greater than the seismic demand corresponding the limit states that have to be considered. The capacity assessment for some connection devices was presented in the previous paragraphs §3.5 and §4.1
The out-of-plane seismic demand for non-structural elements can be determined by applying to them an equivalent static force calculated with the formulation reported in Equation (2.1).
The evaluation of the spectral acceleration S_a is usually performed using the formulation of the floor spectra proposed in (Medina, et al., 2006; and Sullivan, et al, 2013). However, if this formulation could be appropriate for the horizontal panels, that are not directly placed on the ground, it cannot be applied to the vertical panels of one-storey buildings. These vertical panels generally have an edge restrained to the ground. A study for the evaluation of the out-of-plane seismic performance of horizontal panels was carried out by (Belleri, et al., 2018)
The vertical panels placed to the ground are directly stressed by the seismic acceleration and at the top, they are stressed by the action coming from the structure. The structure-to-panel connection, for out-plane actions, is required to absorb both the force generated by the structure-panel interaction and the one generated by the seismic action that directly stressed the panel. In order to understand what might be the force that involves the panel-structure connection, the solution of a simplified structural model was initially searched.
Therefore, some simplifying hypotheses were introduced to make an approximate assessment of the structure's response:

- The real building was schematized in a simplified 2 DOF model (Figure 4-33).
- A rigid roof diaphragm was assumed
- The masses, both of the panel and the structure, were lumped in the points where they were supposed to have the maximum effect (in terms of forces and displacements) during the seismic action.

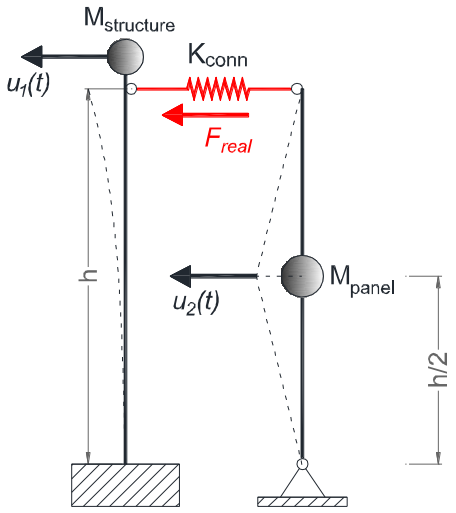

Figure 4-33: Simplified 2 DOF model

The first task to study the 2 DOF system dynamic behaviour is to calculate the stiffness matrix. The complete calculation of the stiffness matrix of the 2 DOF simplified system is reported in Appendix A. The stiffness matrix $\boldsymbol{K}$ can be written as:

$$\boldsymbol{K} = \begin{bmatrix} \frac{3EJ_{col\_e}}{h^3} + \frac{12EJ_{pan\_e} \cdot K_{conn\_e}}{12EJ_{pan\_e} + K_{conn\_e} \cdot h^3} & \frac{24EJ_{pan\_e} \cdot K_{conn\_e}}{K_{conn\_e}h^3 + 12EJ_{pan\_e}} \\ \frac{24EJ_{pan\_e} \cdot K_{conn\_e}}{K_{conn\_e}h^3 + 12EJ_{pan\_e}} & \frac{48EJ_{pan\_e} \cdot K_{conn\_e}}{K_{conn\_e}h^3 + 12EJ_{pan\_e}} \end{bmatrix} \quad (4.7)$$

where:

- E is the concrete elastic modulus.
- J_{col_e} is the equivalent moment of inertia of all columns, equal to $J_{col} \cdot n_{col}$; n_{col} is the number of columns and J_{col} is the moment of inertia of one column.
- J_{pan_e} is the equivalent moment of inertia of all panels placed orthogonally to the earthquake direction, equal to $J_{pan} \cdot n_{pan}$; n_{pan} is the number of panels and J_{pan} is the moment of inertia of one panel.
- K_{conn_e} is the equivalent out-of-plane stiffness of all connection devices mounted on the panels placed orthogonally to the earthquake direction, equal to $K_{conn} \cdot n_{conn}$; n_{conn} is the number of connection and K_{conn} is the out-of-plane stiffness of a single connection device.
- h is the height of both panel and structure.

In this initial study, we assumed that the connection out-of-plane stiffness is infinite. Although this is not correct because the out-of-plane stiffness of the connection devices has a finite value as shown in section 4.1. This is a preliminary study where it is assumed that the structure does not get damaged as well as the connection devices and for simplicity it was assumed that $K_{conn} = \infty$. In this way the stiffnss matrix became:

$$\boldsymbol{K} = \begin{bmatrix} \frac{3EJ_{col\_e}}{h^3} + \frac{12EJ_{pan\_e}}{h^3} & \frac{24EJ_{pan\_e}}{h^3} \\ \frac{24EJ_{pan\_e}}{h^3} & \frac{48EJ_{pan\_e}}{h^3} \end{bmatrix} \quad (4.8)$$

Naming $M_{structure}$ as the whole structure's mass and M_{panel} as the whole panels mass, the differential equation of motion can be written:

$$\boldsymbol{M}\{\ddot{x}\} + \boldsymbol{C}\{\dot{x}\} + \boldsymbol{K}\{x\} = \boldsymbol{M} \cdot \{a_g\} \quad (4.9)$$

If a simple cosinusoidal acceleration, with amplitude A, angular velocity Ω and phase φ, is applied at the base of the undamped structural system, equation of motion become:

$$\begin{bmatrix} M_{structure} & 0 \\ 0 & M_{panel} \end{bmatrix} \begin{bmatrix} \ddot{x}_1 \\ \ddot{x}_2 \end{bmatrix} + \begin{bmatrix} K_{11} & K_{12} \\ K_{21} & K_{22} \end{bmatrix} \begin{bmatrix} x_1 \\ x_2 \end{bmatrix} = \begin{bmatrix} M_{structure} \\ M_{panel} \end{bmatrix} \cdot A \cdot \cos(\Omega t + \varphi) \quad (4.10)$$

In this preliminary hand-calculation study the system was considered undamped for simplicity of calculation. However, damping of 2% was included in the following parametric analyses.
Then, by summing the solution of the homogeneous equation with the particular solution and imposing the following boundary condition:

$$\begin{matrix} u_1(0) = 0; & u_2(0) = 0 \\ \dot{u}_1(0) = 0; & \dot{u}_2(0) = 0 \end{matrix} \quad (4.11)$$

This does it mean that the structure is initially undeformed and also that the initial velocity is zero.
The equation of motion for each degree of freedom can be obtained:

$$x_1(t) = \frac{r_1 C_1 - C_2}{r_1 - r_2} cos\omega_1 t + \frac{C_2 - C_1 r_1}{r_1 - r_2} cos\omega_2 t + C_1 cos\Omega t \quad (4.12)$$

$$x_2(t) = r_1 \frac{r_1 C_1 - C_2}{r_1 - r_2} cos\omega_1 t + r_2 \frac{C_2 - C_1 r_1}{r_1 - r_2} cos\omega_2 t + C_2 cos\Omega t \quad (4.13)$$

Where:

If $\boldsymbol{U} = \begin{bmatrix} U_{11} & U_{12} \\ U_{21} & U_{22} \end{bmatrix}$ is the matrix of the two eigenvectors then $r_1 = \frac{U_{21}}{U_{11}}$ and $r_2 = \frac{U_{22}}{U_{12}}$

and C_1 and C_2 are two constants, calculated during the research of the particular solution.
The step-by-step equation of motion solution is reported in Appendix A.3.

Since the DOFs displacement is computed, is now possible to find the out-of-plane force on a single connection device:

$$F_{real}(t) = \left(x_2(t) \cdot \frac{K_{22}}{2} - x_1(t) \cdot \frac{K_{22}}{4} \right) \cdot \frac{1}{n_{conn}} \quad (4.14)$$

4.4.1 Validating example

Assuming for example the simplified 2 DOF structure of Figure 4-33, with the mass and stiffness values given in Table 4-13:

Structure mass [t]	$M_{structure}$	601

Panel mass [t]	M_{panel}	502
Structure stiffness [kN/m]	K_{col_e}	22312
Panel stiffness [kN/m]	K_{pan_e}	305132

Table 4-13: Mass and stiffness values for validating example

and a with sinusoidal acceleration applied to the base, having the equation:

$$a_g = 9.81 \cdot \sin(4t) \quad (4.15)$$

Then, an OpenSees numerical model of the simplified structure was made and acceleration of equation (4.15) was imputed as ground motion. A manual solution is calculated using the equations (4.12) and (4.13). The results in term of DOFs' displacement (Figure 4-34Figure 4-34: Comparison between numericala) and connection force (Figure 4-34b) obtained with both numerical and hand calculated solution are compared below:

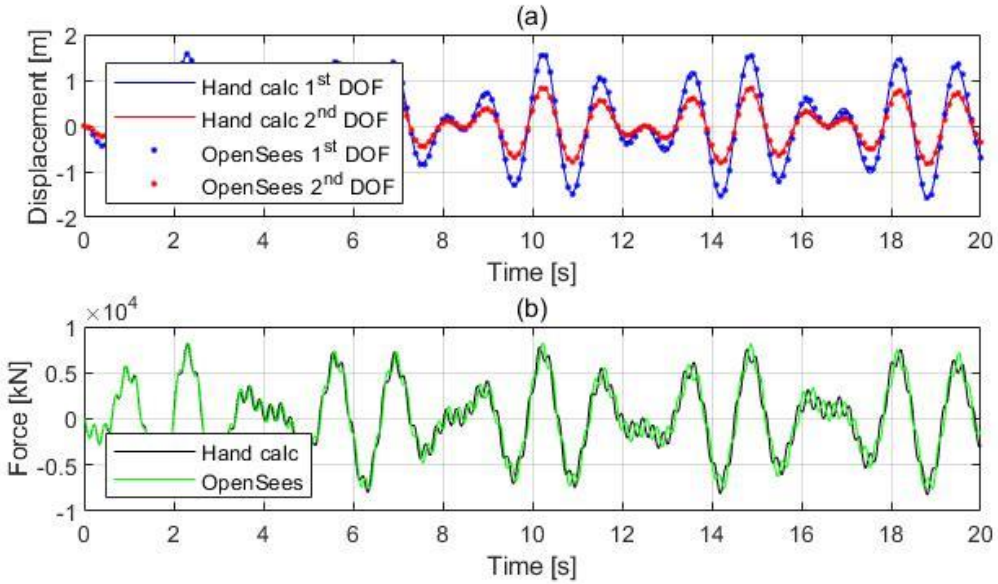

Figure 4-34: Comparison between numerical model and hand calculation results: DOFs' displacement (a) and connection force (b)

The results are in a very good agreement when a simple sinusoid is applied as a ground motion. Therefore, it could be correct to suppose that the solution for random ground motion, such as a recorded accelerogram, can be found by decomposing the acceleration in a Fourier series, through the equation:

$$a_g(t) = \sum_{i=1}^{n} A_i \cdot \cos(2\pi f_i + \varphi_i) \quad (4.16)$$

where:
A_i is the amplitude of each harmonic
f_i is the frequency of each harmonic
φ_i is the phase of each harmonic
n is the signal sampling frequency

The recorded Petrovac E-W acceleration history of Figure 3-6 is chosen as an example and it was scaled to 0.4g. Using Matlab's Fast Fourier Transform function (MATLAB, 2018) it is possible to obtain the amplitude (Figure 4-35a) and phase spectrum (Figure 4-35b):

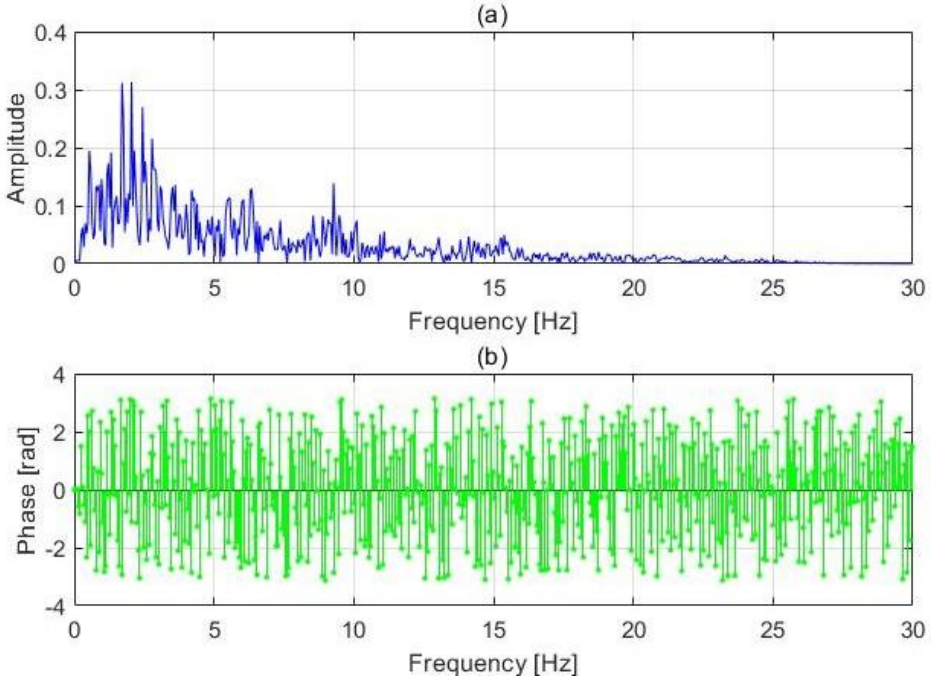

Figure 4-35: Perovac E-W scaled to 0.4g: amplitude spectrum (a) phase spectrum (b)

Considering again the 2 DOF simplified structure of Figure 4-33, with the support of the equations (4.12) and (4.13) it is possible to calculate the system response for each of the 1025 harmonics in which the signal was decomposed. If each obtained response is added together, the overall system solution is obtained. The results are compared, in term of DOFs' displacement (Figure 4-36a) and connection force (Figure 4-36b), with the ones found by using an OpenSees model:

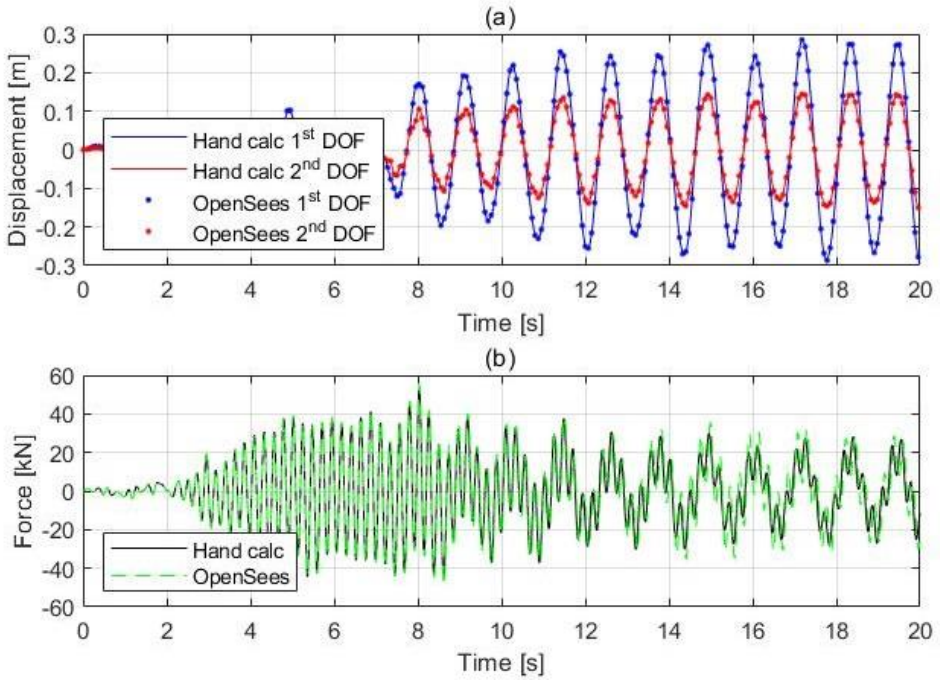

Figure 4-36: Numerical model and hand calculation results comparison for Pertovac 0.4 g scaled accelerogram: DOFs' displacement (a) and connection force (b)

4.4.2 Infinitely stiff structure case

In design practice, panels were often considered as secondary elements. To calculate the connection out-of-plane force, a simply supported beam scheme is assumed for the panel. In this case, the structure and the connection become infinitely rigid although precast RC structures were typically quite flexible. The 2 DOF system of Figure 4-33 becomes a single degree of freedom system (SDOF) (Figure 4-37). Assuming the system undamped for simplicity of calculation, the solution of the equation of motion for sinusoidal ground motion gives:

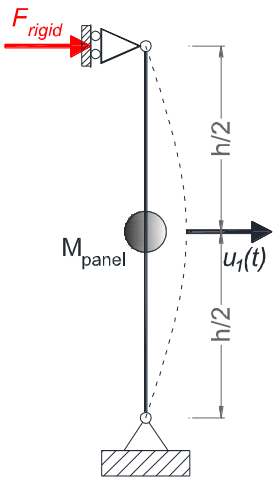

$$\boldsymbol{M}\{\ddot{x}\} + \boldsymbol{K}\{x\} = \boldsymbol{M} \cdot \{a_g\} \quad (4.17)$$

That become:

$$M_{panel}\ddot{x} + \frac{48EJ_{pan\_e}}{h^3} \cdot x = M_{panel} \cdot a_g \quad (4.18)$$

Figure 4-37: SDOF system

The equivalent stiffness of all panel K_{pan_e} is reported in equation (4.18) $\left(\frac{48EJ_{pan\_e}}{h^3}\right)$ and the period of the simply supported panel in Figure 4-37 is:

$$T_{rigid} = 2\pi \cdot \sqrt{\frac{M_{panel} \cdot h^3}{48 E J_{panel\_e}}} \quad (4.19)$$

The solution of equation (4.12) is:

$$u_1(t) = \frac{A}{M_{panel}(\omega^2 - \Omega^2)}(\cos \Omega t - \cos \omega t) \quad (4.20)$$

where:
A is the sinusoidal ground motion amplitude
Ω is the sinusoidal ground motion angular velocity
ω in system angular velocity

the reaction on roller support F_{rigid} can now be calculated as:

$$F_{rigid}(t) = \frac{u_1(t) \cdot K_{pan\_e}}{4} \quad (4.21)$$

the calculation of the force F_{rigid}, that stresses the connection in the case of an infinitely stiff structure, is rather easy.

4.5 The numerical model of the structure-to-panel system

To define a design rule for out-of-plane forces and then determine the out-of-plane force demand that these connections require during a seismic event, the study carried out on the 2 DOF simplified structure needs to be generalized.
For this reason, it was decided to perform a parametric analysis that would allow the relating of the connection force calculated on the simplified structure F_{real} (Figure 4-33) to the connection force evaluated in the case of an infinitely stiff structure F_{rigid} (Figure 4-37).

Starting from the simplified precast structure and assuming that its behaviour is like a cantilever beam with the mass $M_{structure}$ lumped to its top as usually considered in the design practice, a series of period ratios R_T and masses R_M ratios are established, so that:

$$\frac{T_{structure}}{T_{rigid}} = R_T \qquad \frac{M_{structure}}{M_{panel}} = R_M \quad (4.22)$$

So it is possible to write

$$T_{structure} = T_{rigid} \cdot R_T \qquad M_{structure} = M_{panel} \cdot R_M \quad (4.23)$$

if the columns can be assumed as a cantilever beam, then:

$$T_s = 2\pi \sqrt{\frac{M_s h^3}{2 E_s J_s}} \sqrt{\frac{M_s h^3}{3 E_s J_{s\_e}}} \Rightarrow T_s^2 = \frac{4\pi^2 M_s h^3}{3 E_s J_s} \frac{4\pi^2 M_s h^3}{3 E_s J_{s\_e}} \quad (4.24)$$

Where the subscript *structure* was replaced with *s*

By manipulating the equation (4.24), the value of E_s in according to the two ratios R_T and R_M can be computed:

$$E_s = \frac{4\pi^2 M_s h^3}{3E_s T_s^2} \quad (4.25)$$

Therefore introducing the (4.23) in the (4.25), the following is obtained:

$$E_s = \frac{4\pi^2 R_M M_{panel} h^3}{3E_s \left(T_{rigid} R_T\right)^2} \quad (4.26)$$

It is evident that, once the M_{panel} and T_{panel} values are established and a series of i-values of R_M and j-values of R_T are chosen, E_s becomes a matrix with (i, j) components, which defines the stiffness of the structure. In this way, each R_M ratios corresponds to a value of R_T.
Numerical analysis for each value was made to find the maximum of the force F_{real}

To further generalize the result, 28 unscaled accelerograms were chosen, 7 for each seismic zone as defined in the code (OPCM 3274, 2003)
In the OPCM 3274, all Italian municipalities were classified into 4 main categories (Figure 4-38:), indicative of their seismic risk, calculated on the basis of the PGA and for seismic events frequency and intensity:

- Zone 1: high seismicity (PGA over 0.25 g)
- Zone 2: medium-high seismicity (PGA between 0.15 and 0.25 g)
- Zone 3: medium-low seismicity (PGA between 0.05 and 0.15 g).
- Zone 4: low seismicity (PGA less than 0.05 g)

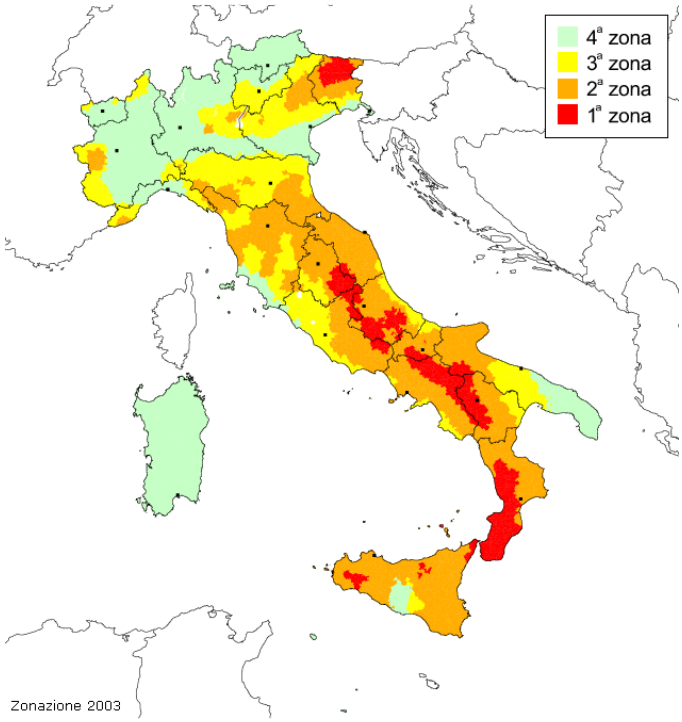

Figure 4-38: Seismic zone classification according to OPCM 3274. Source ("INGV," n.d.)

The main feature of the 28 chosen unscaled accelerograms are reported in the following Table 4-14:

Number	Event name	Station name	Date	PGA [g]	Mw	R [km]	$V_{s,30}$ [m/s]	Duration t_D [s]
Zone 4: PGA≤0.05g								
1	Friuli	BUI	1976-09-11	0.041	5.2	10.2	254	18.95
2	Central Italy	AQG	2009-04-07	0.050	5.1	5.9	696	77.00
3	Central Italy	AQK	2017-01-18	0.025	5.5	22.7	705	92.43
4	Central Italy	GSA	2016-08-24	0.037	6.0	38.8	492	66.03
5	Lazio Abruzzo	RCC	1984-05-07	0.036	5.9	46.8	375	22.71
6	Central Italy	T1217	2016-10-26	0.044	5.9	27.2	-	170.51
7	Emilia 2nd Shock	CAS02	2012-05-29	0.041	6.0	33.0	-	152.00
Zone 3: 0.05g<PGA≤0.15g								
1	Central Italy	MI03	2009-04-07	0.133	5.5	2.8	378	112.58
2	Emilia 2nd Shock	CRP	2012-05-29	0.156	6.0	16.8	-	138.61
3	Central Italy	CSA	1997-10-06	0.110	5.4	21.1	-	28.77
4	Central Italy	MMO	2016-10-26	0.150	5.9	16.2	-	43.45
5	Central Italy	TLO	2016-10-30	0.114	6.5	44.3	-	94.58
6	Central Italy	MDAR	2016-10-26	0.127	5.9	31.6	-	75.18
7	Northern Italy	T0824	2012-05-29	0.137	5.5	12.5	-	100.00
Zone 2: 0.15g<PGA≤0.25g								
1	Umbria-Marche 1st Shock	CLF	1997-09-26	0.247	5.7	2.8	145	44.45
2	Central Italy	CLO	2016-10-26	0.193	5.9	10.8	-	39.26
3	Central Italy	CSC	2016-10-30	0.158	6.5	14.9	698	56.86
4	Central Italy	MMO	2016-10-30	0.189	6.5	19.2	-	60.00
5	Emilia 2nd Shock	MOG0	2012-05-29	0.170	6.0	15.8	-	115.00
6	Central Italy	NOR	2016-08-24	0.180	6.0	15.6	-	39.95
7	Central Italy	T1216	2016-10-26	0.202	5.9	9.2	-	87.30
Zone 1: PGA>0.25g								

1	L'Aquila	AQG	2009-04-06	0.489	6.1	5.0	696	100.00
2	Emilia 1st Shock	MRN	2012-05-20	0.262	6.1	16.1	208	130.15
3	Central Italy	NRC	2016-10-26	0.300	5.4	10.1	498	52.94
4	Friuli 3rd Shock	GMN	1976-09-15	0.255	6.0	4.0	445	9.28
5	Northern Italy	T0819	2012-05-29	0.258	5.5	6.8	208	60.00
6	Central Italy	T1212	2016-10-30	0.278	6.5	10.5	-	61.92
7	L'Aquila	AQU	2009-04-06	0.260	6.1	2.2	696	90.000

Table 4-14: Chosen accelerograms for parametric analysis

where: R is the epicentral distance and M_w is the moment magnitude and t_D the record duration.

In the end, considering 78 values for the vector R_T, 27 values for R_M and 28 accelerograms, 58968 dynamic analysis were performed on 2-DOF structure of Figure 4-33 and the rigid structure depicted in Figure 4-37.
The results obtained for each accelerogram of each seismic zone were averaged with those of the other 6 accelerograms of the same zone according to Eurocode 8 (EN 1998-1-1, 2005) where it is provided that when at least 7 different time-histories acceleration are used, the structure effects are represented by the average of the more adverse values.
Eventually, the results obtained for each of the 4 seismic zones were again average to obtain only one representative function.
The results are represented in terms of R_T, R_M and F_{real}/F_{rigid} ratios in Figure 4-39 with two axonometric view

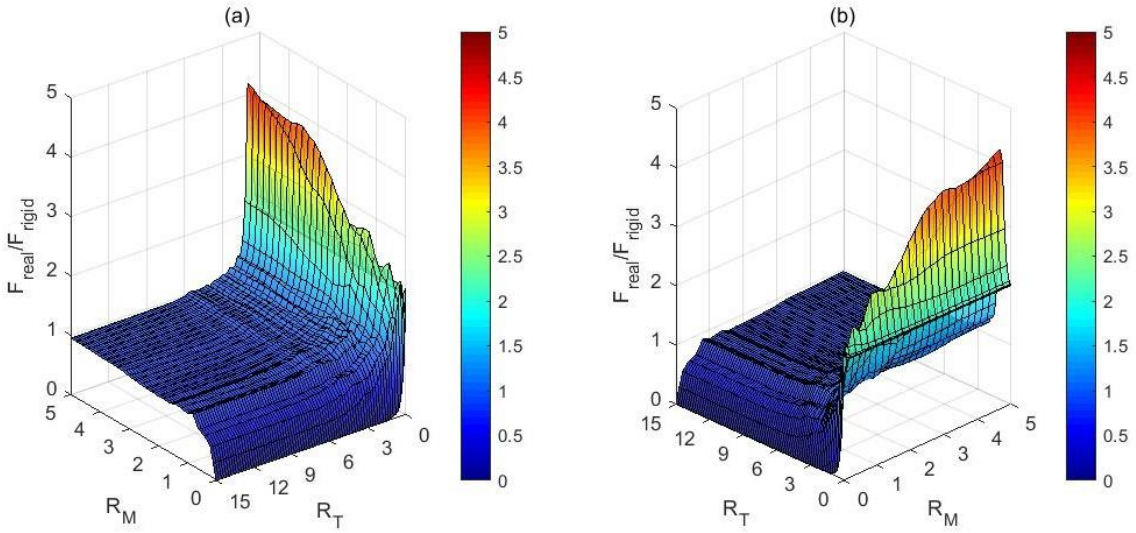

Figure 4-39: Parametric analysis result function: "south-west" view (a) and "south-est view" (b)

Observing the graph in Figure 4-39 it can be immediately noticed that if the ratio R_T, ratio between the period of the structure and the period of the panel, is near to 1.00 there is amplification, up to 4 times, of the connection out-of-plane force F_{real} on real structure with respect to the connection out-of-plane force F_{rigid} on the infinitely stiff structure.

In order to practically explain the surface of the graph in Figure 4-39 let's consider four vertical concrete panels with the elastic modulus E =3.8e7 kN/m^2 and the dimension illustrated in the following Table 4-15 that are typical of panels that can be commonly found on the market.

Panel number	Thickness [m]	Width [m]	Height [m]	Weight [kN/m²]	Panel period T_{panel} [s]	Structure period $T_{structure}$ [s]	Period ratio R_T	Line color
1	0.25	2.40	15	3.04	0.51	1.00	**1.96**	

2	0.30	2.40	15	3.63	0.42	2.00	**4.71**	
3	0.25	2.40	10	3.04	0.23	2.00	**8.81**	
4	0.30	2.40	10	3.63	0.19	1.00	**5.30**	

Table 4-15: Panels characteristics

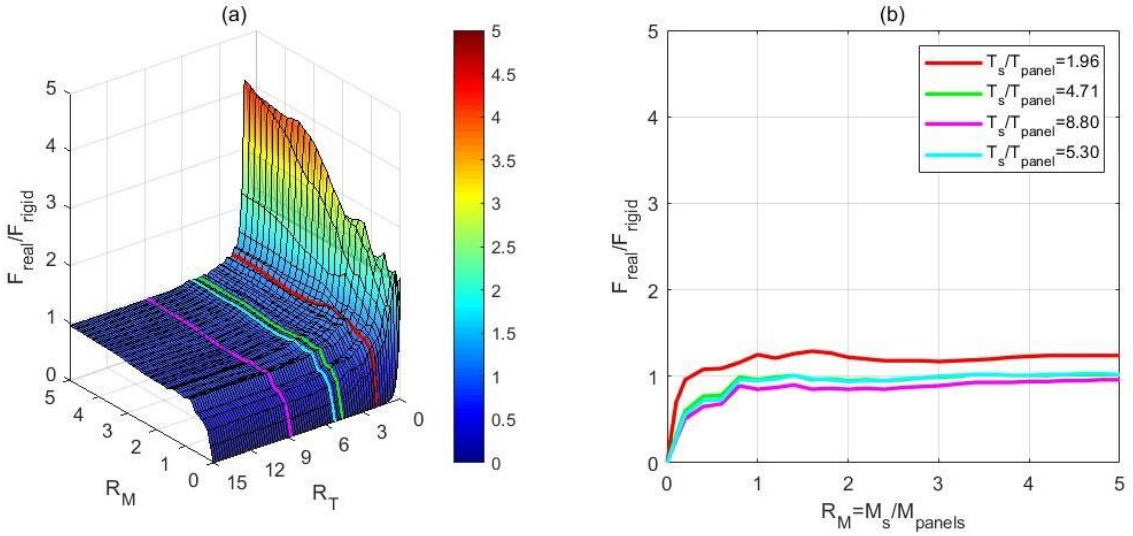

Figure 4-40: Typical panels example: section line at correspondent R_T (a) and section lines projection on R_M-F_{real}/F_{rigid} plane (b)

As can be seen from Table 4-15, each chosen panel, once a vibration period for the main structure is established, defines an R_T value. For each value of R_T, a section line can be drawn on the surface (Figure 4-40a). The section lines are projected on the R_T-F_{real}/F_{rigid} plane (Figure 4-40b)

By examining Figure 4-40b it can be noted that if the R_M ratio tends towards zero then the F_{real}/F_{rigid} ratio also tends towards zero as well. R_M can be zero in 2 cases:

1. if the mass of the structure tends towards zero (Figure 4-41a)
2. or if the panel mass tends towards infinity (Figure 4-41b).

In both cases, to make sure that the R_T remains constant, for example, 1.96 for the purple line, the ratio between masses and stiffnesses cannot change.
In the first case, to ensure that the R_T remains constant when the structure mass tends towards zero, the structure stiffness has to tend towards zero, so the simplified structure of Figure 4-33 becomes almost unstable and the connection force tends towards zero.
In the second case, the mass of the panel is so large that, to ensure a constant R_T, the stiffness of the panel has to be very large so that the structure no longer offers a support to the panel, then there is the same situation as in the previous case.

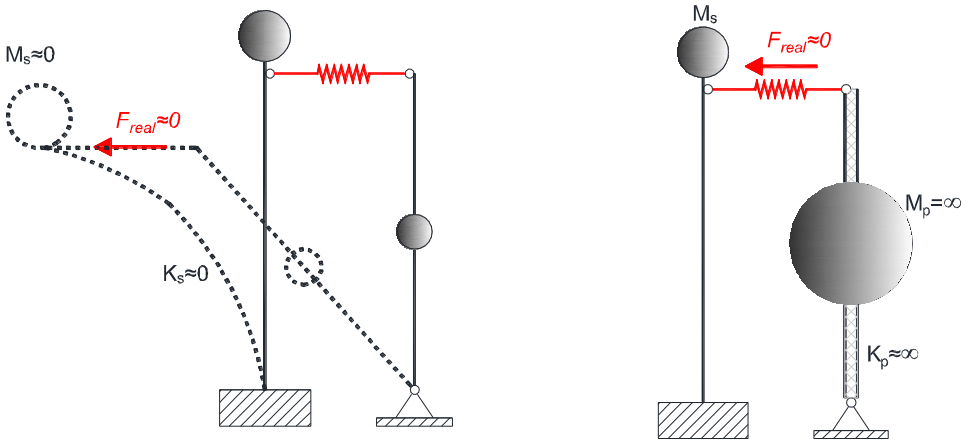

Figure 4-41: Case 1: mass of the structure tends towards zero (a). Case 2: panel mass tends towards infinity (b).

On the contrary, from Figure 4-40b it can be noted that when R_M tends to become very large, the F_{real}/F_{rigid} ratio tends to 1.
R_M can be large in 2 cases:

1. if the mass of the structure tends towards infinity (Figure 4-42a),
2. or the mass of the panel tends towards zero (Figure 4-42b).

In both cases, since the mass of the structure is much larger than that of the panel, due to its large inertia, it tends to become a constraint for the panel. In this way, the structure mass does not transmit force to the panel mass. Therefore, the connection force is due only to the ground motion imposed at the base of the panel.

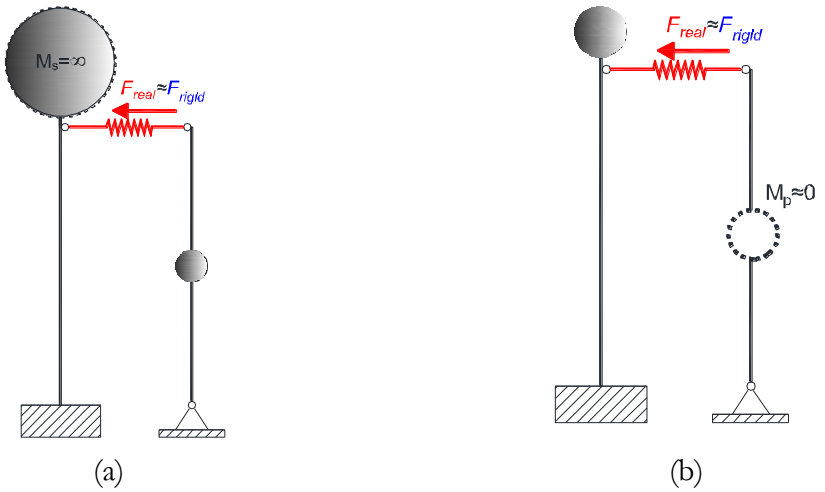

Figure 4-42: Case 1: mass of the structure tends towards infinity (a). Case 2: mass of the panel tends towards zero (b).

Let's now consider four typical R_M ratios for real structures: R_M=0.4 for structures with heavy claddings system, R_M=1 for structures with medium-heavy panels, RM=2 for structures with a light cladding panels system and R_M=4 for structures with a very light claddings system.
Once these four values for R_M have been set, the corresponding section lines on the surface can be traced as shown in Figure 4-43a The section lines are projected into the R_T-F_{real}/F_{rigid} plane as shown in Figure 4-43b.

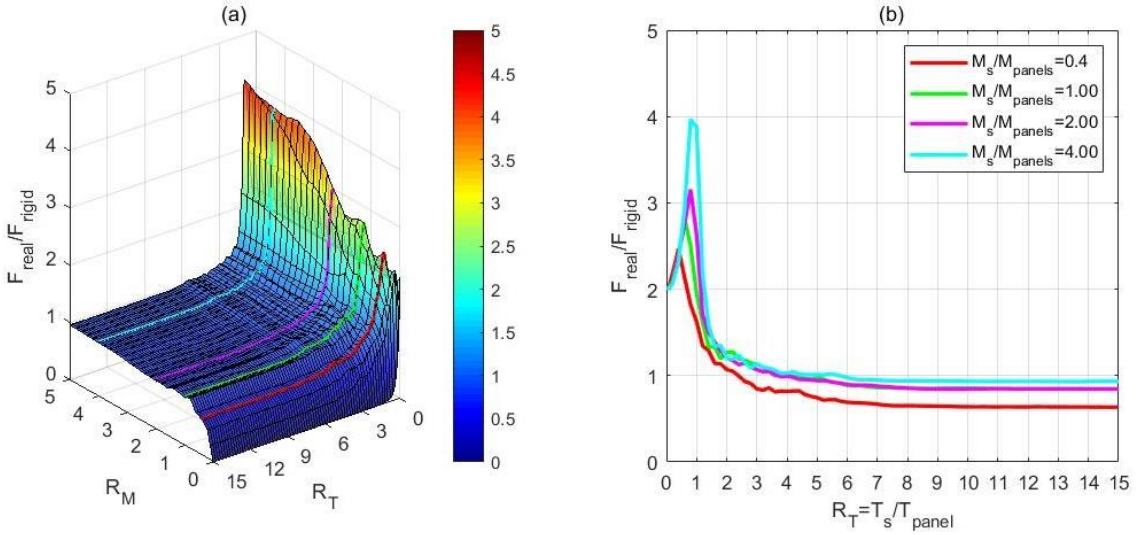

Figure 4-43: Typical masses ratio example: section line at correspondent R_M (a) and section lines projection on R_T-F_{real}/F_{rigid} plane (b)

By examining Figure 4-43b it can be noted that if the R_T ratio tends towards zero when the F_{real}/F_{rigid} ratio tends towards 2. R_T can be zero in 2 cases:

1. if the structure vibration period tends towards zero,
2. or if the panel period tends towards infinity.

Since the R_M ratio between the masses cannot change, the only factor that can be modified is stiffness. In both cases, a system in which the structure is much stiffer than the panel it is obtained. This is the case in the case of an infinitely rigid structure explained in subsection 4.4.2. The ground motion is completely transferred at the panel top, so the panel is accelerated at the base and at the top (Figure 4-44) by the same ground motion and, obviously, the connection force becomes two times larger than in the case when the acceleration is imposed only at the panel base.

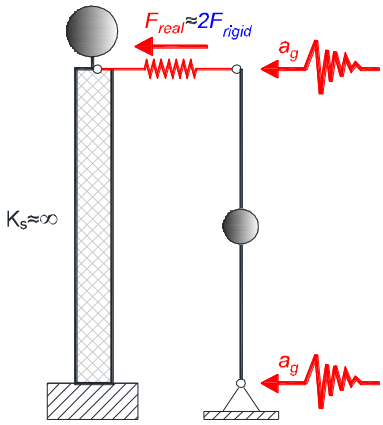

Figure 4-44: Infinitely stiff structure

On the contrary, from Figure 4-43b it can be noted that when R_T tends to become very large, the F_{real}/F_{rigid} ratio tends to 1.

R_T can be large in 2 cases:

1. if the period of the structure tends towards infinity,
2. or the period of the panel tends towards zero.

In both cases, the structure tends to assume the static scheme of a simply supported panel and only the acceleration at the panel base is transmitted to the masses.

In the end, it is evident that when the ratio R_T is near to 1.00, or rather the structure vibration period is about same as that of the panel, we have an amplification of the real structure force F_{real} with respect to the of the infinitely stiff structure force F_{rigid}.

In order to find a mathematical expression for the surface represented in Figure 4-39 the Matlab curve fitting toolbox was used. The numerical data obtained from the parametric analysis were fitted with two different surfaces: one for $R_T > 1$, the green surfaces in Figure 4-45a and one for $R_T \geq 1$, the red surfaces in Figure 4-45b:

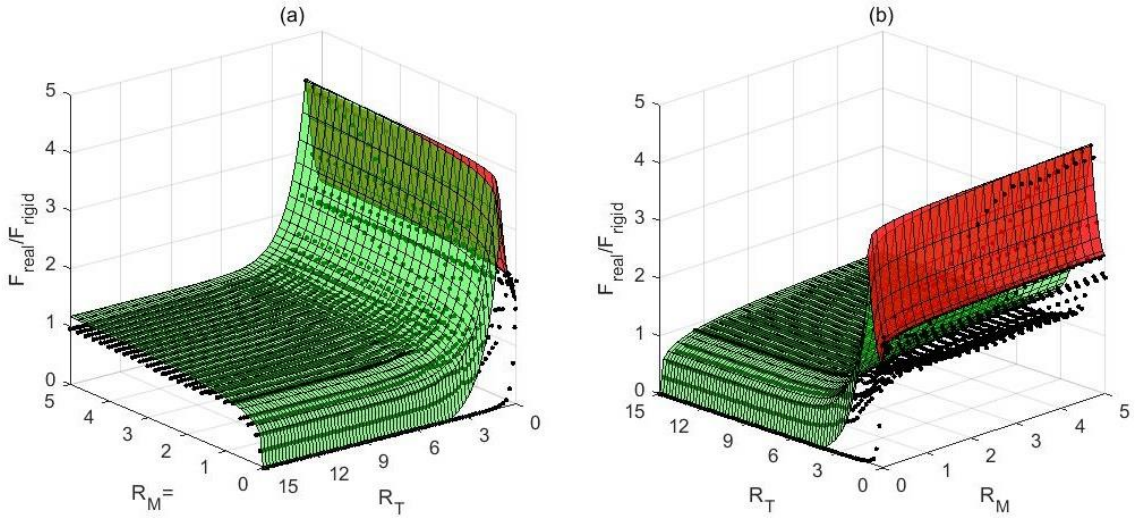

Figure 4-45: Fitting surfaces

The green fitting surface has the equation:

$$\frac{F_{real}}{F_{rigid}} = \left[0.93 + 8.32 \cdot e^{-\frac{T_s}{T_{panel}}} + 0.25\ln\left(\frac{M_s}{M_{panels}}\right)\right] \quad \text{for } \frac{T_s}{T_{panel}} > 1 \qquad (4.27)$$

with an R-square value of 0.607

The red fitting surface has the equation:

$$\frac{F_{real}}{F_{rigid}} = \left[2.27 + 1.82\left(\frac{T_s}{T_{panel}}\right)^2 + 0.07\ln\left(\frac{M_s}{M_{panel}}\right)\right] \quad \text{for } \frac{T_s}{T_{panel}} \leq 1 \qquad (4.28)$$

with an R-square value of 0.548

The R-Square value measures how successful the fit is in explaining the variation of the data. In other words, R-square is the square of the correlation between the response values and the predicted response values. It is also called the square of the multiple correlation coefficient and the coefficient of multiple determination.
R-square is defined as the ratio of the sum of squares of the regression (SSR) and the total sum of squares (SST). SSR is defined as

$$SSR = \sum_{i=1}^{n} (\hat{y}_i - y)^2 \qquad (4.29)$$

SST is also called the sum of squares about the mean, and is defined as

$$SST = \sum_{i=1}^{n} (y_i - \bar{y})^2 \qquad (4.30)$$

R-square is expressed as

$$R_{square} = \frac{SST}{SSR} \qquad (4.31)$$

where
y_i are the observed data;
$\bar{y}$ is their average;
$\hat{y}_i$ are the data estimated from the model obtained by the regression.

It was then regarded as appropriate to try fitting surfaces that had a F_{real}/F_{rigid} value always greater than the one of the surface found with the parametric analysis. This in order to be on the safe side. This is also the reason for why the values of R-square for fitting surfaces are relatively low.

For the panel number 3 of Table 4-15 the following 2 cases are now considered: the first, where the force on the panel, called F_{real}, is calculated by means of the floor spectra (Figure 4-46a) having equation (2.3) and the second case in which the action on the panel, called F_{rigid}, is calculated with the use of the average spectrum (Figure 4-46b) of all the accelerograms within the Table 4-14 and illustrated in the Figure 4-46c

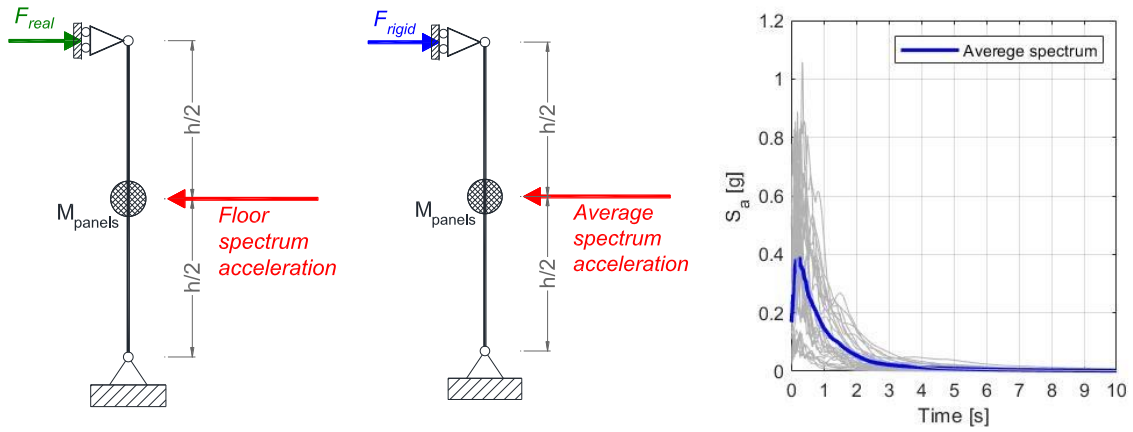

(a) (b) (c)

Figure 4-46: F_{real} calculated with floor spectra (a), F_{rigid} calculated with average spectrum (b), and the average spectrum (c)

The ratio $R_F = F_{real}/F_{rigid}$ is then evaluated for each R_T ratio used for the previous explained parametric analysis. The floor spectra equation (2.3) does not depend on the masses M_{panels} and $M_{structure}$ but only on the periods that was fixed by R_T. What results is a surface that can be compared with the one previously illustrated in Figure 4-39.
The comparison between the two surfaces is depicted in Figure 4-47. The same section lines of Figure 4-43 are traced for the two surfaces and projected on the R_T-F_{real}/F_{rigid} plane. The floor spectra tend to overestimate the connection force for R_T ratios greater than 1.50, in

particular in the range of R_T between 1.00 and 4.50. It is also noted that the amplification peak is, in the same way, in correspondence of R_T value about 1.00. Furthermore, for R_T values close to 0.00 there is a considerable underestimation of the F_{real}/F_{rigid} ratio but this is a limit case that hardly concerns some real buildings.

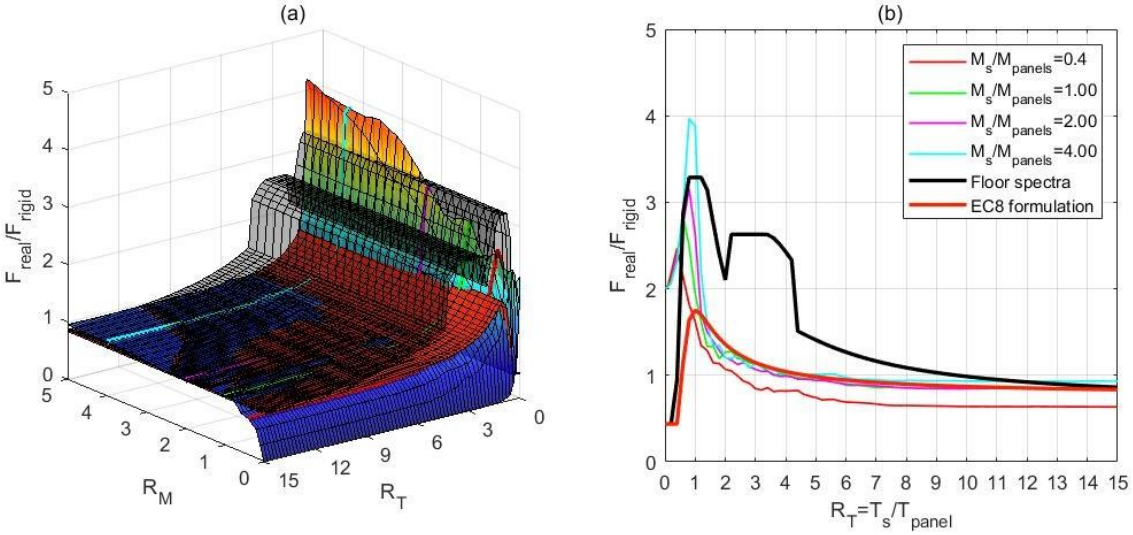

Figure 4-47: Floor spectra and parametric analysis surfaces comparison (a) and section lines projection on R_T-F_{real}/F_{rigid} plane (b)

4.6 Conclusion

In this chapter, the out-of-plane behaviour of connections for vertical panels was studied.
The out-of-plane behaviour of the connections is mainly regulated by their payload in terms of ultimate resistance because in the orthogonal direction to the panels' plane the displacements between the cladding system and the main structure needs to be limited. The connections payload depends on the geometry, materials and the static arrangement adopted for each device. Therefore, it is necessary to carry out laboratory tests before mounting new connection types. Furthermore, the resistance of the devices has to be tested both on the panel and on the structure side and the smaller of the two resistances provides the design resistance.
The out-of-plane resistance of 2 connection devices for vertical panels was tested. The new connection devices for vertical panels called "SismoSafe" showed significantly higher resistance regarding to out-of-plane capacity if compared to the traditional connections (hammer-head straps).
As for the force demand, always in the out-of-plane direction, it is clear that it is determined by the ratio between the panel's mass and the structure's mass and by the ratio between panel's and structure's stiffness of the panel (i.e. the ratio between the vibration periods of the panel and the structure). For this reason, a formulation that relates the force on the connection with the ratios between masses and between periods was investigated. Through a parametric analysis, it was possible to study the relationship between these three quantities and finally an analytical formulation was proposed as an alternative to the use of the floor spectra formulation considered by the Eurocode 8 (EN 1998-1-1, 2005).

5 Parametric study on the seismic response of panel-to-structure connections

5.1 Introduction

In this section, a parametric study on the seismic response of panel-to-structure connections will be performed.
The main purposes of the study are:

- Investigate the influence of types of panel-to-structure connection on the seismic response of precast RC buildings.
- Compare the response of fixed and rocking panels and find the advantages and disadvantages of both configurations.
- Understand in which cases the connection devices do not provide sufficient security against the seismic actions.
- Study the influence between the number of columns and the number of panels on the seismic demand of the panel-to-structure connections.
- Assess whether the critical behaviour of the connections is defined by in-plane or out-of-plane seismic forces imposed

The parametric study will take into account three types of panel-to-structure connection, also examined in the previous sections:

- Short hammer-head strap TA-210
- Long hammer-head strap TA-290
- SismoSafe device

The study will focus exclusively on one-storey RC precast structures with a cladding system made of vertical panels. The panel boundary conditions at the foundation addressed in the study will be two:

- Fixed panels
- Rocking panels

An extensive and systematic parametric study of vulnerability and seismic risk of single-storey prefabricated buildings, typical for Central and Southern Europe, had already been carried out by (Kramar et al., 2010) and (Zoubek, 2015)
In the performed studies the mainly beam-to-column but also the panel-to-structure connections were analysed, although the influence of out-of-plane forces was neglected for the latter because it was assumed that the panel-to-structure connections were able to support, without any damage, the out-of-plane forces imposed by the seismic action.
The study presented below differs from the previously mentioned ones because it will be deterministic rather than probabilistic, it will mainly focus on the panel-structure connections studied in the previous chapters and it will take into account the simultaneous presence of the in and out-of-plane seismic action.
Another important aspect is that the study starts from experimental data obtained from the shaking table test and from numerical models calibrated on such data, both regarding the behaviour of the structure and the connections.
First, in the next section 5.2, the type of buildings designed and dimensioned according to Eurocode 8 (EN 1998-1-1, 2005) will be described. A hinged frame static scheme (see Figure 1-4) was assumed for the load-bearing structure. The scheme is typical of one-storey precast RC buildings. In this scheme, the structure seismic capacity is mainly defined by the columns that need to be properly designed.
The capacity of investigated connections (TA-210, TA-290 and SismoSafe) will be compared with the seismic demand, that will be gradually increased as a function of the peak ground

acceleration, PGA. The parametric study will identify the right building configuration and the PGA value up to which the three chosen connection devices are appropriate. It will also identify which direction in plane and out-of-plane is critical

5.2 Set of buildings studied and dimensioning

For the parametric study, a set of 15 single-storey prefabricated reinforced concrete buildings was selected. The buildings considered were symmetrical along both orthogonal axes and consist of cantilever columns connected in the transverse direction with main roof elements and in the longitudinal direction with secondary roof elements (not drawn in the sketch). On the perimeter of the considered buildings there were edge beams to which the façade panels are usually fixed (Figure 5-1). The columns and the edge beams are meant to be connected employing joints with dowels made in the upper part of the columns or the upper part of column corbels.

For the chosen buildings the spans ranged from 7.5 to 12.5 m and the bays, in the main roof elements direction, are 12 to 30 m long, and the columns were 5, 7 and 9 m height. It has been assumed that the buildings had only two bays in the transverse direction and an indefinite number of spans in the longitudinal direction.
Assuming also that the roof behaved like a rigid diaphragm and provided that all the columns of the structure had the same features, then these buildings could be modelled with a single cantilevered column with a top mass ranging from 20 to 100 tons.
As described in the work of Zoubek (2015), to calculate these masses, a distributed load on the roof equal to $w = 5\ kN/m^2$ was considered for all buildings. The roof elements' dead load is usually $2.5 - 3.5\ kN/m^2$. If we add to this the dead load of the beams ($1\ kN/m^2$) and a costant superdead load ($0.5\ kN/m^2$) we have that the total load on the roof does not exceed $5\ kN/m^2$, the snow load and the live load on the roof were not taken into account for seismic combinations.

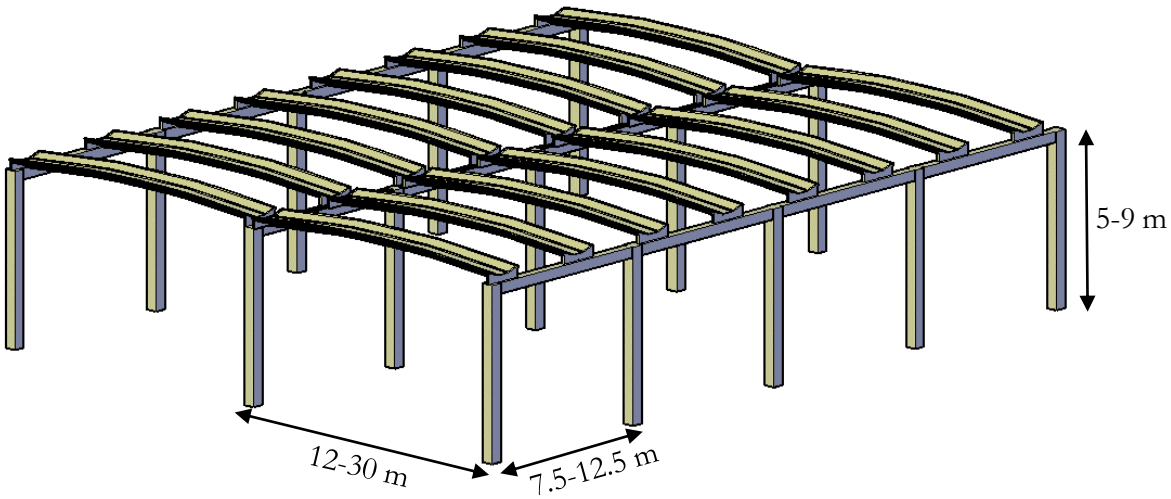

Figure 5-1: Scheme of the structural arrangement of the analysed one-storey industrial buildings.

Since all the considered one-storey buildings were modelled with only one cantilever column, the real range of all the studied buildings can be obtained, in practice, by varying the mass (m) for each equivalent column and by varying its height (H).
Therefore, columns with masses from 20 to 100 t were analysed with an increasing step of 20 t (Table 5-1). For each mass, columns with three different heights H= 5, 7 and 9 m were considered (Table 5-1).
The design of all these buildings according to the Eurocode 8 standard (EN 1998-1-1, 2005) are briefly reported below, following the PhD. thesis of Zoubek (2015).
Assuming that the structures were located in a zone with a bedrock acceleration of 0.25g and are built on a soil type C, the values of the parameters that determine the shape of the response spectrum are: S = 1.15, T_B = 0.2s, T_C = 0.6s and T_D = 2.0s.

Column design

The column design is made according the study of Zoubek (2015).
First of all, the reinforcement steel grade and the concrete class are defined.
A concrete grade C40/50 was chosen. Its properties were determined according to Eurocode 2 (EN 1992-1-1, 2004): f_{ck} = 40 MPa, f_{cd} = 26, 7 MPa, E_{cm} = 35 GPa, ε_{c2} = 2.0‰, ε_{cu2} = 3.5‰.
S500 steel was chosen for the reinforcement bars: f_{yk} = 500 MPa, f_{yd} = 435 MPa, E_s = 200 GPa. It was assumed that the steel is of ductility class C.
This type of steel has a characteristic strain at maximum stress ε_{uk} at least 7.5% and a value of the hardening coefficient k = f_t/f_y between 1.15 and 1.35 (EN 1992-1-1, 2004).
Since the model of the buildings considered is relatively simple (cantilever column with a mass on top), the fundamental vibration period T_1 is evaluated according to the following well-known simple equation:

$$T_1 = 2\pi\sqrt{\frac{m}{k_{ef}}} = 2\pi\sqrt{\frac{mH^3}{3E_{cm}J}} \qquad (5.1)$$

where m is the tributary mass on the considered column, k_{ef} is its actual bending stiffness, H is its height, E_{cm} is the elastic modulus of the concrete and J is the moment of inertia of the column cross-section. The moment of inertia J was calculated considering the reduced moment of inertia, due to the cracking of columns. Therefore, the moment of inertia was reduced by 50% according to the recommendation provided in Eurocode 8.
Starting from the calculated spectrum, according to with Eurocode 8, it was possible to determine the design spectral acceleration S_d (T_1) and the elastic spectral displacement S_{De} (T_1), for the behaviour factor, a value equal to q = 3.0 was chosen (according to with the medium ductility class, DCM).
As reported in some previous studies on the seismic behaviour of reinforced concrete precast structures (Kramar, 2008), the dimensions of the columns are generally determined by the deformation limit state, e.g. the drift limit imposed by the code.
Therefore the initial column sizes were chosen according to the following condition:

$$d_r \upsilon \leq 0.01H \qquad (5.2)$$

where d_r is the design inter-storey drift, calculated by means of the elastic displacement spectrum S_{De} (T), ν is a reduction factor that takes into account the shorter earthquake return period associated with the damage limitation requirement. The value of the factor ν is defined by Eurocode 8 according to the importance class of building. The recommended values of ν are: 0.4 for importance classes III and IV and ν = 0.5 for importance classes I and II. For this study ν = 0.4 has been chosen.

At the same time, the influence of second-order effects shall be checked by the inter-storey drift sensitivity coefficient, θ:

$$\theta = \frac{P_{tot}\, d_r}{V_{tot}\, H} \quad (5.3)$$

where P_{tot} is the total gravity load of the roof and V_{tot} is the total horizontal force due to the seismic action. The Eurocode 8 requires the coefficient θ to be less than 0.3. If $\theta \leq 0.1$, the influence of the second-order effects may be neglected. If, on the other hand, $1 < \theta \leq 0.2$, the second-order effects may approximately be taken into account by multiplying the relevant seismic action effects by a factor equal to $1/(1-\theta)$. The value of the coefficient θ shall, in any case, not exceed 0.3

After the dimensions of the columns were chosen, by determining the moment of inertia *J* such that conditions (5.2) and (5.3) are fulfilled, the amount of longitudinal reinforcement is designed. Longitudinal reinforcement has to be such that the bending capacity of the column M_{Rd} (determined according to EN 1998-1-1, 2005 and EN 1992-1-1, 2004) is higher than required by the following equation:

$$M_{Rd} \geq V_{tot} \frac{H}{1-\theta} \quad (5.4)$$

The number and distance between the longitudinal reinforcement bars were determined from the cross-sectional dimensions of the column (Figure 5-2).

The Eurocode 8 specifies that distance between consecutive longitudinal bars engaged by hoops or cross-ties does not exceed 200 mm.

Only one bar diameter was used within a cross-section.

Based on Table 5-1 data, it is possible to observe that only in five of the fifteen cases considered, equation (5.4) requires more reinforcement than the minimum longitudinal reinforcement condition. Indeed, Eurocode 8, requires the cross-sectional area of the entire longitudinal reinforcement to be at least 1% of the column cross-sectional area.

The condition of minimum longitudinal reinforcement is often critical, due to the large size of the column imposed by the inter-storey drift limit requirement (equation(5.2)). Consequently, the amount of cross-section longitudinal reinforcement is automatically sufficient to withstand design loads imposed by equation(5.4).

The column shear capacity V_{Rd} was determined according to the capacity design rules:

$$V_{Rd} \geq V_{Ed} = \gamma_{Rd}\, M_{Rd}/H \quad (5.5)$$

where the factor γ_{Rd}, which takes into account overstrenght and confinement in the compressed area of the cross-section, is equal to 1.1 for the medium ductility class (DCM). As M_{Rd}, V_{Rd} is determined according to Eurocode 2.

It was decided to use only hoops with a diameter of 8 mm (Figure 5-2), spaced so that condition (5.5) is met.

However, two further checks had to be carried out.

First, it was necessary to verify that the Eurocode 8 requirements for the hoops maximum spacing, s_{max}, are fulfilled:

$$s_{max} = \min(b_0/2; 175mm; 8d_{bL}) \quad (5.6)$$

where b_0 (in millimetres) is the minimum dimension of the concrete core (to the centreline of the hoops); and d_{bL} is the minimum diameter of the longitudinal bars (in millimetres).
In addition to the maximum hoops spacing, it was necessary to verify the mechanical volumetric ratio of confining hoops within the critical regions to justify the ductility that was assumed by choosing the behaviour factor q = 3.0.
According to Eurocode 8, it was necessary to verify that:

$$\alpha\omega_{wd} \geq 30\mu_{\phi}\upsilon_d\varepsilon_{sy,d}\frac{b_c}{b_0} - 0.035 \qquad (5.7)$$

where ω_{wd} is the mechanical volumetric ratio of the confining hoops within the critical regions, μ_{Φ} is the required value of the ductility coefficient in terms of curvature, that depends on the selected behaviour factor q; ν_d is normalized design axial force; $\varepsilon_{sy,d}$ is the design value of the steel strain at yield strength; b_c is the gross cross-sectional width; b_0 is the width of confined core (to the centreline of the hoops) and α confinement effectiveness factor (for the calculation of the individual quantities, see EN 1998-1-1, (2005)).
Furthermore, it is recommended that condition (5.7) provides a minimum value of ω_{wd} equal to 0.08, for DCM design, within the critical region at the base of primary seismic columns.

In seven of the fifteen cases, the maximum distance between the hoops was determined by condition (5.6) (see also Table 5-1). In two cases (m80H5 and m100H5) a reduced spacing between the hoops was required due to the high shear demand, determined by condition (5.5).
In all cases, the amount of transverse reinforcement was always greater or equal than the minimum value of the hoops volumetric ratio $\omega_{wd} \geq 0.08$.
In the investigated columns, equation (5.7) could be easily satisfied since there was a high ductility of curvature μ_{Φ}, the reason could be mainly found in the low level of axial force ν_d, which is quite common in one-storey precast buildings.

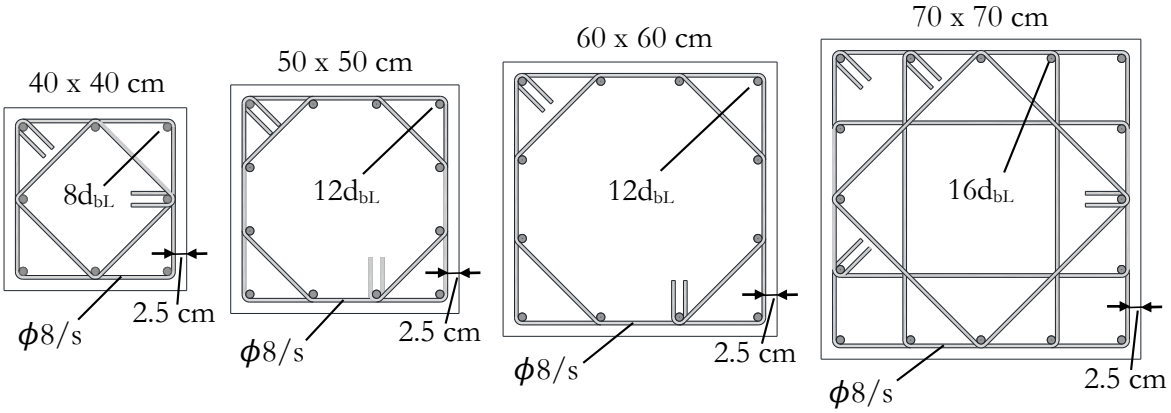

Figure 5-2: Possible column sections of the analysed one-storey buildings (designed according to Eurocode 8)

Label	**m20H5**	**m20H7**	**m20H9**	**m40H5**	**m40H7**	**m40H9**	**m60H5**	**m60H7**	**m60H9**	**m80H5**	**m80H7**	**m80H9**	**m100H5**	**m100H7**	**m100H9**
m [t]	20	20	20	40	40	40	60	60	60	80	80	80	100	100	100
H [m]	5	7	9	5	7	9	5	7	9	5	7	9	5	7	9
h_c [m]	0.4	0.4	0.5	0.5	0.5	0.6	0.5	0.6	0.6	0.6	0.6	0.7	0.6	0.6	0.7
T [s]	0.94	1.56	1.46	0.85	1.41	1.43	1.05	1.2	1.75	0.84	1.39	1.49	0.94	1.55	1.66
S_a [g]	0.152	0.092	0.099	0.168	0.102	0.1	0.137	0.119	0.082	0.171	0.103	0.097	0.153	0.093	0.086
d_r [m]	0.1	0.17	0.16	0.09	0.15	0.15	0.11	0.13	0.19	0.09	0.15	0.16	0.1	0.17	0.18
$d_{r,max}$ [m]	0.13	0.18	0.23	0.13	0.18	0.23	0.13	0.18	0.23	0.13	0.18	0.23	0.13	0.18	0.23
N_{Ed} [kN]	196	196	196	392	392	392	589	589	589	785	785	785	981	981	981
ν	0.046	0.046	0.03	0.059	0.059	0.041	0.089	0.062	0.062	0.083	0.083	0.06	0.1	0.1	0.075
θ	0.133	0.26	0.176	0.109	0.213	0.17	0.163	0.154	0.255	0.105	0.206	0.183	0.131	0.257	0.229
M_{Ed} [kNm]	172	171	211	371	355	427	483	582	583	751	715	836	865	855	990
Long. reinf.	8ø18	8ø18	12ø16	12ø20	12ø20	12ø20	12ø22	12ø22	12ø22	12ø25	12ø25	16ø20	12ø25	12ø28	16ø22
ρ_l	0.013	0.013	0.010	0.015	0.015	0.011	0.018	0.013	0.013	0.016	0.016	0.010	0.016	0.021	0.012
M_{Rd} [kNm]	175	175	261	404	404	513	486	635	635	794	794	880	953	953	1042
V_{Ed} [kN]	39	28	32	89	63	63	107	100	78	175	125	108	210	150	127
s_{max} [cm]	14.4	14.4	12.8	16	16	16	17.5	17.5	17.5	17.5	17.5	16	17.5	17.5	17.5
s [cm]	14	14	12	16	16	12	16	12	12	12	12	16	12	12	16
$V_{Rd,c}$ [kN]	69	69	98	113	113	144	121	153	153	167	167	193	167	180	206
$V_{Rd,s}$ [kN]	170	170	270	202	202	324	202	324	324	324	324	560	324	324	490
ω_{wd}	0.113	0.113	0.109	0.081	0.081	0.089	0.081	0.089	0.089	0.088	0.088	0.093	0.088	0.088	0.093

The condition of minimum longitudinal reinforcement (1% reinforcement) is critical.
The condition of minimum distance between hoops is critical (see expression(5.6)).

Table 5-1: Columns design of the analysed one-storey buildings according to Eurocode 8. (courtesy of Zoubek (2015))

5.3 Accelerograms selection

For each of the constructions analysed, non-linear dynamic analysis with a series of accelerograms was performed.
The accelerograms were selected from the European (ESD) (Luzi et al., 2016) and Italian (ITACA) (Luzi et al., 2019) database of seismic records, using the procedure described in Eurocode 8.
The Eurocode elastic spectra for soil type **A** with maximum peak ground acceleration PGA = 0.05 g, 0.15 g, 0.25 g, 0.35 g and 0.45 g were selected as target spectra, requiring that in the period interval T=0 and T=3.5 s no value of the average elastic spectrum with 5% damping, calculated from all response-histories, is lower than 90%, and greater than 30% of the corresponding value of the target elastic response spectrum with 5% damping. Moreover, some additional conditions have been established, namely that the source of the earthquake is between 0 and 30 km away from the station, that the magnitude M_w of the selected earthquake is between 4 and 8 and that the selection chooses only unscaled records.
The main feature of the chosen **unscaled** accelerograms are reported in Table 5-2, and for each PGA value, the target spectrum, the average spectrum and the selected spectra are depicted in Figure 5-3.

N.	Event name	Station name	Date	PGA [g]	M_w	R [km]	$V_{s,30}$ [m/s]	Duration t_D [s]
Target spectrum PGA=0.05g								
1	Irpinia	ALT	1980-11-23	0.056	6.9	23.4	1018	66.49
2	Northwestern Balkan peninsula	TIG	1979-04-15	0.053	6.9	47.4	-	45.55
3	Central Italy	CSC	2016-10-26	0.066	5.9	23.1	698	52.12
4	Central Italy	PZI1	2016-08-24	0.046	6.0	30.2	-	63.45
5	Central Italy	SLO	2016-10-26	0.059	5.9	14.4	-	59.98
6	Central Italy	TRE1	2016-10-30	0.059	6.5	55.7	-	100.00
7	Northern Italy	MIR06	2012-05-29	0.043	5.5	21.2	-	150.01
Target spectrum PGA=0.15g								
1	Ionian Sea	MIRE	1997-11-18	0.129	6.4	38.3	251	65.44
2	Central Italy	CLO	2016-10-26	0.193	5.9	10.8	-	39.26
3	Umbria-Marche	CSA	1997-09-26	0.172	6.0	22.3	-	55.20
4	Central Italy	NOR	2016-10-26	0.121	5.9	13.3	-	73.86
5	Central Italy	PCB	2016-08-24	0.308	6.0	17.8	-	44.25
6	Irpinia	RNR	1980-11-23	0.099	6.9	35.5	539	79.86
7	Emilia 2nd Shock	T0824	2012-05-29	0.145	6.0	14.2	-	110.01
Target spectrum PGA=0.25g								
1	Central Italy	MZ27	2016-10-26	0.206	5.9	28.8	422	148.84
2	Emilia 2nd Shock	MIRE	2012-05-29	0.177	6.0	4.1	-	61.97
3	Southern Greece	KAL1	1986-09-13	0.232	5.9	6.6	485	30.02
4	Emilia 1st Shock	MRN	2012-05-20	0.262	6.1	16.1	208	130.15
5	Emilia 2nd Shock	T0814	2012-05-29	0.505	6.0	9.2	-	100.01
6	Northern Italy	T0819	2012-05-29	0.258	5.5	6.8	208	60.01
7	Turkey	1201	2003-05-01	0.291	6.3	11.8	528	64.73
Target spectrum PGA=0.35g								
1	Alkion	ST122	1981-02-24	0.283	6.6	19.2	-	80.98
2	Central Italy	MZ63	2016-10-30	0.384	6.5	28.4	562	75.29
3	Central Italy	MZ102	2016-10-30	0.372	6.5	17.4	-	77.15
4	Dinar	AMT	1995-01-10	0.267	6.4	8.3	-	27.98
5	Central Italy	CMI	2016-10-26	0.651	5.9	7.1	-	30.00
6	Emilia 2nd Shock	MIR01	2012-05-29	0.380	6.0	0.5	-	150.05
7	Emilia 2nd Shock	MIR08	2012-05-29	0.248	6.0	8.6	-	170.00
Target spectrum PGA=0.45g								

1	Ducze	1401	1999-12-11	0.731	7.3	36.1	294	55.79
2	Central Italy	CLO	2016-10-30	0.418	6.5	7.8	-	60.00
3	L'Aquila	AQV	2009-04-06	0.657	6.1	4.9	474	100.01
4	L'Aquila	AQV	2009-04-06	0.546	6.1	4.9	474	100.01
5	Central Italy	NOR	2016-10-30	0.312	6.5	4.7	-	60.00
6	Turkey	0302	1995-10-01	0.327	6.0	0.5	198	28.00
7	Emilia 2nd Shock	MIR01	2012-05-29	0.419	6.0	0.5	-	150.01

Table 5-2: Selected accelerograms data.

where: R is the epicentral distance and Mw is the moment magnitude and t_D the record duration.

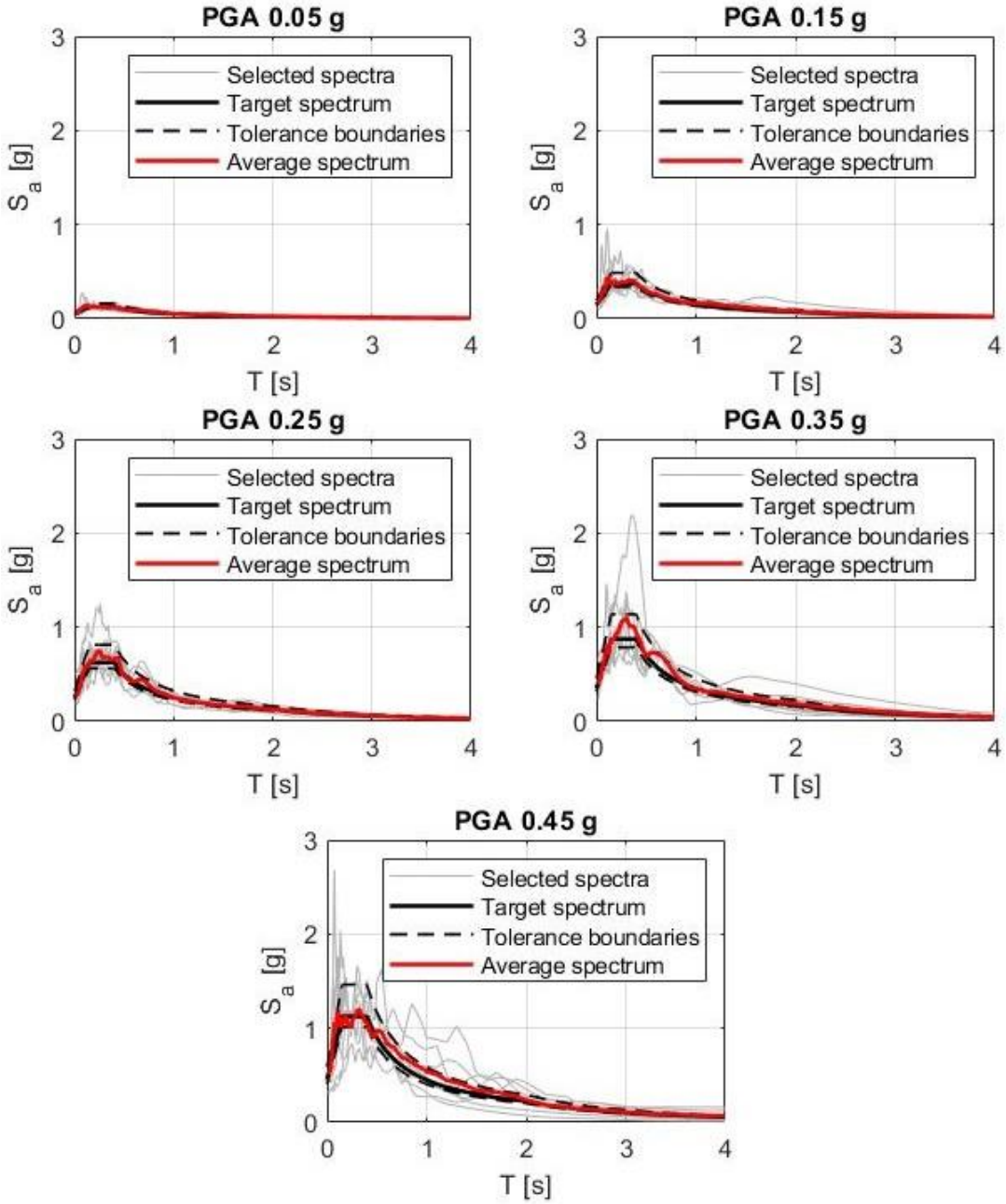

Figure 5-3: Target spectrum, the average spectrum and the selected spectra

5.4 Seismic demand of panel-to-structure connections

In this section, the seismic demand of hammer-head strap connections as well as SismoSafe connections is evaluated and compared with their capacity for each PGA level presented in § 5.3. The dimensions and capacities of the investigated connection were described within section 3.1, and 3.2 for the hammer-head straps and in section 3.5 and 4.1 for the SismoSafe device.
This section also examines the influence of vertical panels anchoring to the foundation beam. In practice, two solutions are often presented: (a) the bottom edges of the panels are joined to the foundation beam with anchorage bars or other steel elements (e.g. angles Figure 5-4a) assuming that they were designed to support maximum actions, or (b) the cladding panels are placed on the foundation beam by a groove and\or rib without additional connecting elements (Figure 5-4b). While solution (a) prevents the panels from being raised, solution (b) allows rocking, i.e. allows the panels to rotate around the lower edges. One of the objectives of this section is to compare the response of the two solutions and find the advantages and disadvantages of both of them. A second purpose is to study the possible influence between the number of columns and the number of panels on the seismic demand of the panel-structure connections.

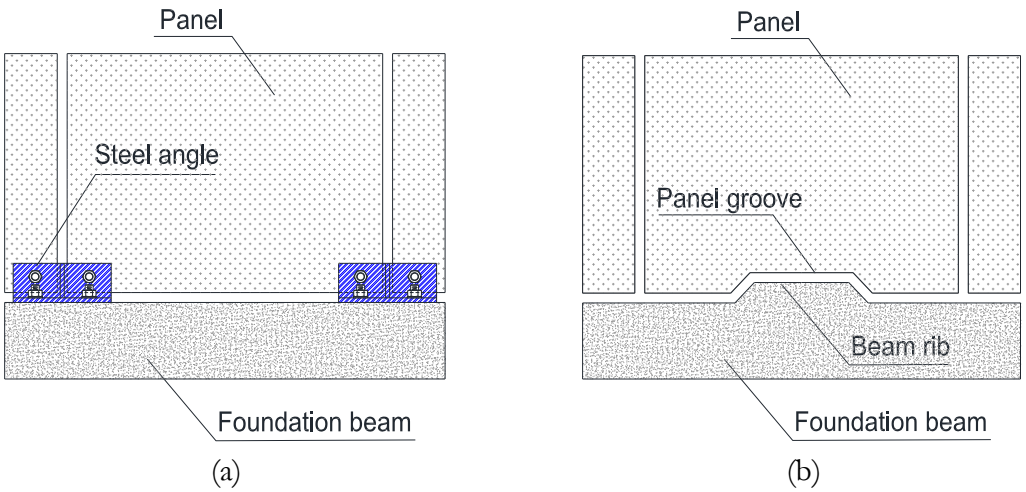

Figure 5-4: Fixed panel solution (a), rocking panel solution (b)

In section 5.4.2, non-linear models of the considered buildings, that take into account the non-linear response of the connections between the panels and the structure, are presented. Inelastic bending response modelling of building columns is described in section 5.4.3.
Concerning the connections, what was developed were non-linear models defined based on the recommendations provided in section 3.3.5 for the hammer-head strap and section 4.3 for the SismoSafe connection. Moreover, in section 5.4.4, the hammer-head strap model is appropriately modified to take into account the simultaneous presence of an in-plane and out-of-plane action. Since an out-of-plane force loads the connections, the critical buckling load for a single connection device is assessed in paragraph 5.4.5. In the last section 5.4.7, the seismic demand of the investigated structures is calculated and the essential results are summarized.

5.4.1 Representative set of building for parametric analysis

As mentioned at the beginning of section 5.2, for the purpose of this parametric study, a set of 15 one-storey precast industrial buildings was selected. Structural system of the analysed buildings is shown in Figure 5-1. It consists of a series of identical cantilever columns. The tops of the columns were tied together by edge beams and roof elements. The edge beams were connected to columns by means of dowel connections. The cladding panels were connected to the edge beam.
In the parametric study the building spans ranged from 7.5 to 12.5 m and the bays, in the main roof elements direction, are 12 to 30 m long (Figure 5-1). The height of the buildings was varied among 5 m 7 m and 9 m. Assuming a rigid diaphragm at the roof level, the lateral load resisting system was modelled with a single equivalent cantilever column. The corresponding mass was concentrated at the top of the column. The mass was defined taking into account the distributed load on the roof of w=5 kN/m^2. Considering the analysed spans (see Figure 5-1), the concentrated mass at the top of the equivalent column was in the range between m = 20 t and m = 100 t.

5.4.2 Models for non-linear dynamic analysis

The simplified mathematical models of single-storey buildings with vertical cladding panels are shown in
Figure 5-5. The non-linear bending behaviour of the columns and the non-linear shear behaviour of the connections between the façade panels and the structure are taken into account. The mass of the vertical panels was computed assuming that the width and thickness of the concrete part of the panel are the same in all considered structures (b_p = 2.5 m, t_p = 0.16 m) and that the height of the panel is equal to the height of the column. The panel was modelled with three lumped masses in order to have a more realistic model end to better evaluate the effect of out-of-plane force.
The columns were modelled by an element with lumped plasticity which will be described in detail in paragraph 5.4.3, the characteristic values of the hysteretic response are given in Table 5-5. The panel was modelled by an elastic frame element with unlimited capacity. Panel cracking was taken into account by a stiffness reduction of 50% according to Eurocode 8.

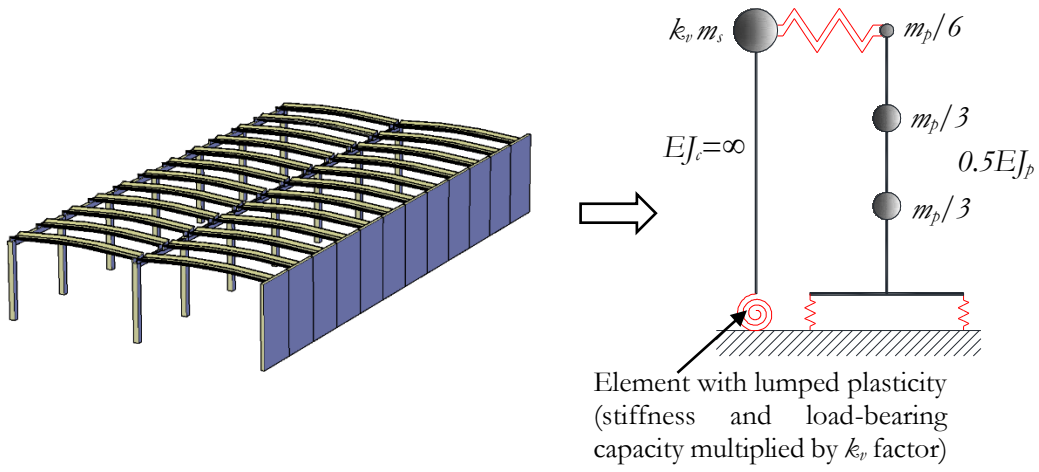

Figure 5-5: Models for non-linear dynamic analysis taking into account non-linear response

Within the parametric study, each structure was modelled with an equivalent column and the panel attached to it. However, the structures were of different ground plan configurations, and the ratio between the number of columns and number of panels differs.
In order to study also the influence of the ratio between the number of columns and panels on the seismic response, according to Zoubek (2015), the mass, stiffness and load-bearing capacity of the columns will be multiplied by the corresponding k_v factor (Figure 4.24). This is possible if a rigid diaphragm is assumed in the roof. The k_v factor is calculated with the following expression:

$$k_v = \frac{n_c}{n_p} = \frac{n_{cx} n_{cy}}{2 \cdot n_{p/r}\, n_r} = \frac{n_{cx} n_{cy}}{2 \cdot n_{p/r}\, (n_{cx} - 1)} \qquad (5.8)$$

where n_c is the number of columns; n_{cx} the number of columns in the longitudinal direction (direction in the plane of the panels); n_{cy} the number of columns in the transverse direction; n_p number of panels; n_r is the number of spans between columns in the longitudinal direction and $n_{p/r}$ number of panels for each span. Expressions (5.8) can be derived relatively easily with the help of Figure 5-5, taking into account that the panels are positioned along both edges of the building in the seismic load direction (see factor 2 in the denominator in equations(5.8)) The actual values of the k_v factor vary between 0.25 and 4. The limit values of the factors k_v are obtained in the case of buildings that are markedly extended in plan. In the shortest direction, the k_v factor is very low and in the longest direction is high.

5.4.3 Modelling the columns inelastic bending response

The response of the columns, designed within the Table 5-1, will be defined with an infinitely stiff elastic beam element coupled with a non-linear rotational spring at its base according to the model proposed by (Giberson, 1967). The spring will be given an appropriate moment rotational behaviour (Figure 5-6b).
The response of a rotational spring in the form of a moment-rotation relationship is determined on the basis of the recommendations, typical for single-storey prefabricated buildings, provided in the work of Fischinger et al., (2008), and considering the formula of Fardis and Biskinis, (2003) for yielding.
Operatively, first the moment-curvature relationship of the cross-section of the columns, taking into account the axial force, was defined (Figure 5-6a).
Section moment-curvature analysis has been performed through the OpenSees software (Mazzoni et al., 2006a).
For concrete, the model proposed by Mander et al,. (1988) was used and it is also included in Eurocode 8-2 - Appendix E, (EN 1998-2, 2009), and the steel of the reinforcement bars was modelled with the Giuffré-Menegotto-Pinto model. The average values of the material characteristics are taken into account (f_{ck}=40MPa, f_{cm} = 48 MPa, f_{ym} = 575 MPa, f_{tm} = 690 MPa).
The cracking moment M_{cr} could be determined, by taking into account the tensile strength of the concrete as $f_{ct} = 0.30 \cdot f_{ck}^{2/3}$, according to the following equation:

$$M_{cr} = W \left(\frac{N}{A_C} + f_{ct} \right) \qquad (5.9)$$

where W is the resistance modulus of the cross-section; N is the axial force (positive if it is in compression) and A_C is the area of the cross-section.

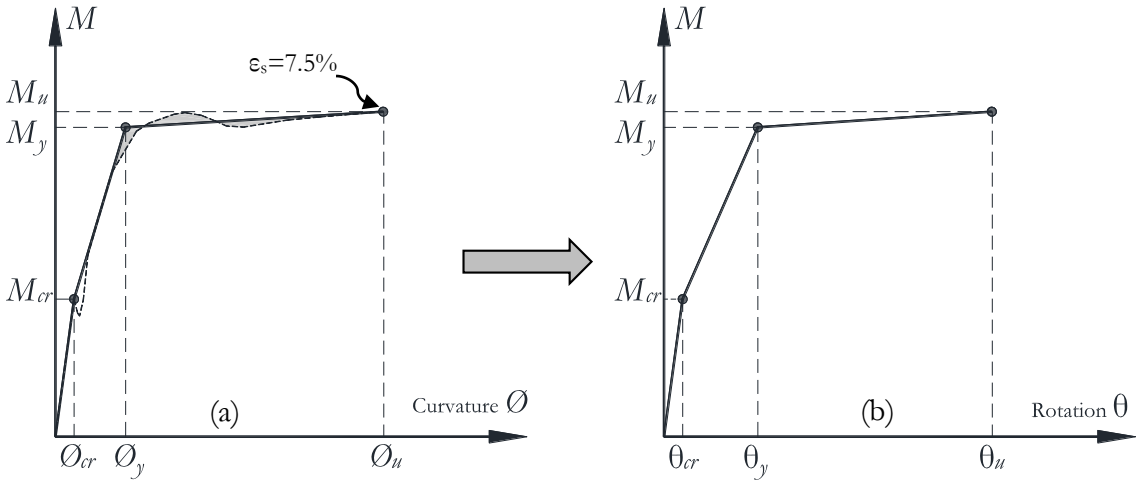

Figure 5-6: Moment-Curvature to Moment-rotation

The moment of inertia was calculated considering the reduced moment of inertia, due to the cracking of columns. According to the recommendations provided in Eurocode 8 (EN 1998-1-1, 2005), the moment of inertia was reduced by 50%.

Therefore cracking curvature $Ø_{cr}$ is then determined by assuming the initial stiffness is $0.5EJ_g$, where EJ_g is the bending stiffness of the cross-section without taking cracking into account.

From the $Ø_{cr}$-M_{cr} point onwards, the curve is idealized using the principle of energy equivalence (observe the shaded area in Figure 5-6a), and imposing the passage of the rectilinear post cracking branch for the first yield point, in this way the $Ø_y$-M_y point is obtained.

The ultimate section curvature $Ø_u$ and the ultimate moment M_u are established when the deformation limit of the reinforcing bars is reached. Limit equal to 7.5% for steel with ductility class C

Once the linearized moment-curvature diagram was obtained, the moment-rotation relationship could be calculated as follows:

Cracking rotation
$$\theta_{cr} = \frac{\phi_{cr} L_v}{3} \quad (5.10)$$

Yielding rotation
$$\theta_y = \frac{\phi_y L_v}{3} + 0.00275 + a_{sl} \frac{0.2 d_{bL} f_y \varepsilon_y}{\sqrt{f_{cc}(d - d')}} \quad (5.11)$$

Ultimate rotation
$$\theta_u = \left(\theta_y + (\phi_u - \phi_y) L_{pl} \left(1 - \frac{0.5 L_{pl}}{L_v} \right) \right) \quad (5.12)$$

where the equation (3.1) is the theoretical formulation for colum rotation. Equation (5.11) is the formula proposed by Fardis and Biskinis, (2003) and the equation (5.12) is the formulation proposed by Eurocode 8 (EN 1998-1-1, 2005) for the ultimate rotation. In which:

$Ø_{cr}$	Cracking curvature
$Ø_y$	Yielding curvature
$Ø_u$	Ultimate curvature
L_v	is the shear span
a_{sl}	variable indicating slip of the longitudinal bars (1=slip, 0=no slip);
d_{bL}	diameter of longitudinal reinforcement
$(d-d')$	is the distance between the tension and compression reinforcement
ε_y	is the yield strain of the tension reinforcement
f_y	is the yield stress of the tension reinforcement in MPa
f_{cc}	is the compressive strength of the concrete in MPa.

For the plastic hinge length L_{pl}, it was suggested by Park and Paulay, (1975) that the equivalent plastic hinge should not be longer than $0.5h_c$, where h_c is the height of the cross-section in the direction of the loading:

$$L_{pl} = 0.5h_c \quad (5.13)$$

The values of θ_{cr}, θ_y and θ_u for all the analysed one-storey buildings, the corresponding moment M_{cr}, M_y and M_u are reported in Table 5-5.

5.4.4 Modelling the hammer-head strap connections response

The hammer-head strap connections could be modelled according to Section 3.3.5 following the formulation proposed by Zoubek et al., (2016). However, this formulation takes into account an out-of-plane force N (see eq. (3.8)), invariant with respect to time, while during a real seismic event the out-of-plane force N, acting on the panel-structure connections, is a function of time and it becomes $N(t)$. In addition, the hammer-head strap is simultaneously stressed by a displacement $d(t)$ in the plane of the panel and when the strap head is stuck into the panel anchor channel, a bending moment $M(t)$ is applied to the neck of the strap as shown in Figure 5-7.

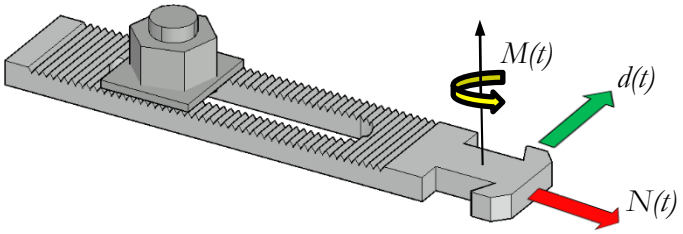

Figure 5-7: Forces applied to the strap during a seismic event

In order to take into account the simultaneous presence of an out-of-plane force, variable over time $N(t)$, and the bending moment $M(t)$, a fibre model has been adopted for the hammer-head strap.
The zone modelled with fibre is only related to the neck (Figure 5-8) because in this area the inelastic behaviour of the element is concentrated, as shown in the works of Isaković et al., (2013) and Zoubek et al., (2016). The fibre element defines both the in-plane and out-of-plane hysteretic behaviour of the connections and couples them.

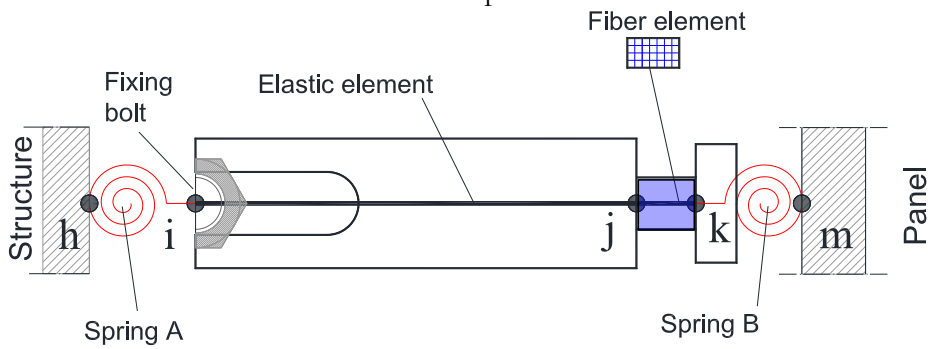

Figure 5-8: Hammer-head strap fibre model

Going further into detail, the hammer-head strap is made of a steel S 275 JR whose mechanical characteristics are: yield strength f_y = 275 MPa; ultimate strength f_u = 430 MPa; ultimate strain $\varepsilon_u(A_{gt})$= 0.18

Within OpenSees software, an elastic element was assigned between the nodes *i* and *j* in which the cross-section geometrical and inertial properties are the same reported in Table 3-2 and Table 3-11.
Between the node *j* and *k,* the *Steel01* material was assigned to each fibre rather a bilinear behaviour with kinematic hardening defined by the following parameters:

f_y yield strength	275	MPa
E_0 initial elastic tangent	210000	MPa
b strain-hardening ratio		-

The strain-hardening ratio *b* is the ratio between post-yield tangent E_p and initial elastic tangent E_0, such that:

$$b = \frac{E_p}{E_0} \quad (5.14)$$

where E_p can be calculated as:

$$E_p = \frac{f_u - f_y}{\varepsilon_u - \frac{f_y}{E_0}} \quad (5.15)$$

The spring between the nodes *h* and *i* (Spring A in Figure 5-8) has only a rotational behaviour defined in OpenSees by an *ElasticPP* material (Figure 5-9a) that simulates the friction force between the straps and the RC beam, due to the tightening torque M_{fr} in the fixing bolt.
The spring between the nodes *j* and *m* (Spring B in Figure 5-8) has a rotational behaviour defined by an *ElasticPPGap* material (Figure 5-9b) that simulates that strap head rotation is restrained by the anchor channel after a free rotation equal to θ_{init} as defined in section 3.3.5.
In the case of panels with rocking, the strap vertical hysteretic behaviour (Figure 5-9c) is assigned to the spring B. This is a simplification that did not allow to couple the strap horizontal and vertical hysteretic behaviour but led to a numerically more stable model.
However, future research and developments would be needed on this point to couple the vertical and horizontal in-plane and out-of-plane behaviour.
According to Table 3-10, the value of M_{fr} can be assumed equal to 45 Nm and the free rotation angle θ_{init} equal to 9° or 0.157 rad.

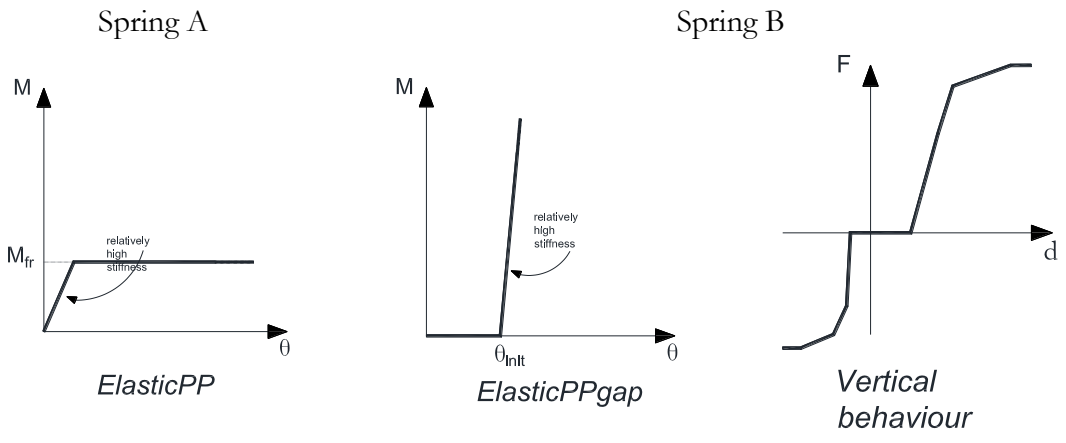

Figure 5-9: Spring A rotational behaviour (a) and spring B rotational restrain (b) and vertical behaviour (c)

Hammer-head strap fibre model validation

In order to validate the steel strap numerical model described above, the strap TA-210 has been modelled with the geometric characteristics shown in Table 3-2 and Figure 5-10a. The displacement history of Figure 5-10b, that is the same used in the experimental campaign carried out within the SAFECLADDING project by the University of Ljubljana (Isaković et al., 2013), was applied to node *m* of Figure 5-8. The results obtained both in the absence and in the presence of out-of-plane force are compared in Figure 5-10c,d.

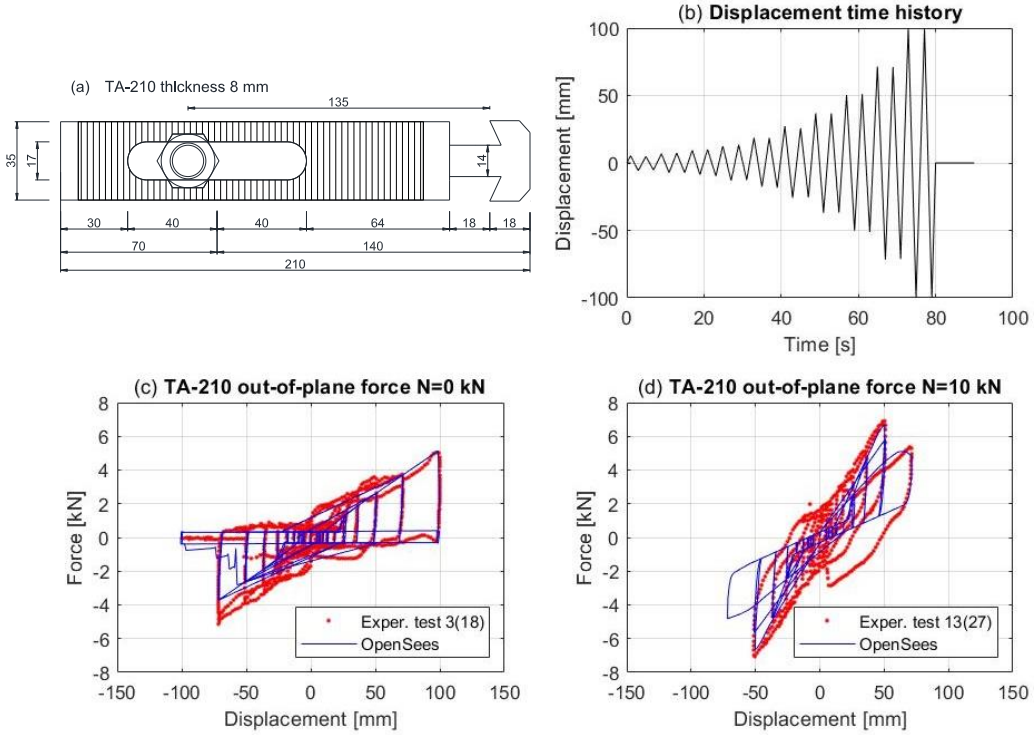

Figure 5-10: Strap TA-210 dimensions (a), SAFECLADDING experimental campaign displacement history (b), Strap hysteretic behaviour without (c) and with (d) an imposed out-of-plane force (c)

Figure 5-10c and d show a good agreement between the proposed model (blue line) and the experimental results (red line).

A second comparison, to validate the steel strap fibre model, was made starting from the numerical model of the building tested on the shaking table and calibrated on the experimental results as described in section 0. The numerical model of the V3 tested with an input acceleration scaled to 0.4g (configuration with fixed panels and short straps TA-210) was taken as reference and the connections were modelled by introducing the fibre model shown in Figure 5-8 instead of a single *zeroLength* element as explained in sub-section 3.3.5.
A static out-of-plane force *N* was applied to each panel as shown in Figure 5-11a. A series of analyses were run and in each of them, the force *N* was linearly increased (Figure 5-11b). The results in terms of maximum displacement, d_{max}, and maximum force, R_{max}, on a single steel strap, in function of the out-of-plane force, are shown in Figure 5-12 and compared with the mathematical model of connections proposed by Zoubek et al., (2016) explained in sub-section 3.3.5.

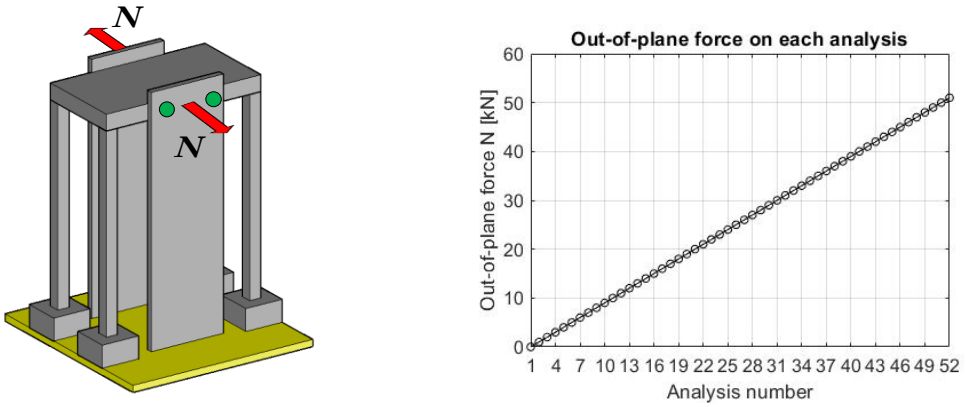

(a) (b)

Figure 5-11: Out-of-plane force N applied on panels(a). Value of N taken in each analysis (b)

To apply equation (3.10) of the mathematical model, it is necessary to calculate the plastic bending moment $M_{p,N}$ of the strap neck as a function of the out-of-plane force N acting on the connection.
Assuming for simplicity, the steel S235JR with an elastic perfectly plastic behaviour, then the bending moment $M_{p,N}$ can be calculated as (Gavin, 2015):

$$M_{p,N} = M_p\left(1 - \left(\frac{N}{N_y}\right)^2\right) \qquad (5.16)$$

where:
N is the actual out-of-plane force on the connection device
M_p is the plastic bending moment when the force out-of-plane N equals zero and can be estimated with the well-known relationship for rectangular sections of homogeneous material (Baldacci, et al., 1974):

$$M_p = \frac{f_y b h^2}{4} \qquad (5.17)$$

N_y is the force out-of-plane (strap's axial force) at the plastic limit and can be estimated as:

$$N_y = f_y b h \qquad (5.18)$$

where b is the base of the neck cross-section, h its height (Figure 5-10a) and f_y is the yield strength of the material.

For the TA-210 hammer-head strap, the characteristic quantities are given in Table 5-3.

b [mm]	h [mm]	f_y [N/mm²]	N_y [kN]	M_p [kNm]
14	8	275	30.8	0.06

Table 5-3: TA-210 strap characteristic quantities

It is worth remembering that the value of N_y refers only to the steel strap. The ultimate out-of-plane capacity of the whole connection takes also into account the capacity of the anchor channel as defined in section 4.1.

Figure 5-12a and b show the comparison between the strap mathematical model carried out by Zoubek et al., (2016) and the proposed fibre model in terms of maximum displacement, d_{max}, and maximum force, R_{max}, in function of the normalized out-of-plane force N/N_y where N_y is defined by eq.(5.18).

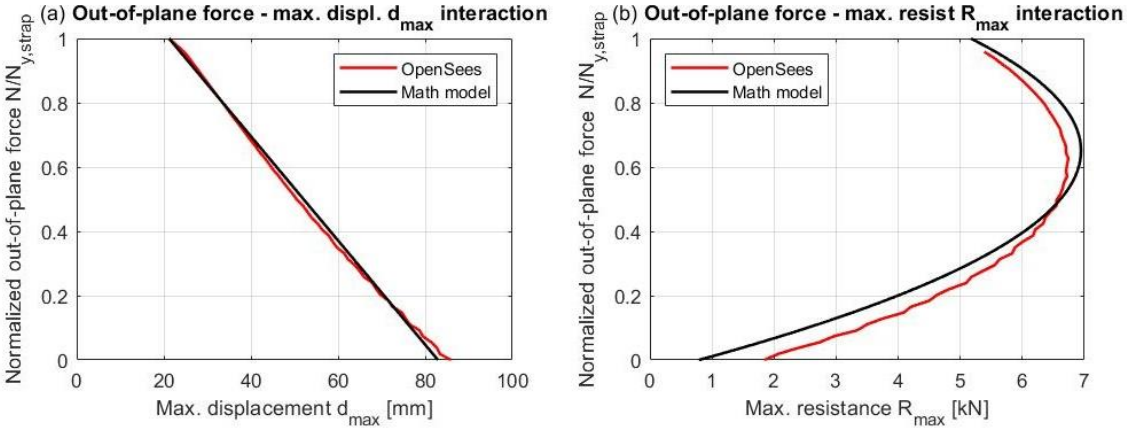

Figure 5-12: N-d_{max} interaction (a) and N-R_{max} interaction (b).

As depicted in Figure 5-12a, the fibre model is in good agreement with the mathematical model, in particular, it is possible to see that the more the force out of plane N increases, the more the displacement capacity of the connection decreases. When the out-of-plane force reaches the value of N_y, due to the hypothesis of a perfectly plastic elastic material, no displacement is possible other than the one relative to the rotation in the fixing bolt (see eq. (3.3)). Unlike the mathematical model, the proposed fibre model allowed to take into account an out-of-plane action that varies over time, $N(t)$, as the one that occurs during a seismic event.

5.4.5 Critical axial bucking load for the hammer-head strap.

In order to assess whether the out-of-plane capacity of whole hammer-head strap connections was limited by the axial buckling load of the steel strap itself, the critical buckling load of strap TA-210 and TA-290 is calculated within this section.

The strap can be attributed to a beam composed of two portions of different areas and with two pinned ends as shown in Figure 5-13, where β^2 is the ratio between the moment of inertia of the two portions J and J_1.

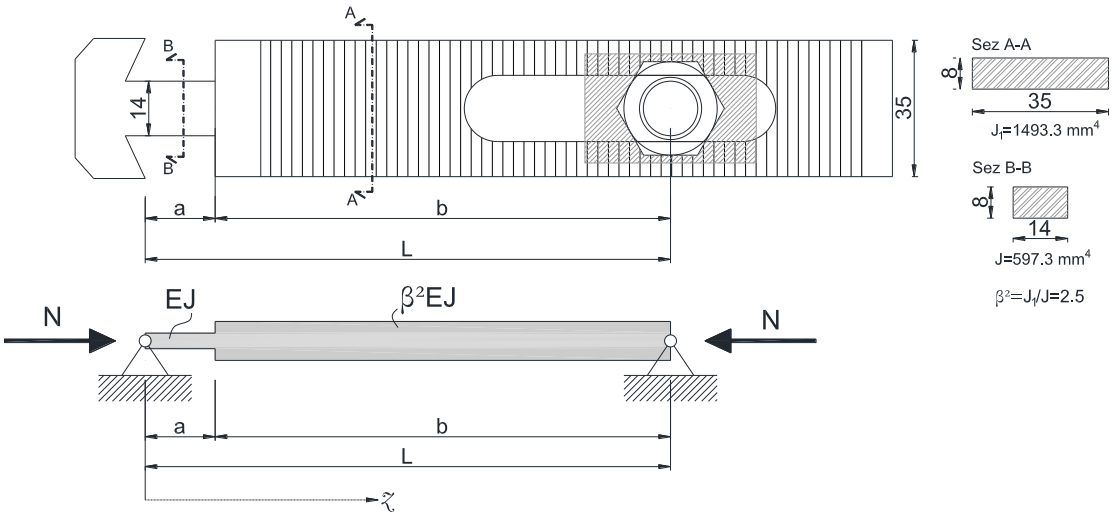

Figure 5-13: Hammer-head strap and the equivalent stepped beam with two pinned ends

The equation of equilibrium for the first and the second portions, respectively, are:

$$\frac{d^2v_1}{dz^2} + \beta^2 k^2 v_1 = 0$$
$$\frac{d^2v_2}{dz^2} + k^2 v_2 = 0 \qquad (5.19)$$

Where $k^2 = P/\beta^2 EJ$ and v is the beam deflection.
The solutions of these equations are, respectively:

$$v_1 = C_1 \sin \beta kz + C_2 \cos \beta kz$$
$$v_2 = C_3 \sin kz + C_4 \cos kz \qquad (5.20)$$

The constants of integration C_1, C_2, C_3 and C_4 are determined from four conditions, namely:

$$v_1 = 0 \text{ at } z = 0$$
$$v_2 = 0 \text{ at } z = L$$
$$v_1 = v_2 \text{ and } \frac{dv_1}{dz} = \frac{dv_2}{dz} \text{ at } z = \frac{L}{2} \qquad (5.21)$$

for continuity.

Applying the first condition gives C_2=0, while the other three conditions yield the equation as:

$$\begin{aligned} &C_1 \sin \beta ka - C_3 \sin ka - C_4 \cos ka = 0 \\ &C_1 \beta \cos \beta ka - C_3 \cos ka + C_4 \sin ka = 0 \\ &C_3 \sin kL + C_4 \cos kL = 0 \end{aligned} \quad (5.22)$$

Now, C_1, C_2 and C_4 have a non-zero solution only if the determinant of the system of linear homogenous equation (5.22) vanishes. i.e.:

$$\begin{vmatrix} \sin \beta ka & -\sin ka & -\cos ka \\ \beta \cos \beta ka & -\cos ka & \sin ka \\ 0 & \sin kL & \cos kL \end{vmatrix} = 0 \quad (5.23)$$

This leads to:

$$\beta \cos \beta ka \cdot \sin k(a-L) - \sin \beta ka \cdot \cos k(a-L) = 0 \quad (5.24)$$

Since $(a-L) = -b$, therefore:

$$\cos \beta ka \cdot \sin kb + \sin \beta ka \cdot \cos kb = 0 \quad (5.25)$$

The determinant roots can be obtained by numerical way. For the short strap TA-210 and long TA-290, assuming the length L equal to 135 and 170 mm respectively (see Figure 3-18) ad substituting the quantities a and b in the eq. (5.25), the results are shown in Table 5-4 and Figure 5-14.

	Strap TA-210	Strap TA-290
L	135 mm	170 mm
a	18L/135	18L/170
b	117L/135	157L/170
Determinant roots		
$(kL)_1$	0.00	0.00
$(kL)_2$	±3.1037	±3.1243
$(kL)_3$	±5.9788	±6.1385
$(kL)_4$	±8.6240	±8.9548

Table 5-4: Determinant roots values

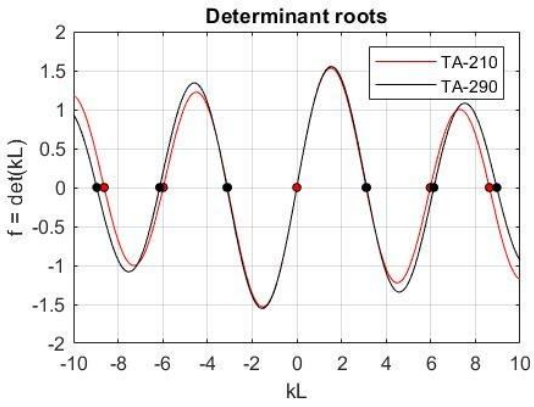

Figure 5-14: Plot of determinant values in function of kL

Considering the smallest non-zero root $(KL)_1$ and recalling that $k^2 = P/\beta^2 EJ$ result in the critical buckling load as:

$$\text{Strap TA-210} \quad P_{cr} = \frac{24.08EJ}{L^2} = 157.86\ kN$$

$$\text{Strap TA-290} \quad P_{cr} = \frac{24.40EJ}{L^2} = 95.19\ kN \quad (5.26)$$

As it is possible to see, the critical buckling load for both types hammer-head strap is relatively high compared to both the yield strength N_y (see Table 5-3) and the beam and panel side resistances obtained from the experimental campaign illustrated in section 4.1. Although an evaluation of the critical buckling load was useful, the value of the load is not crucial for the design and safety evaluation of the connection.

5.4.6 Modelling the panel-foundation and SismoSafe connections response

The panel-foundation connections are modelled in the same way as described in section 3.3.6. For the rocking panel case it necessary to take into account that they are directly placed on the ground and, according to Muthukumar & DesRoches, (2006) contact model, one of the two colliding bodies will have infinite mass m and infinite radius R.
So if we suppose that R_2 and M_2 are infinite then equation (3.18) becomes:

$$\lim_{R_2 \to \infty} \frac{4}{3\pi(h_1+h_2)} \cdot \left[\frac{R_1 R_2}{R_1+R_2}\right]^{1/2} = \frac{4}{3\pi(h_1+h_2)} \cdot [R_1]^{1/2} \qquad (5.27)$$

The equations (3.21)(3.22)(3.24)and(3.25)are modified accordingly assuming that R_2 tends to infinity.
In the parametric analysis, since the height of the panel has been assumed to be equal to the height of the structure, the value of the mass of the panel m_1 will change according to its height and consequently, R_1 will change according to equation (3.20). The values of impact model parameters, K_1 K_2 δy and gap, and the panel mass m_p used in the analysis are shown in Table 5-5.

About the SismoSafe connections, these are modelled using a *Flat Slider Bearing Element* as explained in paragraph 4.3, where the friction coefficient μ is assumed to be 0.4 following the experimental evidence discussed in paragraph 3.5.2.

Label	**m20H5**	**m20H7**	**m20H9**	**m40H5**	**m40H7**	**m40H9**	**m60H5**	**m60H7**	**m60H9**	**m80H5**	**m80H7**	**m80H9**	**m100H5**	**m100H7**	**m100H9**
COLUMN MODEL															
θ_{cr}	0.0028	0.0040	0.0039	0.0025	0.0035	0.0033	0.0028	0.0028	0.0036	0.0022	0.0030	0.0033	0.0023	0.0033	0.0033
θ_{y}	0.0246	0.0333	0.0319	0.0196	0.0263	0.0268	0.0203	0.0224	0.0280	0.0166	0.0228	0.0268	0.0166	0.0231	0.0268
θ_{u}	0.0724	0.0814	0.0763	0.0590	0.0661	0.0707	0.0547	0.0683	0.0741	0.0628	0.0632	0.0710	0.0631	0.0592	0.0642
M_{cr} [kNm]	64	64	116	133	133	212	149	232	232	251	251	366	271	271	389
M_{y} [kNm]	223	223	338	539	539	662	658	836	836	1036	1071	1165	1077	1305	1378
M_{u} [kNm]	244	244	378	553	553	742	664	885	885	1167	1085	1177	1210	1319	1399
HAMMER-HEAD STRAP MODEL TA-210															
M_{fr} [kNm]	45	45	45	45	45	45	45	45	45	45	45	45	45	45	45
θ_{init} [rad]	0.157	0.157	0.157	0.157	0.157	0.157	0.157	0.157	0.157	0.157	0.157	0.157	0.157	0.157	0.157
d_{gap} [mm]	21.20	21.20	21.20	21.20	21.20	21.20	21.20	21.20	21.20	21.20	21.20	21.20	21.20	21.20	21.20
d_{u} [mm]	85	85	85	85	85	85	85	85	85	85	85	85	85	85	85
R_{fr} [kN]	0.34	0.34	0.34	0.34	0.34	0.34	0.34	0.34	0.34	0.34	0.34	0.34	0.34	0.34	0.34
R_{y} [kN]	1.18	1.18	1.18	1.18	1.18	1.18	1.18	1.18	1.18	1.18	1.18	1.18	1.18	1.18	1.18
R_{u} [kN]	9.90	9.90	9.90	9.90	9.90	9.90	9.90	9.90	9.90	9.90	9.90	9.90	9.90	9.90	9.90
HAMMER-HEAD STRAP MODEL TA-290															
M_{fr} [kNm]	45	45	45	45	45	45	45	45	45	45	45	45	45	45	45
θ_{init} [rad]	0.157	0.157	0.157	0.157	0.157	0.157	0.157	0.157	0.157	0.157	0.157	0.157	0.157	0.157	0.157
d_{gap} [mm]	26.70	26.70	26.70	26.70	26.70	26.70	26.70	26.70	26.70	26.70	26.70	26.70	26.70	26.70	26.70
d_{u} [mm]	143	143	143	143	143	143	143	143	143	143	143	143	143	143	143
R_{fr} [kN]	0.26	0.26	0.26	0.26	0.26	0.26	0.26	0.26	0.26	0.26	0.26	0.26	0.26	0.26	0.26
R_{y} [kN]	0.72	0.72	0.72	0.72	0.72	0.72	0.72	0.72	0.72	0.72	0.72	0.72	0.72	0.72	0.72
R_{u} [kN]	8.11	8.11	8.11	8.11	8.11	8.11	8.11	8.11	8.11	8.11	8.11	8.11	8.11	8.11	8.11

…next page…

SISMOSAFE CONNECTION MODEL															
μ [-]	0.4	0.4	0.4	0.4	0.4	0.4	0.4	0.4	0.4	0.4	0.4	0.4	0.4	0.4	0.4
IMPACT MODEL															
m_p [kNs^2/m]	5.10	7.14	9.17	5.10	7.14	9.17	5.10	7.14	9.17	5.10	7.14	9.17	5.10	7.14	9.17
K_1 [kN·10^3/m]	1550	1640	1740	1550	1640	1740	1550	1640	1740	1550	1640	1740	1550	1640	1740
K_2 [kN·10^3/m]	311	329	350	311	329	350	311	329	350	311	329	350	311	329	350
δy [m·10^{-5}]	9.00	9.00	9.00	9.00	9.00	9.00	9.00	9.00	9.00	9.00	9.00	9.00	9.00	9.00	9.00
gap [m·10^{-3}]	1.00	1.00	1.00	1.00	1.00	1.00	1.00	1.00	1.00	1.00	1.00	1.00	1.00	1.00	1.00

Table 5-5: Input data of column, structure-panel, and panel-to-foundation connection models of the analysed one-storey buildings

5.4.7 Modal analysis

A modal analysis was carried out in order to assess the fundamental vibration period T_1 of the building set of building considered within the parametric analysis.
The modal analysis results are grouped for k_v factor and panels support conditions (fixed or rocking) The Figure 5-15 the fundamental vibration period T1 is reported for each considered mass and height values. The numerical value of the periods are reported in Table 5-6.

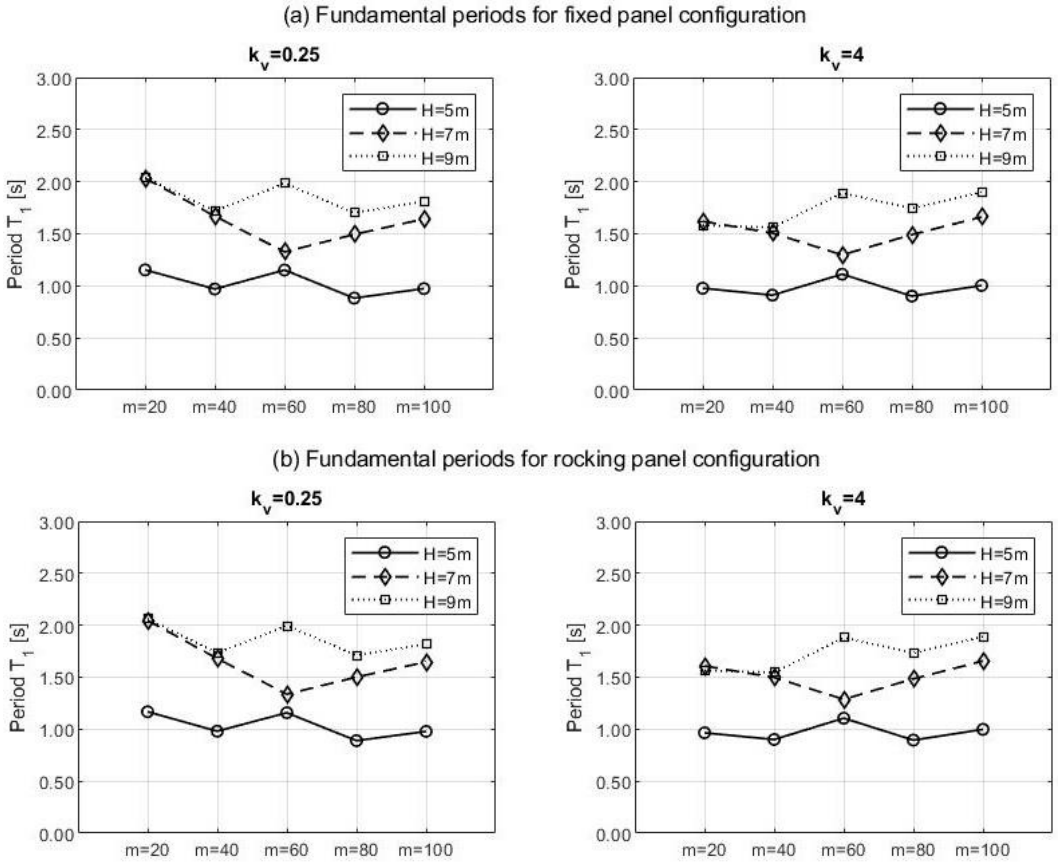

Figure 5-15: Fundamental vibration period of the building set for fixed panel configuration (a) rocking panel configuration (b)

Fundamental vibration period T_1 [s]				
	Fixed panel		Rocking panel	
Label	k_v=0.25	k_v=4	k_v=0.25	k_v=4
m20H5	1.15	0.97	1.17	0.98
m40H5	0.97	0.90	0.98	0.91
m60H5	1.15	1.11	1.16	1.11
m80H5	0.88	0.89	0.89	0.90
m100H5	0.97	1.00	0.98	1.00
m20H7	2.03	1.61	2.05	1.62
m40H7	1.67	1.50	1.68	1.51
m60H7	1.33	1.29	1.34	1.30
m80H7	1.49	1.48	1.50	1.49

m100H7	1.64	1.66	1.65	1.66
m20H9	2.04	1.57	2.06	1.58
m40H9	1.72	1.55	1.73	1.56
m60H9	1.98	1.88	2.00	1.89
m80H9	1.70	1.73	1.71	1.74
m100H9	1.81	1.89	1.82	1.90

Table 5-6: Fundamental vibration period numerical values

5.4.8 Parametric analysis results

In this section, the seismic response for one-storey buildings with vertical panels, considered in the parametric analysis, is illustrated. Figure 5-19 shows with a continuous line the average values of seismic demand for each considered quantity and for all the analysed buildings. The response is obtained, for each PGA value, from at least 7 nonlinear response-history analyses with ground motions. Therefore, the seismic demand value for the considered quantity is the average of the response maxima of the 7 analyses
The dotted lines refer to the 25th and 75th percentile of the data set respectively.
In each diagram, the represented curves are marked in red when the ratio between the number of columns and the number of panels, k_v, is assumed to be 4, and in black when k_v assumes a value of 0.25. Each diagram then shows a pair of curves for each analysed building and also the respective 25th and 75th percentile curves.
The title of each diagram shows the code of each analysed building (for more data on buildings see Table 5-1).
The numerical analyses were carried out for both hammer-head strap and SismoSafe panel-to-structure connections type and the parameters shown in the results diagram are:

in the case of fixed panels:

d	Connection in-plane displacement
N	Connection out-of-plane force
R_b	Shear force at the base of panel (see Figure 4-32)
R_v	Panel uplift force (see Figure 4-32)

in the case of rocking panels:

d	Connection in-plane displacement
d_{vert}	Connection vertical displacement
N	Connection out-of-plane force
R_b	Shear force at the base of panel (see Figure 4-32)

the d, d_{vert} and N quantities for the connection device are compared with the respective capacity. In each diagram, the capacity is shown with a blue dashed line. The F_v and F_u parameters capacity is not shown because it depends on the type of device that is used to avoid the panel rocking movement.

Besides, since the horizontal components of the seismic action shall be considered as acting simultaneously, according to Eurocode 8, the action effects due to the combination of the horizontal components of the seismic action were computed using both the following combinations:

Comb. A: E_{Edx}"+" $0.30E_{Edy}$
Comb. B: $0.30E_{Edx}$"+" E_{Edy}

where:
"+" implies "to be combined with";

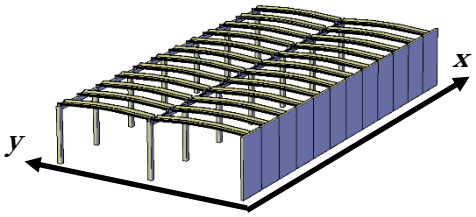

Figure 5-16: Structure main axis

E_{Edx} action effects due to the application of the seismic action along the chosen horizontal axis *x* of the structure (Figure 5-16);
E_{Edy} action effects due to the application of the same seismic action along the orthogonal horizontal axis *y* of the structure (Figure 5-16)
In each result diagram the 2 axes of the abscissae relative to soil type A and soil type C, are repesented.

Within this section, the nomenclature of the Italian Building Code (NTC, 2018) is used. In this nomenclature the ground acceleration is defined as $PGA = a_g \cdot S$.
A preliminary analysis was made for soil type C characterized by the highest PGA value. It was observed that the investigated structures remained substantially in the linear field.
Therefore the results on soil A or B can be obtained by scaling the effects in proportion to the spectral acceleration.
The analyzed structures have a fundamntal vibration period included in the interval T_1=[0.90s; 2.00s] (grey zone in Figure 5-17a,b). In that interval the spectral acceleration on soil C was scaled in order to produce the same effect as that on soil A (Figure 5-17b).

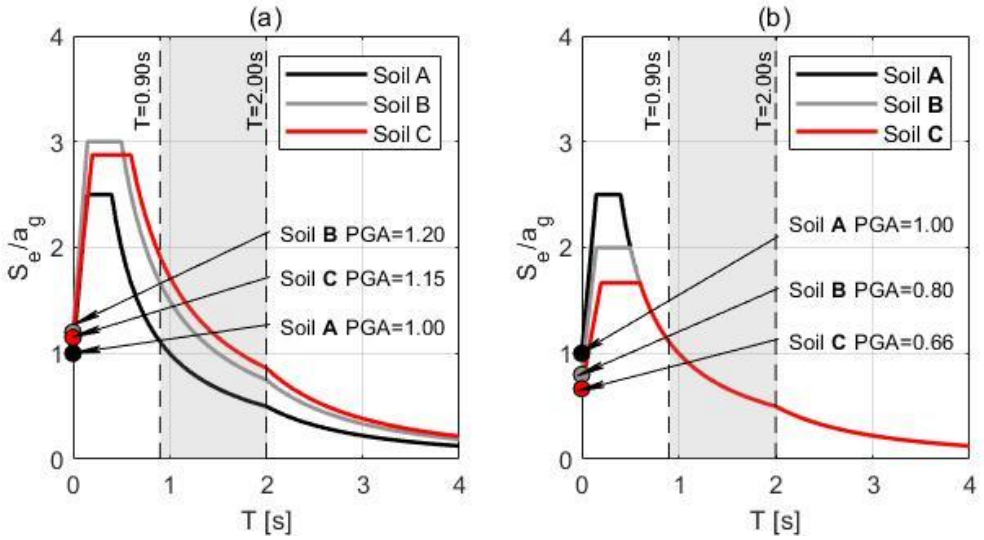

Figure 5-17: Eurocode 8 acceleration spectra for soil A, B and C (a) and scaled spectra by means SF (b)

Since the period interval for the considered structures *T*=[0.90s; 2.00s] is always between T_C and T_D for all soil types then the scale factor, SF, can be calculated as the ratio between the spectrum equations, defined by Eurocode 8 for the branch $T_C<T<T_D$. For example for soil A and C:

$$SF = \frac{a_g \cdot S_{soil\,C} \cdot \eta \cdot 2.5 \cdot \frac{T_C^{soil\,C}}{T}}{a_g \cdot S_{soil\,A} \cdot \eta \cdot 2.5 \cdot \frac{T_C^{soil\,A}}{T}} = \frac{S_{soil\,C} T_C^{soil\,C}}{S_{soil\,A} T_C^{soil\,A}} \quad (5.28)$$

where a_g is the design ground acceleration on type A ground (bedrock); S is the soil factor; T_C is the upper limit of the period of the constant spectral acceleration branch and η is the damping correction factor with a reference value of $\eta = 1$ for 5% viscous damping.
Therefore according to the nomenclature of the Italian Building Code (NTC, 2018), the ratio between the relative ground acceleration, PGA, is:

$$SF_{PGA} = \frac{PGA_{soil\,C} \cdot \eta \cdot 2.5 \cdot \frac{T_C^{soil\,C}}{T}}{PGA_{soil\,A} \cdot \eta \cdot 2.5 \cdot \frac{T_C^{soil\,A}}{T}} = \frac{T_C^{soil\,C}}{T_C^{soil\,A}} \quad (5.29)$$

For all soil types defined by Eurocode 8, the scale factor ratios are obtained as reported in Table 5-7:

Soil type	SF	SF_{PGA}
A	1	1
B	1.50	1.25
C	1.725	1.50
D	2.70	2.00
E	1.75	1.25

Table 5-7: Ratios SF and SF_{PGA} for all the soil types according to Eurocode 8

Summing up, each graph representing the results can be read by following the indications proposed in Figure 5-18.

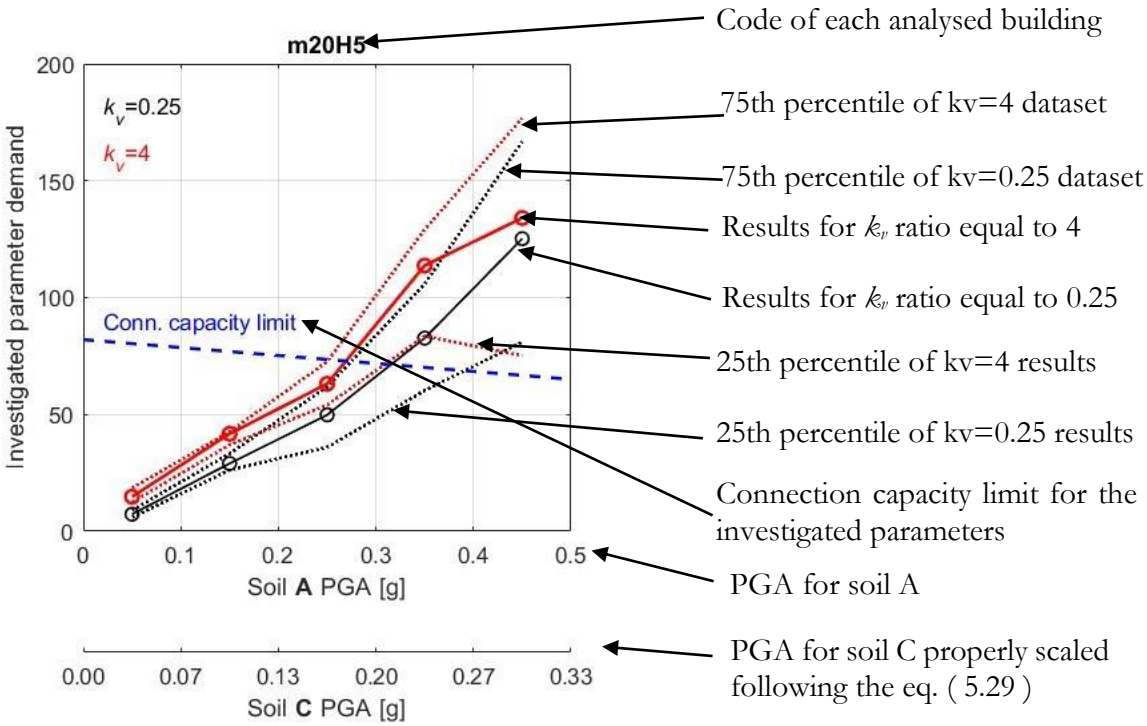

Figure 5-18: Example of result representation graph

In the results, the in-plane capacity of connection is defined in terms of displacement. The ultimate displacement changes according to the out-of-plane force applied, as explained in section 5.4.4.
The out-of-plane capacity of the connections is defined in terms of strength. The ultimate strength was discussed in section 4.1.
Among the investigated structures within the parametric analysis, only the results for in-plane displacement and out-of-plane-force are reported for all investigated cases. For the other investigated quantities only the two most extremal cases (**m20H5** and **m100H9**) are illustrated in the following subsection. The results are grouped by connection type and panel support conditions. The results show the seismic demand for each considered parameters:

in the case of fixed panels:

d	Connection in-plane displacement
N	Connection out-of-plane force
R_b	Shear force at the base of panel
R_v	Panel uplift force (see Figure 4-32)

in the case of rocking panels:

d	Connection in-plane displacement
d_{vert}	Connection vertical displacement
N	Connection out-of-plane force
R_b	Shear force at the base of panel (see Figure 4-32)

The result reported in the following refers only to the most critical load combination (between A and B) for each considered parameters.
Concerning the uplift reaction R_v, it is necessary to specify that this reaction lifts the panel when in the result reported in Figure 5-22, Figure 5-26 and Figure 5-30 it assumes a negative value.

All the results, for all investigated cases and seismic combination, are shown in Appendix B.

5.4.9 Results for fixed panel configuration

Connection Hammer-head strap TA-210

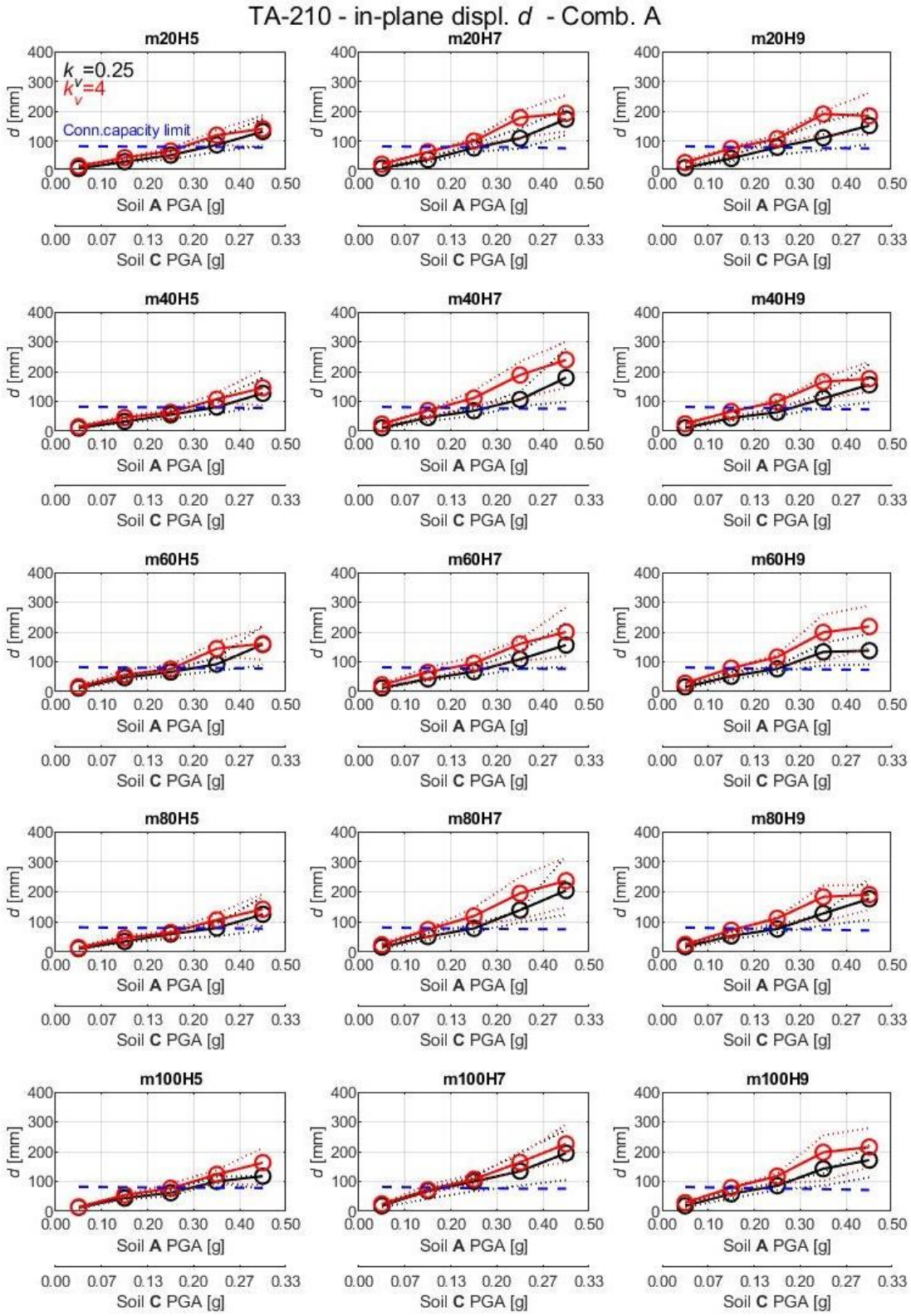

Figure 5-19: Seismic demand and capacity comparison in term of in-plane displacement *d* for hammer-head strap connection TA-210 in the case of fixed panels and seismic combination A.

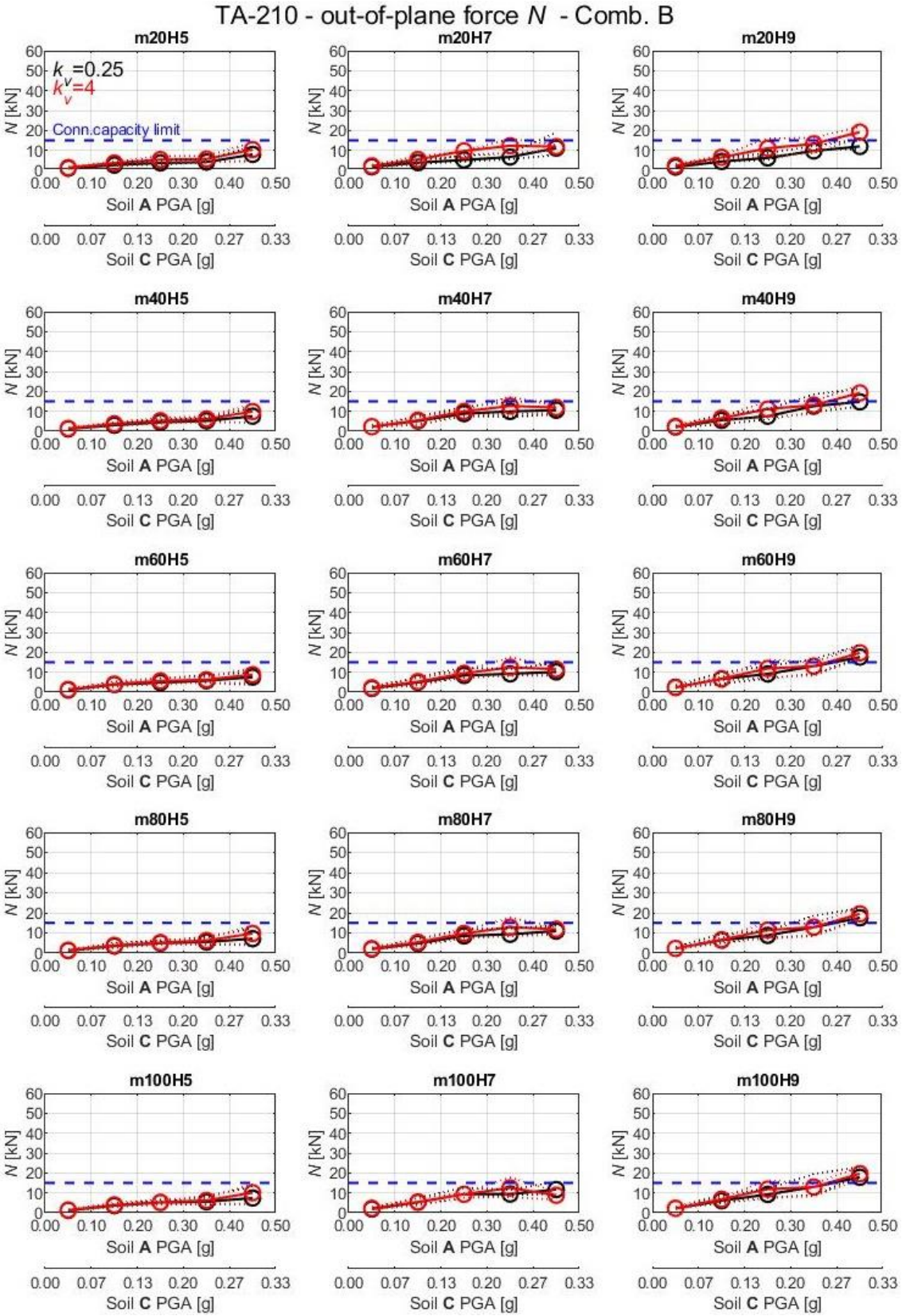

Figure 5-20: Seismic demand and capacity comparison in term in term of out-of-plane force *N* for hammer-head strap connection TA-210 in the case of fixed panels and seismic combination B.

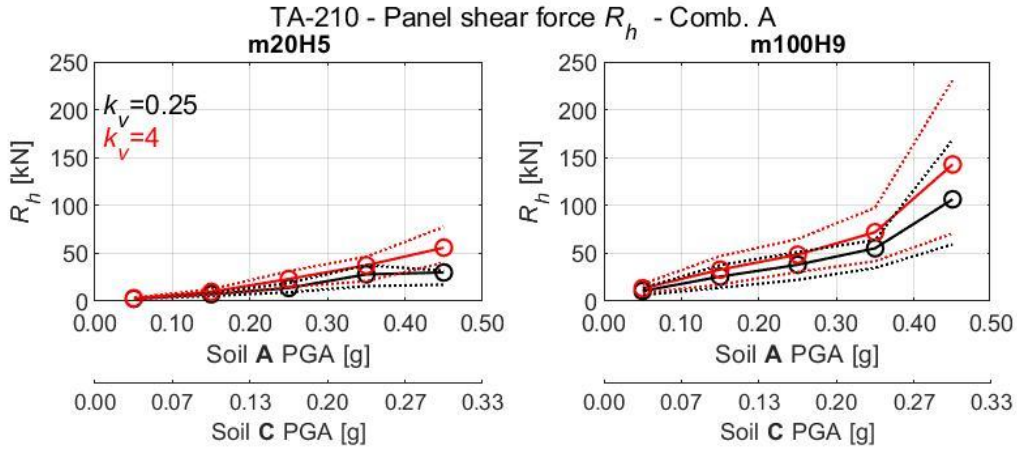

Figure 5-21: Seismic demand in term of shear force R_h at the base of the panel for hammer-head strap connection TA-210 in the case of fixed panels and seismic combination A.

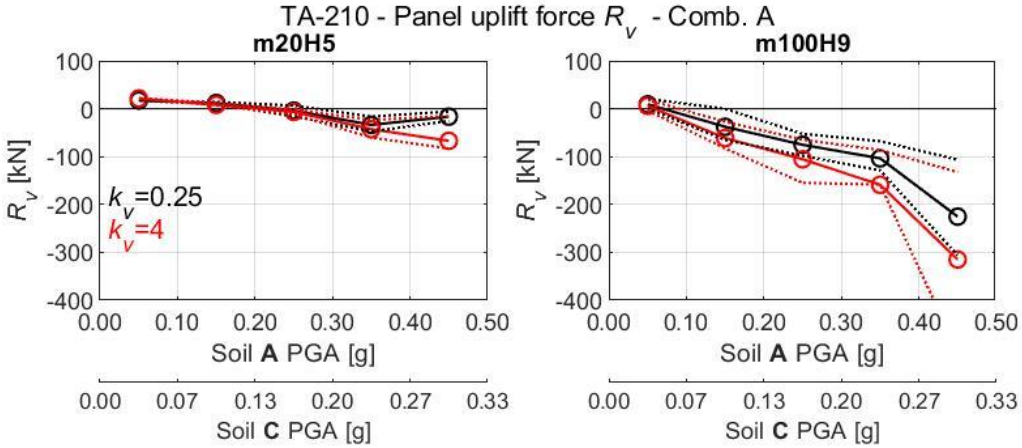

Figure 5-22: Seismic demand in panel uplift force R_v for hammer-head strap connection TA-210 in the case of fixed panels and seismic combination A.

Connection Hammer-head strap TA-290

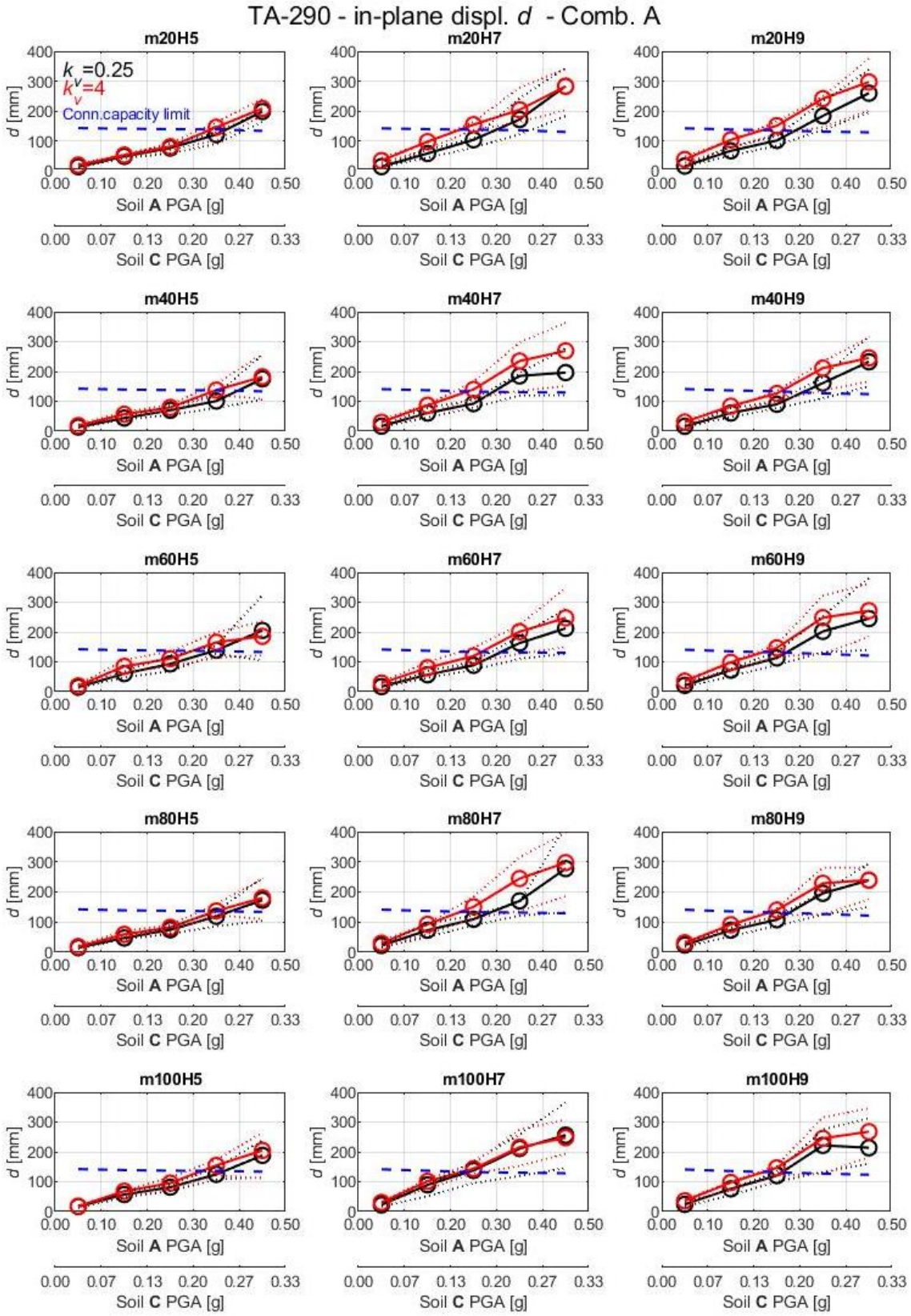

Figure 5-23: Seismic demand and capacity comparison in term of in-plane displacement *d* for hammer-head strap connection TA-290 in the case of fixed panels and seismic combination A.

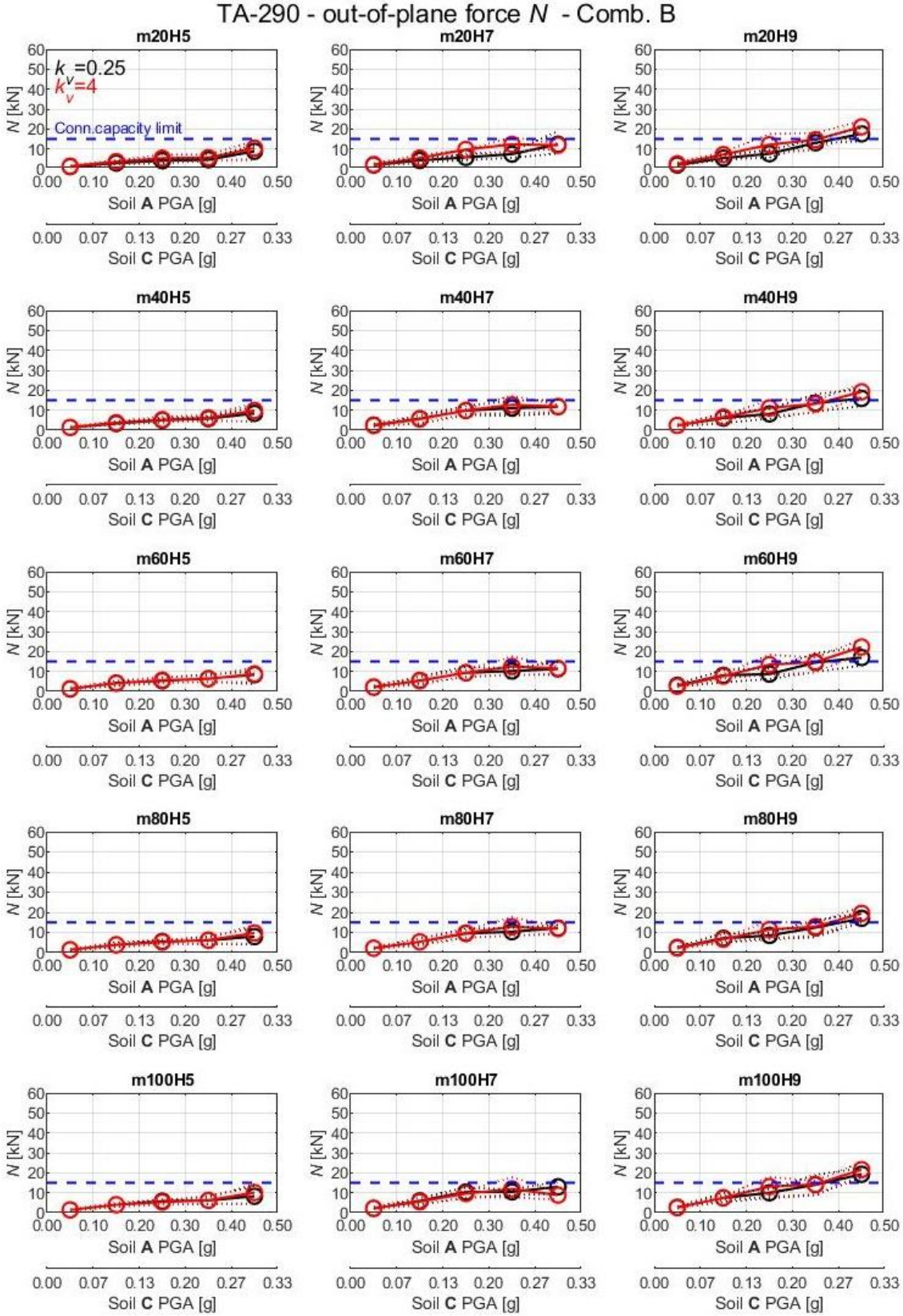

Figure 5-24: Seismic demand and capacity comparison in term in term of out-of-plane force *N* for hammer-head strap connection TA-290 in the case of fixed panels and seismic combination B.

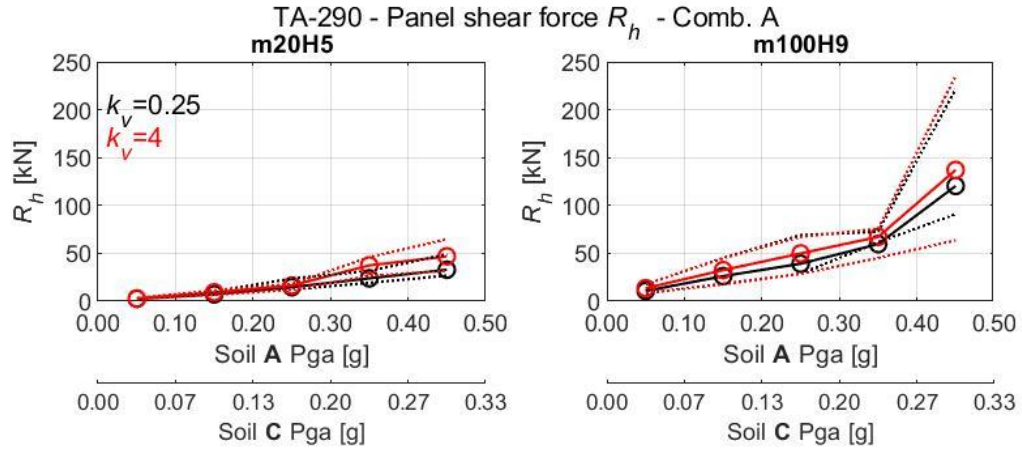

Figure 5-25: Seismic demand in term of shear force R_h at the base of the panel for hammer-head strap connection TA-290 in the case of fixed panels and seismic combination A.

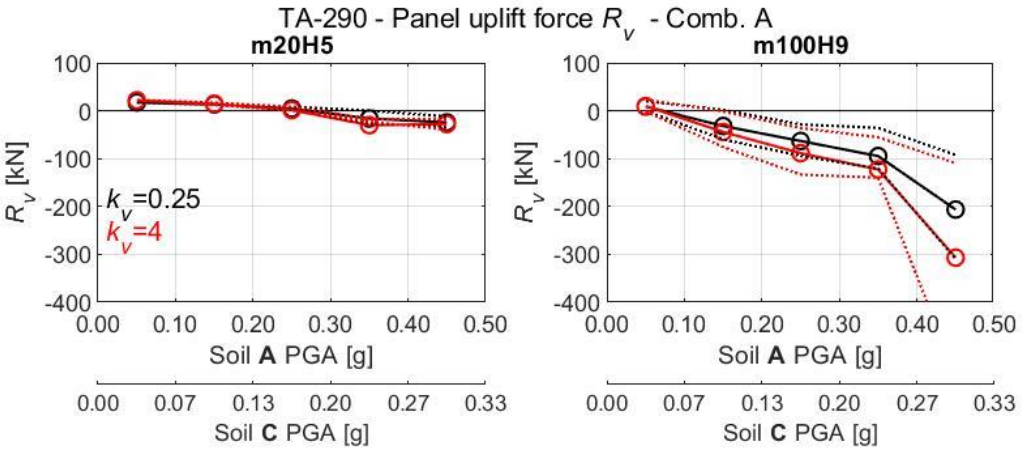

Figure 5-26: Seismic demand in term of shear force R_v at the base of the panel for hammer-head strap connection TA-290 in the case of fixed panels and seismic combination A.

Connection SismoSafe

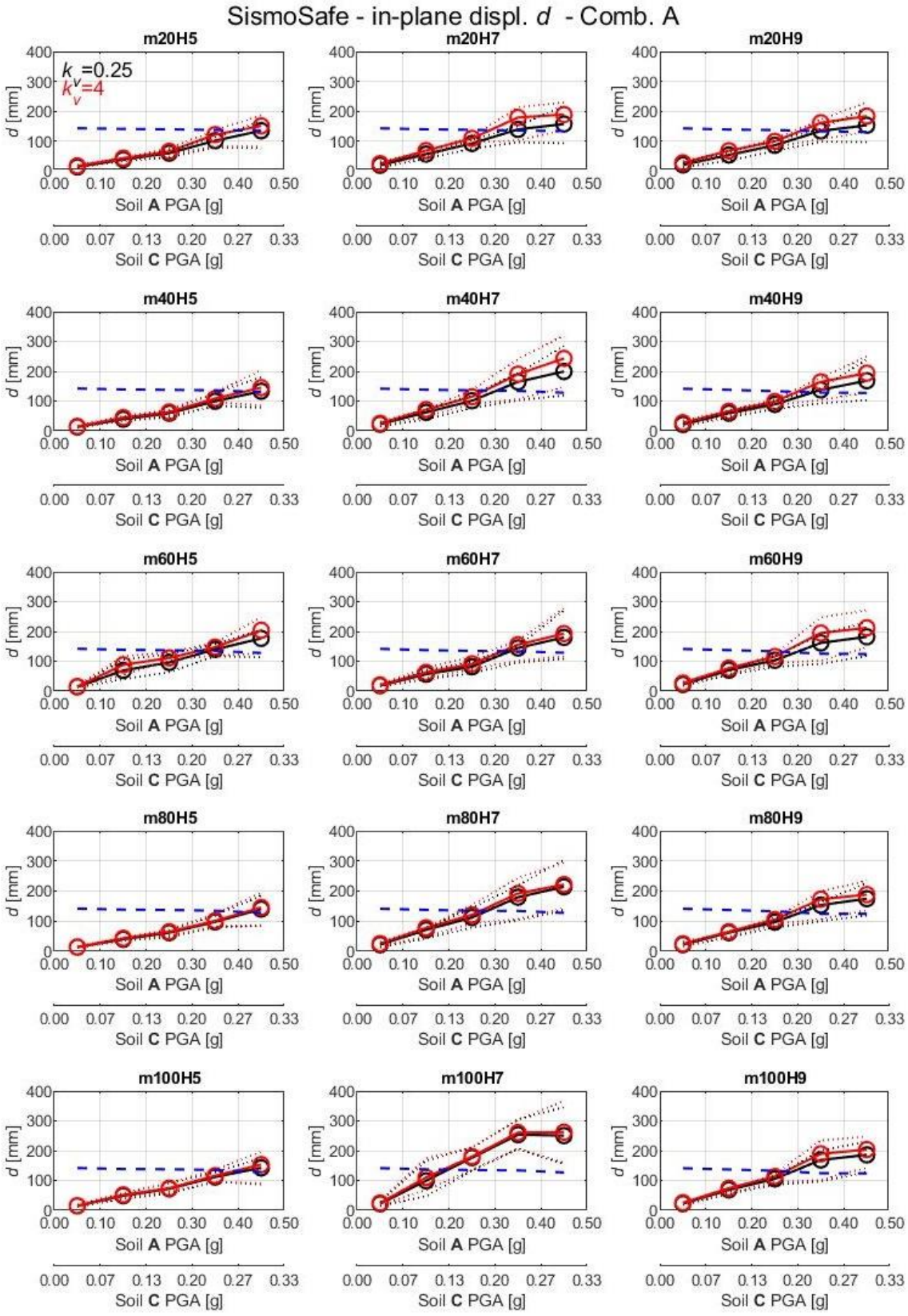

Figure 5-27: Seismic demand and capacity comparison in term of in-plane displacement d for SismoSafe connection in the case of fixed panels and seismic combination A

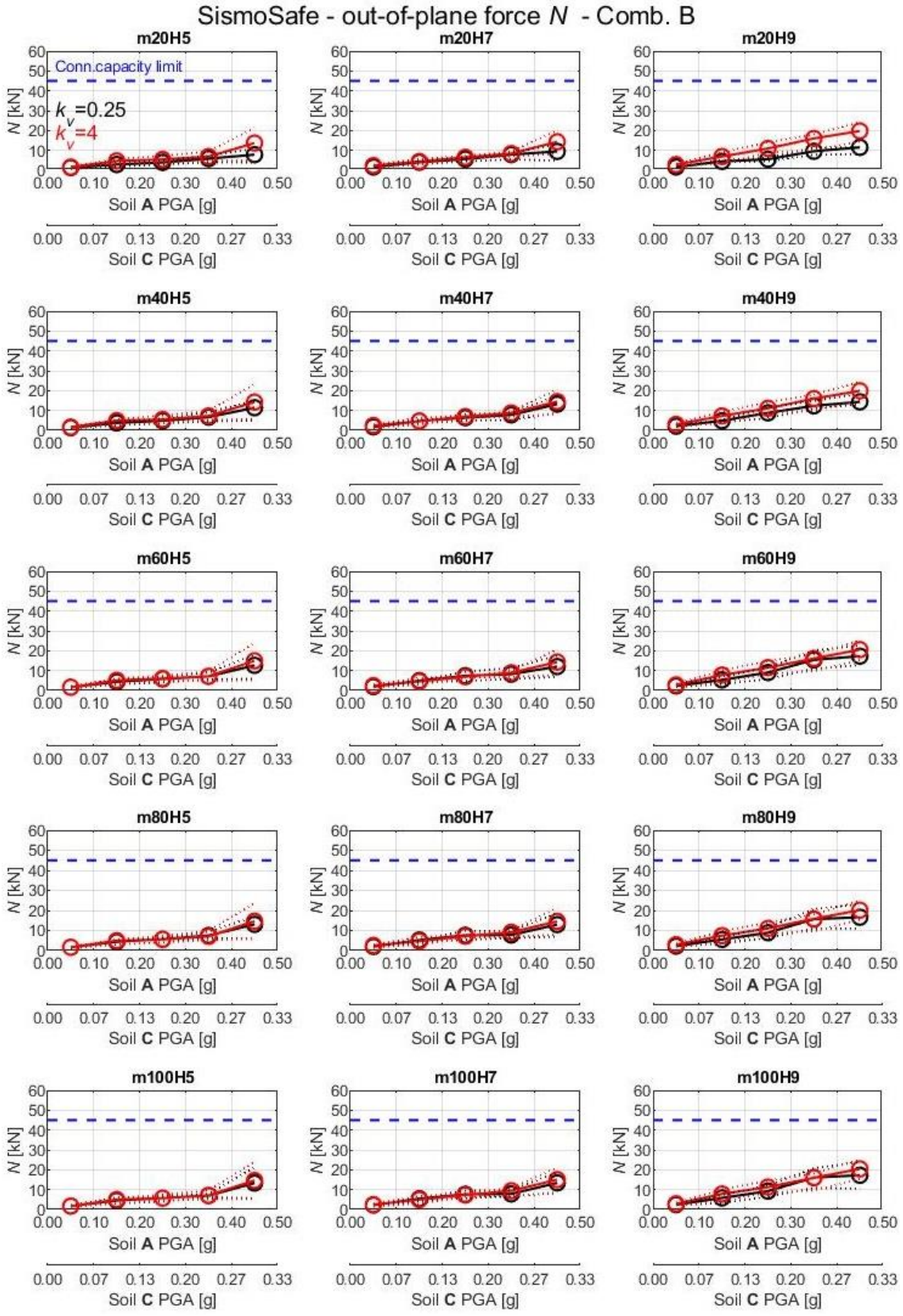

Figure 5-28: Seismic demand and capacity comparison in term in term of out-of-plane force *N* for SismoSafe connection in the case of fixed panels and seismic combination B.

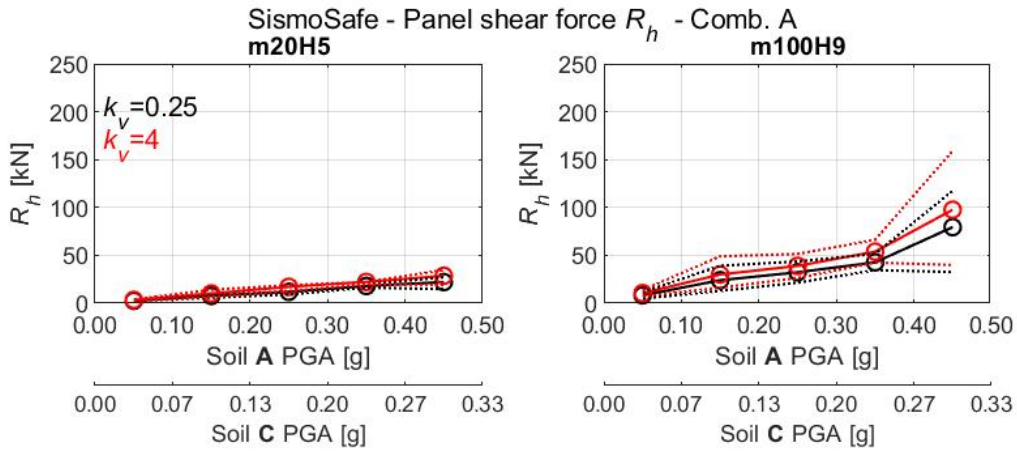

Figure 5-29: Seismic demand in term of shear force R_h at the base of the panel for SismoSafe connection in the case of fixed panels and seismic combination A.

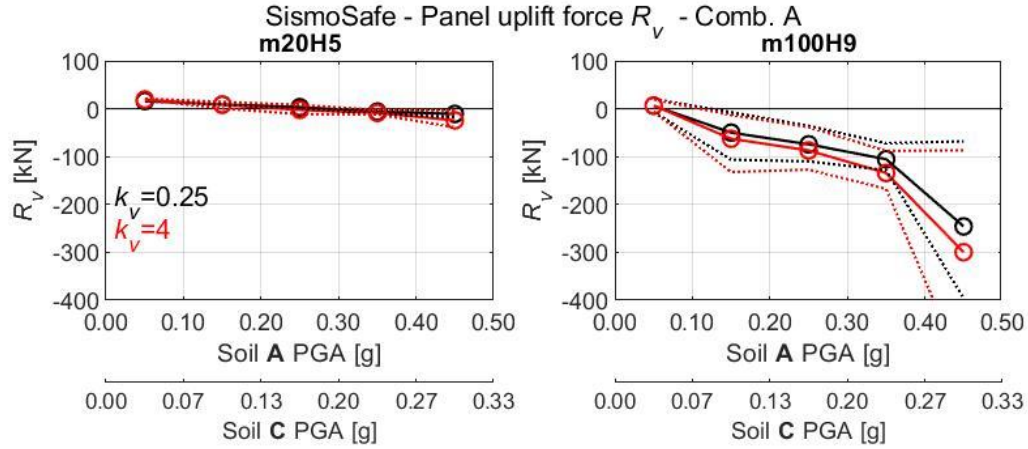

Figure 5-30: Seismic demand in panel uplift force R_v for SismoSafe connection in the case of fixed panels and seismic combination A.

5.4.10 Results for rocking panel configuration
Connection TA-210

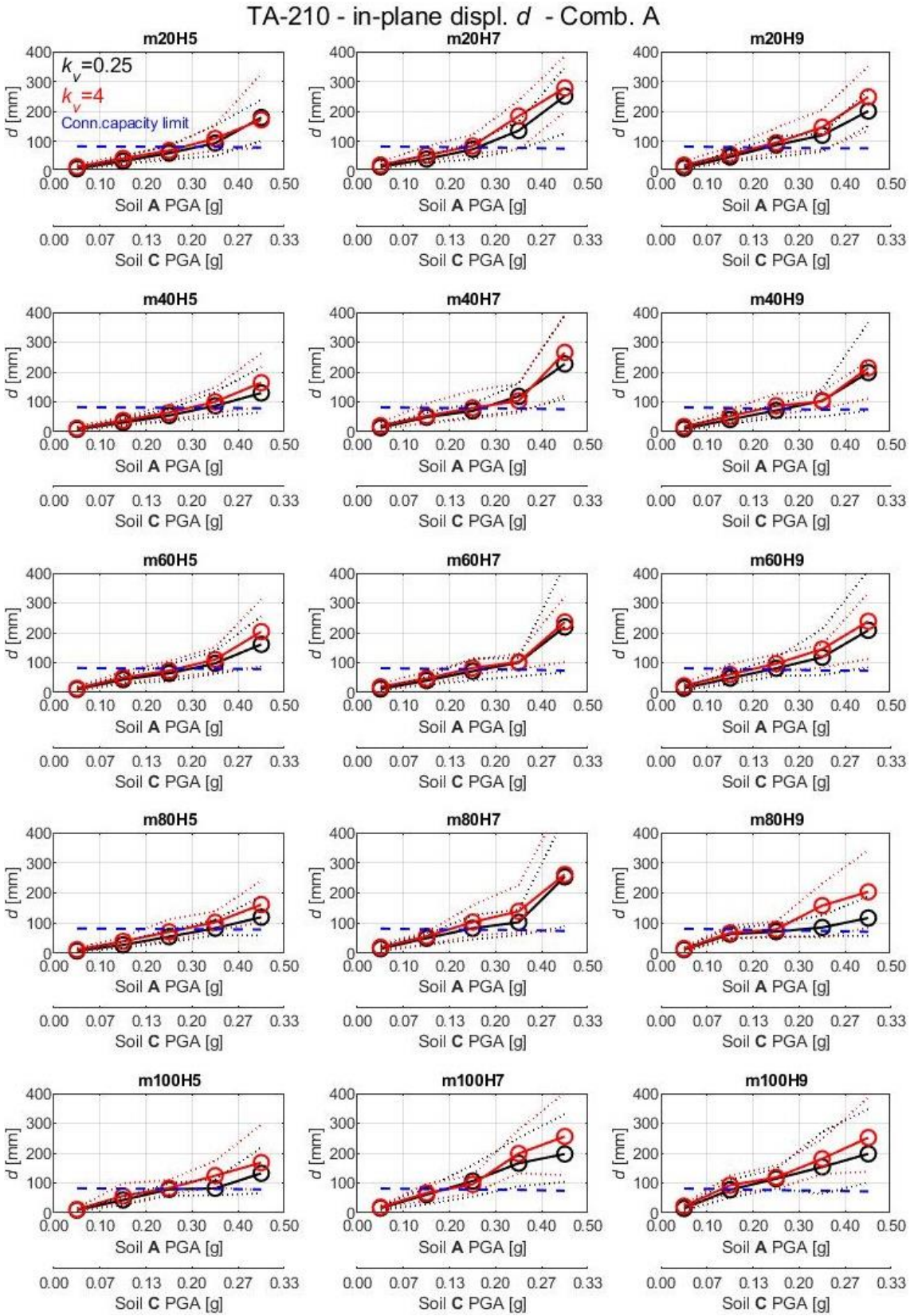

Figure 5-31: Seismic demand and capacity comparison in term of in-plane displacement *d* for hammer-head strap connection TA-210 in the case of rocking panels and seismic combination A.

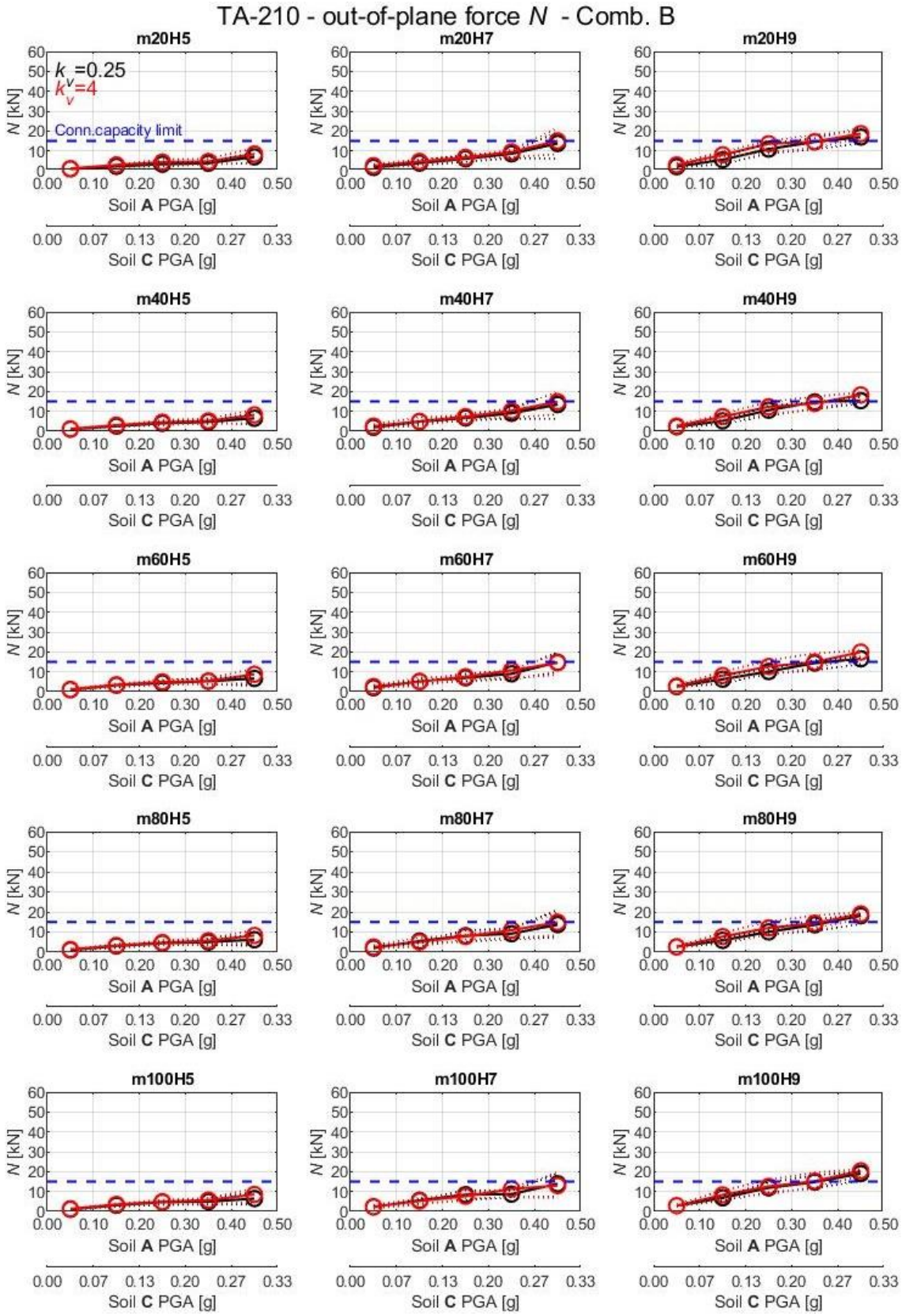

Figure 5-32: Seismic demand and capacity comparison in term in term of out-of-plane force *N* for hammer-head strap connection TA-210 in the case of rocking panels and seismic combination B.

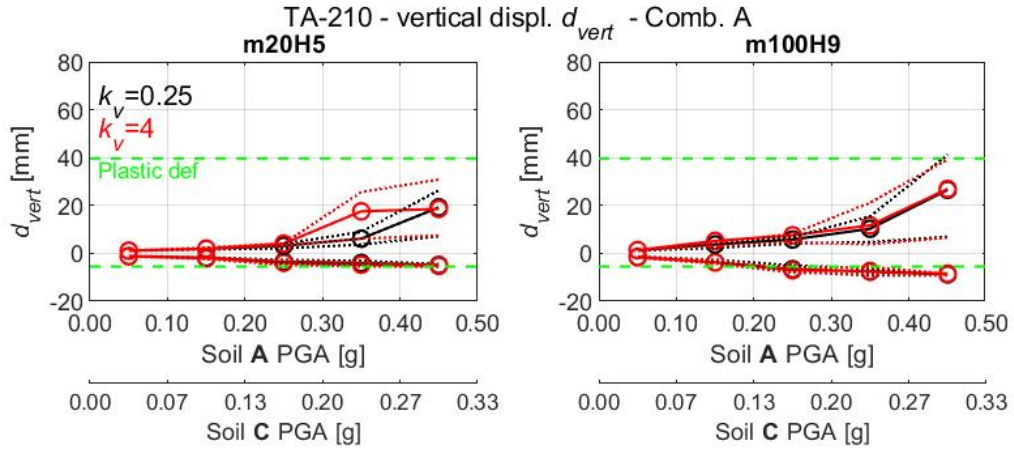

Figure 5-33: Seismic demand and capacity comparison in term of vertical displacement d_{vert} for hammer-head strap connection TA-210 in the case of rocking panels and seismic combination A.

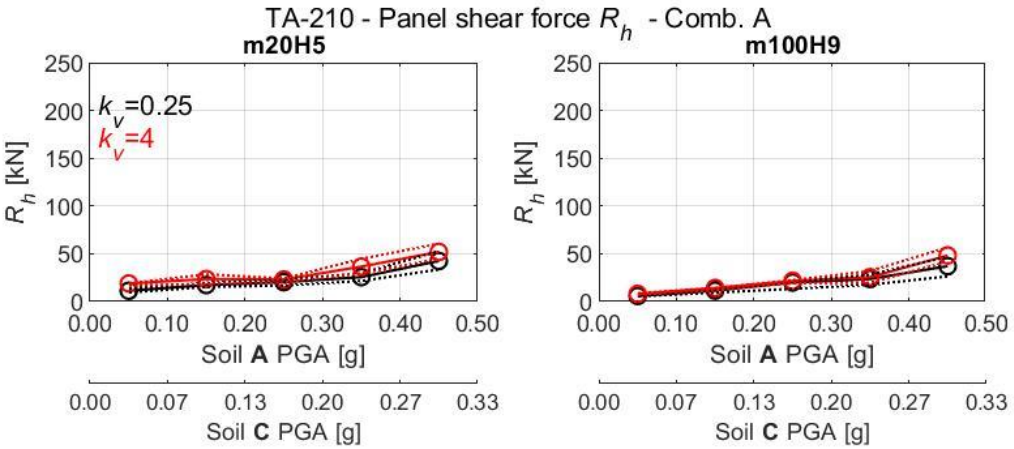

Figure 5-34: Seismic demand in term of shear force R_h at the base of the panel for hammer-head strap connection TA-210 in the case of rocking panels and seismic combination A.

Connection TA-290

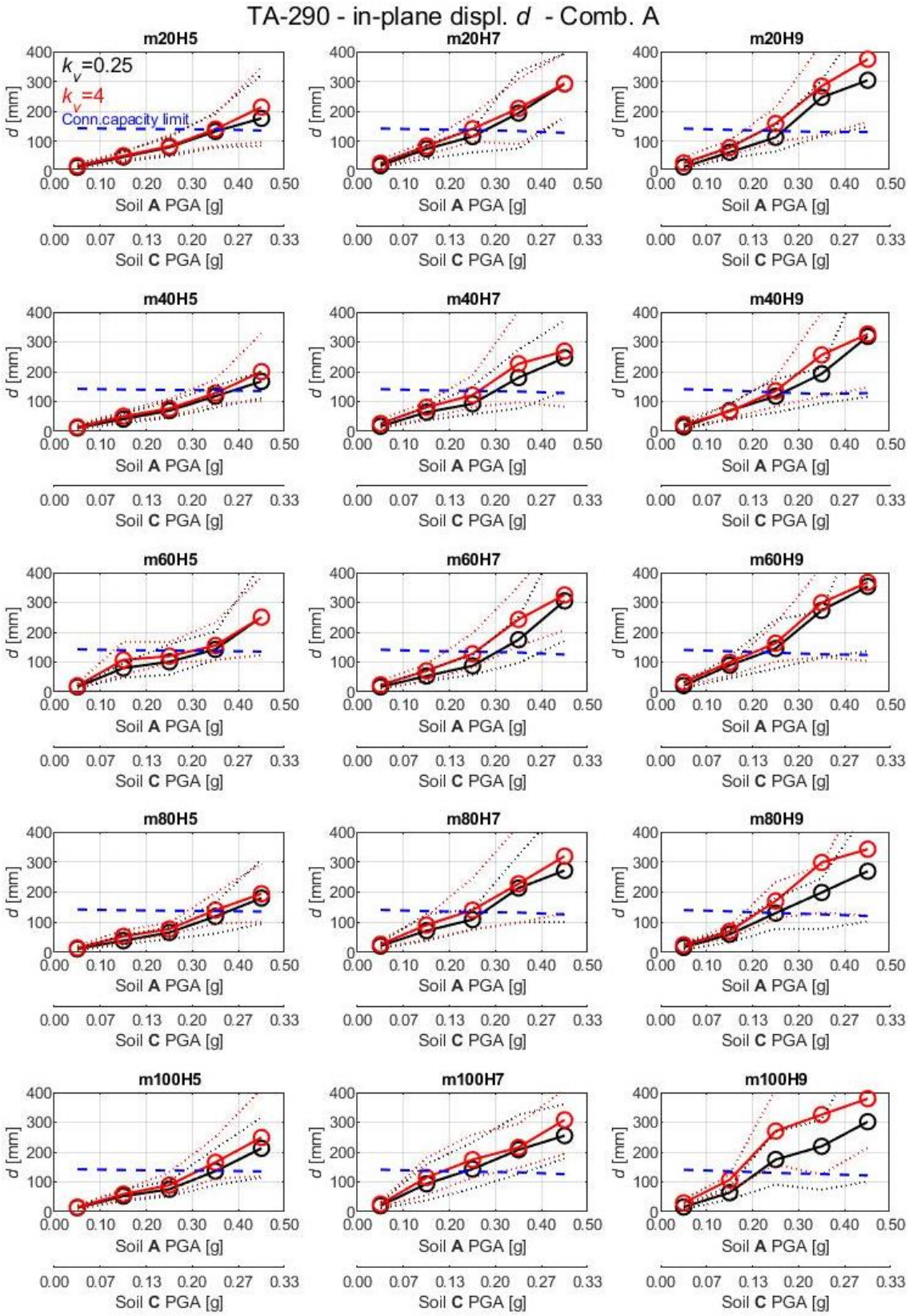

Figure 5-35: Seismic demand and capacity comparison in term of in-plane displacement *d* for hammer-head strap connection TA-290 in the case of rocking panels and seismic combination A.

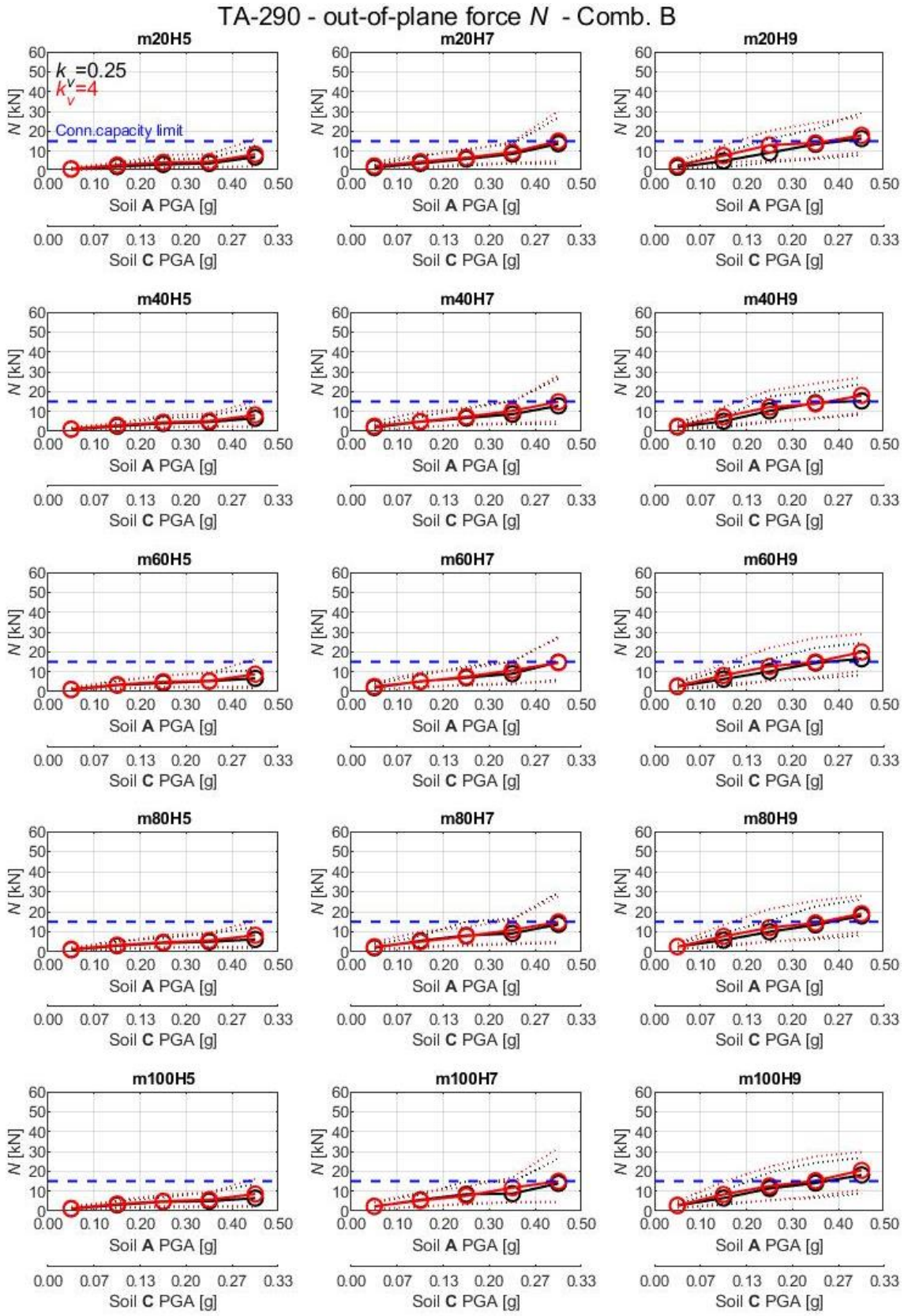

Figure 5-36: Seismic demand and capacity comparison in term in term of out-of-plane force *N* for hammer-head strap connection TA-290 in the case of rocking panels and seismic combination B .

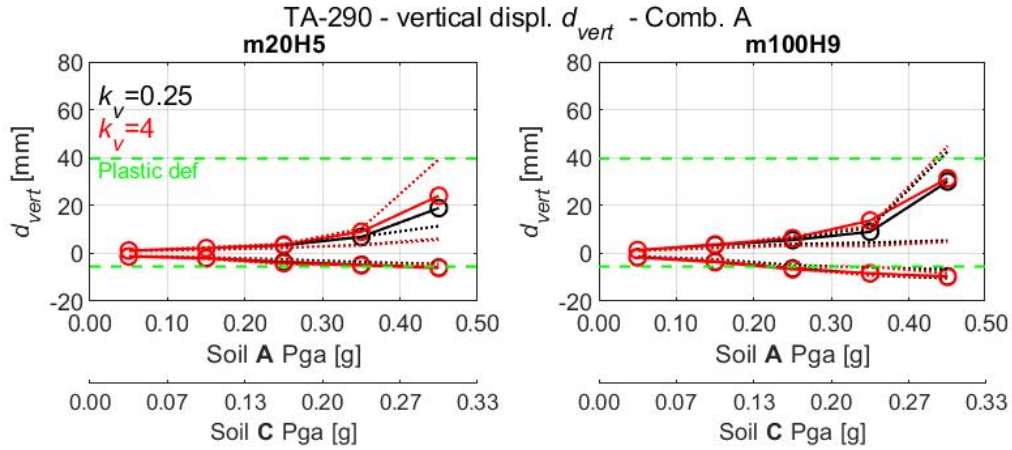

Figure 5-37: Seismic demand and capacity comparison in term of vertical displacement d_{vert} for hammer-head strap connection TA-290 in the case of rocking panels and seismic combination A.

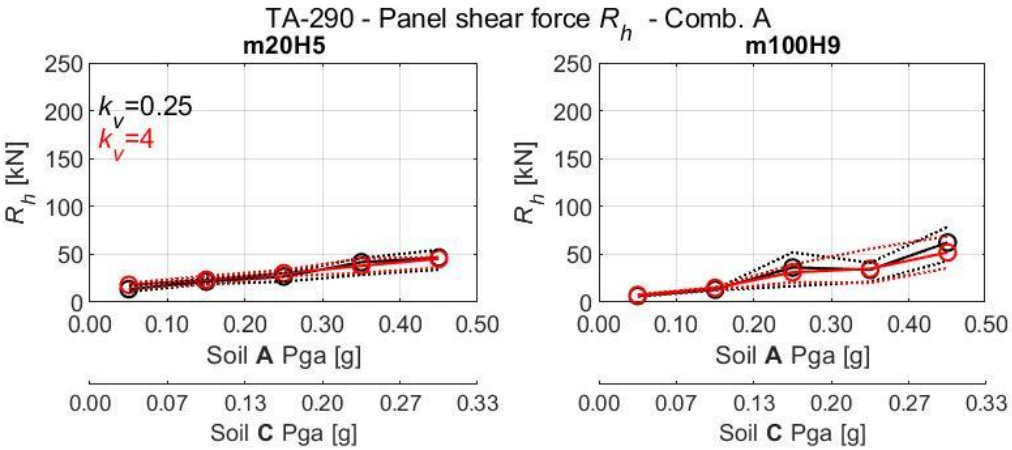

Figure 5-38: Seismic demand in term of shear force R_h at the base of the panel for hammer-head strap connection TA-290 in the case of rocking panels and seismic combination A.

Connection SismoSafe

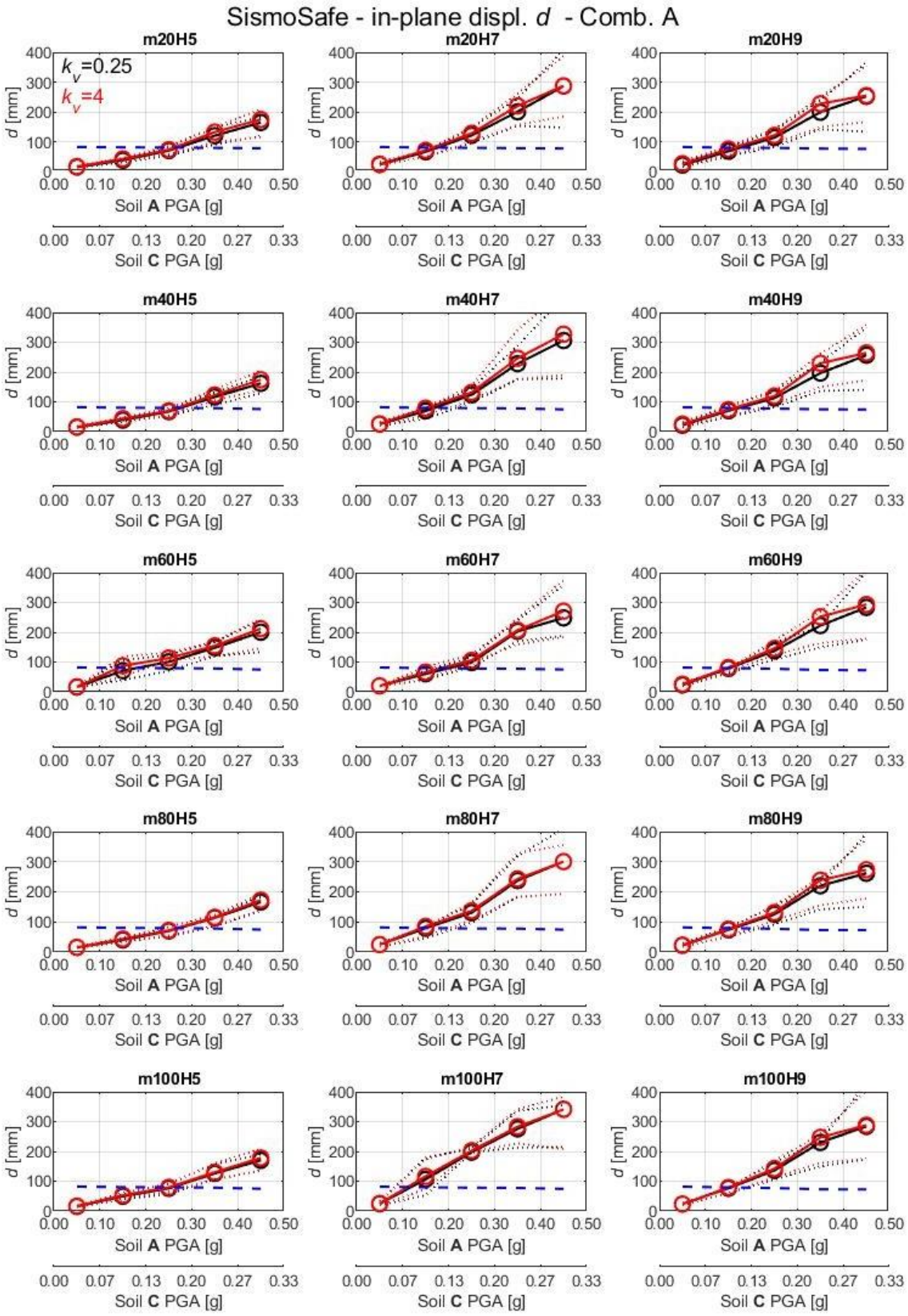

Figure 5-39: Seismic demand and capacity comparison in term of in-plane displacement *d* for SismoSafe connection in the case of rocking panels and seismic combination A

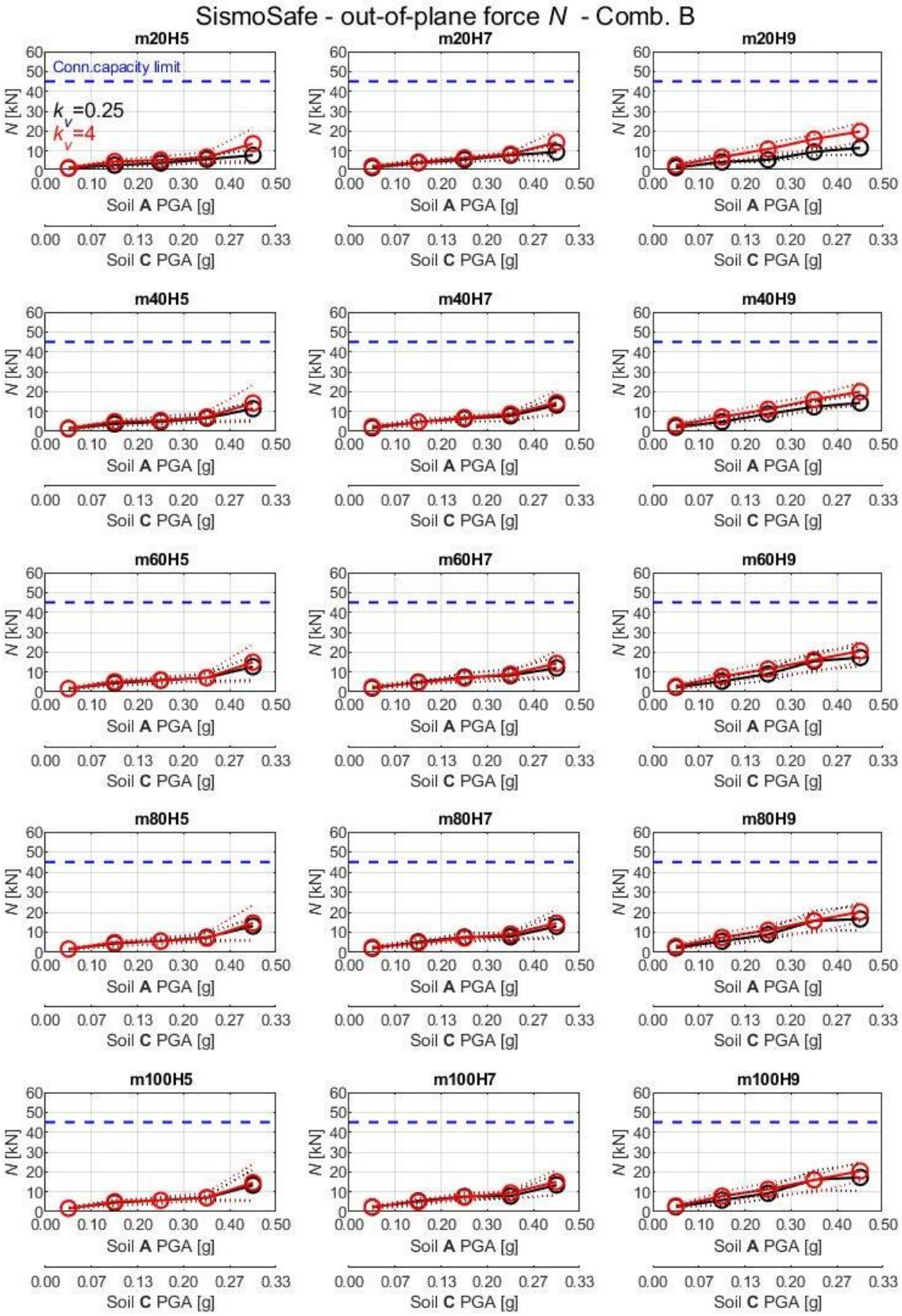

Figure 5-40: Seismic demand and capacity comparison in term in term of out-of-plane force *N* for SismoSafe connection in the case of rocking panels and seismic combination B.

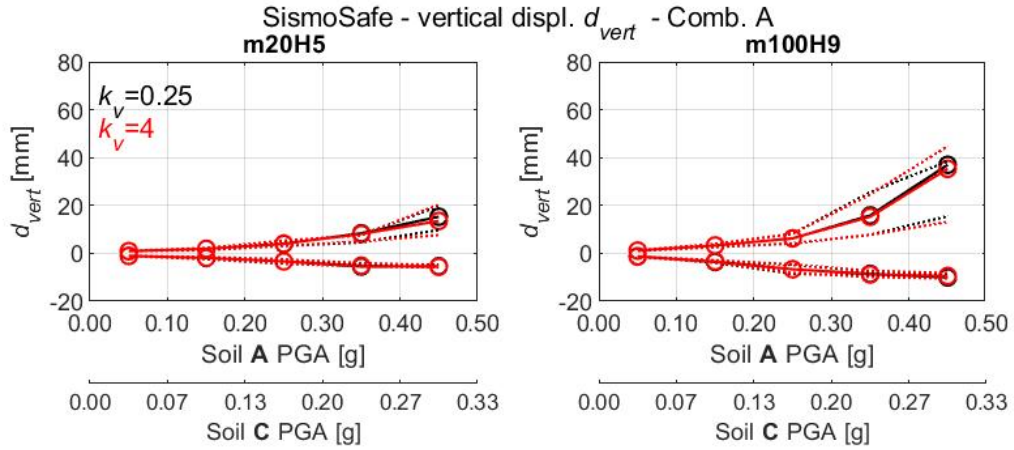

Figure 5-41: Seismic demand in term of vertical displacement d_{vert} for SismoSafe connection in the case of rocking panels and seismic combination A

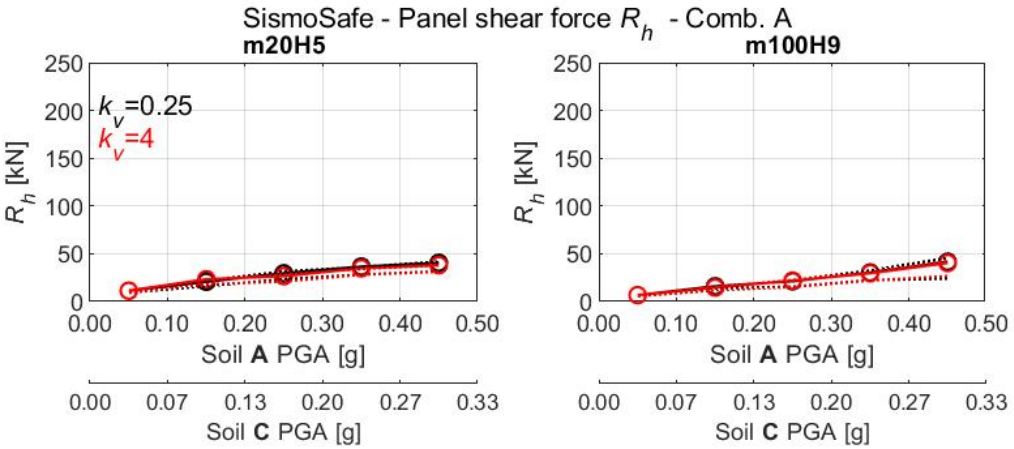

Figure 5-42: Seismic demand in term of shear force R_h at the base of the panel for SismoSafe connection in the case of rocking panels and seismic combination A.

5.5 Summary and conclusions of the parametric study

5.5.1 Considerations on fixed panels

Observing the parametric analysis results, illustrated from Figure 5-19 to Figure 5-42, it can be immediately noted that there is a clear difference in seismic demand between structures with a low and high k_v ratio. The seismic demand increases as the value of k_v increases, consequently, the structures with k_v =4 have larger seismic demand than structures with k_v =0.25. However, it should be highlighted again that only two extreme values of the k_v ratio have been analysed.
For intermediate values of k_v the difference in seismic demand, in term of in-plane displacement and out-of-plane force, could be less noticeable.
In addition, it should be noted that the k_v ratios in one-storey precast industrial buildings are usually different in the two main directions, due to the elongated plan shape of these structures. Therefore, the k_v ratio can be rather low in one direction (for example, k_v = 0.25), but high in the other direction (for example, k_v = 4). In general, lower influence of the k_v ratio can be observed in buildings with a higher average mass.

In general, the demand depends on the vibration period of the structure. And the displacement demand increases in linear proportion to the increase of the fundamental vibration period of the structure T_1. The displacement demand increasing in a rather linear proportion to the period T_1 because T_1 is grater then T_C for all investigated cases. The T_C value for soil A and C is 0.25 according to EC8 while the fundamental periods of the investigated structures are reported in Table 5-6.
This applies both to structures with panels fixed to the foundation beam (Figure 5-19 to Figure 5-30) and to those where rocking is permitted (Figure 5-31 to Figure 5-42). In the structures with higher fundamental period, the displacement demand is higher and consequently, the deformation capacity of the top panel connections (connections between the panel and the structure) is sooner exhausted.

The diagrams in Figure 5-19 and Figure 5-23 show the relationship between the in-plane displacement demand and the capacity of the hammer-head strap connections TA-210 and TA-290 in the case of fixed panels and for the seismic combination A. Seismic combination A indicates the case in which the seismic action is mainly directed in the plane of the panel, as defined at sub-section 5.4.8.

In the diagram of Figure 5-43, the PGA values for which the in-plane displacement demand meets the capacity of the TA-210 hammer-head strap connections are presented.

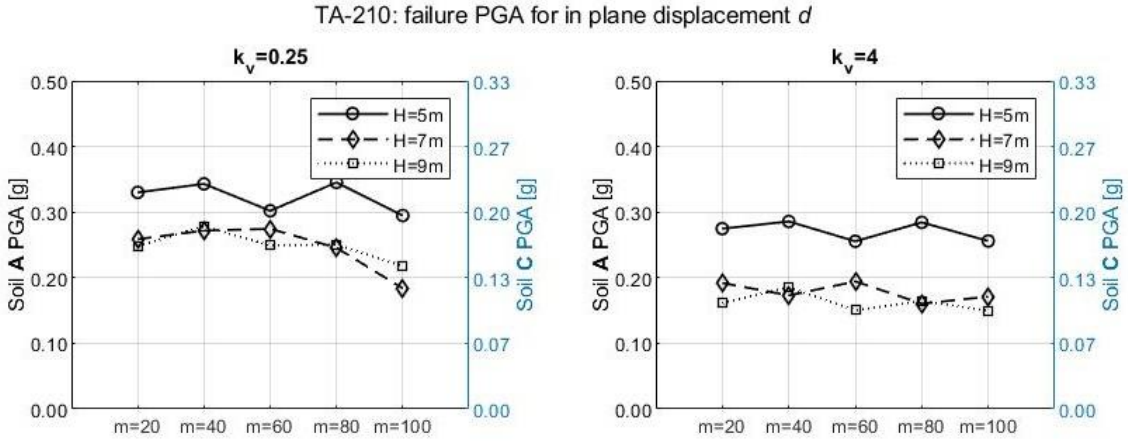

Figure 5-43 PGA values when the in-plane displacement seismic demand *d* equal the capacity for hammer-head strap connection TA-210 in the fixed panel case.

Figure 5-44 instead shows the PGA value for which the in-plane displacement demand meets the capacity of the TA-290 hammer-head strap connections.

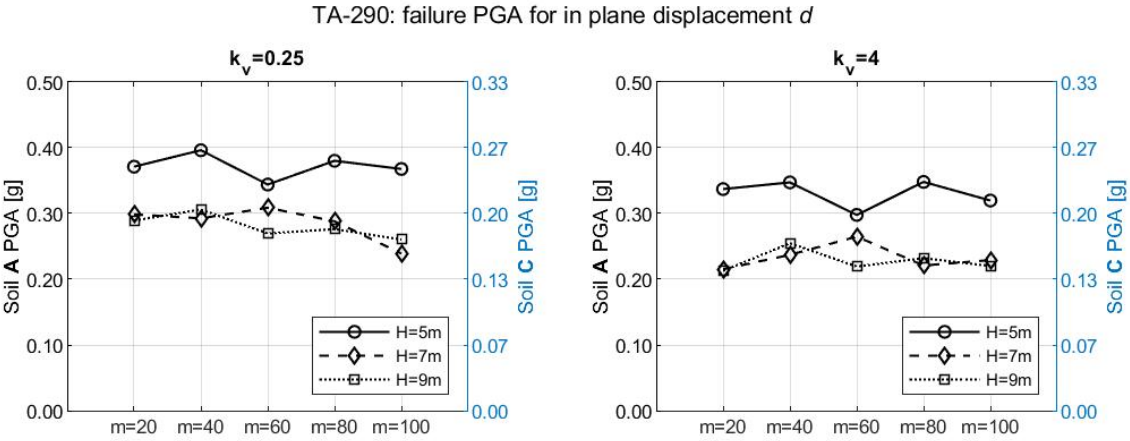

Figure 5-44: PGA values when the in-plane displacement seismic demand *d* meets the capacity for hammer-head strap connection TA-290 in the fixed panel case.

Looking at Figure 5-43 Figure 5-44, it is immediately noticed that the failure PGA trends are similar for both types of hammer-head strap connections, TA-210 and TA-290. However, the failure PGA values for the long strap (TA-290) are higher because their in-plane displacement capacity is larger.

In both cases, when the stiffness of structure increase the displacement demand is reduced. The influence of the k_v factor, which describes the relationship between the number of panels and the number of columns, is also shown.

The PGA collapse limit values for the k_v factor = 0.25 are about 20% larger than the k_v factor = 4 (comparison between left and right diagram in Figure 5-43 Figure 5-44). It is worthy emphasizing once again that the two extreme values of the k_v factor were compared and that the differences for intermediate k_v values may not be so large.

In any case, it can be stated that the failure PGA of the hammer-head strap connections between the vertical panels and the structure is not so high. In particular, for high structures built on type soil C.

A separate consideration can be made for SismoSafe connections whose in-plane displacement demand, in the case of fixed panels, is shown in Figure 5-21. It is seen that there is not a

comparison chart between demand and capacity because, in theory, the SismoSafe devices have an unlimited in-plane displacement capacity as described in section 3.5.
Although, theoretically there is no in-plane displacement limitation for SismoSafe devices from the practical point of view there should be some limitations due to the length of the fixed guide rail and to the assembling tolerance that could prevent the proper sliding of the mobile guide rail.

The diagrams from Figure 5-22 and Figure 5-24 show the relationship between the out-of-plane force demand and the capacity of the hammer-head strap connections TA-210 and TA-290 in the case of fixed panels and for the seismic combination B, which is the case where the seismic action is mainly directed perpendicular to the plane of the panel.

In the diagram of Figure 5-43, he PGA values for which the out-of-plane force demand meets the capacity of the TA-210 hammer-head strap connections are presented.

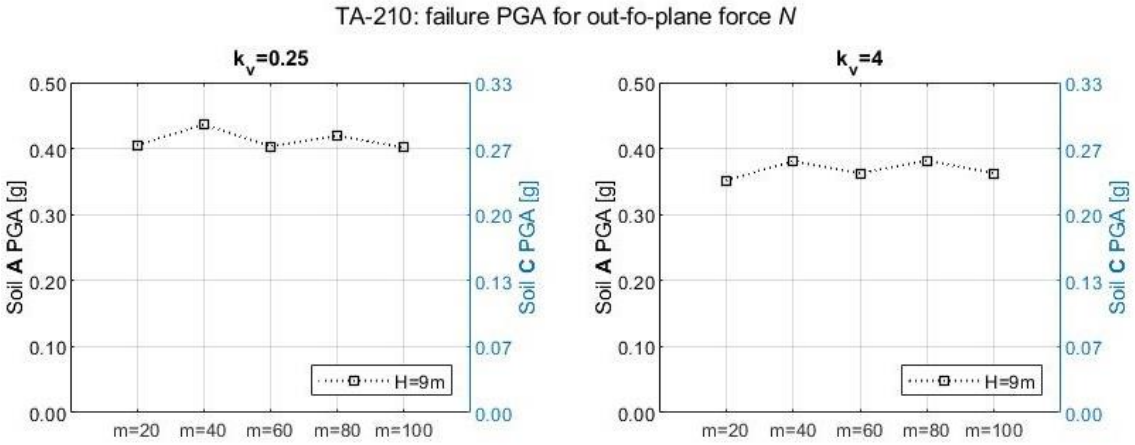

Figure 5-45: PGA values when the out-of-plane force seismic demand *N* meets the capacity for hammer-head strap connection TA-210 in the fixed panel case.

Figure 5-44 shows the PGA value for which the out-of-plane force demand meets the capacity of the TA-290 hammer-head strap connections.

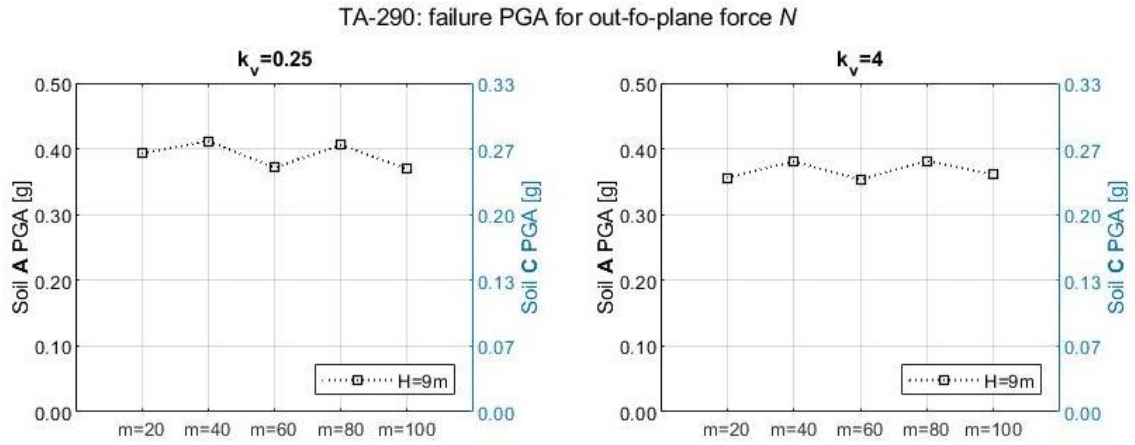

Figure 5-46: PGA values when the out-of-plane force seismic demand *N* meets the capacity for hammer-head strap connection TA-290 in the fixed panel case.

Observing Figure 5-45 and Figure 5-46, it can be seen that failure PGA due to the out-of-plane force, both for short straps (TA-210) and long straps (TA-290), has almost the same

value. The reason is that the out-of-plane force demand is very similar while the capacity is the same and calculated as described in the section 4.1.4.
It is also noted that among all the analysed structures, only in those with grater height (H=9m) the out-of-plane force capacity of the connection is reached. Furthermore, the out-of-plane force capacity is reached for significantly higher PGA values compared with the failure PGA values of in-plane displacement for structures with the same height.
This means that the critical direction for the panel-to-structure connections is the in-plane direction.
About the SismoSafe connections (Figure 5-24), due to their larger out-of-plane force capacity compared to hammer-head straps, in all the performed analysis the limit capacity for out-of-plane force was never reached.

A simple calculation of the out-of-plane force is provided in the following according to the method illustrated in chapter.
Assuming as input acceleration an EC8 spectrum for soil A and acceleration ag=0.25, first of all, the out-of-plane force F_{rigid} on the simply supported panel is evaluated (Figure 5-47).

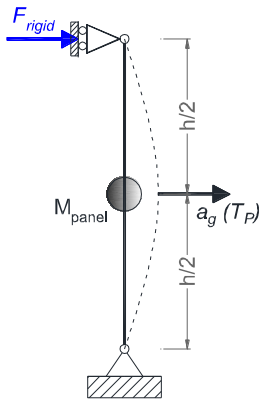

$$F_{rigid} = M_p \cdot a_g(T_P) \quad (5.30)$$

Figure 5-47: Simply supported panel

where: a_g is the spectral acceleration corresponding to the simply supported panel period T_P and M_P is the panel mass.
The values of a_g, T_P, M_P and the panel height H_P, are reported within Table 5-8 for the first three cases of the parametric analysis. In Table 5-8, the panel period T_P calculated considering a 50% reduced stiffness due to the cracking. according to EC8, are also reported:

Case Label	**m20H5**	**m20H7**	**m20H9**
Panel height H_P [m]	5	7	9
Panel mass M_P [t]	5.09	7.13	9.17
Panel period T_P [s]	0.187	0.367	0.60
Spectral acceleration a_g (T_P) [g]	0.625	0.625	0.420
Out-of-plane force F_{rigid} [kN]	15.6	21.87	18.90

Table 5-8. Data for calculation of out-of-plane force F_{rigid}

According to the findings of paragraph 4.4, the dynamic contribution of the structure has to be taken into account. The considered structures have the features reported in Table 5-9. In the table is also reported the ratio between the period of the structure T_s and the period of the panel T_P:

Case Label	**m20H5**	**m20H7**	**m20H9**
Structure height H_s [m]	5	7	9
Structure mass M_s [t]	20	20	20
Structure period T_s [s]	0.93	1.56	1.46
Period ratio T_s/T_P	4.97	4.25	2.43

Table 5-9: Structure features according to Table 5-1

The structure and the panel spectral acceleration, to the corresponding vibration period, are also reported in Figure 5-48.

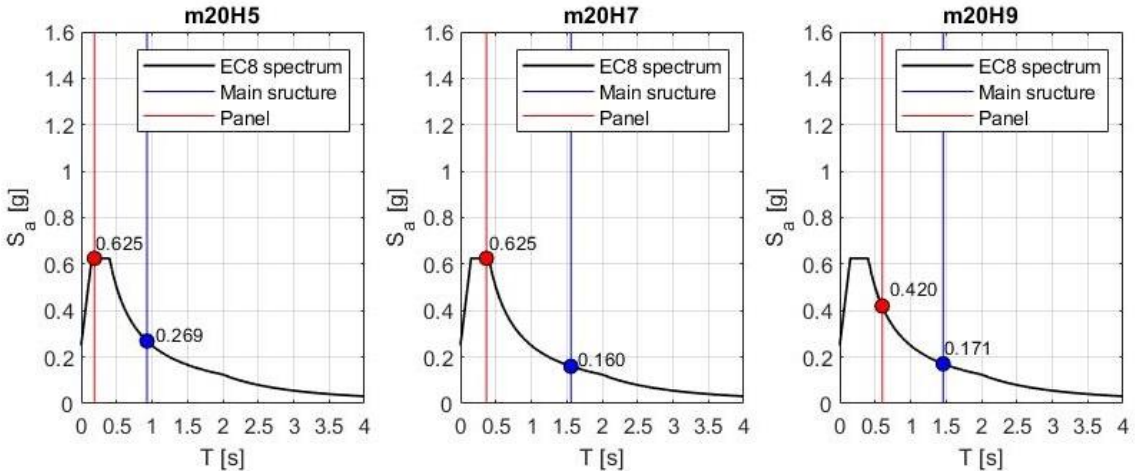

Figure 5-48: Panel and structure spectral acceleration

Since the period ratio T_s/T_P, is lower than 1.00, the amplification of the demand can be evaluated by using eq. (4.27) that is recalled below:

$$\frac{F_{real}}{F_{rigid}} = \left[0.93 + 8.32 \cdot e^{-\frac{T_s}{T_{panel}}} + 0.25\ln\left(\frac{M_s}{M_{panels}}\right)\right] \quad \text{for } \frac{T_s}{T_{panel}} > 1 \qquad (5.31)$$

The demand amplification factor F_{real}/F_{rigid} and the F_{real} value of the out-of-plane force on connection are given in Table 5-10:

Case Label	**m20H5**	**m20H7**	**m20H9**
F_{real}/F_{rigid}	1.31	1.20	1.87
F_{real} [kN]	20.58	28.39	34.81

Table 5-10: Amplification factor and the F_{real} value

If the floor spectra are instead used as described in section 2.3.1, the maximum spectral acceleration $S_a(T_p)$ could be determined by:

$$S_a(T_a) = \begin{cases} \alpha S\left(1+\frac{z}{H_s}\right)\left[\frac{a_p}{1+\left(a_p-1\right)\left(1-\frac{T_p}{aT_s}\right)^2}\right] \geq \alpha S & for\ T_p < aT_s \\ \alpha S\left(1+\frac{z}{H_s}\right) & for\ aT_s \leq T_p < bT_s \\ \alpha S\left(1+\frac{z}{H_s}\right)\left[\frac{a_p}{1+\left(a_p-1\right)\left(1-\frac{T_p}{bT_s}\right)^2}\right] \geq \alpha S & for\ T_p \geq bT_s \end{cases} \quad (5.32)$$

where α is the ratio of the design ground acceleration, a_g, on subsoil type A, and the acceleration of gravity *g*, *S* is the soil factor, z is the height of the non-structural element centroid above the level of application of the seismic action, *H* is the building height measured from the foundation or from the top of a rigid basement, T_a is the fundamental vibration period of the element and T_1 is the fundamental vibration period of the building in the relevant direction; *a*, *b*, a_p, that are parameters depending on the fundamental vibration period of the building in the relevant direction T_1. For this example, α was taken equal to 0.25g and *S* equal to 1. The other parameters are reported in Table 5-11. The panel floor spectral acceleration, to the corresponding vibration period, are also reported inFigure 5-49.

Case Label	**m20H5**	**m20H7**	**m20H9**
Structure height H_s [m]	5	7	9
Structure period T_s [s]	0.93	1.56	1.46
Panel height H_P [m]	5	7	9
Panel centroid height z [m]	2.5	3.5	4.5
Panel mass M_P [t]	5.09	7.13	9.17
Panel period T_P [s]	0.187	0.367	0.60
Floor spectral acceleration *ag* (T_P) [g]	1.131	0.876	0.938
Seismic force on panel centroid F_P [kN]	56.55	61.34	84.38
Out-of-plane force on connections F_c [kN]	28.27	30.67	42.19

Table 5-11: Parameters for floor spectra calculation

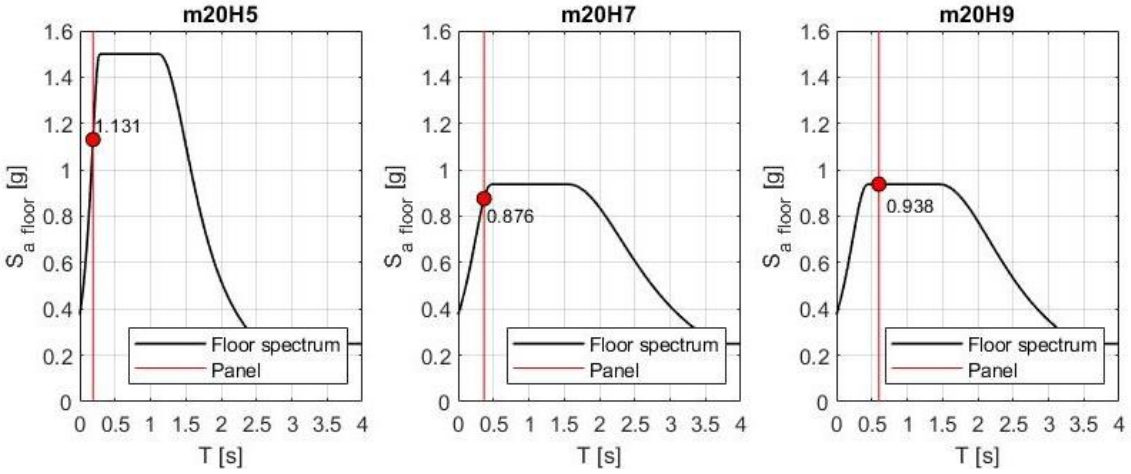

Figure 5-49: Panel floor spectral acceleration

From this example, it can be seen how the out-of-plane force on the panel-to-structure connection is larger for the structure with higher height. Although one may think that if the structure period T_s is longer than T_C, then the accelerations and consequently forces are reduced, it is necessary to take into account the dynamic interaction between the two systems (panel and structure) which depends on the relationship between the period ratio T_s/T_P and the masses M_s/ M_P as shown in chapter 4.
However, in this example, we obtained greater out-of-plane force values than those found with the parametric analysis because in this example we assumed that the panel mass was concentrated at mid-height as shown in Figure 5-47, on the contrary, in the parametric analysis the panel mass was divided into several points as shown in Figure 5-5. This mass distribution contributes to reducing the out-of-plane forces on the connection.
In the case that the panels are fully-fixed at the base, they need connection devices capable of preventing the rocking of the panel as well as the horizontal sliding, so they can withstand the uplifting reaction force R_v and the shear reaction force R_h shown in Figure 5-50 and Figure 4-32 and explained in detail within section 4.3.4.

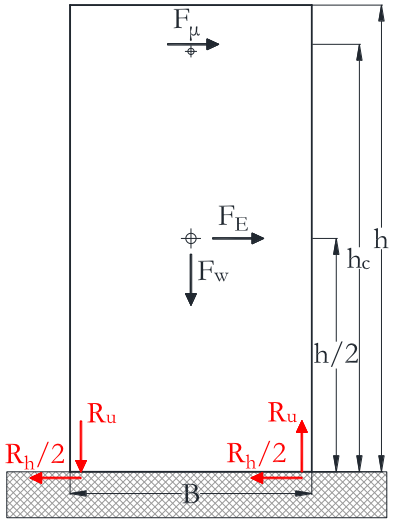

Figure 5-50: Forces acting on the panel for seismic force to the right: $F\mu$ force transmitted by the panel-to-structure connection (due to a relative displacement of the structure to the right), F_E inertial force of the panel, F_w dead weight of the panel, R_h and R_v horizontal and vertical reaction of fixing devices

The seismic demand for the reaction force at the base of the panel, R_v and R_h, resulting from the parametric analysis are shown from Figure 5-25 Figure 5-30 in the case of seismic combination A.
For the shear reaction R_h, both in the case of the hammer-head strap and SismoSafe connections (see Figure 5-25, Figure 5-26 and Figure 5-27), it can be seen that the seismic demand increases with the increase in the height and mass of the building.
Concerning the uplift reaction R_v, first of all, it is necessary to specify that this reaction lifts the panel when in Figure 5-22, Figure 5-26 and Figure 5-30 it assumes a negative value.
The seismic demand trend for R_v, both in the case of the hammer-head strap and SismoSafe connections, increases with the increase in the height and mass of the structure because, at the same time, the height and therefore the mass of the panel also increases. So the horizontal force F_E imposed by the earthquake increase and, to balance the overturning moment, R_v consequently increases. It is also noted that the reaction R_h is slightly dependent on the mass of the structure.

5.5.2 Considerations on rocking panels

The parametric analysis results, for rocking panel configuration, are presented in Figure 5-31 to Figure 5-42.
The diagrams in Figure 5-31 and Figure 5-35 show the relationship between the in-plane displacement demand and the capacity of the hammer-head strap connections TA-210 and TA-290 in the case of rocking panels and for the seismic combination A.

In the diagram of Figure 5-51, the PGA value can be seen, value for which the in-plane displacement demand meets the capacity of the TA-210 hammer-head strap connections for the case of rocking panels.

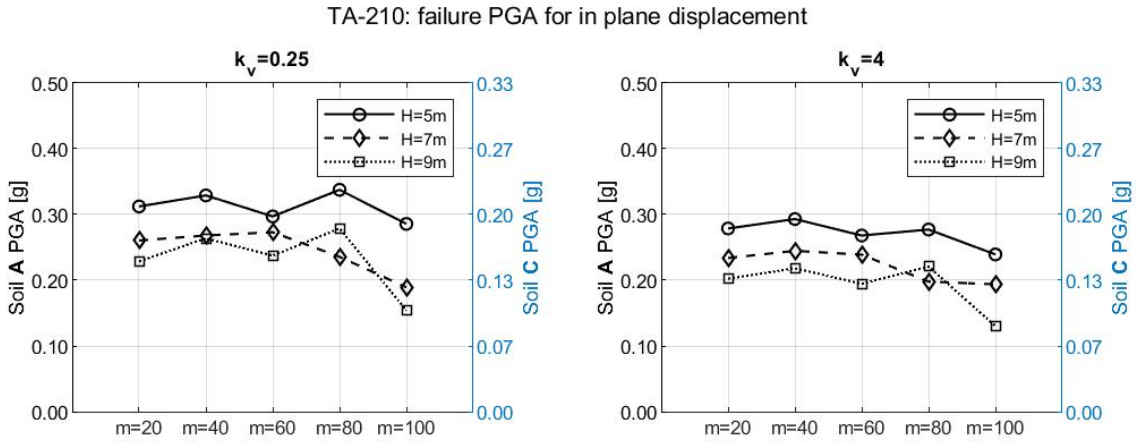

Figure 5-51: PGA values when the in-plane displacement seismic demand *d* meets the capacity for hammer-head strap connection TA-210 in the rocking panel case.

Figure 5-44 instead shows the PGA value for which the in-plane displacement demand meets the capacity of the TA-290 hammer-head strap connections.

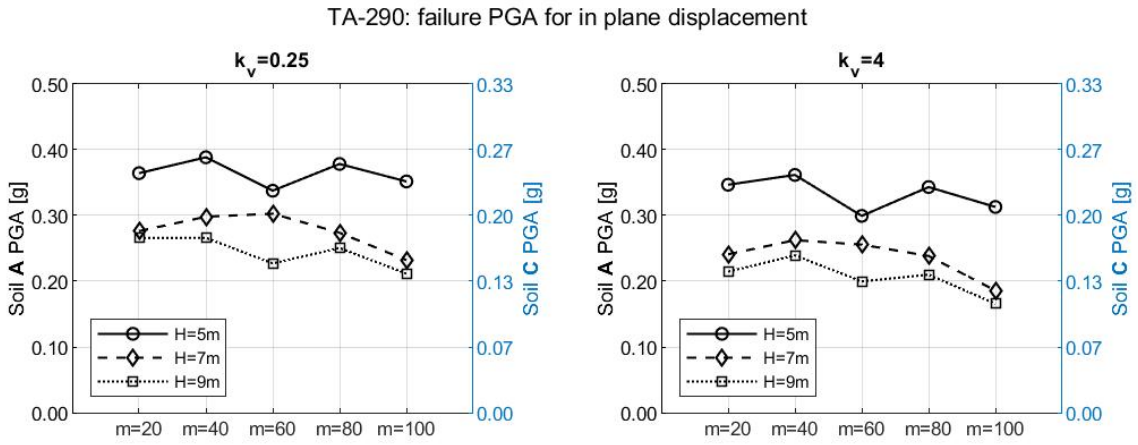

Figure 5-52: PGA values when the in-plane displacement seismic demand *d* meets the capacity for hammer-head strap connection TA-290 in the rocking panel case.

As in the fixed panel case, from Figure 5-51 and Figure 5-52 it can be noticed that the failure PGA trends are similar for both types of hammer-head strap connections, TA-210 and TA-290. However, the failure PGA values for the long strap (TA-290) are higher because their in-plane displacement capacity is larger.

In both cases, the failure PGA decreases with the increasing of the structure period T_1. The fundamental periods are reported in Table 5-6 and Figure 5-15b.
The influence of the k_v factor, which describes the relationship between the number of panels and the number of columns, is also shown.
The PGA collapse limit values for the k_v factor = 0.25 are about 10% larger than the k_v factor = 4 (comparison between left and right diagram in Figure 5-51 and Figure 5-52).
Moreover, the failure PGA values are quite similar between the fixed and the rocking panel configuration because also the period T_1 are similar.
It is also important to recall that during the rocking movement the connections are deformed also in the vertical direction as shown in Figure 5-34 and Figure 5-35. In particular, it is possible to observe that hammer-head strap connections are deformed (plastic limit of the strap is reached) due to vertical displacement in all investigated structures.
A separate consideration can be made for SismoSafe connections whose in-plane displacement demand, in the case rocking panels, is shown in Figure 5-36. It is seen that demand and capacity have not been compared because, in theory, the SismoSafe devices have an in-plane unlimited displacement capacity as described in section 3.5.
However, from the practical point of view, there should be some limitation due to the length of the fixed guide rail and to the assembling tolerance, that could prevent the proper sliding of the mobile guide rail.

The diagrams from Figure 5-37 Figure 5-39 show the relationship between the out-of-plane force demand and the capacity of the hammer-head strap connections TA-210 and TA-290 in the case of rocking panels and for the seismic combination B, which is the case where the seismic action is mainly directed perpendicular to the plane of the panel.

In the diagram of Figure 5-53, the PGA value can be seen, value for which the out-of-plane force demand meets the capacity of the TA-210 hammer-head strap connections.

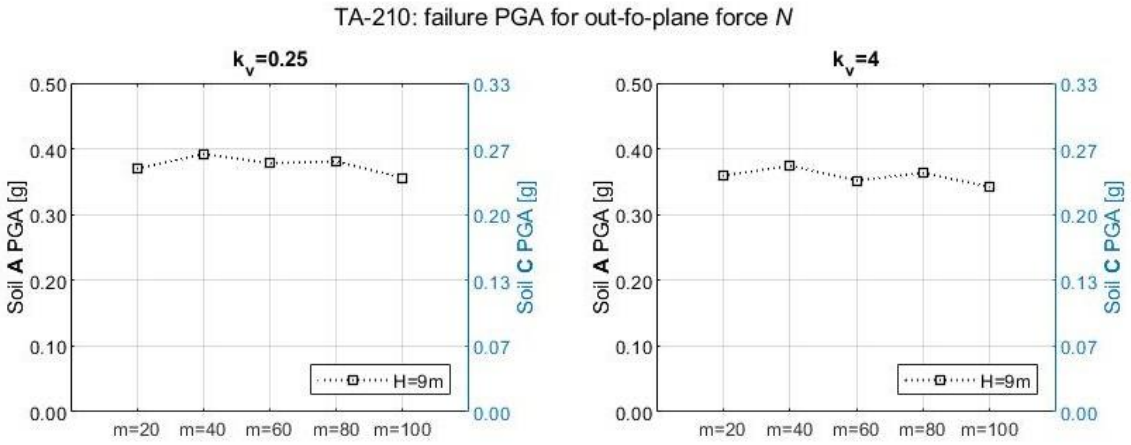

Figure 5-53: PGA values when the out-of-plane force seismic demand *N* meets the capacity for hammer-head strap connection TA-210 in the rocking panel case.

Figure 5-54 shows the PGA value for which the out-of-plane force demand meets the capacity of the TA-290 hammer-head strap connections.

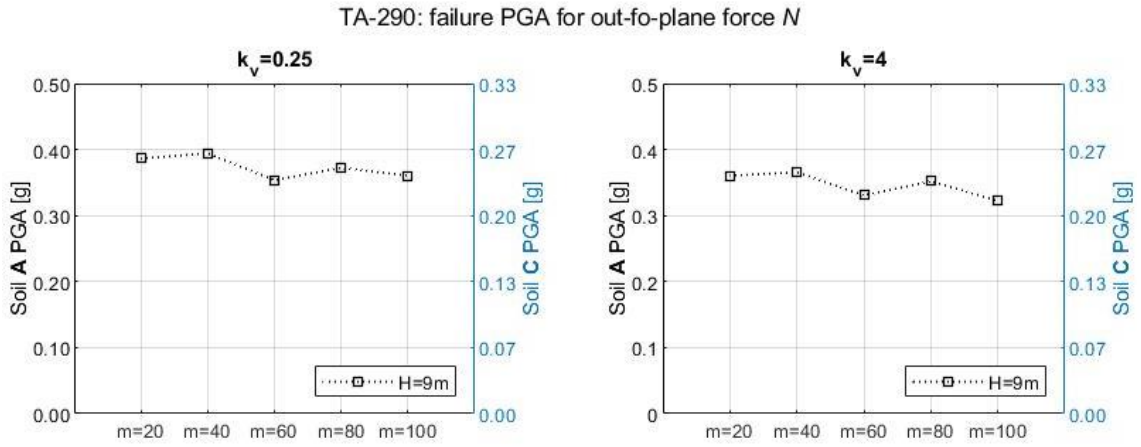

Figure 5-54: PGA values when the out-of-plane force seismic demand *N* meets the capacity for hammer-head strap connection TA-290 in the rocking panel case.

Looking at Figure 5-53 and Figure 5-54, it is possible to notice that the failure PGA for out-of-plane force, both for short straps (TA-210) and long straps (TA-290), is very similar to the one in the fixed panel case.
Among all the analysed structures, the out-of-plane force ultimate capacity of the connection is reached only for the structure with a height of H=9m, the same reasoning made for fixed panels on the mutual dynamic interaction between panel and structure can also be applied in the case of rocking panels.
Also for rocking panels configuration, the failure PGA values are slightly influenced by the coefficient k_v and by the average mass of the column. Indeed, the values of the collapse PGA slightly change as the k_v factor and the mass of the structure change.
About the SismoSafe connections (Figure 5-39), due to their larger out-of-plane force capacity compared to hammer-head straps, in all the performed analysis the limit capacity for out-of-plane force was never reached.

In the case of rocking panels, connection devices capable of preventing only the horizontal sliding are needed at their base. These devices have to only withstand the shear reaction force R_b shown in Figure 5-50.
The seismic demand for the reaction force at the base of the panel, R_b, resulting from the parametric analysis are shown in Figure 5-34, Figure 5-38 and Figure 5-42 in the case of seismic combination A.
The R_b values are up to 50% lower compared with those obtained for the fixed panels configuration.

Finally, some considerations can be made on the dispersion of the results. Observing the results for the rocking panels it can be seen that there is a lager dispersion compared to the fixed panel case. The value of results dispersion is given by the distance between the 75th and 25th percentile curves from the average value curve.
The reason can be found in the less controlled behaviour of the panels, which begin to rotate around their lower edges (i.e. rocking panels) under horizontal seismic load. The relative displacements in the connection between the panels and the structure are no longer the same as the displacements of the structure but can be greater or less since the panel also moves.

This is only a preliminary study that provides some initial indications on the in-plane and out-of-plane seismic demand for vertical panels. However, further investigations are needed to

better understand the seismic response of the panels and to identify which factors influence the demand for connection devices.

6 Conclusions and developments

The main purpose of this dissertation was to evaluate the seismic response of RC vertical cladding panels in RC precast buildings and their influence on seismic response of this type of buildings. The purpose was achieved through the support of extensive experimental and analytical research. The essential contributions of the thesis, are summarized below:

- Based on the analysis of a shaking table test, designed and conducted by the University of Ljubljana, the basic mechanisms of the in-plane response were identified: the basic mechanisms of the panel-to-structure connections and basic mechanisms of panels.
  The influence of the panels on the overall response was studied for different types of panel-to-structure connections (two types of hammer-head straps) and panels-to-foundation connections (fixed and rocking panels)

- The numerical models for the in-plane direction of studied types of connections and panels were developed. In particular, the hysteretic models of the panel-to-structure connections were calibrated on the shaking table test results. For the first time, the vertical behaviour of the hammer-head strap connections was introduced. Therefore, the seismic response obtained during the test was correctly replicated by the numerical models. The calibrated numerical model was used to evaluate the influence of silicone sealant on the seismic behaviour of precast vertical cladding panels.

- The new device, which improves the seismic response of panels, was developed and tested at the University of Florence. It was studied analytically and experimentally. The new device was developed in collaboration with the precast company Baraclit S.p.A. and it was called "SismoSafe" connection. This new device is based on a friction sliding system instead of the hysteresis of the material such as the hammer-head strap device. The appropriate numerical models for the SismoSafe device were developed.

- For the first time, a systematic study of the out-of-plane response of cladding panels was performed. The appropriate numerical models for the analysed connections were developed.

- The in-plane and out-of-plane capacity of the evaluated connections were systematically studied based on the results of the own experiments and that found in the literature.

- Based on the systematic parametric study the critical direction of the connections was identified. In the majority of cases, the in-plane direction was critical.

- Using calibrated models with the results obtained from the experimental campaigns, an extensive parametric study was performed. The parametric study allowed to assess the PGA capacity limit both for the considered connections and fixed and rocking panel configurations.

- Standard and improved connections were evaluated in terms of peak ground accelerations, which corresponds to their capacity.

- For the first time, the response of the rocking and fixed panels were systematically compared.

Within this research work, we came to several results, the most important of which will be listed and described below.

6.1 Main results

In this thesis, the in-plane and out-of-plane seismic response of vertical cladding panels was studied.
Different opinions are presented in the scientific literature about the critical direction for the claddings panels and for their fastening device.

Both an experimental and a numerical study were carried out, in order to identify which direction is more critical.

6.1.1 The in-plane response of connections

Observations from the results of the shaking table experimental campaign
The shaking table experimental campaign, designed by the University of Ljubljana, included a series of tests on a prototype building described in section 3.1. The prototype building was equipped with a couple of vertical panels (one on each side) connected to the main structure by means of hammer-head strap connections (two devices for each panel). Two panel configurations were tested: configuration with fixed panels and configuration with rocking panels. For each panel configuration, both short and long straps were tested.
Examining the results obtained from the shaking table experimental campaign (section 3.2) it was observed that the seismic response mechanism of fixed and rocking panels was considerably different. The displacement seismic demand of rocking panels was about ten times larger than that of fixed panels. The shear force demand in fixed panels was more than two times larger than that in the rocking panels.
More details on the results of the experimental campaign are reported in the work of Isaković et al., (2018). Although in the case of fixed and rocking panels the recorded response was different, the maximum relative displacements between the panels and the main structure in the in-plane panels direction (the displacement demand on panel-to-structure connection) were quantitatively similar.
Besides, both in the case of fixed and rocking panels, during the tests with greater seismic intensity, significant deformation of the hammer-head straps was observed. In the case of fixed panels, the straps were deformed only in the horizontal direction. While, in the case of rocking panels, the hammer-head straps were deformed in both horizontal and vertical directions.
According to the findings of Isaković et al., (2018), it can be said that the configuration with fixed panels may be more appropriate for two reasons:

1. The response of fixed panels is less sensitive to imperfections during assembly and is more controlled and predictable.
2. Hammer-head steel straps are deformed only in their horizontal plane (unlike in the rocking panels configuration, where considerable vertical deformations of the connections were observed.).

It was also possible to understand that within the all testes structure configurations, the stiffness of the panels did not significantly affect the response of the main structure. This was due to the connections since their stiffness and strength was very small compared to that of the panels and the structure. Despite the large differences between the tested panel configurations, the vibration periods and the displacement of the main structure were approximatively the same. Therefore, it can be concluded that the connections, as long as they were effective, isolated the panels from the main structure and allowed the panels to vibrate differently from the main structure.

Moreover, it can be stated that the response of the panels significantly depended on the boundary conditions at the panel foundations. In the case of rocking panels, the response was quite stochastic and influenced by different coincidences and construction imperfections. It was observed that at strong parts of excitation, the main structure controlled the periods of vibrations of the panels. Due to the small stiffness, panels did not significantly influence the overall response.

Numerical modelling – in-plane direction

In order to deeply investigate the seismic behaviour of one-storey precast buildings with vertical cladding panels, a numerical model was made that could be replicate the results obtained during the experimental campaign.
In particular, attention was focused on the proper modelling of the panel-to-structure connections. The mathematical model for hammer-head strap connection proposed by Zoubek et al., (2016), was improved.
The vertical behaviour of hammer-head strap connections was introduced and numerically modelled (see section 3.3.5). It was assumed that in the vertical direction, the strap had a cantilever beam behaviour with two different inflexion lengths, one for the upward direction and one for the downward. The strap cross-section was selected and therefore the elastic-plastic behaviour was studied and implemented in the numerical model.
Another innovative procedure was the simulation of the rocking panel impact with the foundation beam which was described in section 3.3.6. During the shaking table tests, in the rocking panels case, a small amount of damage at lower panel corners was noted and therefore a dissipation of energy occurred in these areas. The impact energy dissipation was simulated introducing in the numerical model an element with non-linear behaviour based on the Hertz contact model whose parameters were calibrated following the indication provided by Muthukumar & DesRoches, (2006).
The developed numerical model was able to replicate the results obtained during the experimental campaign both in terms of displacement and acceleration. This was possible thanks to the implementation of the connections hysteretic models, in particular, the introduction of the connections vertical behaviour and the panel-to-foundation impact model allowed an accurate matching of the results also in the case of rocking panel configuration.
The correctly calibrated numerical model was used to investigate the effect of silicone sealant on the seismic behaviour of precast vertical cladding panels.
The numerical model of the building provided with rocking panels was extended by adding one panel on each side panel. The adjoining panels were connected with a link element that could simulate the silicone sealant shear behaviour. The behaviour of the link element was calibrated based on the experimental results reported in the work of Dal Lago et al., (2017).
Non-linear dynamic analyses were performed on this new model.
The results showed that the presence of the silicone sealant contributed to increasing the displacement demand in the panel-structure connections. However, according to the indications provided by Dal Lago et al., (2017) it is advisable not to take into account the silicone effect when it has a possible beneficial effect on the seismic performance of the structure because silicone is not an engineered material and could be great variability in the mechanical characteristics and the effects of ageing are not well known. On the contrary, the effect of silicone sealant between adjoining panels must be taken into account when it is not on the safe side, for example when assessing the displacement demand of connections.

Development of new connection device

To improve the existing types of connection a new connection device was developed. Since the basic mechanisms of the existing types of connections were not entirely known, they were tested experimentally (cyclic tests + shake table tests) and analytically too.
To avoid the detected deficiencies in the existing connection, the new connections were developed. They were studied experimentally and analytically.
The new connection device was designed in collaboration with the precast company Baraclit S.p.A.
The new SismoSafe device (described in detail in section 3.5.1.2) consists of two vertical steel anchor channels fixed on the panel before casting. Inside the two anchor channels, a sliding block is inserted, to which a mobile guide rail is welded, capable of sliding vertically. This mobile guide rail is suitable to receive a fixed guide rail, which in turn is fixed to the beam through two self-tapping screws and this device allows the mutual horizontal sliding between the panel and the beam.
The experimental campaign showed that the new connection type can properly uncouple the displacement of the panels and the main structure. The devices did not show any significant damage to their metal components during the performed tests due to their behaviour based on relatively low friction forces. It was determined that the value of the friction coefficient, which develops between the mobile guide rail and the fixed guide rail, is 0.45 for static friction and 0.32 for dynamic friction.

6.1.2 The out-of-plane response of connection

The out-of-plane capacity
For the presence of out-of-plane seismic forces, panel-to-structure connections need a satisfactory out-of-plane resistance while out-of-plane relative displacements between the cladding panels and the structure need to be very small to preserve structural integrity. For the first time, an experimental campaign was carried out in the University of Florence laboratory, in order to characterize the out-of-plane of traditional hammer-head strap connections and the new SismoSafe device. Detailed information on the experimental campaign is provided in section 4.1. The experimental tests allowed to evaluate the out-of-plane resistance of the investigated devices, both on beam and panel side. The lesser of the two resistances can be assumed as the ultimate out-of-plane resistance of the device.
Tests showed that traditional hammer-head devices have an out-of-plane resistance on the panel side of about 15 kN, three times less than SismoSafe devices that exhibited a resistance on the panel side of about 45 kN.
To evaluate the out-of-plane force in the panel-to-structure connections of a one-storey precast industrial building equipped with SismoSafe connection, a series of non-linear dynamic analyses were carried out on a case study, considering the four strongest Italian earthquakes of the last 12 years.
The numerical results confirmed that the new SismoSafe devices can safely withstand out-of-plane forces for all four seismic events. In addition, the numerical analyses allowed to highlight the influence of friction at the SismoSafe connections on the seismic response of the structure. As the friction force increases, uplift and shear reaction forces at the base of panels parallel to the earthquake direction also increase, as well as the out-of-plane forces at the top of panels normal to the earthquake direction. Therefore, very low friction would be preferable. However, the manufacturing of low friction devices could be very expensive and not convenient for industrial production.

The out-of-plane capacity was systematically studied for the first time. Traditional and new device were studied. Experiments were performed to estimate this capacity. Capacity of the connections in the out-of-plane direction is defined in terms of forces.
The capacity of traditional devices was about 15 kN.
Besides, during a seismic event, the traditional devices are susceptible to in-plane damage, which could significantly reduce the out-of-plane capacity of hammer-head strap connections.
The capacity of the new device in the out-of-plane direction is considerably larger, about 45 kN. So the number of devices necessary to resist out-of-plane seismic actions can be reduced compared to the number of standard connections, which must be at least three times higher.

The Out-of-plane Seismic demand for panel-to-structure connections

In the common design practice the out-of-plane seismic demand for non-structural elements, like vertical panels, is generally determined by applying to them an equivalent static force. The equivalent static force is usually computed by multiplying the element mass for the spectral acceleration. The spectral acceleration for non-structural elements can be calculated according to the floor spectra proposed by Medina et al., (2006) and Sullivan et al., (2013).
Although the floor spectra formulation may be appropriate for horizontal panels it may not be appropriate for vertical panels of one-storey buildings. The vertical panels generally have edge supported to the ground so they are directly stressed by seismic acceleration. At the top, they are stressed by the action coming from the structure. Therefore, the out-of-plane forces in the panel-to-structure connection are generated by the panel-structure interaction.
In this thesis, a new formulation to compute the out-of-plane force demand in the panel-to-structure connection was proposed.
At the beginning, a one-storey precast building was schematized through a simplified 2-DOF model, introducing the hypothesis of a rigid diaphragm for the roof system. A parametric study was performed through a series of dynamic analysis. The assumed variable parameters are: the ratio between structure panel period, R_T, and the ratio between structure and panel mass, R_M. In each analysis, the out-of-plane F_{real} force in the panel-to-structure connection was monitored.
The parametric analysis led to the definition of a surface that relates the connection out-of-plane force F_{real} with the two variables R_T and R_M. The equation of this surface has been described in detail in section 4.5.
The surface obtained by the parametric numerical analysis was compared with the one obtained through the floor spectra according to the Eurocode 8 (EN 1998-1-1, 2005) formulation.
The comparison between the two surfaces showed that the floor spectra formulation tends to overestimate the connection out-of-plane force for R_T ratios higher than 1.50, particularly in the R_T range between 1.00 and 4.50. Furthermore, it was observed that for R_T values close to 0.00 there is a considerable underestimation of the F_{real} force. However, this is a limit case that can hardly concern some real buildings.

Influence of panel-to-structure connections on seismic response of one-storey precast RC buildings

The parametric study, it was tried to establish in which cases the panel structure connections did not provide sufficient seismic safety.
The parametric study included the three types of connections studied in previous chapters: short straps (TA-210), long straps (TA-290), and the SismoSafe devices. It also included two different panel configurations: fixed and rocking.
Within the parametric study, the parameter k_v, determined by the ratio between the number of columns and the number of panels, was considered. In particular, two extreme real values were estimated and taken into account, namely $k_v = 0.25$ and $k_v = 4$.
The parametric analysis was based on the numerical models calibrated on the results of the shaking test described in Chapter 3, and on the experimental results obtained during the experimental campaigns carried out at the University of Florence. During the parametric analysis, the simultaneous presence of the seismic action in-plane and out-of-plane of the panel was also taken into account.
It was noticed that the demand mainly depends on the vibration period of the structure. And the displacement demand increases proportionally to the increase of the fundamental vibration period of the structure T_1. The displacement demand increasing rather proportional to the period T_1 because T_1 is grater then T_C for all in investigated cases.
In the case of the fixed panel, the analysis showed that the short hammer-head straps failure occurred for average PGA values between 0.35g and 0.10g for soil type A and values between 0.23g and 0.07g for soil type C. For long hammer-head strap, the failure PGA average values were between 0.44g and 0.25g for soil type A and between 0.21g and 0.16g for soil type C. The values changed in these ranges depending on the height, the mass and the stiffness of the main structure.
The SismoSafe connections never reached failure because, in theory, their in-plane displacement capacity depends on the length of the fixed guide rail, and could be considered unlimited. In practice there could be some limitations due to, for example, the length of the fixed guide rail and\or to the assembling tolerance that could prevent the proper sliding of the mobile guide rail. Some further studies are required on this point.

About the out-of-plane force, the analysis showed that the failure of the hammer-head strap occurred for PGA values between 0.42g and 0.38g on soil type A soil between 0.28g and 0.25 g on soil type C. It was observed that among all the analysed structures, only in those with grater height (H=9m) the out-of-plane force capacity of the strap connection is reached.
For the SismoSafe devices, the out-of-plane capacity is never reached
This means that the critical direction for the panel-to-structure connections is the in-plane direction.

In the rocking panel case, the same proportionality between demand and period of structure was observed.
The short hammer-head straps failure occurred for average PGA values between 0.31g and 0.10g for soil type A and values between 0.21g and 0.07g for soil type C. For long hammer-head strap, the failure PGA average values were between 0.38g and 0.16g for soil type A and between 0.25g and 0.10g for soil type C.
It is worthy of notice that the failure PGA values are quite similar between the fixed and the rocking panel configuration because also the periods T_1 are similar.
In addition, the analysis showed that, during the rocking movement of the panels, the connections are also deformed in the vertical direction in all the analysed structures.

As to the SismoSafe connections, their ultimate in-plane displacement capacity was never reached because it could be considered unlimited as previously explained.

In the out-of-plane direction, the analysis showed that the resistance capacity of the connections is reached for PGA values between 0.43g and 0.34g on soil type A and between 0.28g and 0.22 g on soil type C. However, it was observed that the failure PGA, among all the analysed structures, is reached only in those with height equal to 9m. Also, in this case, out-the of-plane capacity of SismoSafe devices is never exhausted.
In can be again stated that the critical direction for the panel-to-structure connections is the in-plane direction, also in the case of rocking panels.

Finally, both the fixed panels and rocking panels layout, the results showed that the effect of a lower ratio between the number of columns and panels, k_n, (or a higher number of panels compared to the number of columns) was favourable, even though relatively limited.
Although the failure PGA values for hammer-head strap connections, in the case of rocking panels, were similar than the PGA values for the fixed panel, the hammer-head are deformed in the vertical direction. Therefore, it can be concluded that: if hammer-head strap connections are used, the rocking configuration has a lower seismic safety than the fixed panel configuration.

6.2 Open topics and future developments

During this research work, some possibilities for further research activities were detected.

Within chapter **3 - The in-plane seismic response of vertical cladding panels**, the results of a shaking table experimental campaign were analysed and discussed. Based on the observations made, numerical models were calibrated to replicate the results obtained during the real tests. The possibilities of further research are mainly located in the following field:

- Further experimental research on other types of panel-structure connections available on the market, as far as their impact on the seismic response is concerned.
- Further experimental research on a larger number of panels (the prototype tested only two) as far as their impact on the seismic response.
- Further experimental and analytical research to better investigate the silicone sealant effects between adjoining cladding panels.
- Study of the combined effect of horizontal and vertical deformation of the hammer-head strap and achievement of an appropriate numerical model that takes into account the interaction between the two behaviours.

Again in Chapter 3, panel-to-structure connection device, which most often used in European practice, were experimentally studied and a new connection device was proposed. Some problems suitable for further research were found, namely:

- Research on how the closing and opening of the gap between the panel and the structure can influence the response of the whole structure.
- Further experimental investigations to define a displacement capacity limit of the new SismoSafe devices. That is because during the laboratory tests everything works perfectly but it would be appropriate to consider possible installing imperfections of the SismoSafe devices.

- Further development of new joints with sufficient deformation capacity, which would allow the complete panel detachment from the structure.
- Additional development of new connection devices where seismic energy could be dissipated.

In Chapter **4 - Out-of-plane vertical panels behaviour**, the out-of-plane connection resistance capacity was assessed and a new formulation is also proposed to evaluate the seismic demand.
In the experimental assessment of the ultimate out-of-plane resistance of hammer-head strap connections, unused devices were employed. However, in a real situation, hammer-head steel straps could be seriously damaged due to in-plane seismic loads, even though they were designed to uncouple the relative in-plane displacement between the panels and the structure. Therefore, the out-of-plane capacity of hammer-head straps was overestimated because the in-plane damage was neglected in the experimental campaign, so further experimental investigation to clarify this point may be desirable. The experimental results for the SismoSafe devices could be considered accurate since they do not suffer any in-plane damage.

In the new formulation for out-of-plane seismic demand assessment, a real structure was schematized with a 2 DOF system, introducing the hypothesis of a rigid diaphragm for the roof system. Further numerical analysis could be performed to remove this hypothesis and evaluate how the out-of-plane demand changes if the roof cannot be considered as a rigid diaphragm.

In Chapter **5 - Parametric study on the seismic response of panel-to-structure connections**, a parametric study was carried out with the aim of understanding in which cases the panel-to-structure connections did not provide sufficient seismic safety. The performed numerical analysis took into account the simultaneous presence of the seismic action in and out of the plane of the panel.
Although the parametric study clearly shows the effects on seismic response of connection types and panel configurations, the connection failure PGA values showed some data dispersion, especially in the case of rocking panels, and therefore they should be taken with caution.
Besides, the numerical models used for nonlinear dynamic analysis were relatively simple and did not capture with sufficient accuracy some important response features of whole structures, such as the stiffness of the roof elements, the failure possibility of the joints between the roof elements and the beams, the interaction between the panels, the contact between the panel and the beam. For this reason, a more detailed review of actual practice in the construction of precast RC buildings would be necessary to assess the actual situation.
Note that some parameters are hard to estimate accurately since they depend on the installation (e.g. the tightening torque in the connection elements of the cladding panels and possible mounting tolerances).

Further aspects that should be studied in detail concern precast multi-storey buildings with vertical cladding system. Understanding the behaviour of the connections and the response of the panels even when they are connected to the structure at multiple points could be useful to assess the overall seismic safety of the building but also to optimize the steel reinforcement of the panels. Since the ultimate goal is to design a cladding system that provides an adequate level of safety under seismic conditions, it would be appropriate to analyse the problems of interaction between the panels at the corners of the building, the possible interaction between the panel and the main columns and other critical points of the cladding system.

7 Razširjeni povzetek (in Slovenian)

V disertaciji prikazujemo rezultate predhodnih eksperimentalnih raziskav prototipov montažnih armiranobetonskih (AB) hal z vertikalnimi paneli in tipičnimi stiki z jekleno ploščico na potresni mizi. Predstavljena je procedura numeričnega modeliranja, ki je omogočila, da smo reproducirali rezultate opravljenih testov.

Nato je predstavljen inovativen stik za vertikalne panele in serija testov za karakterizacijo mehanskega odziva tovrstnih stikov, pri izvedbi katerih smo bili aktivno vključeni. Na koncu je izvedena numerična parametrična študija, s katero smo izboljšali razumevanje sil, ki povzročijo napetosti v povezavah vertikalnih panelov izven svoje ravnine. Na podlagi parametrične študije smo sile, ki vplivajo na povezavo, ocenili kot funkcijo mase in nihajnega časa konstrukcije, s čimer smo razširili področje uporabnosti izsledkov raziskav. Sledijo še preliminarni predlogi za postopke projektiranja obravnavanih sistemov.

V prvih dveh poglavjih disertacije prikazujemo zgodovinski pregled AB montažnih objektov in najsodobnejše raziskave na področju AB montažnih objektov in stikov. Ti dve poglavji omogočata, da izpostavimo pomanjkljivosti potresnega odziva tovrstnega tipa objektov.

V tretjem poglavju predstavljamo eksperimentalne raziskave na potresni mizi, ki so bile predhodno izvedene na UL FGG z namenom preučevanja potresnega odziva enoetažnih AB montažnih objektov z vertikalnimi paneli. Nato predstavimo razvoj numeričnega modela, s katerim smo zanesljivo reproducirali rezultate omenjenih eksperimentov. Kalibrirani numerični model je možno uporabiti za analizo različnih vplivov. V disertaciji smo ga uporabili za oceno vpliva silikonske tesnilne mase na potresno obnašanje montažnega vertikalnega panela. V tem poglavju prikazujemo tudi analitično in eksperimentalno študijo inovativnega stika, ki omogoča disipacijo energije s pomočjo mehanizma trenja.

Cilj omenjenih testov na potresni mizi je bil oceniti vpliv več parametrov na dinamični odziv montažnih industrijskih objektov z armiranobetonskimi fasadnimi paneli. Preučevani parametri v tej študiji so vključevali:

- usmerjenost panelov,
- vrsto povezav med paneli in glavnim konstrukcijskim sistemom objekta (dolg ali kratek stik z jekleno ploščico),
- vrsto povezav panelov s temeljem.

Preizkušenih je bilo osem različnih konfiguracij prototipov. Testi so se razlikovali glede na usmerjenost panelov (vodoravna ali navpična konfiguracija), vrsto povezav med panelom in konstrukcijo, vrsto povezav panelov in temeljev (konzolne ali rotirajoče panele) ter številom panelov (na obeh straneh ali le na eni strani). Glavna okvirna konstrukcija je bila enaka za vseh osem konfiguracij. Ker je namen disertacije karakterizirati potresni odziv vertikalnih panelov, smo obravnavali in komentirali le teste z vertikalnimi paneli.

Numerične modele, ki smo jih je analizirali s programom OpenSees, so lahko z zadovoljivo natančnostjo napovedali rezultate eksperimentov tako za vpete panele kot panele, pri katerih je omogočeno zibanje (v nadaljevanju rotirajoči paneli). Natančnost rezultatov smo dosegli z implementacijo histereznega modela za stike med paneli in konstrukcijo. Natančneje, model za stike z jekleno ploščico, predstavljen v delu, opravljenem na Univerzi v Ljubljani (Zoubek in sod., 2016), smo izboljšali z uvedbo modeliranja vertikalnega obnašanja povezav, s katerim smo lahko upoštevali elastično in plastično nosilnosti ter deformacije. Na ta način smo z

numeričnim modelom lahko simulirali eksperimentalne odzive konstrukcije in panelov v formatu pomikov in pospeškov.

Z numeričnim modelom smo lahko zelo dobro napovedali dejanski odziv panelov, ki so bili vpeti na spodnjem robu, medtem ko je bila napoved manj natančna v primeru rotirajočih panelov, zlasti kadar so bili uporabljeni daljši stiki. Razlog za to je odvisnost odziva panelov od robnih pogojev (načina vpetja v temelje). Odziv rotirajočih panelov je bil precej negotov, saj so nanj vplivali različni parametri in pomanjkljivosti pri izgradnji, ki jih ni mogoče do potankosti modelirati.

Kalibriran numerični model smo uporabili za preučevanje vpliva silikonske tesnilne mase med sosednjima rotirajočima paneloma. Iz rezultatov numeričnih analiz smo ugotovili, da je vzdolžni pomik rotirajočih panelov pri uporabi silikonske tesnilne mase omejen v primerjavi s pomikom panelov brez silikona. Silikonski trakovi, nameščeni med sosednjimi paneli, lahko ugodno vplivajo na kontrolo mejnega stanja uporabnosti, čeprav povzročajo večje potresne zahteve v smislu pomikov v stikih med paneli in konstrukcijo. To pomeni, da pri odzivu konstrukcije blizu mejnega stanja uporabnosti silikonsko tesnilo lahko vpliva na odziv fasadnih panelov.

Silikon ni standarden material, uporabljen v gradbeništvu, zato lahko mehanske lastnosti med različnimi produkti na trgu precej variirajo. Poleg tega ni jasno, kakšni so učinki staranja na silikonsko tesnilno maso, kar prispeva k dodatni negotovosti njegovih mehanskih lastnosti. Nadalje silikon ni primeren za prenos obremenitev pri velikih zamikih med paneli, na primer tistih, ki se pojavijo, ko konstrukcija doseže mejno stanje nosilnosti.

Glede na navedbe Dal Lago in sod. (2017) je priporočljivo, da se vpliv silikona zanemari, kadar ima ta lahko ugoden učinek na potresno obnašanje konstrukcije. Nasprotno se priporoča, da se vpliv silikonske tesnilne mase med sosednjimi paneli upošteva, kadar so ti na nevarni strani, na primer pri oceni potresnih zahtev v smislu pomikov v stikih.

Na Univerzi v Firencah smo v laboratoriju »Laboratory of Tests and Materials of the Department of Civil and Environmental Engineering« izvedli in natančno spremljali serijo eksperimentov, ki je vključevala komercialne stike z jekleno ploščico (v nadaljevanju poimenovani Standard) in inovativne stike (v nadaljevanju poimenovani SismoSafe). Novi stik SismoSafe za vertikalne panele je sestavljen iz dveh jeklenih vertikalnih profilov s kanali, ki se jih pritrdi na panele pred vgradnjo. Znotraj teh dveh kanalov je drsna ploščica, na katero je privarjena premična vodilna tirnica, ki lahko drsi vertikalno. Profil premične vodilne tirnice v panelu se lahko poveže s fiksno vodilno tirnico, ki je pritrjena na gredo z dvema samovreznima vijakoma.

Preizkusi so potrdili nekaj težav stikov Standard, ki so se izkazale kot kritične tudi med nedavnimi potresi v Italiji. Ti stiki so sposobni prenesti pomike panelnega sistema in konstrukcije v ravnini, vendar imajo precej omejeno deformacijsko kapaciteto. Obnašanje stikov je histerezno do nastopa porušitve, ki je običajno posledica upogibne porušitve ploščice v ozkem delu tik pod glavo ploščice, ali zaradi poškodb sidrnega kanala, nameščenega na gredah ali stebrih in izpuljenja vijakov stika z jekleno ploščico. Rezultate testov stikov Standard smo primerjali z rezultati testov iste vrste stikov, opravljenimi na Univerzi v Ljubljani. Primerjava je pokazala, da so preizkušeni stiki v Firencah in v Ljubljani izkazali enako togost, a različno deformacijsko kapaciteto. To je lahko posledica dejstva, da so stiki, čeprav podobni, izdelani s strani različnih proizvajalcev.

Eksperimentalni testi so pokazali, da lahko inovativni stiki SismoSafe prenesejo večje pomike v ravnini panelov in glavne konstrukcije kot stiki Standard, zaradi večje deformacijske kapacitete. Novi stiki med vsemi testi niso utrpeli večjih poškodb na svojih kovinskih komponentah zaradi zelo nizkih sil trenja. Vrednost statičnega koeficienta trenja μ_s je bil približno 0.45, medtem ko so bili dinamični koeficienti μ_d v območju 0.32 - 0.35. Stiki SismoSafe so nekoliko dražji, vendar njihov odziv nakazuje v prid večje varnosti. Poudariti je potrebno, da je povišanje stroškov omejeno, saj stiki SismoSafe ne potrebujejo vnaprej nameščenih elementov na gredi, kar pomeni tudi znižanje stroškov dela. Ker imajo večjo nosilnost za prenos obremenitev izven ravnine kot tradicionalni stiki, pa je za vsak panel potrebno namestiti manjše število tovrstnih stikov.

V četrtem poglavju prikazujemo eksperimentalne preiskave obnašanja stikov z jekleno ploščico Standard izven ravnine. Eksperimenti so bili izvedeni pod našim neposrednim nadzorom. Tekom testov se je pokazalo, da imajo stiki Standard nižjo odpornost izven ravnine kot stiki SismoSafe. Na strani panelov so stiki Standard izkazali trikrat nižjo mejno odpornost kot stiki SismoSafe tako za ciklične kot monotone obremenitve. Poleg tega je potrebno poudariti, da je dejanska nosilnost stikov Standard celo nižja od eksperimentalno določene nosilnost, kajti poškodbe se lahko pojavijo tudi zaradi potresnih sil v ravnini. Stiki SismoSafe se ne poškodujejo zaradi relativnih pomikov v ravnini, zaradi tega so lahko napovedi kapacitet na podlagi testov izven ravnine precej bolj zanesljive. Predlagali smo nov inženirski model za žstike SismoSafe. Model smo uporabili v odprtokodnem programskem okolju za nelinearno analizo konstrukcij OpenSees.

Izvedli smo serijo nelinearnih dinamičnih analiz za oceno sil izven ravnine v stikih SismoSafe med paneli in konstrukcijo na študiji primera enoetažnega industrijskega objekta. V analizah smo upoštevali štiri najmočnejše potrese v Italiji v zadnjih 12 letih. Rezultati numeričnih analiz so potrdili, da bi lahko novi stiki SismoSafe varno zdržali sile izven ravnine zaradi vseh štirih potresnih dogodkov, ne glede na to, ali se sile trenja v ravnini upoštevajo ali ne. Numerične analize so omogočile, da smo podrobneje osvetlili vpliv trenja na stike pri potresnem odzivu konstrukcije. S povečanjem sile trenja se povečajo strižne reakcije na dnu panelov vzporedno z delovanjem potresne obtežbe, kot tudi sile izven ravnine na vrhu panelov pravokotno na delovanje potresne obtežbe. Zato je zaželeno zelo majhno trenje, vendar pa bi bila izdelava stikov z nizkim trenjem lahko zelo draga in verjetno neprimerna za industrijsko proizvodnjo.

Tradicionalni stiki med panelom in konstrukcijo, izdelani z jekleno ploščico, niso mogli prenesti potresnih zahtev sil izven ravnine in pomikov v ravnini za omenjene štiri potresne dogodke. Stiki z jekleno ploščico, ki so na voljo na trgu, imajo omejeno deformacijsko kapaciteto v ravnini, kot tudi omejeno nosilnost izven ravnine (≈ 15 kN). Poleg tega so ti stiki dovzetni za poškodbe v ravnini za potresne dogodke, kar bi lahko znatno zmanjšalo kapaciteto izven ravnine. Nasprotno pa so lahko stiki SismoSafe, tudi če prenašajo sile trenja v ravnini, prenesejo zelo velike pomike v ravnini, kar je odvisno od dolžine fiksnega vodila, znotraj katerega drsi premični kazalec. Kapaciteta odpornosti stikov SismoSafe izven ravnine, ki smo jo ocenili tekom eksperimentov, je znašala približno 45 kN, kar pomeni, da je število stikov, potrebnih za prenos potresnih obtežb izven ravnine, trikrat nižje od števila standardnih stikov. Za nobenega od štirih upoštevanih potresnih dogodkov deformacijska kapaciteta v ravnini, kot tudi kapaciteta odpornosti izven ravnine, ni bila presežena. Poleg tega na drsno obnašanje stikov SismoSafe v ravnini ne vpliva odpornost izven ravnine, zato bi lahko pravilno delovali tudi ob nastopu potresne obtežbe v poljubni smeri.

Potresne obremenitve nekonstrukcijskih elementov izven ravnine se lahko določijo tako, da jih obremenimo z ekvivalentnimi statičnimi silami, ki se izračunajo, na primer, na podlagi

priporočil Evrokoda 8. Spektralne pospeške S_a, ki nam služijo za določevanje sil, navadno določimo z uporabo etažnih spektrov, kot so jih na primer predlagali Medina in sod. (2006) in Sullivan in sod. (2013). Takšno določevanje obremenitev je primerno za horizontalne panele, ki niso v stiku s tlemi, vendar pa se ne more uporabiti za vertikalne panele enoetažnih stavb, saj so tu paneli navadno pritrjeni na tla.

Vertikalni paneli, ki so v stiku s tlemi (pritrjeni na tla), so obremenjeni tako zaradi samega nihanja tal, kot tudi zaradi nihanja konstrukcije, na katero so paneli pritrjeni. Stik med konstrukcijo in panelom za obremenitve v smeri izven ravnine mora prenesti tako obremenitve, ki so posledica vpliva konstrukcije na panel, kot tudi tiste, ki so posledica inercijskih sil samega panela. V disertacijo smo obremenitve na stik določevali s pomočjo poenostavljanega računskega modela, ki sloni na naslednjih predpostavkah:

- Konstrukcijo smo modelirali na poenostavljen način, in sicer z modelom z dvema prostostnima stopnjama,
- Toga diafragma je bila predpostavljena na nivoju etaže,
- Mase panela in konstrukcije smo definirali točkovno, in sicer tako, da njihov vpliv povzroči maksimalne sile in pomike med potresom.

Na podlagi zgoraj omenjenih predpostavk smo nato analitično izvrednotili silo v stiku med konstrukcijo in panelom, ki deluje v smeri izven ravnine F_{real}.

Omenjeni način določevanja sile v stiku se razlikuje od načina, prisotnega v vsakodnevni projektantski praksi, saj projektanti pri določevanju sil v stikih navadno predpostavijo, da sta tako konstrukcija kot tudi stik toga. Na podlagi te predpostavke projektanti nato s pomočjo enostavnega računskega modela (prostoležeči nosilec, pri čemer nosilec predstavlja panel) določijo silo v podpori F_{rigid}, ki se nato uporabi za projektiranje stika. Ker pa so armiranobetonske montažne konstrukcije dejansko precej podajne, vrednost sile F_{rigid} v določenih primer ne predstavlja najboljšega približka dejanski sili v stiku. Zato bi bilo smiselno, da se stike projektira na realnejšo silo, tj. silo F_{real}.

Z namenom definiranja bolj splošnih priporočil za projektiranje stikov na realnejše sile smo izvedli parametrični študijo, ki omogoča, da silo v stiku F_{real}, dobljeno na poenostavljenem modelu, povežemo s silo v stiku F_{rigid}, dobljeno na modelu, v katerem konstrukcijo modeliramo kot neskončno togo. V parametrični študiji smo poskušali zajeti več različnih konfiguracij montažnih stavb. Zato smo variirali dva parametra, in sicer R_M in R_T, ki prestavljata razmerje mas oziroma razmerje nihajnih časov konstrukcije in panela. Rezultate študije smo predstavili v obliki 3D ploskev, kjer prikazujemo razmerje F_{real}/F_{rigid} v odvisnosti od R_T in R_M. Rezultati analize kažejo, da so v primeru, ko je R_T (tj. razmerje nihajnih časov konstrukcije in panela) blizu 1, sile v stiku F_{real} za do faktor 4 večje od sil F_{rigid} (tj. sil, dobljenih z uporabo modela, v katerem konstrukcijo modeliramo kot neskončno togo). Na podlagi dobljenih rezultatov smo tudi predlagali analitično formulacijo za definicijo 3D ploskev, ki se lahko uporabijo kot alternativa etažnim spektrom, predlaganih v Evrokodu 8 (EN 1998-1-1, 2005).

V petem poglavju smo na podlagi spoznanj v zvezi s cikličnim obnašanjem stika panela in konstrukcije prikazali rezultate parametričnih študij, ki smo jih izvedli z namenom preučevanja vpliva tipa stika med panelom in konstrukcijo pri potresnem odzivu armiranobetonskih montažnih stavb. Primerjali smo odziv vpetih panelov in rotirajočih panelov ter iskali prednosti in slabosti obeh načinov pritrjevanja panelov. Iskali smo tudi primere, pri katerih stiki ne zagotavljajo ustrezne potresne odpornosti, in ugotavljali, ali je kritični potresni odziv stikov posledica sil v smeri v ravnini oziroma izven ravnine. Velja tudi omeniti, da smo pri določevanju obremenitev stikov upoštevali različne kombinacije števila stebrov in panelov.

V parametrični študiji smo obravnavali 15 enoetažnih stavb, pri čemer smo variirali višino stebrov (etaže) in maso, ki pripada izbranemu stebru. Uporabili smo tudi tri različne tipe stikov med paneli in konstrukcijo, in sicer stike Standard s kratko jekleno ploščico (tip TA-210), stike Standard z dolgo jekleno ploščico (tip TA-290 in stike SismoSafe. Za analize smo uporabili matematične modele, ki smo jih definirali v prejšnjih poglavjih, pri čemer velja omeniti, da smo model za stika z jekleno ploščico izboljšali na način, ki omogoča sklopljeno simulacijo odziva v smeri v ravnini in v smeri izven ravnine.

Rezultate študije smo prikazali za dva tipa tal (tipa tal A in C po Evrokodu 8) in za naslednje parametre:
v primeru pritrjenih panelov:

d	Pomik stika v ravnini
N	Sila v stiku v smeri izven ravnine
R_h	Prečna sila pri vpetju panela
R_v	Vertikalna sila panela v vpetju

v primeru rotirajočih panelov:

d	Pomik stika v ravnini
d_{vert}	Vertikalni pomik panela
N	Sila v stiku v smeri izven ravnine
R_h	Prečna sila ob vpetju panela

Rezultati parametrične študije kažejo, da razmerje med številom stebrov in številom panelov k_v lahko bistveno vpliva na potresne obremenitve stikov, saj se je izkazalo, da se potresne obremenitve povečujejo z večanjem koeficienta k_v. Tako so lahko obremenitve enoetažnih industrijskih montažnih stavb, ki imajo zaradi samega tlorisa stavb navadno različno razmerje stranic stavbe, v dveh glavnih smereh konstrukcije precej različne. Posledično so tudi sile v stikih precej različne. Vpliv koeficienta k_v je sicer manjši v stavbah z veliko povprečno maso, saj se za te stavbe izkaže, da rezultati potresnega odziva niso pretirano odvisni od razmerja med številom stebrov in panelov (tj. vrednosti parametra k_v). Izkaže se tudi, da se pomik stika linearno povečuje s povečevanjem nihajnega časa konstrukcije T_1, pri čemer velja omeniti, da so bili nihajni časi vseh obravnavanih konstrukcij večji od T_C.

Rezultati analiz za panele, ki so polno vpeti v tla, nadalje kažejo, da je kapaciteta stikov v smislu sile v smeri izven ravnine dosežena pri precej večjih maksimalnih pospeških tal kot v smeri v ravnini. Za stike Standard s kratko jekleno ploščico so se porušitve zaradi sil v smeri v ravnini pojavile pri maksimalnih pospeških tal med 0,35g in 0,10g na tleh tipa A in pri maksimalnih pospeških tal med 0,23g in 0,07g na tleh za tip C. Za stik Standard z dolgo jekleno ploščico smo porušitev stikov v smeri v ravnini zaznali pri maksimalnih pospeških tal med 0,44g in 0,21g za tip tal A in pri maksimalnih pospeških tal med 0,21g in 0,14g za tip tal C. Vrednosti pospeškov so bile odvisne od višine, mase in togosti konstrukcije. Pri stikih tipa SismoSafe porušitve nismo zaznali v nobenem primeru, zato lahko vsaj v teoriji kapaciteto pomika upoštevamo kot neskončno. Dejansko seveda kapaciteta stika ni neskončna zaradi nekaterih omejitev, kot so na primer dolžina fiksne vodilne tirnice oziroma toleranca pri gradnji, ki lahko povzroči nepravilno drsenje premične vodilne tirnice.

Rezultati parametrične študije za panele, ki so polno vpeti v tla, tudi kažejo, da porušitve zaradi obremenitev v smeri izven ravnine za stik tipa SismoSafe, ki ima sicer v primerjavi s stikoma tipa Standard precej večjo kapaciteto v smeri izven ravnine, nismo zaznali v nobenem primeru. Izkaže se tudi, da so maksimalni pospeški tal pri porušitvi zaradi sil, ki delujejo izven ravnine, za stika Standard s kratko (TA-210) in dolgo jekleno ploščico (TA-290) praktično enaki. Ta

rezultat je bil pričakovan, saj so obremenitve na stik v smeri izven ravnine zelo podobne, kapaciteti stikov pa enaki (glej poglavje 4). Naj tudi omenimo, da je bila kapaciteta v smeri izven ravnine dosežena samo za modele, kjer je bila višina stebrov večja od 9m. Čeprav na podlagi odziva sistemov z eno prostostno stopnjo velja, da se pospeški in sile v primeru nihajnih časov, večjih od T_C, zmanjšujejo, je nujno upoštevati tudi dinamično interakcijo med panelom in konstrukcijo, ki je, kot smo pokazali v poglavju 4, odvisna od razmerja nihajnih časov R_T in mas R_M.

V primeru panelov, ki so polno vpeti v tla, je potrebno zagotoviti takšno povezavo (vpetost), ki bo onemogočala rotiranje oz. zibanje in horizontalno drsenje ter posledično bila sposobna prenesti vertikalno dvižno R_v in horizontalno reakcijsko silo R_h. Rezultati analize kažejo, da se horizontalna reakcijska sila tako v primeru stikov tipa Standard kot tudi v primeru sitka tipa SismoSafe povečuje z večanjem višine etaže in mase konstrukcije. Podobno velja za vertikalno reakcijsko silo R_v saj se tudi v tem primeru za vse tipe stikov sila povečuje s večanjem etažne višine in mase konstrukcije. Povečanje sil je neposredna posledica povečanja mase in višine etaže, saj se z njunim večanjem povečuje moment prevrnitve, ki mora biti po drugi strani uravnotežen prav s silama R_v in R_h.

Podobno kot za polno vpete panele so tudi v primeru panelov, ki omogočajo rotiranje, bolj kritične obremenitve v smeri v ravnini. Ugotovili smo, da stiki tipa SismoSafe v smeri v ravnini niso nikoli dosegli svoje kapacitete. Po drugi strani se za stik tipa Standard s kratko jekleno ploščico porušitve zaradi obremenitev v ravnini pojavijo pri maksimalnih pospeških tal med 0,31g in 0,10g za tla tipa A in pri maksimalnih pospeških tal med 0,21g in 0,07g za tla tipa C, za stik tipa Standard z dolgo jekleno ploščico pa pri maksimalnih pospeških tal med 0,38g in 0,16g za tla tipa A ter pri maksimalnih pospeških tal med 0,25g in 0,10g za tla tipa C. Iz prikazanih rezultatov lahko takoj vidimo, da je nosilnost stikov tipa Standard z dolgo jekleno ploščico nekoliko višja kot nosilnost tipa Standard s kratko jekleno ploščico, kar je posledica večje kapacitete stika za pomik v smeri ravnine panelov. Rezultati tudi kažejo, da se v obeh primerih maksimalni pospešek tal pri porušitvi zmanjšuje z večanjem nihajnega časa konstrukcije. Sicer so maksimalni pospeški pri porušitvi v primeru polno vpetih panelov in panelov, ki omogočajo rotiranje, precej podobni, kar je sicer posledica podobnih nihajnih časov konstrukcij. Velja tudi omeniti, da, podobno kot za polno vpete panele, koeficient k_v in povprečna masa, ki odpade na en steber, nekoliko vplivata na vrednosti maksimalnih pospeškov tal pri porušitvi. Iz rezultatov analiz smo tudi razbrali, da se stiki med potresno analizo vseh obravnavanih stavb zaradi rotiranja oz. zibanja panelov precej deformirajo v vertikalni smeri.

Za stik tipa SismoSafe porušitev s smeri izven ravnine nismo nikoli zaznali. Sicer ima ta stik v primerjavi s stikoma tipa Standard precej večjo kapaciteto v smeri izven ravnine. Po drugi strani je bila, podobno kot v primeru polno vpletih panelov, kapaciteta stikov tipa Standard v smeri izven ravnine (v smislu maksimalne sile) dosežena samo za modele, kjer je bila višina stebrov (etaže) večja od 9m. Naj na tem mestu še enkrat ponovimo, da je pri določevanju sil v stiku potrebno upoštevati tudi dinamično interakcijo med panelom in konstrukcijo, ki je, kot smo pokazali v poglavju 4, odvisna od razmerja nihajnih časov R_T in mas R_M.

V primeru vpetih panelov, ki onemogočajo rotiranje oz. zibanje, je potrebno zagotoviti takšno povezavo (vpetost), ki bo onemogočala horizontalno drsenje in bila posledično sposobna prenesti horizontalno R_h reakcijsko silo. Vrednosti reakcijske sile R_h so v primeru panelov, ki omogočajo rotiranje, do 50% manjše kot sile, dobljene v primeru polno vpetih panelov.

Rezultati parametrične študije tudi kažejo, da je disperzija rezultatov za primer panelov, ki omogočajo rotiranje (zibanje) večja kot v primeru polno vpetih panelov. Omenjeni rezultati so posledica manj kontroliranega obnašanja panelov, saj se paneli lahko zibajo pri horizontalnih obremenitvah. Posledično pride tudi do večjega/manjšega relativnega pomika med panelom in konstrukcijo, kar seveda prispeva k večji disperziji rezultatov.

8 Extended abstract (in Italian)

La tesi presenta i risultati di una precedente campagna sperimentale su tavola vibrante di un prototipo di struttura prefabbricata in cemento armato (CA) con pannelli verticali e tipici collegamenti pannello-struttura realizzati con baionette metalliche a testa a martello. Viene presentata la procedura di modellazione numerica, che ha permesso di riprodurre i risultati dei test eseguiti su tavola vibrante.

Successivamente, viene presentato un dispositivo di connessione innovativo per pannelli verticali e una serie di test sperimentali per caratterizzare la risposta meccanica di tal connessione nella cui realizzazione l'autore della tesi è stato attivamente coinvolto. Infine, è stato eseguito uno studio parametrico di tipo numerico per meglio comprendere le forze che causano sollecitazioni fuori piano nelle connessioni dei pannelli verticali. Sulla base dello studio parametrico, le forze che influenzano la connessione sono state stimate in funzione della massa e del periodo oscillazione della struttura, generalizzando così i risultati della ricerca. A seguito di questo studio, sono state proposte indicazioni preliminari da utilizzare nella fase progettuale dei dispositivi di connessione panello-struttura.

Nei primi due capitoli della tesi viene presentato un excursus storico degli edifici prefabbricati in CA e le ultime ricerche scientifiche nel campo della prefabbricazione in CA e dei dispositivi di connessione. Questi due capitoli sono utili per contestualizzare le carenze sismiche di questo tipo di strutture.

Nel terzo capitolo, viene presentata la campagna sperimentale su tavola vibrante, che è stata precedentemente condotta presso UL FGG (Università di Lubiana, Facoltà di Ingegneria Civile e Geodetica) al fine di studiare la risposta sismica di edifici prefabbricati monopiano in CA con pannelli verticali. Successivamente vene illustrato lo sviluppo di un modello numerico con è stato possibile riprodurre in modo affidabile i risultati degli esperimenti citati. Sono state fatte alcune considerazioni sui risultati ottenuti. In particolare, il modello numerico calibrato sui risultati delle prove reali, è stato utilizzato per valutare l'influenza del sigillante siliconico sul comportamento sismico dei pannelli di tamponamento verticali. In questo capitolo viene anche presentato anche uno studio analitico e sperimentale di un dispositivo di connessione pannello-struttura innovativo, che consente la dissipazione di energia per mezzo di un meccanismo ad attrito.

Lo scopo dei test sulla tavola vibrante è stato quello di valutare l'influenza di diversi parametri sulla risposta dinamica di edifici industriali prefabbricati con pannelli tamponamento in cemento armato. In questo studio sono stati esaminati i seguenti parametri:

- orientamento dei pannelli,
- tipo di connessioni tra i pannelli e il sistema strutturale principale (baionette lunghe o corte),
- tipo di collegamento dei pannelli alla fondazione.

Il prototipo strutturale è stato testato con 8 configurazioni diverse. Le prove differivano in base all'orientamento dei pannelli (configurazione orizzontale o verticale), al tipo di collegamenti tra pannello e struttura, al tipo di collegamento tra pannello e fondazione (pannelli fissi o con rocking) e al numero di pannelli (su entrambi i lati o solo su un lato). La struttura principale è stata la stessa per tutte le otto configurazioni. Poiché lo scopo della tesi è quello di caratterizzare la risposta sismica dei pannelli verticali, sono state discusse e commentate solo le prove con pannelli verticali.

I modelli numerici realizzati attraverso il software OpenSees sono stati in grado di replicare i dati sperimentali con una buona approssimazione sia nel caso di pannelli fissi che con rocking. Questo è stato possibile attraverso l'implementazione del modello isterico delle connessioni pannello-struttura. In particolare, il modello per le connessioni a baionetta con testa a martello presentato in un precedente lavoro svolto dall'Università di Lubiana (Zoubek et al., 2016) è stato migliorato introducendo un'adeguata modellazione del comportamento verticale della connessione, in grado di tener conto della loro resistenza e deformazione elastica e plastica in direzione verticale. In questo modo, il modello numerico è stato in grado di simulare correttamente la risposta sperimentale, in termini di spostamenti e accelerazioni, sia della struttura che dei pannelli.

Il modello numerico è stato in grado di approssimare molto bene l'effettiva risposta dei pannelli fissati alla fondazione, mentre l'approssimazione della risposta è stata meno precisa nel caso di pannelli con rocking, soprattutto quando si utilizzavano connessioni a baionetta lunghe. La ragione di ciò è la dipendenza della risposta dei pannelli dalle condizioni al contorno (la tipologia di fissaggio alle fondazioni). La risposta dei pannelli con rocking si è rivelata piuttosto incerta, in quanto influenzata da vari parametri e carenze costruttive non modellabili in dettaglio.

Il modello numerico calibrato è stato utilizzato per studiare l'effetto di un sigillante siliconico tra pannelli con rocking adiacenti. Dai risultati delle analisi numeriche, è emerso che lo spostamento longitudinale dei pannelli con rocking, nel caso in cui si utilizzi il sigillante siliconico, è limitato rispetto allo spostamento dei pannelli senza silicone. Le strisce di silicone installate tra pannelli adiacenti possono avere un effetto benefico nei confronti degli stati limite di esercizio, sebbene contribuiscano ad aumentare la domanda di spostamento nei dispositivi di connessione tra pannello e struttura. Pertanto, negli stati limite di funzionalità, il sigillante siliconico può influenzare le prestazioni sismiche del sistema di pannelli di tamponamento.

Il silicone non è un materiale standard utilizzato nelle costruzioni, quindi le proprietà meccaniche possono variare notevolmente tra i diversi prodotti presenti sul mercato. Inoltre, non è chiaro quali siano gli effetti dell'invecchiamento sul sigillante siliconico, il che contribuisce ad un'ulteriore incertezza delle sue proprietà meccaniche. Inoltre, il silicone non è adatto a sostenere grandi spostamenti tra i pannelli, come quelli che si verificano agli stati limite ultimi.

Secondo le indicazioni fornite da Dal Lago et al., (2017), si raccomanda di trascurare l'effetto del silicone quando ha una possibile conseguenza benefica sulle prestazioni sismiche della struttura. Al contrario, gli effetti del sigillante siliconico tra i pannelli adiacenti devono essere considerati quando non sono a favore di sicurezza, ad esempio quando si valuta la domanda di spostamento delle connessioni

Presso l'Università degli Studi di Firenze, è stata realizzata una campagna sperimentale che ha riguardato sia i collegamenti commerciali in acciaio a testa martello comunemente in uso (di seguito denominati "Standard") che quelli di tipo innovativo (denominati "SismoSafe"). La campagna sperimentale è stata seguita direttamente dall'autore, presso il Laboratorio Prove e Materiali del Dipartimento di Ingegneria Civile e Ambientale dell'Università di Firenze. Il nuovo collegamento "SismoSafe" per pannelli verticali è costituito da due profili canale in acciaio verticali fissati sul pannello prima del getto. All'interno di questi due profili canale sono inserite sue slitte in acciaio che possono scorrere verticalmente alle quali e saldata una guida di scorrimento mobile. La guida mobile viene collegata a una guida fissa, che a sua volta viene assicurata alla trave attraverso due viti autofilettanti.

I test hanno confermato alcune criticità dei dispositivi "Standard" evidenziate anche dai recenti terremoti italiani. I dispositivi "Standard" sono in grado di disaccoppiare gli spostamenti nel piano tra il sistema tamponamento e le struttura, ma hanno una capacità di spostamento piuttosto limitata. I dispositivi "Standard" hanno mostrato un comportamento isteretico fino al collasso, tipicamente dovuto al cedimento flessionale della baionetta, nella parte stretta appena sotto la testa a martello, o al cedimento del profilo canale di ancoraggio installato su travi o colonne e in taluni casi all'espulsione delle viti con testa a martello. Inoltre, i risultati delle prove condotte sui dispositivi "Standard" sono stati confrontati con i risultati ottenuti da una campagna sperimentale condotto presso l'Università di Lubiana sullo stesso tipo di connessione. Il confronto ha evidenziato che le connessioni testate, sia a Firenze che a Lubiana, hanno mostrato la stessa rigidezza ma differenti capacità di spostamento. Ciò può essere dovuto al fatto che le connessioni, sebbene simili, sono realizzate da due produttori diversi.

Le prove sperimentali hanno dimostrato che gli innovativi giunti “SismoSafe” possono sopportare maggiori spostamenti nel piano dei pannelli rispetto ai giunti Standard, grazie alla loro maggiore capacità di deformazione. Questi nuovi dispositivi non hanno mostrato danni significativi nei loro componenti metallici durante tutte le prove, grazie a forze di attrito molto basse. I valori del coefficiente di attrito statico μ_s sono circa 0.45, mentre quelli dinamici μ_d rientrano nell'intervallo 0,32 - 0,35. I giunti "SismoSafe" sono leggermente più costosi ma orientati a favore di una maggiore sicurezza strutturale. Tuttavia, l'aumento dei costi è limitato perché i giunti "SismoSafe" non necessitano di elementi preinstallati sulla trave (con una riduzione anche dei costi di manodopera) e, poiché hanno una maggiore capacità verso i carichi fuori piano rispetto ai giunti tradizionali, è necessario un numero inferiore di dispositivi di fissaggio per ogni pannello.

Nel quarto capitolo, vengono illustrate le indagini sperimentali sul comportamento fuori piano sia delle connessioni “Standard” che dei dispositivi “SismoSafe”. Gli esperimenti sono stati seguiti direttamente dall'autore. I test hanno evidenziato che i dispositivi Standard hanno una resistenza fuori piano inferiore rispetto ai dispositivi SismoSafe. Sul lato del pannello, i dispositivi “Standard” hanno mostrato una resistenza limite tre volte inferiore rispetto ai dispositivi “SismoSafe” sia per carichi ciclici che monotoni. Inoltre, vale la pena sottolineare che la capacità effettiva delle connessioni Standard può ancora più bassa di quella determinata sperimentalmente, in quanto nella realtà possono essere danneggiate dalle forze sismiche che agiscono nel piano del pannello. I dispositivi SismoSafe non vengono danneggiati a causa degli spostamenti nel piano, motivo per cui le previsioni di capacità basate su test fuori piano possono essere ritenute molto più affidabili. È stato proposto un modello ingegneristico per il nuovo dispositivo SismoSafe. Questo modello è stato utilizzato nell'ambiente di programmazione open-source per l'analisi strutturale non lineare OpenSees.

Sono state eseguite una serie di analisi dinamiche non lineari, per stimare le forze fuori al piano nelle connessioni pannello-struttura di tipo SismoSafe, su un caso di studio di un edificio industriale monopiano. Nell'analisi sono stati considerati i quattro terremoti italiani più forti degli ultimi 12 anni. I risultati numerici hanno confermato che i nuovi dispositivi SismoSafe sicurezza alle forze fuori piano per tutti e quattro gli eventi sismici, sia che si consideri o meno la loro forza di attrito nel piano. Le analisi numeriche hanno permesso di evidenziare l'influenza dell'attrito in corrispondenza delle connessioni sulla risposta sismica della struttura. All'aumentare della forza di attrito, aumentano le forze di sollevamento e di taglio (parallelo alla direzione del sisma) alla base dei pannelli, così come le forze fuori piano nelle connessioni pannello-struttura poste in testa ai panelli. Pertanto, un attrito molto basso sarebbe preferibile. Tuttavia, la realizzazione di dispositivi a basso attrito potrebbe essere molto costosa e non conveniente per la produzione industriale.

I collegamenti pannello-struttura di tipo "Standard" realizzati con baionette metalliche con testa a martello non sono state in grado di resistere alla domanda di forza fuori piano e alla domanda di spostamento nel piano piano imposta dai quattro eventi sismici considerati. I dispositivi a baionetta con a martello hanno una limitata capacità di spostamento nel piano, almeno tra quelli disponibili sul mercato e una limitata capacità fuori piano (15 kN). Inoltre, durante un evento sismico, sono suscettibili di danni all'interno del piano, che potrebbero ridurne significativamente la capacità fuori piano. Al contrario, i dispositivi SismoSafe, anche se trasmettono forze di attrito nel piano, possono sostenere spostamenti molto ampi sempre nel piano. Spostamenti che dipendono dalla lunghezza della guida fissa sulla quale scorre il cursore mobile. La capacità di resistenza fuori piano dei dispositivi SismoSafe è di circa 45 kN, come valutato attraverso la campagna sperimentale, quindi il numero di dispositivi necessari per resistere alle azioni sismiche fuori piano è tre volte inferiore rispetto ai collegamenti "Standard". In nessuno dei quattro eventi sismici considerati, la capacità di spostamento nel piano, così come la capacità di resistenza fuori piano, sono mai state superate. Inoltre, la resistenza fuori piano delle connessioni SismoSafe non è influenzata dal comportamento nel piano, per cui potrebbero funzionare correttamente anche in presenza di azioni sismiche comunque inclinate.

La domanda sismica fuori piano di elementi non strutturali può essere determinata applicando ad essi una forza statica equivalente calcolata con la formulazione proposta dall'Eurocodice 8. La valutazione dell'accelerazione spettrale S_a viene solitamente eseguita utilizzando la formulazione degli spettri di piano proposta, ad esempio, da Medina, et al., (2006) e Sullivan, et al., (2013). Tuttavia, se questa formulazione potrebbe essere appropriata per i pannelli orizzontali, che non sono collocati direttamente a terra, non può essere applicata ai pannelli verticali degli edifici degli edifici monopiano. poiché qui i pannelli sono solitamente fissati alla fondazione.

I pannelli verticali che sono a contatto con il suolo (fissati alla fondazione) sono caricati sia dall'azione sismica proveniente dalla fondazione stessa sia dall'azione sismica proveniente della struttura a cui sono fissati i pannelli. Il collegamento tra struttura e pannello, nei riguardi delle azioni fuori piano, deve necessariamente assorbire sia la forza generata dall'interazione struttura-pannello che quella generata dall'azione sismica che sollecita direttamente il pannello. In questo lavoro, la forza fuori piano che sollecita il collegamento pannello-struttura è stata determinata utilizzando un modello computazionale semplificato basato sui seguenti presupposti:

- L'edificio reale è stato schematizzato in un modello semplificato a 2 GDL
- Si è ipotizzato per la copertura un comportamento a diaframma rigido
- Le masse, sia del pannello che della struttura, sono state concentrate nei punti in cui producono il massimo effetto (in termini di forze e spostamenti) durante l'azione sismica.

Risolvendo manualmente il sistema a 2 GDL abbiamo ottenuto la forza fuori piano che agisce sul collegamento pannello-struttura, chiamata F_{real}.

Al fine di definire raccomandazioni generali per la progettazione delle connessioni pannello-struttura nei confronti delle azioni furi piano, è stato eseguito uno studio parametrico che consente di mettere in relazione la forza (fuori piano) nelle connessioni F_{real} ottenuta sul modello semplificato con la forza nelle connessioni F_{rigid} ottenuta su un modello in cui la struttura è modellata come infinitamente rigida. Nello studio parametrico, si è cercato di includere diverse configurazioni differenti di edifici prefabbricati. Di conseguenza sono stati variati due parametri, ovvero R_M e R_T, che rappresentano il rapporto tra la massa della struttura

e quella del panello e il rapporto tra i periodi di vibrazione della struttura e del pannello. I risultati dello studio sono stati presentati sotto forma una superfice 3D, dove viene mostrato il rapporto F_{real} / F_{rigid} in funzione di R_T e R_M. I risultati dell'analisi mostrano che nel caso in cui la R_T (ovvero il rapporto tra i periodi di vibrazione della struttura e del pannello) sia prossimo a 1, le forze di contatto F_{real} sono fino a 4 volte maggiori delle forze F_{rigid} (ovvero le forze ottenute utilizzando il modello in cui la struttura viene modellata come infinitamente rigida). Sulla base dei risultati ottenuti, abbiamo anche proposto una formulazione analitica per la definizione della superfice 3D che può essere utilizzata in alternativa agli spettri di piano proposti nell'Eurocodice 8 (EN 1998-1-1, 2005).

Nel quinto capitolo, sulla base dei risultati relativi al comportamento ciclico del giunto pannello-struttura, presentiamo i risultati di studi parametrici condotti per studiare l'influenza del tipo di contatto pannello-struttura nella risposta sismica di edifici prefabbricati in cemento armato. Abbiamo confrontato la risposta dei pannelli montati e dei pannelli rotanti e abbiamo cercato i vantaggi e gli svantaggi di entrambi i metodi di fissaggio dei pannelli. Abbiamo anche cercato casi in cui i contatti non forniscono un'adeguata resistenza sismica e determinato se la risposta sismica critica dei contatti è dovuta a forze nella direzione nel piano o all'esterno del piano. Vale anche la pena ricordare che nel determinare i carichi di contatto sono state prese in considerazione diverse combinazioni del numero di colonne e pannelli.

Nel quinto capitolo, sulla base dei risultati relativi al comportamento ciclico delle connessioni pannello-struttura, vengono presentati i risultati di studi parametrici condotti con l'obiettivo di studiare l'influenza del tipo di connessione pannello-struttura sulla risposta sismica di edifici prefabbricati in cemento armato. È stata confrontata la risposta dei pannelli fissati alla base e dei pannelli con rocking e sono stato ricercarti gli eventuali vantaggi e svantaggi di entrambe i le configurazioni dei pannelli. Sono stati anche evidenziati casi in cui i le connessioni non forniscono un'adeguata resistenza sismica e è stato determinato se la risposta sismica delle connessioni risulta più critica per azioni nel piano o fuori piano. Vale anche la pena ricordare che nello studio parametrico si è tenuto conto dell'influenza tra il numero di colonne e il numero di pannelli sulla domanda sismica delle connessioni da pannello-struttura.

Nello studio parametrico sono stati considerati 15 edifici monopiano, variando l'altezza dei pilastri, la loro sezione e la massa di competenza del pilastro selezionato. Sono state anche utilizzati tre diversi tipi di connessione pannello-struttura, ovvero connessioni "Standard" con baionetta corta (tipo TA-210), connessioni "Standard" con baionetta lunga (tipo TA-290) e connessioni SismoSafe. I modelli numerici di tali connessioni sono stati definiti nei capitoli precedenti. Vale la pena ricordare però che il modello per le connessioni a baionetta con testa a martello è stato migliorato in modo da consentire una simulazione accoppiata della risposta nel piano e fuori piano.

I risultati dello studio vengono presentati per due tipi di suolo (tipi di suolo A e C secondo l'Eurocodice 8) e per i seguenti parametri:
nel caso di pannelli fissi:

d	Spostamento nel piano della connessione
N	Forza fuori piano della connessione
R_h	Forza di taglio alla base del panello
R_v	Forza di sollevamento del pannello

nel caso di pannelli con rocking:

d	Spostamento nel piano della connessione
d_{vert}	Spostamento verticale della connessione

N Forza fuori piano della connessione
R_b Forza di taglio alla base del panello

I risultati dello studio parametrico mostrano che il rapporto tra il numero di colonne e il numero di pannelli k_n può influenzare in modo significativo i carichi sismici delle connessioni, poiché risulta evidente che i carichi sismici aumentano con l'aumentare del coefficiente k_n. Pertanto, i carichi sismici degli edifici prefabbricati industriali monopiano, che hanno un diverso rapporto di forma dell'edificio k_n a causa delle loro dimensioni in pianta, possono essere abbastanza diversi nelle due principali direzioni di sviluppo dell'edificio stesso. Di conseguenza, anche le forze nelle connessioni sono molto diverse. L'influenza del coefficiente k_n è minore negli edifici con una massa media elevata, in quanto per questi edifici risulta che i risultati della risposta sismica non dipendono eccessivamente dal rapporto tra il numero di colonne e pannelli (ovvero il valore del parametro k_n). Risulta inoltre che lo spostamento delle connessioni aumenta linearmente con l'aumentare del periodo di oscillazione della struttura T_1, vale la pena notare che i periodi di oscillazione di tutte le strutture considerate risultano maggiori di T_C.

I risultati delle analisi per i pannelli incastrati alla base mostrano che la capacità ultima della connessione in termini di forza fuori piano viene raggiunta con accelerazioni massime al suolo (PGA) molto più elevate rispetto alla direzione nel piano. Per connessioni di tipo Standard con baionetta corta, il la rottura dovuta agli spostamenti nel piano si è verificata per accelerazioni massime del terreno comprese tra 0,35 g e 0,10 g sui terreni di tipo A e per accelerazioni massime del terreno tra 0,23 g e 0,07 g sui terreni di tipo C. Per connessioni di tipo Standard con baionetta lunga, la rottura dei dispositivi nel piano piano si è verificata per accelerazioni massime del terreno comprese tra 0,44 g e 0,21 g per il tipo di terreno A e per accelerazioni massime del terreno tra 0,21 g e 0,14 g per il tipo C. I valori delle accelerazioni dipendevano dall'altezza, dalla massa e dalla rigidità della struttura. Nelle connessioni tipo SismoSafe non è stato comunque rilevato alcun danno, quindi almeno in teoria la capacità di spostamento può essere considerata infinita. Ovviamente però, la capacità della connessione non è infinita a causa di alcune limitazioni, come la lunghezza della guida fissa o le tolleranze in fase di montaggio, che possono causare uno scorrimento non corretto della guida mobile.

I risultati dello studio parametrico per i pannelli incastrati alla base a terra hanno mostrato anche che non è stato rilevato alcuna rottura dovuta a carichi in direzione fuori piano per la connessione di tipo SismoSafe, che infatti ha una capacità fuori piano molto superiore rispetto ai contatti di tipo Standard. Risulta inoltre che le PGA che portano alla rottura per forza fuori piano per la connessione Standard con baionetta corta (TA-210) e lunga (TA-290) sono praticamente le stesse. Questo risultato era prevedibile, poiché le forze fuoripiano che agiscono sulla connessione sono molto simili e le capacità fuori piano sono le stesse (vedi Capitolo 4). Va anche notato che la capacità in direzione fuori piano è stata raggiunta solo per i modelli in cui l'altezza delle colonne era la maggiore tra quelle considerate, ovvero 9 m. Sebbene si possa pensare che in strutture con periodo di oscillazione principale più grande di TC le accelerazioni e quindi le forze si riducano all' aumentare del periodo è necessario tenere in conto l'interazione dinamica tra pannello e struttura che, come illustrato nel Capitolo 4, dipende da i rapporti dei periodi di vibrazione R_T e delle masse R_M.

Sempre nel caso di pannelli incastrati alla base, è necessario prevedere alla base un tale collegamento (bloccaggio) che impedisca il rocking e lo scorrimento orizzontale e di conseguenza che sia in grado di sopportare la forza di sollevamento verticale R_v e la forza di taglio orizzontale R_b. I risultati dell'analisi mostrano che la forza di taglio orizzontale aumenta nel caso delle connessioni Standard e SismoSafe con l'aumentare dell'altezza del pannello e

della massa della struttura. Lo stesso vale per la forza di reazione verticale R_v, poiché anche in questo caso, per tutti i tipi di connessione, la forza aumenta con l'aumentare dell'altezza del pannello e della massa della struttura. L'aumento delle forze è conseguenza diretta dell'aumento della massa e dell'altezza del pannello, perché il loro aumento fa aumentare il momento di ribaltante che deve essere bilanciato con dalle forze R_v e R_h.
Analogamente ai pannelli incastrati alla base, nel caso di pannelli con rocking le forze e gli spostamenti nel piano sono più critici. I risultati hanno mostrato che le connessioni di tipo SismoSafe nel piano non hanno mai raggiunto la loro capacità ultima. D'altra parte, le connessioni di tipo Standard con baionette corte, hanno raggiunto la rottura per accelerazioni massime al suolo comprese tra 0,31 g e 0,10 g per il suolo di tipo A e per accelerazioni massime al suolo comprese tra 0,21 g e 0,07 g per il suolo di tipo C. Le connessioni di tipo Standard con baionette lunghe, hanno raggiunto la rottura per accelerazioni massime al suolo comprese tra 0,38 g e 0,16 g per il suolo di tipo A e per accelerazioni massime al suolo comprese tra 0,25 g e 0,10 g per suolo di tipo C.

Dai risultati riportati si può immediatamente vedere che la capacità portante delle connessioni di tipo Standard con baionetta lunga è leggermente superiore alla capacità portante di quelli di tipo Standard con baionetta corta, a causa della maggiore capacità di spostamento nel piano del pannello dei primi. I risultati mostrano anche che in entrambi i casi la PGA di collasso diminuisce con l'aumentare del periodo di vibrazione della struttura. Tuttavia le accelerazioni massime di collasso nel caso di pannelli incastrati alla base e con rocking sono abbastanza simili, ciò è dovuto a periodi di vibrazione simili delle strutture. Va inoltre notato che, analogamente ai pannelli incastrati alla base, il coefficiente k_v e di massa media su ciascuna colonna influenzano leggermente i valori delle accelerazioni massime di collasso della connessione pannello-struttura. Inoltre, le analisi numeriche hanno mostrato che, durante il movimento di rocking dei pannelli, le connessioni a baionetta vengono deformate anche in direzione verticale in tutte le strutture analizzate.

Per le connessioni di tipo SismoSafe, non è mai stata raggiunta la rottura né nel piano né fuori piano. Infatti, questo dispositivo di connessione possiede una capacità, sia nel piano che fuori piano, molto maggiore rispetto alle connessioni di tipo Standard. Anche per in pannelli con rocking, analogamente al caso dei pannelli incastrati alla base, la capacità delle connessioni di tipo Standard in direzione fuori piano (in termini di forza massima) è stata raggiunta solo per nei modelli cui l'altezza delle colonne era la maggiore tra quelle considerate, ovvero 9 m. Si ribadisce che l'interazione dinamica tra il pannello e la struttura deve essere tenuta in considerazione nella determinazione delle forze fuoripiano sulla connessione che, come mostrato nel capitolo 4, dipendono dal rapporto tra i periodi di vibrazione R_T e le masse R_M.

Nel caso di pannelli con rocking, devono essere previsti dispositivi di collegamento alla base in grado di impedire il solo scorrimento orizzontale. Questi dispositivi devono resistere alla sola forza di taglio orizzontale R_h. I valori di R_h sono fino al 50% più bassi rispetto a quelli ottenuti per la configurazione dei pannelli incastrati alla base.

I risultati dello studio parametrico mostrano anche che la dispersione dei risultati per il caso di pannelli che consentono il rocking (pannelli oscillanti) è maggiore rispetto al caso di pannelli incastrati alla base. Questi risultati sono dovuti al comportamento meno controllato dei pannelli con rocking, poiché i pannelli possono oscillare sotto carichi orizzontali attorno ali loro angolo inferiori. Di conseguenza, vi è anche uno spostamento relativo maggiore/minore tra il pannello e la struttura, che ovviamente contribuisce ad una maggiore dispersione dei risultati.

Appendix A

A.1 The stiffness matrix K_{11} term calculation

To find the stiffness matrix of the 2 DOF structure depicted in Figure 4-33, the auxiliary restrains method is used.

Therefore, to compute the K_{11} term of the stiffness matrix, the degree of freedom corresponding to the panel mass M_{panel} was restrained as shown in Figure A-1:

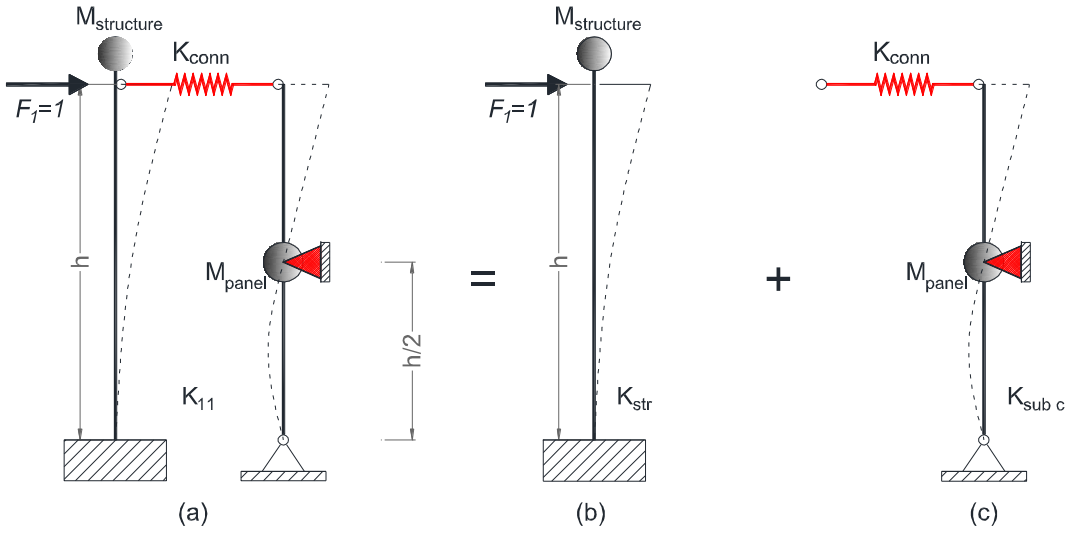

Figure A-1: Auxiliary restrain for K_{11} calculation

The stiffness of structure (a) K_{11} is the sum of the sub-structure (b) stiffness, K_{str}, and the stiffness of the sub-structure (c) $K_{sub\ c}$:

$$K_{11} = K_{str} + K_{sub\ c} \tag{A-1}$$

The stiffness of the sub-structure (b) is easy to calculate since the column act like a cantilever beam, so is possible to set:

$$K_{str} = \frac{3EJ_{column}}{h^3} \tag{A-2}$$

The stiffness of the sub-structure (c) is composed of the out-of-plane stiffness of the connection K_{conn} and the stiffness of the substructure (d) $K_{sub\ d}$, as shown in Figure A-2:

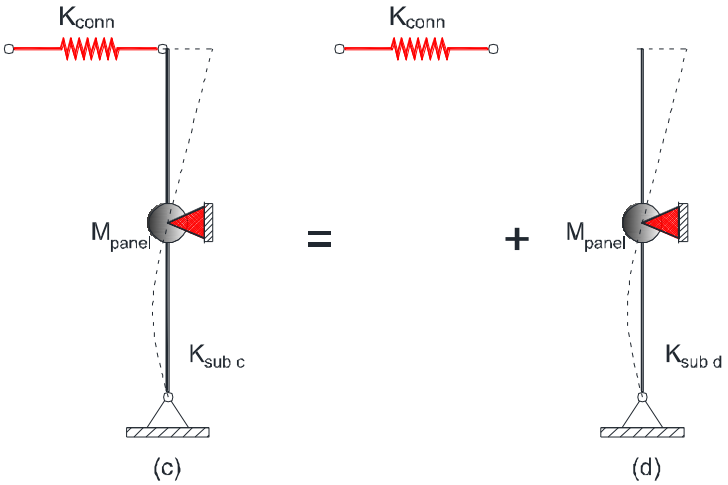

Figure A-2: Stiffness of the sub-structure (c)

The two stiffnesses K_{conn} and $K_{sub\ d}$ acting in series, therefore:

$$K_{sub\ c} = \frac{1}{\frac{1}{K_{conn}} + \frac{1}{K_{sub\ d}}} \tag{A-3}$$

The connection out-of-plane stiffness K_{conn} is a characteristic quantity of the connection devices and has to be provided by the manufacturer or calculated through experimental tests such as those described in section 4.1
Now the translation stiffness of sub-structure (d) $K_{sub\ d}$ has to be calculated. First of all, a force F is applied in correspondence of the point C and the sub-structure moment diagram is calculated:

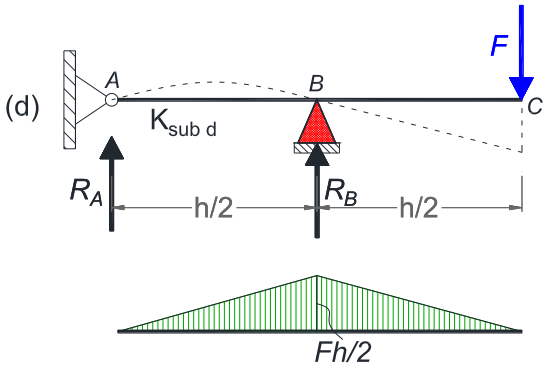

Figure A-3: Sub-structure (d) solution

By imposing the translation equilibrium is possible to write:

$$R_A + R_B - F = 0 \tag{A-4}$$

And then imposing the rotation equilibrium around point A is possible to write:

$$R_B \frac{h}{2} - Fh = 0 \tag{A-5}$$

With the introduction of the equation (A-5) into equation (A-4) the reaction values R_A and R_B are calculated:

$$\begin{aligned} R_B &= 2F \\ R_A &= -F \end{aligned} \tag{A-6}$$

With the two reaction value, the moment diagram can be carried out (Figure A-3).
By the application of virtual work principle, the sub-structure (d) can be divided into a system of real consistent displacements "System 0" and a system of equilibrated virtual forces "System 1" (Figure A-4).

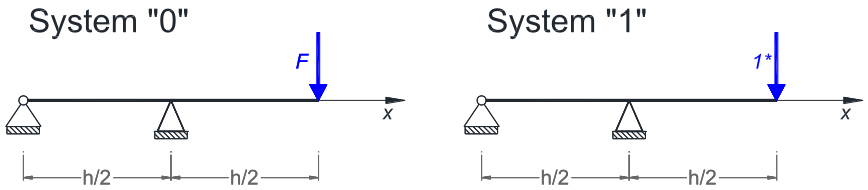

Figure A-4: System 0 and System 1 for virtual work principle application

The equivalence of external and internal work can be written as:

$$W_e = W_i \tag{A-7}$$

$$1^* \cdot \delta = 2 \cdot \int_0^{h/2} \frac{Fx \cdot 1^* x}{EJ} dx \tag{A-8}$$

where 1* is the unitary force applied on "System 1".

By solving the integral relation (A-8), the displacement of the C point when a force F is applied is so calculated:

$$\delta = \frac{Fh^3}{12 \cdot EJ} \tag{A-9}$$

It is now possible to evaluate the sub-structure (d) translation stiffness K_{sub} d by remembering that $K = F/\delta$ and imposing $F = 1$:

$$K_{sub\ d} = \frac{12 \cdot EJ_{panel}}{h^3} \tag{A-10}$$

Therefore, the K_{11} term of the stiffness matrix can be calculated. Recalling equations (A-1) and (A-3) it is possible to write:

$$K_{11} = K_{str} + \frac{1}{\frac{1}{K_{conn}} + \frac{1}{K_{sub\ d}}} \tag{A-11}$$

Introducing the equations (A-2) and (A-10) into (A-11), K_{11} can be definitively calculated:

$$K_{11} = \frac{3EJ_{column}}{h^3} + \frac{12EJ_{panel} \cdot K_{conn}}{12EJ_{panel} + K_{conn} \cdot h^3} \tag{A-12}$$

A.2 The stiffness matrix K_{22} and K_{21} terms calculation

According to the auxiliary restrains method, to compute the K_{22} term of the stiffness matrix, the degree of freedom corresponding to the structure mass $M_{structure}$ was restrained as shown in Figure A-1:

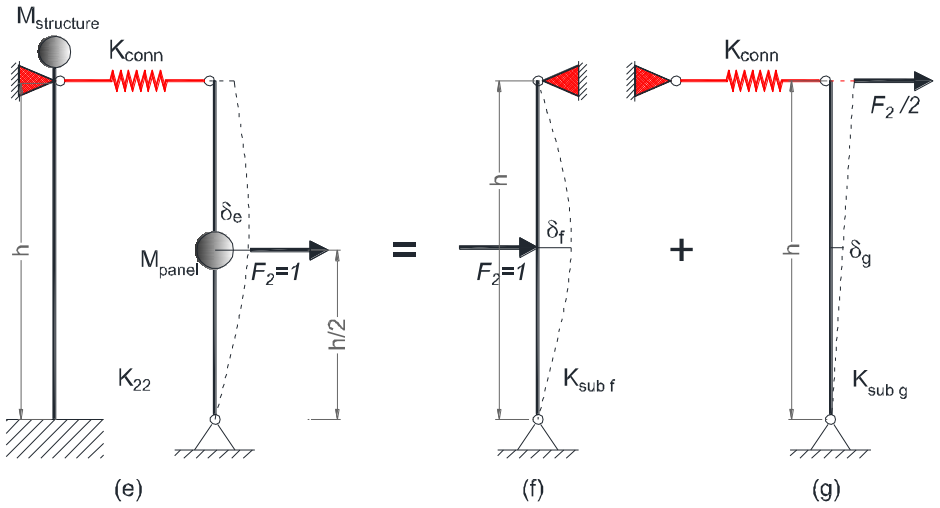

Figure A-5: Auxiliary restrain for K_{22} calculation

The stiffness of structure (e) K_{22} is the sum of the sub-structure (f) stiffness, $K_{sub\,f}$, and the stiffness of the sub-structure (g) $K_{sub\,g}$ that act in parallel:

$$K_{22} = K_{sub\,f} + K_{sub\,g} \tag{A-13}$$

The stiffness of the sub-structure (f) is the translational stiffness of a simply supported beam with a unitary force F_2 applied at mid-span, therefore:

$$K_{sub\,f} = \frac{48EJ_{panel}}{h^3} \tag{A-14}$$

The stiffness of the sub-structure (g) is the reciprocal of the displacement δ_g imposed by the force $F_2/2$ at mid-span of the panel, hence:

$$K_{sub\,g} = \frac{2}{F_2} \cdot \frac{2}{1} \cdot \frac{K_{conn}}{1} \tag{A-15}$$

since F_2=1, then:

$$K_{sub\,g} = 4 \cdot K_{conn} \tag{A-16}$$

Introducing the equations (A-14) and (A-16) into (A-13), K_{22} can be definitively calculated:

$$K_{22} = \frac{48EJ_{panel} \cdot K_{conn}}{K_{conn}h^3 + 12EJ_{panel}} \tag{A-17}$$

Since the force applied at the top of sub-structure (g) is $F_2/2$ then the K21 term is simply:

$$K_{21} = \frac{K_{22}}{2} \tag{A-18}$$

Therefore, the stiffens matrix of the structure is:

$$\boldsymbol{K} = \begin{bmatrix} \frac{3EJ_{column}}{h^3} + \frac{12EJ_{panel} \cdot K_{conn}}{12EJ_{panel} + K_{conn} \cdot h^3} & \frac{K_{22}}{2} \\ \frac{K_{22}}{2} & \frac{48EJ_{panel} \cdot K_{conn}}{K_{conn}h^3 + 12EJ_{panel}} \end{bmatrix} \tag{A-19}$$

A.3 The solution of equation of motion

Assuming the structure does not experience damage as well as the connection devices so it can be hypothesised $K_{conn} = \infty$. In this way the stiffness matrix became:

$$\boldsymbol{K} = \begin{bmatrix} \frac{3EJ_{col\_e}}{h^3} + \frac{12EJ_{pan\_e}}{h^3} & \frac{24EJ_{pan\_e}}{h^3} \\ \frac{24EJ_{pan\_e}}{h^3} & \frac{48EJ_{pan\_e}}{h^3} \end{bmatrix} \tag{A-20}$$

Naming $M_{structure}$ as the whole structure's mass and $M_{panel\ as}$ the whole panels mass the differential equation of motion can be written:

$$\boldsymbol{M}\{\ddot{x}\} + \boldsymbol{C}\{\dot{x}\} + \boldsymbol{K}\{x\} = \boldsymbol{M} \cdot \{a_g\} \tag{A-21}$$

If a simple cosinusoidal acceleration, with amplitude A, angular velocity Ω and phase φ, is applied at the base the undamped structural system, equation of motion become:

$$\begin{bmatrix} M_{structure} & 0 \\ 0 & M_{panel} \end{bmatrix} \begin{bmatrix} \ddot{x}_1 \\ \ddot{x}_2 \end{bmatrix} + \begin{bmatrix} K_{11} & K_{12} \\ K_{21} & K_{22} \end{bmatrix} \begin{bmatrix} x_1 \\ x_2 \end{bmatrix} = \begin{bmatrix} M_{structure} \\ M_{panel} \end{bmatrix} \cdot A \cdot \cos(\Omega t + \varphi) \tag{A-22}$$

Associated homogeneous equation solution

The associated homogeneous equation to the general equation (A-22) is:

$$\begin{bmatrix} M_{structure} & 0 \\ 0 & M_{panel} \end{bmatrix} \begin{bmatrix} \ddot{x}_1 \\ \ddot{x}_2 \end{bmatrix} + \begin{bmatrix} K_{11} & K_{12} \\ K_{21} & K_{22} \end{bmatrix} \begin{bmatrix} x_1 \\ x_2 \end{bmatrix} = \begin{bmatrix} 0 \\ 0 \end{bmatrix} \tag{A-23}$$

If such a solution is assumed (Viola, 2001):

$$\begin{aligned} x_1 &= U_1 \cdot \cos(\omega t - \varphi) \\ x_2 &= U_2 \cdot \cos(\omega t - \varphi) \end{aligned} \tag{A-24}$$

Then is possible to write:

$$\begin{aligned} \ddot{x}_1 &= -\omega^2 U_1 \cdot \cos(\omega t - \varphi) \\ \ddot{x}_2 &= -\omega^2 U_2 \cdot \cos(\omega t - \varphi) \end{aligned} \tag{A-25}$$

Substituting the (A-24) and (A-25) into the (A-23), it is obtained:

$$\left(-\omega^2 \begin{bmatrix} M_{structure} & 0 \\ 0 & M_{panel} \end{bmatrix} + \begin{bmatrix} K_{11} & K_{12} \\ K_{21} & K_{22} \end{bmatrix}\right) \cdot \begin{bmatrix} U_1 \\ U_2 \end{bmatrix} = \begin{bmatrix} 0 \\ 0 \end{bmatrix} \tag{A-26}$$

The (A-26) is an eigenvectors problem, the homogeneous linear system admits a non-zero solution, when its determinant is imposed equal to zero:

$$\det\left(-\omega^2 \begin{bmatrix} M_{structure} & 0 \\ 0 & M_{panel} \end{bmatrix} + \begin{bmatrix} K_{11} & K_{12} \\ K_{21} & K_{22} \end{bmatrix}\right) = 0 \tag{A-27}$$

Therefore, the ω^2_i eigenvalues are:

$$\omega^2_{1,2} = \frac{1}{2}\left\{\frac{M_s K_{22} + M_p K_{11}}{M_s M_p}\right\} \mp \frac{1}{2}\left[\left\{\frac{M_s K_{22} + M_p K_{11}}{M_s M_p}\right\}^2 - 4\left\{\frac{K_{11}K_{22} + K_{12}^2}{M_s M_p}\right\}\right]^{\frac{1}{2}} \tag{A-28}$$

Where the subscript *s* stands for structure and *p* for panel, to lighten notation.
The eigenvalues ω^2_i and associated eigenvectors U_i are found, such that:

$$\boldsymbol{U} = \begin{bmatrix} U_{11} & U_{12} \\ U_{21} & U_{22} \end{bmatrix} \tag{A-29}$$

is the matrix of the two eigenvectors, and it is possible to set:

$$r_1 = \frac{U_{21}}{U_{11}} \quad \text{and} \quad r_2 = \frac{U_{22}}{U_{12}} \tag{A-30}$$

the solution of the system (A-23) is a superposition of the natural vibration modes which are the solution of the equation of motion:

$$\begin{aligned} x_1^{hom}(t) &= U_{11}\cos(\omega_1 t - \varphi_1) + U_{12}\cos(\omega_2 t - \varphi_2) \\ x_2^{hom}(t) &= r_1 U_{11}\cos(\omega_1 t - \varphi_1) + r_2 U_{12}\cos(\omega_2 t - \varphi_2) \end{aligned} \tag{A-31}$$

Recalling the formula:

$$\cos(\omega_i t + \varphi_i) = \cos\omega_i t \cos\varphi_i + \sin\omega_i t \sin\varphi_i \tag{A-32}$$

It is possible to define:

$$\begin{aligned} A_1 &= U_{11}\cos\varphi_1 \quad B_1 = U_{11}\sin\varphi_1 \\ A_2 &= U_{12}\cos\varphi_2 \quad B_2 = U_{12}\sin\varphi_2 \end{aligned} \tag{A-33}$$

By substituting the (A-33) into the (A-31) the homogeneous solution became:

$$\begin{aligned} x_1^{hom}(t) &= A_1\cos\omega_1 t + B_1\sin\omega_1 t + A_2\cos\omega_2 t + B_2\sin\omega_2 t \\ x_2^{hom}(t) &= r_1 A_1\cos\omega_1 t + r_1 B_1\sin\omega_1 t + r_2 A_2\cos\omega_2 t + r_2 B_2\sin\omega_2 t \end{aligned} \tag{A-34}$$

Particular solution

A particular solution is searched for, with the expression:

$$\begin{aligned} x_1^p(t) &= C_1\cos(\Omega t + \phi) \\ x_2^p(t) &= C_2\cos(\Omega t + \phi) \end{aligned} \tag{A-35}$$

Therefore:

$$\begin{aligned} x_1^p(t) &= \begin{bmatrix} x_1^p \\ x_2^p \end{bmatrix} = \begin{bmatrix} C_1 \\ C_2 \end{bmatrix}\cos\Omega t \\ \ddot{x}_1^p(t) &= \begin{bmatrix} x_1^p \\ x_2^p \end{bmatrix} = -\Omega^2\begin{bmatrix} C_1 \\ C_2 \end{bmatrix}\cos\Omega t \end{aligned} \tag{A-36}$$

If the (A-36) is replaced into the general equation (A-22), it is obtained:

$$\begin{bmatrix} K_{11} - \Omega^2 M_s & K_{12} \\ K_{21} & K_{22} - \Omega^2 M_p \end{bmatrix} \cdot \begin{bmatrix} C_1 \\ C_2 \end{bmatrix} = \begin{bmatrix} M_s \\ M_p \end{bmatrix} \cdot A \tag{A-37}$$

By solving the system (A-37), by Cramer method, the two amplitudes of the particular solution C_1 and C_2 are obtained:

$$\begin{aligned} C_1 &= \frac{\left(K_{22} - \Omega^2 M_p\right)M_s A - K_{12}M_p A}{\left(K_{11} - \Omega^2 M_s\right)\left(K_{22} - \Omega^2 M_p\right) - K_{21}K_{12}} \\ C_2 &= \frac{\left(K_{11} - \Omega^2 M_s\right)M_p A - K_{21}M_s A}{\left(K_{11} - \Omega^2 M_s\right)\left(K_{22} - \Omega^2 M_p\right) - K_{21}K_{12}} \end{aligned} \tag{A-38}$$

The general solution of the motion equation (A-22) is the sum of the associated homogeneous solution (A-34) and the particular solution (A-35), therefore:

$$\begin{aligned} x_1(t) &= A_1 \cos\omega_1 t + B_1 \sin\omega_1 t + A_2 \cos\omega_2 t + B_2 \sin\omega_2 t + C_1 \cos(\Omega t + \phi) \\ x_2(t) &= r_1 A_1 \cos\omega_1 t + r_1 B_1 \sin\omega_1 t + r_2 A_2 \cos\omega_2 t + r_2 B_2 \sin\omega_2 t + C_2 \cos(\Omega t + \phi) \end{aligned} \quad \text{(A-39)}$$

by deriving, is obtained:

$$\begin{aligned} \dot{x}_1(t) &= -\omega_1 A_1 \sin\omega_1 t + \omega_1 B_1 \cos\omega_1 t - \omega_2 A_2 \sin\omega_2 t + \omega_2 B_2 \cos\omega_2 t \\ &\quad - \Omega C_1 \sin(\Omega t + \phi) \\ \dot{x}_2(t) &= -\omega_1 r_1 A_1 \sin\omega_1 t + \omega_1 r_1 B_1 \cos\omega_1 t - \omega_2 r_2 A_2 \sin\omega_2 t + \omega_2 r_2 B_2 \cos\omega_2 t \\ &\quad - \Omega C_2 \sin(\Omega t + \phi) \end{aligned} \quad \text{(A-40)}$$

imposing the following boundary condition:

$$\begin{aligned} u_1(0) = 0; \quad u_2(0) = 0 &\implies \text{initially undeformed structure} \\ \dot{u}_1(0) = 0; \quad \dot{u}_2(0) = 0 &\implies \text{starting with zero velocity} \end{aligned} \quad \text{(A-41)}$$

It is possible to write the system:

$$\begin{bmatrix} 1 & 1 & 0 & 0 \\ r_1 & r_2 & 0 & 0 \\ 0 & 0 & \omega_1 & \omega_2 \\ 0 & 0 & r_1\omega_1 & r_2\omega_2 \end{bmatrix} \begin{bmatrix} A_1 \\ A_2 \\ B_1 \\ B_2 \end{bmatrix} = \begin{bmatrix} -C_1 \cos\phi \\ -C_2 \cos\phi \\ \Omega C_1 \sin\phi \\ \Omega C_2 \sin\phi \end{bmatrix} \quad \text{(A-42)}$$

The system (A-42) can be solved using, for example, the Gauss-Jordan method, and the quantities are computed:

$$\begin{aligned} A_1 &= \frac{C_2 - C_1 r_2}{r_2 - r_1} \cos\phi \quad B_1 = \left(\frac{C_1 r_2 - C_2}{r_2 - r_1}\right) \frac{\Omega}{\omega_1} \sin\phi \\ A_2 &= \frac{C_1 r_1 - C_2}{r_2 - r_1} \cos\phi \quad B_1 = \left(\frac{C_2 - C_1 r_1}{r_2 - r_1}\right) \frac{\Omega}{\omega_2} \sin\phi \end{aligned} \quad \text{(A-43)}$$

By substituting (A-43) the into the general solution (A-39) and with the position (A-38) for C1 and C2, the final solution of the motion equation for the 2-DOF system can be written:

$$\begin{aligned} x_1(t) &= \frac{r_1 C_1 - C_2}{r_1 - r_2} cos\omega_1 t + \frac{C_2 - C_1 r_1}{r_1 - r_2} cos\omega_2 t + C_1 cos\Omega t \\ x_2(t) &= r_1 \frac{r_1 C_1 - C_2}{r_1 - r_2} cos\omega_1 t + r_2 \frac{C_2 - C_1 r_1}{r_1 - r_2} cos\omega_2 t + C_2 cos\Omega t \end{aligned} \quad \text{(A-44)}$$

Appendix B

B.1 Result for fixes panels

Connection: hammer-head strap TA-210

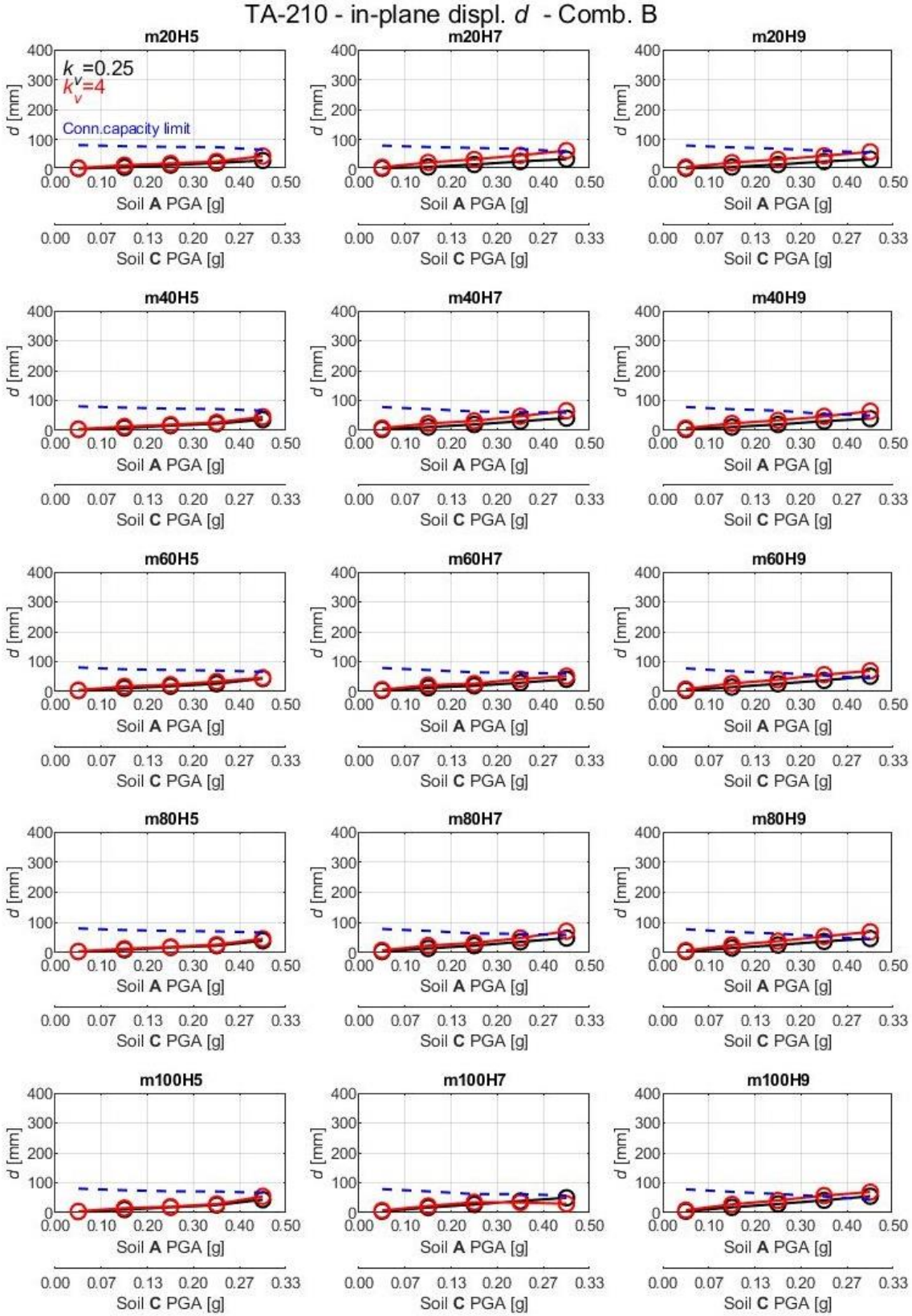

Figure B-1: Seismic demand and capacity comparison in term of in-plane displacement *d* for hammer-head strap connection TA-210 in the case of fixed panels and seismic combination B.

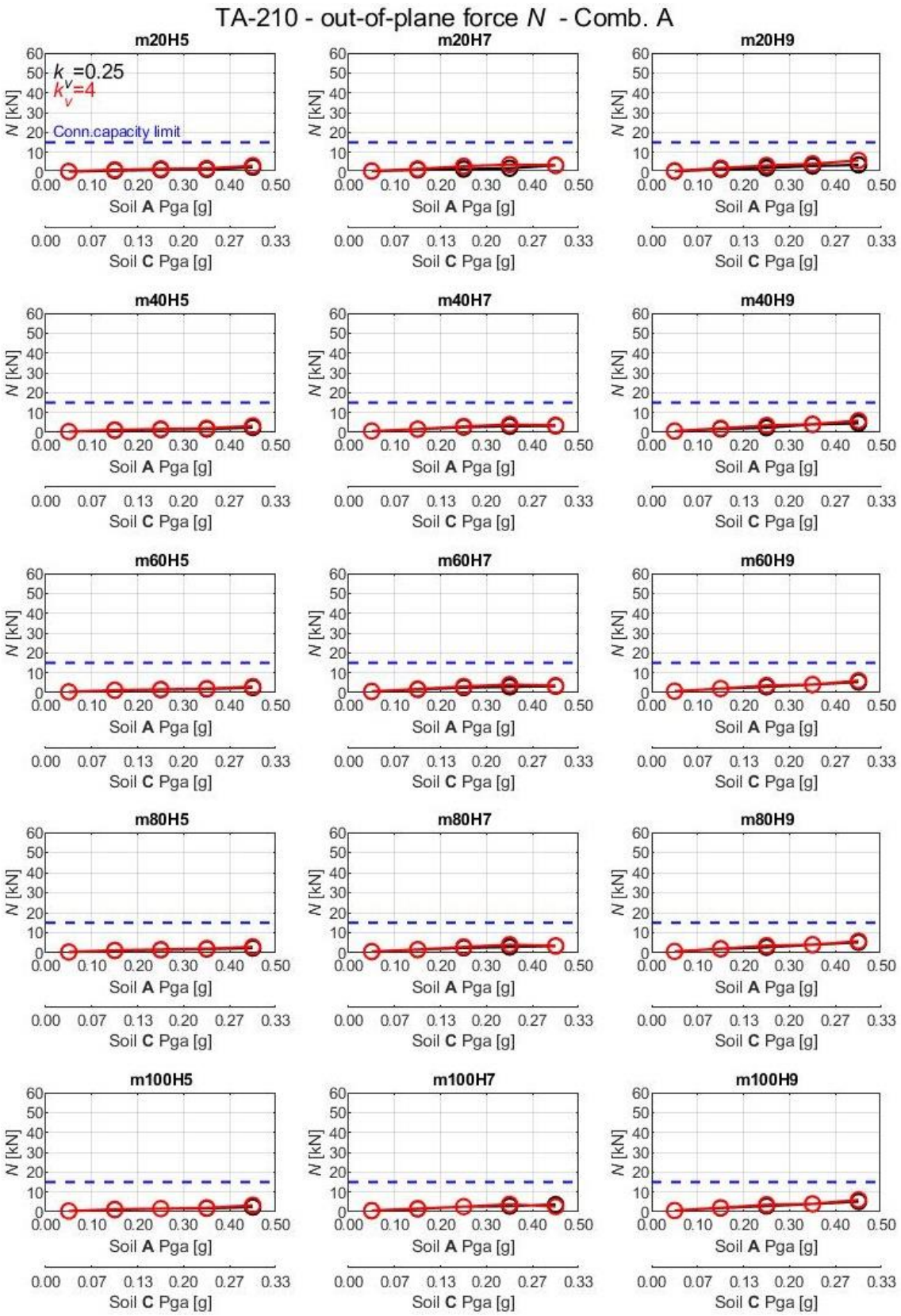

Figure B-2: Seismic demand and capacity comparison in term of out-of-plane force *N* for hammer-head strap connection TA-210 in the case of fixed panels and seismic combination A.

.

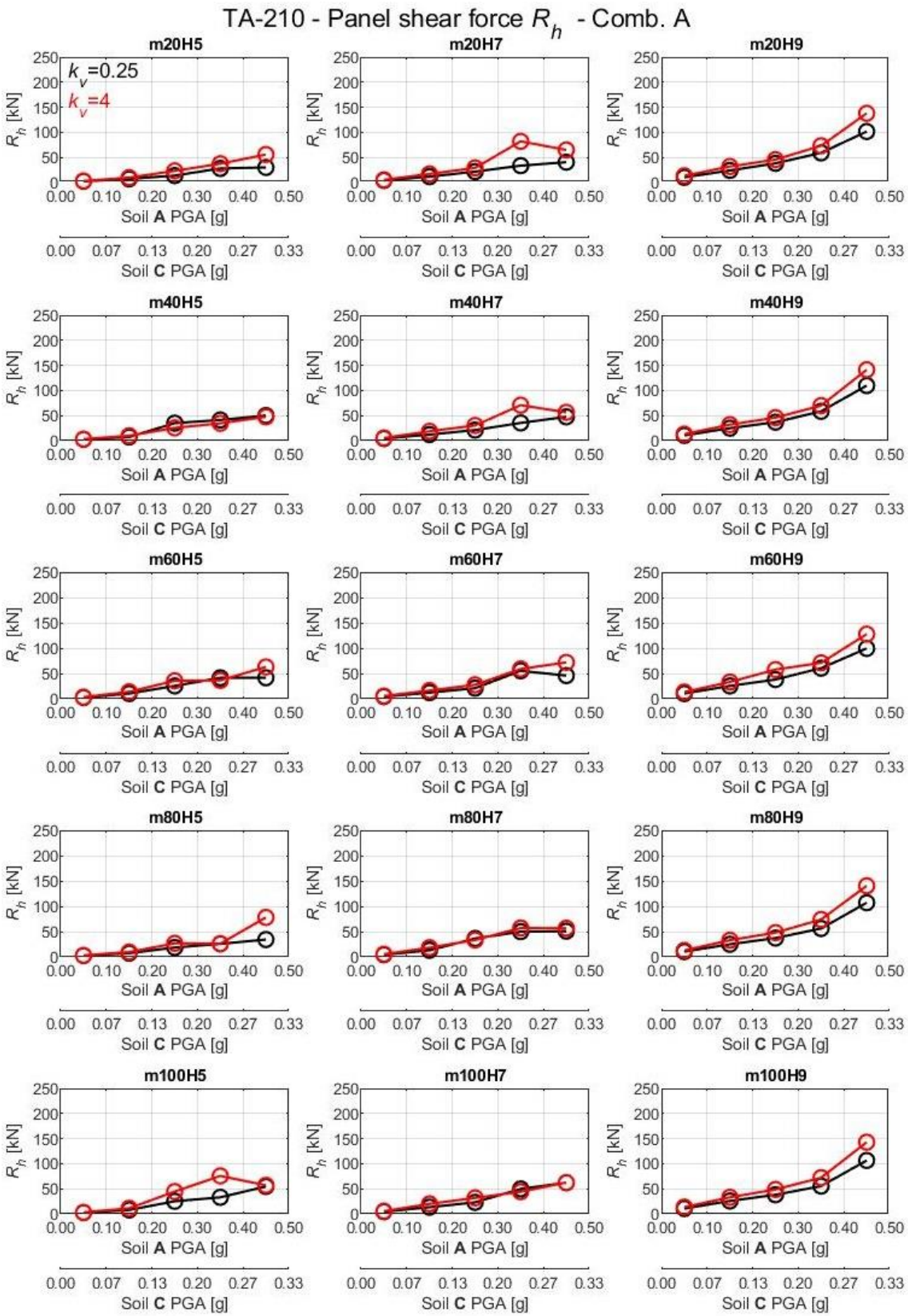

Figure B-3: Seismic demand in term of shear force R_h at the base of the panel for hammer-head strap connection TA-210 in the case of fixed panels and seismic combination A.

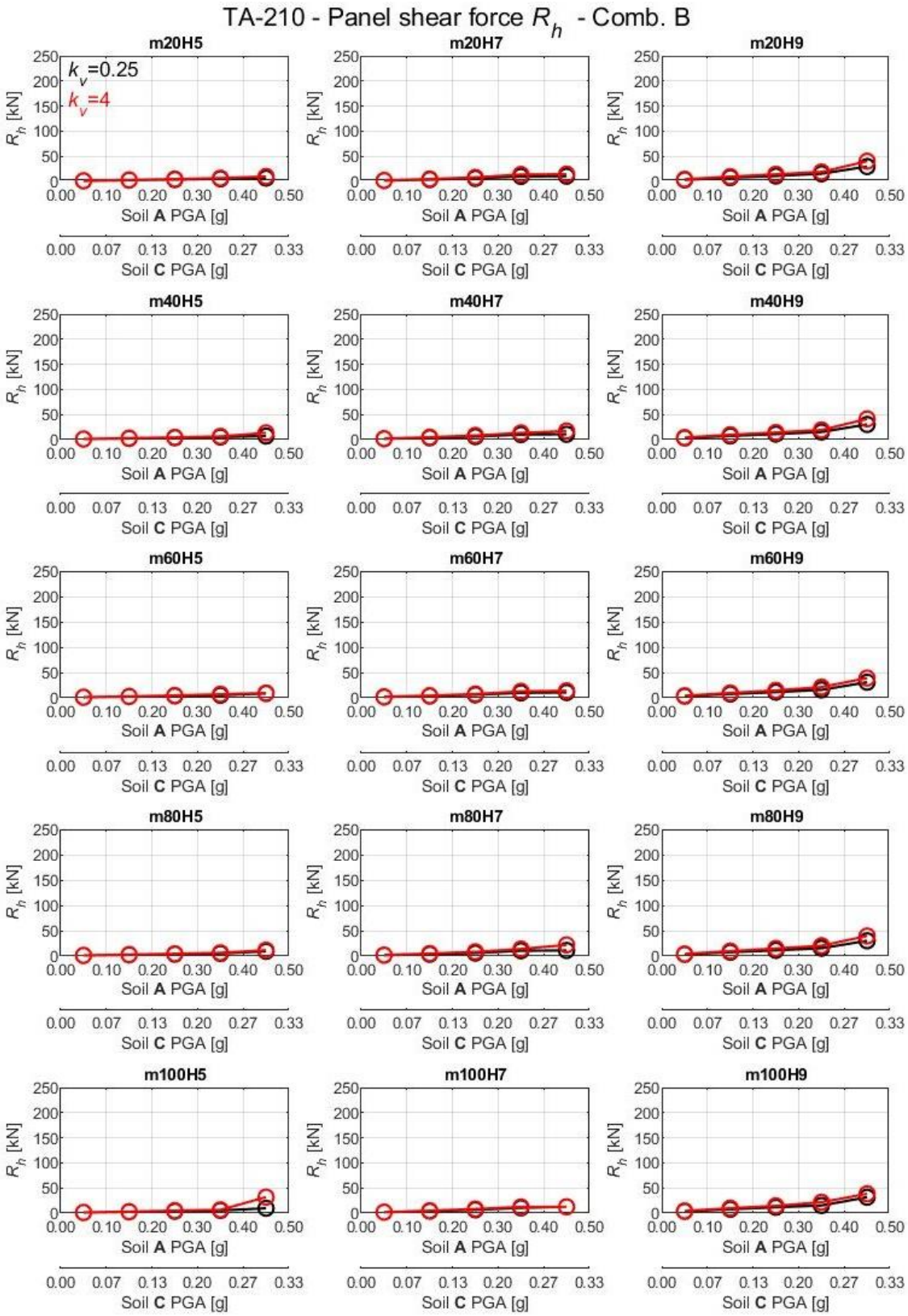

Figure B-4: Seismic demand in term of shear force R_h at the base of the panel for hammer-head strap connection TA-210 in the case of fixed panels and seismic combination B.

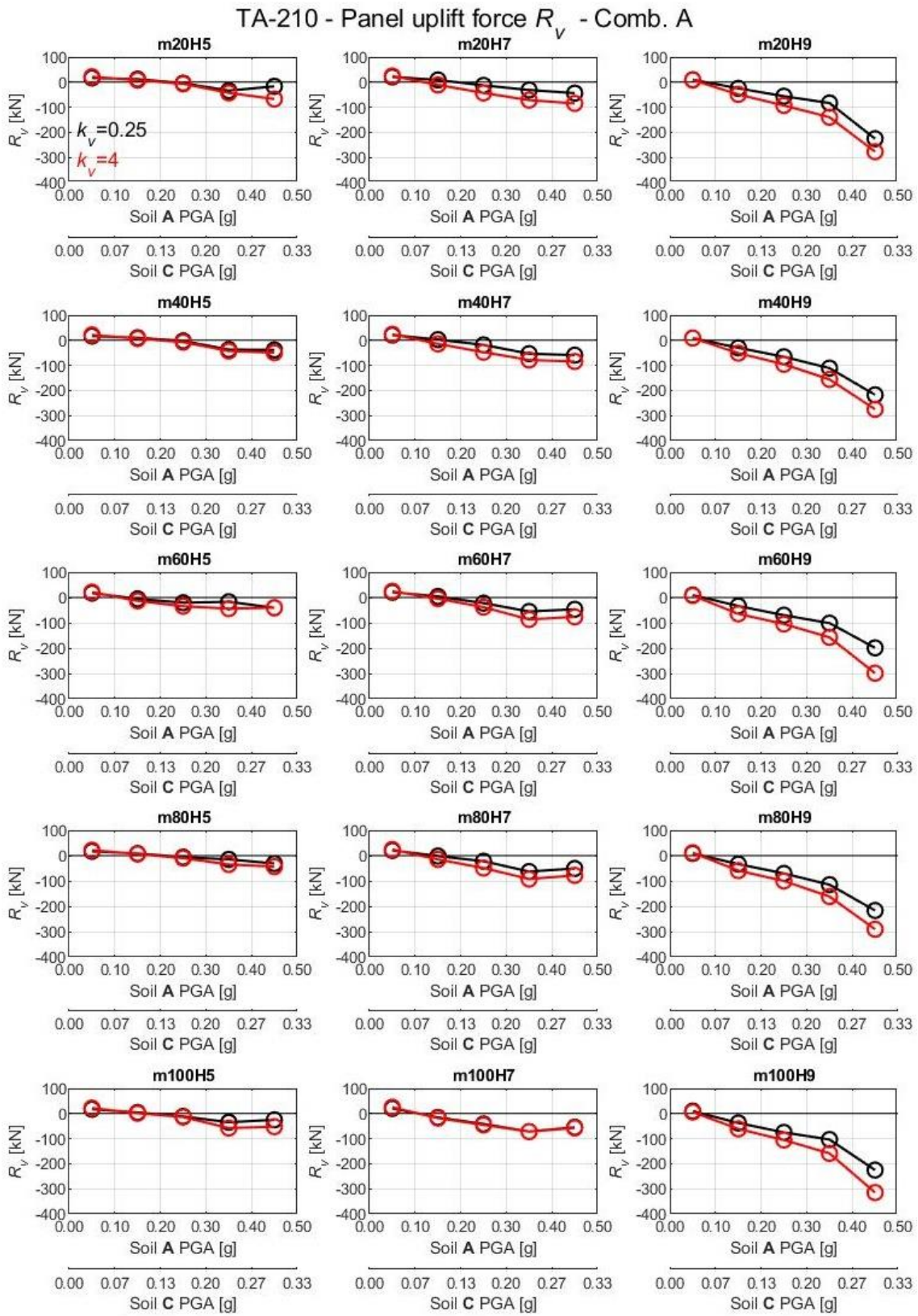

Figure B-5: Seismic demand in panel uplift force R_v for hammer-head strap connection TA-210 in the case of fixed panels and seismic combination A.

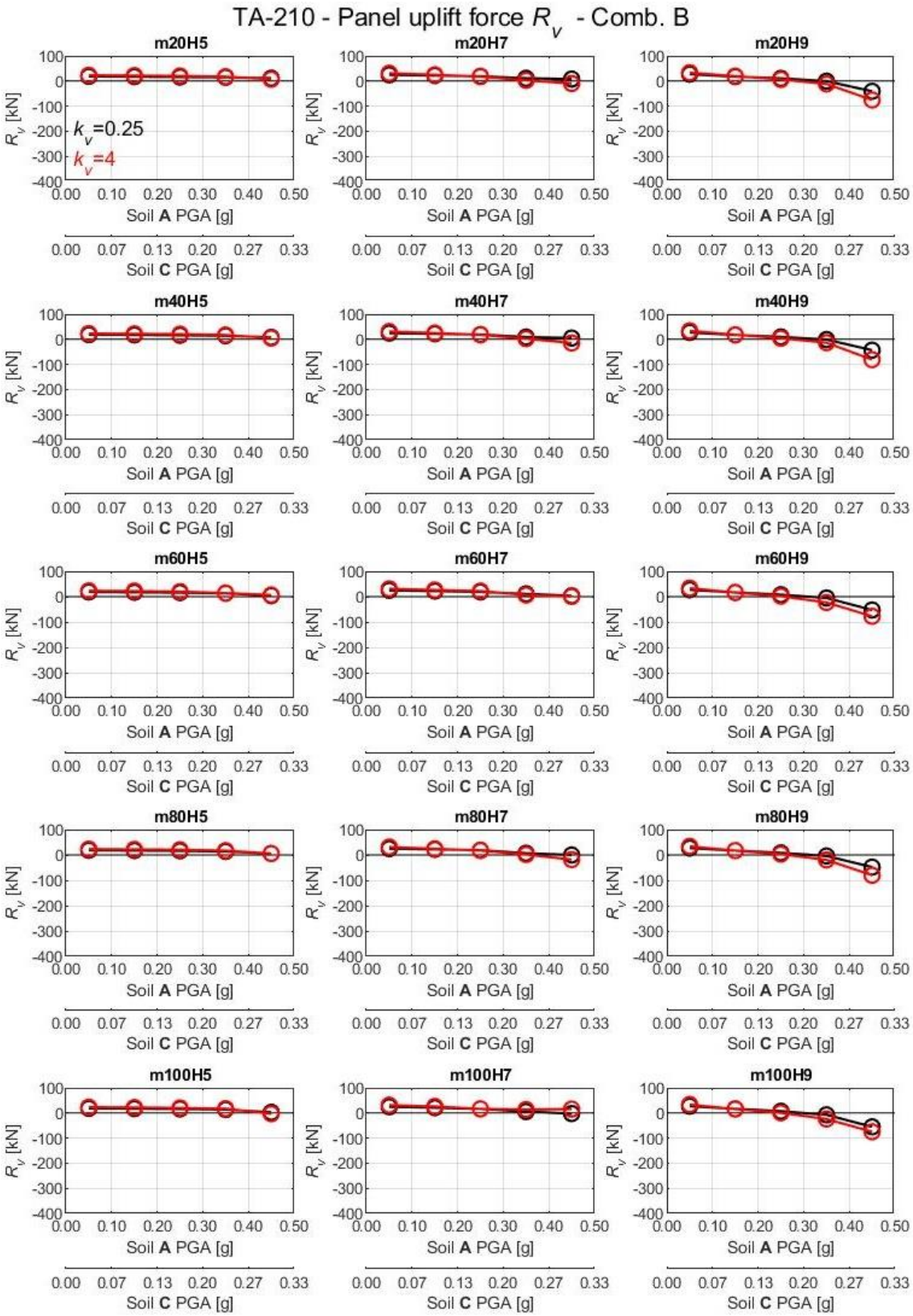

Figure B-6: Seismic demand in panel uplift force R_v for hammer-head strap connection TA-210 in the case of fixed panels and seismic combination B.

Connection: hammer-head strap TA-290

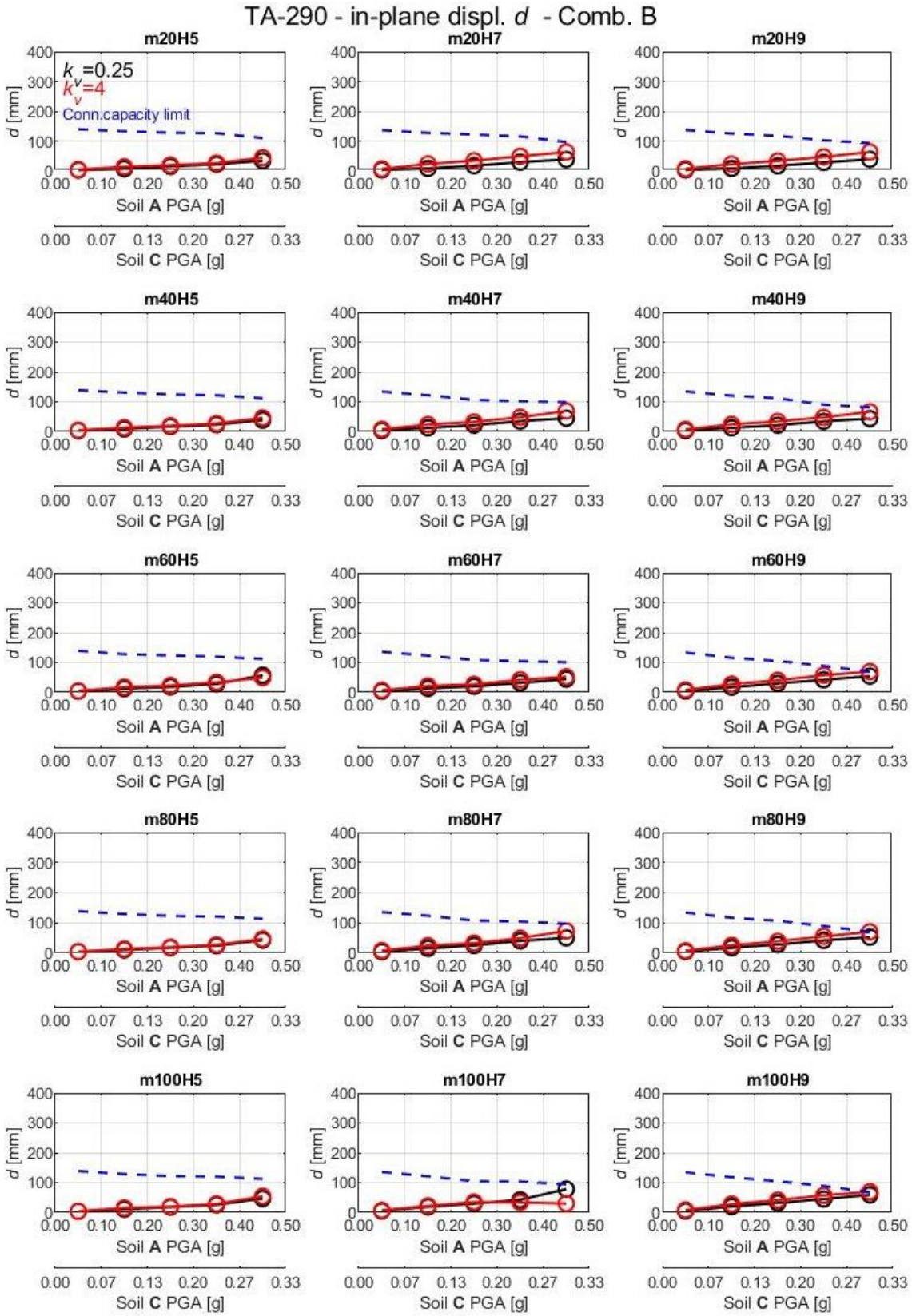

Figure B-7: Seismic demand and capacity comparison in term of in-plane displacement *d* for hammer-head strap connection TA-290 in the case of fixed panels and seismic combination B.

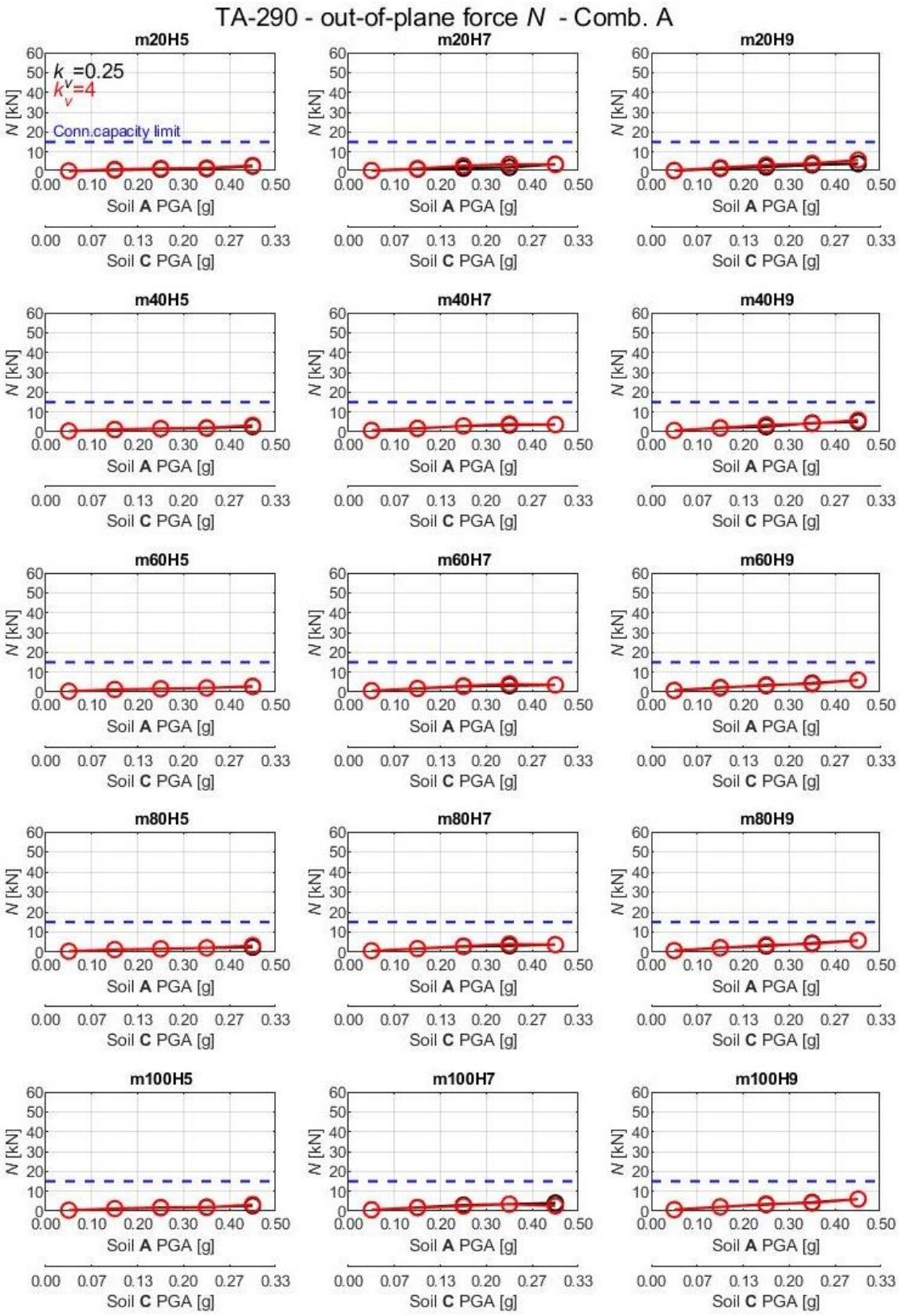

Figure B-8: Seismic demand and capacity comparison in term of out-of-plane force *N* for hammer-head strap connection TA-290 in the case of fixed panels and seismic combination A.

.

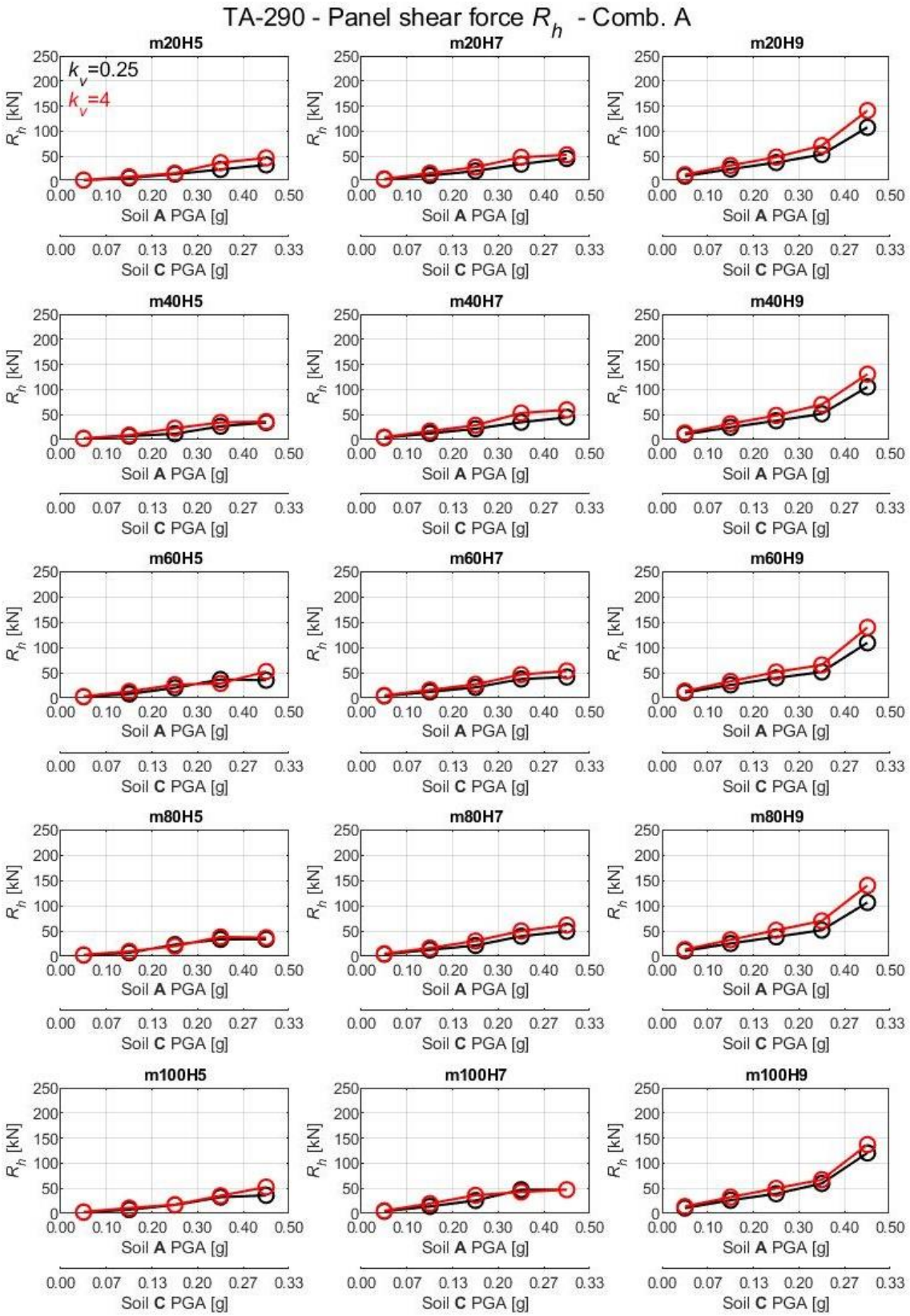

Figure B-9: Seismic demand in term of shear force R_h at the base of the panel for hammer-head strap connection TA-290 in the case of fixed panels and seismic combination A.

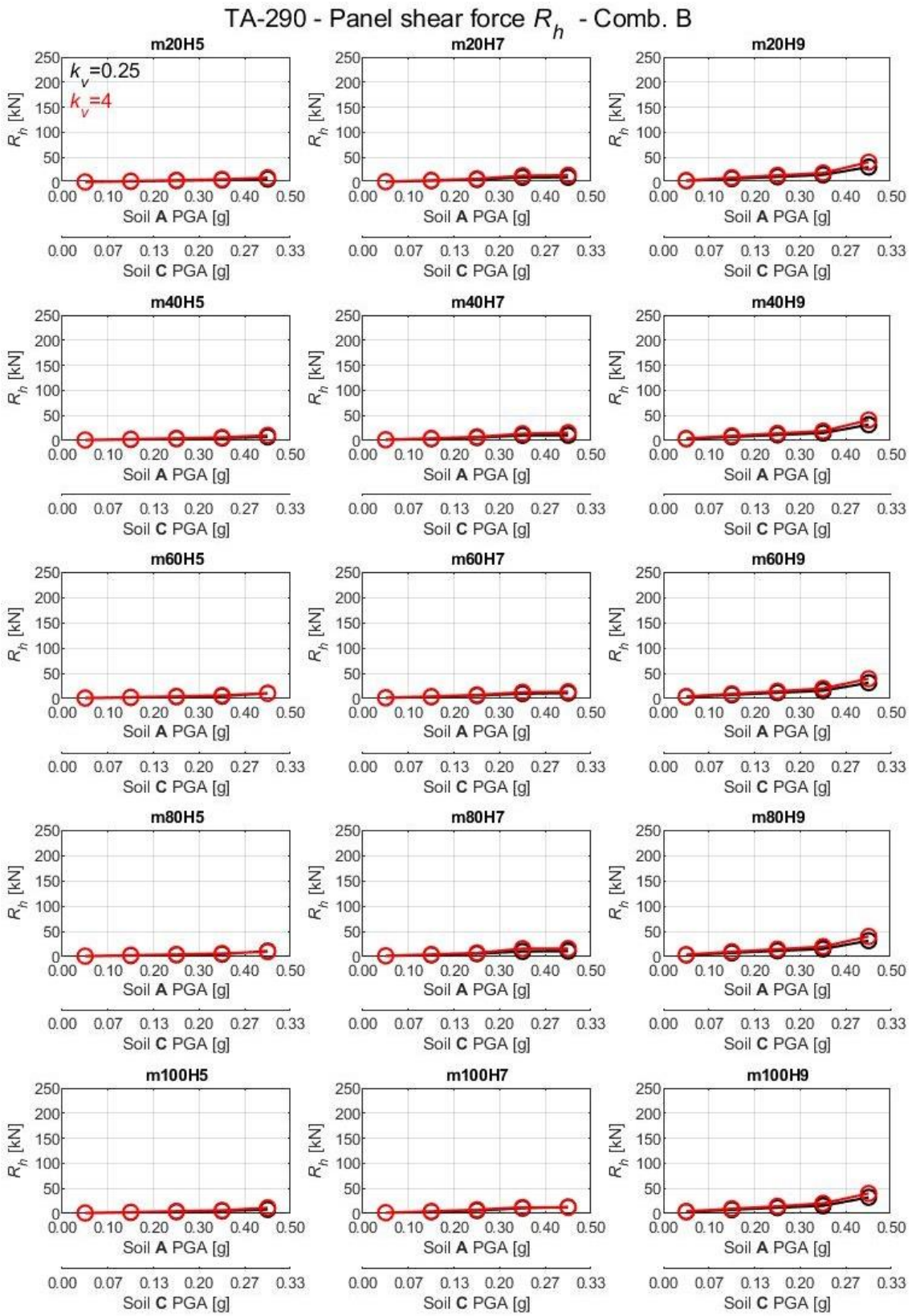

Figure B-10: Seismic demand in term of shear force R_h at the base of the panel for hammer-head strap connection TA-290 in the case of fixed panels and seismic combination B.

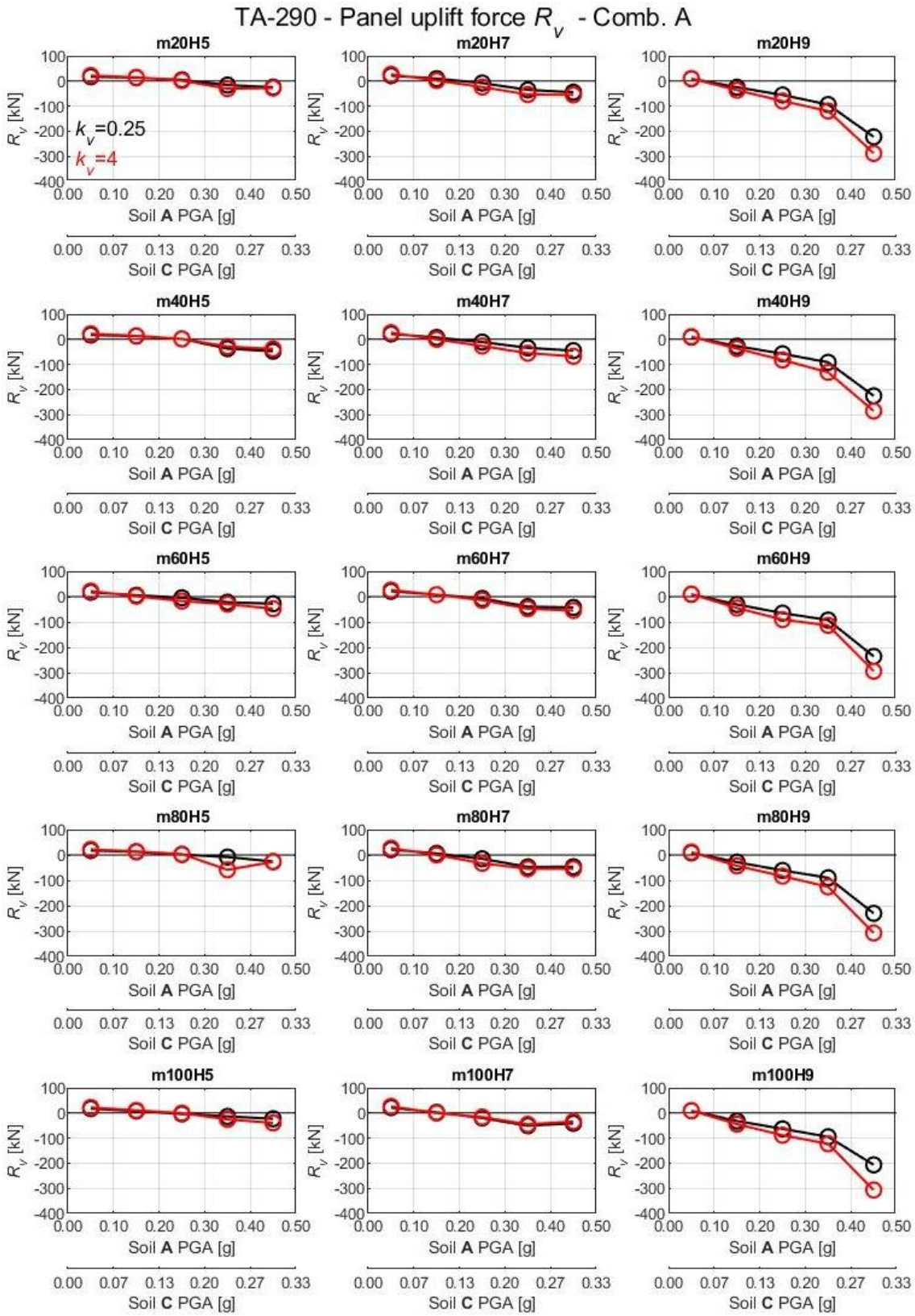

Figure B-11: Seismic demand in panel uplift force R_v for hammer-head strap connection TA-290 in the case of fixed panels and seismic combination A.

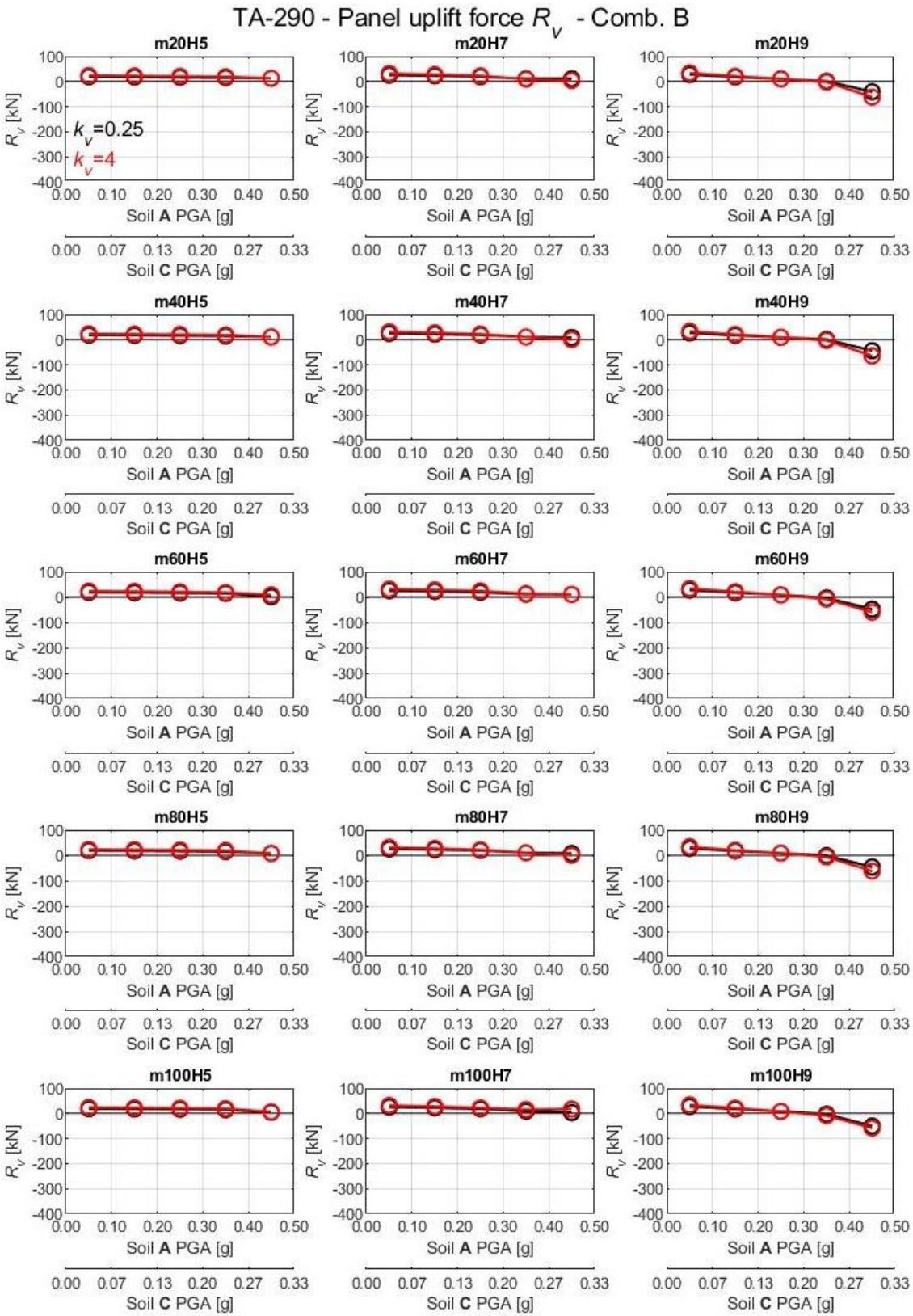

Figure B-12: Seismic demand in panel uplift force R_v for hammer-head strap connection TA-290 in the case of fixed panels and seismic combination B.

Connection: SismoSafe device

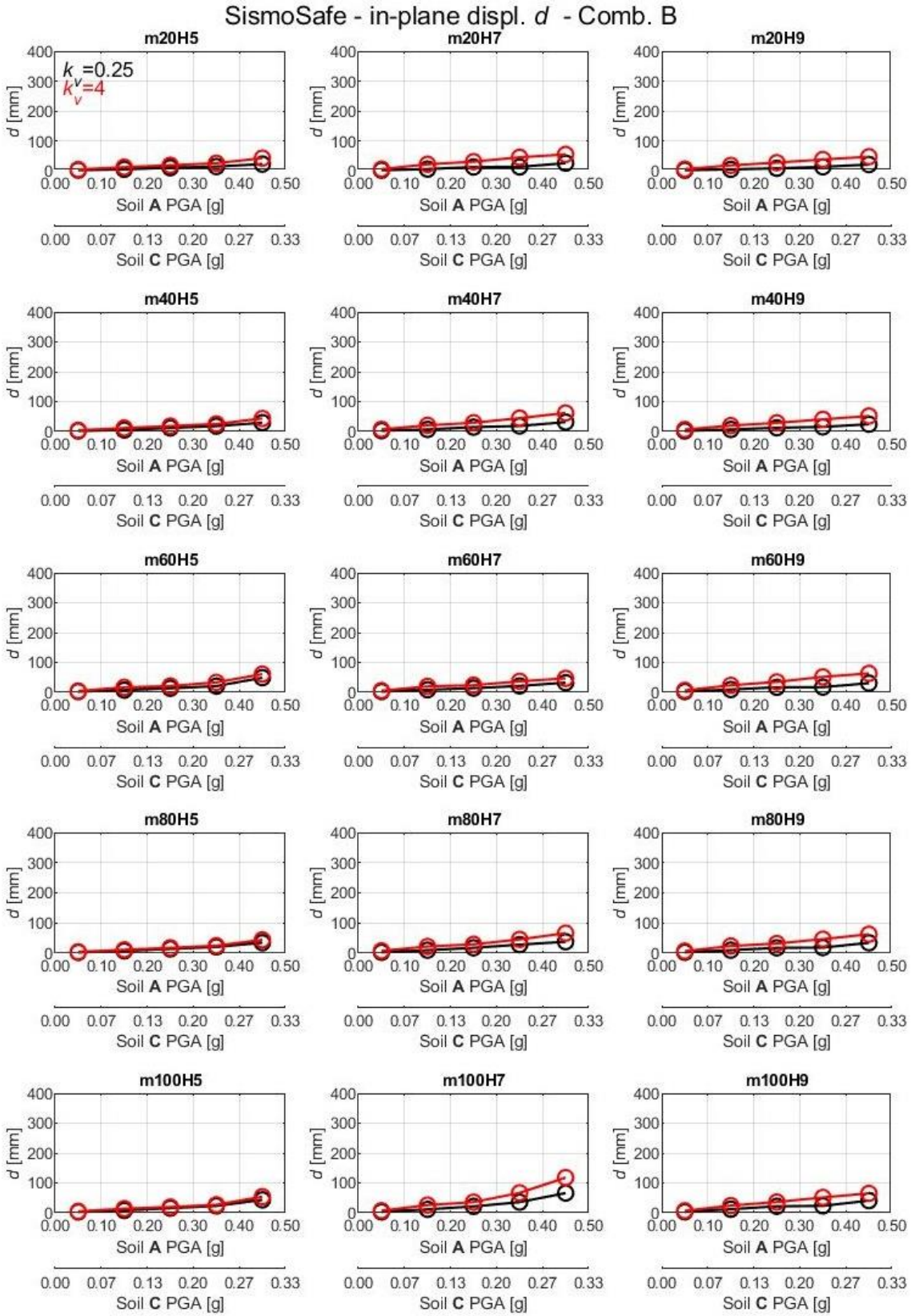

Figure B-13: Seismic demand and capacity comparison in term of in-plane displacement *d* for SismoSafe connection in the case of fixed panels and seismic combination B.

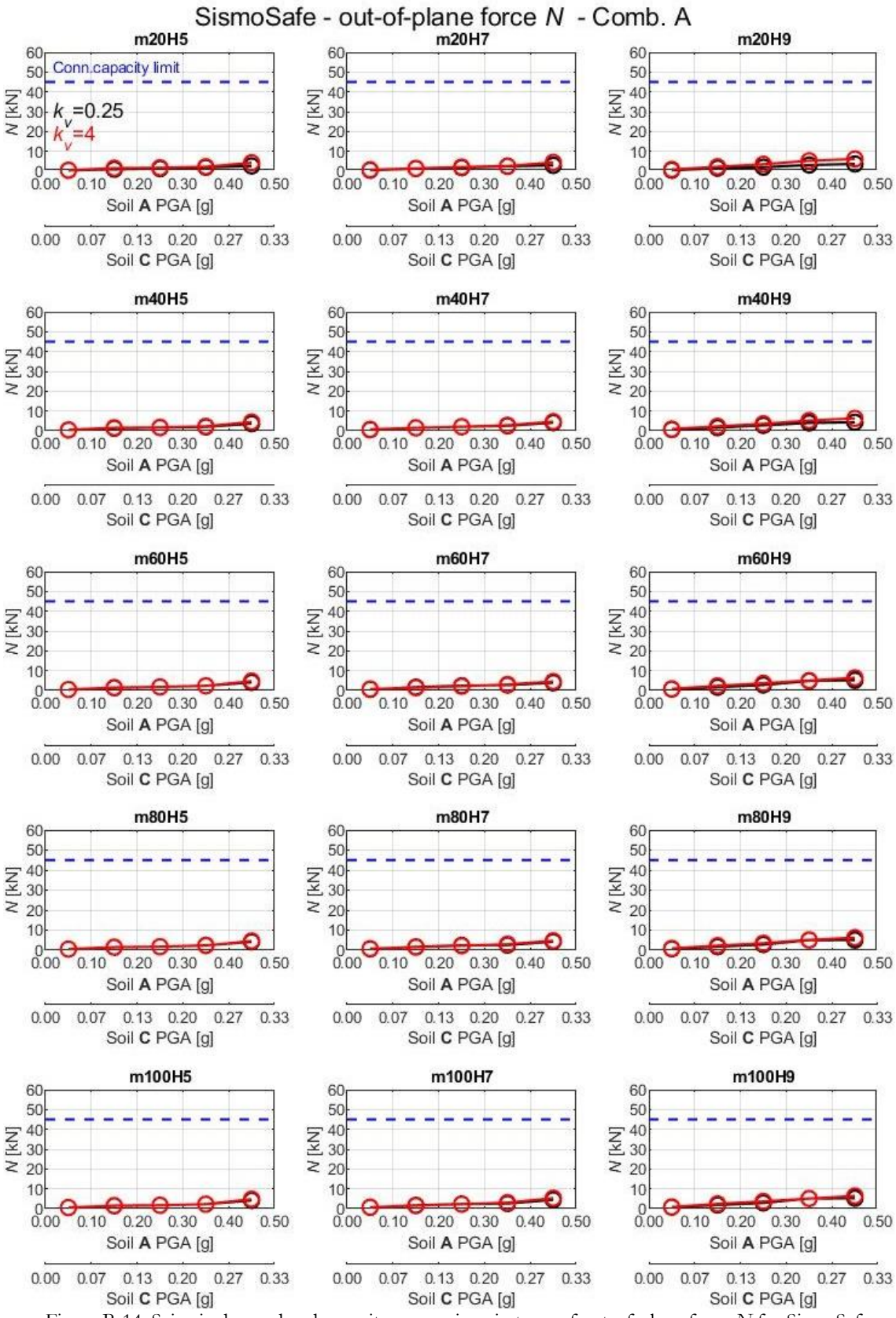

Figure B-14: Seismic demand and capacity comparison in term of out-of-plane force *N* for SismoSafe connection in the case of fixed panels and seismic combination A.

.

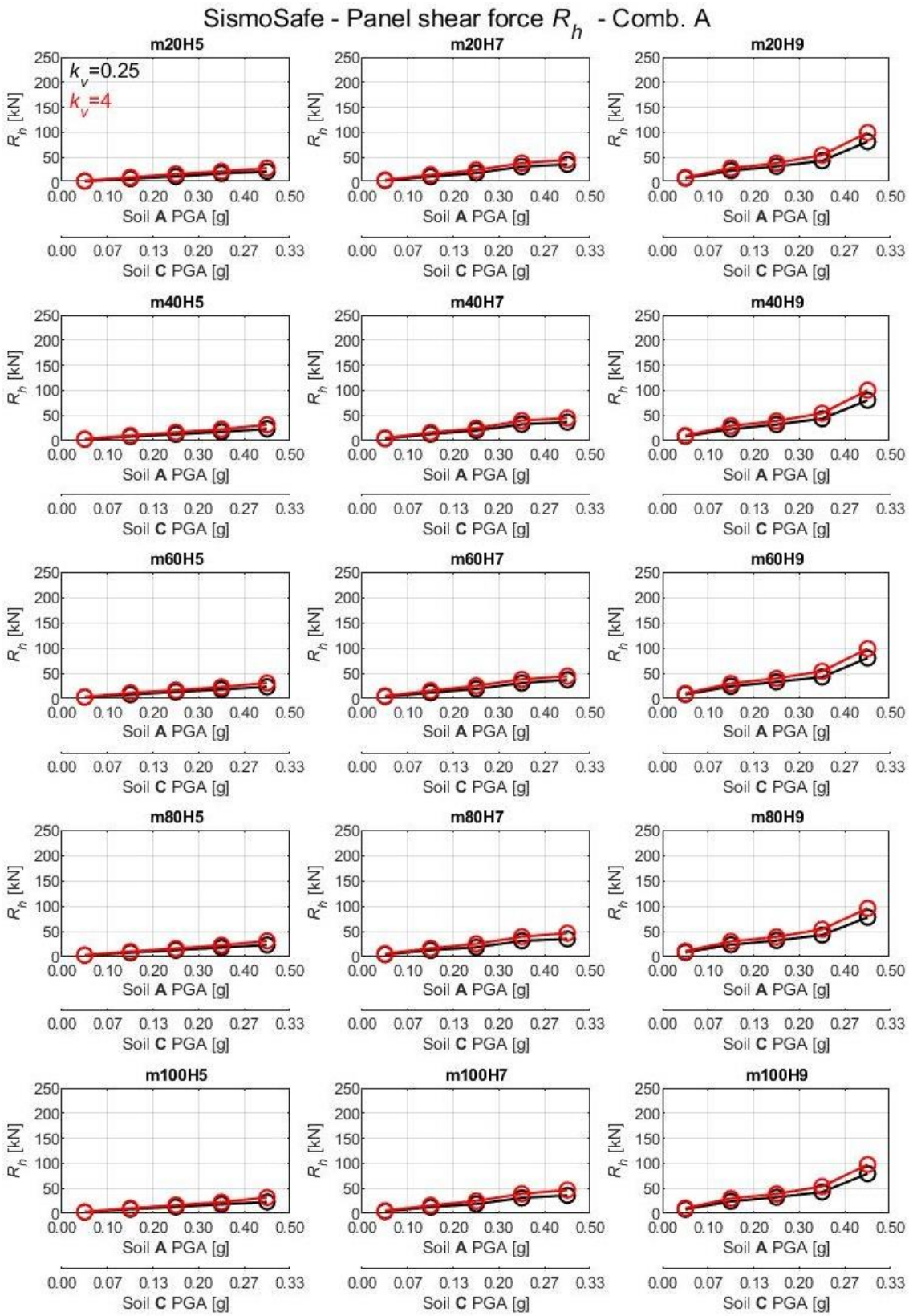

Figure B-15: Seismic demand in term of shear force R_h at the base of the panel for SismoSafe connection in the case of fixed panels and seismic combination A.

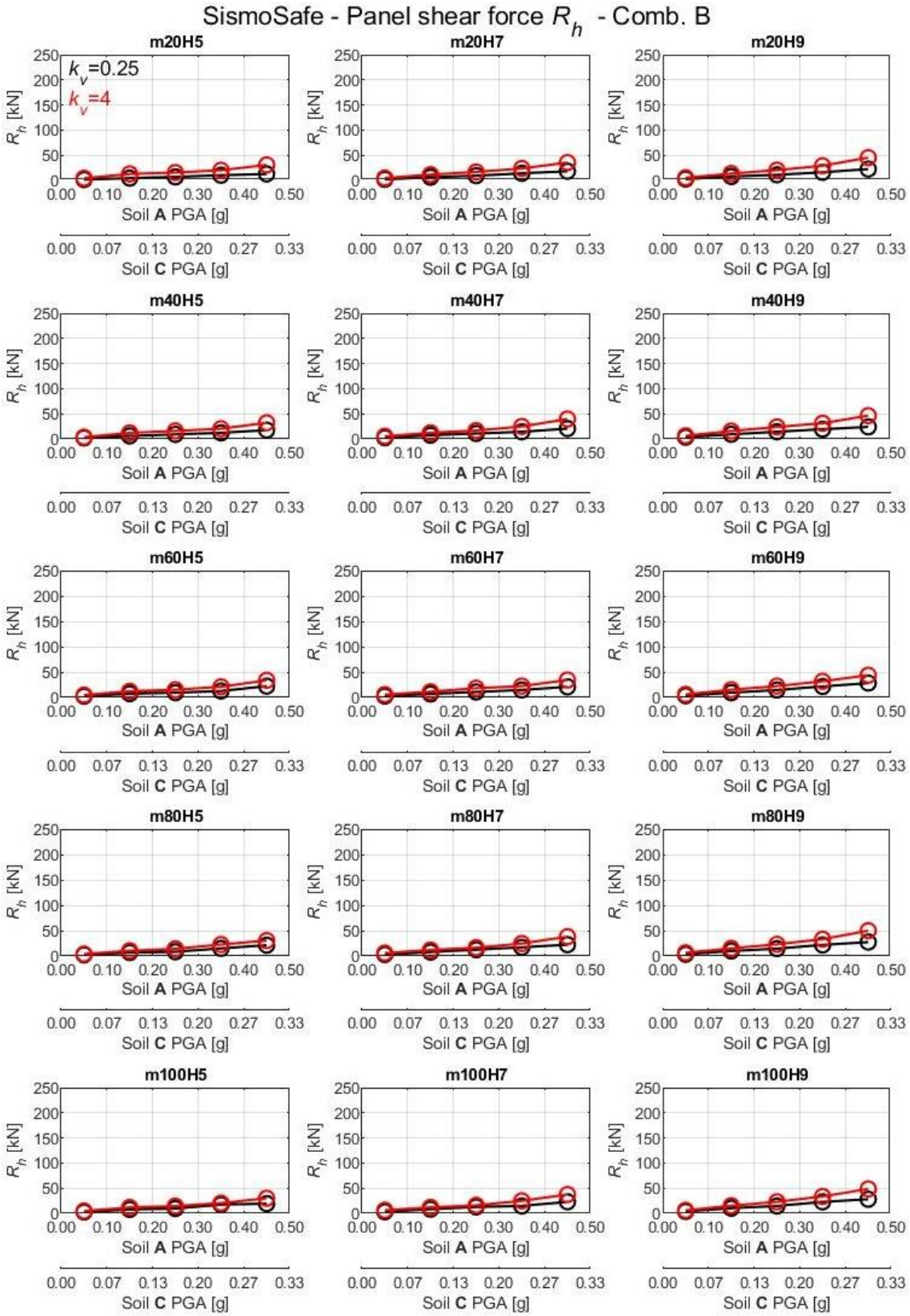

Figure B-16: Seismic demand in term of shear force R_h at the base of the panel for SismoSafe connection in the case of fixed panels and seismic combination B.

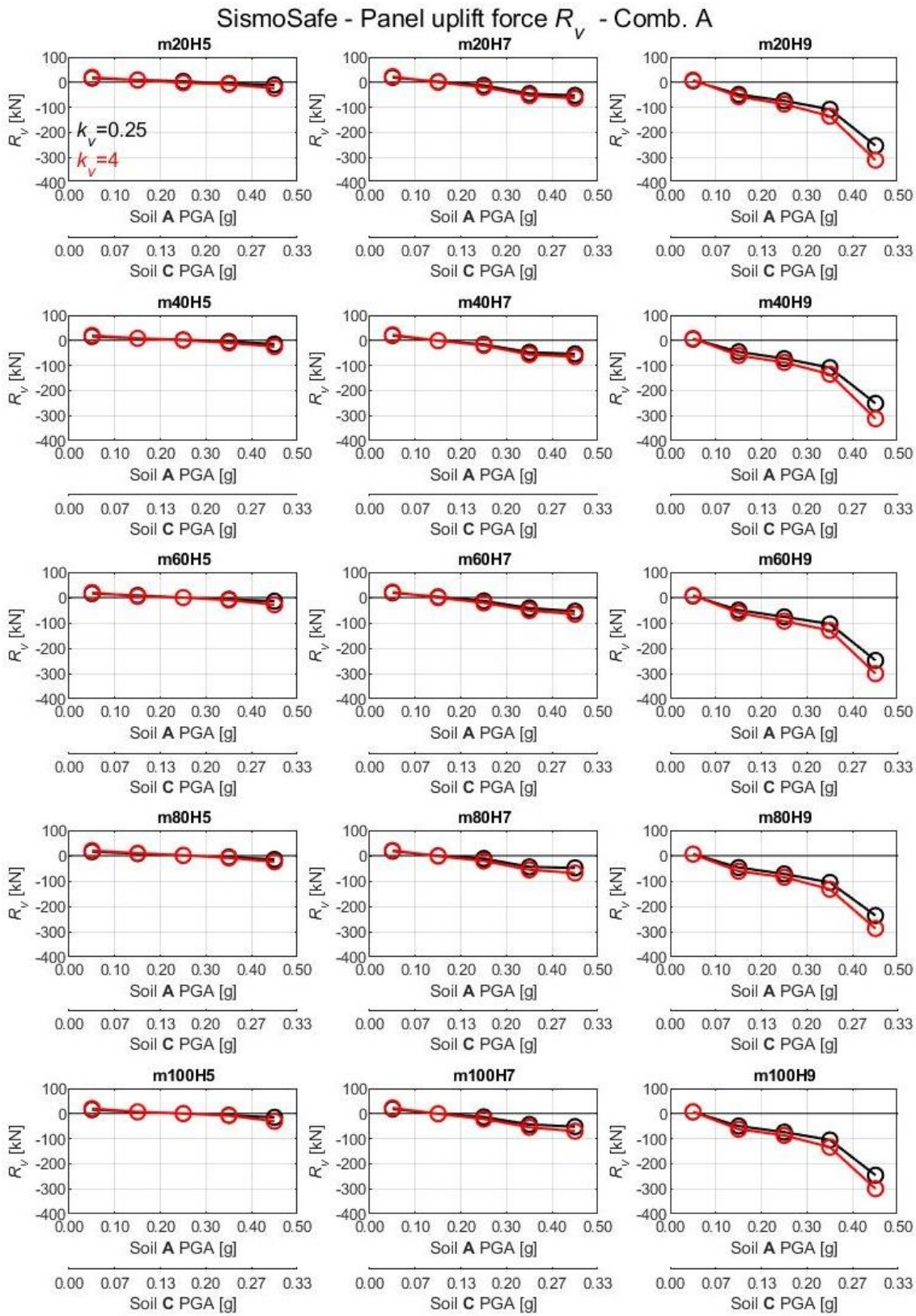

Figure B-17: Seismic demand in panel uplift force R_v for SismoSafe connection in the case of fixed panels and seismic combination A.

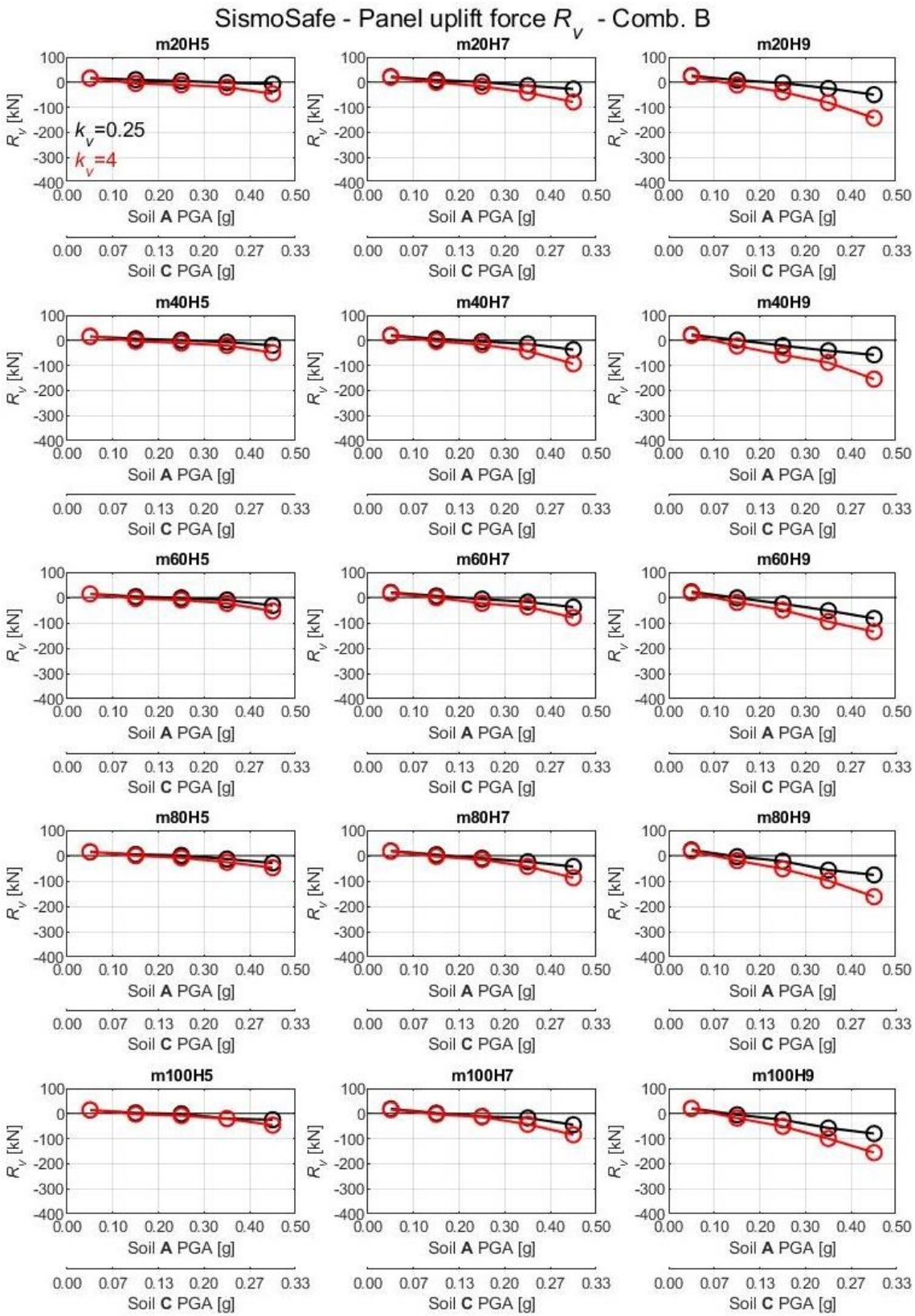

Figure B-18: Seismic demand in panel uplift force R_v for SismoSafe connection in the case of fixed panels and seismic combination B.

B.2 Result for rocking panels
Connection: hammer-head strap TA-210

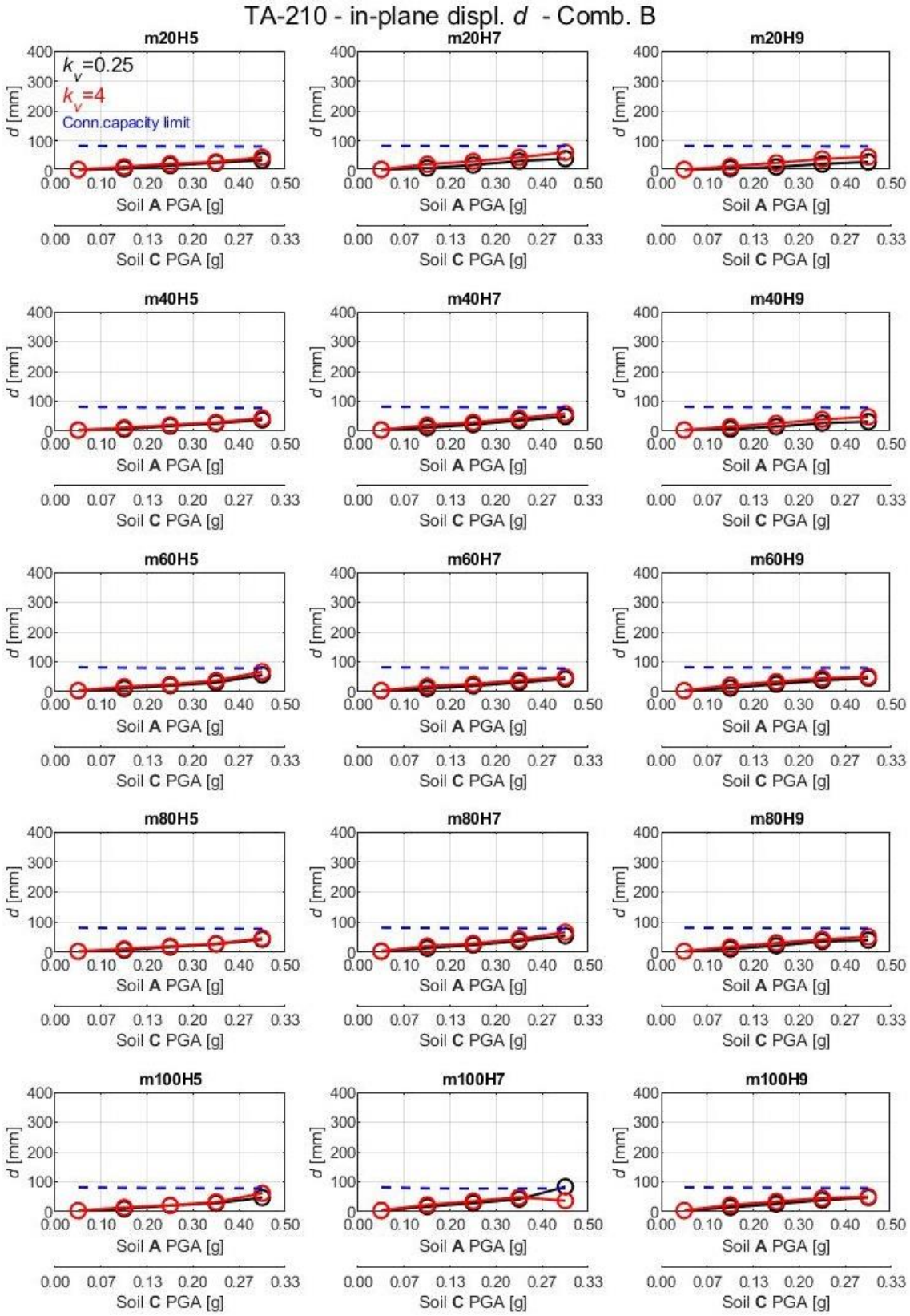

Figure B-19: Seismic demand and capacity comparison in term of in-plane displacement *d* for hammer-head strap connection TA-210 in the case of rocking panels and seismic combination B.

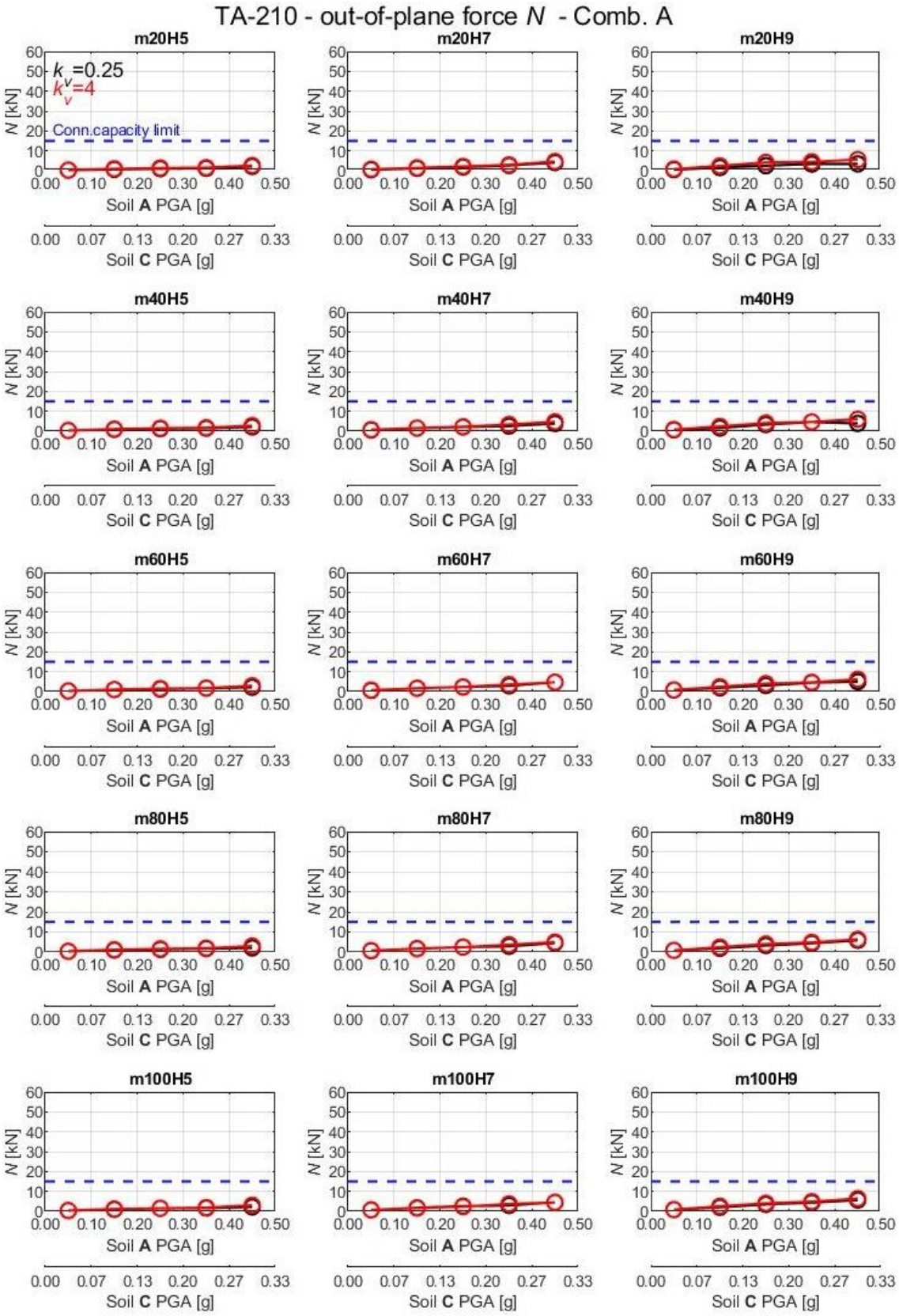

Figure B-20: Seismic demand and capacity comparison in term of out-of-plane force *N* for hammer-head strap connection TA-210 in the case of rocking panels and seismic combination A.

.

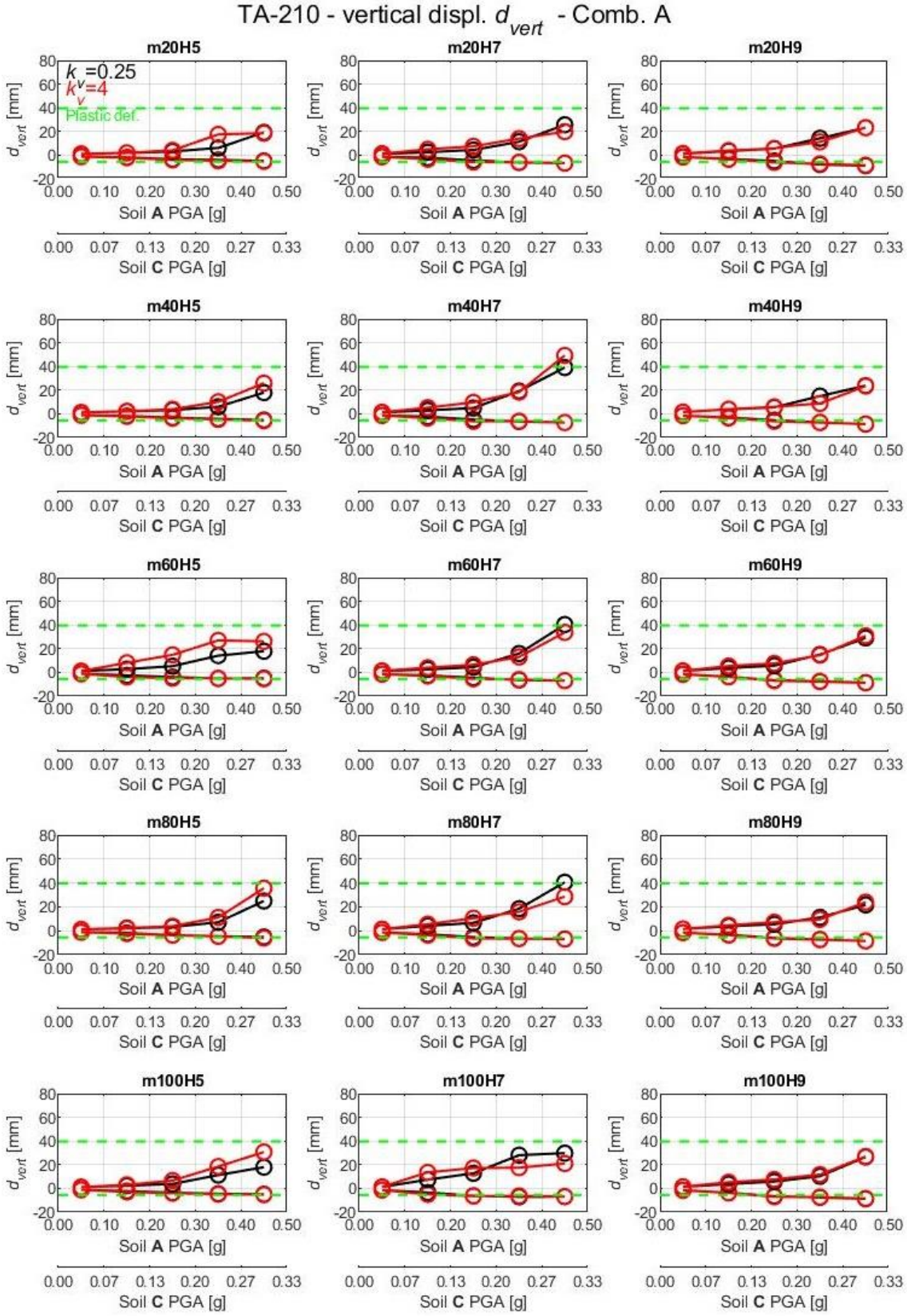

Figure B-21: Seismic demand and capacity comparison in term of vertical displacement d_{vert} for hammer-head strap connection TA-210 in the case of rocking panels and seismic combination A.

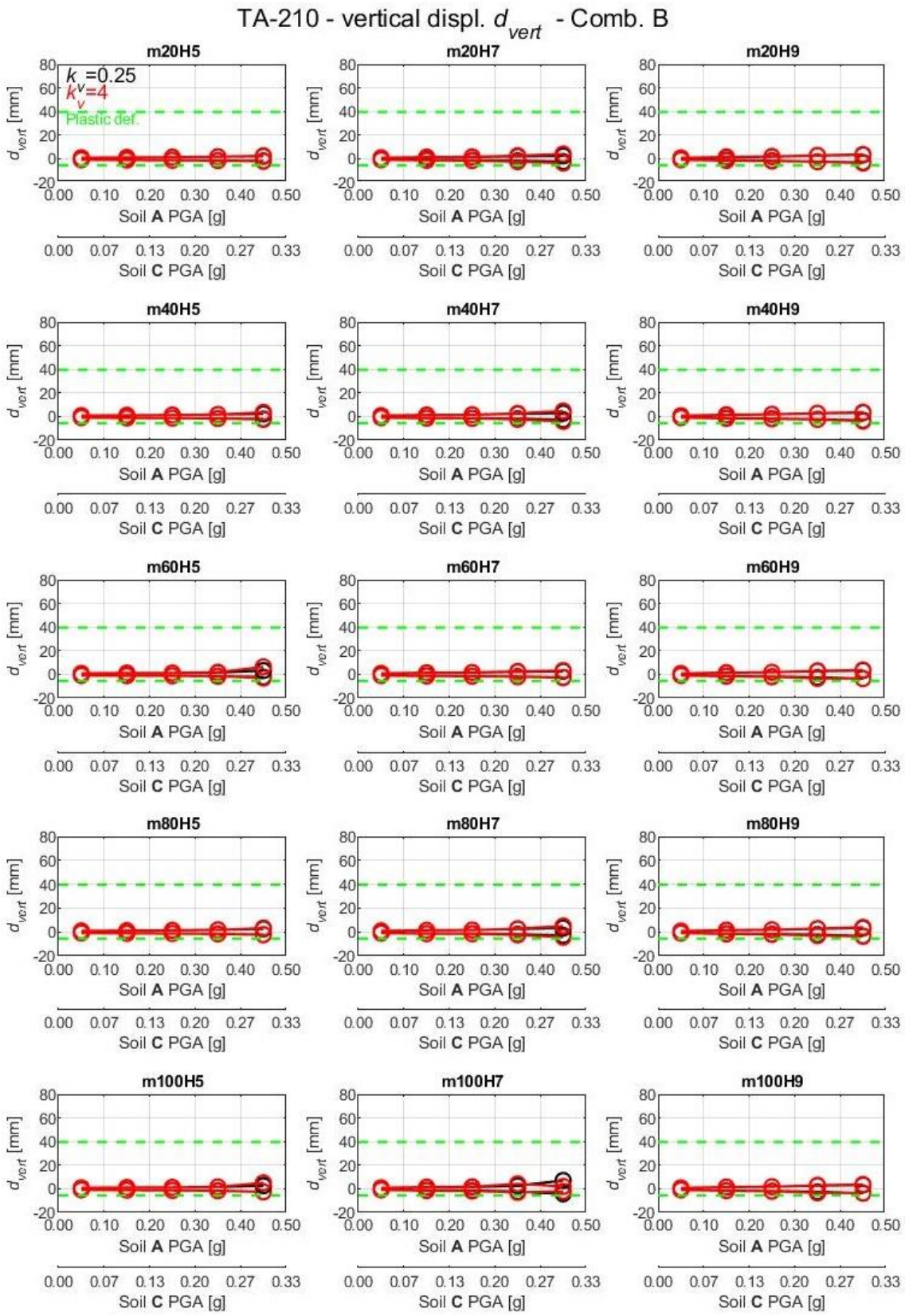

Figure B-22: Seismic demand and capacity comparison in term of vertical displacement d_{vert} for hammer-head strap connection TA-210 in the case of rocking panels and seismic combination B.

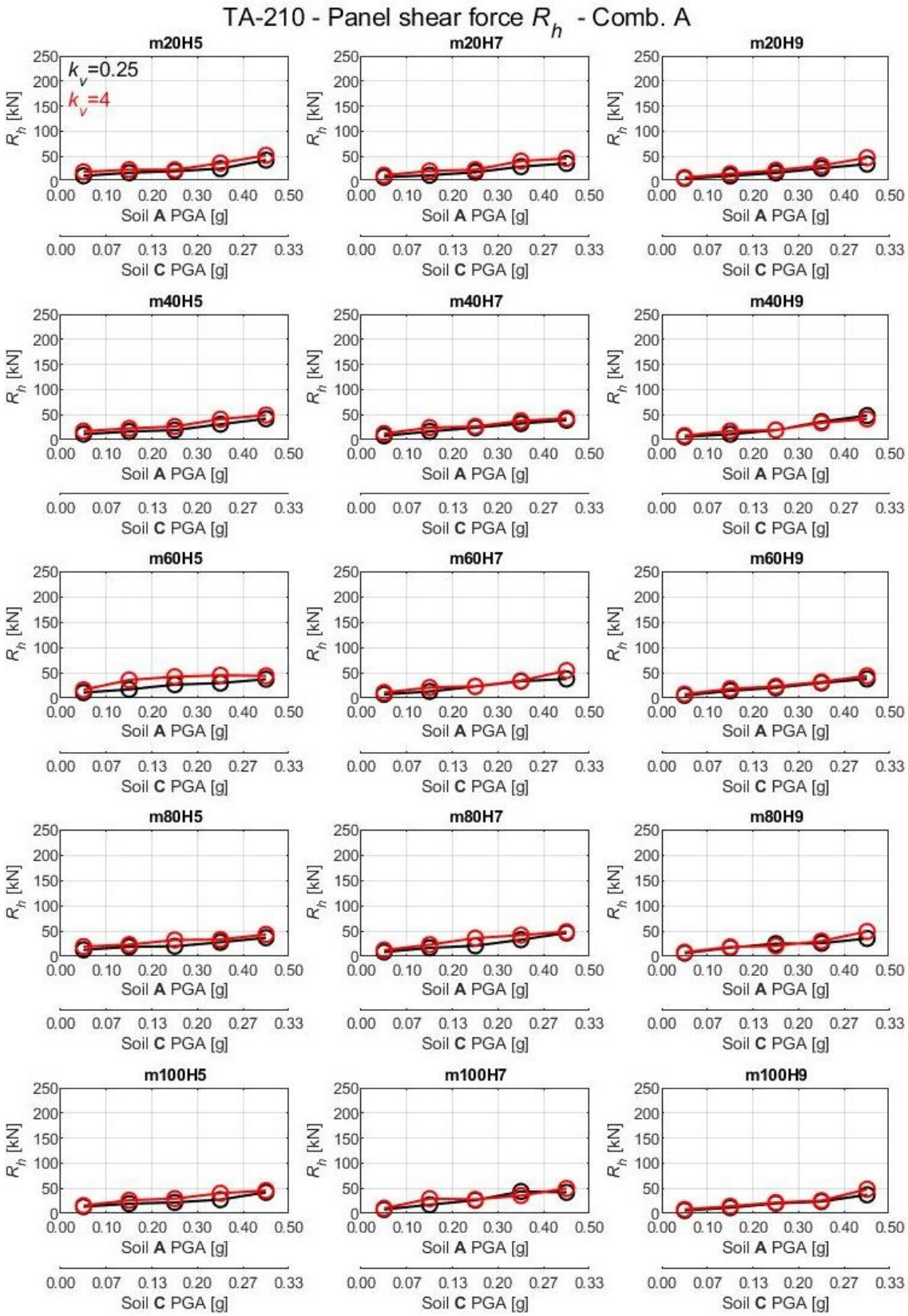

Figure B-23: Seismic demand in term of shear force R_h at the base of the panel for hammer-head strap connection TA-210 in the case of rocking panels and seismic combination A.

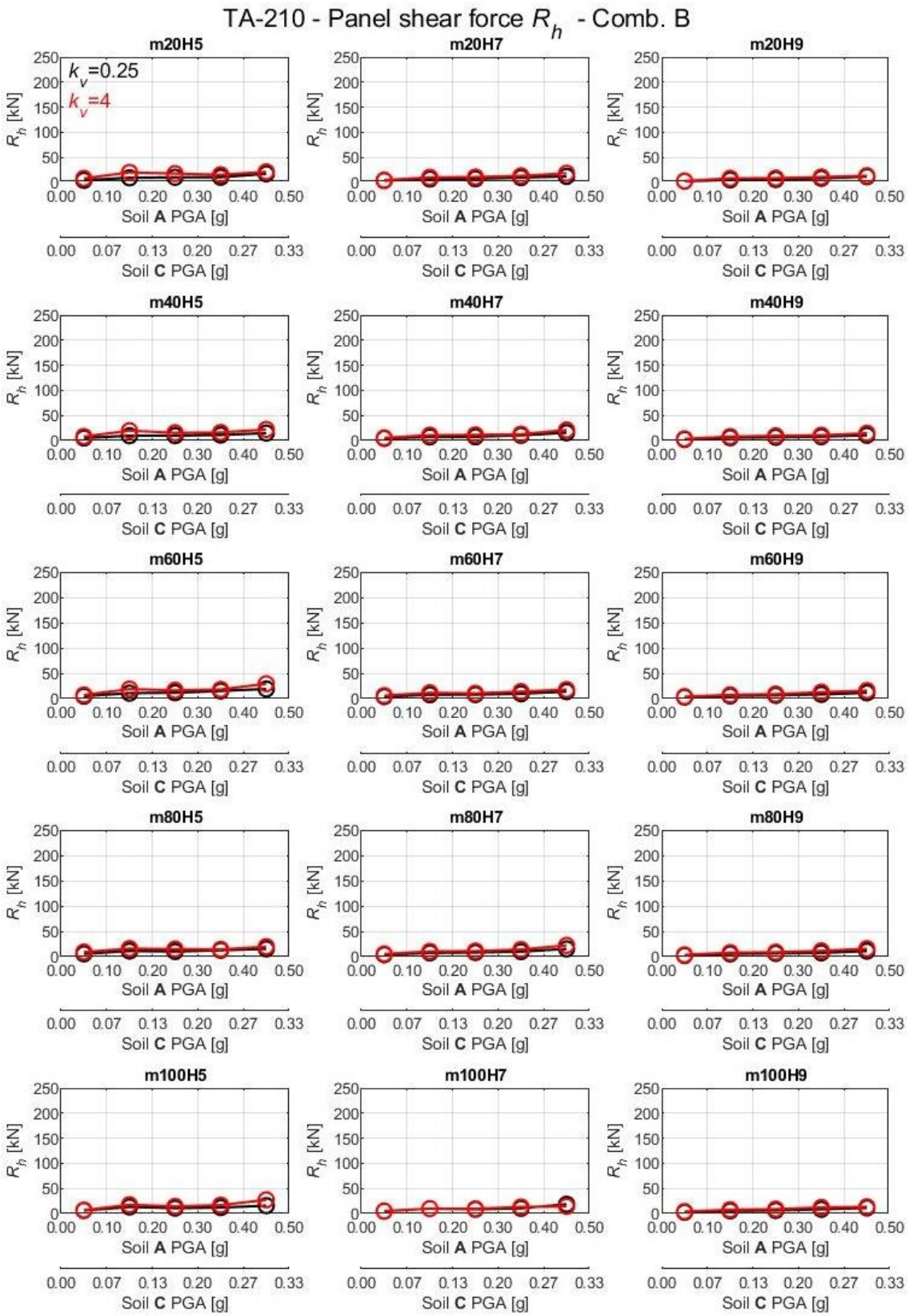

Figure B-24: Seismic demand in term of shear force R_h at the base of the panel for hammer-head strap connection TA-210 in the case of rocking panels and seismic combination B.

Connection: hammer-head strap TA-290

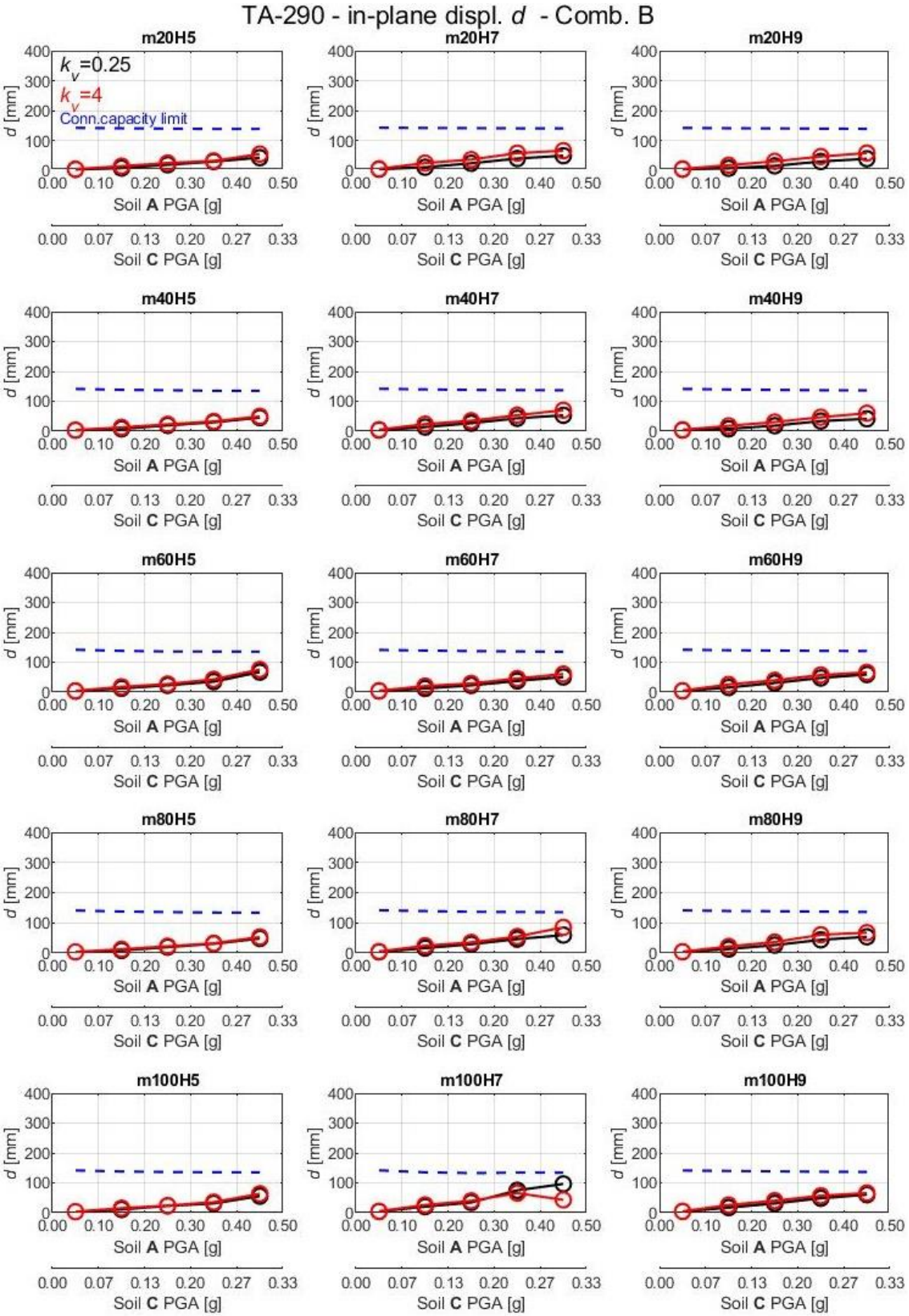

Figure B-25: Seismic demand and capacity comparison in term of in-plane displacement *d* for hammer-head strap connection TA-290 in the case of rocking panels and seismic combination B.

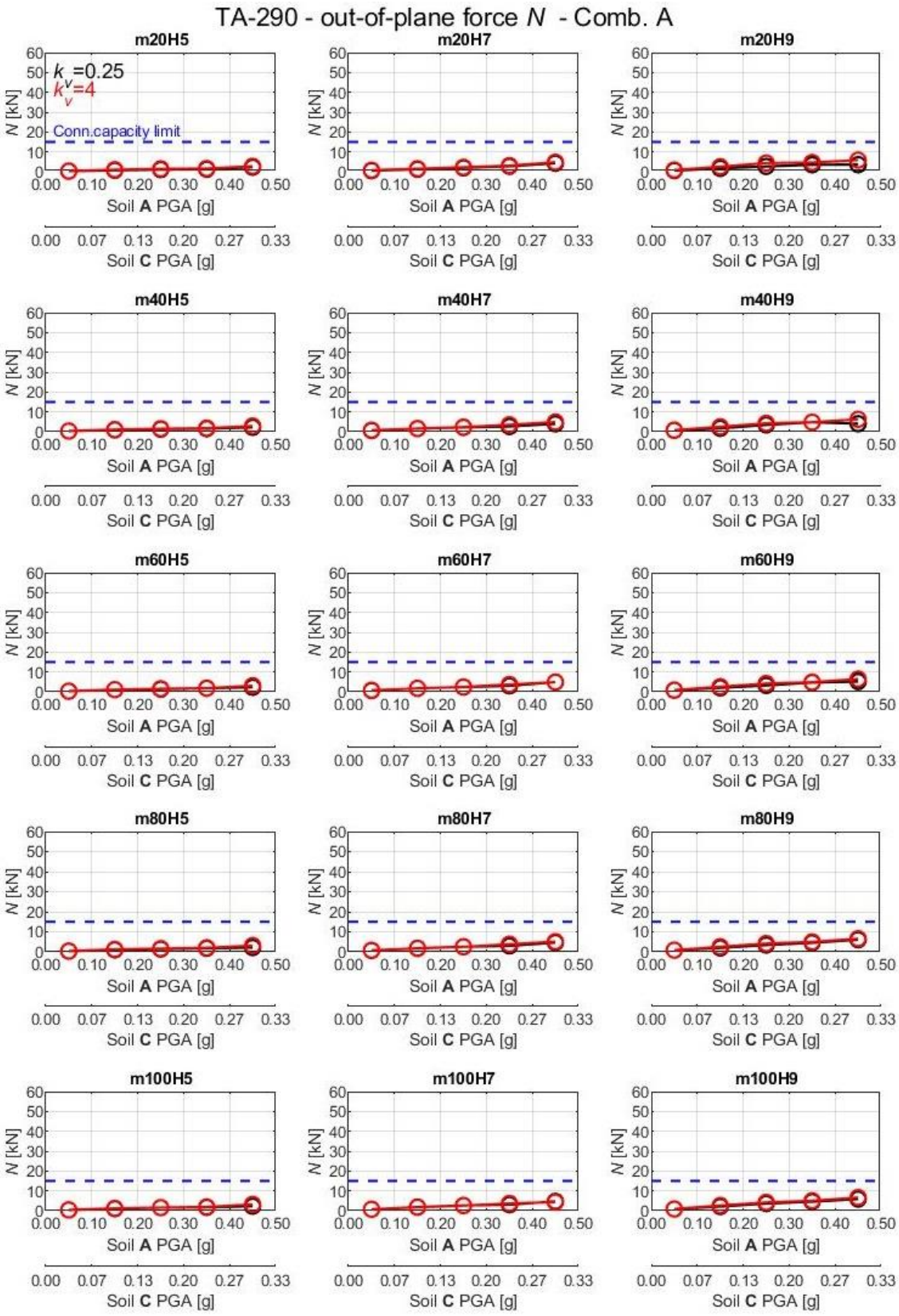

Figure B-26: Seismic demand and capacity comparison in term of out-of-plane force *N* for hammer-head strap connection TA-290 in the case of rocking panels and seismic combination A.

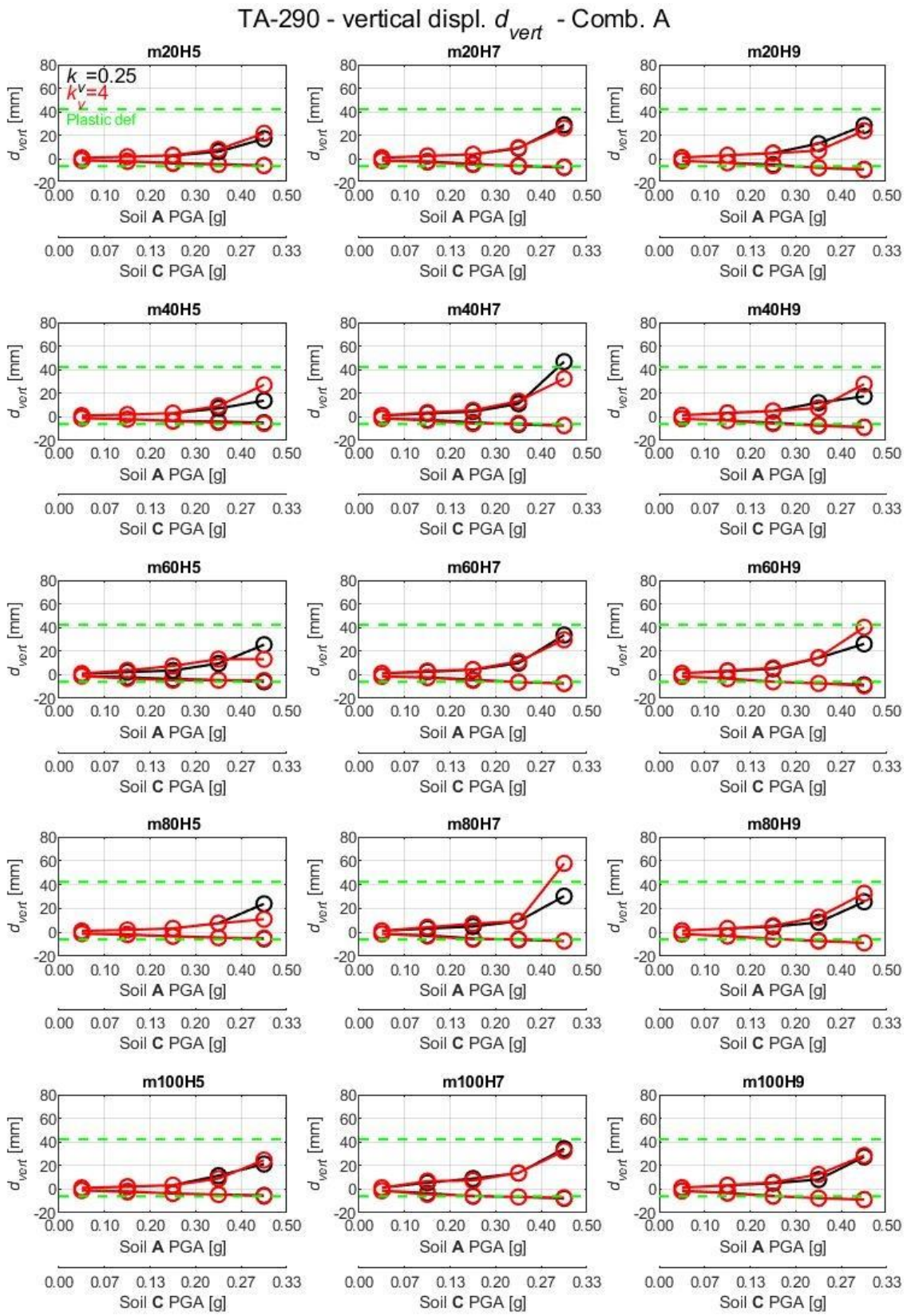

Figure B-27: Seismic demand and capacity comparison in term of vertical displacement d_{vert} for hammer-head strap connection TA-290 in the case of rocking panels and seismic combination A.

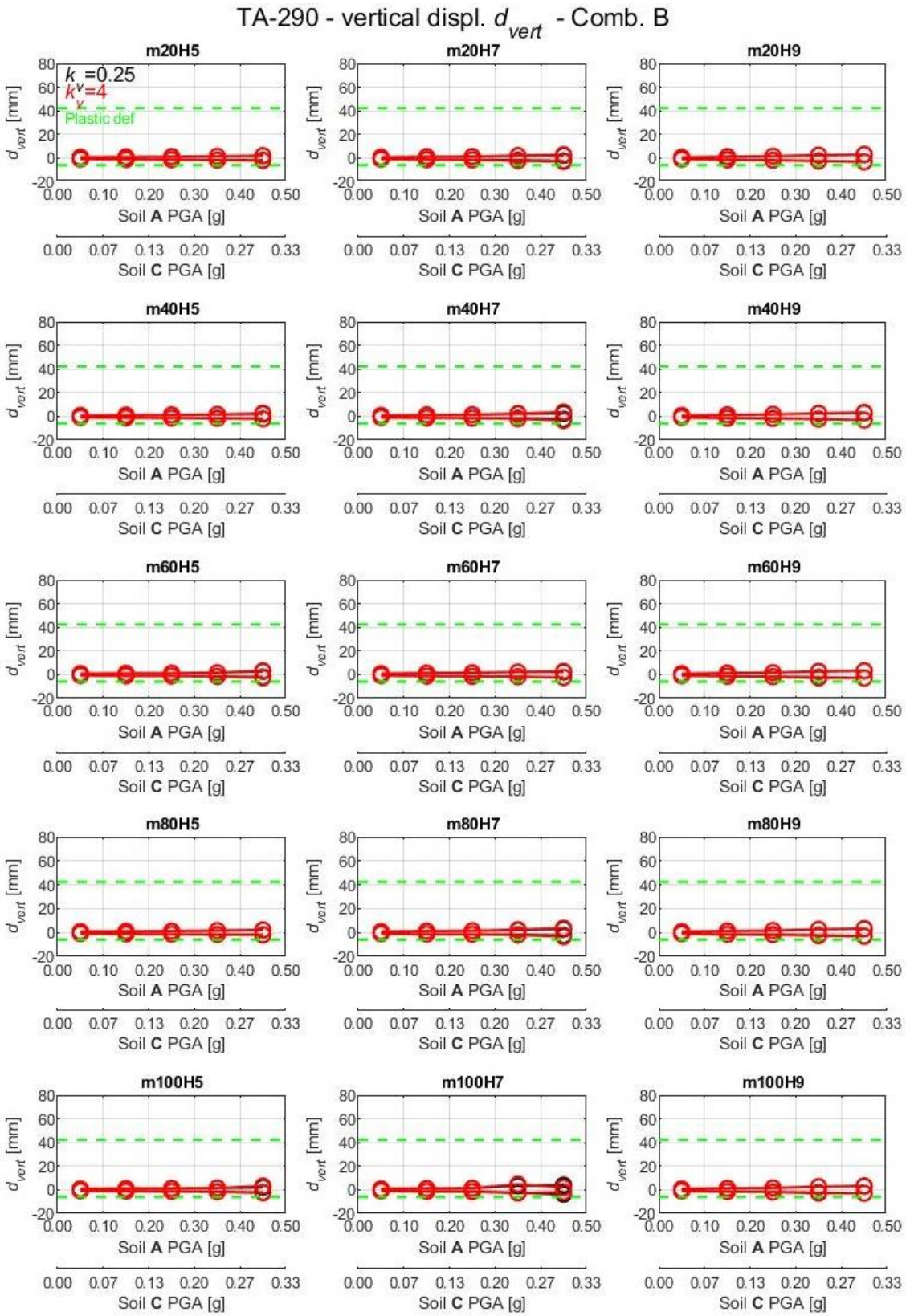

Figure B-28: Seismic demand and capacity comparison in term of vertical displacement d_{vert} for hammer-head strap connection TA-290 in the case of rocking panels and seismic combination A.

.

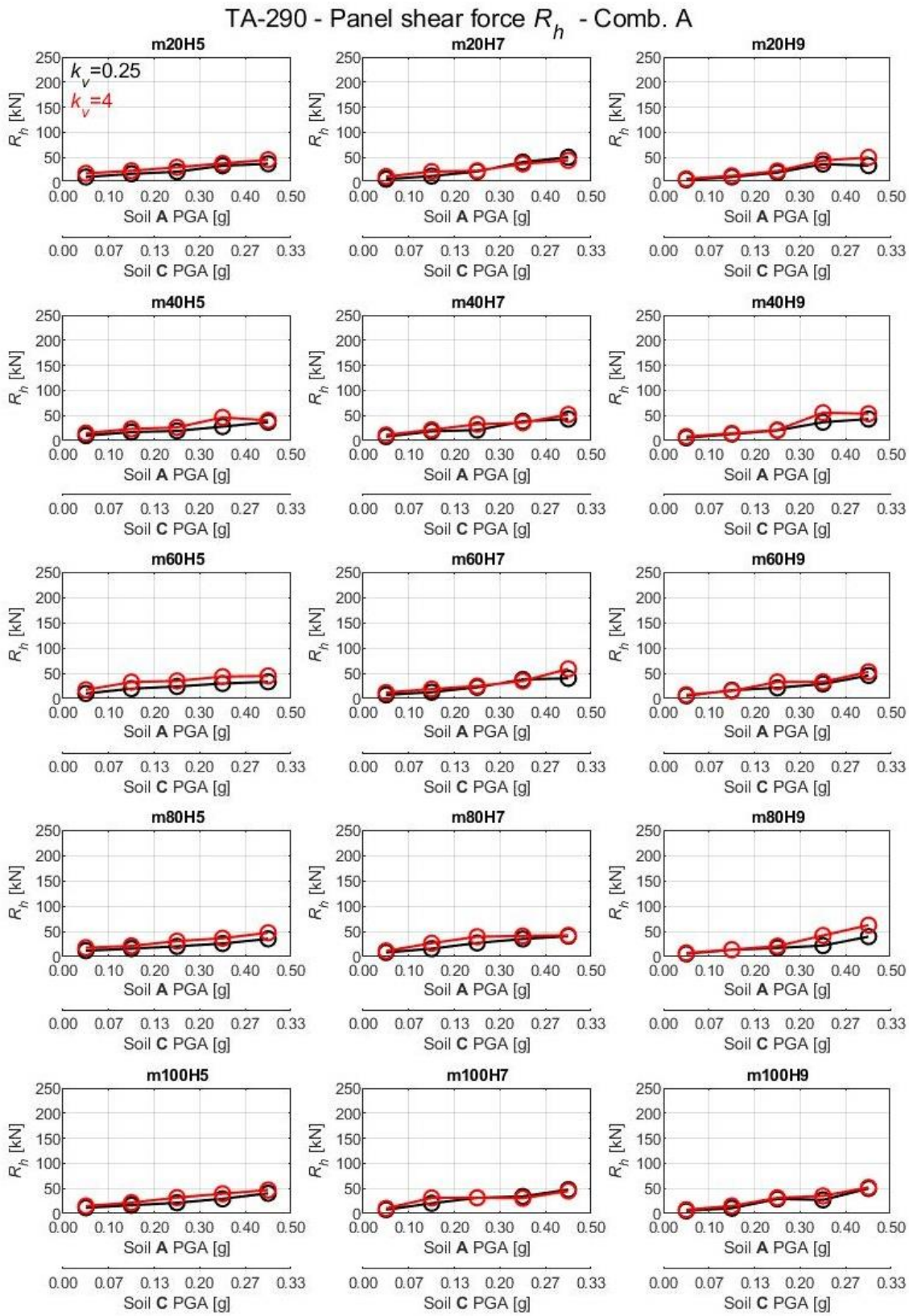

Figure B-29: Seismic demand in term of shear force R_h at the base of the panel for hammer-head strap connection TA-290 in the case of rocking panels and seismic combination A.

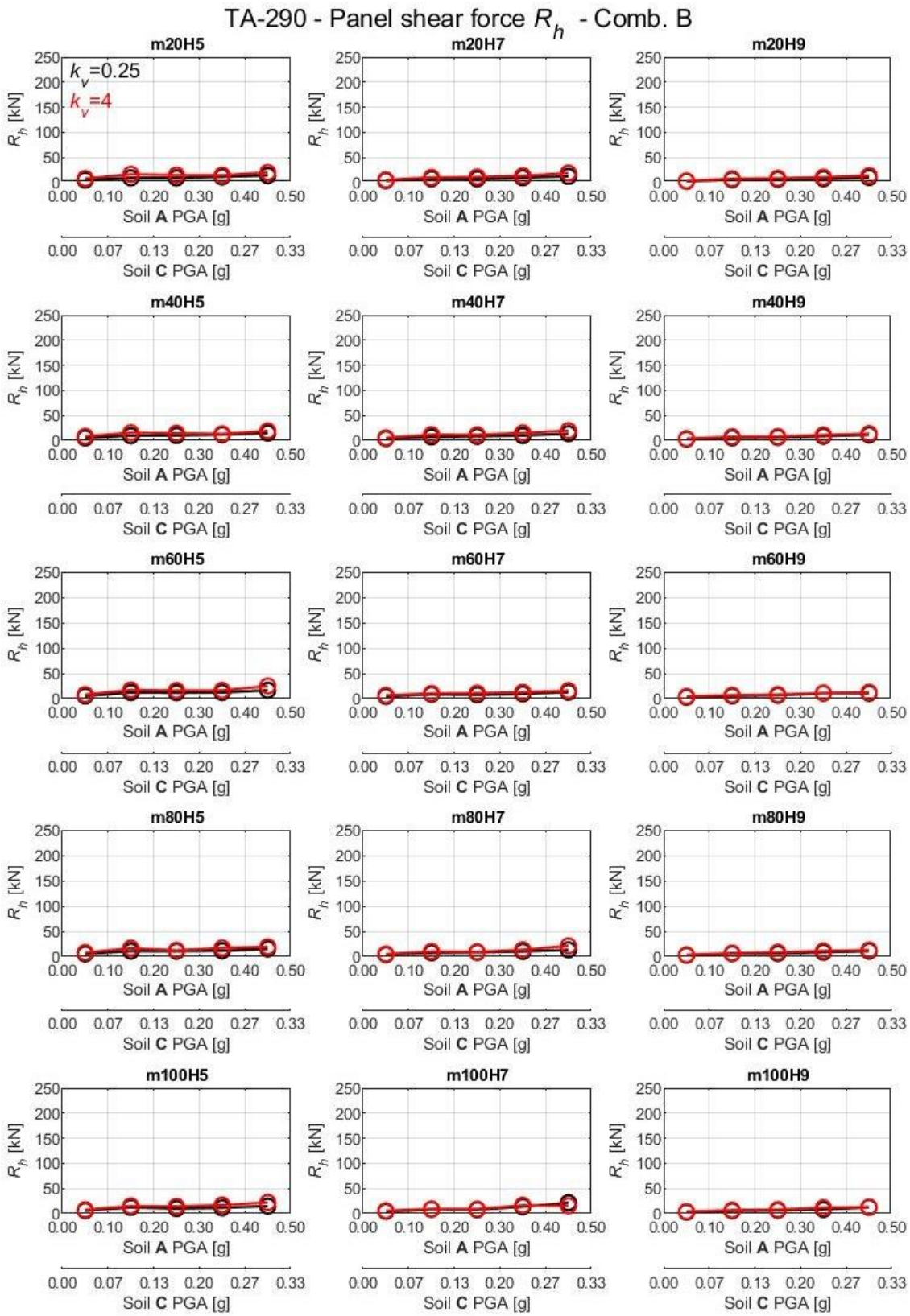

Figure B-30: Seismic demand in term of shear force R_h at the base of the panel for hammer-head strap connection TA-290 in the case of rocking panels and seismic combination B..

Connection: SismoSafe device

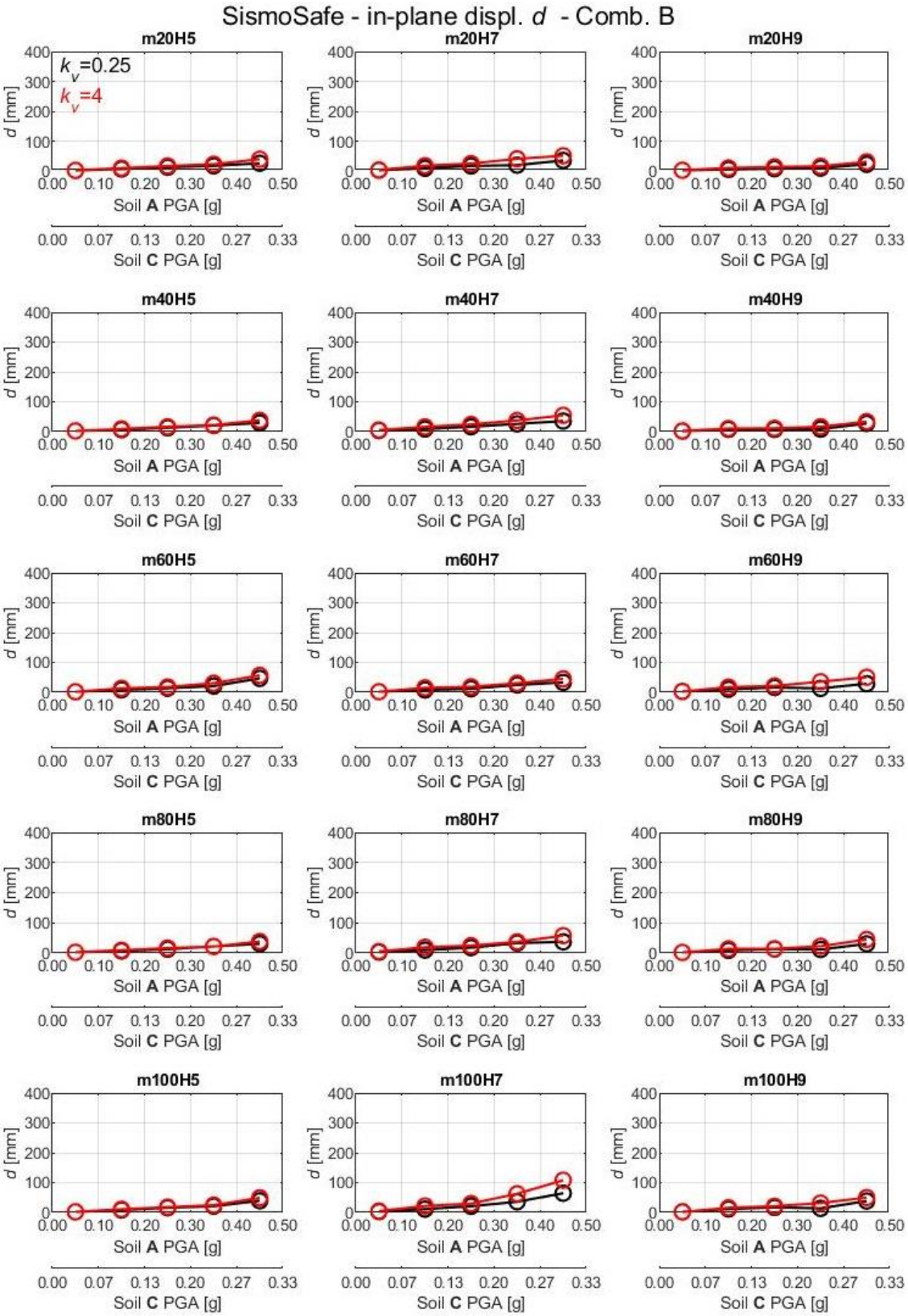

Figure B-31: Seismic demand and capacity comparison in term of in-plane displacement *d* for SismoSafe connection in the case of rocking panels and seismic combination B.

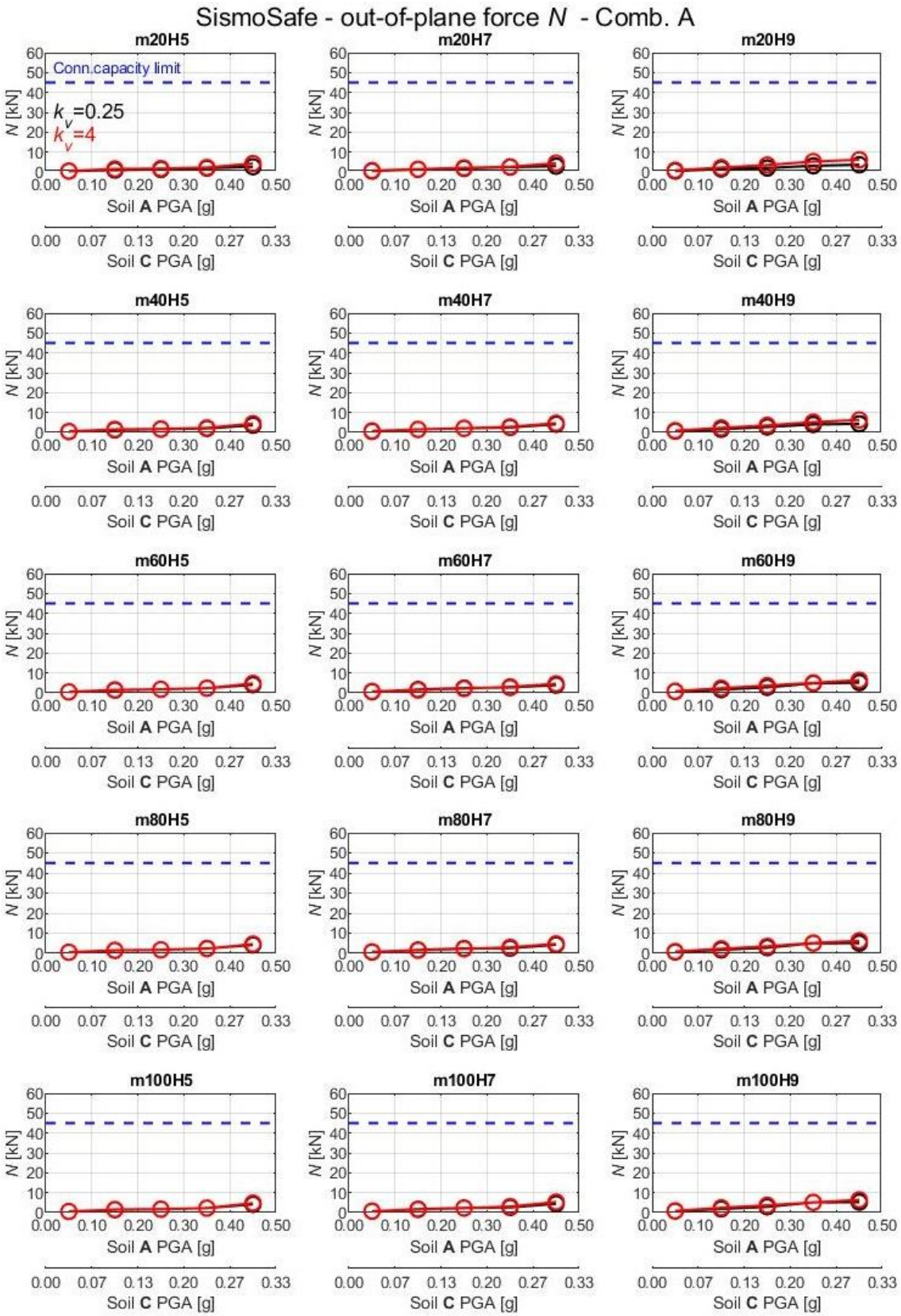

Figure B-32: Seismic demand and capacity comparison in term of out-of-plane force *N* for SismoSafe connection in the case of rocking panels and seismic combination A.

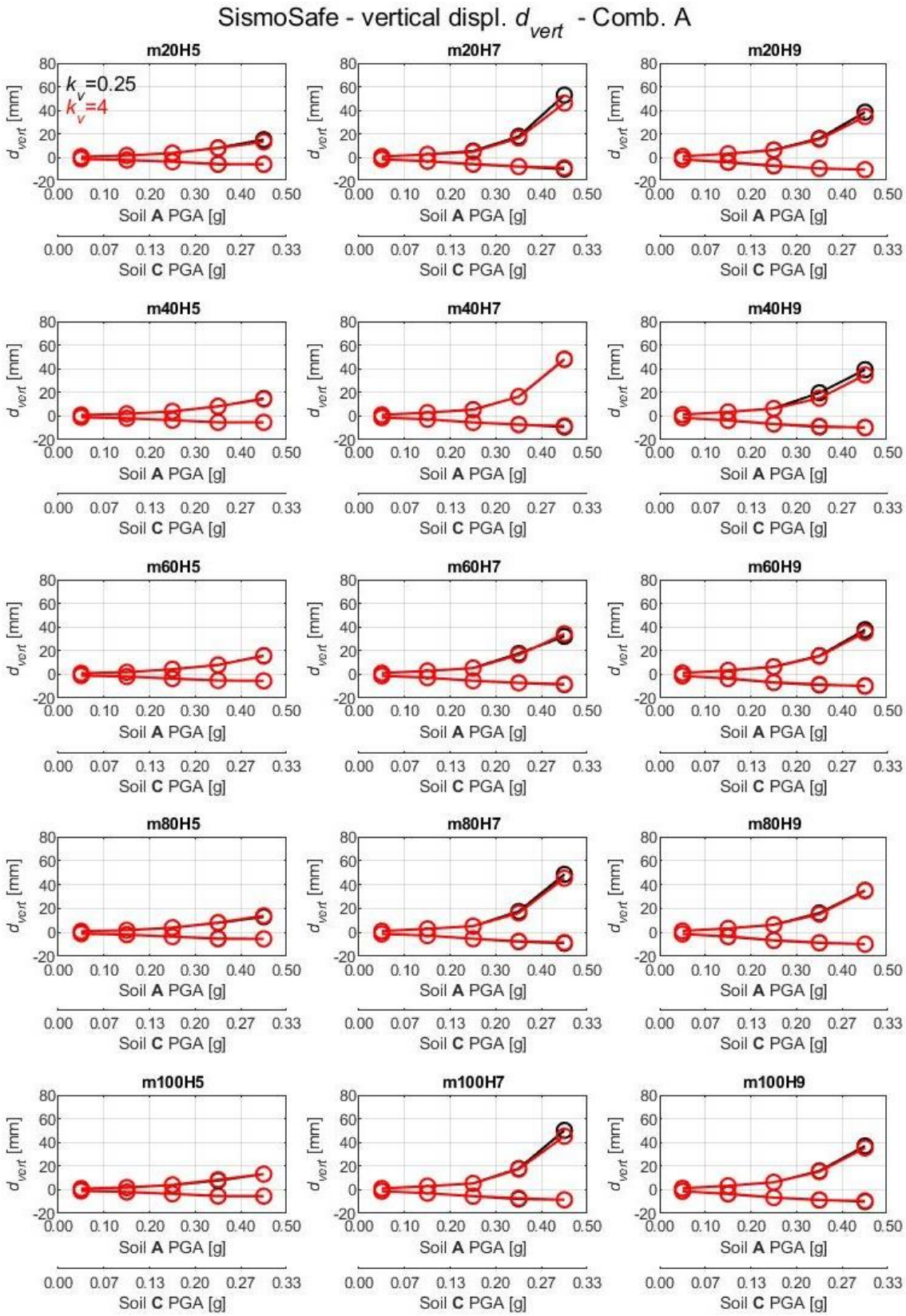

Figure B-33: Seismic demand and capacity comparison in term of vertical displacement d_{vert} for SismoSafe connection in the case of rocking panels and seismic combination A.

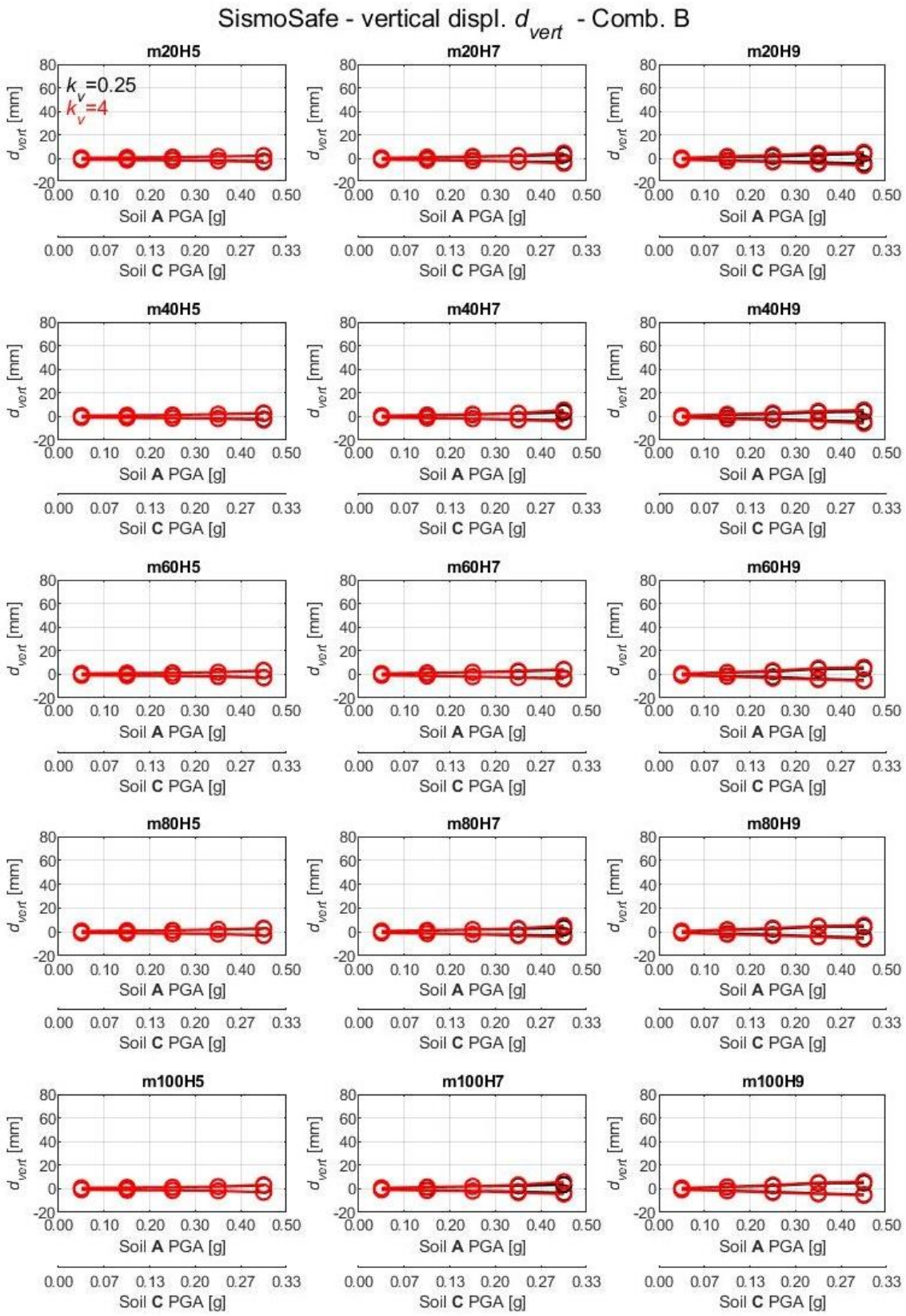

Figure B-34: Seismic demand and capacity comparison in term of vertical displacement d_{vert} for SismoSafe connection in the case of rocking panels and seismic combination B.

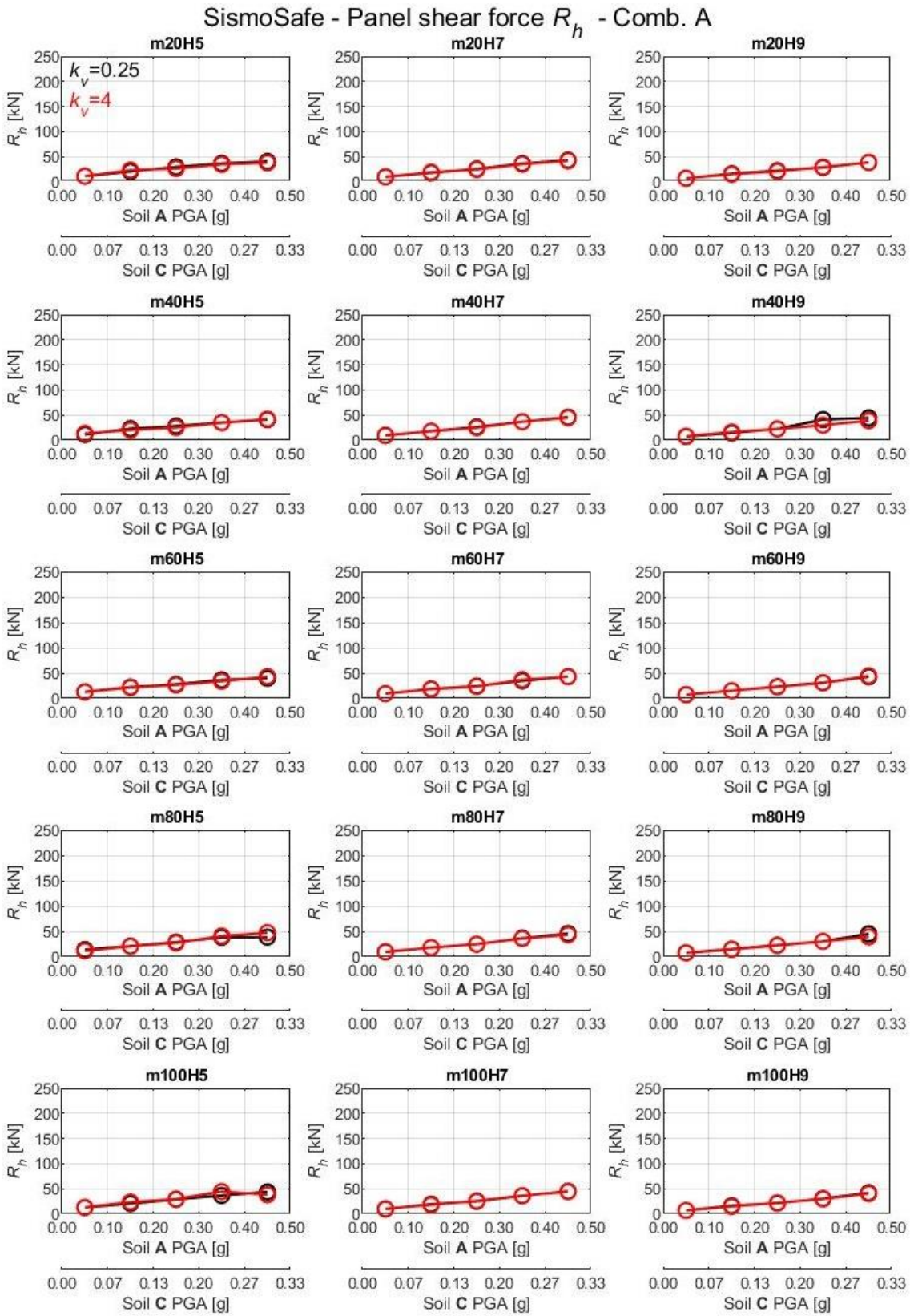

Figure B-35: Seismic demand in term of shear force R_h at the base of the panel for SismoSafe connection in the case of rocking panels and seismic combination A.

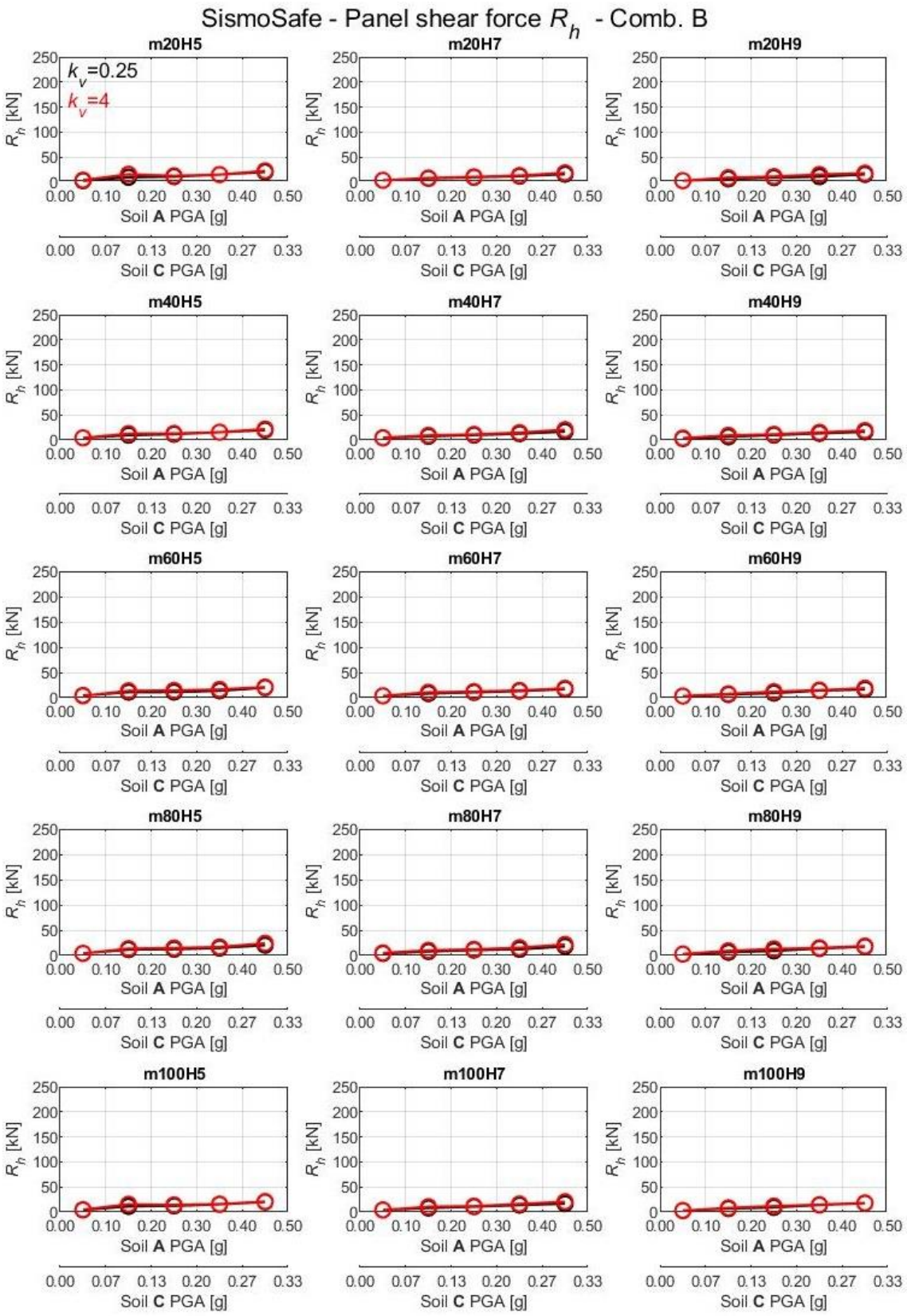

Figure B-36: Seismic demand in term of shear force R_h at the base of the panel for SismoSafe connection in the case of rocking panels and seismic combination B.

Bibliography

Angotti, F., Orlando, M., & Vignoli, A. (2010). Le unioni a secco tra elementi prefabbricati in c.a.: i risultati di un'indagine sperimentale. In C. T. E. C. dei T. della I. Edilizia (Ed.), *Atti del 18° Congresso CTE* (p. 640). Brescia.

Arnold, C. (1989). Cladding Design: Recent Architectural Trends and Their Impact on Seismic Design. *International Symposium on Architectural Precast Concrete Cladding - Its Contribution to Lateral Resistance of Buildings*. Chicago.

ASSOBETON, & ReLuis. (2007). *Schedario dei collegamenti in strutture prefabbricate*. Milano: ASSOBETON.

Bachman, R. E., & Bonneville, D. R. (2000). The Seismic Provisions of the 1997 Uniform Building Code. *Earthquake Spectra*, *16*(1), 85–100. https://doi.org/10.1193/1.1586084

Baird, A., Diaferia, R., Palermo, A., & Pampanin, S. (2011a). *Numerical modelling of local cladding-structure interaction*.

Baird, A., Diaferia, R., Palermo, A., & Pampanin, S. (2011b). Parametric investigation of seismic interaction between precast concrete cladding systems and moment resisting frames. *Structures Congress 2011*, 1286–1297.

Baird, A., Palermo, A., & Pampanin, S. (2012). Understanding cladding damage: A numerical investigation into a Christchurch earthquake case study. *New Zealand Society for Earthquake Engineering (NZSEE) Conference*. Christchurch, New Zealand.

Baldacci, R., Ceradini, G., & Giangreco, E. (1974). *Plasticità* (Centro italiano sviluppo impieghi acciaio, ed.). Cisia.

Belleri, A., Cornali, F., Passoni, C., Marini, A., & Riva, P. (2018). Evaluation of out-of-plane seismic performance of column-to-column precast concrete cladding panels in one-storey industrial buildings. *Earthquake Engineering & Structural Dynamics*, *47*(2), 397–417.

Belleri, A., Torquati, M., Marini, A., & Riva, P. (2016a). Horizontal cladding panels: in-plane seismic performance in precast concrete buildings. *Bulletin of Earthquake Engineering*, *14*(4), 1103–1129. https://doi.org/10.1007/s10518-015-9861-8

Belleri, A., Torquati, M., Marini, A., & Riva, P. (2016b). Horizontal cladding panels: in-plane seismic performance in precast concrete buildings. *Bulletin of Earthquake Engineering*, *14*(4), 1103–1129. https://doi.org/10.1007/s10518-015-9861-8

Belleri, A., Torquati, M., & Riva, P. (2013). *Seismic performance of ductile connections between precast beams and roof elements*.

Belletti, B., Baroni, L., Gasperi, A., & Stocchi, A. (2013). Il ruolo dei collegamenti fra elementi di copertura e travi principali nella definizione del comportamento a diaframma di edifici prefabbricati. *Atti Del XV Convegno Dell'Associazione Nazionale Di Ingegneria Sismica "L'ingegneria Sismica in Italia", Padova*, *30*.

Belletti, B., Gasperi, A., & Spagnoli, A. (2015). Capacity Design–Based Seismic Forces in Floor-to-Beam Connections of Precast Concrete Frames. *Journal of Performance of Constructed Facilities*, *29*(6), 4014161. https://doi.org/10.1061/(ASCE)CF.1943-5509.0000649

Beschi, C., Metelli, G., Riva, P., & Luitprandi, G. (2010). Studio sperimentale del comportamento isteretico di una connessione tegolo-trave per strutture prefabbricate. *18° Congresso CTE (Collegio Dei Tecnici Della Industrializzazione Edilizia)*, 111–122.

Biondini, F., Dal Lago, B. A., & Toniolo, G. (2010). *Influenza delle connessioni tra pannelli sulla risposta sismica di costruzioni prefabbricate*.

Biondini, F., Dal Lago, B. A., & Toniolo, G. (2013). Role of wall panel connections on the seismic performance of precast structures. *Bulletin of Earthquake Engineering*, *11*, 1061–

1081. https://doi.org/10.1007/s10518-012-9418-z

Biondini, F., Dal Lago, B., & Toniolo, G. (2017). Experimental tests on dissipative cladding connection systems of precast structures. *Sixteen World Conference on Earthquake Engineering (16th WCEE), Santiago, Chile*, 9–13.

Biondini, F., Ferrara, L., Negro, P., & Toniolo, G. (2004). Results of pseudodynamic test on a prototype of precast RC frame. *International Conference on Advances in Concrete and Structures (ICACS)*, 1–10. RILEM.

Biondini, F., & Toniolo, G. (2009). Probabilistic calibration and experimental validation of the seismic design criteria for one-story concrete frames. *Journal of Earthquake Engineering*, *13*(4), 426–462.

Bournas, D., & Negro, P. (2012). Seismic Performance of Mechanical Connections in the SAFECAST Precast Building. *15th World Conference on Earthquake Engineering (15 WCEE)*, *3*(1988), 10. https://doi.org/10.1007/s00422-012-0521-7

Chan, K. (2003). *Experimental investigation of push-pull precast cladding connections*.

Charney, F. A., & Harris, J. R. (1989). The effect of architectural precast concrete cladding on the lateral response of multistory buildings. *Memorias Del Architectural Precast Concrete Cladding*, 80–96.

Chen, M. C., Pantoli, E., Wang, X., Astroza, R., Ebrahimian, H., Hutchinson, T. C., … Faghihi, M. (2015). Full-Scale Structural and Nonstructural Building System Performance during Earthquakes: Part I – Specimen Description, Test Protocol, and Structural Response. *Earthquake Spectra*, *32*(2), 737–770. https://doi.org/10.1193/012414EQS016M

Cohen, J. M. (1995). Seismic Performance of Cladding: Responsibility Revisited. *Journal of Performance of Constructed Facilities*, *9*(4), 254–270. https://doi.org/10.1061/(ASCE)0887-3828(1995)9:4(254)

Cohen, J. M., & Powell, G. H. (1993). A design study of an energy-dissipating cladding system. *Earthquake Engineering & Structural Dynamics*, *22*(7), 617–632.

Craig, J. I., Goodno, B. J., Keister, M. J., & Fennell, C. J. (1986). Hysteretic Behavior of Precast Cladding Connections. *Dynamic Response of Structures*, 817–826. ASCE.

Craig, J. I., Leistikow, R., & Fennell, C. J. (1988). Experimental Studies of the Performance of Precast Cladding Connections. *Proceed'tzs Ninth World Conference on Earthquake Engineering, Held in Tokyo and Kyoto, Japr& On*, *6*, 201–206.

Dal Lago, B. A. (2015). *Seismic performance of precast structures with dissipative cladding panel connections*. Politecnico di Milano.

Dal Lago, B. A., Biondini, F., & Toniolo, G. (2018). Experimental Investigation on Steel W-Shaped Folded Plate Dissipative Connectors for Horizontal Precast Concrete Cladding Panels. *Journal of Earthquake Engineering*, *22*(5), 778–800. https://doi.org/10.1080/13632469.2016.1264333

Dal Lago, B. A., Biondini, F., Toniolo, G., & Lamperti Tornaghi, M. (2017). Experimental investigation on the influence of silicone sealant on the seismic behaviour of precast façades. *Bulletin of Earthquake Engineering*, *15*(4), 1771–1787. https://doi.org/10.1007/s10518-016-0045-y

Dal Lago, B. A., Lamperti Tornaghi, M., & Dal Lago, A. (2012). Studio sul comportamento bidirezionale di connessioni meccaniche scorrevoli pannello-telaio. *19° Convegno CTE*, 131–140.

Dal Lago, B. A., Lamperti Tornaghi, M. G., & Toniolo, G. (2013). Experimental behaviour of semi-dry column-foundation connections for precast buildings. In *Studies and Researches - Volume 32* (Edizioni I). Milano.

Dal Lago, B. A., Toniolo, G., & Lamperti Tornaghi, M. (2016). Influence of different mechanical column-foundation connection devices on the seismic behaviour of precast structures. *Bulletin of Earthquake Engineering*, *14*(12), 3485–3508. https://doi.org/10.1007/s10518-016-0010-9

Dassori, E. (2001). *La prefabbricazione in calcestruzzo: guida all'utilizzo nella progettazione* (Editrice BE-MA, Ed.). Milano.

DM. (1987). Decreto Ministeriale del 3 Dicembre 1987. *Norme Tecniche per La Progettazione, Esecuzione e Collaudo Delle Costruzioni Prefabbricate*. Rome: Ministero dei Lavori Pubblici.

DM. (1996). Decreto Ministeriale del 16 Gennaio 1996. *Norme Tecniche per Le Costruzioni in Zone Sismiche*. Rome: Ministero dei Lavori Pubblici.

EN 1992-1-1. *Eurocode 2: Design of concrete structures. Part 1-1: General rules and rules for buildings*. , (2004).

EN 1998-1-1. *Eurocode 8: Design of structures for earthquake resistance. Part 1: General rules, seismic actions and rules for buildings*. , (2005).

EN 1998-2. *Eurocode 8: Design of structures for earthquake resistance. Part 2: Bridges*. , (2009).

Ercolino, M, Magliulo, G., & Manfredi, G. (2016). Failure of a precast RC building due to Emilia-Romagna earthquakes. *Engineering Structures*, *118*, 262–273.

Ercolino, Marianna. (2014). *Seismic behavior of one-story precast buildings*. Università degli Studi di Napoli Federico II.

Ercolino, Marianna, Capozzi, V., Magliulo, G., & Manfredi, G. (2013). Influence of cladding panels on dynamic behaviour of one-storey precast building. *Opensees Days Italia: Atti Del Covegno*, 190–241.

Fardis, M. N., & Biskinis, D. E. (2003). Deformation capacity of RC members, as controlled by flexure or shear. *Otani Symposium*, *511530*.

Ferrara, L., Felicetti, R., Toniolo, G., & Zenti, C. (2011). Friction dissipative devices for cladding panels in precast buildings: An experimental investigation. *European Journal of Environmental and Civil Engineering*, *15*(9), 1319–1338. https://doi.org/10.1080/19648189.2011.9714857

Filiatrault, A., & Christopoulos, C. (2001). *Guidelines, Specifications, and Seismic Performance Characterization of Nonstructural Building Components and Equipment*.

Fischinger, M., Kramar, M., & Isaković, T. (2008). *Cyclic response of slender RC columns typical of precast industrial buildings*. 519–534. https://doi.org/10.1007/s10518-008-9064-7

Fischinger, M., Zoubek, B., Kramar, M., & Isaković, T. (2012). Cyclic response of dowel connections in precast structures. *15th World Conference on Earthquake Engineering*.

Gaiotti, R., & Smith, B. S. (1992). Stiffening of moment-resisting frame by precast concrete cladding. *PCI Journal*, *37*(5), 80–92.

Gavin, H. P. (2015). *Plastic Design of a Fixed-Fixed Beam-Column*. Durham, North Carolina USA: CEE 201L. Uncertainty, Design, and Optimization.

Germano, F., Tiberti, G., Plizzari, G., & Colombo, A. (2015). Experimental behavior of precast HSFRC columns in steel socket foundation under cyclic loads. *Engineering Structures*, *102*, 230–248. https://doi.org/10.1016/j.engstruct.2015.07.052

Giberson, M. F. (1967). *The response of nonlinear multi-story structures subjected to earthquake excitation*.

Giuffrè, A., & Pinto, P. (1970). Il comportamento del cemento armato per sollecitazioni cicliche di forte intensità. *Giornale Del Genio Civile*.

Gjelsvik, A. (1974). Interaction between frames and precast panel walls. *Journal of the Structural Division*, *100*(2), 405–426.

Goodno, Barry J, Will, K. M., & Palsson, H. (1980). Effect of cladding on building response to moderate ground motion. *Proc. 7th WCEE*, 449–456.

Goodno, Barry John, & Craig, J. (1989). Historical Overview of Studies on the Contribution of Cladding to Lateral Resistance of Buildings. *Architectural Precast Concrete Cladding–Its Contribution to Lateral Resistance of Buildings*, 36–47.

Goodno, Barry John, & Craig, J. (1998). Ductile cladding connection systems for seismic design. *Nist Gcr; 98-758*.

Goodno, Barry John, & Palsson, H. (1986). Analytical Studies of Building Cladding. *Journal of Structural Engineering*, *112*(4), 665–676. https://doi.org/10.1061/(ASCE)0733-

9445(1986)112:4(665)

Henry, R. M., & Roll, F. (1986). Cladding-frame interaction. *Journal of Structural Engineering*, *112*(4), 815–834.

Hunt, J. P., & Stojadinovic, B. (2010). Seismic performance assessment and probabilistic repair cost analysis of precast concrete cladding systems for multistory buildings. *PEER Report*.

IBC. International Building Code. , International Code Council, USA § (2018).

INGV. (n.d.). Retrieved October 24, 2019, from Istituto Nazionale di Geofisica e Vulcanologia website: http://zonesismiche.mi.ingv.it/class2004.html

International Federation for Structural Concrete. (2003). *Seismic Design of Precast Concrete Building Structures: State-of-the-art Report*. Retrieved from https://books.google.it/books?id=SSebCJWyhx4C

Isaković, T., Zoubek, B., & Fischinger, M. (2018). Full-scale shake table tests of cladding panels. *16th European Conference on Earthquake Engineering (16 ECEE)*. Tessaloniki.

Isakovic, T., Zoubek, B., Lopatic, J., & Fischinger, M. (2014). Experimental research of typical cladding panel connections in industrial buildings. *Proceedings of 2nd ECEES*, 24–29.

Isaković, T., Zoubek, B., Lopatič, J., Urbas, M., & Fischinger, M. (2013). *Report and card files on the tests performed on existing connections* (p. 104). p. 104. 1.2, SAFECLADDING - Improved fastening systems of cladding wall panels of precast buildings in seismic zones.

Iverson, J. K., & Hawkins, N. M. (1994). Performance of precast/prestressed building structures during Northridge earthquake. *PCI Journal*, *39*(2).

Karadogan, F., Yuksel, E., & Bal, I. E. (2012). The Seismic Behavior of An Asymmetric Exterior Precast Beam-Column Connection. *Proceedings of the 15th World Conference on Earthquake Engineering*.

Karadoğan, F., Yüksel, E., Khajehdehi, A., Özkaynak, H., Güllü, A., & Şenol, E. (2019). Cyclic behavior of reinforced concrete cladding panels connected with energy dissipative steel cushions. *Engineering Structures*, *189*, 423–439. https://doi.org/https://doi.org/10.1016/j.engstruct.2019.03.092

Kramar, M. (2008). *Seismic vulenrability of the precast reinforced concrete structures*. Fakulteta za gradbeništvo in geodezijo, Univerza v Ljubljani.

Kramar, M., Isaković, T., & Fischinger, M. (2010). Seismic collapse risk of precast industrial buildings with strong connections. *Earthquake Engineering & Structural Dynamics*, *39*(8), 847–868.

Luzi, L., Pacor, F., & Puglia, R. (2019). Italian Accelerometric Archive v 3.0 Istituto Nazionale di Geofisica e Vulcanologia, Dipartimento della Protezione Civile Nazionale. https://doi.org/10.13127/itaca.3.0

Luzi, L., Puglia, R., Russo, E., & ORFEUS WG5. (2016). Engineering Strong Motion Database, version 1.0. Istituto Nazionale di Geofisica e Vulcanologia, Observatories & Research Facilities for European Seismology. https://doi.org/10.13127/ESM

Magliulo, G., Capozzi, V., Fabbrocino, G., & Manfredi, G. (2011). Neoprene-concrete friction relationships for seismic assessment of existing precast buildings. *Engineering Structures*. https://doi.org/10.1016/j.engstruct.2010.11.011

Magliulo, G., Ercolino, M., & Manfredi, G. (2015). Influence of cladding panels on the first period of one-story precast buildings. *Bulletin of Earthquake Engineering*, *13*(5), 1531–1555. https://doi.org/10.1007/s10518-014-9657-2

Magliulo, G., Ercolino, M., Petrone, C., Coppola, O., & Manfredi, G. (2014). The Emilia Earthquake: Seismic Performance of Precast Reinforced Concrete Buildings. *Earthquake Spectra*, *30*(2), 891–912. https://doi.org/10.1193/091012EQS285M

Magliulo, G., Fabbrocino, G., & Manfredi, G. (2008). Seismic assessment of existing precast industrial buildings using static and dynamic nonlinear analyses. *Engineering Structures*, *30*(9), 2580–2588.

Mandelli Contegni, M., Palermo, A., & Toniolo, G. (2007). Strutture prefabbricate: scheadario

dei collegamenti. *Italian Civil Protection Department, ReLUIS and Assobeton*.

Mander, B. J., Priestley, N. M. J., & Park, R. (1988). Theoretical Stress-Strain Model for Confined Concrete. *Journal of Structural Engineering*, *114*(8), 1804–1826. https://doi.org/10.1061/(ASCE)0733-9445(1988)114:8(1804)

Marinini, L., Spatti, P., Riva, P., Nascimbene, R., Izzo, L., Spadavecchia, A., & Maffioletti, M. (2008). Sviluppo di una connessione dissipativa per strutture prefabbricate. In C.T.E. (Ed.), *17° Congresso C.T.E.* Roma.

MATLAB. (2018). *MATLAB 2018b*. Natick, Massachusetts: The MathWorks Inc.

Mazzoni, S., McKenna, F., Scott, M. H., & Fenves, G. L. (2006a). OpenSees: A Framework for Earthquake Engineering Simulation. *Pacific Earthquake Engineering Research (PEER) Center*. Retrieved from https://opensees.berkeley.edu/

Mazzoni, S., McKenna, F., Scott, M. H., & Fenves, G. L. (2006b). OpenSees command language manual. *Pacific Earthquake Engineering Research (PEER) Center*, *264*.

McMullin, K., Wong, T., Choi, C., & Chan, K. (2004). Seismic performance states of precast concrete cladding connections. *Memorias Del XIII Congreso Mundial de Ingeniería Sísmica*, (3379).

Medina, R. A., Sankaranarayanan, R., & Kingston, K. M. (2006). Floor response spectra for light components mounted on regular moment-resisting frame structures. *Engineering Structures*, *28*(14), 1927–1940. https://doi.org/https://doi.org/10.1016/j.engstruct.2006.03.022

Memari, A. M., Hathairat, M., & Yousef, B. (2004). Study of the Effect of Near-Source Vertical Ground Motion on Seismic Design of Precast Concrete Cladding Panels. *Journal of Architectural Engineering*, *10*(4), 167–184. https://doi.org/10.1061/(ASCE)1076-0431(2004)10:4(167)

Menegotto, M. (2009). Experiences from L'Aquila 2009 earthquake. *Proceedings of the 3rd Fib Congress*.

Menichini, G. (2016). *Il ruolo dei collegamenti in copertura nella risposta sismica di edifici prefabbricati monopiano* (Università di Firenze). Retrieved from https://sol.unifi.it/tesi/consultazione

Menichini, G., Del Monte, E., Falsini, C., Bartoli, G., & Boschi, S. (2017). Analysis of a tile-beam connection for precasted industrial buildings and its influence on the global seismic response of the structure. *XXVII Convegno ANIDIS L'ingegneria Sismica in Italia*, 35–46. Pistoia: Pisa University Press.

Metelli, G., Beschi, C., & Riva, P. (2011). Cyclic behaviour of a column to foundation joint for concrete precast structures. *European Journal of Environmental and Civil Engineering*. https://doi.org/10.3166/EJECE.15.1297-1318

Muthukumar, S., & DesRoches, R. (2006). A Hertz contact model with non-linear damping for pounding simulation. *Earthquake Engineering & Structural Dynamics*, *35*(7), 811–828.

Negro, P., & Lamperti Tornaghi, M. (2017). Seismic response of precast structures with vertical cladding panels: The SAFECLADDING experimental campaign. *Engineering Structures*, *132*, 205–228. https://doi.org/https://doi.org/10.1016/j.engstruct.2016.11.020

NIST. (1995). *Literature review on seismic performance of building cladding systems*. Emeryville, California, U.S.A.: National Institue of Standards and Technology.

NPCA. (2012). *Architectural precast concrete wall panels: connection guide*. Carmel, Illinois, U.S.A.: National Precast Concrete Association (NPCA) Document.

NTC. NTC 2008 - norme tecniche per le costruzioni. , Decreto Ministeriale § (2008).

NTC. Decreto Ministeriale del 17-01-2018. , Norme Tecniche per le Costruzioni § (2018).

OPCM 3274. Ordinanza del Presidente del Consiglio dei Ministri n. 3274. , Primi elementi in materia di criteri generali per la classificazione sismica del territorio nazionale e di normative tecniche per le costruzioni in zona sismica § (2003).

Oppenheim, I. J. (1973). Dynamic behavior of tall buildings with cladding. *Proceedings, Fifth*

World Conference on Earthquake Engineering, Rome, Italy, 2769–2773.

Orlando, M., & Piscitelli, L. R. (2018). Experimental investigation on static and cyclic behaviour of flanged unions for precast reinforced concrete columns. *European Journal of Environmental and Civil Engineering*, *22*(8), 927–945. https://doi.org/10.1080/19648189.2016.1229226

Pall, A. S. (1989). Friction damped connections for precast concrete cladding. *Proceedings of the International Symposium on Architectural Precast Concrete Cladding*.

Palsson, H., & Goodno, B. J. (1988). Influence of interstory drift on cladding panels and connections. *Ninth World Conference on Earthquake Engineering*, 213–218.

Palsson, H., Goodno, B. J., Craig, J. I., & Will, K. M. (1984). Cladding influence on dynamics response of tall buildings. *Earthquake Engineering & Structural Dynamics*, *12*(2), 215–228.

Pantoli, E. (2016). *Seismic Behavior of Architectural Precast Concrete Cladding Panels and Connections*. UC San Diego.

Pantoli, E., Chen, M. C., Wang, X., Astroza, R., Ebrahimian, H., Hutchinson, T. C., … Faghihi, M. (2015). Full-Scale Structural and Nonstructural Building System Performance during Earthquakes: Part II – NCS Damage States. *Earthquake Spectra*, *32*(2), 771–794. https://doi.org/10.1193/012414EQS017M

Park, R., & Paulay, T. (1975). *Reinforced concrete structures*. John Wiley & Sons.

PCI. (2007). *Architectural Precast Concrete* (Third edit). Chicago: Pecast/Prestress Concrete Institute.

Pinelli, J., & Craig, J. I. (1989). Experimental Studies on the Performance of Mexican Precast Cladding Connections. *Architectural Precast Concrete Cladding–Its Contribution to Lateral Resistance of Buildings*, 159–176.

Pinelli, J., Craig, J. I., & Goodno, B. J. (1995). Energy-Based Seismic Design of Ductile Cladding Systems. *Journal of Structural Engineering*, *121*(3), 567–578. https://doi.org/10.1061/(ASCE)0733-9445(1995)121:3(567)

Pinelli, J., Craig, J. I., Goodno, B. J., & Hsu, C. (1993). Passive Control of Building Response Using Energy Dissipating Cladding Connections. *Earthquake Spectra*, *9*(3), 529–546. https://doi.org/10.1193/1.1585728

Pinelli, J., Moor, C., Craig, J. I., & Goodno, B. J. (1992). Experimental testing of ductile cladding connections for building facades. *The Structural Design of Tall Buildings*, *1*(1), 57–72.

Pinelli, J., Moor, C., Craig, J. I., & Goodno, B. J. (1996). Testing of energy dissipating cladding connections. *Earthquake Engineering & Structural Dynamics*, *25*(2), 129–147.

Popa, V., Papurcu, A., Cotofana, D., & Pascu, R. (2015). Experimental testing on emulative connections for precast columns using grouted corrugated steel sleeves. *Bulletin of Earthquake Engineering*. https://doi.org/10.1007/s10518-014-9715-9

Psycharis, I. N., Kalyviotis, I. M., & Mouzakis, H. P. (2018). Experimental investigation of the response of precast concrete cladding panels with integrated connections under monotonic and cyclic loading. *Engineering Structures*, *159*, 75–88. https://doi.org/https://doi.org/10.1016/j.engstruct.2017.12.036

Psycharis, I. N., & Mouzakis, H. P. (2012a). Assessment of the seismic design of precast frames with pinned connections from shaking table tests. *Bulletin of Earthquake Engineering*. https://doi.org/10.1007/s10518-012-9372-9

Psycharis, I. N., & Mouzakis, H. P. (2012b). Shear resistance of pinned connections of precast members to monotonic and cyclic loading. *Engineering Structures*, *41*, 413–427. https://doi.org/10.1016/j.engstruct.2012.03.051

Psycharis, I. N., Mouzakis, H. P., & Carydis, P. G. (2012). Experimental investigation of the seismic behaviour of precast structures with pinned beam-to-column connections. *Geotechnical, Geological and Earthquake Engineering*. https://doi.org/10.1007/978-94-007-1977-4_18

Restrepo, J., Fleischman, R. B., Schoettler, M. J., Nigbor, R., & Deutsch, D. (2012). *RAPID: Mapping of Damage in Precast Concrete Buildings from the February 2011 Christchurch, New Zealand Earthquake*.

Rihal, S. S. (1988). Seismic behavior and design of precast facades, cladding and connections in low/medium rise buildings. *Report ARCE R88-1, California Institute of Technology*.

Rihal, S. S. (1989). *Earthquake resistance and behavior of architectural precast cladding and connections*. California Polytechnic State University: Earthquake Research Unit.

Romão, X., Costa, A. A., Paupério, E., Rodrigues, H., Vicente, R., Varum, H., & Costa, A. (2013). Field observations and interpretation of the structural performance of constructions after the 11 May 2011 Lorca earthquake. *Engineering Failure Analysis*, *34*, 670–692. https://doi.org/https://doi.org/10.1016/j.engfailanal.2013.01.040

Sack, R. L., Beers, R. J., & Thomas, D. L. (1989). Seismic behavior of architectural precast cladding. *Proceedings, Architectural Precast Concrete Cladding-Its Contribution to Lateral Resistance of Buildings*, 141–158.

Saisi, A. E., & Toniolo, G. (1998). Precast rc columns under cyclic loading: an experimental programme oriented to EC8. *Studi e Ricerche-Politecnico Di Milano. Scuola Di Specializzazione in Costruzioni in Cemento Armato*, (19), 373–413.

Savoia, M., Buratti, N., & Vincenzi, L. (2017). Damage and collapses in industrial precast buildings after the 2012 Emilia earthquake. *Engineering Structures*, *137*, 162–180. https://doi.org/https://doi.org/10.1016/j.engstruct.2017.01.059

Simeonov, S. (1985). *Building construction under seismic conditions in the balkan region: design and construction of prefabricated reinforced concrete building systems*. United Nations Industrial Development Organization, executing agency for the ….

Singh, M. P., Moreschi, L. M., Suarez, L. E., & Matheu, E. E. (2006a). Seismic design forces. I: Rigid nonstructural components. *Journal of Structural Engineering*, *132*(10), 1524–1532.

Singh, M. P., Moreschi, L. M., Suarez, L. E., & Matheu, E. E. (2006b). Seismic design forces. II: Flexible nonstructural components. *Journal of Structural Engineering*, *132*(10), 1533–1542.

Smith, B. S., & Gaiotti, R. (1989). Interaction of precast concrete cladding with a story-height frame module. *Proceedings of the Architectural Precast Concrete Cladding-Its Contribution to Lateral Resistance of Buildings*, 48–61.

Soroushian, P., Obaseki, K., Rojas, M., & Najm, H. S. (1987). BEHAVIOR OF BARS IN DOWEL ACTION AGAINST CONCRETE COVER. *ACI Structural Journal*.

Spacone, E., Filippou, F. C., & Taucer, F. F. (1996). Fibre beam–column model for non-linear analysis of R/C frames: Part I. Formulation. *Earthquake Engineering & Structural Dynamics*, *25*(7), 711–725.

Starešinič, G., Zoubek, B., Gams, M., Isaković, T., & Fischinger, M. (2020). Modelling in-plane dynamic response of a fastening system for horizontal concrete facade panels in RC precast buildings. *Engineering Structures*, *224*, 111210. https://doi.org/https://doi.org/10.1016/j.engstruct.2020.111210

Sullivan, T. J., Calvi, P. M., & Nascimbene, R. (2013). Towards improved floor spectra estimates for seismic design. *Earthquakes and Structures*, *4*(1), 109–132.

Thiel, C. C., Elsesser, E., Lindsay, J., Kelly, T., Bertero, V. V, Filippou, F., & McCann, R. (1986). Seismic energy absorbing cladding system: A feasibility study. *Proc. ATC-17 Seminar and Workshop on Base Isolation and Passive Energy Dissipation, ATC, San Francisco, CA*.

Toniolo, G. (2014). Ruolo dei sistemi di connessione dei pannelli di tamponamento nel comportamento sismico degli edifici prefabbricati. *20° Congresso C.T.E. (Collegio Dei Tecnici Della Industrializzazione Edilizia)*. Milano.

Toniolo, G., & Colombo, A. (2012). Precast concrete structures: the lessons learned from the L'Aquila earthquake. *Structural Concrete*, *13*(2), 73–83. https://doi.org/10.1002/suco.201100052

Vassiliou, M. F., Mackie, K. R., & Stojadinovic, B. (2016). A finite element model for seismic

response analysis of deformable rocking frames. *Earthquake Engineering & Structural Dynamics*. https://doi.org/10.1002/eqe.2799

Vassiliou, M. F., Mackie, K. R., & Stojadinović, B. (2014). Dynamic response analysis of solitary flexible rocking bodies: modeling and behavior under pulse-like ground excitation. *Earthquake Engineering & Structural Dynamics*, *43*(10), 1463–1481.

Vintzeleou, E., & Tassios, T. (1985). Mechanisms of load transfer along interfaces in reinforced concrete: prediction of shear force vs. shear displacement curves. *Studi e Ricerche - Corso Di Perfezionamento per Le Costruzioni in Cemento Armato Fratelli Pasenti*.

Viola, E. (2001). *Fondamenti di dinamica e vibrazione delle strutture* (Pitagora, Ed.). Bologna.

Wang, M. L. (1986a). Full Scale Tests of Cladding Components. *Dynamic Response of Structures*, 497–504. ASCE.

Wang, M. L. (1986b). *Nonstructural Element Test Phase: US-Japan Cooperative Research Project on a Full Scale Steel Test Frame*. Center for Environmental Design Research.

Wang, M. L. (1987). Cladding Performance on a Full Scale Test Frame. *Earthquake Spectra*, *3*(1), 119–173. https://doi.org/10.1193/1.1585423

Wang, M. L., Sakamoto, I., & Bassler, B. L. (1992). Design of cladding for earthquakes. *Cladding. McGraw-Hill, Inc., New York, NY*, 71–87.

Weidlinger, P. (1973). Shear field panel bracing. *Journal of the Structural Division*, *99*(7), 1615–1631.

Wilkinson, S., Grant, D., Williams, E., Paganoni, S., Fraser, S., Boon, D., … Free, M. (2013). Observations and implications of damage from the magnitude Mw 6.3 Christchurch, New Zealand earthquake of 22 February 2011. *Bulletin of Earthquake Engineering*, *11*(1), 107–140. https://doi.org/10.1007/s10518-012-9384-5

Zoubek, B. (2015). *Influence of the connections on the seismic response of precast reinforced concrete structures*. Doctoral dissertation. University of Ljubljana, Faculty of civil and ….

Zoubek, B., Fahjan, Y., Fischinger, M., & Isaković, T. (2014). Nonlinear finite element modelling of centric dowel connections in precast buildings. *Computers and Concrete*. https://doi.org/10.12989/cac.2014.14.4.463

Zoubek, B., Fischinger, M., & Isaković, T. (2014). Estimation of the cyclic capacity of beam-to- column dowel connections in precast industrial buildings. *Bulletin of Earthquake Engineering*, (July). https://doi.org/10.1007/s10518-014-9711-0

Zoubek, B., Fischinger, M., & Isaković, T. (2016). Cyclic response of hammer-head strap cladding-to-structure connections used in RC precast building. *Engineering Structures*, *119*, 135–148. https://doi.org/https://doi.org/10.1016/j.engstruct.2016.04.002

Zoubek, B., Fischinger, M., & Isaković, T. (2018). Seismic response of short restrainers used to protect cladding panels in RC precast buildings. *Journal of Vibration and Control*, *24*(4), 645–658. https://doi.org/10.1177/1077546316659780

"It is not his possession of knowledge, of irrefutable truth, that makes the man of science, but his persistent and recklessly critical quest for truth."

"Non il possesso della conoscenza, della verità irrefutabile, fa l'uomo di scienza, ma la ricerca critica, persistente e inquieta, della verità."

[Karl Popper]